UNIVERSIDAD NACIONAL AUTÓNOMA DE MÉXICO

DOCTORADO EN CIENCIAS BIOMÉDICAS
FACULTAD DE MEDICINA

EL 17BETA-ESTRADIOL INDUCE HIPERREACTIVIDAD DE LAS VÍAS AÉREAS DE COBAYO POR LA INHIBICIÓN DE LA ATPASA DE CALCIO DE LA MEMBRANA PLASMÁTICA

TESIS
QUE PARA OPTAR POR EL GRADO DE:
DOCTOR EN CIENCIAS

PRESENTA:
BIANCA SUSANA ROMERO MARTÍNEZ

DIRECTOR DE TESIS

DR. LUIS MANUEL MONTAÑO RAMÍREZ
FACULTAD DE MEDICINA, UNAM
Apruebo esta versión de la tesis 07/04/2025

COMITÉ TUTOR

DR. CARLOS PÉREZ PLASENCIA
FACULTAD DE ESTUDIOS SUPERIORES IZTACALA, UNAM
Apruebo esta versión de la tesis 07/04/2025

DR. MARCO ANTONIO CERBÓN CERVANTES
FACULTAD DE MEDICINA, UNAM
Apruebo esta versión de la tesis 07/04/2025

MÉXICO, D. F. 7 DE ABRIL DE 2025

Agradecimientos

Al Programa de Doctorado en Ciencias Biomédicas de la Universidad Nacional Autónoma de México por mis estudios durante mi formación.

Al Consejo Nacional de Humanidades Ciencias y Tecnología (CONHACYT) por la beca otorgada durante la realización del posgrado con el número de solicitud: 2020-000013-01NACF-12778. Número de CVU: 469822.

A la Dirección General de Asuntos del Personal Académico (DGAPA), Universidad Nacional Autónoma de México por el apoyo otorgado al Dr. Luis Manuel Montaño (IN200522) y al Dr. Jorge Reyes García (IA203924) para la realización de este proyecto de tesis.

Esta tesis contó con el respaldo institucional otorgado al Dr. Edgar Flores Soto por la División de Investigación de la Facultad de Medicina de la Universidad Nacional Autónoma de México, mediante el proyecto identificado con la clave FM/DI/123/2024.

A mi tutor principal el Dr. Luis Manuel Montaño y a los miembros de mi comité tutoral conformado por el Dr. Carlos Pérez Plasencia y el Dr. Marco Antonio Cerbón Cervantes por su apoyo y enseñanzas a lo largo de mi formación durante el posgrado.

Al Dr. Edgar Flores Soto por su invaluable guía y enseñanzas durante todo mi posgrado, así como su apoyo y amistad, pero sobre todo por creer en mí.

Al Dr. Héctor Solís Chagoyán por su amistad y enseñanzas.

A Rosalba Rodríguez Linares y a Pilar Romo por su apoyo y amistad.

A mi madre y mi familia, por su apoyo incondicional, por sus palabras de aliento y por acompañarme para cumplir mis sueños.

A Briseyda Sofia Hernández Peña y a Brenda Elisa Valladares Hernández por ser mis amigas y compañeras durante este camino de aprendizaje.

Muchas gracias a todos.

Índice

Abreviaturas

Abreviatura	Término	Abreviatura	Término
$[Ca^{2+}]_e$	Concentraciones extracelulares de calcio	CYP11A1	Citocromo P450scc
$[Ca^{2+}]_i$	Concentraciones de calcio intracelular	CYP17A1	Citocromo P450 17A1
$[Ca^{2+}]_{RS}$	Concentraciones de calcio en el retículo sarcoplásmico	CYP19A1	Aromatasa
°C	Grados Celsius	D600	Clorhidrato de metoxiverapamilo
µL	Microlitro	DHEA	Dehidroepiandrosterona
µM	Micromolar	DPN	Diarilpropionitrilo (Agonista específico del receptor REβ)
17β-HSD	17β-Hidroxiesteroide deshidrogenasa	E2	17β-estradiol
3β-HSD	3β-Hidroxiesteroide deshidrogenasa	E3	Estriol
AA	Aminoácido	EE	Error estándar de la media
ABC	Área bajo la curva	EGTA	Ácido aminopolicarboxílico
AC	Adenilato ciclasa	ERE	Elementos de respuesta estrogénica
AM	Alérgenos mixtos	ERK1/2	Cinasas reguladas por señales extracelulares 1/2
AMPc	Adenosín monofosfato cíclico	FCCP	Cianuro de carbonilo 4-(trifluorometoxi)fenilhidrazona
ARNm	Ácido ribonucleico mensajero	FeNO	Óxido nítrico exhalado
ATP	Trifosfato de Adenosina	FSH	Hormona folículo estimulante
Ca^{2+}	Calcio	Fura-2 AM	Fura-2-acetoximetil éster
$CaCl_2$	Cloruro de Calcio	g	Gramo
CAM	Calmodulina	GPCR	Receptor membranal acoplado a proteínas G
CCDV-L	Canal de calcio dependiente de voltaje tipo-L	GPR30	Receptor membranal estrogénico acoplado a proteína G
Cch	Carbacol	h	Hora
CE	Carboxieosina	H^+	Hidrógeno
CE_{50}	Concentración efectiva 50	NMDA	N-metil-D-aspartato
CI_{50}	Concentración inhibitoria 50	IgE	Inmunoglobulina E
CO_2	Dióxido de carbono	IL-13	Interleucina 13
CREB	Proteína de unión al elemento de respuesta de AMPc	IL-4	Interleucina 4
HR	Hiperreactividad	PDE4	Fosfodiesterasa 4
CPA	Ácido ciclopiazónico	IP_3	Inositol 1,4,5-trifosfato

Kcal/mol	Kilo caloría/mol	PKA	Proteínas cinasas A
KCl	Cloruro de Potasio	PKC	Proteínas cinasas C
kDa	kiloDaltons	PKG	Proteína cinasa G
Kg	Kilogramo	PLCβ	Fosfolipasa C Beta
Ki	Constante de inhibición	pM	Picomolar
La^{3+}	Lantano	PMCA	ATPasa de Ca^{2+} de la membrana plasmática
LH	Hormona luteinizante	PPT	Propilpirazoltriol (Agonista específico del receptor REα)
MAPK	Proteínas cinasas activadas por mitógenos	RE	Receptor estrogénico
mg	Miligramo	rpm	Revoluciones por minuto
Mg^{2+}	Magnesio	RS	Retículo sarcoplásmico
$MgSO_4$	Sulfato de magnesio	RyR	Receptor de Rianodina
Min	Minuto	SERCA	ATPasa de Ca^{2+} del retículo sarcoplásmico
mL	Mililitro	StAR	Proteína reguladora aguda esteroidogénica STARD1
MLVA	Músculo liso de vía aérea	STIM1	Molécula de interacción estromal 1
mM	Milimolar	Th17	Linfocitos T cooperadores tipo 17
Na^+	Sodio	Th2	Linfocito T cooperador tipo 2
NaCl	Cloruro de sodio	TM	Transportador mitocondrial
$NaHCO_3$	Bicarbonato de Sodio	TNF-α	Factor de necrosis tumoral alfa
NCX	Intercambiador Na^+/Ca^{2+}	U-0126	Inhibidor de ERK 1/2
nM	Nanomolar	WAY-200070	Agonista específico del receptor REβ
O_2	Oxígeno	ΔG	Delta G

Índice de figuras

RESUMEN

Introducción: En mujeres asmáticas, las fluctuaciones en las concentraciones séricas del 17β-estradiol (E2) están asociadas con el desarrollo y la gravedad de la enfermedad del asma. Según reportes epidemiológicos sobre el asma, en la infancia existe mayor incidencia en niños, comparado con niñas, y esta relación se invierte una vez que inicia la pubertad, afectando primordialmente a las mujeres. Esto sugiere que la hiperreactividad de las vías aéreas es influenciada por el E2. Se conoce que el E2 tiene efectos no genómicos a través de mecanismos que regulan las concentraciones de Ca^{2+} intracelular ($[Ca^{2+}]_i$); sin embargo, se desconoce su efecto sobre la ATPasa de Ca^{2+} de la membrana plasmática (PMCA), la ATPasa de Ca^{2+} del retículo sarcoplásmico (SERCA) y el intercambiador Na^+/Ca^{2+} (NCX). **Métodos:** Se utilizaron cobayos machos de la cepa Hartley de 300-400 gramos. En miocitos traqueales de cobayo se midieron las concentraciones de Ca^{2+} intracelular por medio de microfluorometría. En anillos traqueales de cobayo se midió la contracción del músculo liso de vía aérea (MLVA) por medio de órganos aislados. Mediante Western blot, se midió la expresión de la PMCA. Por medio de la técnica de acoplamiento molecular, se analizó la interacción entre los estrógenos y las ATPasas de Ca^{2+}. **Resultados:** En los anillos traqueales de cobayo, la incubación aguda de E2 produjo un incremento en la máxima contracción muscular inducida por carbacol (Cch). En miocitos aislados del área traqueal, la incubación con E2 (5 min) produjo una meseta de Ca^{2+} sostenida en la respuesta transitoria de Ca^{2+} inducida por cafeína. El bloqueo del canal de Ca^{2+} dependiente de voltaje tipo L (CCDV-L) con D600 no modificó la cinética de la respuesta transitoria de Ca^{2+} inducida por cafeína. La inhibición de SERCA con ácido ciclopiazónico y la inhibición de las cinasas reguladas por señales extracelulares ERK1/2 con U-0126 no modificaron la cinética del efecto de E2 en la respuesta de Ca^{2+} inducida por cafeína. La entrada capacitativa de Ca^{2+} y la actividad del transportador mitocondrial no fueron afectadas por la incubación aguda de E2. La incubación con los inhibidores de PMCA, lantano y carboxieosina (CE), revirtió parcialmente la meseta de Ca^{2+} sostenida producida por el E2 en la respuesta de cafeína. En el MLVA se demostró la expresión de las isoformas de los genes PMCA1 y PMCA4 por medio del análisis por Western blot. A través de experimentos de órganos aislados en anillos traqueales de cobayo, se observó que la inhibición de PMCA con CE (15 min) induce hiperreactividad a la contracción inducida por Cch. Mediante la técnica de acoplamiento molecular se observó que el E2 puede interactuar con ambas isoformas de la PMCA. **Conclusión:** El 17β-estradiol indujo la hiperreactividad de las vías aéreas mediante la inhibición de la PMCA, probablemente representando uno de los mecanismos de participación en la exacerbación de la sintomatología de la enfermedad del asma en mujeres asociado con la menstruación o durante el embarazo.

ABSTRACT

Introduction: In asthmatic women, fluctuations in serum 17β-estradiol (E2) concentrations are associated with the development and severity of the disease of asthma. According to epidemiological reports on asthma, there exists a higher incidence in boys, compared with girls during childhood, and this relationship is reversed once puberty begins, primarily affecting women. This suggests that airway hyperreactivity is influenced by E2. 17β-estradiol is known to have non genomic effects through mechanisms that regulate intracellular Ca^{2+} concentrations ($[Ca^{2+}]_i$); however, its effect on the plasma membrane Ca^{2+} ATPase (PMCA), the sarcoplasmic reticulum Ca^{2+} ATPase (SERCA) and the Na^{+}/Ca^{2+} exchanger (NCX) are unknown. **Methods:** Male guinea pigs of the Hartley strain weighing 300-400 grams were used. Intracellular Ca^{2+} concentrations were measured in guinea pig tracheal myocytes by microfluorometry. Airway smooth muscle (ASM) contraction was measured in guinea pig tracheal rings through organ baths. PMCA expression was measured by Western blot. The interaction between estrogens and with the Ca^{2+} ATPases was analyzed by the technique of molecular docking. **Results:** In guinea pig tracheal rings, acute incubation with E2 produced an increase in the maximum muscular contraction induced by carbachol (Cch). In isolated myocytes from the tracheal area, incubation with E2 (5 min) produced a sustained Ca^{2+} plateau in the caffeine-induced transient Ca^{2+} response. Blockade of the L-type voltage-dependent Ca^{2+} channel (L-VDCC) with D600 did not modify the kinetics of the caffeine-induced Ca^{2+} transient response. Inhibition of SERCA with cyclopiazonic acid and inhibition of the extracellular signal-regulated kinases 1/2 with U-0126 did not modify the kinetics of the effect of E2 on the caffeine-induced Ca^{2+} response. Capacitative Ca^{2+} entry and mitochondrial transporter activity were not affected by acute E2 incubation. Incubation with the PMCA inhibitors lanthanum and carboxyeosin (CE) partially reversed the sustained Ca^{2+} plateau produced by E2 in the caffeine response. In the ASM, the expression of the genes PMCA1 and PMCA4 isoforms was demonstrated by Western blot analysis. Through organ bath experiments in guinea pig tracheal rings, it was observed that the inhibition of PMCA with CE (15 min) induced hyperreactivity to the Cch-induced contraction. Through the molecular docking technique, it was observed that E2 could interact with both PMCA isoforms. **Conclusion:** 17β-estradiol induced airway hyperreactivity by inhibiting PMCA; probably representing one of the mechanisms participating in the exacerbation of asthma symptoms in women associated with menstruation or during pregnancy.

1. Introducción

1.1 Asma

El asma es una enfermedad multifactorial caracterizada por inflamación crónica, hiperreactividad (HR), obstrucción reversible de las vías respiratorias y diversos síntomas respiratorios, que incluyen dificultad para respirar, sibilancias, opresión en el pecho y tos[1]. El asma afecta a todos los grupos de edad y es una enfermedad crónica que afecta aproximadamente a 300 millones de personas en todo el mundo[1]. Los datos clínicos sugieren que el desarrollo y la gravedad del asma están influenciados por la edad y el sexo[2,3]. En la infancia, el asma predomina en los niños. Sin embargo, después de la pubertad esta relación se invierte ya que se observa una mayor frecuencia de asma en las mujeres durante la adolescencia y durante toda la edad adulta, coincidiendo con el incremento y ciclos de las hormonas sexuales femeninas[2-4]. La gravedad del asma se ha relacionado con cambios en las concentraciones hormonales séricas durante el ciclo menstrual, lo que se correlaciona con niveles elevados de estrógenos y progesterona y afecta entre el 11 y el 45% de las mujeres asmáticas[2,3,5,6]. En estas pacientes, el embarazo es una preocupación específica ya que se ha observado que, durante la gestación, un tercio de las gestantes presenta empeoramiento de los síntomas, un tercio mejora y un tercio no presenta cambios[2,7].

Durante sus años reproductivos, las mujeres experimentan fluctuaciones significativas en la concentración de hormonas sexuales, lo que influye en el tiempo de exposición a estas en las células blanco (músculo liso de vía aérea (MLVA)[8,9], neurona[10,11], eritrocitos[12], hepatocitos[13], etc.), teniendo efectos tanto genómicos (ejecutados en horas o días) como no genómicos (inducidos en segundos a minutos). Los efectos del 17β-

estradiol (E2) pueden ocurrir mediante la ocupación de receptores estrogénicos (RE) específicos α, β y GPR30, y mediante la interacción directa con diferentes proteínas[2,8,14-16]. En este sentido, a través de efectos no genómicos, se ha demostrado que el E2 activa una multitud de vías, incluyendo la producción de adenosina monofosfato cíclico (AMPc)[9], proteínas cinasas activadas por mitógenos (MAPK)[10,11,17,18], proteínas cinasas A (PKA)[19,20], proteínas cinasas C (PKC)[20] y cinasas de residuos de tirosina[10]. La actividad de esta hormona no se limita a las funciones reproductivas, y es un importante regulador de multitud de procesos fisiológicos en otros órganos. Las células del MLVA expresan receptores REα y REβ[8] que se ha demostrado que modulan la concentración de Ca^{2+} intracelular, lo que probablemente contribuye al dimorfismo sexual observado en la prevalencia y gravedad del asma[2,8,14].

1.2 Influencia de las hormonas sexuales femeninas sobre el asma

Las hormonas sexuales desempeñan un papel importante en el desarrollo y la severidad de la enfermedad del asma. Durante la infancia, más niños que niñas son diagnosticados con asma, presenta un riesgo cuatro veces mayor hasta los 14 años de edad[2,21,22]. Durante la pubertad se invierte este riesgo, dado que la frecuencia comienza a afectar más a las niñas y sigue esta tendencia durante la edad reproductiva de la mujer[2,23-25]. Esta misma tendencia es observada en la población mexicana[26]. Interesantemente, las niñas con un inicio de pubertad temprana, es decir, menarca antes de los 12 años, presentan aumento en el riesgo a desarrollar asma durante la pubertad en comparación con aquellas que presentan una menarca tardía[2,27,28].

En la etapa adulta, el 40% de las mujeres asmáticas presentan asma perimenstrual, caracterizadas por cambios en la severidad o exacerbación del asma en relación con el ciclo menstrual[2,29-31]. Un estudio encontró que el asma perimenstrual se asoció con la fase lútea del ciclo menstrual, donde se observó un incremento en las concentraciones séricas de E2, en comparación con mujeres asmáticas sin asma perimenstrual y con las mujeres sin asma[5]. Este empeoramiento de la sintomatología en mujeres asmáticas genera una mayor necesidad de broncodilatadores, una mayor frecuencia de hospitalizaciones[2,23,29,32] y un riesgo elevado de intubación y de mortalidad[5,33]. Esta severidad podría estar relacionada con las fluctuaciones hormonales que presentan las mujeres. Incluso, se ha reportado que, en algunas mujeres asmáticas con asma leve o moderado, pero no en casos severos, las exacerbaciones causadas por el asma perimenstrual pueden mejorar con el uso de anticonceptivos orales, posiblemente debido a la disminución de la variabilidad hormonal[2,34-36]. Debido a la naturaleza heterogénea del asma, los pacientes han sido clasificados en distintos grupos según sus características demográficas, clínicas o fisiopatológicas, llamados “fenotipos del asma”[1] con el objetivo de mejorar su manejo. Se ha propuesto un nuevo fenotipo del asma que afecta predominantemente a mujeres, se presenta de forma tardía y se caracteriza por sintomatología perimenstrual cíclica y recurrente[5,37].

Considerando que las grandes fluctuaciones hormonales influyen en la severidad del asma, el embarazo representa un gran desafío para las mujeres asmáticas. Se ha reportado un deterioro sintomático durante el embarazo en mujeres con asma severa[2,38,39]. Además, el riesgo de desarrollar asma aumenta en mujeres multíparas[36]. Durante el tercer trimestre del embarazo, cuando las concentraciones hormonales

alcanzan su punto máximo, un tercio de las mujeres asmáticas reporta un empeoramiento de la sintomatología, otro tercio presenta mejoría y el último tercio no reporta cambios[2,38,40].

Durante la menopausia, un estado fisiológico que ocurre después del periodo reproductivo de la mujer, se observa una disminución en las concentraciones séricas de estradiol[2,41,42]. Además, se ha reportado una frecuencia de asma similar a la de los hombres de la misma edad[2], junto con una reducción en las hospitalizaciones por asma en comparación con mujeres entre 20 y 30 años[2,42].

Los efectos de las hormonas sexuales sobre el sistema respiratorio y, en particular, su papel en la fisiopatología del asma aún se desconoce con exactitud. Sin embargo, el papel del estradiol sigue siendo objeto de debate, ya que los estudios han reportado resultados contradictorios, lo que impide clasificarlo como un factor protector o de riesgo. En modelos de ratones sensibilizados, las hembras no ovariectomizadas (OVX), bajo la influencia de las hormonas sexuales femeninas, presentaron un incremento en la respuesta inmune mediada por linfocitos T cooperadores tipo 2 (Th2) y la producción de interleucina 13 (IL-13). Además, un incremento en los linfocitos T cooperadores tipo 17 (Th17) y su producción de IL-17A, así como en la infiltración de eosinófilos y neutrófilos en el lavado broncoalveolar, en los niveles séricos de inmunoglobulina E (IgE) y en la HR[43].

En otro estudio se compararon ratones hembras y machos de 6 y 12 semanas de edad, para evaluar la reactividad de las vías aéreas mediante la prueba de metacolina. Se observó que, en la sexta semana de edad, los machos presentaban una mayor

reactividad que las hembras. Sin embargo, en la duodécima semana esta relación se invirtió, observándose una reactividad mayor en las hembras, lo que sugiere que las hormonas sexuales y la edad influyen sobre la HR[44]. Además, se ha asociado el incremento de la HR con el REα, debido a que en ratones hembras con silenciamiento génico para REα se observaron alteraciones en la función pulmonar y en la reactividad ante la prueba de metacolina y serotonina[45].

En mujeres sanas, se han evaluado los niveles de óxido nítrico exhalado (FeNO), presentándose los niveles más altos a la mitad del ciclo menstrual, cuando las concentraciones de E2 sérico son mayores[46]. El óxido nítrico tiene un efecto broncodilatador sobre la vía aérea y se ha reportado que el E2 incrementa su producción en el epitelio bronquial[47]. Sin embargo, la medición del FeNO se utiliza como un marcador de inflamación pulmonar y su aumento en relación con las fluctuaciones del ciclo menstrual podría actuar como un mecanismo compensatorio contra el estado inflamatorio del asma perimenstrual[2,48]. Además este incremento se ha asociado con la sintomatología diurna y un mayor número de eosinófilos en esputo[49].

Además, se ha descrito un aumento en la HR bronquial ante la prueba de metacolina y un incremento de las concentraciones séricas de inmunoglobulina E (IgE), una mayor producción de interleucina 4 (IL-4) y de eotaxina durante la fase lútea, en pacientes con asma perimenstrual en comparación con mujeres sin esta condición. Estas evidencias sugieren una asociación entre la respuesta inmune de tipo 2 y el asma perimenstrual[50]. Asimismo, en mujeres con asma severa también se ha descrito una respuesta inmune de tipo 2 caracterizada por un aumento de células Th2 circulantes, una mayor producción de interleucina 13 (IL-13) y un aumento en la tasa de hospitalización en comparación con

mujeres con asma leve a moderada o con hombres. Esta respuesta inmune fue mediada por la activación del REα y del receptor glucocorticoide[51].

En este sentido, se han reportado que el E2 presenta efectos broncodilatadores mediante la modulación de mecanismos regulatorios de Ca^{2+}, inhibiendo de manera aguda los canales de calcio dependientes de voltaje tipo L (CCDV-L)[8] e incrementando los niveles de AMPc[9]. Mientras que de manera crónica el E2, a través de la regulación del REβ disminuye las concentraciones de Ca^{2+} intracelular ($[Ca^{2+}]_i$) al inhibir los CCDV-L y aumentar el almacenamiento de Ca^{2+} hacia el retículo sarcoplásmico (RS)[52]. Además, en bronquios de porcinos, el E2, a concentraciones suprafisiológicas (40 micromolar [μM]) potenció 10.6 veces la relajación inducida por isoprenalina, un agonista de los receptores β-adrenérgicos[53].

Existe una gran variedad de evidencia científica que demuestra la influencia de las hormonas sexuales, en especial del E2, en la fisiopatología del asma, favoreciendo la inflamación y modulando la respuesta inmune y la reactividad de las vías aéreas. A lo largo de la vida de la mujer, existen periodos de grandes fluctuaciones hormonales que afectan la severidad, prevalencia y manejo del asma. Una mayor comprensión de los mecanismos que involucran las hormonas sexuales es necesaria para desarrollar estrategias terapéuticas para las mujeres afectadas por el asma.

1.3 Influencia del Ca^{2+} en la contracción y la relajación del músculo liso de las vías aéreas

El MLVA se considera el órgano blanco en la fisiopatología del asma; una alteración en su contractilidad puede contribuir a la HR, definida como una respuesta contráctil exagerada del MLVA a los estímulos en comparación con los individuos sanos[54]. En condiciones normales, la contracción del MLVA comienza con un incremento en las $[Ca^{2+}]_i$ que se encuentra aproximadamente entre 100-150 nanomolar (nM) en condiciones basales[55]. El Ca^{2+} es un segundo mensajero que regula diversos procesos intracelulares, dependiendo de sus incrementos en las concentraciones intracelulares a lo largo del tiempo. Entre las funciones que modula se incluyen la contracción muscular, la exocitosis, la transcripción génica, la proliferación celular, la apoptosis, entre otros[14,56].

Un incremento en las $[Ca^{2+}]_i$ puede ocurrir por una entrada de Ca^{2+} extracelular, a través de los CCDV-L, el canal de Ca^{2+} operado por el almacén (CCOA) o una liberación de las reservas internas desde el retículo sarcoplásmico (RS)[55,57] y la mitocondria a través del transportador mitocondrial (TM)[14,56,58,59]. Adicionalmente, se ha identificado que los canales de potencial transitorio de receptor (PTR), en particular el PTR canónico 3 (PTRC3) y el PTR vanilloide (PTRV) participan en la regulación de la entrada de Ca^{2+} en el MLVA[14,55]. El equilibrio en las $[Ca^{2+}]_i$ debe restablecerse rápidamente; por lo tanto, el Ca^{2+} es extruido al espacio extracelular a través de proteínas especializadas como el Intercambiador Na^+/Ca^{2+} (NCX) y la ATPasa de Ca^{2+} de la membrana plasmática (PMCA), ambos localizados en la membrana plasmática. Además, el Ca^{2+} intracelular se almacena en el RS mediante la actividad de la ATPasa de Ca^{2+} del retículo sarcoplásmico (SERCA) situada en la membrana de este organelo, el RS llega a resguardar

concentraciones de Ca^{2+} de hasta 5-10 mM[14,55,56]. PMCA y SERCA eliminan la mayor cantidad de Ca^{2+} del medio intracelular después de la estimulación de MLVA por un agonista excitador (Figura 1)[60,61].

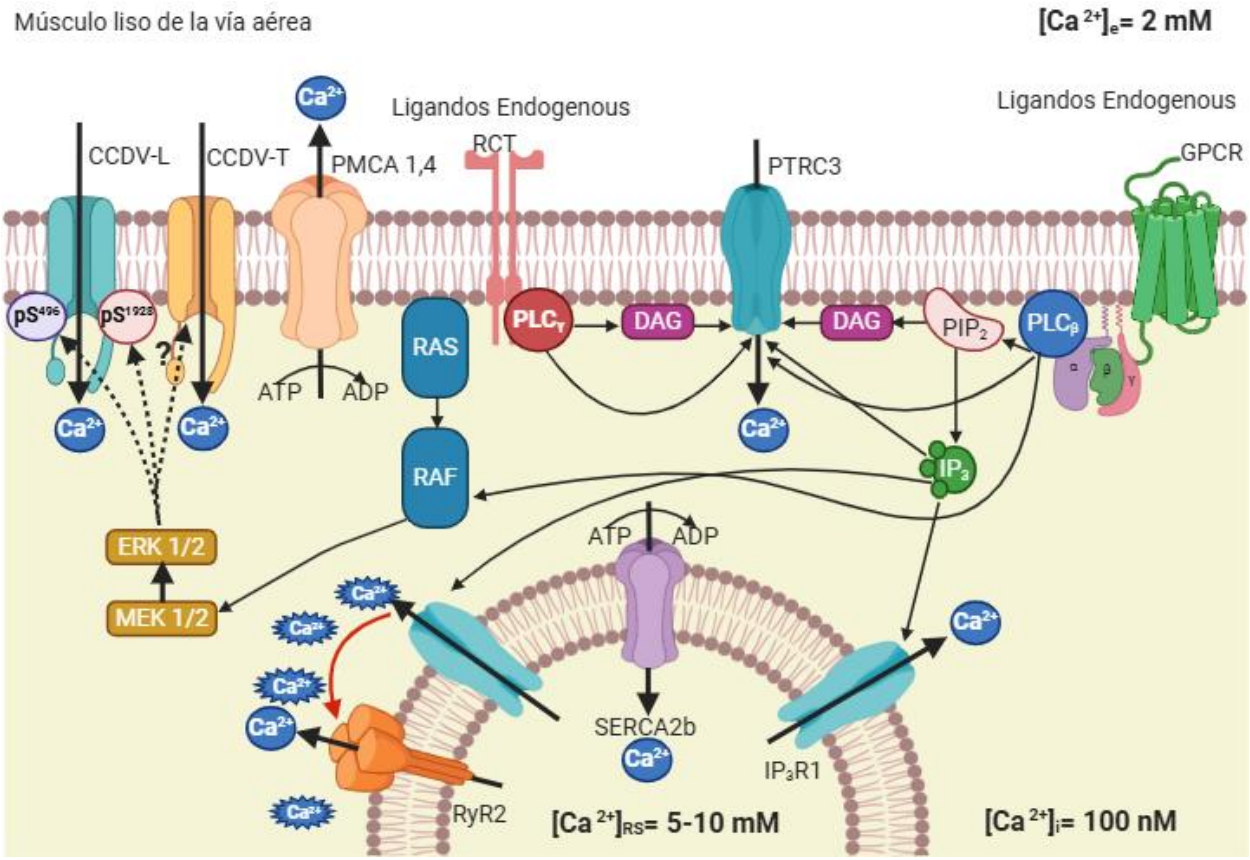

Figura 1. Mecanismos encargados del mantenimiento de las concentraciones intracelulares de calcio $[Ca^{2+}]_i$. En la membrana celular hay canales que tienen actividad constitutiva bajo condiciones basales, incluyendo el CCDV-L, CCDV-T y TRPC3, los cuales son regulados por distintas vías de señalización intracelular como la fosforilación del CCDV-L, en los residuos Ser^{496} de la subunidad β2 y Ser^{1928} de la subunidad α1, y la posible fosforilación del CCDV-T mediada por la señalización de la proteína cinasa ERK1/2, que es activada por mitógenos. La activación de los receptores acoplados a proteínas G (GPCR) por ligandos endógenos (ej. acetilcolina, histamina y leucotrienos) induce la producción de diacilglicerol (DAG) e inositol trifosfato (IP_3) por medio de la activación de la fosfolipasa C beta (PLCβ). El IP_3, al activar su receptor IP_3R1 en el retículo sarcoplásmico, promueve la liberación de Ca^{2+} al citosol, lo cual genera "chispas" de Ca^{2+} liberado de los RyR2. También el DAG, generado por la PLCβ o por la fosfolipasa C gamma (PLCγ) que es activada por los receptores cinasa de tirosina (RCT) al unirse a sus ligandos, activa los TRPC3 que ingresan Ca^{2+} al citosol. Para mantener la homeostasis de $[Ca^{2+}]_i$, este es regulado por las bombas SERCA2b y PMCA (PMCA1 o PMCA4). CCDV-L, canal dependiente de voltaje de tipo L; CCDV-T, canal de Ca^{2+} dependiente de voltaje de tipo T; PTRC3, potencial transitorio de receptor canónico 3; ERK1/2, cinasas reguladas por señales extracelulares 1/2; GPCR, receptor acoplado a proteína G; RCT, receptor de cinasa de tirosina; DAG, diacilglicerol; IP_3, inositol 1,4,5-trifosfato; PLC, fosfolipasa C; IP_3R1, receptor de IP_3; RyR2, receptor de rianodina 2; SERCA2b, ATPasa de Ca^{2+} del retículo sarcoplásmico 2b; PMCA, ATPasa de Ca^{2+} de la membrana plasmática; $[Ca^{2+}]_e$, concentraciones extracelulares de calcio; $[Ca^{2+}]_{RS}$, concentraciones de calcio en el retículo sarcoplásmico. (Figura modificada de Reyes-García, et al., 2018)[55].

La PMCA tiene cuatro isoformas (PMCA1-4), cada una codificada por un gen diferente y con distintas variantes de corte y empalme[55,62,63]. El corte y empalme es un proceso que ocurre en la expresión génica de células eucariotas, en el cual se eliminan los intrones (las secuencias no codificantes) de un ARN mensajero (ARNm), y se unen solo los exones (las secuencias codificantes), formando un ARNm maduro y funcional. Se ha reportado que en los seres humanos hasta un 95% de los genes que codifican proteínas contienen intrones y requieren ser sometidos a este proceso, lo cual produce múltiples variantes de la proteína a través del mismo gen, aumentando la diversidad proteica[64,65]. La expresión de la isoforma cambia de manera específica según el tejido[62,63]. Se ha observado que las células del MLVA de rata expresan las isoformas PMCA1 y PMCA4[62]. Esta proteína pertenece a la familia de las ATPasas tipo P. La PMCA es una proteína conformada por 10 dominios transmembranales con los extremos N- y C-terminal encontrados en la cara citosólica[66-68]. Un dominio consiste en una secuencia de aproximadamente 100 a 250 residuos plegados de forma compacta que es estructuralmente independiente y funcional. Aunque estén físicamente separadas, estas estructuras se conectan por segmentos de cadenas polipeptídicas[69]. Uno de los principales motivos preservados en la proteína se encuentra en el extremo C-terminal, donde se localiza el sitio de unión autoinhibitorio de unión de calmodulina (CaM)[66,70,71].

Un motivo es una secuencia corta de 5 a 20 aminoácidos de la estructura secundaria, ya sea α-hélice o β-plegada, que usualmente realiza una función específica y corresponde a patrones conservados[69]. Este motivo de unión a CaM interactúa con el sitio catalítico de PMCA (en el primer y segundo bucle citosólico) cuando se encuentra en un estado de reposo a $[Ca^{2+}]_i$ bajas, inhibiendo así la proteína. Una vez que se incrementan las

$[Ca^{2+}]_i$, el complejo Ca^{2+}/CaM se une a su sitio de unión, induciendo un cambio conformacional en la proteína y reduce su afinidad por el sitio catalítico e incrementa la actividad de la PMCA[66,71].

Además, en el extremo C-terminal también se encuentra un motivo de unión PDZ, denominado así por las iniciales de las tres primeras proteínas descubiertas que presentaban el dominio: la proteína de densidad postsináptica 95 (PSD95), el supresor tumoral disc grande de Drosophila (Dlg1) y la proteína zonula occludens-1 (zo-1). Se ha observado que este dominio es necesario para la dimerización de PMCA e incrementa su actividad[66,72,73]. En el extremo C-terminal también se encuentran sitios de regulación por PKC y PKA[66] (Figura 2).

Por otro lado, en el extremo N-terminal se encuentra un motivo inhibitorio de unión 14-3-3[66,74,75]. En el bucle citosólico que se encuentra entre los dominios transmembranales 2 y 3, se sitúa un sitio de unión a fosfolípidos ácidos[66,76,77], y un sitio de acople y empalme A[66,78-80]. El sitio catalítico está formado por los bucles entre los dominios transmembranales 2 y 3, y en parte por el bucle citosólico entre los dominios transmembranales 4 y 5[66,81]. El sitio de unión a Ca^{2+} está formado por el residuo E433 en el dominio transmembranal 4 y en los residuos D895 y N891 en el dominio 6. El poro que transporta Ca^{2+} está formado por los dominios transmembranales 1, 2, 3 y 4[71] (Figura 2), tiene alta afinidad por el Ca^{2+} pero baja capacidad de transporte, con una relación estequiométrica de 1:1 de Ca^{2+}/ATP y, con una reacción electroneutra mediante el intercambio Ca^{2+}/H^{+}[55,63].

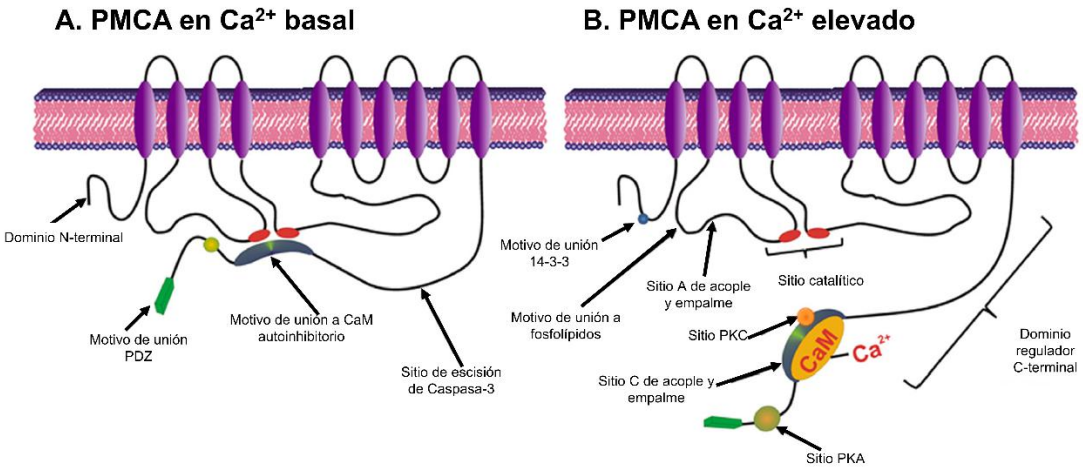

Figura 2. Estructura bidimensional de la ATPasa de Ca^{2+} de la membrana plasmática. A. En un estado de reposo, el sitio catalítico (círculos rojos) de la ATPasa de Ca^{2+} de la membrana plasmática (PMCA) se encuentra inhibido por el sitio autoinhibitorio del motivo de unión a calmodulina (CaM) en la cola C-terminal. B. Durante un estado de incremento de las concentraciones de Ca^{2+} intracelular, el complejo Ca^{2+}/CaM se une al sitio de unión a CaM, induciendo un cambio conformacional que provoca su disociación del sitio catalítico, permitiendo la activación de PMCA (Tomada de Bruce, 2018)[66].

Por otro lado, SERCA tiene tres isoformas (SERCA1-3), así como muchas variantes de corte y empalme, siendo la isoforma más predominante SERCA2b en las células de MLVA[14,55,82]. Similarmente a la PMCA, la SERCA pertenece a la familia de las ATPasas tipo P. Esta proteína transporta el Ca^{2+} al interior del RS en contra de un gradiente, con una diferencia de concentración 1,000 veces mayor a las $[Ca^{2+}]i$[83,84]. Estructuralmente la SERCA está compuesta por 10 dominios transmembranales que pueden dividirse en 3 grupos: los dominios transmembranales 1, 2, 3 y 4, y los dominios 5-10[83,85,86]. Específicamente, SERCA2b tiene una hélice transmembranal adicional, el dominio transmembranal 11 (Gly1013-Tyr1030). Este segmento adicional incrementa la afinidad de la variante por el Ca^{2+} más de 2 veces y disminuye la actividad enzimática de SERCA2b en comparación con las variantes de SERCA1a y SERCA2a[83,87]. En la cara citosólica se distinguen 3 dominios, el dominio actuador (A), un sitio de unión a nucleótidos (N) y un sitio de fosforilación (P)[83,85,86]. Específicamente el residuo D351 en el sitio P es el sitio de fosforilación[88]. Durante un ciclo de actividad la ATPasa transporta

a dos iones Ca^{2+}. Se ha descrito que los seis residuos que participan en la unión a Ca^{2+} son: E309 en el dominio transmembranal 4, E771 en el dominio 5, N796, T799 y D800 en el dominio 6, y por último, E908 está situado en el dominio transmembranal 8[88] (Figura 3). Se ha demostrado que ambas ATPasas participan en funciones de las células de MLVA como la homeostasis del Ca^{2+} [89], contracción[90], HR[90,91], proliferación[62], e incluso apoptosis[62].

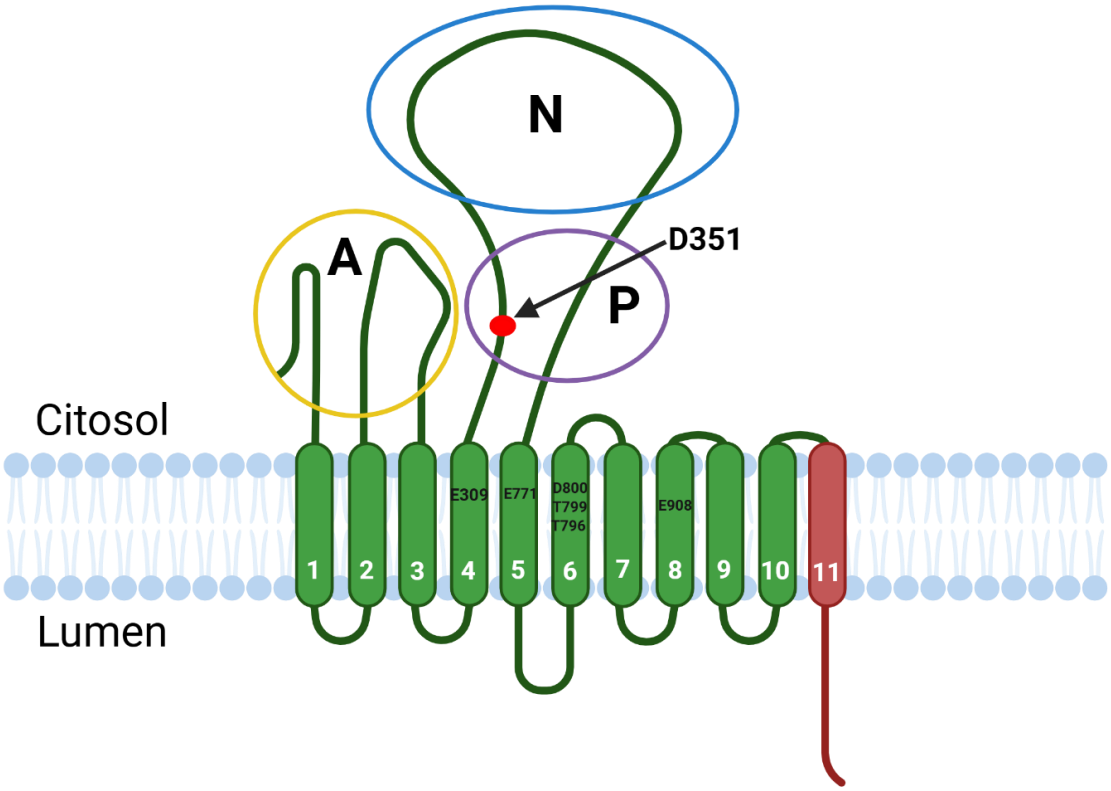

Figura 3. Estructura bidimensional de la ATPasa de Ca^{2+} del retículo sarcoplásmico 2b. La variante de la ATPasa de Ca^{2+} del retículo sarcoplásmico 2b (SERCA2b) está conformada por 11 segmentos transmembranales, el segmento adicional está marcado en rojo. SERCA conserva 3 dominios extramembranales en la cara citosólica, el dominio actuador (A, círculo amarillo), el dominio de fosforilación (P, círculo morado), y el sitio de unión a nucleótidos (N, círculo azul). El residuo D351 es el sitio de fosforilación, y los seis residuos E309, E771, T796, T799, D800 y E908 son los sitios de unión a Ca^{2+}[83,88].

1.3 Papel del estradiol en el músculo liso de las vías aéreas

1.3.1 Biosíntesis

Las hormonas sexuales conforman una familia de hormonas esteroideas derivadas del colesterol, compartiendo una base compuesta de 4 anillos llamado ciclopentanoperhidrofenantreno, un hidrocarburo policíclico. Los estrógenos pertenecen a la familia de las hormonas sexuales, y sus tres principales formas fisiológicas son: la estrona (E1), el estradiol (E2), y el estriol (E3)[15,16,92]. Este grupo hormonal comparte una estructura base que contiene 18 carbonos ($C_{18}H_{24}O_2$), conociéndose como esteroides C18 y su estructura contiene un anillo A fenólico (el cual es un anillo aromático con un grupo hidroxilo posicionado en el carbono 3), diferenciándose por la cantidad de grupos hidroxilo que presentan, siendo un grupo hidroxilo en E1, dos en el E2 y tres grupos hidroxilos en el E3[93,94]. El E2 es el estrógeno con mayor producción y el más potente durante el periodo reproductivo de la mujer y sus niveles séricos presentan amplias fluctuaciones a través de los distintos periodos de la vida, ciclo menstrual (80 pM-1.5 nM), embarazo (1-150 nM) y menopausia (40-120 pM)[2]. La biosíntesis de los estrógenos primordialmente sucede en los ovarios, el cuerpo lúteo y la placenta, pero existe una producción significativa en sitios de síntesis extragonadales (glándula suprarrenal, hígado, tejido adiposo, corazón, piel, pulmón, cerebro, etc.), los cuales son la fuente predominante de estrógenos en mujeres postmenopáusicas y en hombres. La producción de estrógenos en los ovarios es, en su mayoría, liberada al torrente sanguíneo para ejercer sus efectos, transportados por la globulina transportadora de hormonas sexuales o por la albúmina hasta el sitio de acción. En cambio, aquellos

producidos en los sitios extragonadales funcionan de manera paracrina y/o autocrina, ejerciendo su efecto en procesos fisiológicos locales (Figura 4)[15,92,95-98].

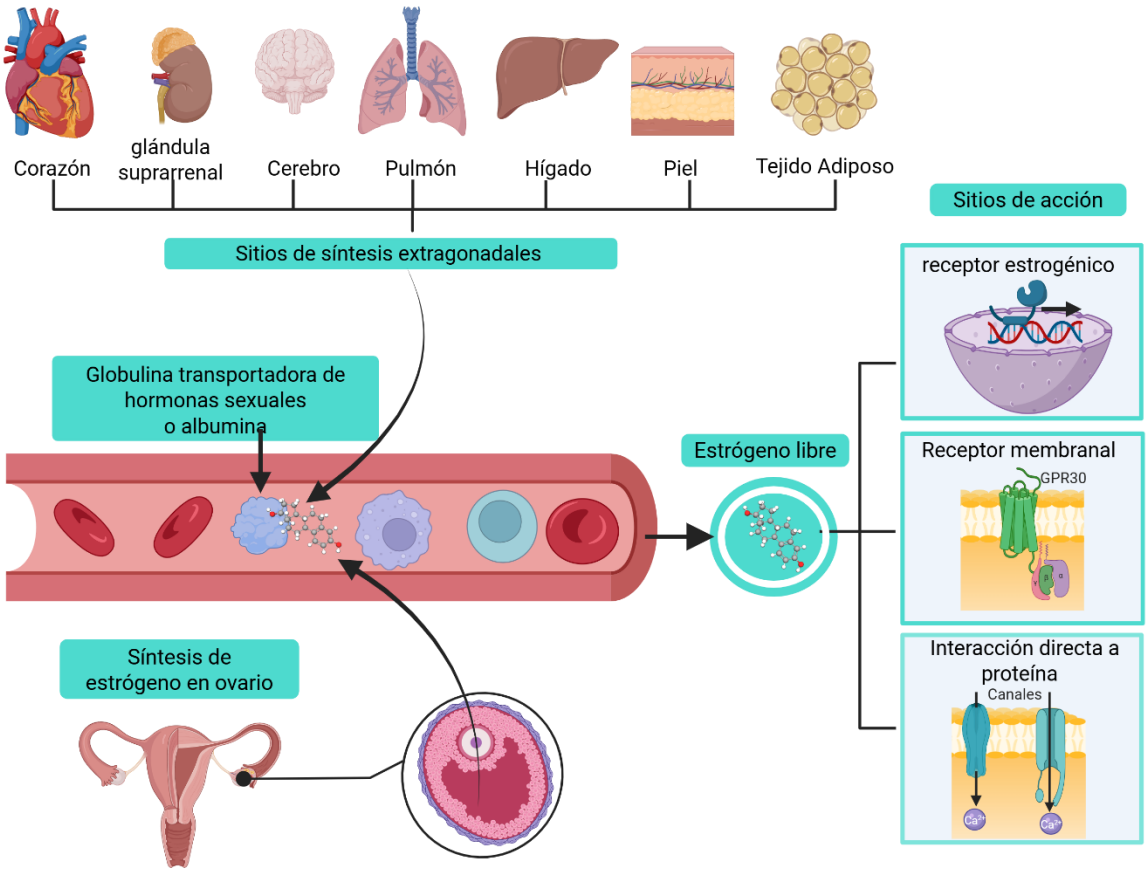

Figura 4. Sitios de biosíntesis estrogénica y sitios de acción. El principal sitio de biosíntesis estrogénica es el ovario; sin embargo, existen sitios de síntesis extragonadal, los cuales requieren la expresión de la aromatasa en estos tejidos para su producción. Cuando se sintetiza el estrógeno, este puede tener actividad local en el sitio de producción o ser liberado al torrente sanguíneo, donde será transportado a su sitio de acción a través de su unión a la globulina transportadora de hormonas sexuales o a la albúmina. Una vez que el estrógeno llega a su sitio de acción, ejerce su efecto a través de tres modos de acción: 1. a través de la activación de los receptores estrogénicos ERα y ERβ, 2. activación de su receptor membranal GPR30 o 3. interacción directa con una proteína. GPR30, receptor acoplado a proteína G 30. (Figura modificada de Romero-Martínez, 2023).[14]

En los ovarios, la síntesis de estradiol ocurre parcialmente en las células de la teca y en las células de la granulosa. Las células de la teca no pueden producir E2 directamente, pero sí generan andrógenos, que actúan como precursores del E2. Por otro lado, las células de la granulosa no pueden producir andrógenos a partir de la progesterona, pero tienen la capacidad de realizar la conversión del andrógeno a 17β-estradiol. Para iniciar

la biosíntesis de las hormonas esteroideas, el colesterol es transportado a la membrana mitocondrial interna a través de la proteína reguladora aguda esteroidogénica STARD1 (StAR), un paso que regula la velocidad de la producción de esteroides[93]. En las células de la teca, la hormona luteinizante (LH) regula la esteroidogénesis a través de la regulación de la expresión de StAR. Cuando la LH se une a su receptor acoplado a la proteína Gs, activa a la enzima adenilato ciclasa (AC) para producir monofosfato de adenosina cíclico (AMPc). Este AMPc activa la proteína cinasa A (PKA), que fosforila a la proteína de unión al elemento de respuesta de AMPc (CREB), promoviendo la transcripción de StAR[93,99].

Una vez que el colesterol ingresa a la célula, la síntesis comienza con la escisión de la cadena lateral del colesterol por el citocromo P450scc (CYP11A1), un punto esencial para la síntesis de las hormonas esteroideas, convirtiéndolo en pregnenolona, precursora de todas las hormonas esteroideas. La biosíntesis puede continuar en la célula de la teca, permitiendo la difusión de la pregnenolona a las células circundantes. Similarmente, en la célula de la granulosa, de manera similar, la hormona folículo estimulante (FSH) activa la expresión de StAR a través de la unión a su receptor membranal[93,99]. La pregnenolona puede ser convertida a 17α-hidroxipregnenolona, por el citocromo P450 17α-hidroxilasa (CYP17A1), la cual es nuevamente hidroxilada por el CYP17A1 a dehidroepiandrosterona (DHEA). Por medio de la 3β-hidroxiesteroide deshidrogenasa (3β-HSD), la pregnenolona también puede ser convertida a progesterona. La progesterona y la DHEA son precursores de la androstenediona. La DHEA puede ser biotransformada a testosterona por la 17β-hidroxiesteroide deshidrogenasa (17β-HSD), o a estrona por medio de la aromatasa (CYP19A1). Finalmente, la testosterona y la

estrona son los precursores del E2, catalizándose su transformación a través de la aromatasa y la 17β-HSD, respectivamente (Figura 5)[15,92,93].

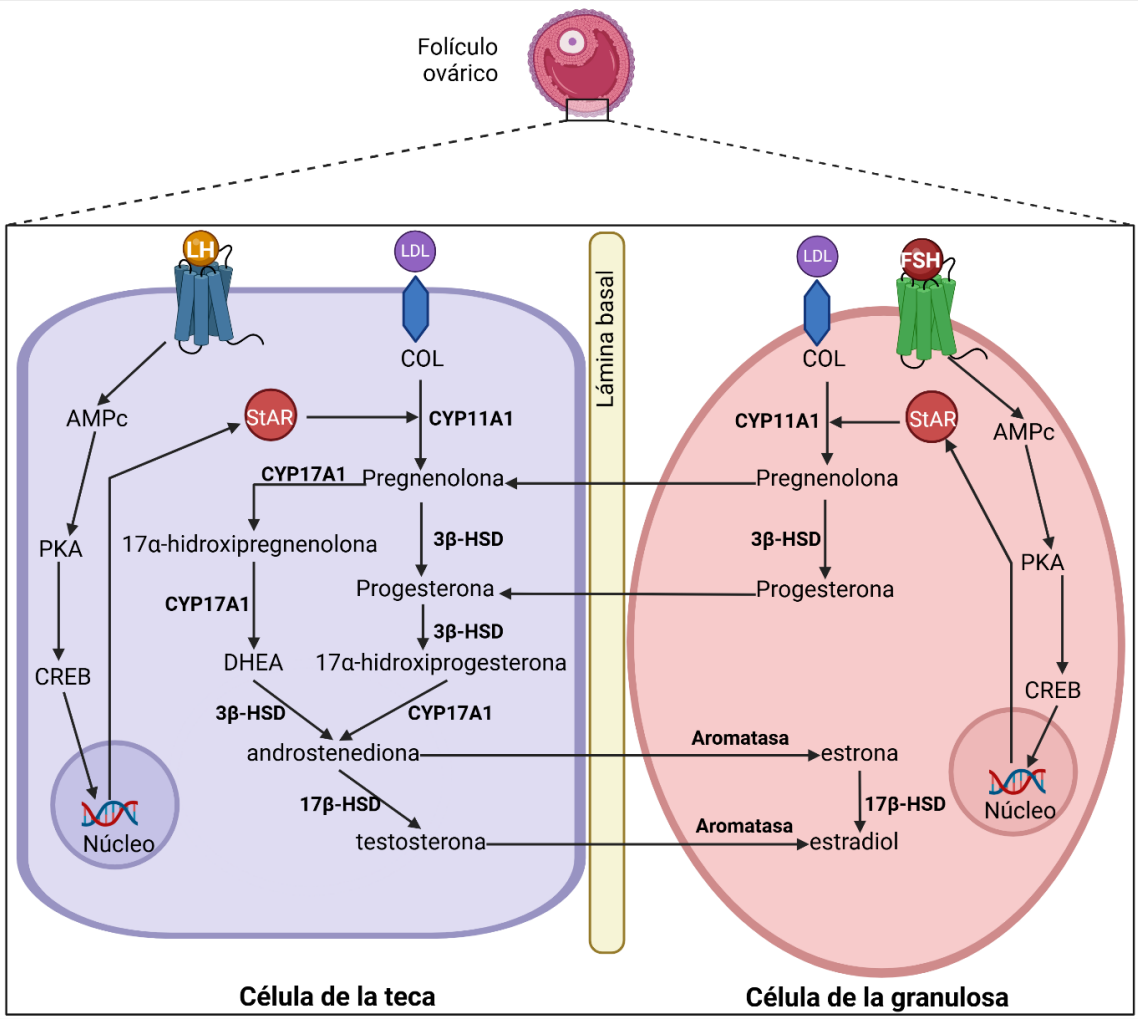

Figura 5. Biosíntesis estrogénica en el ovario. En el folículo ovárico, la biosíntesis del estradiol se lleva a cabo parcialmente en las células de la teca y de la granulosa. La hormona luteinizante (LH) y folículo estimulante (FSH) inducen la producción de esteroides al promover la expresión de la proteína reguladora aguda de esteroides (StAR), que facilita la translocación del colesterol. El colesterol se convierte en pregnenolona mediante la escisión de la cadena lateral por la enzima CYP11A1. Esta, a su vez, es convertida a 17α-hidroxipregnenolona por el citocromo P450 17α-hidroxilasa (CYP17A1) en las células de la teca, o a progesterona por la 3β-hidroxiesteroide deshidrogenasa (3β-HSD). Posteriormente, la 17α-hidroxipregnenolona es nuevamente hidroxilada por el CYP17A1, convirtiéndose en dehidroepiandrosterona (DHEA). En las células de la teca, la progesterona se convierte en 17α-hidroxiprogesterona por la 3β-HSD. Tanto la DHEA como la 17α-hidroxiprogesterona se transforman en androstenediona a través de la 3β-HSD y el CYP17A1, respectivamente. La androstenediona puede transformarse en testosterona por la 17β-hidroxiesteroide deshidrogenasa (17β-HSD) en las células de la teca, o aromatizarse en estrona en las células de la granulosa. Por último, en las células de la granulosa, la testosterona puede aromatizarse en 17β-estradiol, o la estrona puede convertirse en estradiol por la 17β-HSD (Modificada de Fuentes, 2019)[93].

El paso limitante en la biosíntesis del estradiol es la aromatasa, la cual es ampliamente expresada en diversos tejidos, siendo esta enzima un indicador de la producción local. En los ovarios, las células de la teca son responsables de la síntesis esteroidea hasta la producción de andrógeno, que posteriormente se convierte en E2 en las células de la granulosa mediante la aromatización, para luego viajar por el torrente sanguíneo y ejercer sus efectos en tejidos reproductivos y órganos no reproductivos. Es importante resaltar que la conversión local a E2 en tejidos extragonadales depende de la expresión de la enzima aromatasa en estos tejidos[15], de la cual se ha reportado su presencia en el pulmón, aunque su expresión es mínima y tiene mayor relevancia en procesos patológicos como el cáncer o la enfermedad pulmonar obstructiva crónica[96,97].

1.3.2 Efectos genómicos y no genómicos de los estrógenos

Los efectos fisiológicos que ejercen los estrógenos son a través de efectos genómicos y no genómicos. Los efectos no genómicos se presentan de segundos a minutos, y no requieren de la activación de un receptor estrogénico citoplasmático[2,16,92,100,101]. Recientemente, se ha propuesto que los estrógenos activan a un receptor membranal (GPR30) para producir sus efectos no genómicos[2,16,92]. Por otro lado, los efectos genómicos se presentan en horas, involucran a su receptor estrogénico citoplasmático (RE) los cuales presentan dos isoformas (REα y el REβ) que activan distintas vías de señalización[2,16,92,100]. Los RE pertenecen a la superfamilia de receptores nucleares que modulan la transcripción de genes, codificados por los genes ESR1 y ESR2, respectivamente, localizados en diferentes cromosomas[15]. El REα está compuesto por una cadena en 595 aminoácidos y tiene un peso molecular de 67 kiloDaltons (kDa), mientras que el REβ está formado por 530 aminoácidos y tiene un peso de 59 kDa. La

principal diferencia entre ambos radica en que el REβ posee un dominio N-terminal más corto[93]. Estructuralmente estos receptores están compuestos por varios dominios funcionales conocidos como A/B, C, D y E/F, y en la región C se encuentra localizado el dominio de unión al ADN (DUA)[93]. Estos receptores cuando se unen al estradiol inducen un cambio conformacional que promueve la dimerización, tanto en forma de homodímeros (REα/REα, REβ/REβ) como de heterodímeros (REα/REβ). Este complejo procede a translocarse al núcleo, donde se une a secuencias de elementos de respuesta estrogénica (ERE) en el ADN por medio de los dominios de unión al ADN (Figura 6)[93,102].

Recientemente, en el genoma humano y de ratón se han identificado más de 70,000 ERE a través de un estudio de detección de genoma completo[93,103]. Interesantemente, estos receptores tienen funciones biológicas distintas, y su expresión varía según el tejido y el tipo celular[15]. Además, se ha descrito que hasta un 35% de los genes regulados por el E2 no contienen secuencias de ERE[93,95,104]. En estos casos, la regulación de dichos genes ocurre a través de la interacción de los RE con otros componentes de las vías de señalización, como factores de transcripción, en lugar de un contacto directo con el ADN.

El GPR30, es una proteína de membrana que actúa de manera independiente de los REs, y puede inducir respuestas rápidas mediante efectos no genómicos[15]. Entre estos mecanismos incluyen la activación de las vías de señalización de nucleótidos cíclicos, PKC, PKA y proteína cinasa G o PKG (Figura 6)[2,14-16]. Cabe mencionar que este receptor no es exclusivo de E2, ya que se ha reportado que también puede activarse por quimiocinas[15].

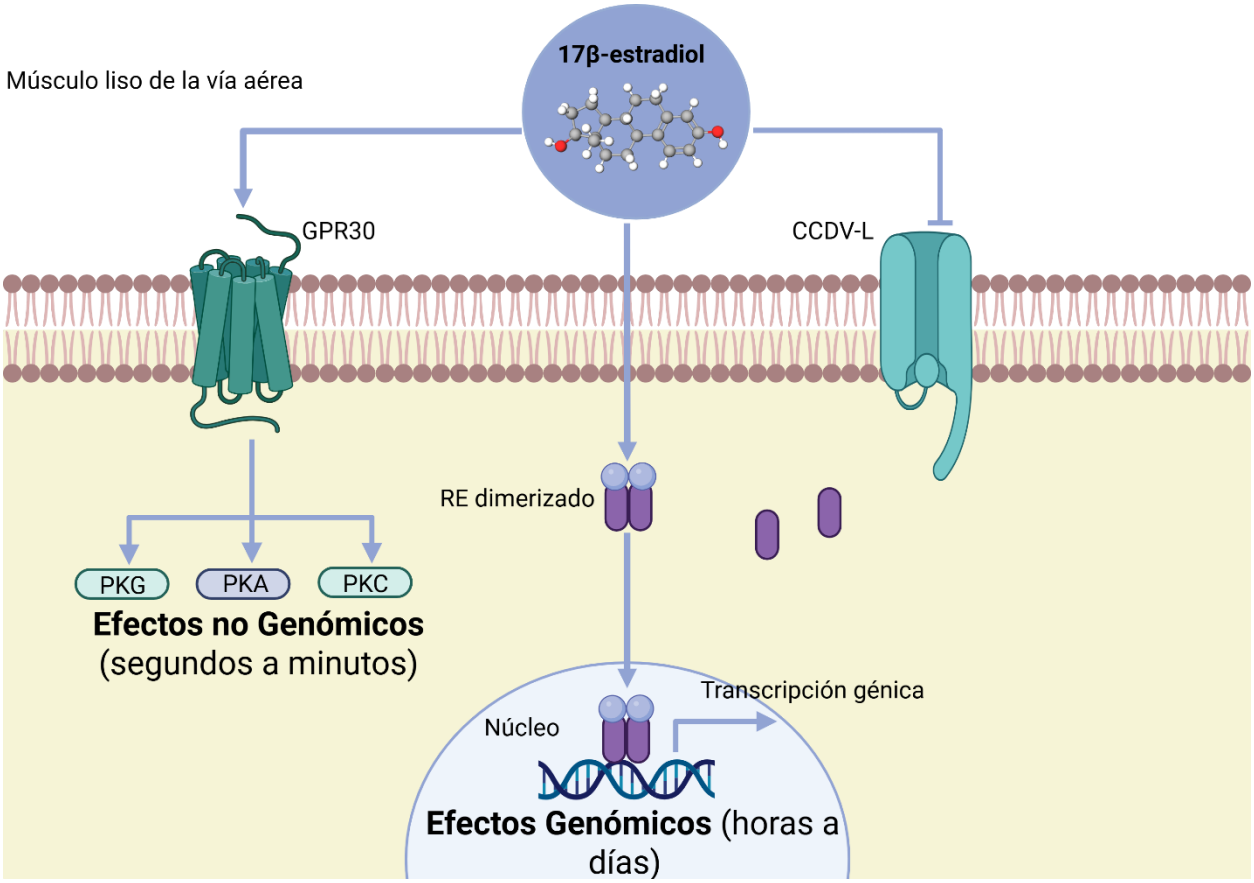

Figura 6. Efectos del 17β-estradiol (E2). El 17β-estradiol puede ejercer efectos no genómicos, que ocurren en un rango de segundos a minutos, a través de su actividad sobre su receptor acoplado a proteína G (GPR30), o a través de su interacción directa con proteínas blanco, como el canal de calcio dependiente de voltaje tipo L (CCDV-L). También el E2 puede activar efectos genómicos, que toman de horas a días, mediante la activación de los receptores estrogénicos (RE) α y β, los cuales, tras interactuar con E2, se dimerizan y se translocan al núcleo para unirse a los elementos de respuesta estrogénica (ERE) e iniciar la transcripción génica. PKC, proteína cinasa C; PKA, proteína cinasa A; PKG, proteína cinasa G.

1.4 Antecedentes

Es conocido que el E2 juega un papel controversial en la modulación de las $[Ca^{2+}]_i$ en el MLVA. Se ha observado, que los efectos ejercidos por esta hormona son dependientes de la concentración y varían de acuerdo con el tiempo de exposición[9,16,92,101]. Se ha visto que a niveles fisiológicos (rango nanomolar) y suprafisiológicos (rango micromolar) el E2 inhibe de manera no genómica al CCDV-L en el MLVA[8,105], indicando un efecto concentración-dependiente. Aunque el mecanismo exacto por el cual el E2 inhibe al CCDV-L aún se desconoce, se ha reportado que su unión directa en el sitio dihidropiridínico de los CCDV-L puede potenciar su actividad en neuronas hipocampales[106]. También existe la hipótesis de que este efecto sea mediado por la vía de ERK 1/2, dado que en el miocardio de rata se ha reportado que ERK1/2 puede disminuir la actividad del CCDV-L a través de la fosforilación de la subunidad β2 en el sitio Ser496[55,107]. Dado que el E2 puede activar ERK1/2 a través de mecanismos no genómicos[11,17], esta activación podría ser el mecanismo por el cual E2 inhibe el CCDV-L. Hasta el momento se desconoce si el E2 tiene algún efecto no genómico sobre SERCA, en cambio, existe un reporte sobre efectos de la exposición crónica del E2 sobre SERCA[52]. En células del MLVA de humano tratadas con TNF-α o lL-13 se observa una disminución de la función de SERCA, y la incubación crónica con un agonista específico del REβ revierte este efecto, el cual no se presenta en presencia de E2 o de un agonista específico del REα. Se atribuye esto a los efectos genómicos sobre la expresión de SERCA, en donde el TNF-α o lL-13 disminuyen su expresión, pero es revertido ante la incubación con el agonista del REβ (WAY-200070) pero no con el agonista de REα (PPT)

o E2[52]. Actualmente no existen evidencia de los efectos que podría tener el E2 sobre NCX y PMCA.

En estudios preliminares en el laboratorio de Investigación de Asma, encontramos que la incubación de los miocitos traqueales de cobayo con 10 nM de E2 durante 5 min induce una ligera disminución en las $[Ca^{2+}]_i$ basal. Al ser estimulada la célula con cafeína (10 milimolar [mM]), un modulador del receptor de rianodina (RyR), en la presencia de E2, se observa una disminución en la amplitud de la respuesta; sin embargo, se modifica la cinética transitoria de la cafeína, produciendo una meseta sostenida en las $[Ca^{2+}]_i$. Estos resultados nos permitirán explorar efectos del E2 sobre los mecanismos reguladores de las $[Ca^{2+}]_i$ en el MLVA.

2. Planteamiento del problema

Las variaciones de las concentraciones séricas de estrógenos se asocian a la severidad de la sintomatología en mujeres asmáticas. Este fenómeno sugiere la relación que presenta la edad y el sexo en la enfermedad del asma[2,44,100]. El estradiol presenta una respuesta bifásica, i.e., favoreciendo o protegiendo de la hiperreactividad de la vía aérea, la cual es dependiente del tiempo de exposición. Por lo tanto, en este proyecto, se explorarán los efectos del E2 sobre los mecanismos involucrados en la regulación de las $[Ca^{2+}]_i$ del músculo liso traqueal de cobayo.

3. Pregunta de investigación

¿La exposición aguda al 17β-estradiol a concentraciones fisiológicas, participará en la regulación de las $[Ca^{2+}]_i$ en el músculo liso traqueal de cobayo?

4. Hipótesis

El 17β-estradiol a concentraciones fisiológicas, a través de efectos no genómicos, inhibe la actividad de las proteínas reguladoras de Ca^{2+} intracelular PMCA, SERCA y NCX en el músculo liso traqueal de cobayo.

5. Objetivo general

Determinar si el 17β-estradiol a concentraciones fisiológicas tiene efectos sobre los mecanismos que regulan las concentraciones intracelulares de Ca^{2+} $[Ca^{2+}]_i$ del músculo liso traqueal de cobayo.

5.1 Objetivos particulares

1. Caracterizar el efecto del 17β-estradiol en la contracción de músculo liso de las vías aérea inducida por carbacol.
2. Analizar el efecto de la carboxieosina sobre la actividad de la ATPasa de Ca^{2+} de la membrana plasmática (PMCA) y durante la contracción de musculo liso de las vías aérea inducida por carbacol.
3. Estudiar el efecto del 17β-estradiol sobre la liberación de Ca^{2+} del retículo sarcoplásmico mediante la activación del receptor de rianodina (RyR) con cafeína (modulador del RyR) y caracterizar los mecanismos involucrados en los miocitos traqueales de cobayo utilizando microfluorometría.
4. Determinar el efecto del 17β-estradiol sobre la ATPasa de Ca^{2+} de membrana plasmática (PMCA) en el incremento de Ca^{2+} inducida por cafeína utilizando el inhibidor inespecífico de PMCA, el lantano, y el inhibidor especifico carboxieosina.

5. Estudiar el efecto del 17β-estradiol sobre la ATPasa de Ca^{2+} de retículo sarcoplásmico (SERCA) en el incremento de Ca^{2+} inducida por cafeína utilizando los inhibidores específicos tapsigargina y ácido ciclopiazónico (CPA).
6. Explorar el efecto del 17β-estradiol sobre la actividad del intercambiador Na^{+}/Ca^{2+} (NCX) utilizando cloruro de colina.
7. Estudiar la participación de la vía de señalización de la proteína cinasa regulada por señales extracelulares 1/2 (ERK 1/2) en el efecto del 17β-estradiol sobre la actividad de la ATPasa de Ca^{2+} de membrana plasmática (PMCA) utilizando el inhibidor de ERK 1/2 (U-0126).
8. Determinar la modulación específica de los agonistas específicos de los receptores estrogénicos alfa (REα) y beta (REβ) (Propilpirazoletriol [PPT] y Diarilpropionitrilo [DPN] respectivamente) sobre la ATPasa de Ca^{2+} de membrana plasmática (PMCA).
9. Estudiar el efecto del 17β-estradiol sobre la entrada la entrada capacitativa de Ca^{2+} a través de los canales operados por almacén (CCOA), mediante la estimulación con cafeína y ácido ciclopiazónico (CPA) en un medio libre de Ca^{2+}.
10. Estudiar el efecto del 17β-estradiol sobre la actividad del transportador mitocondrial de Ca^{2+} utilizando el activador cianuro de carbonilo 4-(trifluorometoxi)fenilhidrazona (FCCP), con el fin de comprender su impacto en la regulación de la señalización intracelular mediada por Ca^{2+}.
11. Estudiar, mediante modelos computacionales de acoplamiento molecular, la posible interacción entre el 17β-estradiol, el agonista selectivo del receptor de estrógenos α Propilpirazoletriol (PPT), el agonista selectivo del receptor de estrógenos β

Diarilpropionitrilo (DPN) y la carboxieosina con las isoformas 1 y 4 de la ATPasa de Ca^{2+} de la membrana plasmática (PMCA1 y PMCA4).

12. Evaluar, mediante modelos computacionales de acoplamiento molecular, la posible interacción entre E2, PPT, DPN y el inhibidor de SERCA, ácido ciclopiazónico, con la isoforma 2b de la ATPasa de Ca^{2+} del retículo sarcoplásmico (SERCA2b), con el fin de caracterizar sus posibles sitios de unión y mecanismos de modulación.

META: Analizar el papel del 17β-estradiol (E2) en la regulación del Ca^{2+} intracelular y la contracción del músculo liso en miocitos traqueales de cobayo, utilizando métodos experimentales y computacionales.

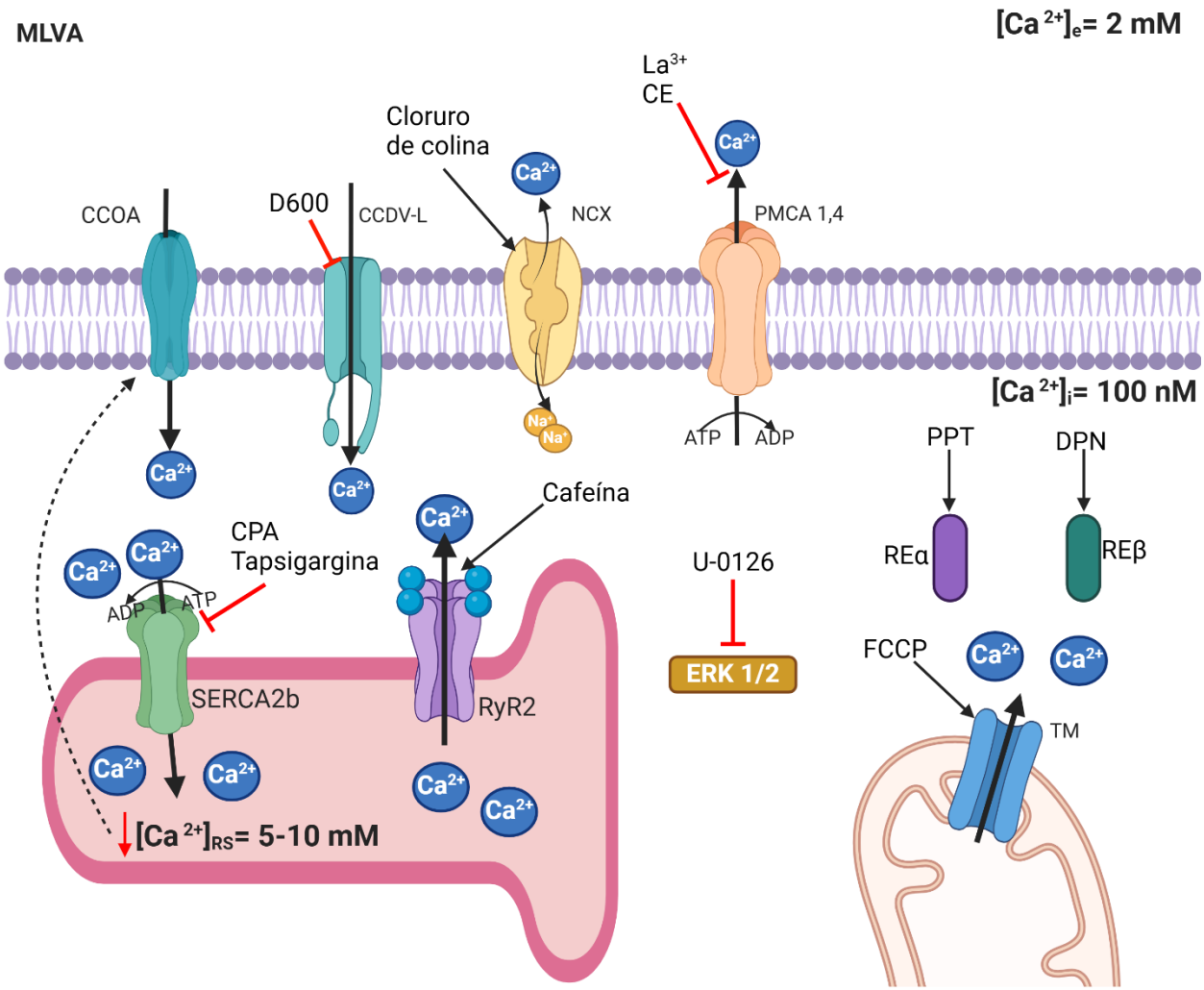

Figura 7. Propósitos particulares del estudio. Se utilizó la cafeína como herramienta farmacológica para inducir la liberación del Ca^{2+} del retículo sarcoplásmico (RS) por la apertura del receptor de rianodina (RyR2). Se utilizó el inhibidor de los canales de calcio dependientes de voltaje tipo L (CCDV-L) denominado D600. Para estudiar la actividad de la ATPasa de Ca^{2+} de la membrana plasmática (PMCA), se utilizaron los inhibidores lantano (La^{3+}) y carboxieosina (CE). Para estudiar la actividad de la ATPasa de Ca^{2+} del retículo sarcoplásmico (SERCA), se utilizaron los inhibidores tapsigargina y ácido ciclopiazónico (CPA). Para estudiar el efecto sobre el intercambiador Na^{+}/Ca^{2+} (NCX), se utilizó el cloruro de colina. Para estudiar la participación de la vía de señalización de las cinasas reguladas por señales extracelulares 1/2 (ERK 1/2), se utilizó el inhibidor especifico U-0126. Para estudiar la participación de los receptores estrogénicos (RE), se utilizaron los agonistas específicos Propilpirazoletriol (PPT, agonista de REα) y Diarilpropionitrilo (DPN, agonista de REβ). Para estudiar el efecto sobre los canales de Ca^{2+} operados por el almacén (CCOA), se empleó una estrategia en medio sin Ca^{2+} y con CPA. Para estudiar la actividad sobre el transportador mitocondrial (TM), se utilizó el activador cianuro de carbonilo 4-(trifluorometoxi)fenilhidrazona (FCCP).

6. Relevancia e impacto del proyecto

Las mujeres a lo largo de su vida reproductiva presentan fluctuaciones en las concentraciones plasmáticas de las hormonas sexuales, principalmente del 17β-estradiol. Se ha descrito que hasta un 40% de las mujeres presentan exacerbación del asma perimenstrual, lo que sugiere una relación entre la severidad del asma y las hormonas sexuales. Durante el embarazo, el 33% de las mujeres asmáticas presentan exacerbación de los síntomas, otro 33% presenta mejora durante el tercer trimestre, y el último tercio no presenta cambio alguno. Los cambios en las concentraciones hormonales presentes durante este periodo podrían estar afectando la reactividad del músculo liso de las vías aéreas a través de la regulación de los mecanismos de la contracción, como aquellos que regulan las $[Ca^{2+}]_i$. Por lo anterior, es relevante determinar los mecanismos inducidos por los estrógenos sobre la regulación de las $[Ca^{2+}]_i$ para brindar estrategias terapéuticas personalizadas a las mujeres asmáticas.

7. Métodos

7.1 Modelo animal

Se utilizaron cobayos machos de la cepa Hartley de 300-400 g. El manejo de animales se realizó de acuerdo con la norma: NOM-062-Z00-1999. Proyecto aprobado por la Comisión de Investigación y Ética de la Facultad de Medicina, UNAM: FM- DI/084/2023.

7.2 Evaluación de la hiperreactividad del músculo liso de la vía aérea mediante la técnica de órganos aislados

Se eutanizaron los cobayos con una dosis letal de pentobarbital sódico por vía intraperitoneal (200 mg/kg). Se disecó la tráquea y fue colocada en una caja de disección

donde posteriormente se eliminó el exceso de tejido conectivo. Todo el proceso fue realizado con el tejido sumergido en solución de Krebs Ringer con la siguiente composición (mM): $NaHCO_3$ (25), NaCl (118), KCl (4.77), KH_2PO_4 (1.20), $MgSO_4$ (1.20), $CaCl_2$ (2.5) y Glucosa (11). Se cortó la tráquea en 6 anillos (~3 milímetros) conteniendo cuatro anillos de cartílago, cada anillo se colocó en una cámara de órganos aislados de 10 mL de capacidad con 5 mL de solución de Krebs. Las preparaciones se mantuvieron a 37°C y se burbujearon continuamente con 5% CO_2 y 95% O_2 a un pH de 7.4.

Cada anillo traqueal se sujetó a un transductor de fuerza isométrica modelo FT03 (Grass Instruments, West Warwick, RI, EUA) conectado a un sistema amplificador de señales Cyberamp 380 (Axon Instruments, Foster City, CA, EUA) y a una interfaz análogo-digital Digidata 1440A (Axon Instrruments). Los experimentos se almacenaron en una computadora y se analizaron con el software AxoScope versión 10.2 (Axon Instruments, EUA).

Los tejidos se sometieron a una tensión de reposo de 1 g durante 30 min al inicio de estos experimentos para permitir la estabilización del tejido y la optimización del aparato contráctil, se estimularon tres veces consecutivas con KCl (60 mM) hasta alcanzar la respuesta máxima de contracción del tejido (~20 min) con un intervalo de 1 h entre cada estimulación. Posteriormente, se realizaron los protocolos experimentales descritos a continuación. Se construyó una curva concentración-respuesta acumulativa a carbacol (Cch, 0.1, 0.32, 1, 3.2 y 10 µM). Para los grupos experimentales, después de 45 min posteriores al tercer estímulo de KCl, se incubo por 15 min con E2 (10 nM), la concentración elegida fue estandarizada a través de una curva concentración-respuesta en un rango fisiológico previamente realizada. Otro grupo experimental fue incubado con

carboxeosina (CE, 100 nM) 15 min previos a iniciar la curva concentración-respuesta acumulativa con carbacol, elegida por su constante inhibitoria (Ki) de 100 nM[108].

7.3 Medición de las concentraciones de Ca^{2+} intracelular en célula única mediante la técnica de microfluorometría

Para estos experimentos, otro grupo de cobayos machos de la cepa Hartley de 300-400 g fueron eutanizados con una sobredosis de pentobarbital sódico (200 mg/Kg) intraperitoneal, se les extrajo la tráquea y se colocó en una placa de disección en solución de Krebs Ringer con la siguiente composición (mM): $NaHCO_3$ (25), NaCl (118), KCl (4.77), KH_2PO_4 (1.20), $MgSO_4$ (1.20), $CaCl_2$ (2.5) y Glucosa (11). Posteriormente se eliminó el exceso de tejido conjuntivo adyacente bajo microscopio estereoscópico. Inmediatamente después se realizó la disección del músculo liso traqueal, se cortó longitudinalmente la tráquea en la parte cartilaginosa, exponiendo la parte membranosa, esta después se fijó con alfileres al fondo de la caja de Petri con Sylgard® (Dow Corning Co. Midland, Mi, EUA). Al obtener el músculo liso traqueal, se incubó en 5 ml de solución de Hanks (Gibco, New York, EUA) con 35 µL de papaína (Worthington-Biochem, New Jersey, EUA) (56 mg/mL) y 2 mg de L-cisteína durante 10 min a 37°C. Después se lavó el tejido con medio mínimo esencial (Minimal Essential Medium, Gibco, New York, EUA) durante 1 min para desactivar y remover la papaína y L-cisteína. Posteriormente, se incubó el tejido en 5 ml de solución Hanks con 50 µg de colagenasa tipo 1 (Worthington-Biochem, New Jersey, EUA) durante dos periodos de 10 min a 37°C. Al finalizar cada periodo se procede a disgregar mecánicamente el tejido utilizando una pipeta Pasteur aspirando y soltando el tejido a través de la pipeta hacia las paredes del tubo ~40 veces. Al finalizar este proceso revisamos las células bajo un microscopio para corroborar la

efectividad de la disgregación. Una vez disgregado el tejido, la actividad enzimática se detiene adicionando medio mínimo esencial. El tejido se centrifugó dos veces a 1000 rpm durante 6 min, desechando el sobrenadante entre cada repetición. Ya obtenidas las células, se incubaron con fura-2-acetoximetil éster (Fura 2-AM; 2.5 µM, Sigma, Missouri, EUA)[57] en concentraciones bajas de Ca^{2+} (0.1 mM) durante 1 h a temperatura ambiente (22-25°C) y en obscuridad.

Las células previamente incubadas con Fura 2-AM se colocaron en una cámara con una cubierta de vidrio durante 30 min con el objetivo de que las células se adhieran a la base del vidrio, posteriormente la cámara se montó en un microscopio invertido (Diaphot 200, Nikon, Tokio, Japón) y se perfundieron con solución de Krebs calentada a 37°C con un flujo de 2-3 ml/min de la solución Krebs. Las células incubadas con el Fura 2-AM fueron excitadas al recibir pulsos alternos de luz de excitación con una longitud de onda 340 y 380 nm, y la luz de emisión se colectó a 510 nm utilizando un microfotómetro de Photon Technology International Modelo D-104 (PTI, Princeton, Nueva Jersey, EUA).

Para determinar las concentraciones de Ca^{2+} intracelular ($[Ca^{2+}]_i$), se realizó en una célula aislada que se localizó a través del microscopio, se empleó la fórmula de Grynkiewicz[109], con una Kd=386 nM para el Fura 2-AM. La fluorescencia se registró cada 0.5 seg, Rmax y Rmin, fueron 6.6 y 0.39, Rmax y Rmin corresponden a los cocientes de fluorescencia 340/380 respectivamente. Los datos fueron almacenados en una computadora y luego analizados con un software especializado (Felix, versión 1.21, PTI).

En los miocitos traqueales de cobayo, se investigaron los mecanismos afectados por el E2 (10 nM) para modificar la liberación de Ca^{2+} inducida por la cafeína (10 mM).

Las células fueron estimuladas con cafeína 10 mM y se observó un incremento de la $[Ca^{2+}]_i$, después de 15 min de lavado se volvió a dar un segundo estímulo con cafeína. Estas mismas células fueron preincubadas durante 5 min con E2 (10 nM) o D600 (30 µM)[57] previos a la segunda estimulación de cafeína y se midieron las concentraciones de $[Ca^{2+}]_i$ y la cinética de la respuesta inducida por cafeína en el miocito aislado de cobayo.

Para valorar el efecto del E2 sobre el intercambiador Na^+/Ca^{2+} en su forma reversa (NCX_{rev}) se evaluó la respuesta de Ca^{2+} a la sustitución de NaCl 118 mM en Krebs con cloruro de colina (143 mM)[110,111] seguida de una respuesta inmediata de cafeína (10 mM) con o sin E2 (10 nM).

Para evaluar el transportador mitocondrial (TM), los miocitos se estimularon con cianuro de carbonilo 4-(trifluorometoxi)fenilhidrazona (FCCP, 10 µM, un activador del TM)[112] con o sin E2 (10 nM).

Para inducir la entrada capacitativa de Ca^{2+}, las células se estimularon con cafeína (10 nM), y luego se perfundió una solución de Krebs libre de Ca^{2+} que contenía EGTA 0,1 mM durante 10 min, con ácido ciclopiazónico (CPA, 10 µM)[113] añadido durante los últimos 5 min antes de restaurar la perfusión de Krebs que contiene Ca^{2+} con o sin E2 (10 nM).

En el siguiente protocolo, después de un estímulo inicial de cafeína 10 mM con su respectivo lavado de 10 min, se incubó la célula con U-0126 (10 µM)[55,114] durante 5 min, se estimuló nuevamente con cafeína (10 mM). Posteriormente, se repitió el

procedimiento, incubando primero con U-0126 (10 µM) durante 7 min, adicionando E2 (10 nM) durante los últimos 5 min, seguido por un segundo estímulo con cafeína 10 mM.

Para los siguientes experimentos, se realizó un primer estímulo con cafeína 10 mM, seguido por un lavado de 10 min y posteriormente se incubó la célula con propilpirazoltriol (PPT, 10 nM, un agonista específico del REα)[8,52] o diarilpropionitrilo (DPN, 10 nM, un agonista del REβ)[8,52] durante 5 min, seguido por un segundo estimulo con cafeína 10 mM.

En otro grupo experimental, se realizó un primer estímulo con cafeína 10 mM, después de 10 min de lavado se incubó la célula primero con E2 (10 nM) y después se agregó lantano (La^{3+}, 100 µM, establecida a través de una curva concentración respuesta) durante 3 min, seguido por un segundo estímulo con cafeína 10 mM.

Posteriormente, se realizó el siguiente protocolo dando un primer estímulo con cafeína 10 mM, seguido de un lavando durante 10 min se incubó durante 5 min con E2 (10 nM) y después se agregó carboxieosina (CE, 100 nM); establecida a través de una curva concentración respuesta y por su Ki de 100 nM[108] durante 4 min, estimulando la célula con cafeína y midiendo el incremento de $[Ca^{2+}]_i$.

En otro grupo experimental, se realizó un primer estímulo con cafeína 10 mM, después se dio un lavado con solución Krebs durante 10 min, después se incubó durante 2.5 min la tapsigargina a diferentes concentraciones (0.125, 0.25, 0.5, 1, 1.5 y 2 µM), basado en concentraciones de trabajos anteriores[55], y se estimuló con cafeína (10 mM). Posterior a un lavado de 15 min se realizó un último estímulo con cafeína (10 mM).

En el último protocolo, se estimuló la célula con cafeína 10 mM, después de un lavado de 15 min la célula se incubó con CPA (10 µM)[113] durante 2.5 min, seguido por un lavado con solución Krebs de 5 min, posterior a esto se estimuló la célula con cafeína. Después del estímulo se lavó la célula durante 15 min. Nuevamente se incubó la célula durante 2.5 min con CPA, y enseguida se retira el CPA y se incubó durante 5 min con E2 (10 nM), al finalizar se estimula nuevamente a la célula con cafeína en presencia del E2.

7.4 Identificación de la presencia de PMCA a través de la técnica de Western Blot

Se disecaron tiras de músculo liso traqueal de cobayo libres de epitelio y tejido conectivo. Se usó un mortero de pellets (Kimble, DWK Life Sciences, Massachusetts, EUA) para homogeneizar cada tejido en 30 µl de tampón de lisis RIPA (Santa Cruz Biotechnology, cat. No. sc-24948, Santa Cruz, CA, EUA) que contenía un cóctel de inhibidores de proteasas (Sigma, cat. No. P8340). Las muestras homogeneizadas se centrifugaron a 5000 rpm y 4°C durante 15 min. Se utilizó un kit comercial (RC DC Protein Assay, catálogo 500–0119, Bio-Rad, Hercules, CA, EUA) para medir la concentración de proteína total. Las muestras (30 µg cada una) se dividieron en diferentes carriles de gel de poliacrilamida-SDS al 10% y se sometieron a electroforesis en condiciones reductoras. Las proteínas se transfirieron a una membrana de fluoruro de polivinilideno (Bio-Rad, Hercules, CA, EUA) y se bloquearon con leche en polvo descremada al 5% en PBS tween (Tween 20, 0.1%, Sigma, EUA) durante 1 h a temperatura ambiente. Se incubaron con anticuerpos policlonales de conejo (GTX130858; dilución 1:500, GeneTex, Irvine, CA, EUA) y con monoclonales de ratón (GTX22783; dilución 1:1000, GeneTex) preparados contra PMCA1 y PMCA4, respectivamente, en las membranas a 4ºC durante una noche. Posteriormente, las membranas se trataron durante 2 h a temperatura

ambiente con un anticuerpo secundario IgG de cabra anti-conejo, anti-ratón (1:500, GeneTex, Irvine, CA, EUA) acoplado con peroxidasa de rábano. Se utilizó β-actina (A1978, Merck KGaA, Darmstadt, Alemania) como control de carga. Se utilizó un reactivo quimioluminiscente mejorado (Luminol; Santa Cruz Biotechnology, cat. No. sc-2048 CA, EUA) para detectar las proteínas en la membrana tras la inmunotransferencia. La señal generada fue capturada y analizada mediante un escáner C-DiGit. (LI-COR Biotechnology, Lincoln, NE, EUA).

7.5 Análisis de acoplamiento molecular

Para evaluar la posible interacción del 17β-estradiol (E2) o de sus agonistas específicos de los receptores estrogénicos sobre la PMCA y la SERCA, considerando que se ha reportado que el E2 puede unirse a otras proteínas y regular su actividad, como ocurre con el CCDV-L[106] y el canal de potasio activado por Ca^{2+}[101,115,116]. Además, se ha reportado que otros agonistas estrogénicos (DPN, PPT, bisfenol A) pueden regular estos canales[101,117,118], lo que nos sugirió un posible mecanismo de acción similar entre el E2 y las ATPasas. Mediante la técnica de acoplamiento molecular, nos fue posible predecir y visualizar la afinidad y estabilidad de la interacción entre E2 y las ATPasas, mostrando evidencia estructural que respalda la hipótesis de una regulación directa por parte de esta hormona.

7.5.1 Preparación de las proteínas para el acoplamiento molecular

Se inicio por la preparación de las estructuras de proteínas para el análisis de acoplamiento de la siguiente manera. Tanto las estructuras proteicas de PMCA-1 (ID PDB: 6A69, plasma membrane calcium-transporting ATPase 1) con 1220 aminoácidos,

y de SERCA2b (ID PDB: 6LN7, sarco/endoplasmic reticulum Ca^{2+} ATPase) con 1042 aminoácidos, se obtuvieron del Protein Data Bank (//www.rcsb.org/). Mientras que la estructura de la proteína PMCA-4 (ID AF: P23634, Plasma membrane calcium-transporting ATPase 4) con 1241 aminoácidos se obtuvo de la base de datos AlphaFold Protein Structure Database (https://alphafold.ebi.ac.uk/). Todas las estructuras de las proteínas se refinaron utilizando el software USCF Chimera versión 1.15 (//www.cgl.ucsf.edu/chimera, Resource for Biocomputing, Visualization, and Informatics (RBVI), CA, EUA). Se eliminaron restos de solventes y residuos de aminoácidos individuales, se adicionaron hidrógenos, se adicionaron las cargas teniendo en cuenta las interacciones electrostáticas, también se consideró el campo de fuerza del aminoácido AMBER ff14SB[119]. En el caso de las proteínas, se conservaron tanto los iones de Ca^{2+} como de Mg^{2+}.

7.5.2 Preparación de los ligandos para el acoplamiento molecular

Las estructuras de los ligandos (5(6)-carboxyeosina (CE, SID: 44119976), el 17β-estradiol (E2, SID: 349982835), el ácido ciclopiazónico (CPA, SID: 198943370), el diarilpropionitrilo (DPN, SID: 405282160) y el propilpirazoltriol (PPT, SID: 5 040063) se obtuvieron de la base de datos PubChem (https://pubchem.ncbi.nlm.nih.gov). Se descargaron las estructuras de los ligandos en formato SDF y fueron optimizados geométricamente, corrigiendo posibles distorsiones en los ángulos y enlaces para minimizar su energía y obtener una estructura más estable y realista antes de realizar la simulación, para esto se utilizó el software Avogadro (versión de software 1.2.0 https://avogadro.cc/). El posible estado de ionización se generó a valores de pH de 7.0 ± 0.5. Las cargas parciales de los átomos del ligando se calcularon según el método de

Gasteiger[120], utilizando el software USCF Chimera versión 1.15 (https://www.cgl.ucsf.edu/chimera).

7.5.3 Acoplamiento molecular

Después de la preparación de las estructuras de las proteínas y de las estructuras de los ligandos, se realizaron cálculos de acoplamiento molecular utilizando un acoplamiento molecular ciego y rígido ya que son los modelos de unión proteína-ligando más utilizados para nuestro objetivo. Los acoplamientos se realizaron con el software AutoDock 4.2.6. software (https://autodock.scripps.edu/, Scripps Research, CA, EUA) y la extensión AutoDock Vina Versión 1.1.2[121], ejecutándolos desde la base de USCF Chimera Versión 1.15 y Discovery Studio Visualizer versión 21.1.0, CA, EUA (https://www.3ds.com/). Los mejores modelos de unión proteína-ligando se obtuvieron utilizando funciones de puntuación específicas basadas en términos de energía (ΔG).

7.6 Fármacos y reactivos

17β-estradiol

El 17β-estradiol [1,3,5(10)-estratrieno-3-17β-E2] es una hormona sexual esteroidea perteneciente al grupo de los estrógenos[15,92]. El rango fisiológico en la mujer es de 40 pM durante la menopausia hasta alcanzar los 150 nM durante el embarazo, con un rango de 80 pM-1.5 nM durante el ciclo menstrual[2]. Para determinar la concentración de los experimentos de microfluorometría se realizó una curva preliminar de concentración-respuesta en donde se observó que el E2 alcanzaba su máximo efecto sobre la respuesta de Ca^{2+} inducida por cafeína a la concentración de 10 nM, por lo que esta concentración fue elegida durante los protocolos de microfluorometría. Para los experimentos de

órganos aislados se utilizó un rango fisiológico de E2 con concentraciones de 1, 32 y 100 nM. El E2 se obtuvo de Sigma Chemical Co. (St. Louis, MO, EUA).

Cafeína

La cafeína (1,3,7-trimetilxantina) es un alcaloide perteneciente al grupo de las metilxantinas encontrado naturalmente en una variedad de plantas como el café, té, cacao, yerba mate, entre otras. Su naturaleza hidrofóbica le permite difundirse rápidamente a través de la membrana plasmática, teniendo múltiples blancos farmacológicos[122,123]. En el MLVA la cafeína es conocida por ser un modulador del RyR a una concentración de ~10 mM[122-126]. Además, actúa como un antagonista de los receptores de adenosina, con una concentración inhibitoria 50 (CI_{50}) de 98 μM[122,123,127], y como un agonista de los receptores amargos (300 μM)[122,123,128-130]. También puede inhibir a la fosfodiesterasa 4 (PDE4) con un CI_{50} en el rango de 500 μM-1 mM[122,123,131,132]. La cafeína es una herramienta farmacológica utilizada para incrementar la probabilidad de apertura de RyR al incrementar su sensibilidad al Ca^{2+}, su agonista endógeno. Su rápida y reversible unión con el RyR[122,123], ofrece varias ventajas experimentales. Para los experimentos de microfluorometría se utilizó la concentración de 10 mM y se obtuvo de Sigma Chemical Co. (St. Louis, MO, EUA).

Fura-2 AM

El fura-2-acetoximetil éster, o Fura-2 AM, es un indicador fluorescente del Ca^{2+} que es permeable a la membrana. Una vez dentro de la célula, sus grupos acetoximetilo son eliminados por esterasas intracelulares, liberando la molécula en su forma ácida (Fura-2). En esta forma, con sus cuatro grupos carboxilos expuestos, puede unirse a los iones

divalentes (Ca^{2+}). Esta molécula es utilizada para la medición de las concentraciones de Ca^{2+} libre intracelular, utilizando un método de proporción f de fluorescencia[133]. Para los experimentos de microfluorometría se utilizó la concentración de 2.5 µM[57] y fue obtenido de Sigma Chemical Co. (St. Louis, MO, EUA).

D600

El D600 (clorhidrato de metoxiverapamilo), también conocido como galopamil, es un análogo del verapamil, perteneciente al grupo de los bloqueadores del CCDV-L, específicamente del grupo de las fenilalquilamina. Como es característico de este grupo, el D600 bloquea la corriente lenta interna dependiente de entrada de Ca^{2+} a través de la membrana plasmática. A este fármaco se le conoce por su acción en el sistema cardiovascular, empleándose en la clínica como tratamiento para la hipertensión, angina, isquemia miocárdica e incluso como un antiarrítmico[134,135]. Para los experimentos de microfluorometría se utilizó la concentración de 30 µM[57] y fue obtenido de Sigma Chemical Co. (St. Louis, MO, EUA).

Lantano (La^{3+})

El lantano (tricloro lantano III) es el primer elemento de la serie de lantánidos. Estos elementos son ampliamente utilizados por su capacidad de desplazar al Ca^{2+} de sus sitios de unión[136,137]. Sin embargo, el lantano es un fármaco inespecífico, pues no se restringe únicamente a sitios de unión del Ca^{2+}. Además, puede reemplazar al magnesio (Mg^{2+}) u otros iones en su unión a varias proteínas. Específicamente en las proteínas regulatorias de Ca^{2+} intracelular, se ha reportado que el lantano inhibe la actividad de PMCA al desplazar tanto al Ca^{2+} y/o al Mg^{2+} en sus sitios de unión de alta afinidad. Dado

que la PMCA requiere del Mg^{2+} para el recambio rápido del grupo fosfato, la sustitución de MgATP por La^{3+}ATP como sustrato, ralentiza la disociación del fosfato, inhibiendo la actividad de PMCA[136]. Similarmente, en SERCA, el lantano se une al sitio citoplasmático de transporte de Ca^{2+} y Mg^{2+}, inhibiendo el recambio de la fosfoenzima[137]. Adicionalmente, se ha descrito que el lantano tiene la capacidad de bloquear el CCDV-L al unirse a la zona permeable del poro, bloqueando la corriente interna de Ca^{2+} del canal[138]. Para los experimentos de microfluorometría se realizó una curva de concentración-respuesta tomando en cuenta concentraciones utilizadas en trabajos anteriores del laboratorio[55], continuando con la concentración de 100 µM dado que fue la menor concentración en la que se observó su efecto. El lantano fue obtenido de Sigma Chemical Co. (St. Louis, MO, EUA).

Carboxieosina (CE)

La 5(6)-Carboxieosina (CE), es una molécula similar a la eosina, con la adición de un grupo carboxilo. Estos compuestos son análogos de la fluoresceína, y se han observado que tienen potentes efectos inhibitorios sobre PMCA. La CE tiene una alta afinidad por PMCA (Ki=100 nM), se une de manera reversible a un sitio alostérico, por lo que no compite con el ATP por su sitio de unión, presentando una actividad inhibitoria independiente de la concentración de ATP[108]. A concentraciones más altas (40 µM), se ha observado que la CE puede afectar a PMCA y a SERCA, pero no interfiere con NCX[108,139]. Para los experimentos de microfluorometría se realizó una curva de concentración-respuesta tomando en cuenta su Ki. Se seleccionó la concentración de 100 nM para continuar el protocolo. Para los experimentos de órganos aislados se

seleccionaron concentraciones basadas en su Ki y se utilizaron las concentraciones de 32 y 100 nM. La CE se obtuvo de Abcam (Cambridge, Reino Unido).

Carbacol (Cch)

El carbacol (cloruro de carbamilcolina, Cch) es un análogo de la acetilcolina con actividad agonista sobre los receptores colinérgicos muscarínicos y nicotínicos. Estructuralmente es similar a la acetilcolina, ya que es una amina cuaternaria que tiene una carga positiva. A diferencia de la acetilcolina, el Cch no se hidroliza por colinesterasas. Debido a su acción sobre los receptores colinérgicos y su estabilidad en soluciones acuosas, se utiliza ampliamente en la investigación. En el ámbito terapéutico, el Cch se utilizaba para provocar la contracción del esfínter del iris y los músculos ciliares en el ojo durante el tratamiento del glaucoma, aunque en la actualidad ha sido reemplazado por otros fármacos con mayor efectividad y menos efectos secundarios[140]. Para los experimentos de órganos aislados se realizaron curvas de concentración-respuesta a Cch (0.1, 0.32, 1, 3.2 y 10 µM); las concentraciones fueron seleccionadas basadas en trabajos anteriores del laboratorio[141]. El Cch se obtuvo de Sigma Chemical Co. (St. Louis, MO, EUA).

Ácido ciclopiazónico (CPA)

El ácido ciclopiazónico (CPA) es un metabolito indólico tetramínico, producido como micotoxina por especies de Aspergillus y Penicillium. Su presencia en productos agrícolas representa un riesgo para la salud humana y animal cuando consumen los productos agrícolas contaminados con la toxina. Se ha descrito que el CPA actúa inhibiendo a SERCA de manera específica y reversible[142,143]. La inhibición por parte del CPA ocurre al estabilizar a SERCA en una conformación inactiva de la enzima,

deteniendo la fosforilación mediada por ATP[142]. La concentración de CPA (10 µM) para los experimentos de microfluorometría fue establecida a través de trabajos anteriores del laboratorio[113] y mediante una curva de concentración-respuesta (1, 3.2 y 10 µM), además, fue obtenido de Sigma Chemical Co. (St. Louis, MO, EUA).

Tapsigargina

La tapsigargina es una lactona sesquiterpénica del tipo guaianolida, que se encuentra en abundancia en una hierba mediterránea, *Thapsia garganica* o "zanahoria mortal," llamada así por su toxicidad cuando es ingerida por el ganado[144]. La tapsigargina es reconocida por ser un potente inhibidor de SERCA, afectando tanto la velocidad de carga como la actividad de la ATPasa Ca^{2+}-dependiente de manera dosis-dependiente[144,145]. Su efecto se presenta a concentraciones bajas en el rango nanomolar, sin afectar a PMCA o NCX. SERCA presenta dos estados; el estado E1 ocurre cuando la ATPasa se encuentra activada al unirse a dos iones Ca^{2+} (un estado de alta afinidad por el Ca^{2+}), y E2 es el estado en el que se liberan los iones al interior del RS (con baja afinidad por el Ca^{2+}). Durante el estado E2 (libre de Ca^{2+}), la tapsigargina forma un complejo irreversible con SERCA, inactivando catalíticamente la proteína, evitando la unión de Ca^{2+} y bloqueando la unión de ATP, evitando su activación[144,145]. Para los experimentos de microfluorometría se realizó una curva de concentración-respuesta (0.125, 0.25, 0.5, 1, 1.5 y 2 µM) basada en concentraciones de trabajos anteriores del laboratorio[55], y la tapsigargina fue obtenido de Sigma Chemical Co. (St. Louis, MO, EUA).

U-0126

El U-0126 es un inhibidor indirecto de ERK1/2, ya que actúa inhibiendo de manera directa y no competitiva a las cinasas de las ERK1/2 (MEK-1 y MEK-2). Su inhibición es altamente selectiva y no se ha observado efecto sobre otras cinasas[146]. Para los experimentos de microfluorometría se utilizó la concentración de 10 µM, escogida por una curva de concentración-respuesta basada en trabajos previos del laboratorio[55,114], y se obtuvo de Sigma Chemical Co. (St. Louis, MO, EUA).

Propilpirazoltriol (PPT)

El propilpirazoltriol (PPT) es un compuesto derivado de pirazol caracterizado por ser un agonista selectivo del REα. Presenta una alta afinidad de unión a este receptor, ~50% en comparación con el E2, y una alta selectividad de unión por REα sobre REβ, con una diferencia de afinidad de 410 veces, siendo el pirazol con mayor afinidad y selectividad[147]. Para los experimentos de microfluorometría con PPT, se utilizó la concentración de 10 nM basada en concentraciones utilizadas en la literatura[52,148], y se obtuvo de Sigma Chemical Co. (St. Louis, MO, EUA).

Diarilpropionitrilo (DPN)

El diarilpropionitrilo (DPN) es un compuesto análogo de nitrilo con una alta selectividad hacia el REβ. Aunque actúa como un agonista para ambos subtipos de RE, su afinidad relativa de unión por a REβ es 70 veces mayor que la de REα, y su potencia relativa para la transcripción mediada por REβ es 170 veces mayor que para REα. Además, tiene una selectividad de potencia para REβ 78 veces mayor (CE_{50} = 0.85 nM para REβ; CE_{50} = 66 nM para REα)[149]. Para los experimentos de microfluorometría con DPN, se utilizó la

concentración de 10 nM basado en concentraciones utilizada en la literatura[8,52,148], y se obtuvo de Sigma Chemical Co. (St. Louis, MO, EUA).

Cloruro de colina

El cloruro de colina es una sal de amonio cuaternario ampliamente utilizada en la industria de alimentos para la producción pecuaria[150]. Para demostrar la presencia y función del NCX_{rev} en estas células, realizamos la sustitución de NaCl y $NaHCO_3$ por cloruro de colina, el cual induce un incremento transitorio de las $[Ca^{2+}]_i$, lo cual corresponde a la activación del intercambiador en su modo reverso, ingresando Ca^{2+} al interior de la célula y extrayendo Na^+[110,111]. Para los experimentos de microfluorometría con cloruro de colina, se utilizó la concentración de 143 mM, basada en trabajos previos del laboratorio[110,111], y se obtuvo de Sigma Chemical Co. (St. Louis, MO, EUA).

Cianuro de carbonilo 4-(trifluorometoxi)fenilhidrazona (FCCP)

El cianuro de carbonilo 4-(trifluorometoxi)fenilhidrazona (FCCP, 10 µM) es un protonóforo (ionóforo H^+) y desacoplador de la fosforilación oxidativa en las mitocondrias. Tiene la capacidad de despolarizar las membranas plasmáticas y mitocondriales[151], además de presentar diversos efectos sobre el Ca^{2+} celular. En estudios previos realizados en nuestro laboratorio, se evaluó la respuesta de Ca^{2+} ante el estímulo con FCCP en fibroblastos para activar al transportador mitocondrial[112]. Para los experimentos de microfluorometría con FCCP, se utilizó la concentración de 10 µM[112], y se obtuvo de Sigma Chemical Co. (St. Louis, MO, EUA).

7.7 Análisis estadístico

Los resultados de las $[Ca^{2+}]_i$ de célula única se evaluaron mediante un análisis de varianza de una vía seguido de la prueba de Dunnett. La comparación entre grupos en los experimentos de órganos aislados se llevó a cabo mediante un análisis de varianza de una vía seguido de la prueba de Dunnett. La significancia estadística se fijó en $p<0.05$ bimarginalmente. La reactividad al Cch se evaluó mediante la concentración efectiva 50% (CE_{50}) y la respuesta máxima. La CE_{50} se calculó a partir de la curva concentración-respuesta acumulativa mediante regresión lineal como -Log utilizando el software ED50plus v1.0 y se expresó como concentración nM. El área bajo la curva (ABC) se analizó en Graphpad Prism 9.0.2, expresado como la media ± error estándar de la media (EE), la significancia se determinó mediante un análisis de varianza de una vía seguido de la prueba de Dunnett.

8. Resultados

8.1 Efecto del 17β-estradiol sobre la contracción inducida por carbacol

En los anillos traqueales de cobayo, el Cch indujo una contracción dependiente de la concentración. La preincubación con E2 durante 15 min aumentó la respuesta máxima de contracción a Cch (Figura 8A, n = 5). En el grupo control (circulo negro), se realizó una curva acumulativa con Cch (100, 320 nM, 1, 3.2 y 10 µM). La incubación con E2 a 10 nM, (triángulo blanco) produce un aumento significativo en la contracción a Cch a las concentraciones de 1, 3.2 y 10 µM comparado con el grupo control. Mientras, en el grupo con E2 a 32 nM (rombo blanco), hubo un incremento significativo de la contracción con Cch a la concentración de 3.2 y 10 µM al compararse con el grupo control. Finalmente,

el grupo con E2 a 1 nM (cuadro blanco), solo se observan diferencias significativas en la contracción a la concentración de 10 µM de Cch contra el grupo control. Cabe mencionar, que las concentraciones de E2 utilizadas en estos experimentos fueron en un rango fisiológico. Cuando se analizó la CE_{50}, no se observaron diferencias en ninguno de los grupos (Figura 8B).

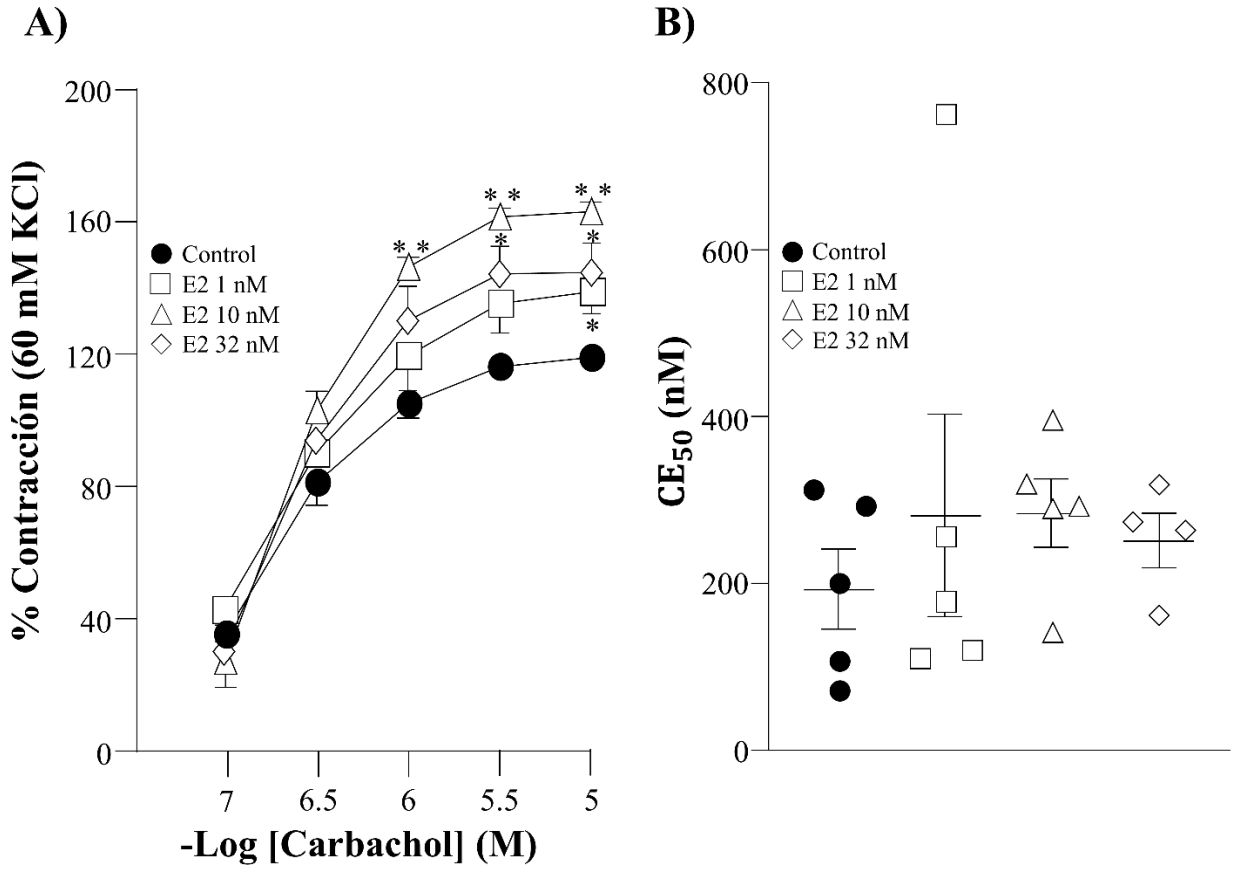

Figura 8. Efecto del estradiol E2 sobre la contracción del músculo liso traqueal de cobayo inducida por carbacol. A) Curvas concentración-respuesta acumulativa de carbacol con y sin 17β-estradiol (E2) en anillos traqueales de cobayo. B) Gráfico que ilustra los valores de la CE_{50} para las curvas a Cch con y sin E2. Los símbolos representan la media ± el error estándar de la media (EE). *p<0.05, **p < 0.01 al compararse contra el grupo de E2, evaluado mediante análisis de varianza de una vía seguido de la prueba de Dunnett. n=5 para Control, E2 1 nM y 10 nM; n=4 para E2 32 nM.

8.2 El efecto del 17β-estradiol sobre el aumento de Ca^{2+} en respuesta a la cafeína

En los miocitos del MLVA de cobayo, la estimulación con cafeína indujo un aumento de las $[Ca^{2+}]_i$, observado como un pico transitorio con un rápido retorno a los niveles basales. Esta respuesta a la cafeína se repitió dos veces (Figura 9A, n=5). La incubación con E2 (10 nM) durante 5 min antes de la estimulación con cafeína disminuyó la amplitud de la respuesta de las $[Ca^{2+}]_i$ y el pico transitorio se modificó, produciendo una meseta; una subsecuente estimulación con cafeína posterior a un lavado de 15 min sin E2, produce una respuesta de Ca^{2+} similar a la primera (Figura 9B, n=8). La incubación con D600 (un bloqueador del CCDV-L) durante 5 min mostró una disminución en las $[Ca^{2+}]_i$ basales. Hubo una disminución en la amplitud de la respuesta a cafeína sin modificar el pico transitorio. Seguido a un lavado de 15 min sin presencia de D600, se volvió a estimular con cafeína, observando una respuesta de Ca^{2+} similar a la primera respuesta (Figura 9C, n=5).

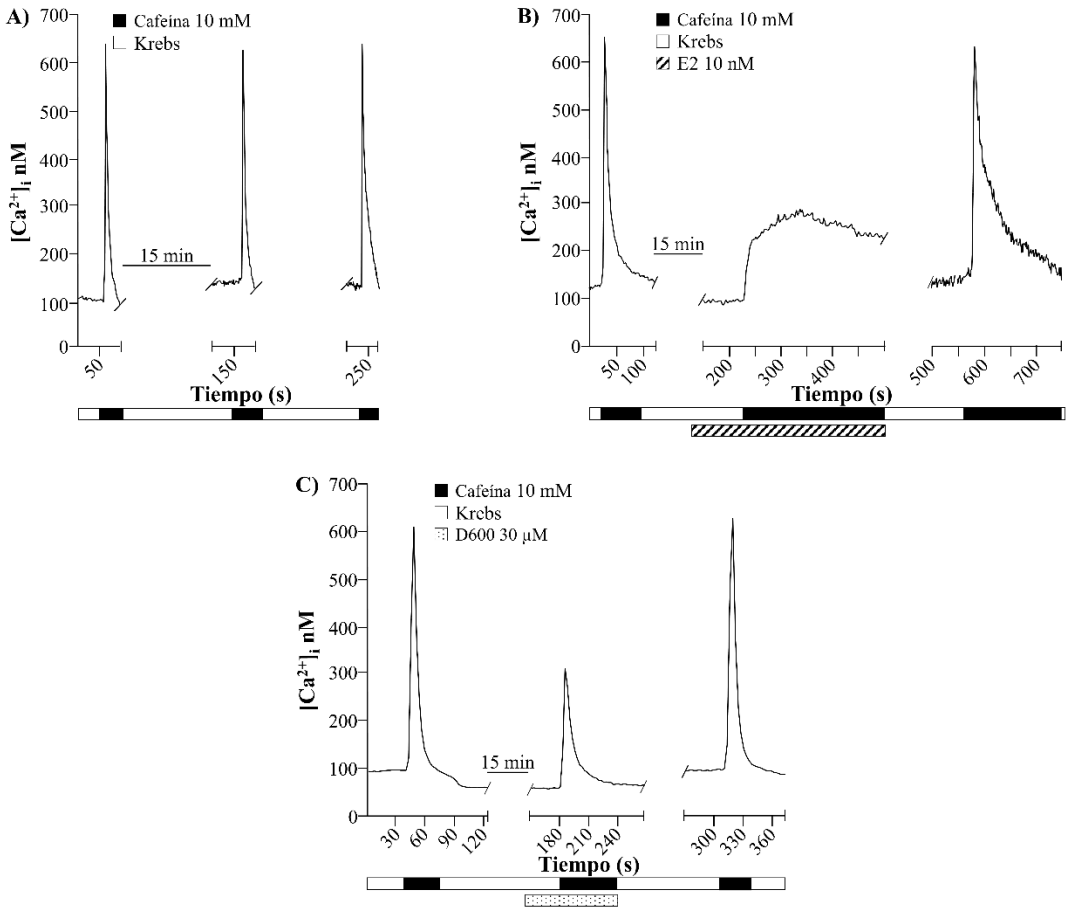

Figura 9. Efecto del 17β-estradiol sobre la respuesta de cafeína. A) Los miocitos traqueales de cobayo, fueron estimulados con cafeína (10 mM) durante 3 ocasiones, entre intervalos de lavado de 15 min, induciendo incrementos en las $[Ca^{2+}]_i$ (control). Los miocitos fueron incubados previamente durante 5 min con B) 17β-estradiol (E2, 10 nM) o C) D600 (30 µM; bloqueador del CCDV-L) subsecuentemente fueron estimulados con cafeína (10 mM) induciendo aumento en las $[Ca^{2+}]_i$. n=8 para E2, n=5 para D600.

8.3 Efecto de los agonistas específicos de los receptores estrogénicos sobre la respuesta de Ca^{2+} inducida por la cafeína

En miocitos traqueales de cobayo, las células se estimularon con cafeína, induciendo un pico transitorio de Ca^{2+}. Después de un lavado de 15 min con Krebs, las células se incubaron con los agonistas específicos de los RE, PPT (10 nM, agonista del REα) y DPN (10 nM, agonista del REβ). Se observó una meseta de Ca^{2+} similar a la producida por E2 cuando las células se incubaron con PPT (Figura 10A, C, n=4) pero no con DPN

(Figura 10B, C, n=5), lo que indica una señalización diferencial entre los agonistas específicos de su RE.

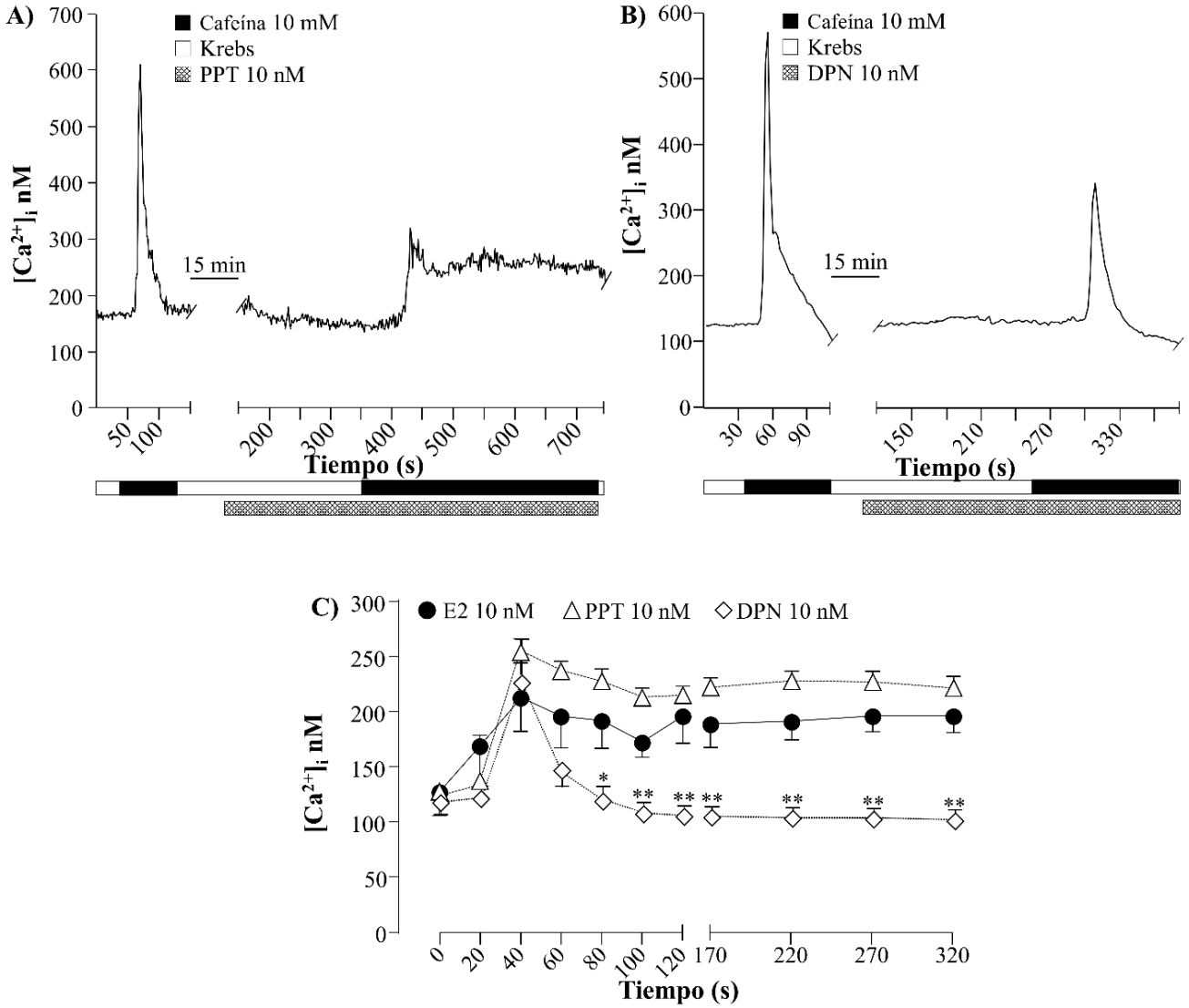

Figura 10. Comparación entre la respuesta de cafeína en presencia de los agonistas específicos de los receptores de estrógeno (RE). A) Registro de la primera estimulación de cafeína mostrando un pico de Ca^{2+}. Después de un lavado de 15 min con solución de Krebs, la célula se incubó con PPT (10 nM; agonista del REα) durante 5 min antes del segundo estímulo de cafeína, induciendo una meseta de Ca^{2+}. B) Se estimuló a la célula con cafeína, seguido por un lavado de 15 min con Krebs y después la célula se incubó durante 5 min con DPN (10 nM; agonista del REβ). Posteriormente, la célula fue estimulada con cafeína produciendo un pico transitorio de Ca^{2+}. C) Comparación de la evolución temporal de las respuestas de Ca^{2+} inducidas por la cafeína en presencia de E2, PPT o DPN. Los símbolos representan la media ± error estándar de la media (EE). El análisis se realizó mediante un análisis de varianza unidireccional seguido de la prueba de Dunnett. *p<0,05, **p<0,01. n=8 para E2, n=5 para D600, n=4 para PPT y n=5 para DPN.

8.4 Análisis del efecto del estradiol y los agonistas específicos de los receptores de estrógeno sobre la respuesta de Ca^{2+} inducida por la cafeína

Se procedió a analizar las respuestas de Ca^{2+} inducidas por la cafeína en presencia de E2, D600, PPT y DPN. En el análisis del área bajo la curva (ABC) se observaron diferencias significativas en la comparación de E2 vs PPT y altamente significativas en la comparación de E2 vs D600 y E2 vs DPN (Figura 11). Aunque la respuesta de Ca^{2+} inducida por cafeína mostró una meseta tanto con E2 como con PPT, PPT tuvo un ABC mayor que E2, lo que podría deberse a la inespecificidad de E2. No obstante, la respuesta de Ca^{2+} inducida por cafeína con DPN fue un pico transitorio y su ABC fue menor en comparación con E2, lo que sugiere que el efecto de E2 no está mediado por el ERβ.

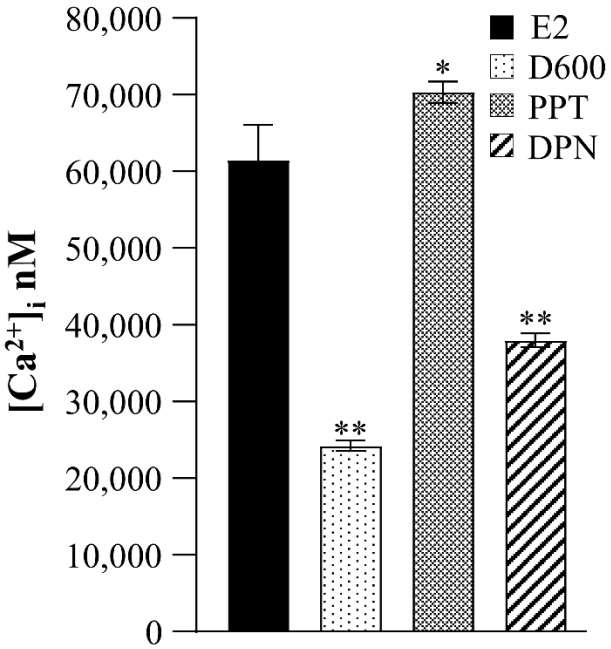

Figura 11. Comparación del área bajo la curva (ABC) de la respuesta de Ca^{2+} inducida por cafeína en presencia de E2, D600, PPT o DPN. Análisis de ABC de la respuesta de Ca^{2+} inducida por cafeína en presencia de E2 (10 nM), D600 (30 µM; bloqueador del CCDV-L), PPT (10 nM; agonista del REα) o DPN (10 nM; agonista del REβ). Los datos representan el ABC ± EE. Los datos se analizaron mediante un análisis de varianza de una vía seguido de la prueba de Dunnett, analizados todos contra el grupo de E2. *p<0,05, **p<0,01. n=8 para E2, n=5 para D600, n=4 para PPT y n=5 para DPN.

8.5 Efecto del U-0126 sobre la respuesta de Ca^{2+} inducida por la cafeína

Para corroborar que el fenómeno observado con E2 no fue mediado por la vía de señalización celular de las cinasas 1 y 2 reguladas por señales extracelulares (ERK 1/2), utilizamos U-0126 (un inhibidor de MEK1/2, 10 µM)[55]. En miocitos traqueales de cobayo, la incubación con U-0126 durante 5 min disminuyó la amplitud del pico transitorio de Ca^{2+} inducido por cafeína (Figura 12A, n=3). Además, se incubó U-0126 durante 7 min y se añadió E2 durante los últimos 5 min, seguido de un estímulo de cafeína que produjo una meseta de Ca^{2+} (Figura 12B, n=3).

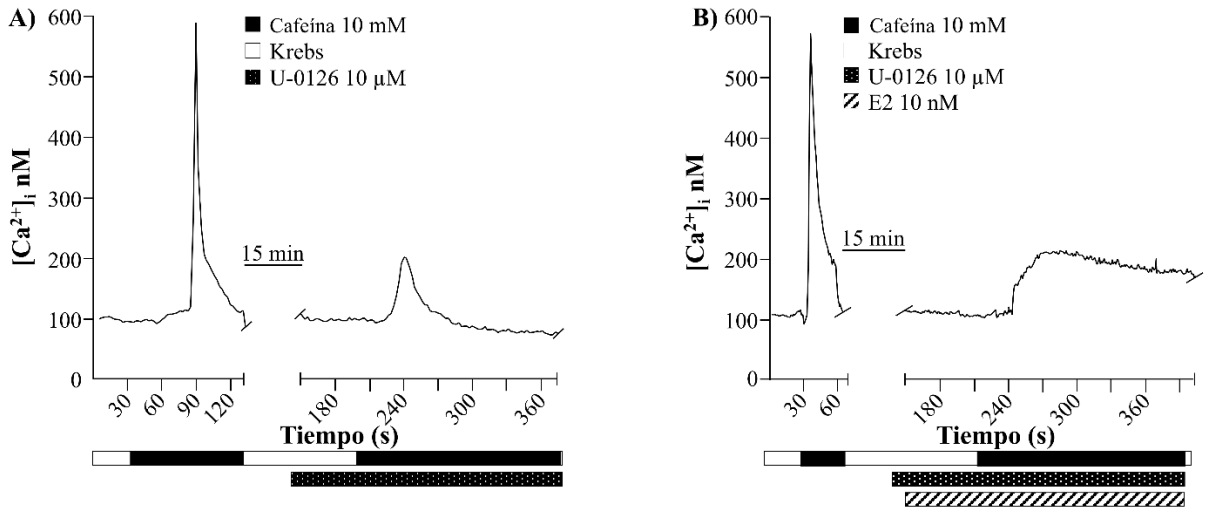

Figura 12. Comparación de los efectos del E2 sobre diferentes mecanismos implicados en el manejo de las $[Ca^{2+}]_i$. A) Registro original de la primera respuesta de Ca^{2+} a cafeína (10 mM). Después de un lavado de 10 min, se incubó U-0126 (10 µM, inhibidor de MEK1/2, n=3) durante 5 min antes de un segundo estímulo de cafeína, induciendo un pico transitorio de Ca^{2+} de menor amplitud. B) La estimulación del miocito con cafeína indujo un incremento en las $[Ca^{2+}]_i$. Posterior a un lavado de 10 min, la célula se incubó con U-0126 durante 2 min y luego se añadió E2 (10 nM) durante 5 mi (el período de incubación de U-0126 duró 7 minutos, n=3). Un estímulo final de cafeína produjo una meseta de Ca^{2+}. Tanto U-0126 como E2 estuvieron presentes durante el estímulo.

8.6 Efecto del estradiol sobre el intercambiador Na^+/Ca^{2+}

Para inducir la inversión del NCX (NCX_{rev}) y estudiar si estaba involucrado en el fenómeno producido por E2, se sustituyó el NaCl (118 mM) por cloruro de colina (143 mM; sustituto equivalente milimolar del Na^+) en la solución normal de Krebs, induciendo

un incremento transitorio de Ca^{2+} cuando inmediatamente después se estimularon las células con cafeína y se observó que el pico de Ca^{2+} no estaba alterado (Figura 13A). Después de un período de incubación de 5 min con E2, la respuesta a cloruro de colina se redujo significativamente (Figura 13B); sin embargo, la estimulación con cafeína después de la respuesta con cloruro de colina no afectó la meseta de Ca^{2+} inducida por cafeína.

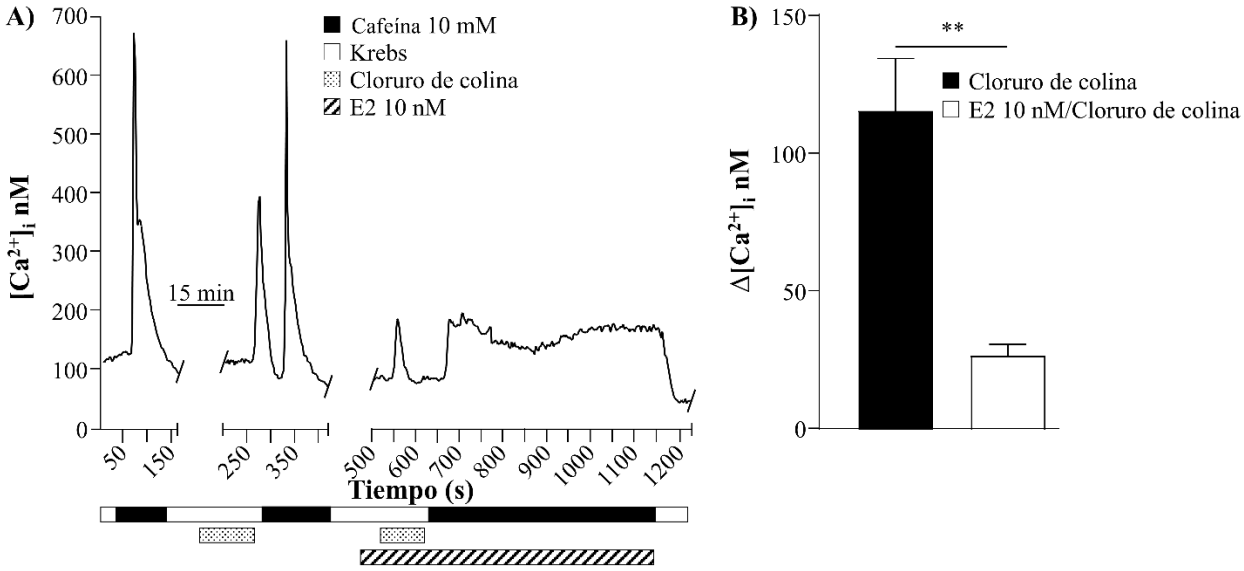

Figura 13. Efecto del estradiol sobre el intercambiador Na^+/Ca^{2+}. A) Respuesta inicial de Ca^{2+} a cafeína (10 mM), seguida de un lavado de 15 min. Luego, la célula se estimuló con una solución de Krebs sustituyendo el NaCl 118 mM con cloruro de colina (143 mM, sustituto equivalente milimolar del NaCl), induciendo un incremento transitorio en las $[Ca^{2+}]_i$. La estimulación inmediata con cafeína tras la retirada de cloruro de colina produce un pico de Ca^{2+} comparable al primero. Después de un lavado de 10 min, se añadió nuevamente E2 (10 nM) y después de 5 min se administró cloruro de colina, lo que mostró una respuesta transitoria disminuida. Posterior a la eliminación de cloruro de colina, la respuesta de Ca^{2+} inducida por cafeína es una meseta. B) El incremento transitorio de las $[Ca^{2+}]_i$ inducido por cloruro de colina fue significativamente diferente del producido por E2/cloruro de colina. Los datos se expresan como la media ± EE. El análisis fue mediante la prueba t de Student; **p<0,01. n = 10.

8.7 Efecto del 17β-estradiol sobre el transportador mitocondrial

Se utilizó FCCP para evaluar si E2 afectaba al TM. FCCP indujo un aumento transitorio de Ca^{2+}, que no se alteró después de una incubación de 5 min con E2 (Figura 14A y B). Indicando que el E2 no afecta la actividad del TM bajo estas condiciones experimentales.

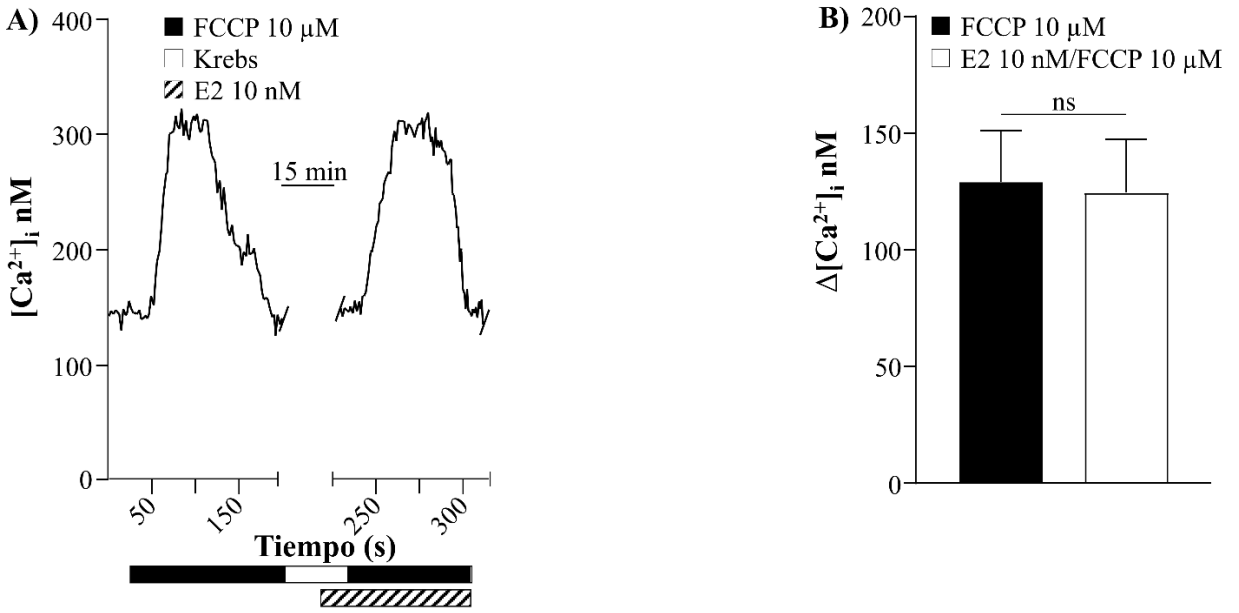

Figura 14. Efecto del estradiol sobre el transportador mitocondrial. A) La respuesta de Ca^{2+} al estímulo con FCCP (10 µM; activador del transportador mitocondrial) y la respuesta subsecuente al FCCP después de una incubación de 5 min con E2 mostraron en ambas un incremento transitorio en las $[Ca^{2+}]_i$ sin diferencias estadísticas significativas entre ellas (B). Los datos se expresan como la media ± EE. El análisis fue mediante la prueba t de Student, n = 6.

8.8 Efecto del 17β-estradiol sobre los canales de Ca^{2+} operados por el almacén

Además, se evaluaron los canales de Ca^{2+} operados por el almacén (CCOA) midiendo la entrada capacitiva de Ca^{2+} después de restaurar el Ca^{2+} a la solución de perfusión. No se observaron diferencias en la entrada capacitiva de Ca^{2+} después de la incubación con E2 (Figura 15A y B).

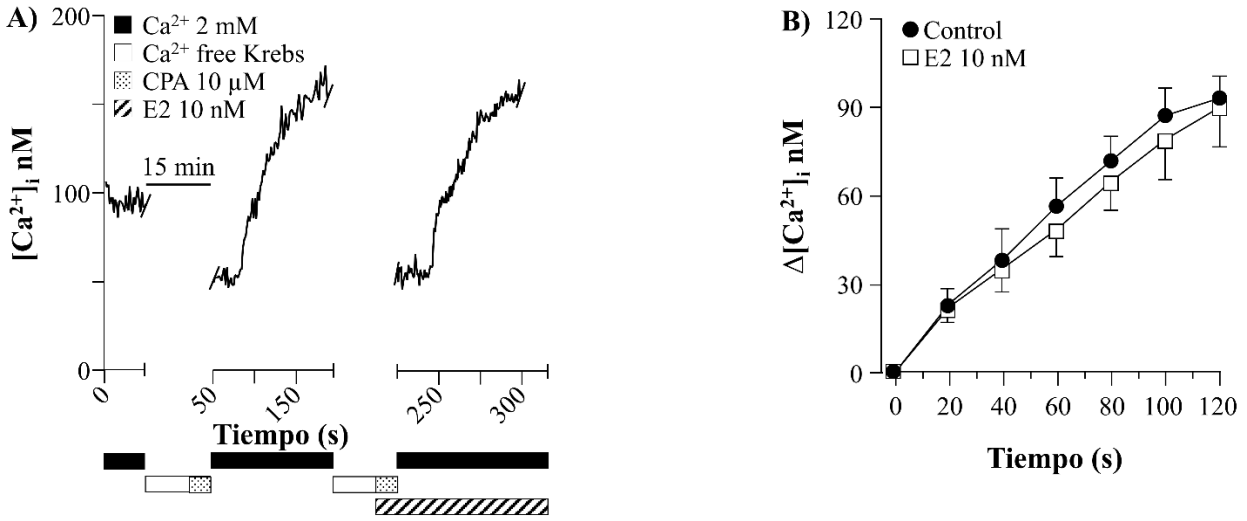

Figura 15. Efecto del estradiol sobre los canales de calcio operados por el almacén. A) Para inducir la entrada capacitativa de Ca^{2+}, la célula fue estimulada por cafeína (10 mM) seguido de 10 min en medio libre de Ca^{2+} (EGTA 0,1 mM). Luego se añadió CPA (10 µM) durante los últimos 5 min. Posteriormente, la célula se perfundió únicamente con Krebs que contenía Ca^{2+} y con E2. B) No se observaron diferencias en la entrada capacitiva de Ca^{2+}. Los datos se expresan como la media ± EE. El análisis fue mediante la prueba t de Student, n = 7.

8.9 Efecto de la inhibición de la ATPasa de Ca^{2+} de la membrana plasmática sobre la respuesta de Ca^{2+} a la cafeína

Para explorar el efecto que podría tener E2 sobre PMCA, se realizó una curva concentración-respuesta con lantano (La^{3+}, 100 µM, 1 mM y 3 mM, Figura 16A) y carboxeosina (CE, 1, 32, 100, 320, 1000 nM, Figura 16B)[108,136]. Observamos un incremento característico en las $[Ca^{2+}]_i$ a La^{3+} y a CE de acuerdo con lo reportado en la literatura[55,62]. Se eligieron La^{3+} 100 µM y CE 100 nM para los experimentos adicionales ya que eran las concentraciones más bajas que aumentaban las $[Ca^{2+}]_i$ (Figura 16A y B).

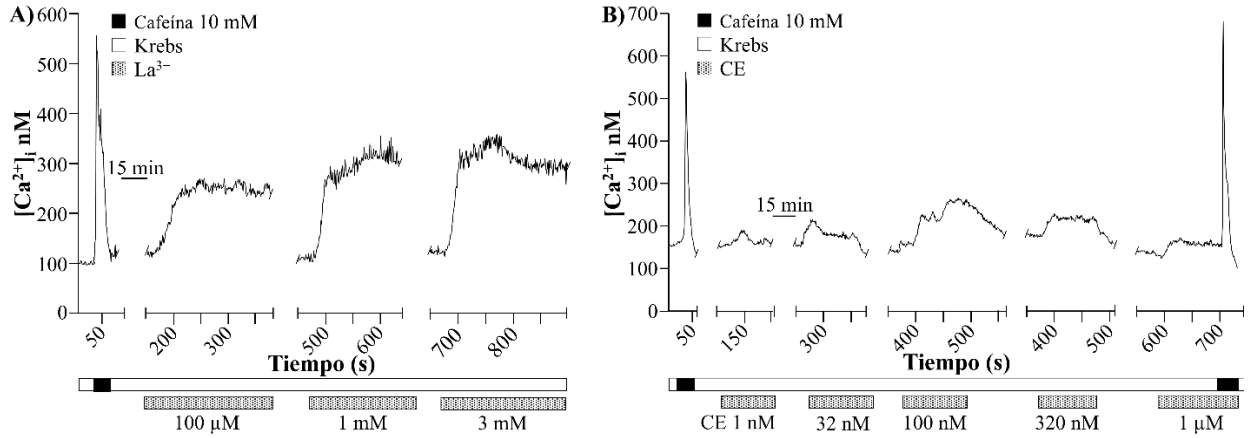

Figura 16. Registro de la curva concentración respuesta de inhibidores de la ATPasa de Ca^{2+} de la membrana plasmática. A) Incrementos de las $[Ca^{2+}]_i$ inducidas por el estímulo de lantano (La^{3+}, 100 µM, 1 mM y 3 mM; inhibidor inespecífico de PMCA). B) Curva concentración-respuesta a carboxeosina (CE, 1, 32, 100, 320, 1000 nM; inhibidor especifico de PMCA) y los correspondientes incrementos de las $[Ca^{2+}]_i$.

En los experimentos posteriores, los miocitos del MLVA se incubaron con E2 durante 5 min y La^{3+} o CE durante los últimos 4 min antes del segundo estímulo de cafeína. Tanto E2 como La^{3+} o CE permanecieron presentes durante el estímulo de cafeína. Ni La^{3+} ni CE modificaron las $[Ca^{2+}]_i$ (Figura 17A y B), como es la respuesta característica de la inhibición de la PMCA. La segunda respuesta a la cafeína con La^{3+} mostró un pico de Ca^{2+} que lentamente cayó hasta una meseta sostenida durante la presencia de cafeína (Figura 17A), mientras que con CE fue un pico transitorio (Figura 17B). Observamos diferencias significativas en las $[Ca^{2+}]_i$ de 170-320 s entre los grupos E2 vs E2/La^{3+} (Figura 17C, n=6 en el grupo E2 y n=5 en el grupo E2/La^{3+}) y de 80-320 s en el grupo E2 vs grupo E2/CE (Figura 17C, n=6 en el grupo E2 y n=6 para el grupo E2/CE).

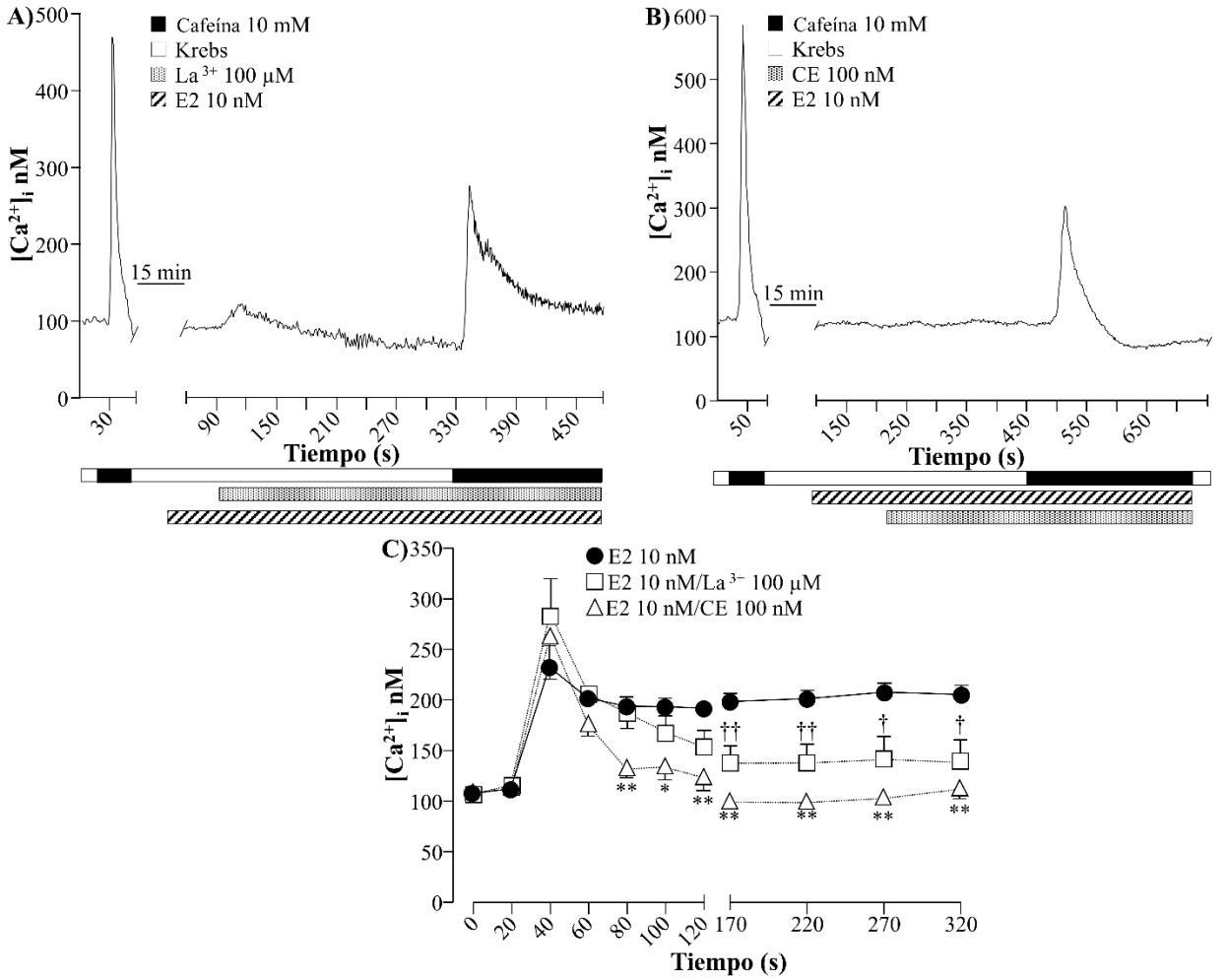

Figura 17. Efecto de la inhibición de la ATPasa de Ca^{2+} de la membrana plasmática (PMCA) sobre la respuesta de Ca^{2+} a la cafeína en presencia de E2 en miocitos traqueales de cobayo. A) Las células fueron estimuladas con cafeína (10 mM), induciendo un incremento en las $[Ca^{2+}]_i$ (control). Después de un lavado de 10 min, la célula se incubó con E2 (10 nM) durante 1 min y luego se añadió La^{3+} (100 µM; inhibidor inespecífico de PMCA) durante 4 min (E2 tuvo un período total de incubación de 5 min), seguido por la segunda respuesta a cafeína, produciendo un pico de Ca^{2+} que lentamente cayó hasta una meseta. Tanto E2 como La^{3+} estuvieron siempre presentes. B) La estimulación con cafeína indujo un incremento en las $[Ca^{2+}]_i$, después de un lavado de 10 min, la célula se incubó con E2 durante 5 min, añadiéndose CE (100 nM; inhibidor específico de PMCA) durante los últimos 4 min de la incubación. Posteriormente, la estimulación con cafeína (10 mM) en presencia de estos fármacos indujo un pico transitorio de Ca^{2+} de menor magnitud, que lentamente cayó por debajo de la línea base de Ca^{2+} inicial. C) Comparación de la evolución temporal de las respuestas de Ca^{2+} inducidas por la cafeína en presencia de E2, E2/La^{3+} o E2/CE. *p<0,05, **p<0,01, †p<0,05, ††p<0,01 al compararse contra el grupo de E2. n=6 para E2, n=5 para E2/La^{3+}, n=6 para E2/CE. Para el análisis se realizó un análisis de varianza seguido de la prueba de Dunnett.

8.10 Efecto de la inhibición de la ATPasa de Ca^{2+} de la membrana plasmática sobre la contracción inducida por carbacol

Para investigar el efecto que podría tener E2 sobre PMCA, se utilizó CE (100 nM). En el músculo liso traqueal de cobayo, el Cch indujo una contracción dependiente de la concentración (0.1, 0.32, 1, 3.2, 10 µM). Las respuestas a 0.32 µM y concentraciones adicionales de Cch aumentaron significativamente cuando los tejidos se incubaron durante 15 min con 100 nM de CE (Figura 18A); no se observaron diferencias en la CE_{50} (Figura 18B).

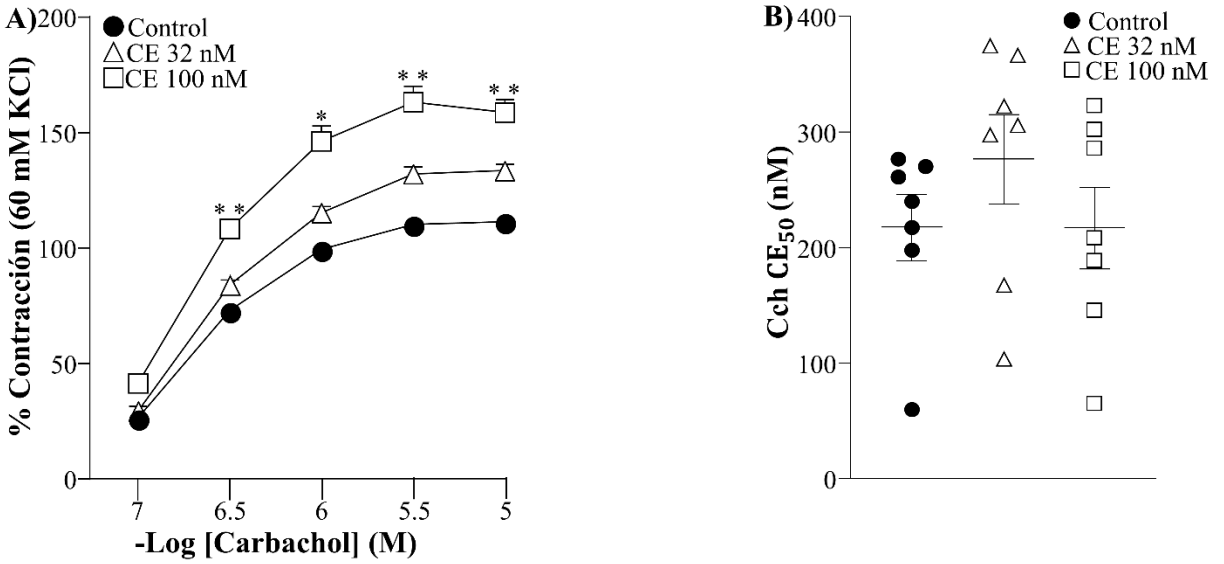

Figura 18. Efecto de la inhibición de la ATPasa de Ca^{2+} de la membrana plasmática sobre la contracción de los anillos traqueales de cobayo. A) La inhibición farmacológica de PMCA mediante la preincubación con CE (100 nM; inhibidor especifico de PMCA) en órganos aislados indujo un aumento significativo en la respuesta a Cch (0.32, 1, 3.2, 10 µM). *p < 0.05, **p < 0.01, n = 7. G) No hubo modificación en el CE_{50}. Los símbolos representan las medias ± error estándar de las medias (EE). Para el análisis se realizó un análisis de varianza seguido de la prueba de Dunnett.

8.11 Comparación del efecto de la inhibición de la ATPasa de Ca^{2+} de la membrana plasmática sobre la respuesta de Ca^{2+} inducida por cafeína

En el análisis del ABC se observaron diferencias altamente significativas en la comparación de E2 vs La^{3+} y E2 vs CE (Figura 19). El ABC de la respuesta de Ca^{2+} inducida por cafeína en presencia de La^{3+} y CE es menor en comparación con el grupo

de E2, lo que sugiere que el área de la meseta inducida por E2 se reduce cuando se revierte con La^{3+} y CE.

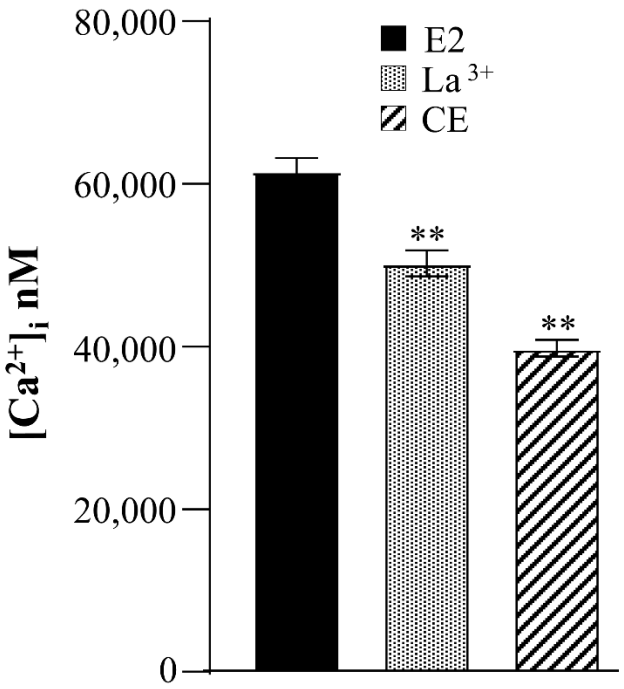

Figura 19. Comparación del área bajo la curva (ABC) de la respuesta de Ca^{2+} inducida por cafeína en presencia de E2, La^{3+}/E2 o CE/E2. Análisis del ABC de la respuesta de Ca^{2+} a cafeína en presencia de E2 (10 nM), La^{3+} (100 µM) o CE (100 nM). Los datos representan el ABC ± EE. Los datos se analizaron mediante un análisis de varianza de una vía seguido de la prueba de Dunnett, analizados todos contra el grupo de E2. **p<0,01. n=6 para E2, n=5 para La^{3+} y n=6 para CE.

8.12 Expresión de la ATPasa de Ca^{2+} de la membrana plasmática en el músculo liso de las vías aéreas

El análisis de Western blot en tejido de MLVA de cobayo confirmó la presencia de PMCA1 y PMCA4 (Figuras 20A, B) como se describió previamente en MLVA de rata[62].

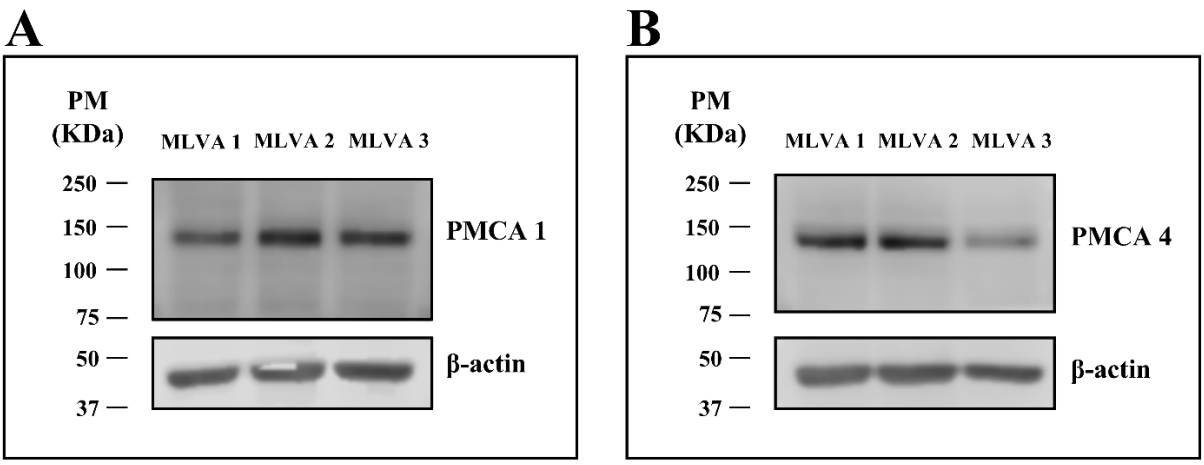

Figura 20. Western blot que muestra la presencia de las proteínas PMCA1 y PMCA4 en el músculo liso de las vías aéreas (MLVA) de cobayos. Se recolectaron tejidos de nueve animales y se combinaron en tres muestras diferentes (MLVA 1, MLVA 2 y MLVA 3). El panel A ilustra transferencias representativas de la expresión de PMCA1 con una masa molecular de 139 kDa, mientras que el panel B muestra transferencias de la expresión para PMCA4, también con un peso molecular de 138 kDa. La masa molecular se expresa según las especificaciones de las hojas de datos comerciales de anticuerpos. Se utilizó β-actina (42 kDa) como control de carga de proteínas.

8.13 Efecto de la inhibición de la ATPasa de Ca^{2+} del retículo sarcoplásmico sobre la respuesta de Ca^{2+} a la cafeína

Para estudiar la participación de SERCA sobre el efecto del E2 en la respuesta de Ca^{2+} inducida por cafeína utilizamos al inhibidor especifico, la tapsigargina. Se realizó una curva concentración respuesta de tapsigargina en las células (0.125, 0.25, 0.5, 1, 1.5 y 2 µM) (figura 21), donde se observó que la incubación con tapsigargina genera un ligero incremento con una subsecuente disminución en las $[Ca^{2+}]_i$, respuesta característica de tapsigargina según los reportado en la literatura[55] (Figura 21). Después de la incubación con tapsigargina (0.125, 0.25, 0.5 y 1 µM; n=13), al estimular con cafeína en presencia de esta, la respuesta de Ca^{2+} se abolía por completo (Figura 22). Ya que la tapsigargina es un fármaco irreversible, y que en presencia de este inhibidor no se genera una respuesta de Ca^{2+} inducida por cafeína, no era una herramienta optima y se decidió cambiar de inhibidor.

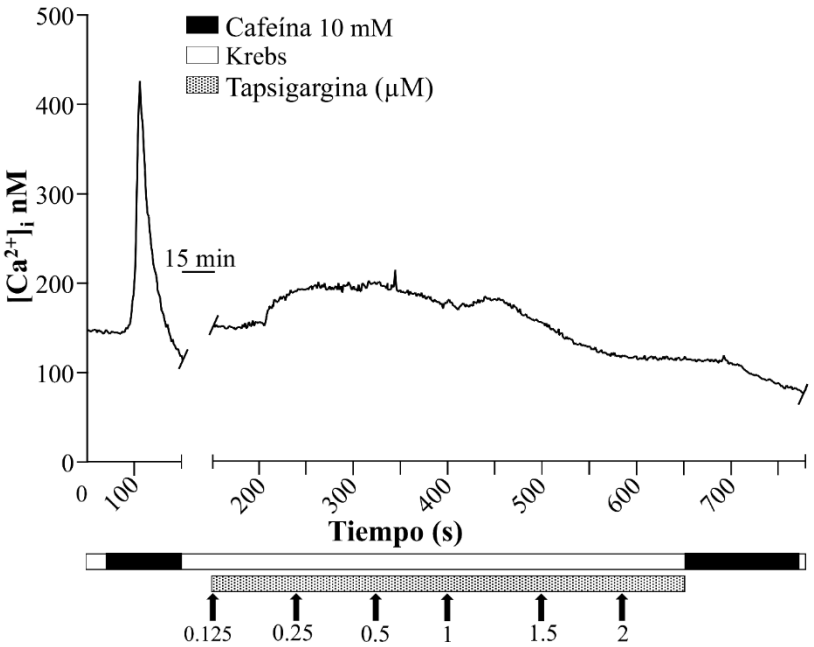

Figura 21. Registro original de la curva concentración-respuesta de tapsigargina en miocitos traqueales de cobayo. Se observa un incremento inicial con una subsecuente disminución de las $[Ca^{2+}]_i$ cuando se incubó las células con tapsigargina (0.125, 0.25, 0.5, 1, 1.5 y 2 µM), sin que se genere una respuesta a la estimulación con cafeína (10 mM), n=3.

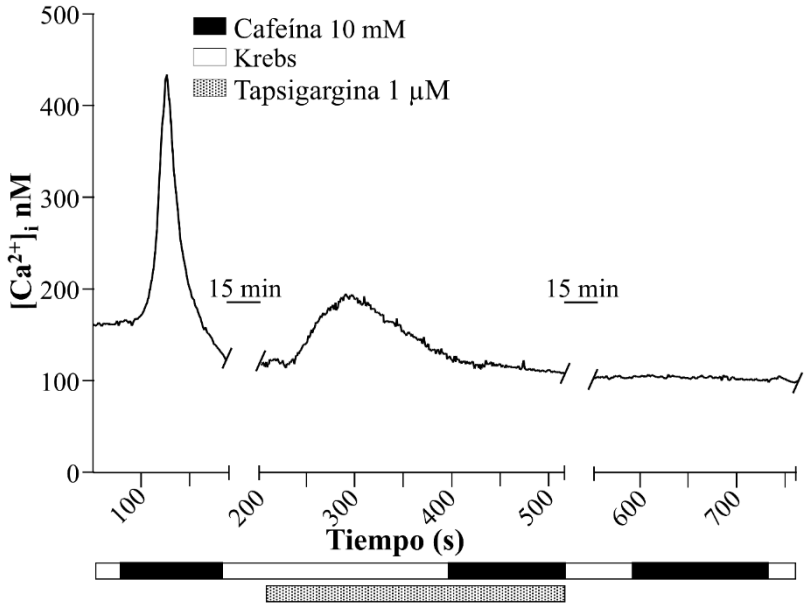

Figura 22. Registro original de la respuesta de Ca^{2+} inducida por cafeína en miocitos traqueales en presencia de tapsigargina. La célula se estimuló con cafeína (10 mM), observando un pico transitorio de Ca^{2+}. Al incubar a la célula con tapsigargina, se observó un incremento transitorio en las $[Ca^{2+}]_i$. Sin embargo, al estimular la célula con cafeína en presencia de tapsigargina no se modificó las $[Ca^{2+}]_i$. Luego de un nuevo lavado con Krebs durante 15 min, se realizó un último estímulo con cafeína (10 mM) y no se observa una respuesta de Ca^{2+}.

Para explorar el efecto que podría tener el E2 sobre SERCA, y al no poder utilizar la tapsigargina, se decidió utilizar el CPA, un inhibidor específico y reversible de SERCA. Se realizó una curva concentración respuesta a CPA en las células (1, 3.2 y 10 µM), donde se observó que la incubación con esta substancia genera un ligero incremento en las $[Ca^{2+}]i$, respuesta ya anteriormente reportada en la literatura[152] (figura 23, n=3). Decidimos utilizar 10 µM ya que es la concentración donde mejor se aprecia su efecto y ha sido utilizada en trabajos anteriores[113]. Sin embargo, después de la incubación con CPA durante 2.5 min, al estimular con cafeína (10 mM), no se observó una respuesta de Ca^{2+} (Figura 23), esta abolición de la respuesta de cafeína en presencia de CPA ya estaba reportada en la literatura[152].

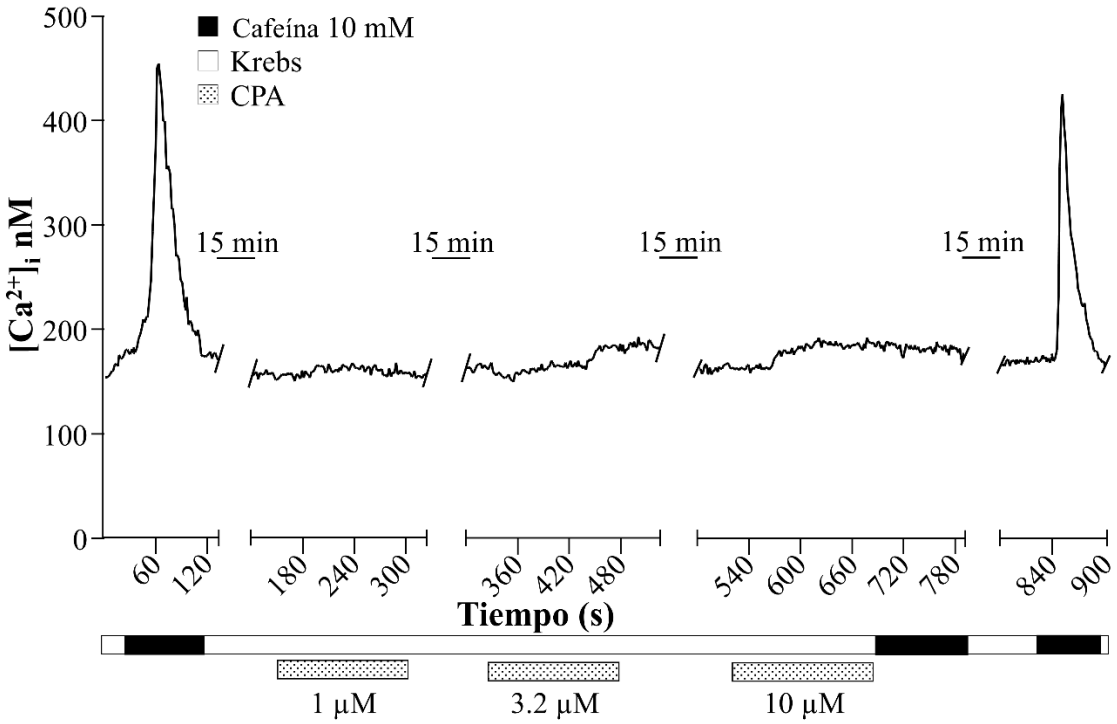

Figura 23. Registro original de la curva concentración-respuesta de ácido ciclopiazónico en miocitos traqueales de cobayo. Se observa un ligero incremento en las $[Ca^{2+}]_i$ cuando se incubó a la célula con ácido ciclopiazónico (CPA; inhibidor de SERCA; 1, 3.2 y 10 µM) durante 2.5 min, con intervalos de 15 min de lavado entre cada incubación. Al estimular con cafeína (10 mM) en presencia de CPA o inmediatamente después de retirar el fármaco, no induce un incremento de las $[Ca^{2+}]_i$. Cabe mencionar que el CPA es un inhibidor reversible y después de un periodo de lavado con Krebs sin presencia del fármaco la respuesta de cafeína es restaurada, induciendo un incremento de las $[Ca^{2+}]_i$ transitorio. n= 3.

El CPA actúa como un inhibidor reversible, lo que permite la recuperación de la respuesta de Ca^{2+} inducida por cafeína. Se decidió analizar el porcentaje de atenuación de la respuesta de cafeína inducida por la incubación de CPA posterior a un intervalo de lavado con Krebs (1, 3 y 5 min). Se observó que a 1 y 3 min se atenúa casi completamente la respuesta de cafeína en comparación con el pico inicial de Ca^{2+} inducido por cafeína (de un 4.36% y 7.78% respectivamente) (Figura 24A, n=5). A los 5 min de lavado, el incremento de Ca^{2+} era de un 56.44% de la respuesta de Ca^{2+} inducida por cafeína. Realizamos un análisis de varianza seguida de una prueba de Dunnett mostrando diferencias significativas en todos los grupos ($p<0.01$) (Figura 24B, n=5).

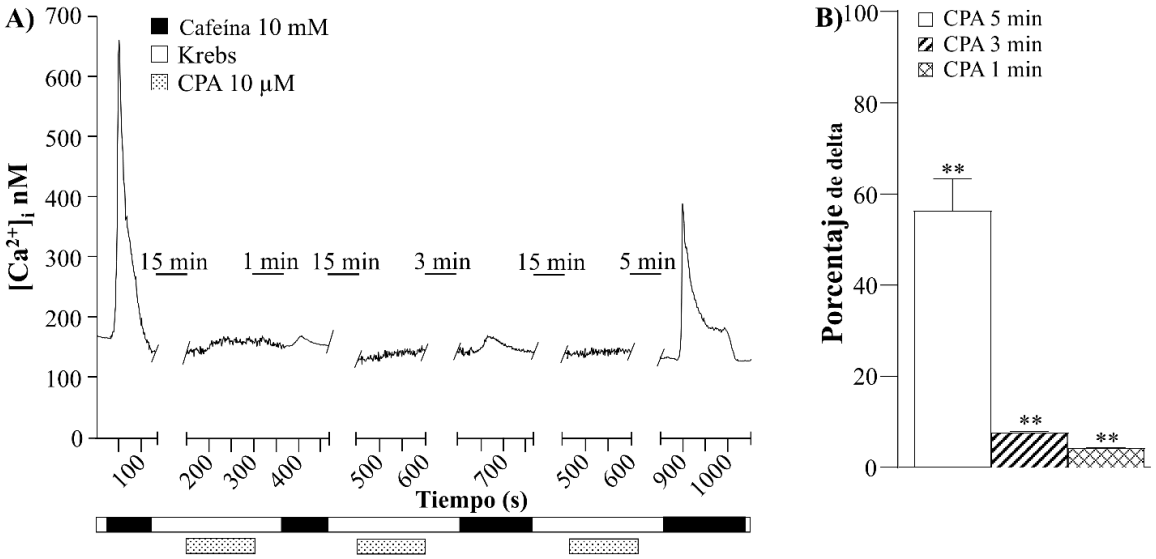

Figura 24. Curso temporal de la respuesta de Ca^{2+} inducida por cafeína en presencia de ácido ciclopiazónico. A. Registro original de miocitos traqueales de cobayo, se realizó un estímulo inicial con cafeína (10 mM) induciendo un pico transitorio de Ca^{2+}. Después de un lavado de 15 min con Krebs, las células fueron incubadas con ácido ciclopiazónico (CPA; inhibidor de SERCA; 10 µM) durante 2.5 min, seguidos de un lavado con Krebs (1, 3 y 5 min) y estimulación con cafeína (10 mM). Este proceso fue realizado entre intervalos de lavados de 15 min con Krebs. Se observa que la respuesta con cafeína tras 1 y 3 min de lavados está casi completamente atenuada, mientras que después de 5 min la respuesta de Ca^{2+} inducida por cafeína empieza a restablecerse, produciendo un pico transitorio de Ca^{2+}. B. Grafica de barras que muestra el porcentaje del incremento de Ca^{2+} inducido por cafeína, tomando como referencia el 100% de la respuesta control (n=5). Se identifican diferencias altamente significativas en la respuesta después de 1, 3 y 5 min de lavado. Las barras representan la media más el error estándar de la media (EE). Para la evaluación estadística se realizó un análisis de varianza seguido por una prueba de Dunnett. **p< 0.01.

Las células fueron incubadas con CPA (10 µM, 2.5 min), lo cual no modificó el fenómeno provocado por la incubación de E2 en la respuesta de Ca^{2+} inducida por cafeína, lo que indica que los mecanismos activados son independientes de la actividad de SERCA (Figura 25A-B). Debe tenerse bajo consideración que la respuesta de cafeína resulto después de un periodo de 5 min después de la eliminación de CPA, durante el cual fue incubado el E2. Tenga en cuenta que después de la eliminación del CPA transcurrieron 5 min antes de que se provocara la respuesta a la cafeína. Si no se retira el CPA, no se desarrolla ninguna respuesta de Ca^{2+} (Figura 23).

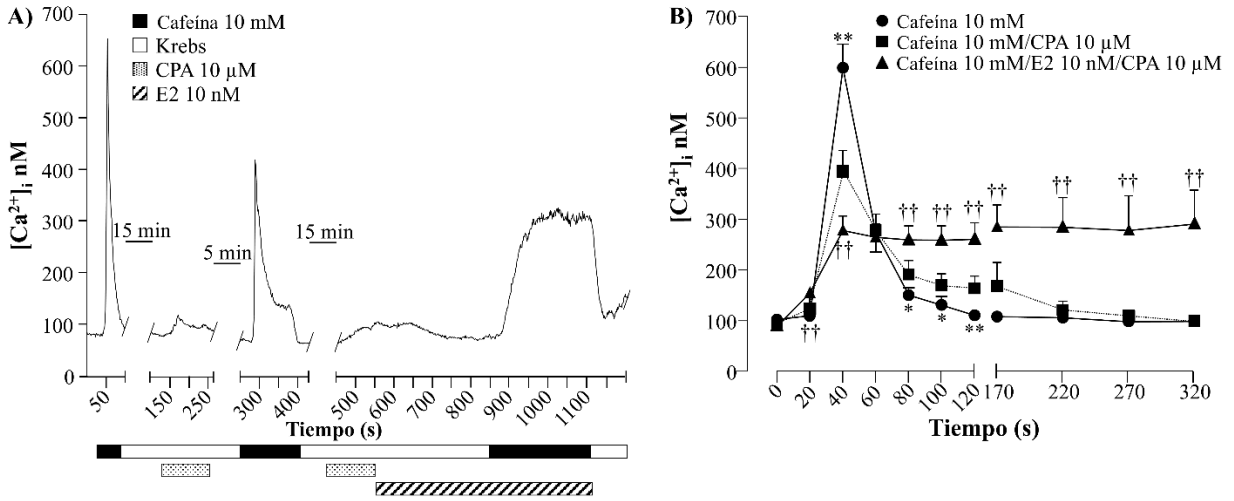

Figura 25. Efecto de la inhibición de la ATPasa de Ca^{2+} del retículo sarcoplásmico sobre la respuesta de Ca^{2+} a la cafeína en presencia de E2. A) Registro del primer pico de Ca^{2+} de cafeína (10 mM) control; el segundo pico de Ca^{2+} es la respuesta de cafeína después de la incubación con CPA (10 µM durante 2,5 min). Después de la incubación con CPA y E2 (10 nM), la adición de cafeína indujo una meseta de Ca^{2+}. B) Evolución temporal de la respuesta de Ca^{2+} inducida por cafeína solo, con CPA o CPA más E2. Los símbolos representan las medias ± error estándar de la media (EE). Para el análisis se realizó un análisis de varianza unidireccional seguido de la prueba de Dunnett. *p<0,05, **p<0,01 para cafeína vs cafeína/CPA, ††p<0,01 para cafeína vs cafeína/E2/CPA; n= 7 para todos los grupos.

8.14 El 17β-estradiol interactúa con PMCA1 de manera similar a los agonistas de los receptores estrogénicos

Realizamos un acoplamiento molecular para predecir la afinidad de unión entre el 17β-estradiol y los agonistas específicos de los RE, PPT y DPN con la isoforma PMCA1. En la Figura 26, el PMCA1 se representa orientado hacia la membrana plasmática y los sitios de modulación para la fosforilación de Ca^{2+}/calmodulina y PKA están etiquetados como referencia (en los sitios 1100-1117 y Ser-1178 respectivamente).

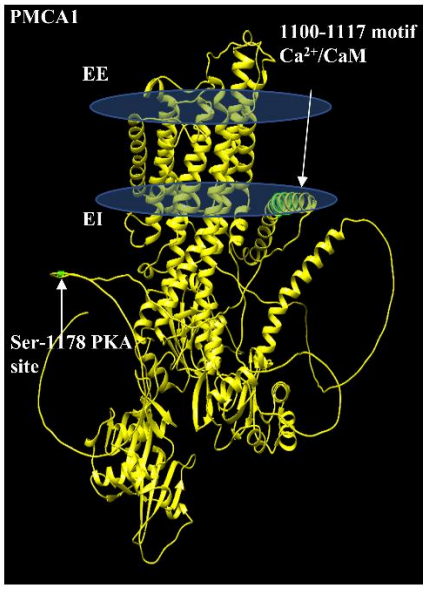

Figura 26. Ilustración que muestra el sitio de unión de Ca^{2+}-calmodulina (Ca^{2+}/CaM) (motivo 1100-1117) y el sitio de activación de PKA (Ser-1178) de PMCA1[66,71]. Para facilitar la comprensión de la orientación de PMCA1, la membrana plasmática está representada por dos discos paralelos horizontales azules. EE: espacio extracelular. EI: espacio intracelular.

La interacción E2-PMCA1 muestra una conformación estable (Figura 27A, ΔG= -8.9 Kcal/mol, cuanto más negativo es el ΔG, más equilibrio tiene la reacción) en los aminoácidos (AAs) ARG182, ARG458, LEU460, PHE1144, HIS1147 y PHE181. Curiosamente, los resultados de la Figura 27B muestran que CE se une a PMCA1 (ΔG = -7,1 Kcal/mol) mediante interacciones con diferentes AAs en comparación con E2-PMCA1 (ILE90, PRO91, PRO92, LYS93, LYS94, PHE288, THR289, GLY292, ALA293 y

GLU296); tales interacciones se estabilizan mediante enlaces de hidrógeno, enlaces de van der Waals, uniones Pi-alquilo y Pi-anión. Por otro lado, también realizamos el acoplamiento entre PPT y PMCA1 (Figura 27C, ΔG= -8,6 Kcal/mol) y, curiosamente, dicha interacción es similar (LYS177, ARG458, PRO1148, ARG182, LEU460 y PHE181) en comparación a la conformación entre E2 y PMCA1, estos sitios de interacción no son compartidos por CE. También realizamos el acoplamiento entre DPN y PMCA1. Según los resultados, la interacción DNP-PMCA1 (Figura 27D, ΔG=-6,4 Kcal/mol) se estabiliza mediante ASN543, LYS583, ALA603, ILE648 y PHE578; aunque se trata de diferentes AAs que estabilizan la interacción entre CE, E2 o PTT y PMCA1.

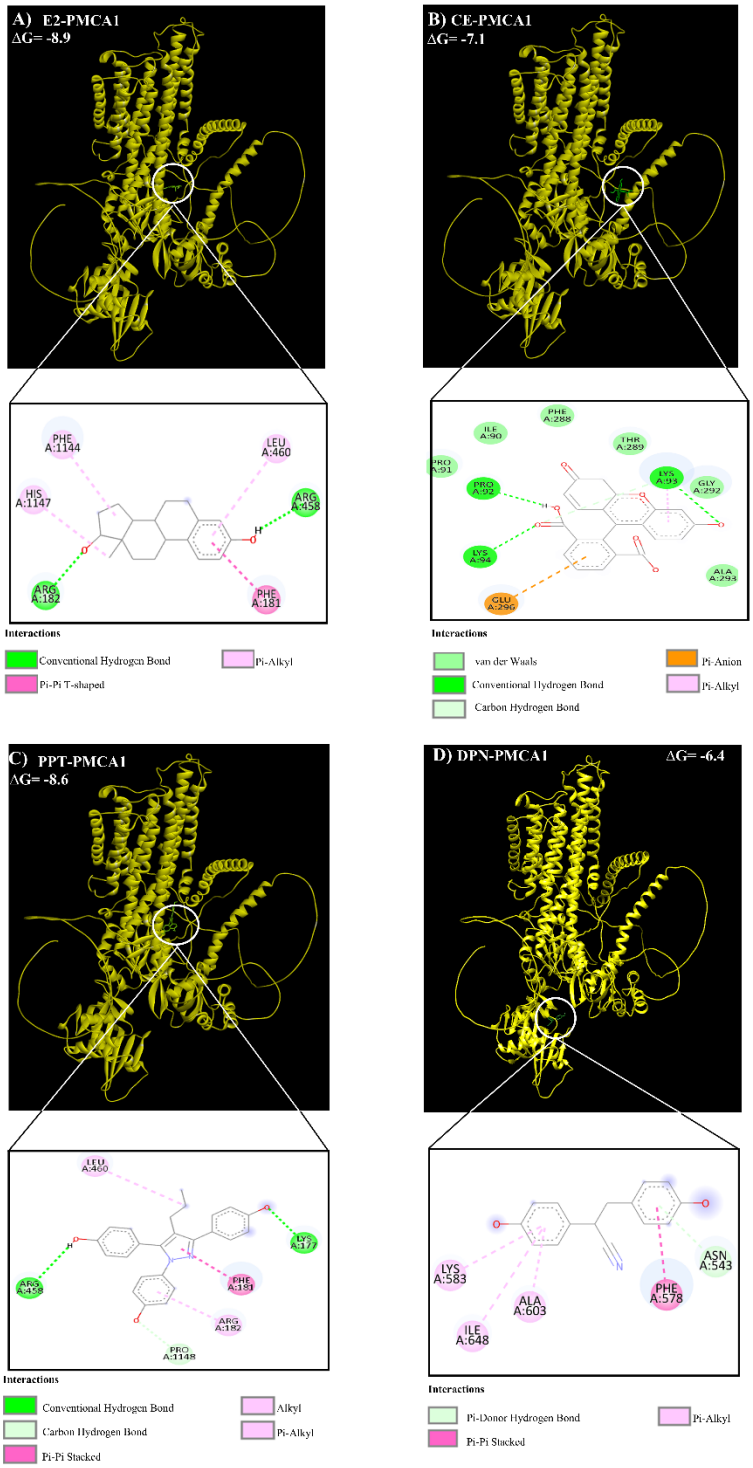

Figura 27. Acoplamiento molecular de las interacciones entre el estradiol (E2), carboxeosina (CE) y los agonistas específicos de los receptores de estrógeno (RE), propilpirazoltriol (PPT; REα) y diarilpropionitrilo (DPN; REβ) con la ATPasa de Ca^{2+} de la membrana plasmática 1 (PMCA1). La membrana plasmática está representada por dos discos paralelos horizontales azules. EE: espacio extracelular. EI: espacio intracelular. A) Ilustración que muestra posibles interacciones moleculares entre E2 y PMCA1. B) Representación gráfica de las probables interacciones de CE con PMCA1. C) Imagen de la proteína PMCA1 y sus interacciones propuestas con PPT. D) Imagen de PMCA1 que presenta interacciones moleculares probables con DPN.

8.15 El 17β-estradiol interactúa con PMCA4 de manera similar a los agonistas de los receptores estrogénicos

También realizamos el acoplamiento entre PMCA4 y los ligandos CE, E2, PPT y DPN. La Figura 28 representa PMCA4 en orientación hacia la membrana plasmática y marca el sitio de unión de Ca^{2+}/calmodulina en los AAs 1086-1103.

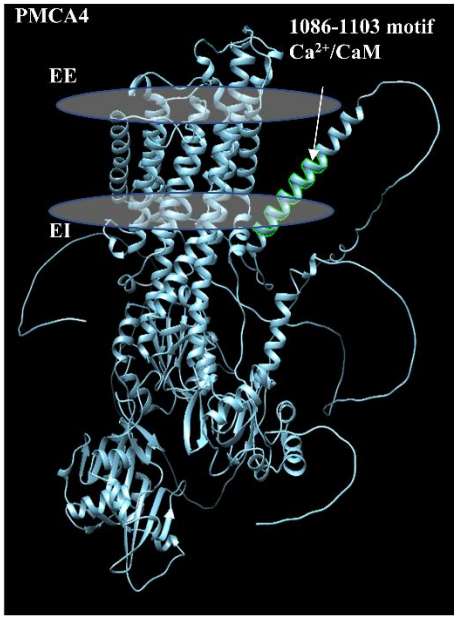

Figura 28. Ilustración que muestra el sitio de unión de Ca^{2+}-calmodulina (Ca^{2+}/CaM) (motivo 1086-1103) de $PMCA4^{153-155}$. Para facilitar la comprensión de la orientación de PMCA4, la membrana plasmática está representada por dos discos paralelos horizontales grises. EE: espacio extracelular. EI: espacio intracelular.

Nuestros resultados muestran que ninguna de las interacciones entre PMCA4 y los ligandos (E2-PMCA4, ΔG de -8,1 Kcal/mol; CE-PMCA4, ΔG de -7,5 Kcal/mol; PPT-PMCA4, ΔG de -7,6 Kcal/mol; y DPN ΔG de -6,7 Kcal/mol, Figuras 29A-D, respectivamente) es tan prominente como con PMCA1.

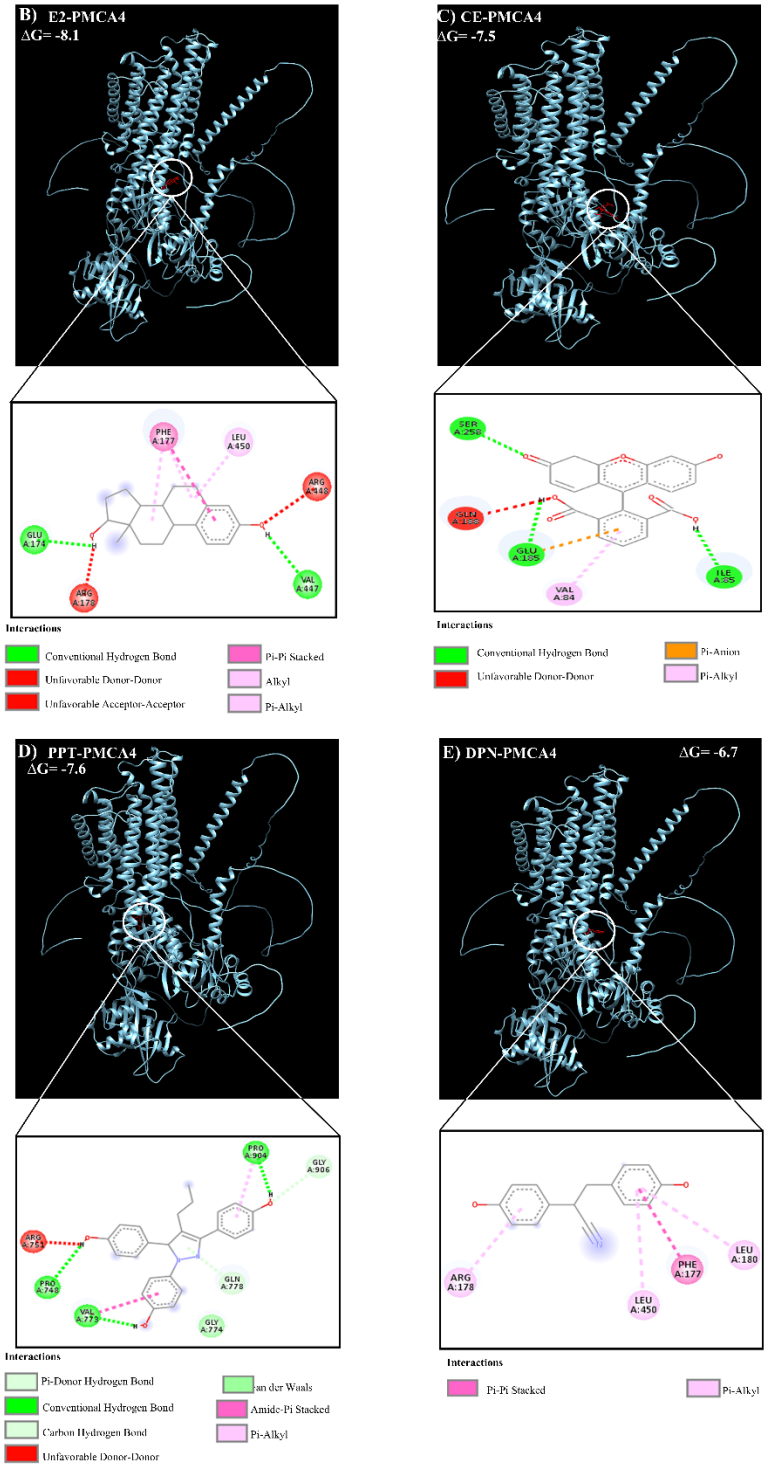

Figura 29. Acoplamiento molecular de las interacciones entre el estradiol (E2), carboxeosina (CE) y los agonistas específicos de los receptores de estrógeno (RE), propilpirazoltriol (PPT; REα) y diarilpropionitrilo (DPN; REβ) con la ATPasa de Ca^{2+} de la membrana plasmática 4 (PMCA4). La membrana plasmática está representada por dos discos paralelos horizontales grises. CE: espacio extracelular. IC: espacio intracelular. A) Ilustración que muestra posibles relaciones moleculares entre E2 y PMCA4. B) Representación gráfica de las probables interacciones de CE con PMCA4. C) Imagen de la proteína PMCA4 y sus uniones propuestas con PPT. D) Pantalla de PMCA4 que presenta interacciones moleculares factibles con DPN.

8.16 Interacción entre el 17β-estradiol y los agonistas de los receptores estrogénicos con SERCA2b

Finalmente, también realizamos el acoplamiento entre SERCA2b y los ligandos (E2, CPA, PPT y DPN) (Figura 30A-D), y encontramos que estas interacciones son muy bajas, con excepción de CPA (ΔG de -8,1 Kcal/mol).

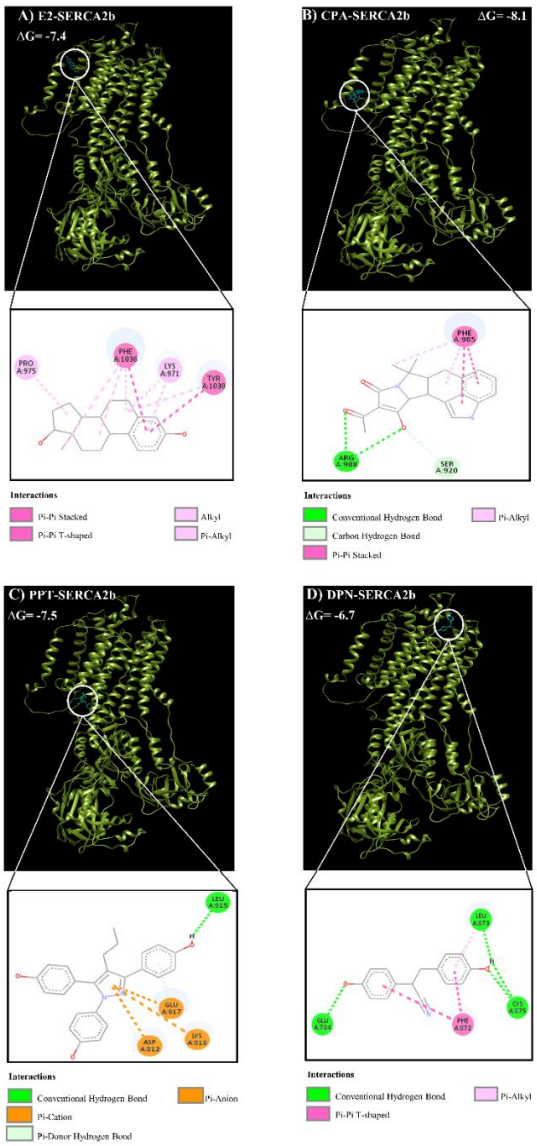

Figura 30. Acoplamiento molecular de las interacciones del estradiol (E2), el ácido ciclopiazónico (CPA) y los agonistas específicos para los receptores de estrógeno (RE) propilpirazoltriol (PPT) y diarilpropionitrilo (DPN) con la ATPasa de Ca^{2+} del retículo sarcoplásmico 2b (SERCA2b). A) Ilustración que muestra posibles relaciones moleculares entre E2 y SERCA2b. B) Representación gráfica de las probables interacciones de CPA con SERCA2b. C) Imagen de la proteína SERCA2b y sus interacciones propuestas con PPT. D) Imagen de SERCA2b que presenta interacciones moleculares probables con DPN.

9. Discusión

Nuestros hallazgos sugieren que, en el músculo liso de las vías aéreas de cobayo, el 17β-estradiol (E2) induce una hiperreactividad a la estimulación con carbacol (Cch) a través de la inhibición no genómica de la ATPasa de Ca^{2+} de la membrana plasmática (PMCA). Además, este efecto parece estar relacionado con una interacción directa entre el E2 o su agonista específico del receptor estrogénico α propilpirazoltriol (PPT) y la PMCA, según lo evidenciado por los análisis de acoplamiento molecular y los experimentos de medición de Ca^{2+} intracelular. Hasta donde tenemos conocimiento, este es el primer estudio que reporta los efectos no genómicos del E2 sobre la PMCA en células del músculo liso de las vías aéreas.

En muchos tipos de células, la señalización de Ca^{2+} constituye un fenómeno vital. Para mantener las células en condiciones óptimas, la homeostasis del Ca^{2+} se mantiene mediante un conjunto de herramientas de Ca^{2+} compuesto por canales, bombas e intercambiadores. Estos mecanismos están sujetos a influencias internas y externas, incluida la regulación hormonal[14]. En el MLVA, Townsend y cols. exploraron el efecto agudo del E2 sobre los canales de Ca^{2+} y se ha establecido que la exposición a este estrógeno inhibe el CCDV-L y parcialmente los CCOA [8].

Por lo general, en el MLVA, la cafeína induce un pico transitorio de Ca^{2+} debido a la liberación de Ca^{2+} del RS, previamente rellenado con Ca^{2+} proporcionado por la actividad de CCDV-L y CCOA[57]. El bloqueo del CCDV-L no altera la cinética de la respuesta de Ca^{2+} inducida por cafeína, como se observa en la Figura 9C; sólo disminuye la amplitud del pico de Ca^{2+}. Debido a que la respuesta de Ca^{2+} a cafeína en presencia de E2 no muestra un pico de Ca^{2+}, sino una respuesta sostenida, se señala la implicación de otras

proteínas reguladoras de Ca^{2+}. Excluimos la contribución del NCX_{rev}, TM o entrada capacitiva de Ca^{2+} ya que no participaron en este fenómeno (Figura 3C-H). Pocas investigaciones, generalmente centradas en los efectos genómicos, han examinado las posibles consecuencias del E2 sobre la PMCA.

En un estudio previo, se investigó que el tratamiento con E2 (40 µg/kg/día) durante 72 h en ratas hembra prepúberes disminuyó la expresión de PMCA1 en el esófago[156]. En células sinoviales humanas similares a fibroblastos y a macrófagos de ratón, E2 redujo la expresión de PMCA2 y PMCA4[157] y PMCA1 en el útero de ratón[158]. A través de mecanismos genómicos, E2 aumenta la expresión de PMCA4b en células MCF-7[159] y PMCA1 en endometrio humano[160]. Curiosamente, en las células renales del túbulo distal, la incubación con E2 durante 24 h mejoró la actividad de PMCA sin alterar su expresión[161]. En nuestro trabajo, debido a que la incubación de E2 fue por un período corto, los resultados sugieren que, al inhibir directamente (efecto no genómico) la bomba PMCA, E2 altera la fase de caída de la respuesta de cafeína, produciendo la meseta de Ca^{2+}.

Se ha demostrado que el estradiol, a través de sus efectos no genómicos, activa una multitud de vías de señalización. En células del MLVA humanas, la incubación aguda de E2 incrementaba la producción de AMPc, favoreciendo la relajación[9]. En otro estudio, la incubación durante 10 min o 24 h con E2 en células hipocampales inducía un efecto neuroprotector contra la neurotoxicidad mediada por los receptores de N-metil-D-aspartato (NMDA) y de kainato, al activar la fosforilación de estos canales por las vías de Src (cinasa de tirosina) y la vía de proteínas cinasas activadas por mitógenos (MAPK)[10]. En neuronas del ganglio de la raíz dorsal, la incubación durante 10 min con

E2 inducía la fosforilación de la proteína de unión al elemento de respuesta de AMPc (CREB) a través de la activación de la vía de ERK1/2. Este efecto no se observó en células del ganglio autonómico pélvico, indicando un efecto específico dependiente del tipo celular[11]. En células de neuroblastoma humano de la línea SK-N-SH, la incubación con E2 aumentaba la actividad de la vía de ERK1/2[17], y en otro estudio activo a la PKA y a la PKC[20]. Además, se ha demostrado que la PMCA está sujeta a la modulación por cinasas[162-164]. En células HEK293T, se demostró que E2 disminuye de forma no genómica la fosforilación de la molécula de interacción estromal 1 (STIM1), una proteína que participa en la entrada capacitativa de Ca^{2+}, inhibiendo su movilidad y activación[165]. Curiosamente, la incubación durante 24 h con E2 de células del MLVA también produjo un efecto similar, inhibiendo la fosforilación de STIM1, disminuyendo así la entrada de Ca^{2+} a través de CCOA inducida por histamina potenciada por el extracto de humo de cigarro[166].

En concreto, en el MLVA se sabe que la vía ERK1/2 regula la activación basal de los CCDV-L[55], lo que explica la disminución de la amplitud del pico de Ca^{2+} inducido por cafeína en presencia de U-0126, un inhibidor indirecto de ERK1/2 (Figura 3A). Además, se ha demostrado que el E2 activa la vía ERK en diferentes tejidos[2,167,168], incluido el MLVA[18]. También, se ha propuesto que la actividad de PMCA está regulada por los efectos no genómicos del estradiol en sinaptosomas corticales de rata, eritrocitos humanos[12] y hepatocitos[13]. Además, en el endotelio vascular, se demostró que el E2 disminuye la actividad de PMCA a través de efectos genómicos. La activación del receptor GPR30 por E2 activa al receptor del factor de crecimiento epidérmico, y este inicia la vía de señalización de ERK1/2, que incrementa la expresión de calmodulina

(CaM). El E2 incrementa la unión de CaM con PMCA, promoviendo un aumento en la actividad de la ATPasa. No obstante, también estimula la fosforilación de PMCA en residuos de tirosina, prolongando la señalización de Ca^{2+} intracelular. Esto conduce a un aumento en las $[Ca^{2+}]_i$ y a una mayor interacción con el complejo Ca^{2+}-CaM[169].

Cabe señalar que en las células del MLVA, la expresión de GPR30 no es significativa[170]. En este contexto, la meseta de Ca^{2+} inducida por cafeína producida por la incubación con E2 no fue modificada por la adición previa de U-0126. Por lo tanto, se puede descartar la participación de las cinasas ERK1/2 en este fenómeno (Figura 10B). Sin embargo, es posible que otras vías de fosforilación estén implicadas. Se necesitan experimentos adicionales, como la mutagénesis dirigida, para confirmar la interacción directa del E2 con PMCA y esclarecer su papel en este proceso.

Por otro lado, los efectos del E2 sobre SERCA se estudiaron en células del MLVA sometidas a mediadores inflamatorios. Las células del MLVA de humano incubadas con TNF-α o lL-13 mostraron una expresión disminuida de SERCA2 que fue revertida por un agonista específico de REβ (WAY-200070 10 nM). Esta respuesta no se observó con E2 ni con el agonista específico de REα (PPT). La activación de REβ disminuyó la $[Ca^{2+}]_i$ en un estado proinflamatorio en células del MLVA[52]. Sin embargo, no hay ningún reporte previo de un efecto no genómico de E2 sobre las ATPasas de Ca^{2+}. En este sentido, E2 produjo una meseta de Ca^{2+} en respuesta a los estímulos con cafeína. La inhibición de PMCA con La^{3+} o CE en una célula previamente incubada con E2 no modificó las $[Ca^{2+}]_i$ basales, y cuando se estimuló con cafeína, la meseta de Ca^{2+} observada en presencia de E2 solo se revirtió parcialmente con La^{3+} y totalmente con CE, lo que indica que E2 está inhibiendo a PMCA. Alternativamente, cuando los miocitos fueron estimulados con

CPA y E2, la meseta de Ca^{2+} no se alteró, lo que indica que E2 no está afectando a SERCA.

En este contexto, E2, a través de mecanismos no genómicos, desregula las $[Ca^{2+}]_i$ bloqueando los CCDV-L y disminuyendo la amplitud del pico al limitar el Ca^{2+} disponible para el llenado del RS y al inhibir la bomba PMCA, el E2 altera la fase de caída de la respuesta de cafeína, produciendo la meseta de Ca^{2+}.

Posiblemente, cualquier modificación en los mecanismos de manejo de Ca^{2+} que conduzca a concentraciones elevadas de las $[Ca^{2+}]_i$ podría predisponer al MLVA a la hiperreactividad. En una curva de concentración-respuesta acumulativa del agonista, la HR puede interpretarse como hipersensibilidad (un desplazamiento hacia la izquierda de la curva) o un aumento en la respuesta contráctil máxima[54]. Si bien existen mecanismos compartidos entre estas características distintivas de la HR, también pueden presentarse de forma independiente, involucrando distintos mecanismos[171,172]. La HR puede ser causada por un aumento en la contractilidad del MLVA, ya sea a través de un aumento en las $[Ca^{2+}]_i$ o mecanismos de sensibilidad al calcio[54,90,173,174]. Esta posibilidad fue explorada a través de nuestros experimentos con órganos aislados. La inhibición de PMCA por CE indujo hiperreactividad a Cch en los anillos traqueales de cobayo. Se ha documentado que la inhibición de PMCA o SERCA conduce a un incremento de las $[Ca^{2+}]_i$[55,62] y podría provocar HR, una probabilidad confirmada en nuestra investigación. Curiosamente, se ha reportado de una mayor actividad de la ATPasa de Ca^{2+} en células de MLVA de cobayos sensibilizados, probablemente como un mecanismo compensatorio activado en respuesta al incremento de las $[Ca^{2+}]_i$[90]; no obstante, aún queda por explorar si este mecanismo compensatorio se ve alterado por la adición de E2. En este sentido,

nuestros resultados usando La^{3+} o CE más E2 podrían estar señalando un mecanismo compensatorio de manejo de Ca^{2+}, dado que el La^{3+} es un fármaco inespecífico, su efecto no se revierte completamente, a diferencia de lo que ocurre con CE. Los resultados sugieren que la inhibición de PMCA induce hiperreactividad en las vías aéreas, lo que está relacionado con un aumento en las concentraciones intracelulares de Ca^{2+}.

La curva concentración-respuesta a Cch en presencia de E2 mostró un efecto similar al provocado por CE, con significancia estadística para la respuesta máxima. Este hallazgo respalda nuestra propuesta de que el E2 inhibe la PMCA y, en consecuencia, induce hiperreactividad. Se ha documentado que los agonistas específicos de los receptores estrogénicos α y β (PPT y DPN, respectivamente) pueden unirse directamente al canal de potasio activado por Ca^{2+} y regular su actividad[117], lo que concuerda con nuestros experimentos de Ca^{2+}, donde se observa que el fenómeno también ocurre con el PPT, probablemente a través de una interacción directa con la PMCA.

Dado que exploramos las consecuencias que la exposición aguda al E2 podría causar en el MLVA, es posible que estos resultados estén relacionados con el asma perimenstrual, un período de exacerbación de los síntomas que sufren muchas mujeres asmáticas. Con respecto al papel del E2 en la HR, se comparó la respuesta de reactividad de las vías respiratorias a la metacolina en ratones macho y hembra prepúberes con la respuesta de los ratones de 12 semanas de edad. En el primer protocolo experimental, los machos demostraron una respuesta significativamente mayor que las hembras. A las 12 semanas, este efecto se revirtió y se observó un aumento significativo de la HR, lo que indica que la respuesta estaba relacionada con la edad y el sexo de los ratones[44]. Teniendo en cuenta que la investigación de McKenzie et al. se

realizó en ratones no sensibilizados, entonces esto implica que los cambios hormonales podrían ser responsables de la HR encontrada en las hembras de mayor edad. Al comparar ratones ovariectomizados (OVX) sensibilizados con ovoalbúmina (OVA) tratados con E2 con un grupo sin intervención, un grupo sin intervención con OVA y un grupo OVX-OVA, el grupo OVX-OVA-E2 presentó una mayor resistencia de las vías aéreas al reto con metacolina[175]. En otro estudio, la función pulmonar y la capacidad de respuesta de las vías aéreas a la metacolina y la serotonina inhalada en ratones hembra con silenciamiento génico para el REα mejoraron en comparación con sus contrapartes hembras de tipo normal o con ratones hembra con REβ-silenciado[45]. Este cambio en el grupo del REα-silenciado se asoció con una expresión reducida del receptor muscarínico M2 y de su función en el pulmón. Además, cuando se sometieron a una sensibilización con ovoalbúmina, los ratones con el REα-silenciado tuvieron un aumento de la HR pero sin aumento de la inflamación, lo que indica que el REα es crucial en la respuesta de las vías aéreas a los agonistas broncoconstrictores y su desregulación puede conducir a la HR. La capacidad de respuesta de las vías aéreas parece estar bajo la regulación de la activación diferencial de los RE y esto afecta la gravedad del asma en las mujeres, como lo indican Ambhore, et al. 2019, a través de estudios *in vitro*, donde los miocitos del MLVA de pacientes asmáticos mostraron una mayor expresión de REβ y una disminución en la remodelación de las vías aéreas mediada por agonistas de REβ[100]. En cuanto a los parámetros de función respiratoria, un estudio realizado en ratones hembra, macho y OVX expuestos a alérgenos mixtos (AM) mostró que las hembras tenían una mayor resistencia de las vías respiratorias con una menor distensibilidad. Cuando estas hembras fueron tratadas con un agonista de REβ (WAY-200070), los cambios inducidos

por MA se revirtieron, fenómeno que no se observó en el caso de un agonista del REα (PPT). Además, la exposición a AM provocó un aumento en la expresión del ARNm y de las proteínas tanto para REα como para el REβ, así como para genes de remodelación, lo que se revirtió con el tratamiento con WAY-200070, indicando así que el REβ podría regular negativamente la HR y la remodelación de las vías aéreas[100].

Por otra parte, la inflamación es una característica distintiva del asma atópico. En este sentido, el papel que desempeña el E2 sobre las células inflamatorias es un tema de investigación importante. Por ejemplo, se ha observado que, en células mononucleares de sangre periférica de pacientes con asma leve a moderada, el tratamiento con E2 (10 nM), progesterona (1 µM) o una combinación de E2+progesterona aumentó los niveles de expresión de GATA-3 y la producción de IL-4. GATA-3 es un factor de transcripción que regula la producción de citocinas relacionadas con Th2, e IL-4 es un producto de la respuesta inflamatoria tipo 2, lo que sugiere que E2 y la progesterona podrían mantener el estado inflamatorio observado en el asma[176]. De manera similar, en modelos de ratones, las hormonas ováricas aumentaron la respuesta inmune tipo 2, así como la producción de IL-17 y la infiltración de eosinófilos y neutrófilos[43].

El E2 puede ejercer efectos directos independientes de sus receptores o por la activación de otras vías de señalización. De manera aguda, el E2 puede unirse al receptor nicotínico neural humano α4β2 en la secuencia AGMI, localizada en el extremo C-terminal de la subunidad α4, lo que potencia la actividad del receptor[177]. También se ha visto que el E2 puede regular de manera no genómica diversos canales. En células hipocampales, la exposición aguda a E2 en concentraciones del rango pM potencia la actividad del CCDV-L a través de la unión directa al sitio dihidropiridínico del canal[106]. En células HEK293, la

incubación aguda con E2 (10 nM-5 µM) puede regular la actividad del canal de potasio activado por Ca^{2+} mediante la unión a la subunidad β del canal[115,116]. Asimismo, se ha reportado que otros agentes estrogénicos (PPT, DPN y bisfenol A) pueden regular de manera aguda la actividad del canal de potasio activado por Ca^{2+}[117,118].

Las secuencias proteicas y funciones de proteínas individuales están bien caracterizadas y pueden consultarse en bases de datos como UniProt donde están indexadas y son de fácil acceso [178,179]. Sin embargo, las proteínas rara vez actúan de manera aislada; por el contrario, tienden a formar complejos o integrarse en maquinarias que interactúan dinámicamente para llevar a cabo funciones biológicas o procesos celulares. En este contexto, ha surgido el término de "interactoma," el cual hace referencia al mapeo completo de todas las posibles interacciones proteína-proteína que pueden ocurrir en un organismo vivo[180]. Para que una interacción entre dos proteínas sea considerada legítima, deben cumplirse ciertos criterios específicos: 1) Deben tener contacto físico que genere un acoplamiento molecular, ya sea de manera permanente o transitoria. 2) La interacción debe ser intencional, es decir, debe de ocurrir por fuerzas o eventos específicos y no de manera accidental o aleatoria. 3) Aunque el contacto físico es un requisito, este debe ser específico, no genérico, y debe tener un propósito o finalidad en particular[181].

Similarmente, las proteínas pueden interactuar con otras moléculas, como los lípidos y los ácidos nucleicos. Las interacciones proteína-lípido pueden ocurrir de forma específica o no específica y son esenciales en diversos procesos, como la función y el mantenimiento de la estructura de la membrana[182]. Estas interacciones se clasifican en tres tipos: los lípidos en masa, lípidos anulares y lípidos no anulares.

Las interacciones con lípidos en masa no son directas con la proteína, pero pueden afectar su función o estructura al modificar el ambiente lipídico[182,183]. Se ha observado que estas modificaciones en el ambiente de los lípidos en masa pueden incluso alterar procesos de señalización celular[184-186] y transporte[187,188].

En el caso de los lípidos anulares, estos se encuentran alrededor de las proteínas, formando un anillo alrededor de los dominios transmembranales. La interacción con las proteínas es de manera no específica[182,189]. Se ha visto que dicha interacción puede regular la actividad de SERCA. En estudios previos, la SERCA del RS de músculo esquelético fue reconstruida en bicapas de fosfatidilcolina, y se encontró que la velocidad de hidrólisis era más rápida cuando la longitud de la cadena acilo graso era de 18 carbonos. En contraste, tanto cadenas más cortas o largas se asociaron a una menor actividad enzimática[189-192].

En el caso de PMCA, se ha observado que cuando se reconstituye en micelas mixtas de fosfolípidos y detergente, esta mezcla genera la transición de las micelas a una bicapa, lo que prolonga el tiempo en que la ATPasa permanece en su conformación fosforilada, disminuyendo su actividad enzimática. Además, las interacciones específicas entre proteínas y lípidos desempeñan un papel en la regulación de la actividad de PMCA. Las bicapas de 1,2-dimiristoil-sn-glicero-3-fosfocolina mostraban compatibilidad óptima con la actividad de PMCA. Además, la modificación de fosfolípidos alteraba el grosor de la membrana lipídica, reportándose que un grosor de 24 Å es el óptimo para la actividad enzimática de PMCA[193]. Finalmente, los lípidos no anulares interactúan de manera específica con las proteínas, uniéndose a motivos de unión lipídicos específicos[182,194,195].

Estas interacciones pueden modular directamente la conformación y función de la proteína[182,196,197].

También se ha descrito que las proteínas pueden interactuar con ácidos nucleicos, ya sea con ADN o ARN. Estas interacciones son esenciales para múltiples procesos biológicos. En el caso de los procesos que involucran al ADN, estas interacciones participan en la replicación, transcripción, reparación y reorganización del material genético, entre otros procesos[198,199]. Las interacciones se pueden clasificar en dos tipos: específicas, cuando una proteína se une a un sitio de reconocimiento específico, y no específicas, como las interacciones de histonas-ADN[198,200]. Por otro lado, las interacciones proteínas-RNA participan en procesos de corte y empalme, el transporte, la traducción y el silenciamiento génico[199]. Estas interacciones pueden ser específicas, requiriendo de dominios de unión al RNA, o no específicas dependiendo del contexto molecular [198,201,202].

Con respecto a una interacción ligando-proteína, la afinidad de unión se refiere a la fuerza de interacción entre ambas moléculas, determinada por el equilibrio entre la tasa de unión y disociación, lo que indica la estabilidad de dicho complejo formado. Por otro lado, la selectividad de la interacción ligando-proteína indica la capacidad del ligando para unirse de manera preferente a su objetivo, discriminando otras proteínas basándose en la estructura y conformación[203].

De acuerdo con nuestros resultados, tanto PMCA1 como PMCA4 se expresan en células MLVA de cobayo, pero el efecto del E2 sobre las $[Ca^{2+}]_i$ puede estar mediado por su interacción con PMCA1, ya que el acoplamiento molecular de dicha conformación

sugiere que esta es la interacción más estable, incluso en comparación con la interacción entre CE y PMCA1. Las diferencias entre los ΔG de ambas interacciones se deben en parte a los AAs que subyacen a la unión de los ligandos (E2 y CE) con PMCA1, lo que sugiere que los sitios de unión son diferentes para cada ligando, y esta observación puede estar respaldada por los resultados de los experimentos con $[Ca^{2+}]_i$. Sin embargo, es necesario explorar más a fondo si la interacción del complejo E2 y PMCA1 también induce cambios conformacionales. Interesantemente, los sitios de unión identificados en los análisis de acoplamiento molecular se encuentran en la cara citosólica de la ATPasa, pero no corresponden con sitios de importancia ya descritos en la proteína, como el motivo de unión de CaM o el sitio catalítico[66,71]. Sin embargo, algunos de los aminoácidos que forman enlaces se encuentran en el extremo C-terminal y están en proximidad al motivo de unión de CaM. En la interacción E2-PMCA1 destacan los residuos de los AA PHE1144 y HIS1147, mientras que en la interacción PPT-PMCA1 se observa la participación del residuo PRO1148. Además, dado que PMCA4 es otra isoforma expresada en células MLVA, también exploramos la contribución de PMCA4 en el efecto del E2. De manera similar a las interacciones observadas con PMCA1, las interacciones con PMCA4 ocurren en la cara citosólica de la proteína, sin involucrar sitios previamente descritos como esenciales, como el motivo autoinhibitorio de unión a CaM o el sitio catalítico de PMCA[66,71]. No obstante, a diferencia de PMCA1, en las interacciones de PMCA4 no se muestra la participación de ningún AA en la región C-terminal. Curiosamente, los experimentos de acoplamiento muestran que a pesar de que la conformación de E2-PMCA4 es altamente estable en comparación con las demás (CE-PMCA4 y PPT-PMCA4), la conformación E2-PMCA1 sigue siendo la más adecuada.

Este resultado confirma en parte que los efectos observados sobre las $[Ca^{2+}]_i$ pueden estar mediados principalmente por PMCA1, y puede ser interesante profundizar en la comprensión del potencial efecto sinérgico de PMCA4 en este modelo. Cabe señalar que se ha demostrado que PMCA4 participa en procesos fisiológicos en células del MLVA[62].

Podría decirse que una limitación del presente estudio es el uso de cobayos machos en lugar de hembras. No obstante, el empleo de cobayos macho prepúberes podría limitar la influencia de las hormonas sexuales endógenas en los resultados descritos en este documento. Además, se ha demostrado que el MLVA tiene una expresión similar de receptores de estrógenos en hombres y mujeres, y ambos sexos se han utilizado como modelos de estudio para la influencia de los estrógenos y los RE en el asma y la regulación del manejo del Ca^{2+}[52,148,170]. El uso de un modelo con cobayos machos permitió evitar la variable adicional asociada a la producción estrogénica por el inicio del ciclo estral de las hembras, ya que se ha reportado que puede existir una considerable incidencia en el inicio temprano de la madurez en las hembras (antes de los 21 días de edad o bien 300 g de peso)[204]. Se estableció la correlación entre la edad (en días) y el peso corporal (en gramos) en sujetos con menos de 21 días de edad o un peso inferior a 300 g, con el objetivo de identificar la relación entre ambos parámetros durante las primeras etapas del desarrollo.

Finalmente, existe evidencia que relaciona el papel de la edad y el E2 con el desarrollo y la gravedad de la enfermedad del asma en las mujeres, lo cual es especialmente relevante durante períodos de grandes fluctuaciones hormonales como el embarazo y merece mayor investigación en modelos asmáticos.

10. Conclusiones

Mediante nuestros resultados podemos concluir que:

1. Las concentraciones fisiológicas de 17β-estradiol inducen la hiperreactividad del músculo liso de las vías aéreas en el cobayo a través de efectos no genómicos, posiblemente mediante la inhibición directa de la ATPasas de Ca^{2+} de la membrana plasmática (PMCA).
2. El agonista del receptor estrogénico α (PPT) podría también estar induciendo este efecto a través de una inhibición directa de la PMCA.
3. El mecanismo no genómico inducido por el E2 en el músculo liso de las vías aéreas no involucra la vía de ERK1/2.
4. El E2 si inhibe la actividad de la forma reversa del intercambiador Na^{+}/Ca^{2+}, pero esta inhibición no participa en la hiperreactividad inducida por el E2 en las vías aéreas.
5. La inhibición de la PMCA por E2 podría estar relacionada con los mecanismos involucrados en el desarrollo de la hiperreactividad en mujeres que padecen asma perimenstrual y en la exacerbación de los síntomas del asma durante el embarazo y es un hallazgo que podría contribuir al desarrollo de estrategias innovadoras para un tratamiento personalizado.

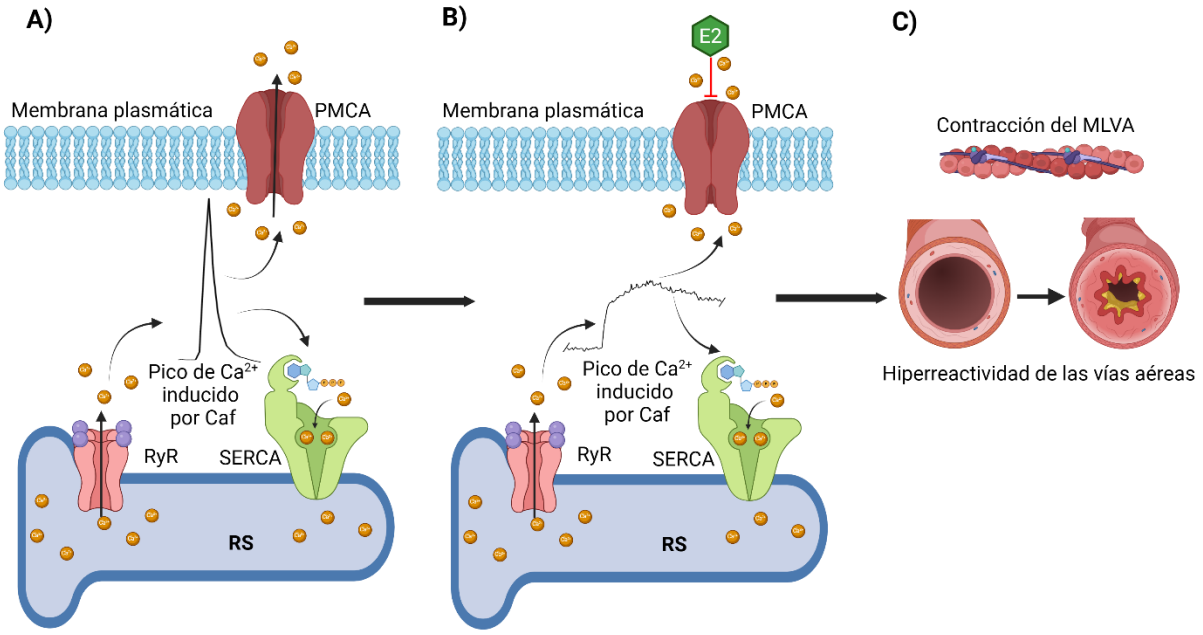

Figura 31. Efecto no genómico del 17β-estradiol sobre la respuesta de Ca^{2+} inducida por cafeína. A) La estimulación del músculo liso de las vías aéreas (MLVA) con cafeína induce un pico transitorio de Ca^{2+} producido por la liberación de Ca^{2+} del retículo sarcoplásmico (RS) a través del receptor de rianodina (RyR), mientras que la fase de disminución rápida del Ca^{2+} citosólico se debe por la activación de la ATPasa de Ca^{2+} de la membrana plasmática (PMCA) y la ATPasa de Ca^{2+} del retículo sarcoplásmico (SERCA). B) La incubación aguda (5 min) de 17β-estradiol (E2) inhibe la PMCA, posiblemente a través de una interacción directa. Al estimular la célula con cafeína después de la incubación con E2, se modifica la respuesta de Ca^{2+}, induciendo una meseta de Ca^{2+}. C) Este incremento sostenido en las concentraciones intracelulares de Ca^{2+} provoca la hiperreactividad de las vías respiratorias.

11. Perspectivas

- Estudiar los efectos genómicos del 17β-estradiol sobre la expresión y función de la ATPasa de Ca^{2+} de la membrana plasmática (PMCA).
- Explorar los efectos del 17β-estradiol sobre la reactividad de la vía aérea en animales sensibilizados.
- Investigar la interacción del 17β-estradiol con PMCA mediante técnicas de mutagénesis.

12. Referencias

1. Levy ML, Bacharier LB, Bateman E, et al. Key recommendations for primary care from the 2022 Global Initiative for Asthma (GINA) update. *npj Primary Care Respiratory Medicine*. 2023;33(1). doi:10.1038/s41533-023-00330-1
2. Townsend EA, Miller VM, Prakash YS. Sex Differences and Sex Steroids in Lung Health and Disease. *Endocrine Reviews*. 2012;33(1):1-47. doi:10.1210/er.2010-0031
3. Radzikowska U, Golebski K. Sex hormones and asthma: The role of estrogen in asthma development and severity. *Allergy*. 2023;78(3):620-622. doi:10.1111/all.15548
4. Bulkhi AA, Shepard KV, Casale TB, Cardet JC. Elevated Testosterone Is Associated with Decreased Likelihood of Current Asthma Regardless of Sex. *The Journal of Allergy and Clinical Immunology: In Practice*. 2020;8(9):3029-3035.e4. doi:10.1016/j.jaip.2020.05.022
5. Semik-Orzech A, Skoczyński S, Pierzchała W. Serum estradiol concentration, estradiol-toprogesterone ratio and sputum IL-5 and IL-8 concentrations are increased in luteal phase of the menstrual cycle in perimenstrual asthma patients. *European Annals of Allergy and Clinical Immunology*. 2017;49(04):161. doi:10.23822/eurannaci.1764-1489.09
6. Sánchez-Ramos JL, Pereira-Vega AR, Alvarado-Gómez F, Maldonado-Pérez JA, Svanes C, Gómez-Real F. Risk factors for premenstrual asthma: a systematic review and meta-analysis. *Expert review of respiratory medicine*. 2017;11(1):57–72. doi:https://doi.org/10.1080/17476348.2017.1270762
7. Giles W, Murphy V. Asthma in pregnancy: a review. *Obstetric Medicine*. 2013;6(2):58-63. doi:10.1258/om.2012.120008
8. Townsend EA, Thompson MA, Pabelick CM, Prakash YS. Rapid effects of estrogen on intracellular Ca^{2+} regulation in human airway smooth muscle. *American journal of physiology Lung cellular and molecular physiology*. 2010;298(4):L521-30. doi:doi: 10.1152/ajplung.00287.2009
9. Townsend EA, Sathish V, Thompson MA, Pabelick CM, Prakash YS. Estrogen effects on human airway smooth muscle involve cAMP and protein kinase A. *American journal of physiology Lung cellular and molecular physiology*. 2012;303(10):L923–L928. doi:https://doi.org/10.1152/ajplung.00023.2012
10. Bi R, Broutman G, Foy MR, Thompson RF, Baudry M. The tyrosine kinase and mitogen-activated protein kinase pathways mediate multiple effects of estrogen in hippocampus. *Proceedings of the National Academy of Sciences*. 2000;97(7):3602-3607. doi:10.1073/pnas.97.7.3602
11. Purves-Tyson TD, Keast JR. Rapid actions of estradiol on cyclic amp response-element binding protein phosphorylation in dorsal root ganglion neurons. *Neuroscience*. 2004;129(3):629–637. doi:https://doi.org/10.1016/j.neuroscience.2004.08.019
12. Szemraj J, Kawecka I, Lachowicz L, Zylińska L. Non-genomic effect of estradiol on plasma membrane calcium pump activity in vitro. *Pol J Pharmacol*. 2003;55(5):887-93.
13. Stratton RC, Squires PE, Green AK. 17β-Estradiol Elevates cGMP and, via Plasma Membrane Recruitment of Protein Kinase GIα, Stimulates Ca^{2+} Efflux from Rat Hepatocytes. *Journal of Biological Chemistry*. 2010;285(35):27201-27212. doi:10.1074/jbc.m110.103630
14. Romero-Martínez BS, Sommer B, Solís-Chagoyán H, et al. Estrogenic Modulation of Ionic Channels, Pumps and Exchangers in Airway Smooth Muscle. *International Journal of Molecular Sciences*. 2023;24(9):7879. doi:https://doi.org/10.3390/ijms24097879
15. Cui J, Shen Y, Li R. Estrogen synthesis and signaling pathways during aging: from periphery to brain. *Trends in Molecular Medicine*. 2013;19(3):197-209. doi:10.1016/j.molmed.2012.12.007
16. Heldring N, Pike A, Andersson S, et al. Estrogen receptors: how do they signal and what are their targets. *Physiological reviews*. 2007;87(3):905-31. doi:doi: 10.1152/physrev.00026.2006
17. Watters JJ, Campbell JS, Cunningham MJ, Krebs EG, Dorsa DM. Rapid Membrane Effects of Steroids in Neuroblastoma Cells: Effects of Estrogen on Mitogen Activated Protein Kinase Signalling

Cascade and c-fos Immediate Early Gene Transcription. *Endocrinology*. 1997;138(9):4030-4033. doi:10.1210/endo.138.9.5489
18. Stamatiou R, Paraskeva E, Papagianni M, Molyvdas PA, Hatziefthimiou A. The mitogenic effect of testosterone and 17β-estradiol on airway smooth muscle cells. *Steroids*. 2011;76(4):400-8. doi: 10.1016/j.steroids.2010.12.010.
19. Harrison DA, Carr DW, Meizel S. Involvement of protein kinase A and A kinase anchoring protein in the progesterone-initiated human sperm acrosome reaction. *Biol Reprod*. 2000;62(3):811–820. doi:https://doi.org/10.1095/biolreprod62.3.811
20. Vasudevan N, Kow L-M, Pfaff DW. Early membrane estrogenic effects required for full expression of slower genomic actions in a nerve cell line. *Proceedings of the National Academy of Sciences*. 2001;98(21):12267-12271. doi:10.1073/pnas.221449798
21. Caracta CF. Gender differences in pulmonary disease. *Mt Sinai J Med*. 2003;70(4):215-24.
22. Bjornson CL, Mitchell I. Gender differences in asthma in childhood and adolescence. *J Gend Specif Med*. 2000;3(8):57-61.
23. Melgert BN, Ray A, Hylkema MN, Timens W, Postma DS. Are there reasons why adult asthma is more common in females? *Curr Allergy Asthma Rep*. 2007;7(2):143-50. doi:10.1007/s11882-007-0012-4
24. Redline S, Gold D. Challenges in interpreting gender differences in asthma. *Am J Respir Crit Care Med*. 1994;150(5)(Pt 1):1219-21. doi:10.1164/ajrccm.150.5.7952543
25. Schatz M, Camargo CA, Jr. The relationship of sex to asthma prevalence, health care utilization, and medications in a large managed care organization. *Ann Allergy Asthma Immunol*. 2003;91(6):553-8. doi:10.1016/S1081-1206(10)61533-5
26. Vargas MH. Epidemiología del asma. *Neumol Cir Torax*. 2009;68(Suppl: 2):91-97.
27. Salam MT, Wenten M, Gilliland FD. Endogenous and exogenous sex steroid hormones and asthma and wheeze in young women. *J Allergy Clin Immunol*. 2006;117(5):1001-7. doi:10.1016/j.jaci.2006.02.004
28. Postma DS. Gender differences in asthma development and progression. *Gend Med*. 2007;4(Suppl B):S133-46. doi:10.1016/s1550-8579(07)80054-4.
29. Vrieze A, Postma DS, Kerstjens HA. Perimenstrual asthma: a syndrome without known cause or cure. *The Journal of allergy and clinical immunology*. 2003;112(2):271–282. doi:https://doi.org/10.1067/mai.2003.1676
30. Chhabra SK. Premenstrual asthma. *Indian J Chest Dis Allied Sci*. 2005;47(2):109–116.
31. Farha S, Asosingh K, Laskowski D, et al. Effects of the menstrual cycle on lung function variables in women with asthma. *Am J Respir Crit Care Med*. 2009;180(4):304-10. doi:10.1164/rccm.200904-0497OC
32. Gibbs CJ, Coutts II, Lock R, Finnegan OC, White RJ. Premenstrual exacerbation of asthma. *Thorax*. 1984;39(11):833-6. doi:10.1136/thx.39.11.833
33. Brenner BE, Holmes TM, Mazal B, Camargo CA, Jr. Relation between phase of the menstrual cycle and asthma presentations in the emergency department. *Thorax*. 2005;60(10):806-9. doi:10.1136/thx.2004.033928
34. Dratva J, Schindler C, Curjuric I, et al. Perimenstrual increase in bronchial hyperreactivity in premenopausal women: Results from the population-based SAPALDIA 2 cohort. *Journal of Allergy and Clinical Immunology*. 2010;125(4):823-829. doi:10.1016/j.jaci.2009.12.938
35. Forbes L, Jarvis D, Burney P. Do hormonal contraceptives influence asthma severity? *European Respiratory Journal*. 1999;14(5):1028-1033. doi:10.1183/09031936.99.14510289
36. Jenkins MA, Dharmage SC, Flander LB, et al. Parity and decreased use of oral contraceptives as predictors of asthma in young women. *Clin Exp Allergy*. 2006;36(5):609-13. doi:10.1111/j.1365-2222.2006.02475.x

37. Moore WC, Meyers DA, Wenzel SE, et al. Identification of Asthma Phenotypes Using Cluster Analysis in the Severe Asthma Research Program. *American Journal of Respiratory and Critical Care Medicine*. 2010;181(4):315-323. doi:10.1164/rccm.200906-0896oc
38. Juniper EF, Daniel EE, Roberts RS, Kline PA, Hargreave FE, Newhouse MT. Improvement in airway responsiveness and asthma severity during pregnancy. A prospective study. *Am Rev Respir Dis*. 1989;140(4):924-31. doi:10.1164/ajrccm/140.4.924
39. Schatz M, Harden K, Forsythe A, et al. The course of asthma during pregnancy, post partum, and with successive pregnancies: a prospective analysis. *J Allergy Clin Immunol*. 1988;81(3):509-17.
40. Schatz M, Dombrowski MP, Wise R, et al. Asthma morbidity during pregnancy can be predicted by severity classification. *J Allergy Clin Immunol*. 2003;112(2):283-8. doi:10.1067/mai.2003.1516
41. Kohler PC, Trump DL. Ectopic hormone syndromes. *Cancer Invest*. 1986;4(6):543-54. doi:10.3109/07357908609039834
42. Balzano G, Fuschillo S, Melillo G, Bonini S. Asthma and sex hormones. *Allergy*. 2001;56(1):13-20. doi:10.1034/j.1398-9995.2001.00128.x
43. Fuseini H, Yung JA, Cephus JY, et al. Testosterone Decreases House Dust Mite–Induced Type 2 and IL-17A–Mediated Airway Inflammation. *The Journal of Immunology*. 2018;201(7):1843-1854. doi:10.4049/jimmunol.1800293
44. McKenzie R, Burton MD, Royce SG, Tang ML. Age and sex influences on airway hyperresponsiveness. *The Journal of asthma : official journal of the Association for the Care of Asthma*. 2010;47(6):651–654. doi:https://doi.org/10.3109/02770901003692801
45. Carey MA, Card JW, Bradbury JA, et al. Spontaneous airway hyperresponsiveness in estrogen receptor-alpha-deficient mice. *American journal of respiratory and critical care medicine*. 2007;175(2):126–135. doi:https://doi.org/10.1164/rccm.200509-1493OC
46. Kharitonov SA, Logan-Sinclair RB, Busset CM, Shinebourne EA. Peak expiratory nitric oxide differences in men and women: relation to the menstrual cycle. *Heart*. 1994;72(3):243-245. doi:10.1136/hrt.72.3.243
47. Townsend EA, Meuchel LW, Thompson MA, Pabelick CM, Prakash YS. Estrogen Increases Nitric-Oxide Production in Human Bronchial Epithelium. *The Journal of Pharmacology and Experimental Therapeutics*. 2011;339(3):815-824. doi:10.1124/jpet.111.184416
48. Mandhane PJ, Hanna SE, Inman MD, et al. Changes in exhaled nitric oxide related to estrogen and progesterone during the menstrual cycle. *Chest*. 2009;136(5):1301-1307. doi:10.1378/chest.09-0604
49. Oguzulgen IK, Turktas H, Erbas D. Airway inflammation in premenstrual asthma. *J Asthma*. 2002;39(6):517-22. doi:10.1081/jas-120004921
50. Skoczynski S, Semik-Orzech A, Sozanska E, et al. Bronchial hyperreactivity in perimenstrual asthma is associated with increased Th-2 response in lower airways. *Journal of Thoracic Disease*. 2017;9(7):2015-2021. doi:10.21037/jtd.2017.06.121
51. Vijeyakumaran M, Jawhri MA, Fortunato J, et al. Dual activation of estrogen receptor alpha and glucocorticoid receptor upregulate CRTh2-mediated type 2 inflammation; mechanism driving asthma severity in women? *Allergy*. 2023;78(3):767-779. doi:10.1111/all.15543
52. Bhallamudi S, Connell J, Pabelick CM, Prakash YS, Sathish V. Estrogen receptors differentially regulate intracellular calcium handling in human nonasthmatic and asthmatic airway smooth muscle cells. *American Journal of Physiology-Lung Cellular and Molecular Physiology*. 2020;318(1):L112-L124. doi:10.1152/ajplung.00206.2019
53. Foster PS, Goldie RG, Paterson JW. Effect of steroids on β-adrenoceptor-mediated relaxation of pig bronchus. *British Journal of Pharmacology*. 1983;78(2):441-445. doi:10.1111/j.1476-5381.1983.tb09409.x

54. Hirota S, Helli PB, Cataldi A, Chew A, Janssen LJ. Airway smooth muscle excitation-contraction coupling and airway hyperresponsiveness. *Canadian journal of physiology and pharmacology*. 2005;83(8-9):725–732. doi:https://doi.org/10.1139/y05-070
55. Reyes-García J, Flores-Soto E, Carbajal-García A, Sommer B, Montaño L. Maintenance of intracellular Ca^{2+} basal concentration in airway smooth muscle (Review). *International Journal of Molecular Medicine*. 2018;42(6):2998-3008. doi:10.3892/ijmm.2018.3910
56. Berridge MJ, Bootman MD, Roderick HL. Calcium signalling: dynamics, homeostasis and remodelling. *Nature Reviews Molecular Cell Biology*. 2003;4(7):517-529. doi:10.1038/nrm1155
57. Flores-Soto E, Reyes-García J, Sommer B, Montaño LM. Sarcoplasmic reticulum Ca^{2+} refilling is determined by L-type Ca^{2+} and store operated Ca^{2+} channels in guinea pig airway smooth muscle. *European Journal of Pharmacology*. 2013;721(1-3):21-28. doi:10.1016/j.ejphar.2013.09.060
58. Chalmers S, Mccarron JG. The mitochondrial membrane potential and Ca^{2+} oscillations in smooth muscle. *Journal of Cell Science*. 2008;121(1):75-85. doi:10.1242/jcs.014522
59. Pan S, Conaway S, Deshpande DA. Mitochondrial regulation of airway smooth muscle functions in health and pulmonary diseases. *Archives of Biochemistry and Biophysics*. 2019;663:109-119. doi:10.1016/j.abb.2019.01.002
60. Montaño LM, Flores-Soto E, Reyes-García J, Chagoyán HS, Perusquía M, Sommer B. Airway smooth muscle functioning in basal, agonists stimulated conditions and novel androgen asthma therapy. In: Berhardt LV, ed. *Advances in Medicine and Biology*. Nova Science Publishers; 2020.
61. Webb RC. Smooth muscle contraction and relaxation. *Advances in physiology education*. 2003;27(1-4):201–206. doi:https://doi.org/10.1152/advan.00025.2003
62. Chen YF, Cao J, Zhong JN, et al. Plasma membrane Ca^{2+}-ATPase regulates Ca^{2+} signaling and the proliferation of airway smooth muscle cells. *European journal of pharmacology*. 2014;740:733–741. doi:https://doi.org/10.1016/j.ejphar.2014.05.055
63. Brini M, Carafoli E. Calcium pumps in health and disease. *Physiological reviews*. 2009;89(4):1341–1378. doi:https://doi.org/10.1152/physrev.00032.2008
64. Majoros WH, Holt C, Campbell MS, Ware D, Yandell M, Reddy TE. Predicting gene structure changes resulting from genetic variants via exon definition features. *Bioinformatics*. 2018;34(21):3616-3623. doi:10.1093/bioinformatics/bty324
65. Alberts B, Johnson A, Lewis J, et al. *Molecular Biology of the Cell.* 6th ed. Garland Science; 2017.
66. Bruce JIE. Metabolic regulation of the PMCA: Role in cell death and survival. *Cell Calcium*. 2018;69:28–36. doi:https://doi.org/10.1016/j.ceca.2017.06.001
67. Monteith GR, Wanigasekara Y, Roufogalis BD. The plasma membrane calcium pump, its role and regulation: new complexities and possibilities. *J Pharmacol Toxicol Methods*. 1998;40(4):183-90. doi:10.1016/s1056-8719(99)00004-0
68. Strehler EE, Zacharias DA. Role of alternative splicing in generating isoform diversity among plasma membrane calcium pumps. *Physiol Rev*. 2001;81(1):21-50. doi:10.1152/physrev.2001.81.1.21
69. Lodish H, Berk A, Kaiser CA, et al. *Biología celular y molecular*. 7ª Ed. ed. Médica Panamericana; 2016.
70. James P, Maeda M, Fischer R, et al. Identification and primary structure of a calmodulin binding domain of the Ca^{2+} pump of human erythrocytes. *The Journal of biological chemistry*. 1988;263(6):2905-10.
71. Gong D, Chi X, Ren K, et al. Structure of the human plasma membrane Ca^{2+}-ATPase 1 in complex with its obligatory subunit neuroplastin. *Nature Communications*. 2018;9(1). doi:10.1038/s41467-018-06075-7
72. Vorherr T, Kessler T, Hofmann F, Carafoli E. The calmodulin-binding domain mediates the self-association of the plasma membrane Ca^{2+} pump. *J Biol Chem*. 1991;266(1):22-7.

73. Kosk-Kosicka D, Bzdega T. Activation of the erythrocyte Ca^{2+}-ATPase by either self-association or interaction with calmodulin. *J Biol Chem*. 1988;263(34):18184-9.
74. Linde CI, Di Leva F, Domi T, Tosatto SC, Brini M, Carafoli E. Inhibitory interaction of the 14-3-3 proteins with ubiquitous (PMCA1) and tissue-specific (PMCA3) isoforms of the plasma membrane Ca^{2+} pump. *Cell Calcium*. 2008;43(6):550-61. doi:10.1016/j.ceca.2007.09.003
75. Rimessi A, Coletto L, Pinton P, Rizzuto R, Brini M, Carafoli E. Inhibitory Interaction of the 14-3-3ϵ Protein with Isoform 4 of the Plasma Membrane Ca^{2+}-ATPase Pump. *Journal of Biological Chemistry*. 2005;280(44):37195-37203. doi:10.1074/jbc.m504921200
76. Zvaritch E, James P, Vorherr T, Falchetto R, Modyanov N, Carafoli E. Mapping of functional domains in the plasma membrane Ca^{2+} pump using trypsin proteolysis. *Biochemistry*. 1990;29(35):8070-6. doi:10.1021/bi00487a012
77. Brodin P, Falchetto R, Vorherr T, Carafoli E. Identification of two domains which mediate the binding of activating phospholipids to the plasma-membrane Ca^{2+} pump. *European Journal of Biochemistry*. 1992;204(2):939-946. doi:10.1111/j.1432-1033.1992.tb16715.x
78. Chicka MC, Strehler EE. Alternative Splicing of the First Intracellular Loop of Plasma Membrane Ca2+-ATPase Isoform 2 Alters Its Membrane Targeting. *Journal of Biological Chemistry*. 2003;278(20):18464-18470. doi:10.1074/jbc.m301482200
79. Grati MH, Aggarwal N, Strehler EE, Wenthold RJ. Molecular determinants for differential membrane trafficking of PMCA1 and PMCA2 in mammalian hair cells. *Journal of Cell Science*. 2006;119(14):2995-3007. doi:10.1242/jcs.03030
80. Hill JK, Williams DE, LeMasurier M, Dumont RA, Strehler EE, Gillespie PG. Splice-site A choice targets plasma-membrane Ca^{2+}-ATPase isoform 2 to hair bundles. *J Neurosci*. 2006;26(23):6172-80. doi:10.1523/JNEUROSCI.0447-06.2006
81. Falchetto R, Vorherr T, Brunner J, Carafoli E. The plasma membrane Ca^{2+} pump contains a site that interacts with its calmodulin-binding domain. *J Biol Chem*. 1991;266(5):2930-6.
82. Mahn K, Hirst SJ, Ying S, et al. Diminished sarco/endoplasmic reticulum Ca^{2+} ATPase (SERCA) expression contributes to airway remodelling in bronchial asthma. *Proceedings of the National Academy of Sciences*. 2009;106(26):10775-10780. doi:10.1073/pnas.0902295106
83. Zhang Y, Inoue M, Tsutsumi A, et al. Cryo-EM structures of SERCA2b reveal the mechanism of regulation by the luminal extension tail. *Science Advances*. 2020;6(33):eabb0147. doi:10.1126/sciadv.abb0147
84. Meldolesi J, Pozzan T. The endoplasmic reticulum Ca^{2+} store: a view from the lumen. *Trends Biochem Sci*. 1998;23(1):10-4. doi:10.1016/s0968-0004(97)01143-2
85. Olesen C, Picard M, Winther AM, et al. The structural basis of calcium transport by the calcium pump. *Nature*. 2007;450(7172):1036-42. doi:10.1038/nature06418.
86. Toyoshima C, Nomura H. Structural changes in the calcium pump accompanying the dissociation of calcium. *Nature*. 2002;418(6898):605-11. doi:10.1038/nature00944
87. Lytton J, Westlin M, Burk SE, Shull GE, MacLennan DH. Functional comparisons between isoforms of the sarcoplasmic or endoplasmic reticulum family of calcium pumps. *J Biol Chem*. 1992;267(20):14483-9.
88. Inesi G, Tadini-Buoninsegni F. Ca^{2+}/H^{+} exchange, lumenal Ca^{2+} release and Ca^{2+}/ATP coupling ratios in the sarcoplasmic reticulum ATPase. *Journal of Cell Communication and Signaling*. 2014;8(1):5-11. doi:10.1007/s12079-013-0213-7
89. Zhang W-B, Kwan C-Y. Pharmacological evidence that potentiation of plasmalemmal Ca^{2+}-extrusion is functionally coupled to inhibition of SR Ca^{2+}-ATPases in vascular smooth muscle cells. *Naunyn-Schmiedeberg's Archives of Pharmacology*. 2016;389(4):447-455. doi:10.1007/s00210-016-1209-7

90. Jain D, Raj HG, Gangal SV, Chhabra SK. Relationship between Intracellular Calcium and Airway Reactivity in Guinea Pigs. *The Japanese Journal of Physiology*. 2001;51(5):577-583. doi:10.2170/jjphysiol.51.577
91. Sathish V, Thompson MA, Bailey JP, Pabelick CM, Prakash YS, Sieck GC. Effect of proinflammatory cytokines on regulation of sarcoplasmic reticulum Ca^{2+} reuptake in human airway smooth muscle. *American journal of physiology Lung cellular and molecular physiology*. 2009;29(1): L26–L34. doi:https://doi.org/10.1152/ajplung.00026.2009
92. Sathish V, Martin YN, Prakash YS. Sex steroid signaling: Implications for lung diseases. *Pharmacology & Therapeutics*. 2015;150:94-108. doi:10.1016/j.pharmthera.2015.01.007
93. Fuentes N, Silveyra P. Estrogen receptor signaling mechanisms. *Advances in Protein Chemistry and Structural Biology*. Elsevier; 2019:135-170.
94. Shoham Z, Schachter M. Estrogen biosynthesis--regulation, action, remote effects, and value of monitoring in ovarian stimulation cycles. *Fertil Steril*. 1996;65(4):687-701. doi:10.1016/s0015-0282(16)58197-7
95. Vrtačnik P, Ostanek B, Mencej-Bedrač S, Marc J. The many faces of estrogen signaling. *Biochemia Medica*. 2014;24(3):329-342. doi:10.11613/bm.2014.035
96. Konings GFJ, Reynaert NL, Delvoux B, et al. Increased levels of enzymes involved in local estradiol synthesis in chronic obstructive pulmonary disease. . *Mol Cell Endocrinol*. 2017;443:23-31. doi:10.1016/j.mce.2016.12.001
97. Pezzi V, Mathis JM, Rainey WE, Carr BR. Profiling transcript levels for steroidogenic enzymes in fetal tissues. *J Steroid Biochem Mol Biol*. 2003;87(2-3):181-9. doi:10.1016/j.jsbmb.2003.07.006
98. Peng J, Meireles SI, Xu X, et al. Estrogen metabolism in the human lung: impact of tumorigenesis, smoke, sex and race/ethnicity. *Oncotarget*. 2017;8(63):106778-106789. doi:10.18632/oncotarget.22269
99. Manna PR, Dyson MT, Stocco DM. Regulation of the steroidogenic acute regulatory protein gene expression: present and future perspectives. *Mol Hum Reprod*. 2009;15(6):321-33. doi:10.1093/molehr/gap025
100. Ambhore NS, Kalidhindi RSR, Loganathan J, Sathish V. Role of Differential Estrogen Receptor Activation in Airway Hyperreactivity and Remodeling in a Murine Model of Asthma. *American journal of respiratory cell and molecular biology*. 2019;61(4):469–480. doi:https://doi.org/10.1165/rcmb.2018-0321OC
101. Kow L-M, Pfaff DW. Rapid estrogen actions on ion channels: A survey in search for mechanisms. *Steroids*. 2016;111:46-53. doi:10.1016/j.steroids.2016.02.018
102. Cui R, Wang Y, Wang L, et al. Cyclopiazonic acid, an inhibitor of calcium-dependent ATPases with antiviral activity against human respiratory syncytial virus. *Antiviral Research*. 2016;132:38-45. doi:10.1016/j.antiviral.2016.05.010
103. Bourdeau V, Deschênes J, Métivier R, et al. Genome-Wide Identification of High-Affinity Estrogen Response Elements in Human and Mouse. *Molecular Endocrinology*. 2004;18(6):1411-1427. doi:10.1210/me.2003-0441
104. Marino M, Galluzzo P, Ascenzi P. Estrogen Signaling Multiple Pathways to Impact Gene Transcription. *Current Genomics*. 2006;7(8):497-508. doi:10.2174/138920206779315737
105. Flores-Soto E, Reyes-García J, Carbajal-García A, et al. Sex steroids effects on guinea pig airway smooth muscle tone and intracellular Ca^{2+} basal levels. *Molecular and Cellular Endocrinology*. 2017;439:444-456. doi:10.1016/j.mce.2016.10.004
106. Sarkar SN, Huang R-Q, Logan SM, Yi KD, Dillon GH, Simpkins JW. Estrogens directly potentiate neuronal L-type Ca^{2+} channels. *Proceedings of the National Academy of Sciences*. 2008;105(39):15148-15153. doi:10.1073/pnas.0802379105

107. Xu KY, Zhu W, Xiao R-P. Serine^{496} of β_2 subunit of L-type Ca^{2+} channel participates in molecular crosstalk between activation of (Na^++K^+)-ATPase and the channel. *Biochemical and Biophysical Research Communications*. 2010;402(2):319-323. doi:10.1016/j.bbrc.2010.10.024
108. Gatto C, Milanick MA. Inhibition of the red blood cell calcium pump by eosin and other fluorescein analogues. *Am J Physiol*. 1993;264(6)(Pt 1):C1577-86. doi:10.1152/ajpcell.1993.264.6.C1577
109. Grynkiewicz G, Poenie M, Tsien RY. A new generation of Ca^{2+} indicators with greatly improved fluorescence properties. *The Journal of biological chemistry*. 1985;260(6):3440–3450.
110. Bazán-Perkins B, Sánchez-Guerrero E, Carbajal V, Barajas-López C, Montaño LM. Sarcoplasmic reticulum Ca^{2+} depletion by caffeine and changes of $[Ca^{2+}]_i$ during refilling in bovine airway smooth muscle cells. *Arch Med Res*. 2000;31(6):558-63. doi:10.1016/s0188-4409(00)00156-9
111. Flores-Soto E, Reyes-García J, Sommer B, Chavez J, Barajas-López C, Montaño LM. PPADS, a P2X receptor antagonist, as a novel inhibitor of the reverse mode of the Na^+/Ca^{2+} exchanger in guinea pig airway smooth muscle. *Eur J Pharmacol*. 2012;674(2-3):439-44.
112. Luis-García ER, Becerril C, Salgado-Aguayo A, et al. Mitochondrial Dysfunction and Alterations in Mitochondrial Permeability Transition Pore (mPTP) Contribute to Apoptosis Resistance in Idiopathic Pulmonary Fibrosis Fibroblasts. *International Journal of Molecular Sciences*. 2021;22(15):7870. doi:10.3390/ijms22157870
113. Perusquía M, Flores-Soto E, Sommer B, et al. Testosterone-induced relaxation involves L-type and store-operated Ca^{2+} channels blockade, and PGE_2 in guinea pig airway smooth muscle. *Pflügers Archiv - European Journal of Physiology*. 2015;467(4):767-777. doi:10.1007/s00424-014-1534-y
114. Reyes-García J, Flores-Soto E, Solís-Chagoyán H, et al. Tumor Necrosis Factor Alpha Inhibits L-Type Ca^{2+} Channels in Sensitized Guinea Pig Airway Smooth Muscle through ERK 1/2 Pathway. *Mediators of Inflammation*. 2016;2016:1-13. doi:10.1155/2016/5972302
115. Korovkina VP, Brainard AM, Ismail P, Schmidt TJ, England SK. Estradiol Binding to Maxi-K Channels Induces Their Down-regulation via Proteasomal Degradation. *Journal of Biological Chemistry*. 2004;279(2):1217-1223. doi:10.1074/jbc.m309158200
116. Valverde MA, Rojas P, Amigo J, et al. Acute activation of Maxi-K channels (hSlo) by estradiol binding to the beta subunit. *Science*. 1999;285(5435):1929-31. doi:10.1126/science.285.5435.1929
117. Wang YJ, Lin MW, Wu SN, Sung RJ. The activation by estrogen receptor agonists of the BK_{Ca}-channel in human cardiac fibroblasts. *Biochem Pharmacol*. 2007;73(9):1347-57. doi:10.1016/j.bcp.2006.12.029
118. Rottgen TS, Fancher IS, Asano S, Widlanski TS, Dick GM. Bisphenol A activates BK channels through effects on α and β1 subunits. *Channels*. 2014;8(3):249-257. doi:10.4161/chan.27709
119. Pearlman DA, Case DA, Caldwell JW, et al. AMBER, a package of computer programs for applying molecular mechanics, normal mode analysis, molecular dynamics and free energy calculations to simulate the structural and energetic properties of molecules. *Computer Physics Communications*. 1995;91(1-3):1–41. doi:https://doi.org/10.1016/0010-4655(95)00041-D
120. Gasteiger, J., Marsili M. Iterative partial equalization of orbital electronegativity—a rapid access to atomic charges. *Tetrahedron*. 1980;36(22):3219–3228. doi:https://doi.org/10.1016/0040-4020(80)80168-2
121. Eberhardt J, Santos-Martins D, Tillack AF, Forli S. AutoDock Vina 1.2.0: New Docking Methods, Expanded Force Field, and Python Bindings. *Journal of Chemical Information and Modeling*. 2021;61(8):3891-3898. doi:10.1021/acs.jcim.1c00203
122. Sommer B, Montaño LM, Flores-Soto E, Romero-Martínez BS, González-Avila G, Solís-Chagoyán H. Coffee and Caffeine Respiratory Health Benefits: A Review. In: Berhardt LV, ed. *Advances in Medicine and Biology*. Nova Science Publishers, Inc.; 2021:chap 3.
123. Romero-Martínez BS, Montaño LM, Solís-Chagoyán H, et al. Possible Beneficial Actions of Caffeine in SARS-CoV-2. *International Journal of Molecular Sciences*. 2021;22(11):5460. doi:10.3390/ijms22115460

124. Guerreiro S, Marien M, Michel PP. Methylxanthines and ryanodine receptor channels. *Handb Exp Pharmacol*. 2011;(200):135-50. doi:10.1007/978-3-642-13443-2_5.
125. Kong H, Jones PP, Koop A, Zhang L, Duff J, Henry, Chen W, R., S. Caffeine induces Ca^{2+} release by reducing the threshold for luminal Ca^{2+} activation of the ryanodine receptor. *Biochemical Journal*. 2008;414(3):441-452. doi:10.1042/bj20080489
126. Shi D, Padgett WL, Daly JW. Caffeine analogs: effects on ryanodine-sensitive calcium-release channels and GABAA receptors. *Cell Mol Neurobiol*. 2003;23(3):331-47. doi:10.1023/a:1023688604792
127. Franco R, Oñatibia-Astibia A, Martínez-Pinilla E. Health Benefits of Methylxanthines in Cacao and Chocolate. *Nutrients*. 2013;5(10):4159-4173. doi:10.3390/nu5104159
128. Devillier P, Naline E, Grassin-Delyle S. The pharmacology of bitter taste receptors and their role in human airways. *Pharmacol Ther*. 2015;155:11-21. doi:10.1016/j.pharmthera.2015.08.001
129. Deshpande DA, Wang WCH, Mcilmoyle EL, et al. Bitter taste receptors on airway smooth muscle bronchodilate by localized calcium signaling and reverse obstruction. *Nature Medicine*. 2010;16(11):1299-1304. doi:10.1038/nm.2237
130. Shaik FA, Singh N, Arakawa M, Duan K, Bhullar RP, Chelikani P. Bitter taste receptors: Extraoral roles in pathophysiology. . *Int J Biochem Cell Biol*. 2016;77(Pt B):197-204. doi:10.1016/j.biocel.2016.03.011
131. Rabe KF, Magnussen H, Dent G. Theophylline and selective PDE inhibitors as bronchodilators and smooth muscle relaxants. *European Respiratory Journal*. 1995;8(4):637-642. doi:10.1183/09031936.95.08040637
132. Ruangkittisakul A, Ballanyi K. Methylxanthine reversal of opioid-evoked inspiratory depression via phosphodiesterase-4 blockade. *Respir Physiol Neurobiol*. 2010;172(3):94-105. doi:10.1016/j.resp.2010.04.025
133. Oakes SG, Martin WJ, 2nd, Lisek CA, Powis G. Incomplete hydrolysis of the calcium indicator precursor fura-2 pentaacetoxymethyl ester (fura-2 AM) by cells. *Anal Biochem*. 1988;169(1):159-66. doi:10.1016/0003-2697(88)90267-9
134. Fleckenstein-Grün G. Gallopamil: cardiovascular scope of action of a highly specific calcium antagonist. *J Cardiovasc Pharmacol*. 1992;20(Suppl 7):S1-10. doi:10.1097/00005344-199200207-00002.
135. Brogden RN, Benfield P. Gallopamil. A review of its pharmacodynamic and pharmacokinetic properties, and therapeutic potential in ischaemic heart disease. *Drugs*. 1994;47(1):93-115. doi:10.2165/00003495-199447010-00007
136. Herscher CJ, Rega AF. Pre-Steady-State Kinetic Study of the Mechanism of Inhibition of the Plasma Membrane Ca^{2+}-ATPase by Lanthanum. *Biochemistry*. 1996;35(47):14917-14922. doi:10.1021/bi961879r
137. Fujimori T, Jencks WP. Lanthanum inhibits steady-state turnover of the sarcoplasmic reticulum calcium ATPase by replacing magnesium as the catalytic ion. *J Biol Chem*. 1990;265(27):16262-70.
138. Mlinar B, Enyeart JJ. Block of current through T-type calcium channels by trivalent metal cations and nickel in neural rat and human cells. *J Physiol*. 1993;469:639-52. doi:10.1113/jphysiol.1993.sp019835
139. Fierro L, Dipolo R, Llano I. Intracellular calcium clearance in Purkinje cell somata from rat cerebellar slices. *The Journal of Physiology*. 1998;510(2):499-512. doi:10.1111/j.1469-7793.1998.499bk.x
140. Hoover DB. Carbachol. *Reference Module in Biomedical Sciences*. Elsevier; 2016.
141. Montaño LM, Flores-Soto E, Reyes-García J, et al. Testosterone induces hyporesponsiveness by interfering with IP_3 receptors in guinea pig airway smooth muscle. *Molecular and Cellular Endocrinology*. 2018;473:17-30. doi:10.1016/j.mce.2017.12.010
142. Seidler NW, Jona I, Vegh M, Martonosi A. Cyclopiazonic acid is a specific inhibitor of the Ca^{2+}-ATPase of sarcoplasmic reticulum. *J Biol Chem*. 1989;264(30):17816-23.
143. Yao S, Gallenkamp D, Wölfel K, Lüke B, Schindler M, Scherkenbeck J. Synthesis and SERCA activities of structurally simplified cyclopiazonic acid analogues. *Bioorg Med Chem*. 2011;19(15):4669-78. doi:10.1016/j.bmc.2011.06.001

144. Jaskulska A, Janecka AE, Gach-Janczak K. Thapsigargin—From Traditional Medicine to Anticancer Drug. *International Journal of Molecular Sciences*. 2020;22(1):4. doi:10.3390/ijms22010004
145. Kijima Y, Ogunbunmi E, Fleischer S. Drug action of thapsigargin on the Ca^{2+} pump protein of sarcoplasmic reticulum. *J Biol Chem*. 1991;266(34):22912-8.
146. Favata MF, Horiuchi KY, Manos EJ, et al. Identification of a Novel Inhibitor of Mitogen-activated Protein Kinase Kinase. *Journal of Biological Chemistry*. 1998;273(29):18623-18632. doi:10.1074/jbc.273.29.18623
147. Stauffer SR, Coletta CJ, Tedesco R, et al. Pyrazole ligands: structure-affinity/activity relationships and estrogen receptor-alpha-selective agonists. *J Med Chem*. 2000;43(26):4934-47. doi:10.1021/jm000170m
148. Ambhore NS, Katragadda R, Raju Kalidhindi RS, et al. Estrogen receptor beta signaling inhibits PDGF induced human airway smooth muscle proliferation. *Molecular and Cellular Endocrinology*. 2018;476:37-47. doi:10.1016/j.mce.2018.04.007
149. Meyers MJ, Sun J, Carlson KE, Marriner GA, Katzenellenbogen BS, Katzenellenbogen JA. Estrogen receptor-beta potency-selective ligands: structure-activity relationship studies of diarylpropionitriles and their acetylene and polar analogues. *J Med Chem*. 2001;44(24):4230-51. doi:10.1021/jm010254a
150. Frauenkron M, Melder J-P, Ruider G, Rossbacher R, Höke H. *Ethanolamines and Propanolamines* . 2001. doi:https://doi.org/10.1002/14356007.a10_001
151. Park K-S, Jo I, Pak Y, et al. FCCP depolarizes plasma membrane potential by activating proton and Na+ currents in bovine aortic endothelial cells. *Pflügers Archiv - European Journal of Physiology*. 2002;443(3):344-352. doi:10.1007/s004240100703
152. Wu C, Sui G, Fry CH. The role of the L-type Ca^{2+} channel in refilling functional intracellular Ca^{2+} stores in guinea-pig detrusor smooth muscle. *The Journal of Physiology*. 2002;538(2):357-369. doi:10.1113/jphysiol.2001.013191
153. Brini M, Calì T, Ottolini D, Carafoli E. The plasma membrane calcium pump in health and disease. *Febs j*. 2013;280(21):5385-97. doi:10.1111/febs.12193
154. Caride AJ, Filoteo AG, Penniston JT, Strehler EE. The Plasma Membrane Ca2+ Pump Isoform 4a Differs from Isoform 4b in the Mechanism of Calmodulin Binding and Activation Kinetics. *Journal of Biological Chemistry*. 2007;282(35):25640-25648. doi:10.1074/jbc.m701129200
155. Corradi GR, Mazzitelli LR, Petrovich GD, De Tezanos Pinto F, Rochi L, Adamo HP. Plasma Membrane Ca2+ Pump PMCA4z Is More Active Than Splicing Variant PMCA4x. *Frontiers in Cellular Neuroscience*. 2021;15doi:10.3389/fncel.2021.668371
156. Kim K, Lee D, Ahn C, et al. Effects of estrogen on esophageal function through regulation of Ca^{2+}-related proteins. *Journal of gastroenterology*. 2017;52(8):929-939. doi:10.1007/s00535-016-1305-y
157. El-Beialy W, Galal N, Deyama Y, et al. Effects of Estrogen on PMCA 2 and 4 in Human Fibroblast-like Synovial Cells and Mouse Macrophage-like Cells. *Endocrine Journal*. 2010;57(1):93-97. doi:10.1507/endocrj.k09e-247
158. Tran DN, Jung E-M, Ahn C, Lee J-H, Yoo Y-M, Jeung E-B. Effects of Bisphenol A and 4-tert-Octylphenol on Embryo Implantation Failure in Mouse. *International Journal of Environmental Research and Public Health*. 2018;15(8):1614. doi:10.3390/ijerph15081614
159. Varga K, Hollósi A, Pászty K, et al. Expression of calcium pumps is differentially regulated by histone deacetylase inhibitors and estrogen receptor alpha in breast cancer cells. *BMC Cancer*. 2018;18(1)doi:10.1186/s12885-018-4945-x
160. Yang H, Choi KC, Hyun SH, Jeung EB. Coexpression and estrogen-mediated regulation of TRPV6 and PMCA1 in the human endometrium during the menstrual cycle. *Molecular reproduction and development*. 2011;78(4):274–282. doi:https://doi.org/10.1002/mrd.21303

161. Dick IM, Liu J, Glendenning P, Prince RL. Estrogen and androgen regulation of plasma membrane calcium pump activity in immortalized distal tubule kidney cells. *Molecular and cellular endocrinology*. 2003;212(1)(2):11-18. doi:https://doi.org/10.1016/j.mce.2003.09.028
162. Babnigg G, Zagranichnaya T, Wu X, Villereal ML. Differential Tyrosine Phosphorylation of Plasma Membrane Ca^{2+}-ATPase and Regulation of Calcium Pump Activity by Carbachol and Bradykinin. *Journal of Biological Chemistry*. 2003;278(17):14872-14882. doi:10.1074/jbc.m210418200
163. Bruce JIE, Yule DI, Shuttleworth TJ. Ca^{2+}-dependent Protein Kinase-A Modulation of the Plasma Membrane Ca^{2+}-ATPase in Parotid Acinar Cells. *Journal of Biological Chemistry*. 2002;277(50):48172-48181. doi:10.1074/jbc.m208393200
164. Wright LC, Chen S, Roufogalis BD. Regulation of the activity and phosphorylation of the plasma membrane Ca^{2+}-ATPase by protein kinase C in intact human erythrocytes. *Arch Biochem Biophys*. 1993;306(1):277–284. doi:https://doi.org/10.1006/abbi.1993.1512
165. Sheridan JT, Gilmore RC, Watson MJ, Archer CB, Tarran R. 17β-Estradiol Inhibits Phosphorylation of Stromal Interaction Molecule 1 (STIM1) Protein. *Journal of Biological Chemistry*. 2013;288(47):33509-33518. doi:10.1074/jbc.m113.486662
166. Sathish V, Freeman MR, Long E, Thompson MA, Pabelick CM, Prakash YS. Cigarette Smoke and Estrogen Signaling in Human Airway Smooth Muscle. *Cellular Physiology and Biochemistry*. 2015;36(3):1101-1115. doi:10.1159/000430282
167. Endoh H, Sasaki H, Maruyama K, et al. Rapid activation of MAP kinase by estrogen in the bone cell line. *Biochem Biophys Res Commun*. 1997;235(1):99-102. doi: 10.1006/bbrc.1997.6746
168. Migliaccio A, Piccolo D, Castoria G, et al. Activation of the Src/p21ras/Erk pathway by progesterone receptor via cross-talk with estrogen receptor. *EMBO J*. 1998;17(7):2008-18. doi: 10.1093/emboj/17.7.2008
169. Tran Q-K, Firkins R, Giles J, et al. Estrogen Enhances Linkage in the Vascular Endothelial Calmodulin Network via a Feedforward Mechanism at the G Protein-coupled Estrogen Receptor 1. *Journal of Biological Chemistry*. 2016;291(20):10805-10823. doi:10.1074/jbc.m115.697334
170. Aravamudan B, Goorhouse KJ, Unnikrishnan G, et al. Differential Expression of Estrogen Receptor Variants in Response to Inflammation Signals in Human Airway Smooth Muscle. *Journal of Cellular Physiology*. 2017;232(7):1754-1760. doi:10.1002/jcp.25674
171. Moreno RH, Hogg JC, Paré PD. Mechanics of airway narrowing. *The American review of respiratory disease*. 1986;133(6):1171–1180. doi:https://doi.org/10.1164/arrd.1986.133.6.1171
172. Prieto L, Gutiérrez V, Morales C, Marín J. Differences in sensitivity, maximal response and position of the concentration-response curve to methacholine between asthmatics, patients with allergic rhinitis and healthy subjects. *Respiratory medicine*. 1998;92(1):88–94. doi:https://doi.org/10.1016/s0954-6111(98)90038-5
173. Perez-Zoghbi JF, Karner C, Ito S, Shepherd M, Alrashdan Y, Sanderson MJ. Ion channel regulation of intracellular calcium and airway smooth muscle function. *Pulmonary Pharmacology & Therapeutics*. 2009;22(5):388-397. doi:10.1016/j.pupt.2008.09.006
174. Somlyo AP, Somlyo AV. Ca^{2+} sensitivity of smooth muscle and nonmuscle myosin II: modulated by G proteins, kinases, and myosin phosphatase. *Physiological reviews*. 2003;83(4):1325–1358. doi:https://doi.org/10.1152/physrev.00023.2003
175. Warren KJ, Deering-Rice C, Huecksteadt T, et al. Steady-state estradiol triggers a unique innate immune response to allergen resulting in increased airway resistance. *Biology of Sex Differences*. 2023;14(1). doi:10.1186/s13293-022-00483-7
176. Nejatbakhsh Samimi L, Fallahpour M, Khoshmirsafa M, et al. The impact of 17β-estradiol and progesterone therapy on peripheral blood mononuclear cells of asthmatic patients. *Molecular Biology Reports*. 2021;48(1):297-306. doi:10.1007/s11033-020-06046-6

177. Paradiso K, Zhang J, Steinbach JH. The C terminus of the human nicotinic α4β2 receptor forms a binding site required for potentiation by an estrogenic steroid. *J Neurosci*. 2001;21(17):6561-8. doi:10.1523/JNEUROSCI.21-17-06561.2001
178. Consortium U. The Universal Protein Resource (UniProt) in 2010. *Nucleic Acids Research*. 2010;38(suppl_1):D142-D148. doi:10.1093/nar/gkp846
179. Jain E, Bairoch A, Duvaud S, et al. Infrastructure for the life sciences: design and implementation of the UniProt website. *BMC Bioinformatics*. 2009;10(1):136. doi:10.1186/1471-2105-10-136
180. Cusick ME, Klitgord N, Vidal M, Hill DE. Interactome: gateway into systems biology. *Hum Mol Genet*. 2005;14(*Spec No. 2*):R171-81. doi:10.1093/hmg/ddi335
181. De Las Rivas J, Fontanillo C. Protein–Protein Interactions Essentials: Key Concepts to Building and Analyzing Interactome Networks. *PLoS Computational Biology*. 2010;6(6):e1000807. doi:10.1371/journal.pcbi.1000807
182. Sych T, Levental KR, Sezgin E. Lipid–Protein Interactions in Plasma Membrane Organization and Function. *Annual Review of Biophysics*. 2022;51(1):135-156. doi:10.1146/annurev-biophys-090721-072718
183. Javanainen M, Enkavi G, Guixà-Gonzaléz R, et al. Reduced level of docosahexaenoic acid shifts GPCR neuroreceptors to less ordered membrane regions. *PLOS Computational Biology*. 2019;15(5):e1007033. doi:10.1371/journal.pcbi.1007033
184. Blouin CM, Hamon Y, Gonnord P, et al. Glycosylation-Dependent IFN-γR Partitioning in Lipid and Actin Nanodomains Is Critical for JAK Activation. *Cell*. 2016;166(4):920-934. doi:10.1016/j.cell.2016.07.003
185. Özhan G, Sezgin E, Wehner D, et al. Lypd6 Enhances Wnt/β-Catenin Signaling by Promoting Lrp6 Phosphorylation in Raft Plasma Membrane Domains. *Developmental Cell*. 2013;26(4):331-345. doi:10.1016/j.devcel.2013.07.020
186. Sezgin E, Azbazdar Y, Ng XW, et al. Binding of canonical Wnt ligands to their receptor complexes occurs in ordered plasma membrane environments. *The FEBS Journal*. 2017;284(15):2513-2526. doi:10.1111/febs.14139
187. Brown DA, Rose JK. Sorting of GPI-anchored proteins to glycolipid-enriched membrane subdomains during transport to the apical cell surface. . *Cell*. 1992;68(3):533-44. doi:10.1016/0092-8674(92)90189-j
188. Lajoie P, Nabi IR. Lipid rafts, caveolae, and their endocytosis. *Int Rev Cell Mol Biol*. 2010;282:135-63. doi:10.1016/S1937-6448(10)82003-9
189. Lee AG. Lipid-protein interactions. *Biochem Soc Trans*. 2011;39(3):761-6. doi:10.1042/BST0390761
190. Starling AP, East JM, Lee AG. Effects of phosphatidylcholine fatty acyl chain length on calcium binding and other functions of the (Ca^{2+}-Mg^{2+})-ATPase. *Biochemistry*. 1993;32(6):1593–1600.
191. Froud RJ, Earl CR, East JM, Lee AG. Effects of lipid fatty acyl chain structure on the activity of the (Ca^{2+} + Mg^{2+})-ATPase. *Biochim Biophys Acta*. 1986;860(2):354-60. doi:10.1016/0005-2736(86)90532-8.
192. Froud RJ, East JM, Jones OT, Lee AG. Effects of lipids and long-chain alkyl derivatives on the activity of (Ca^{2+} -Mg^{2+})-ATPase. *Biochemistry*. 1986;25(23):7544–7552. doi:https://doi.org/10.1021/bi00371a043
193. Pignataro MF, Dodes-Traian MM, González-Flecha FL, Sica M, Mangialavori IC, Rossi JPFC. Modulation of Plasma Membrane Ca^{2+}-ATPase by Neutral Phospholipids. *Journal of Biological Chemistry*. 2015;290(10):6179-6190. doi:10.1074/jbc.m114.585828
194. Cannarozzo C, Fred SM, Girych M, et al. Cholesterol-recognition motifs in the transmembrane domain of the tyrosine kinase receptor family: The case of TRKB. *European Journal of Neuroscience*. 2021;53(10):3311-3322. doi:10.1111/ejn.15218
195. Stahelin RV. Lipid binding domains: more than simple lipid effectors. *J Lipid Res*. 2009;50 Suppl:S299-304. doi:10.1194/jlr.R800078-JLR200

196. Chavent M, Karia D, Kalli AC, et al. Interactions of the EphA2 Kinase Domain with PIPs in Membranes: Implications for Receptor Function. *Structure*. 2018;26(7):1025-1034.e2. doi:10.1016/j.str.2018.05.003
197. Yen HY, Hoi KK, Liko I, et al. PtdIns(4,5)P_2 stabilizes active states of GPCRs and enhances selectivity of G-protein coupling. *Nature*. 2018;559(7714):423-427. doi:10.1038/s41586-018-0325-6
198. Cozzolino F, Iacobucci I, Monaco V, Monti M. Protein–DNA/RNA Interactions: An Overview of Investigation Methods in the -Omics Era. *Journal of Proteome Research*. 2021;20(6):3018-3030. doi:10.1021/acs.jproteome.1c00074
199. Wang L, Brown SJ. BindN: a web-based tool for efficient prediction of DNA and RNA binding sites in amino acid sequences. *Nucleic Acids Research*. 2006;34:W243-W248. doi:10.1093/nar/gkl298
200. Lin M, Guo J-T. New insights into protein–DNA binding specificity from hydrogen bond based comparative study. *Nucleic Acids Research*. 2019;47(21):11103-11113. doi:10.1093/nar/gkz963
201. Jankowsky E, Harris ME. Specificity and nonspecificity in RNA-protein interactions. *Nat Rev Mol Cell Biol*. 2015;16(9):533-44. doi:10.1038/nrm4032
202. Guenther UP, Yandek LE, Niland CN, et al. Hidden specificity in an apparently nonspecific RNA-binding protein. . *Nature*. 2013;502(7471):385-8. doi:10.1038/nature12543
203. Spassov DS. Binding Affinity Determination in Drug Design: Insights from Lock and Key, Induced Fit, Conformational Selection, and Inhibitor Trapping Models. *International Journal of Molecular Sciences*. 2024;25(13):7124. doi:10.3390/ijms25137124
204. Matos ASD, Kugelmeier T, Guimarães DADA, Silva KSMD. Early puberty in short-haired Guinea pigs kept in laboratory animal facilities. *Animal Reproduction*. 2022;19(1)doi:10.1590/1984-3143-ar2021-0068

13. Anexos

Anexo 1. Artículo requerido para la obtención del grado.
Romero-Martínez BS, Flores-Soto E, Sommer B, Reyes-García J, Arredondo-Zamarripa D, Solís-Chagoyán H, Lemini C, Rivero-Segura NA, Santiago-de-la-Cruz JA, Pérez-Plascencia C, Montaño LM. 17β-estradiol induces hyperresponsiveness in guinea pig airway smooth muscle by inhibiting the plasma membrane Ca^{2+}-ATPase. Mol Cell Endocrinol. 2024;590:112273. doi: 10.1016/j.mce.2024.112273.

Anexo 2. Artículo de revisión.
Romero-Martínez BS, Sommer B, Solís-Chagoyán H, Calixto E, Aquino-Gálvez A, Jaimez R, Gomez-Verjan JC, González-Avila G, Flores-Soto E, Montaño LM. Estrogenic Modulation of Ionic Channels, Pumps and Exchangers in Airway Smooth Muscle. Int J Mol Sci. 2023;24(9):7879. doi: 10.3390/ijms24097879.

Anexo 3. Artículo original.
Sánchez-Florentino ZA, Romero-Martínez BS, Flores-Soto E, Montaño LM, Sommer B, Valdés-Tovar M, Argueta J, Calixto E, Aquino-Gálvez A, Castillejos-López M, Serrano H, Gomez-Verjan JC, López-Riquelme GO, Benítez-King GA, Jaimez R, Solís-Chagoyán H. Altered PLCβ/IP_3/Ca^{2+} Signaling Pathway Activated by GPRCs in Olfactory Neuronal Precursor Cells Derived from Patients Diagnosed with Schizophrenia. Biomedicines. 2024;12(10):2343. doi: 10.3390/biomedicines12102343.

Anexo 4. Artículo de revisión.
Montaño LM, Sommer B, Solís-Chagoyán H, Romero-Martínez BS, Aquino-Gálvez A, Gomez-Verjan JC, Calixto E, González-Avila G, Flores-Soto E. Could Lower Testosterone in Older Men Explain Higher COVID-19 Morbidity and Mortalities? Int J Mol Sci. 2022;23(2):935. doi: 10.3390/ijms23020935.

Anexo 5. Artículo de revisión.
Montaño LM, Sommer B, Gomez-Verjan JC, Morales-Paoli GS, Ramírez-Salinas GL, Solís-Chagoyán H, Sanchez-Florentino ZA, Calixto E, Pérez-Figueroa GE, Carter R, Jaimez-Melgoza R, Romero-Martínez BS, Flores-Soto E. Theophylline: Old Drug in a New Light, Application in COVID-19 through Computational Studies. Int J Mol Sci. 2022;23(8):4167. doi: 10.3390/ijms23084167.

Anexo 6. Artículo de revisión.
Romero-Martínez BS, Montaño LM, Solís-Chagoyán H, Sommer B, Ramírez-Salinas GL, Pérez-Figueroa GE, Flores-Soto E. Possible Beneficial Actions of Caffeine in SARS-CoV-2. Int J Mol Sci. 2021 May 22;22(11):5460. doi: 10.3390/ijms22115460.

Molecular and Cellular Endocrinology 590 (2024) 112273

Contents lists available at ScienceDirect

Molecular and Cellular Endocrinology

journal homepage: www.elsevier.com/locate/mce

17β-estradiol induces hyperresponsiveness in guinea pig airway smooth muscle by inhibiting the plasma membrane Ca^{2+}-ATPase

Bianca S. Romero-Martínez [a], Edgar Flores-Soto [a], Bettina Sommer [b], Jorge Reyes-García [a], David Arredondo-Zamarripa [a], Héctor Solís-Chagoyán [c], Cristina Lemini [a], Nadia A. Rivero-Segura [d], José A. Santiago-de-la- Cruz [d], Carlos Pérez-Plascencia [e,f], Luis M. Montaño [a,*]

[a] Departamento de Farmacología, Facultad de Medicina, Universidad Nacional Autónoma de México, Av. Universidad No. 3000, Alcaldía de Coyoacán, CP 04510, CDMX, México
[b] Departamento de Investigación en Hiperreactividad Bronquial, Instituto Nacional de Enfermedades Respiratorias, Calz. De Tlalpan 4502, Col. Sección XVI, Alcaldía de Tlalpan, CP 14080, CDMX, México
[c] Neurociencia Cognitiva Evolutiva, Centro de Investigación en Ciencias Cognitivas, Universidad Autónoma Del Estado de Morelos, CP 62209, Morelos, México
[d] Dirección de Investigación, Instituto Nacional de Geriatría (INGER), Ciudad de México, CP 10200, México
[e] Unidad de Genómica y Cáncer, Subdirección de Investigación Básica, INCan, SSA, Av. San Fernando 22, Alcaldía de Tlalpan, CP 14080, CDMX, México
[f] Facultad de Estudios Superiores Iztacala, Av. de Los Barrios S/N Los Reyes Ixtacala Tlalnepantla de Baz, Edo. de México, CP 54090, Tlalnepantla de Baz, México

ARTICLE INFO

Handling Editor: Carolyn M. Klinge

Keywords:
17β-estradiol
Asthmatic women
Airway smooth muscle
Airway hyperresponsiveness
Plasma membrane Ca^{2+}-ATPase pump

ABSTRACT

High serum estrogen concentrations are associated with asthma development and severity, suggesting a link between estradiol and airway hyperresponsiveness (AHR). 17β-estradiol (E2) has non-genomic effects via Ca^{2+} regulatory mechanisms; however, its effect on the plasma membrane Ca^{2+}-ATPases (PMCA1 and 4) and sarcoplasmic reticulum Ca^{2+}-ATPase (SERCA) is unknown. Hence, in the present study, we aim to demonstrate if E2 favors AHR by increasing intracellular Ca^{2+} concentrations in guinea pig airway smooth muscle (ASM) through a mechanism involving Ca^{2+}-ATPases.

In guinea pig ASM, Ca^{2+} microfluorometry, muscle contraction, and Western blot were evaluated. Then, we performed molecular docking analysis between the estrogens and Ca^{2+} ATPases.

In tracheal rings, E2 produced AHR to carbachol. In guinea pig myocytes, acute exposure to physiological levels of E2 modified the transient Ca^{2+} peak induced by caffeine to a Ca^{2+} plateau. The incubation with PMCA inhibitors (lanthanum and carboxyeosin, CE) partially reversed the E2-induced sustained plateau in the caffeine response. In contrast, cyclopiazonic acid (SERCA inhibitor), U-0126 (an inhibitor of ERK 1/2), and choline chloride did not modify the Ca^{2+} plateau produced by E2. The mitochondrial uniporter activity and the capacitative Ca^{2+} entry were unaffected by E2. In guinea pig ASM, Western blot analysis demonstrated PMCA1 and PMCA4 expression. The results from the docking modeling demonstrate that E2 binds to both plasma membrane ATPases. In guinea pig tracheal smooth muscle, inhibiting the PMCA with CE, induced hyperresponsiveness to carbachol. 17β-estradiol produces hyperresponsiveness by inhibiting the PMCA in the ASM and could be one of the mechanisms responsible for the increase in asthmatic crisis in women.

1. Introduction

Asthma is a multifactorial disease characterized by chronic inflammation, airway hyperresponsiveness (AHR), reversible airway obstruction, and various respiratory symptoms, including shortness of breath, wheezing, chest tightness, and coughing (Levy et al., 2023). Asthma affects all age groups and is a lifelong illness affecting approximately 300 million people worldwide (Levy et al., 2023). Clinical data suggest that asthma development and severity are influenced by age and gender (Radzikowska and Golebski, 2023; Townsend, Miller, et al., 2012a). In

* Corresponding author. Departamento de Farmacología, Edificio de Investigación, sexto piso, laboratorio de Investigación en Asma Facultad de Medicina, Universidad Nacional Autónoma de México, Ciudad Universitaria, CP 04510, CDMX, México.
E-mail address: lmmr@unam.mx (L.M. Montaño).

https://doi.org/10.1016/j.mce.2024.112273
Received 13 December 2023; Received in revised form 16 May 2024; Accepted 17 May 2024
Available online 18 May 2024

childhood, asthma is predominant in boys. However, after puberty, this relation is inverted since greater asthma frequency is observed in women during adolescence and throughout adulthood, coinciding with the increment and cycles of female sexual hormones (Bulkhi et al., 2020; Radzikowska and Golebski, 2023; Townsend, Miller, et al., 2012a). Asthma severity has been linked to changes in serum hormone concentrations during the menstrual cycle, correlating with increased levels of estrogen and progesterone and affecting between 11 and 45% of asthmatic women (Radzikowska and Golebski, 2023; Semik-Orzech et al., 2017; Sánchez-Ramos et al., 2017; Townsend, Miller, et al., 2012a). In asthmatic women, pregnancy is a specific concern since it has been observed that, during gestation, one-third of the pregnant women present worsening symptoms, one-third improve, and one-third present no changes (Giles and Murphy, 2013; Townsend, Miller, et al., 2012a).

During their reproductive years, women experience significant fluctuations in sex hormone concentration, time of exposure, and targeted tissue, having both genomic (executed in hours or days) and non-genomic effects (induced in minutes). 17β-estradiol (E2) effects can happen through the occupation of specific estrogenic receptors (ER) α, β and GPR30, and through direct interaction with target proteins (Cui et al., 2013; Heldring et al., 2007; Romero-Martínez et al., 2023; Townsend, Miller, et al., 2012a; Townsend et al., 2010). In this regard, through non-genomic effects, E2 has been shown to activate a multitude of pathways including cAMP production (Townsend, Sathish, et al., 2012b), mitogen-activated protein kinases (MAPK) (Bi et al., 2000; Purves-Tyson and Keast, 2004; Stamatiou et al., 2011; Watters et al., 1997), protein kinase A (Harrison et al., 2000; Vasudevan et al., 2001), protein kinase C (Vasudevan et al., 2001) and tyrosine kinase (Bi et al., 2000). The activity of this hormone is not limited to reproductive activities, and it is an important regulator of a multitude of physiological processes in other organs. Airway smooth muscle (ASM) cells express ERα and ERβ receptors (Townsend et al., 2010) that have been shown to modulate Ca^{2+} handling mechanisms, probably contributing to the gender dimorphism observed in asthma prevalence and severity (Romero-Martínez et al., 2023; Townsend, Miller, et al., 2012a; Townsend et al., 2010). ASM is considered a primary target of asthma pathophysiology; an alteration in its contractility can contribute to AHR, defined as an exaggerated ASM contractile response to stimuli compared to normal individuals (Hirota et al., 2005). Under normal conditions, ASM contraction begins with an increment in intracellular Ca^{2+} concentrations ($[Ca^{2+}]_i$) that lay approximately between 100 and 150 nM (Reyes-García et al., 2018). An increment in $[Ca^{2+}]_i$ can occur as an influx of extracellular Ca^{2+} or release from internal stores from the sarcoplasmic reticulum (SR) (Reyes-García et al., 2018; Romero-Martínez et al., 2023). Equilibrium in $[Ca^{2+}]_i$ must promptly be re-established. Therefore, Ca^{2+} is extruded to the extracellular space through specialized proteins such as the Na^+/Ca^{2+} Exchanger (NCX) and the plasma membrane Ca^{2+}-ATPase (PMCA), both localized on the plasma membrane. Besides, intracellular Ca^{2+} is stored into the SR through the activity of the sarcoplasmic reticulum Ca^{2+}-ATPase (SERCA) situated on the membrane of this organelle (Reyes-García et al., 2018; Romero-Martínez et al., 2023). PMCA and SERCA remove the highest amount of Ca^{2+} from the intracellular space after ASM stimulation by a contractile agonist (Montaño et al., 2020; Webb, 2003).

PMCA has four isoforms (PMCA1-4), each encoded by a different gene and several splicing variants (Brini and Carafoli, 2009; Chen et al., 2014; Reyes-García et al., 2018). The isoform expression changes in a tissue-specific manner (Brini and Carafoli, 2009; Chen et al., 2014). It has been observed that rat ASM cells express PMCA1 and 4 isoforms (Chen et al., 2014). It has a high affinity for Ca^{2+} but a low transport capacity, with a stochiometric relation of 1:1 of Ca^{2+}/ATP, with an electroneutral reaction via the Ca^{2+}/H^+ exchange (Brini and Carafoli, 2009; Reyes-García et al., 2018). On the other hand, SERCA has three isoforms (SERCA1-3) as well as many splicing variants, with the most predominant isoform being SERCA2b in ASM cells (Mahn et al., 2009; Reyes-García et al., 2018; Romero-Martínez et al., 2023). Both ATPases have been shown to participate in ASM cell functions like Ca^{2+} homeostasis (Zhang and Kwan, 2016), contraction (Jain et al., 2001), AHR (Jain et al., 2001; Sathish et al., 2009), proliferation (Chen et al., 2014), and even apoptosis (Chen et al., 2014).

In the present study, we explored if E2 modulates PMCA and/or SERCA activity in guinea pig ASM cells and if this modulation could lead to a reduction in intracellular Ca^{2+} clearance that could lead to AHR in asthmatic women.

2. Materials and methods

2.1. Animals

Male Hartley prepubescent guinea pigs between 350 and 400 g were used (4–6 weeks old). Animals were bred in our institutional animal facilities with standard conditions: filtered conditioned air, 21 ± 1 °C, 50–70% humidity, and sterilized bed, and had food and sterilized water *ad libitum*. Scientific and Bioethics committees of the Facultad de Medicina, Universidad Nacional Autónoma de México approved the experimental protocol. During the experiments, the Guiding Principles for the Care and Use of Vertebrate Animals in Research and Training published by the American Physiological Society 2014 and the National Institutes of Health Guide for the Care and Use of Laboratory Animals were followed. The Mexican National Laws on Animal Protection and the General Health Law Related to Health Research (NOM-062-Z00-1999) were also observed.

2.2. Organ baths

Guinea pig tracheal rings were placed in an organ bath as previously described (Flores-Soto et al., 2013). Tissues were submitted to a resting tension of 1 g for a duration of 30 min at the start of these experiments. To allow tissue conditioning and optimization of the contractile apparatus, three consecutive KCl (60 mM) stimulations were given. A cumulative concentration-response curve to carbachol (Cch) was constructed in the absence or presence of E2 or carboxyeosin (CE).

2.3. Intracellular Ca^{2+} measurements in tracheal myocytes

Guinea pig tracheal smooth muscles were disaggregated as previously described (Flores-Soto et al., 2013). Briefly, myocytes loaded with 2.5 μM Fura 2-AM were kept in low Ca^{2+} (0.1 mM) at room temperature (~21 °C) for 1 h. Then, cells were settled into a heated perfusion chamber with a glass cover at the bottom, and the chamber was mounted on an inverted microscope (Diaphot 200, Nikon, Tokyo, Japan). Cells were given alternating pulses of 340 and 380 nm excitation light, and emission light was collected at 510 nm using a microphotometer from Photon Technology International Model D-104 (PTI, Princeton, NJ, USA).

To determine intracellular Ca^{2+} concentration ($[Ca^{2+}]_i$), the Grynkiewicz formula (Grynkiewicz et al., 1985), with a Kd for fura 2-AM of 386 nM, was employed. Fluorescence was registered every 0.5 s, and the mean 340/380 fluorescence ratios Rmax and Rmin were 6.6 and 0.39, respectively. Data were stored in a computer and afterwards analyzed with a specialized software (Felix, version 1.21, PTI).

After basal Ca^{2+} concentrations measurement, cells were stimulated with Caffeine (Caf, 10 mM) in the presence of E2, Propylpyrazoletriol (PPT, an ERα specific agonist), Diarylpropionitrile (DPN, an ERβ agonist), U-0126 (an inhibitor of ERK 1/2) or Ca^{2+} ATPases inhibitors lanthanum (La^{3+}), carboxyeosin (CE) and cyclopiazonic acid (CPA). The Ca^{2+} response to the substitution of the 118 mM NaCl in Krebs with choline chloride (CC, 143 mM) followed by an immediate Caf (10 mM) response with or without E2 (10 nM) was assessed. To evaluate the mitochondrial Ca^{2+} uniporter (MCU), the myocytes were stimulated with carbonyl cyanide 4-(trifluoromethoxy)phenylhydrazone (FCCP, 10 μM, an activator of MCU) with or without E2 (10 nM). To induce the

capacitative Ca^{2+} entry, the cells were stimulated with Caf (10 nM), and afterwards a Ca^{2+}-free Krebs solution containing 0.1 mM EGTA was perfused for 10 min, with cyclopiazonic acid (10 μM) added for the las 5 min before restoring the Ca^{2+}-containing Krebs perfusion with or without E2 (10 nM).

2.4. Western blot

Guinea pig tracheal smooth muscle strips freed of epithelium and connective tissue were collected. A pellet pestle (Kimble, DWK Life Sciences) was used to homogenize each tissue in 30 μL RIPA lysis buffer (Santa Cruz Biotechnology, cat. No. sc-24948, Santa Cruz, CA, USA) containing protease inhibitor cocktail (Sigma, cat. No. P8340). The homogenized samples were centrifuged at 5000 rpm and 4 °C for 15 min. A commercial kit (RC DC Protein Assay, catalog 500–0119, Bio-Rad, Hercules, CA, USA) was used to measure total protein concentration. Samples (30 μg each) were split into different lanes of 10% SDS-polyacrylamide gel and electrophoresed under reducing conditions. Proteins were transferred to a Bio-Rad polyvinylidene fluoride membrane and blocked with 5% nonfat dry milk in PBS tween (Tween 20, 0.1%) for 1 h at room temperature. A rabbit polyclonal (GTX130858; 1:500 dilution, GeneTex, Irvine, CA, USA) and mouse monoclonal (GTX22783; 1:1000 dilution, GeneTex) antibodies prepared against PMCA1 and PMCA4, respectively, were incubated on the membranes at 4 °C for an entire night. Subsequently, the membranes were treated for 2 h at room temperature with a goat anti-rabbit and anti-mouse IgG secondary antibody (1:500) coupled with horseradish peroxidase, respectively. β-actin (A1978, Merck KGaA, Darmstadt, Germany) was used as a loading control. An improved chemiluminescent reactant (Luminol; Santa Cruz Biotechnology, cat. No. sc-2048 CA, USA) was used to generate immunoblots, and scanned with a C-DiGit Blot Scanner (LI-COR Biotechnology, Lincoln, NE).

2.5. Docking modeling

First, we prepared protein structures for the docking analysis, as follows. Both PMCA1 (ID PDB: 6A69) and SERCA2b (ID PDB: 6LN7) protein structures were obtained from the Protein Data Bank (https://www.rcsb.org/). Additionally, the PMCA4 (ID: P23634) protein structure was obtained from the AlphaFold Protein Structure Database (https://alphafold.ebi.ac.uk/). All protein structures were refined using the USCF Chimera software version 1.15 (https://www.cgl.ucsf.edu/chimera) as previously described (Barrera-Vazquez et al., 2023). The AMBER ff14SB amino acid force field was also considered (Pearlman et al., 1995). Both the Ca^{2+} and Mg^{2+} ions were preserved. Then, ligands (5(6)-Carboxyeosin (SID: 44119976), 17β-Estradiol (SID: 349982835), Cyclopiazonic acid (SID: 198943370), Diarylpropionitrile (SID: 405282160), Propylpyrazoletriol (SID: 5 040063), (R,R)-5,11-Diethyl-5,6,11,12-tetrahydro-2,8-chrysenediol (SID: 341713655) were obtained from the PubChem database (https://pubchem.ncbi.nlm.nih.gov) and were geometrically optimized using Avogadro software (software version 1.2.0 https://avogadro.cc/). The possible ionization state was generated at pH values of 7.0 ± 0.5. The calculation for the partial charges of the ligand atoms were done according to the Gasteiger method (Gasteiger and Marsili, 1980), using the USCF Chimera software version 1.15 (https://www.cgl.ucsf.edu/chimera). Blind and rigid docking analyses were performed using the AutoDock 4.2.6 software (https://autodock.scripps.edu/) and the AutoDock Vina Version 1.1.2 extension (Pettersen et al., 2004). Linkages, interactions, and distances among protein and ligands were obtained with USCF Chimera software Version 1.15 and Discovery Studio Visualizer Version 21.1.0, CA, USA (https://www.3ds.com/). Only the most stable configurations of protein-ligand binding, based on terms of energy (ΔG), were considered for this study.

2.6. Drugs and reagents

17β-estradiol [1,3,5(10)-estratriene-3-17β-E2; 10 and 32 nM], carbamylcholine chloride (carbachol; 0.1, 0.32, 1, 3.2 and 10 μM), methoxyverapamil (D600, 30 μM), lanthanum (100 μM), (5(6)-Carboxyeosin (32 and 100 nM), Cyclopiazonic Acid (10 μM), U-0126 (10 μM), Diarylpropionitrile (10 nM), Propylpyrazoletriol (10 nM), Choline chloride (CC, 143 mM) and Carbonyl cyanide 4-(trifluoromethoxy) phenylhydrazone (FCCP, 10 μM) were obtained from Sigma Chemical Co. (St. Louis, MO, USA). Carboxyeosin was obtained from Abcam (Cambridge, UK).

2.7. Statistical analysis

Single-cell $[Ca^{2+}]_i$ results were evaluated through a one-way analysis of variance followed by Dunnett's. Comparison among groups in the organ baths experiments was carried out through a one-way analysis of variance followed by Dunnett's test. Statistical significance was set at $p < 0.05$ bimarginally. Reactivity to Cch was evaluated through the effective concentration 50% (EC_{50}) and maximum response. The EC_{50} was calculated from the cumulative concentration–response curve by straight-line regression as -Log using the ED50plus v1.0 software and is expressed as nM concentration. The area under the curve (AUC) was analyzed in Graphpad Prism 9.0.2, expressed as the mean ± SEM, the significance was determined by a one-way analysis of variance followed by Dunnett's test.

3. Results

3.1. Effect of estradiol on the carbachol-induced contraction

In guinea pig tracheal rings, Cch induced a concentration-dependent contraction; preincubation with E2 for 15 min augmented the maximum response to Cch (Fig. 1A, n = 5). Increased responsiveness began at 1 μM Cch when incubated with E2 (32 nM); at 3.2 μM Cch, differences were observed in the E2 10 and 32 nM groups, and at 10 μM Cch, all E2 groups had a significant increment. No differences were observed in the EC_{50} in any of the groups (Fig. 1B).

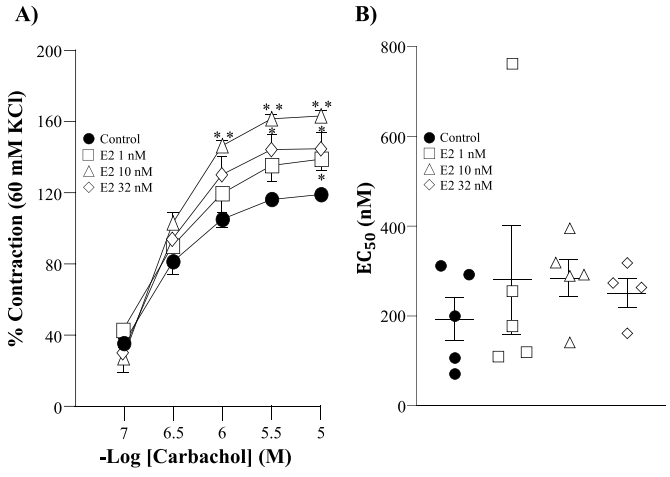

Fig. 1. Effect of estradiol on the guinea pig tracheal smooth muscle contraction induced by carbachol. **A)** Cumulative concentration-response curves to carbachol with and without 17β-estradiol (E2) in guinea pig tracheal rings. **B)** Graph illustrating EC_{50} values for the Cch curves with and without E2. The symbols represent the mean ± the standard error of the mean (SEM). *$p < 0.05$, **$p < 0.01$ when comparing with the control group, evaluated through one-way analysis of variance followed by Dunnett's test. n = 5 for Control, E2 1 nM and 10 nM; n = 4 for E2 32 nM.

3.2. The effect of estradiol and their specific agonist receptors on the Ca^{2+} increase in response to caffeine

In guinea pig tracheal smooth muscle myocytes, stimulation with Caf induces an increase in $[Ca^{2+}]_i$, observed as a transient peak with a quick return to basal levels. This caffeine response was repeated twice (Fig. 2A, n = 5). The incubation with E2 (10 nM) for 5 min before the caffeine stimulation decreased the amplitude of the $[Ca^{2+}]_i$ response, and the transient peak was modified, producing a plateau that was only diminished when the drugs were withdrawn (Fig. 2B, n = 8). Incubation with D600 (an L-type voltage-dependent Ca^{2+} channel [L-VDCC] blocker) for 5 min showed a decrease in basal $[Ca^{2+}]_i$. There was a decrease in the amplitude of the response to Caf without modifying the transient peak (Fig. 2C, Table 1, n = 5). A similar Ca^{2+} plateau as that produced by E2 was observed when cells were incubated with PPT (10 nM, Fig. 2D–F, Table 1, n = 4) but not with DPN (10 nM, Fig. 2E, F,

Table 1
Comparison of the area under the curve (AUC) of the caffeine-induced Ca^{2+} response in the presence of E2, D600, PPT or DPN.

Treatment groups	AUC ± SEM
E2	61534 ± 4672
D600	24352 ± 648.7**
PPT	70489 ± 1368*
DPN	38117 ± 911**

AUC analysis of the Ca^{2+} response to Caffeine in the presence of E2 (10 nM), D600 (30 μM), PPT (10 nM), or DPN (10 nM). Data represented as AUC ± SEM. The data were analyzed by a one-way variance analysis followed by Dunnett's test. *p < 0.05, **p < 0.01, when comparing with E2 group. n = 8 for E2, n = 5 for D600, n = 4 for PPT and n = 5 for DPN.

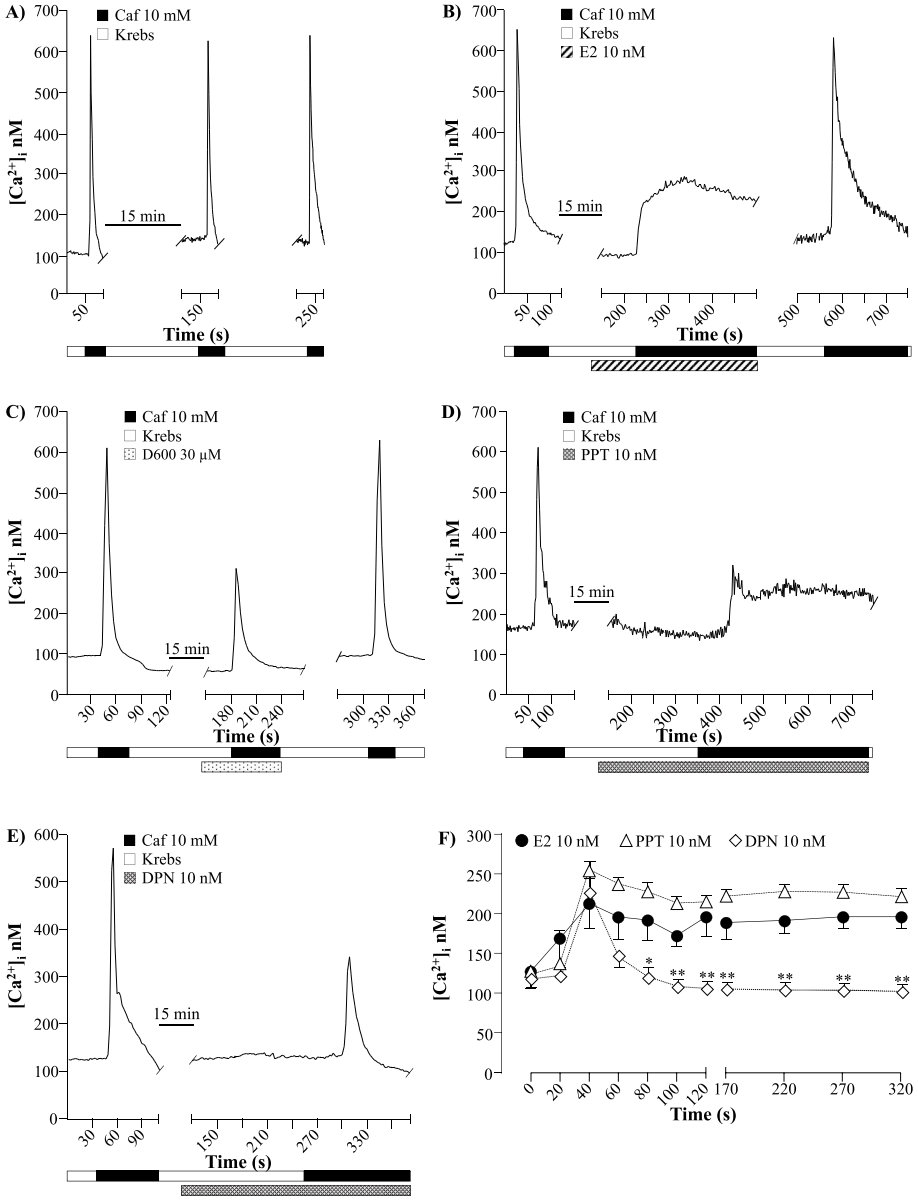

Fig. 2. Comparison between the caffeine response in the presence of estradiol and specific estrogen receptors (ER) agonists in tracheal myocytes. **A)** Control recording of the increment in $[Ca^{2+}]_i$ induced by repeated caffeine (Caf, 10 mM) stimulations after 15 min washouts. Caf $[Ca^{2+}]_i$ response after a 5 min incubation period with **B)** 17β-estradiol (E2, 10 nM), **C)** D600 (30 μM), **D)** PPT (10 nM) or **E)** DPN (10 nM). **F)** Comparison of the time course of the Ca^{2+}responses induced by caffeine in the presence of E2, PPT or DPN. The symbols represent the mean ± standard error of the mean (SEM). The analysis was carried out through a one-way analysis of variance followed by Dunnett's test. *p < 0.05, **p < 0.01 when comparing with E2 group. n = 8 for E2, n = 5 for D600, n = 4 for PPT and n = 5 for DPN.

Table 1, n = 5).

To corroborate that the phenomenon observed with E2 was not mediated by the cellular signaling pathway of extracellular signal-regulated kinases 1 and 2 (ERK 1/2), we utilized U-0126 (an inhibitor of ERK 1/2, 10 μM) (Reyes-García et al., 2018). In guinea pig tracheal myocytes, the incubation with U-0126 for 5 min diminished the amplitude of the transient Ca^{2+} peak induced by Caf (Fig. 3A, n = 3). Additionally, U-0126 was incubated for 7 min, and E2 was added during the last 5 min, followed by a Caf stimulus producing a Ca^{2+} plateau that was only diminished after withdrawing the drugs (Fig. 3B, n = 3).

To induce the inversion of the NCX (NCXrev), and study if it was involved in the phenomenon produced by E2, the 118 mM NaCl was substituted with choline chloride (CC, 143 mM) in normal Krebs solution, inducing a transient Ca^{2+} increment, when immediately afterwards the cells were stimulated with Caf and it was observed that the Ca^{2+} peak was not altered (Fig. 3C). After a 5 min incubation period with E2, the response to CC was significantly reduced (Fig. 3D); however, the stimulation with Caf following the response with CC did not affect the Caf-induced Ca^{2+} plateau. FCCP was used to evaluate whether E2 affected the mitochondrial Ca^{2+} uniporter (MCU). FCCP induced a transient Ca^{2+} increase, which was not altered after a 5 min incubation with E2 (Fig. 3E–F). Additionally, store-operated Ca^{2+} channels (SOCCs) were evaluated by measuring the capacitative Ca^{2+} entry after restoring Ca^{2+} back to the perfusion solution. No differences were observed in the capacitative Ca^{2+} entry after E2 incubation (Fig. 3G–H).

3.3. Effect of the inhibition of the plasma membrane and sarcoplasmic reticulum calcium ATPases on the Ca^{2+} response to caffeine and in the carbachol-induced contraction

To explore the effect that E2 could have on PMCA, a concentration-response curve was performed with lanthanum (La^{3+}, 100 μM, 1 mM, and 3 mM, Fig. 4A) and carboxyeosin (CE, 1, 32, 100, 320, 1000 nM, Fig. 4B) (Gatto and Milanick, 1993; Herscher and Rega, 1996). We observed a characteristic increment in the $[Ca^{2+}]_i$ to La^{3+} and CE in accordance with those reported in the literature (Chen et al., 2014; Reyes-García et al., 2018). La^{3+} 100 μM and CE 100 nM were chosen for further experiments since they were the lowest concentrations that increased the $[Ca^{2+}]_i$ (Fig. 4A and B). In the subsequent experiments, ASM myocytes were incubated with E2 for 5 min and La^{3+} or CE for the last 4 min before the 2nd caffeine stimulus. Both E2 and La^{3+} or CE remained present during Caf stimulus. Neither La^{3+} nor CE modified the $[Ca^{2+}]_i$ (Fig. 4C and D), as is the characteristic response of the inhibition of PMCA. The 2nd response to caffeine with La^{3+} showed a Ca^{2+} peak that slowly fell to a plateau sustained during the presence of caffeine (Fig. 4C), while with CE it was a transient peak (Fig. 4D). We observed significant differences in $[Ca^{2+}]_i$ from 170 to 320 s between E2 vs E2/La^{3+} groups (Fig. 4E, Table 2, n = 6 in the E2 group and n = 5 in the E2/La^{3+} group) and from 80 to 320 s in the E2 vs E2/CE groups (Fig. 4E, Table 2, n = 6 in the E2 group and n = 6 for E2/CE group).

To investigate the effect that E2 could have on PMCA, CE (100 nM) was used. In guinea pig tracheal smooth muscle, Cch induced a concentration-dependent (0.1, 0.32, 1, 3.2, 10 μM) contraction. Responses to 0.32 μM and further concentrations of Cch were significantly increased when tissues were incubated for 15 min with 100 nM of CE (Fig. 4F); no differences were observed in the EC_{50} (Fig. 4G).

Western blot analysis in guinea pig ASM tissue confirmed the presence of PMCA1 and PMCA4 (Fig. 5A and B) as previously described in rat ASM (Chen et al., 2014).

The addition of CPA (10 μM, 2.5 min) did not modify the phenomenon caused by E2 incubation in the Ca^{2+} response induced by Caf, indicating that the mechanisms activated are independent of SERCA activity (Fig. 6A–B). Note that after CPA removal 5 min elapse before the caffeine response was elicited. If CPA is not withdrawn no Ca^{2+} response is developed.

3.4. 17β-estradiol interacts with PMCA1 and PMCA4 similarly to ER agonists

We performed molecular docking to predict the binding affinity between 17β-estradiol and the ER-specific agonists PPT and DPN with the isoforms PMCA1 and 4. In Fig. 7A, the PMCA1 is depicted in orientation to the plasma membrane and the modulation sites for Ca^{2+}/calmodulin and PKA phosphorylation are labeled for reference (in the 1100–1117 and the Ser-1178 sites respectively). The interaction E2-PMCA1 shows a stable conformation (Fig. 7B, ΔG = −8.9 kcal/mol, the more negative the ΔG is, the more equilibrium the reaction has) in the amino acids (AAs) ARG182, ARG458, LEU460, PHE1144, HIS1147, and PHE181. Interestingly, the results in Fig. 7C show that CE binds to PMCA1 (ΔG = −7.1 kcal/mol) by interactions with different AAs in comparison to the E2-PMCA1 (ILE90, PRO91, PRO92, LYS93, LYS94, PHE288, THR289, GLY292, ALA293, and GLU296); such interactions are stabilized by hydrogen bonds, van der Waals bonds, Pi-Alkyl and Pi-Anion unions. On the other hand, we also performed the docking between PPT and PMCA1 (Fig. 7D, ΔG = −8.6 kcal/mol), and interestingly, such interaction is similar (LYS177, ARG458, PRO1148, ARG182, LEU460, and PHE181) in comparison to the conformation between E2 and PMCA1. Additionally, to find out if the ligands (CE, E2, and PPT) have similar effects on PMCA, we also performed the docking between DPN and PMCA1. According to the results, the interaction DNP-PMCA1 (Fig. 7E, ΔG = −6.4 kcal/mol) is stabilized by ASN543, LYS583, ALA603, ILE648, and PHE578; although these are different AAs that stabilize the interaction between CE, E2 or PTT and PMCA1.

We also performed the docking between PMCA4 and the ligands CE, E2, or PPT. Fig. 8A depicts PMCA4 in orientation to the plasma membrane and labels the Ca^{2+}/calmodulin binding site in the 1086–1103 AAs. Our results show that none of the interactions between PMCA4 and the ligands (E2-PMCA4, ΔG of −8.1 kcal/mol; CE- PMCA4, ΔG of −7.5 kcal/mol; and PPT-PMCA4, ΔG of −7.6 kcal/mol, Fig. 8B–E, respectively) is as prominent as with PMCA1. Finally, we also performed the docking between SERCA2b and the ligands (E2, CPA, PPT, and DPN) (Fig. 9A–D), and found that these interactions are also very low.

4. Discussion

Our results indicate that in guinea pig ASM, E2 induces AHR to Cch via the non-genomic inhibition of the plasma membrane Ca^{2+}-ATPase. Furthermore, this effect appears to be through the direct interaction between E2 or PPT and PMCA, as suggested by the molecular docking results and Ca^{2+} measurement experiments. To our knowledge, this is the first report of E2 non-genomic effects on PMCA in ASM cells.

In many cell types, Ca^{2+} signaling constitutes a vital phenomenon. To keep cells in optimal condition, Ca^{2+} homeostasis is maintained by a Ca^{2+} toolkit comprised of channels, pumps, and exchangers. These mechanisms are subjected to internal and external influences, including hormonal regulation (Romero-Martínez et al., 2023). In ASM, E2 acute effect on Ca^{2+} channels has been explored, and it has been established that E2 exposure inhibits the L-VDCC and partially the SOCCs, a response mediated by the ERα (Flores-Soto et al., 2017; Townsend et al., 2010).

Usually, in ASM, Caf induced a Ca^{2+} transient peak due to Ca^{2+} release from the SR, previously refilled with Ca^{2+} provided by the L-VDCC and SOCCs activity (Flores-Soto et al., 2013). However, the sole blockade of L-VDCCs does not alter the kinetics of the Ca^{2+} response induced by Caf, as observed in Fig. 2C; it only decreases the amplitude of the Ca^{2+} peak. Because the Ca^{2+} response to Caf in the presence of E2 does not show a Ca^{2+} peak, but instead, a sustained response, the implication of other Ca^{2+}-handling proteins is pointed out. We excluded the participation of NCXrev, MCU, or capacitative Ca^{2+} entry as they did not participate in this phenomenon. In this sense, scant research, mainly exploring genomic effects, considers what consequences E2 might exert on the PMCA.

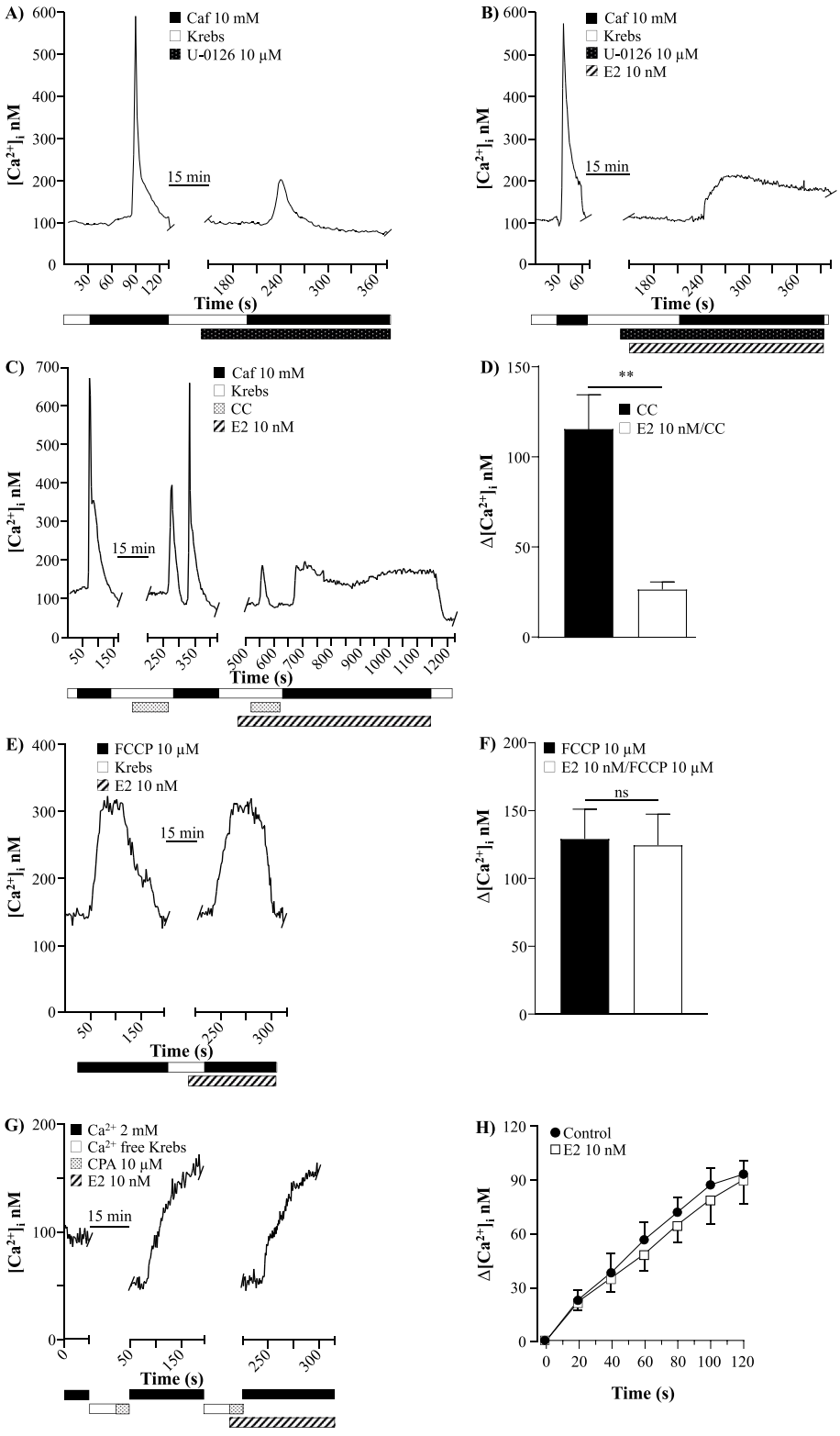

(caption on next page)

Fig. 3. Comparison of E2 effects on different mechanisms involved in handling $[Ca^{2+}]_i$ in tracheal myocytes. **A)** Original recording of the first Ca^{2+} response to Caf (10 mM). After a 10-min washout, U-0126 (10 μM, n = 3) was incubated for 5 min before a 2nd Caf stimulus, inducing a transient Ca^{2+} peak. **B)** Recording of the Caf control Ca^{2+} peak. After a 10-min washout, the cell was incubated with U-0126 for 2 min, and then E2 (10 nM) was added for 5 min (U-0126 incubation period lasted 7 min, n = 3). A final Caf stimulus produced a Ca^{2+} plateau. Both U-0126 and E2 were present during the stimulus. **C)** Initial Ca^{2+} response to Caf (10 mM), followed by a 15 min washout. The cell is then stimulated with a choline chloride (CC, 143 mM) substitution of the 118 mM NaCl in the Krebs solution, inducing a transient increment in the $[Ca^{2+}]_i$. The immediate stimulation with Caf after CC withdrawal, produces a Ca^{2+} peak comparable to the first one. After a 10 min washout, E2 (10 nM) was added again and after 5 min CC was given, showing a diminished response. After CC removal, the Caf-induced Ca^{2+} response is a plateau. **D)** The $[Ca^{2+}]_i$ increment induced by CC was significantly different from that produced by E2/CC. The statistical analysis was a Student's *t*-test; $^{**}p < 0.01$. n = 10. **E)** Ca^{2+} response to the stimulus with FCCP (10 μM) and FCCP after a 5 min incubation with E2, and no statistical differences were found, n = 6 **(F)**. **G)** To induce the capacitative Ca^{2+} entry, the cell was incubated for 10 min in Ca^{2+}-free medium (0.1 mM EGTA) and CPA (10 μM) for 5 min. Afterwards, the cell was perfused with Ca^{2+}-containing Krebs and a slow increment in $[Ca^{2+}]$i was observed. Then, the cell was again perfused with Ca^{2+}-free Krebs solution for 10 min and CPA/E2 for 5 min. Ca^{2+} was restored in the presence of E2 only and a similar Ca^{2+} response was appreciated. **H)** Graphs depicting no statistical differences in the capacitative Ca^{2+} entry due to E2 incubation, n = 7. Data in all figures are expressed as the mean ± SEM.

One study reported that E2 treatment (40 μg/kg/day) for 72 h in prepubescent female rats decreased the expression of PMCA1 in the esophagus (Kim et al., 2017). In human fibroblast-like synovial cells and mouse macrophage-like cells, E2 reduced the expression of PMCA2 and 4 (El-Beialy et al., 2010), and PMCA1 in mouse uterus (Tran et al., 2018). Through genomic mechanisms, E2 increases the expression of PMCA4b in MCF-7 cells (Varga et al., 2018) and PMCA1 in human endometrium (Yang et al., 2011). Interestingly, in distal tubule kidney cells, E2 incubation for 24 h enhanced PMCA activity without altering its expression (Dick et al., 2003). Because the incubation of E2 lasted a short period, our results hint that, by directly (non-genomic effect) inhibiting the PMCA pump, E2 alters the decay phase of the Caf response, producing the Ca^{2+} plateau.

Estradiol has been shown to activate a multitude of pathways including cAMP production (Townsend, Sathish, et al., 2012b), mitogen-activated protein kinases (MAPK) (Bi et al., 2000; Purves-Tyson and Keast, 2004; Stamatiou et al., 2011; Watters et al., 1997), protein kinase A (Harrison et al., 2000; Vasudevan et al., 2001), protein kinase C (Vasudevan et al., 2001) and tyrosine kinase (Bi et al., 2000). Furthermore, PMCA has been shown to be subjected to kinase modulation (Babnigg et al., 2003; Bruce et al., 2002; Wright et al., 1993). Additionally, in HEK293T cells, E2 was shown to nongenomically decrease the phosphorylation of the stromal interaction molecule 1 (STIM1, a capacitative Ca^{2+} entry structure), inhibiting its mobility and activation (Sheridan et al., 2013). Interestingly, the incubation of ASM cells during 24 h with E2 also produced a similar effect, inhibiting the phosphorylation of STIM1, thus decreasing the SOCCs histamine-induced Ca^{2+} response enhanced by cigarette smoke extract (Sathish et al., 2015).

Specifically, in the ASM, the ERK 1/2 and MAPK pathway is known to regulate the basal activation of the L-VDCCs (Reyes-García et al., 2018), which explains the diminished amplitude of the Caf-induced Ca^{2+} peak produced in the presence of U-0126, an ERK1/2 inhibitor (Fig. 3A). Furthermore, E2 has been shown to activate the ERK pathway in various tissue models (Endoh et al., 1997; Migliaccio et al., 1998; Townsend, Miller, et al., 2012a), including ASM (Stamatiou et al., 2011). Meanwhile, PMCA activity has been reported to be regulated by non-genomic estradiol effects in rat cortical synaptosomes and human erythrocytes (Szemraj et al., 2003), and hepatocytes (Stratton et al., 2010). Furthermore, in vascular endothelium, it was demonstrated that E2 decreases the activity of PMCA by a GPR30/ERK1/2/MAPK/calmodulin (CaM) pathway by genomically regulating the expression of CaM, resulting in higher $[Ca^{2+}]_i$ and Ca^{2+}-CaM interactions (Tran et al., 2016). It should be noted that in ASM cells, the expression of the GPR30 is not significant (Aravamudan et al., 2017). The Caf-induced Ca^{2+} plateau produced by the incubation with E2 was not modified by the previous addition of U-0126. Therefore, the participation of the ERK 1/2 in this phenomenon can be ruled out (Fig. 3B). However, the possibility of other phosphorylation pathways as well as the direct interaction of E2 on PMCA still requires further studies to clarify if they participate in this phenomenon.

Meanwhile, E2 effects on SERCA were studied in ASM cells subjected to inflammatory mediators. Human ASM incubated with TNF-α or IL-13 showed diminished SERCA2 expression that was reverted by an ERβ specific agonist (WAY 10 nM). This response was not observed with E2 or with the ERα specific agonist PPT. The activation of ERβ decreases $[Ca^{2+}]_i$ in a proinflammatory state in ASM cells (Bhallamudi et al., 2020). However, there has been no previous report of a non-genomic effect of E2 over the Ca^{2+} ATPases. In this sense, E2 produced a Ca^{2+} plateau in response to the stimuli with Caf. The inhibition of PMCA with La^{3+} or CE in a cell previously incubated with E2 did not modify the basal $[Ca^{2+}]_i$, and when stimulated with Caf, the Ca^{2+} plateau observed in the presence of E2 alone was partially reverted, indicating that E2 is inhibiting PMCA. Alternatively, when myocytes were stimulated with CPA and E2, the Ca^{2+} plateau was not altered, indicating that E2 is not affecting SERCA.

In this context, E2, through non-genomic mechanisms, dysregulates the $[Ca^{2+}]_i$ by blocking L-VDCCs, and decreasing the amplitude of the peak by limiting the Ca^{2+} available for the SR refilling, and by inhibiting the PMCA pump, E2 alters the decay phase of the Caf response, producing the Ca^{2+} plateau.

Conceivably, any modification in the Ca^{2+} handling mechanisms that leads to a higher $[Ca^{2+}]_i$, could predispose ASM to hyperresponsiveness. This phenomenon is observed as a leftward shift of the agonist cumulative response curve or an increase in the maximum contractile response (Hirota et al., 2005). AHR can be caused by an increase in contractility of the ASM, either through an increase in $[Ca^{2+}]_i$ or mechanisms of Ca^{2+} sensitivity (Hirota et al., 2005; Jain et al., 2001; Perez-Zoghbi et al., 2009; Somlyo and Somlyo, 2003). This possibility was explored through our organ bath experiments. The inhibition of PMCA by CE induced hyperresponsiveness to Cch in the guinea pig tracheal rings. It has been documented that the inhibition of PMCA or SERCA leads to an increment in $[Ca^{2+}]_i$ (Chen et al., 2014; Reyes-García et al., 2018) and could cause AHR, a probability confirmed in our research. Interestingly, a higher activity of the Ca^{2+}-ATPase in ASM cells from sensitized guinea pigs has been reported, probably as a compensatory mechanism activated in response to the higher $[Ca^{2+}]_i$ (Jain et al., 2001); nonetheless, it still remains to find out if this compensatory mechanism is altered by E2 addition. In this regard, our results using La^{3+} or CE plus E2 could be pointing out a compensatory Ca^{2+} handling mechanism (probably SERCA) as might be seen in Fig. 4E. Furthermore, when La^{3+} or CE are added alone (Fig. 4A and B) increases in the basal Ca^{2+} concentration are seen. Interestingly, this Ca^{2+} concentration increment is abolished after the incubation with E2 and the subsequent addition of La^{3+} or CE (Fig. 4C and D).

The concentration-response curve to Cch in the presence of E2 showed a similar effect as that elicited by CE, with statistical significance for the maximum response. This finding sustains our proposal that E2 inhibits PMCA, consequently inducing hyperresponsiveness. The Ca^{2+} experiments performed with the ER-specific agonists indicate that the phenomenon also occurs with PPT through a direct interaction with the PMCA.

Since we explored the consequences that acute exposure to E2 might cause in ASM, it is possible that these results could be related to perimenstrual asthma, a period of symptom exacerbation suffered by many

asthmatic women. Regarding the role of E2 in AHR, the airway reactivity response to methacholine in prepubescent male and female mice was compared to the response of the 12-week-old mice. In the first experimental protocol, males demonstrated a significantly greater response than females. At 12 weeks, this effect was reversed, and a significantly increased AHR was observed, indicating that the response was linked to the age and sex of the mice (McKenzie et al., 2010). When comparing ovalbumin (OVA)-sensitized ovariectomized (OVX) mice treated with E2 to a sham group, an OVA-sham group, and an OVX-OVA group, the OVX-OVA-E2 group presented increased airway resistance to the methacholine challenge (Warren et al., 2023). Note that the McKenzie et al. research was done in non-sensitized mice, implying that

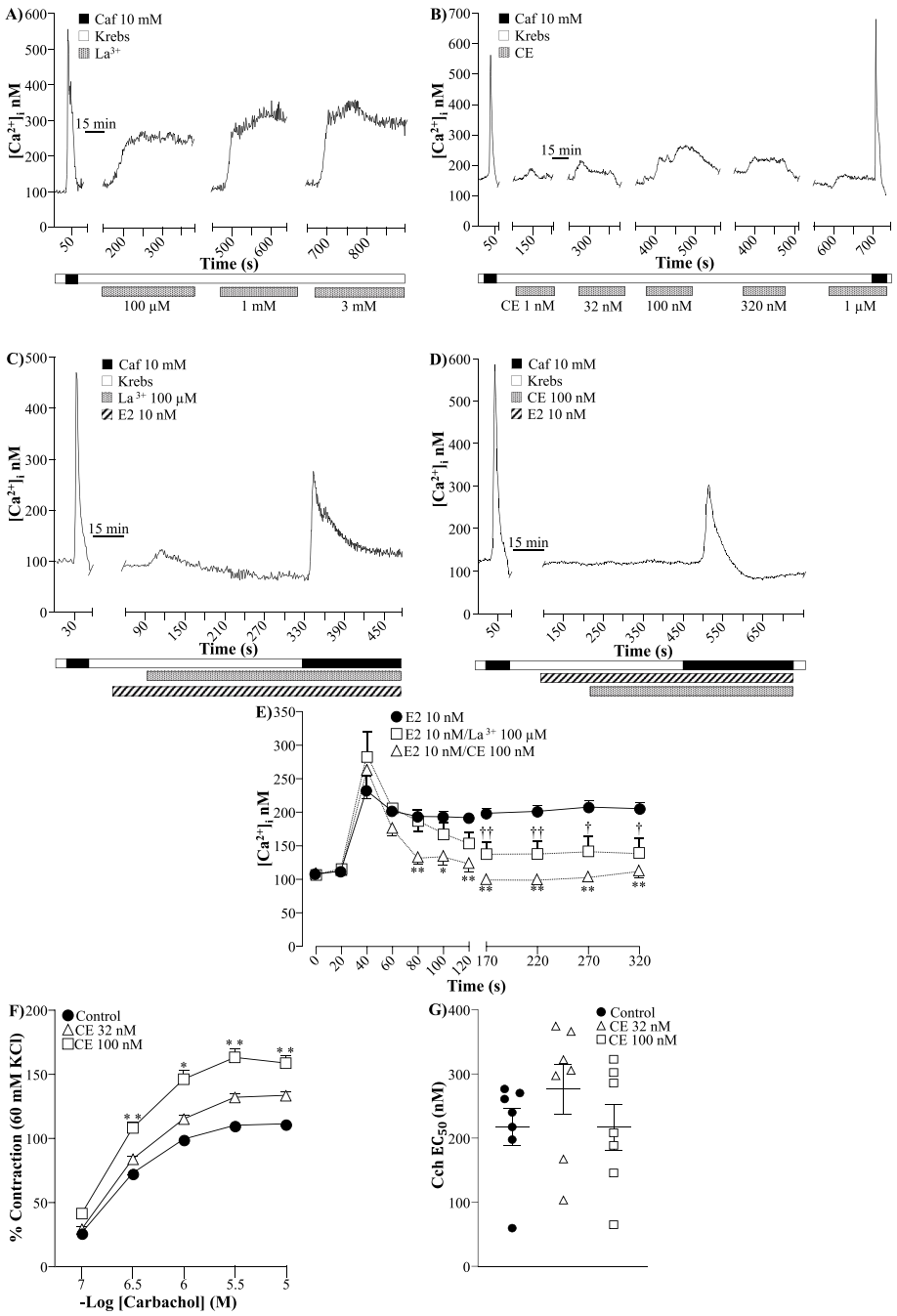

Fig. 4. Effect of the inhibition of the plasma membrane Ca^{2+}-ATPase (PMCA) on the Ca^{2+} response to caffeine (Caf) and the carbachol-induced contraction in the presence of E2. **A)** After corroborating cell viability with Caf a concentration-response curve of the sustained increase in $[Ca^{2+}]_i$ induced by lanthanum (La^{3+}) is illustrated. **B)** Concentration-response curve to carboxyeosin (CE) and the corresponding increases in $[Ca^{2+}]_i$. **C)** Recording of the first control Caf (10 mM) Ca^{2+} peak. After a 10-min washout, the cell was incubated with E2 (10 nM) for 1 min, and then La^{3+} (100 µM) was added for 4 min (E2 had a total of 5 min incubation period), followed by the 2nd Caf response, producing a Ca^{2+} peak that slowly fell to a plateau. Both E2 and La^{3+} were always present. **D)** After the first Caf stimulation showing a Ca^{2+} peak, following a 10-min washout, the cell was incubated with E2 for 5 min, and during the last 4 min with CE (100 nM) as well and then a second Caf stimulus was given. This last procedure also induced a Ca^{2+} peak, although smaller in magnitude, that slowly fell below the initial Ca^{2+} baseline. **E)** Comparison of the time course of the Ca^{2+}responses induced by caffeine in the presence of E2, E2/La^{3+} or E2/CE. *p < 0.05, **p < 0.01, †p < 0.05, ††p < 0.01 when compared to E2 group. n = 6 for E2, n = 5 for E2/La^{3+}, n = 6 for E2/CE. **F)** The pharmacological inhibition of PMCA through CE 100 nM preincubation in organ baths induced a significant increase in the maximum response to Cch. *p < 0.05, **p < 0.01, n = 7. **G)** There was no modification in the EC_{50}. The symbols represent the mean ± standard error of the mean (SEM). For the analysis a one-way analysis of variance followed by Dunnett's test was performed.

Table 2
Comparison of the area under the curve (AUC) of the caffeine-induced Ca^{2+} response in the presence of E2, La^{3+}/E2 or CE/E2.

Treatment groups	AUC ± SEM
E2	62778 ± 1749
La^{3+}	50235 ± 3593**
CE	39780 ± 2540**

AUC analysis of the Ca^{2+} response to Caffeine in the presence of E2 (10 nM), La^{3+} (100 μM) or CE (100 nM). Data represented as AUC ± SEM. The data were analyzed by a one-way variance analysis followed by Dunnett's test. **$p < 0.01$ when comparing with E2 group. $n = 6$ for E2, $n = 5$ for La^{3+}, and $n = 6$ for CE.

hormonal changes might be responsible for the AHR found in the older female mice. In another study, the lung function and airway responsiveness to inhaled methacholine and serotonin in ERα-knockout female mice was enhanced when compared to wildtype female counterparts or to ERβ-knockout female mice (Carey et al., 2007). This change in the ERα-KO group was associated with a reduced expression of the muscarinic M2 receptor and function in the lung. Furthermore, when submitted to ovalbumin sensitization, the ERα-KO mice had increased AHR without increased inflammation, indicating that ERα is crucial in the airway response to bronchoconstrictor agonists and dysregulation may lead to AHR. Airway responsiveness seems to be under regulation of differential ER activation and this impacts asthma severity in women, as indicated by Ambhore et al., 2019, through in vitro studies, where ASM myocytes from asthmatic patients showed a higher expression of ERβ, and an ERβ agonist-mediated decrease in airway remodeling (Ambhore et al., 2019). Regarding respiratory function parameters, a study done in female, male and OVX-mice exposed to mixed allergens (MA) showed that females had a higher airway resistance, elastance and tissue-dampening, with a lower compliance. When these females were treated with an ERβ agonist (WAY), the changes induced by MA were reverted, a phenomenon that was not observed in the case of an ERα agonist (PPT). Additionally, MA exposure caused an increase in mRNA and protein expression for both ERα and ERβ as well as remodeling genes, which was reverted with WAY treatment, indicating that ERβ might downregulate AHR and airway remodeling (Ambhore et al., 2019).

On the other hand, inflammation is a hallmark of atopic asthma. In this sense, the role played by E2 on inflammatory cells is an important research topic. For instance, it has been observed that, in peripheral blood mononuclear cells (PBMCs) from patients with mild to moderate asthma, treatment with E2 (10 nM), progesterone (1 μM) or a combination of E2+progesterone increased the expression levels of GATA-3 and the production of IL-4. GATA-3 is a transcription factor that regulates the production of Th2-related cytokines, and IL-4 is a product of the type 2 inflammatory response, suggesting that E2 and progesterone could be sustaining the inflammatory state seen in asthma (Nejatbakhsh Samimi et al., 2021). Similarly, in mice models, ovarian hormones

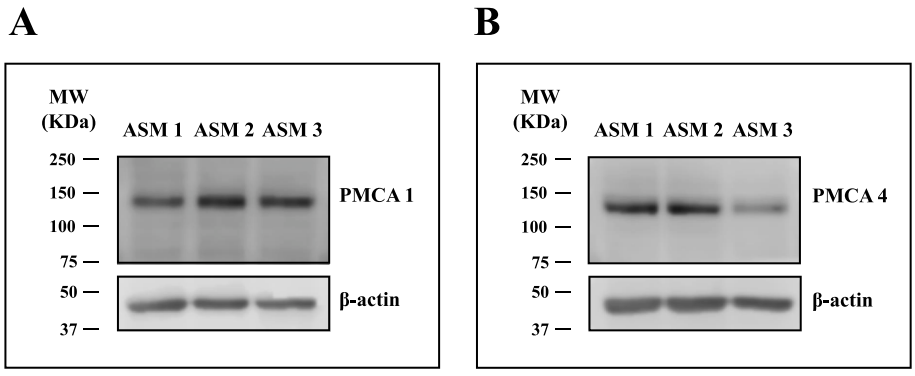

Fig. 5. Western blot showing PMCA1 and PMCA4 in guinea pig airway smooth muscle (ASM). Tissues from nine animals were collected and pooled in three different samples (ASM 1, ASM 2, and ASM 3). Panel **A** illustrates representative blots of PMCA1 with a molecular mass of 139 kDa, while panel **B** displays blots for PMCA4, with a molecular mass of 138 kDa. The molecular mass is expressed according to the specifications of the commercial antibody data sheets. β-Actin (42 kDa) was blotted as a control for protein load.

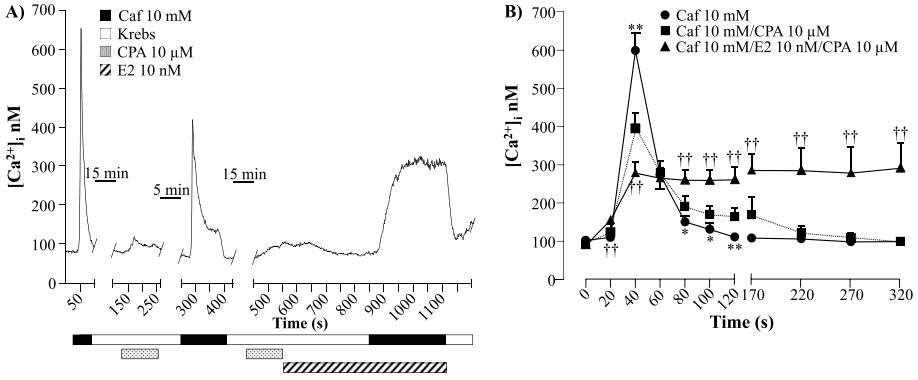

Fig. 6. Effect of the inhibition of the sarcoplasmic reticulum Ca^{2+}-ATPase on the Ca^{2+} response to caffeine in the presence of E2. **A)** Recording of the first control Caf (10 mM) Ca^{2+} peak; the second Ca^{2+} peak is the Caf response after CPA (10 μM during 2.5 min) incubation. After incubation with CPA and E2 (10 nM), adding Caf induced a Ca^{2+} plateau. **B)** Time course of the Ca^{2+} response induced by Caf alone, with CPA or CPA plus E2. The symbols represent the mean ± standard error of the mean (SEM). For the analysis a one-way analysis of variance followed by Dunnett's test was performed. *$p < 0.05$, **$p < 0.01$ when comparing with Caf/CPA group, ††$p < 0.01$ when comparing with Caf group; $n = 7$ for all groups.

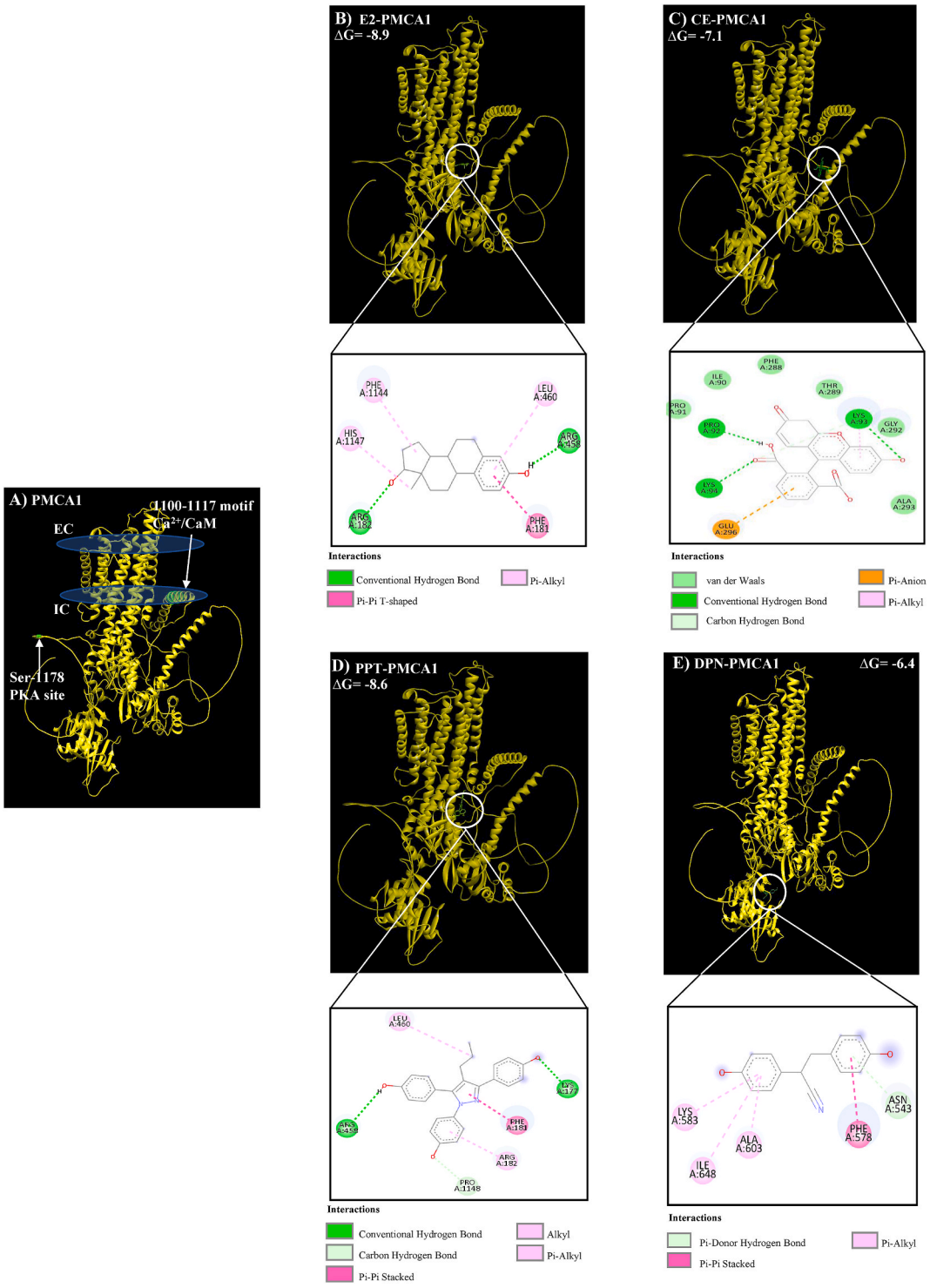

Fig. 7. Molecular docking studies illustrating interactions between estradiol (E2), carboxyeosin (CE), and the estrogen receptor (ER) specific agonists Propylpyrazoletriol (PPT) and Diarylpropionitrile (DPN) with the plasma membrane Ca^{2+}-ATPase 1 (PMCA1). **A)** Illustration depicting Ca^{2+}-calmodulin (Ca^{2+}/CaM) binding site (1100–1117 motif) and PKA activation site (Ser-1178) of the PMCA1 (Bruce, 2018; Gong et al., 2018). To facilitate comprehension of the PMCA1 orientation, the plasma membrane is represented by two blue horizontal parallel discs. EC: extracellular space. IC: intracellular space. **B)** Illustration showing possible molecular relations between E2 and PMCA1. **C)** Graphic representation of the probable interactions of CE with PMCA1. **D)** Picture of the PMCA1 protein and its proposed connections with PPT. **E)** PMCA1 display presenting feasible molecular interactions with DPN.

increased type 2 immune response as well as IL-17 production and eosinophil and neutrophil infiltration (Fuseini et al., 2018).

Moreover, in accordance with our results, both PMCA1 and PMCA4 are expressed in guinea pig ASM cells, but the effect of E2 on $[Ca^{2+}]_i$ may be mediated by its interaction with PMCA1 since the molecular docking of such conformation suggests that this is the most stable interaction, even in comparison to the interaction between CE and PMCA1. The differences between the ΔGs of both interactions are in part due to the AAs that underlie the binding of the ligands (E2 and CE) with PMCA1, suggesting that the binding sites are different for each ligand,

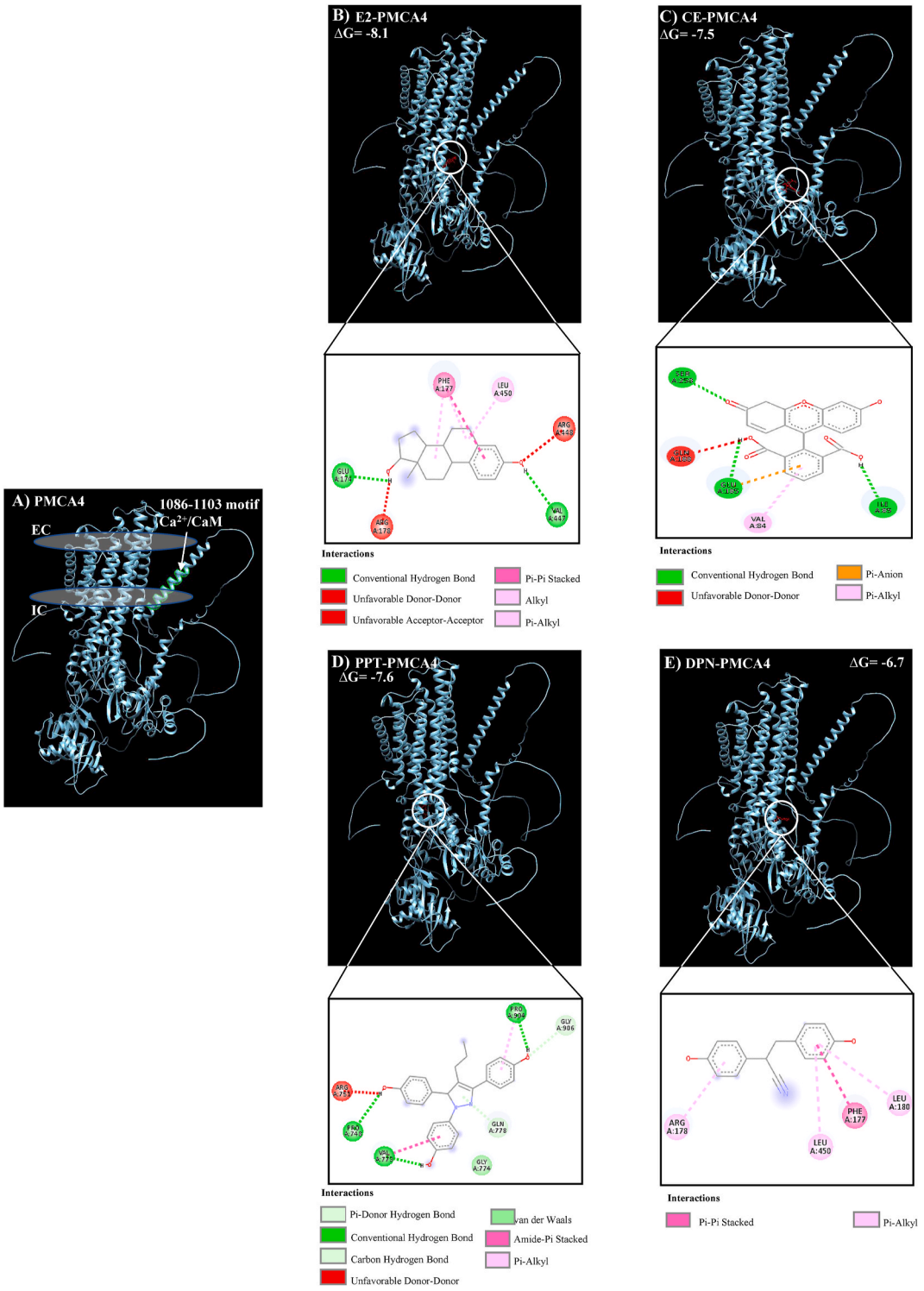

Fig. 8. Molecular docking studies illustrating interactions between estradiol (E2), carboxyeosin (CE), and the estrogen receptor (ER) specific agonists Propylpyrazoletriol (PPT) and Diarylpropionitrile (DPN) with the plasma membrane Ca^{2+}-ATPase 4 (PMCA4) (Brini et al., 2013; Caride et al., 2007; Corradi et al., 2021). **A)** Illustration depicting Ca^{2+}-calmodulin (Ca^{2+}/CaM) binding site (1086–1103 motif) of the PMCA4. To facilitate comprehension of the PMCA4 orientation, the plasma membrane is represented by 2 Gy horizontal parallel discs. EC: extracellular space. IC: intracellular space. **B)** Illustration showing possible molecular relations between E2 and PMCA4. **C)** Graphic representation of the possible interactions of CE with PMCA4. **D)** Picture of the PMCA4 protein and its proposed connections with PPT. **E)** PMCA4 display presenting feasible molecular interactions with DPN.

and this observation may be supported by the results from the $[Ca^{2+}]_i$ experiments. Nevertheless, it is necessary to explore further whether the interaction of the complex E2 and PMCA1 also induces conformational changes. Additionally, since PMCA4 is another isoform expressed in ASM cells, we also explored the contribution of PMCA4 in the effect of E2. Interestingly, docking experiments show that despite the conformation of E2-PMCA4 being highly stable in comparison to the others (CE-PMCA4 and PPT-PMCA4), the E2-PMCA1 remains the most suitable conformation. This result confirms in part that the observed effects on the $[Ca^{2+}]_i$ may be mediated by PMCA1 mainly, and it may be

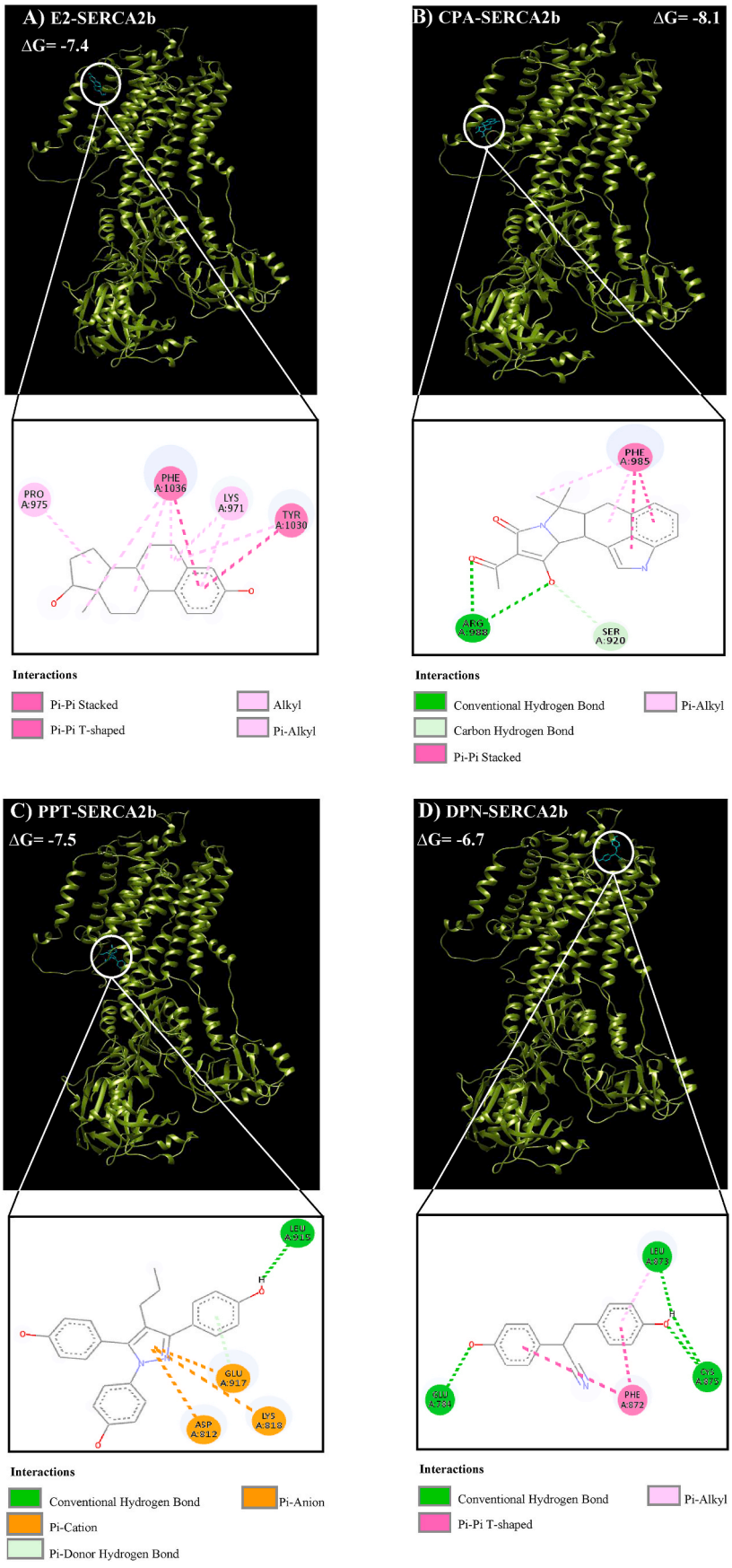

(caption on next page)

Fig. 9. Molecular docking illustrating estradiol (E2), cyclopiazonic acid (CPA), and the estrogen receptor (ER) specific agonists Propylpyrazoletriol (PPT) and Diarylpropionitrile (DPN) interactions with the sarcoplasmic reticulum Ca^{2+}-ATPase2b (SERCA2b). **A)** Illustration showing possible molecular relations between E2 and SERCA2b. **B)** Graphic representation of the probable interactions of CPA with SERCA2b. **C)** Picture of the SERCA2b protein and its proposed connections with PPT. **D)** SERCA2b display presenting feasible molecular interactions with DPN.

interesting to delve into understanding the potential synergistic effect of PMCA4 in this model. It should be noted that PMCA4 has been shown to participate in physiological processes in ASM cells (Chen et al., 2014).

Arguably, a limitation of the present study could be using male guinea pigs instead of females. Nonetheless, the employment of prepubescent male guinea pigs might sensibly limit the influence of endogenous sex hormones on the results described herein. Furthermore, it has been shown that the airway smooth muscle has a similar expression of estrogen receptors in males and females, and both genders have been used as study models for the influence of estrogen and the ERs in asthma and Ca^{2+} handling regulation (Ambhore et al., 2018; Aravamudan et al., 2017; Bhallamudi et al., 2020; Kalidhindi et al., 2020).

Finally, there is evidence linking the role of age and E2 with the development and severity of asthma in women, which is especially relevant during periods of major hormonal fluctuations such as pregnancy and merits further research in asthmatic models.

5. Conclusion

In summary, in guinea pig ASM, E2 at a physiological concentration induces AHR via non-genomic effects, possibly by directly inhibiting PMCA. This phenomenon might be related to mechanisms participating in the development of AHR in women suffering from perimenstrual asthma and in pregnant women that present symptom worsening and is a finding that could lead to novel personalized treatment strategies.

Funding

This study was partly supported by grants from the Dirección General de Asuntos del Personal Académico (DGAPA), the Universidad Nacional Autónoma de México (IN200522), and CONAHCYT (CF-2019/137725) to L.M. Montaño, and DGAPA, the Universidad Nacional Autónoma de México (IA203924) and CONAHCYT (CBF2023-24-1074) to J. Reyes-García.

CRediT authorship contribution statement

Bianca S. Romero-Martínez: Writing – original draft, Methodology, Investigation, Formal analysis, Conceptualization. **Edgar Flores-Soto:** Writing – review & editing, Investigation, Conceptualization. **Bettina Sommer:** Writing – review & editing, Supervision, Investigation. **Jorge Reyes-García:** Methodology, Formal analysis, Data curation. **David Arredondo-Zamarripa:** Methodology, Formal analysis. **Héctor Solís-Chagoyán:** Investigation, Data curation. **Cristina Lemini:** Investigation, Data curation. **Nadia A. Rivero-Segura:** Methodology, Investigation, Data curation. **José A. Santiago-de-la- Cruz:** Methodology, Investigation, Data curation. **Carlos Pérez-Plascencia:** Supervision, Conceptualization. **Luis M. Montaño:** Writing – review & editing, Writing – original draft, Visualization, Validation, Supervision, Investigation, Funding acquisition, Formal analysis, Conceptualization.

Declaration of competing interest

The authors declare that they have no known competing financial interests or personal relationships that could have appeared to influence the work reported in this paper.

Data availability

Data will be made available on request.

Acknowledgements

This publication is required for the accomplishment of the Ph.D. degree from Bianca S. Romero-Martínez who is grateful to the Programa de Doctorado en Ciencias Biomédicas, Universidad Nacional Autónoma de México, for the instruction received during her studies. She received a fellowship from the Consejo Nacional de Humanidades Ciencias y Tecnología, México (application # 2020-000013-01NACF-12778; CVU 469822).

References

Ambhore, N.S., Kalidhindi, R.S.R., Loganathan, J., Sathish, V., 2019. Role of differential estrogen receptor activation in airway hyperreactivity and remodeling in a murine model of asthma. Am. J. Respir. Cell Mol. Biol. 61 (4), 469–480. https://doi.org/10.1165/rcmb.2018-0321OC.

Ambhore, N.S., Katragadda, R., Raju Kalidhindi, R.S., Thompson, M.A., Pabelick, C.M., Prakash, Y.S., Sathish, V., 2018. Estrogen receptor beta signaling inhibits PDGF induced human airway smooth muscle proliferation. Mol. Cell. Endocrinol. 476, 37–47. https://doi.org/10.1016/j.mce.2018.04.007.

Aravamudan, B., Goorhouse, K.J., Unnikrishnan, G., Thompson, M.A., Pabelick, C.M., Hawse, J.R., Prakash, Y.S., Sathish, V., 2017. Differential expression of estrogen receptor variants in response to inflammation signals in human airway smooth muscle. J. Cell. Physiol. 232 (7), 1754–1760. https://doi.org/10.1002/jcp.25674.

Babnigg, G., Zagranichnaya, T., Wu, X., Villereal, M.L., 2003. Differential tyrosine phosphorylation of plasma membrane Ca^{2+}-ATPase and regulation of calcium pump activity by carbachol and bradykinin. J. Biol. Chem. 278 (17), 14872–14882. https://doi.org/10.1074/jbc.m210418200.

Barrera-Vazquez, O., Santiago-De-La-Cruz, J.A., Rivero-Segura, N.A., Estrella-Parra, E.A., Morales-Paoli, G.S., Flores-Soto, E., Gomez-Verjan, J.C., 2023. Data-driven approaches used for compound library design for the treatment of Parkinson's disease. Int. J. Mol. Sci. 24 (2), 1134. https://doi.org/10.3390/ijms24021134.

Bhallamudi, S., Connell, J., Pabelick, C.M., Prakash, Y.S., Sathish, V., 2020. Estrogen receptors differentially regulate intracellular calcium handling in human nonasthmatic and asthmatic airway smooth muscle cells. Am. J. Physiol. Lung Cell Mol. Physiol. 318 (1), L112–L124. https://doi.org/10.1152/ajplung.00206.2019.

Bi, R., Broutman, G., Foy, M.R., Thompson, R.F., Baudry, M., 2000. The tyrosine kinase and mitogen-activated protein kinase pathways mediate multiple effects of estrogen in hippocampus. Proc. Natl. Acad. Sci. USA 97 (7), 3602–3607. https://doi.org/10.1073/pnas.97.7.3602.

Brini, M., Calì, T., Ottolini, D., Carafoli, E., 2013. The plasma membrane calcium pump in health and disease. FEBS J. 280 (21), 5385–5397. https://doi.org/10.1111/febs.12193.

Brini, M., Carafoli, E., 2009. Calcium pumps in health and disease. Physiol. Rev. 89 (4), 1341–1378. https://doi.org/10.1152/physrev.00032.2008.

Bruce, J.I.E., 2018. Metabolic regulation of the PMCA: role in cell death and survival. Cell Calcium 69, 28–36. https://doi.org/10.1016/j.ceca.2017.06.001.

Bruce, J.I.E., Yule, D.I., Shuttleworth, T.J., 2002. Ca^{2+}-dependent protein kinase-A modulation of the plasma membrane Ca^{2+}-ATPase in parotid acinar cells. J. Biol. Chem. 277 (50), 48172–48181. https://doi.org/10.1074/jbc.m208393200.

Bulkhi, A.A., Shepard, K.V., Casale, T.B., Cardet, J.C., 2020. Elevated testosterone is associated with decreased likelihood of current asthma regardless of sex. J. Allergy Clin. Immunol. Pract. 8 (9), 3029–3035.e3024. https://doi.org/10.1016/j.jaip.2020.05.022.

Carey, M.A., Card, J.W., Bradbury, J.A., Moorman, M.P., Haykal-Coates, N., Gavett, S.H., Graves, J.P., Walker, V.R., Flake, G.P., Voltz, J.W., Zhu, D., Jacobs, E.R., Dakhama, A., Larsen, G.L., Loader, J.E., Gelfand, E.W., Germolec, D.R., Korach, K.S., Zeldin, D.C., 2007. Spontaneous airway hyperresponsiveness in estrogen receptor-alpha-deficient mice. Am. J. Respir. Crit. Care Med. 175 (2), 126–135. https://doi.org/10.1164/rccm.200509-1493OC.

Caride, A.J., Filoteo, A.G., Penniston, J.T., Strehler, E.E., 2007. The plasma membrane Ca^{2+} pump isoform 4a differs from isoform 4b in the mechanism of calmodulin binding and activation kinetics. J. Biol. Chem. 282 (35), 25640–25648. https://doi.org/10.1074/jbc.m701129200.

Chen, Y.F., Cao, J., Zhong, J.N., Chen, X., Cheng, M., Yang, J., Gao, Y.D., 2014. Plasma membrane Ca^{2+}-ATPase regulates Ca^{2+} signaling and the proliferation of airway smooth muscle cells. Eur. J. Pharmacol. 740, 733–741. https://doi.org/10.1016/j.ejphar.2014.05.055.

Corradi, G.R., Mazzitelli, L.R., Petrovich, G.D., De Tezanos Pinto, F., Rochi, L., Adamo, H. P., 2021. Plasma membrane Ca^{2+} pump PMCA4z is more active than splicing variant PMCA4x. Front. Cell. Neurosci. 15 https://doi.org/10.3389/fncel.2021.668371.

Cui, J., Shen, Y., Li, R., 2013. Estrogen synthesis and signaling pathways during aging: from periphery to brain. Trends Mol. Med. 19 (3), 197–209. https://doi.org/10.1016/j.molmed.2012.12.007.

Dick, I.M., Liu, J., Glendenning, P., Prince, R.L., 2003. Estrogen and androgen regulation of plasma membrane calcium pump activity in immortalized distal tubule kidney

cells. Mol. Cell. Endocrinol. 212 (1), 11–18. https://doi.org/10.1016/j.mce.2003.09.028.
El-Beialy, W., Galal, N., Deyama, Y., Yoshimura, Y., Suzuki, K., Tei, K., Totsuka, Y., 2010. Effects of estrogen on PMCA 2 and 4 in human fibroblast-like synovial cells and mouse macrophage-like cells. Endocr. J. 57 (1), 93–97. https://doi.org/10.1507/endocrj.k09e-247.
Endoh, H., Sasaki, H., Maruyama, K., Takeyama, K., Waga, I., Shimizu, T., Kawashima, H., 1997. Rapid activation of MAP kinase by estrogen in the bone cell line. Biochem. Biophys. Res. Commun. 235 (1), 99–102. https://doi.org/10.1006/bbrc.1997.6746.
Flores-Soto, E., Reyes-García, J., Carbajal-García, A., Campuzano-González, E., Perusquía, M., Sommer, B., Montaño, L.M., 2017. Sex steroids effects on Guinea pig airway smooth muscle tone and intracellular Ca^{2+} basal levels. Mol. Cell. Endocrinol. 439, 444–456. https://doi.org/10.1016/j.mce.2016.10.004.
Flores-Soto, E., Reyes-García, J., Sommer, B., Montaño, L.M., 2013. Sarcoplasmic reticulum Ca^{2+} refilling is determined by L-type Ca^{2+} and store operated Ca^{2+} channels in Guinea pig airway smooth muscle. Eur. J. Pharmacol. 721 (1–3), 21–28. https://doi.org/10.1016/j.ejphar.2013.09.060.
Fuseini, H., Yung, J.A., Cephus, J.Y., Zhang, J., Goleniewska, K., Polosukhin, V.V., Peebles Jr., R.S., Newcomb, D.C., 2018. Testosterone decreases house dust mite–induced type 2 and IL-17a–mediated airway inflammation. J. Immunol. 201 (7), 1843–1854. https://doi.org/10.4049/jimmunol.1800293.
Gasteiger, J., Marsili, M., 1980. Iterative partial equalization of orbital electronegativity—a rapid access to atomic charges. Tetrahedron 36 (22), 3219–3228. https://doi.org/10.1016/0040-4020(80)80168-2.
Gatto, C., Milanick, M.A., 1993. Inhibition of the red blood cell calcium pump by eosin and other fluorescein analogues. Am. J. Physiol. 264 (6 Pt 1), C1577–C1586. https://doi.org/10.1152/ajpcell.1993.264.6.C1577.
Giles, W., Murphy, V., 2013. Asthma in pregnancy: a review. Obstet. Med. 6 (2), 58–63. https://doi.org/10.1258/om.2012.120008.
Gong, D., Chi, X., Ren, K., Huang, G., Zhou, G., Yan, N., Lei, J., Zhou, Q., 2018. Structure of the human plasma membrane Ca^{2+}-ATPase 1 in complex with its obligatory subunit neuroplastin. Nat. Commun. 9 (1) https://doi.org/10.1038/s41467-018-06075-7.
Grynkiewicz, G., Poenie, M., Tsien, R.Y., 1985. A new generation of Ca^{2+} indicators with greatly improved fluorescence properties. J. Biol. Chem. 260 (6), 3440–3450.
Harrison, D.A., Carr, D.W., Meizel, S., 2000. Involvement of protein kinase A and A kinase anchoring protein in the progesterone-initiated human sperm acrosome reaction. Biol. Reprod. 62 (3), 811–820. https://doi.org/10.1095/biolreprod62.3.811.
Heldring, N., Pike, A., Andersson, S., Matthews, J., Cheng, G., Hartman, J., Tujague, M., Ström, A., Treuter, E., Warner, M., Gustafsson, J.A., 2007. Estrogen receptors: how do they signal and what are their targets. Physiol. Rev. 87 (3), 905–931. https://doi.org/10.1152/physrev.00026.2006.
Herscher, C.J., Rega, A.F., 1996. Pre-steady-state kinetic study of the mechanism of inhibition of the plasma membrane Ca^{2+}-ATPase by lanthanum. Biochemistry 35 (47), 14917–14922. https://doi.org/10.1021/bi961879r.
Hirota, S., Helli, P.B., Catalli, A., Chew, A., Janssen, L.J., 2005. Airway smooth muscle excitation-contraction coupling and airway hyperresponsiveness. Can. J. Physiol. Pharmacol. 83 (8–9), 725–732. https://doi.org/10.1139/y05-070.
Jain, D., Raj, H.G., Gangal, S.V., Chhabra, S.K., 2001. Relationship between intracellular calcium and airway reactivity in Guinea pigs. Jpn. J. Physiol. 51 (5), 577–583. https://doi.org/10.2170/jjphysiol.51.577.
Kalidhindi, R.S.R., Ambhore, N.S., Bhallamudi, S., Loganathan, J., Sathish, V., 2020. Role of estrogen receptors α and β in a murine model of asthma: exacerbated airway hyperresponsiveness and remodeling in ERβ knockout mice. Front. Pharmacol. 10 (1499) https://doi.org/10.3389/fphar.2019.01499.
Kim, K., Lee, D., Ahn, C., Kang, H.Y., An, B.S., Seong, Y.H., Jeung, E.B., 2017. Effects of estrogen on esophageal function through regulation of Ca^{2+}-related proteins. J. Gastroenterol. 52 (8), 929–939. https://doi.org/10.1007/s00535-016-1305-y.
Levy, M.L., Bacharier, L.B., Bateman, E., Boulet, L.-P., Brightling, C., Buhl, R., Brusselle, G., Cruz, A.A., Drazen, J.M., Duijts, L., Fleming, L., Inoue, H., Ko, F.W.S., Krishnan, J.A., Mortimer, K., Pitrez, P.M., Sheikh, A., Yorgancıoğlu, A., Reddel, H.K., 2023. Key recommendations for primary care from the 2022 Global Initiative for Asthma (GINA) update. npj Primary Care Respiratory Medicine 33 (1). https://doi.org/10.1038/s41533-023-00330-1.
Mahn, K., Hirst, S.J., Ying, S., Holt, M.R., Lavender, P., Ojo, O.O., Siew, L., Simcock, D.E., McVicker, C.G., Kanabar, V., Snetkov, V.A., O'Connor, B.J., Karner, C., Cousins, D.J., Macedo, P., Chung, K.F., Corrigan, C.J., Ward, J.P., Lee, T.H., 2009. Diminished sarco/endoplasmic reticulum Ca^{2+} ATPase (SERCA) expression contributes to airway remodelling in bronchial asthma. Proc. Natl. Acad. Sci. USA 106 (26), 10775–10780. https://doi.org/10.1073/pnas.0902295106.
McKenzie, R., Burton, M.D., Royce, S.G., Tang, M.L., 2010. Age and sex influences on airway hyperresponsiveness. J. Asthma : official journal of the Association for the Care of Asthma 47 (6), 651–654. https://doi.org/10.3109/02770901003692801.
Migliaccio, A., Piccolo, D., Castoria, G., Di Domenico, M., Bilancio, A., Lombardi, M., Gong, W., Beato, M., Auricchio, F., 1998. Activation of the Src/p21ras/Erk pathway by progesterone receptor via cross-talk with estrogen receptor. EMBO J. 17 (7), 2008–2018. https://doi.org/10.1093/emboj/17.7.2008.
Montaño, L.M., Flores-Soto, E., Reyes-García, J., Chagoyán, H.S., Perusquía, M., Sommer, B., 2020. Airway smooth muscle functioning in basal, agonists stimulated conditions and novel androgen asthma therapy. In: Berhardt, L.V. (Ed.), Advances in Medicine and Biology, vol. 157. Nova Science Publishers.
Nejatbakhsh Samimi, L., Fallahpour, M., Khoshmirsafa, M., Moosavi, S.A.J., Bayati, P., Baharlou, R., Falak, R., 2021. The impact of 17β-estradiol and progesterone therapy on peripheral blood mononuclear cells of asthmatic patients. Mol. Biol. Rep. 48 (1), 297–306. https://doi.org/10.1007/s11033-020-06046-6.
Pearlman, A.D., Case, D.A., Caldwell, J.W., Ross, W.S., Cheatham, T.E., DeBolt, S., Ferguson, D., Seibel, G., Kollman, P., 1995. AMBER, a package of computer programs for applying molecular mechanics, normal mode analysis, molecular dynamics and free energy calculations to simulate the structural and energetic properties of molecules. Comput. Phys. Commun. 91 (1–3), 1–41. https://doi.org/10.1016/0010-4655(95)00041-D.
Perez-Zoghbi, J.F., Karner, C., Ito, S., Shepherd, M., Alrashdan, Y., Sanderson, M.J., 2009. Ion channel regulation of intracellular calcium and airway smooth muscle function. Pulm. Pharmacol. Therapeut. 22 (5), 388–397. https://doi.org/10.1016/j.pupt.2008.09.006.
Pettersen, E.F., Goddard, T.D., Huang, C.C., Couch, G.S., Greenblatt, D.M., Meng, E.C., Ferrin, T.E., 2004. UCSF Chimera–a visualization system for exploratory research and analysis. J. Comput. Chem. 25 (13), 1605–1612. https://doi.org/10.1002/jcc.20084.
Purves-Tyson, T.D., Keast, J.R., 2004. Rapid actions of estradiol on cyclic amp response-element binding protein phosphorylation in dorsal root ganglion neurons. Neuroscience 129 (3), 629–637. https://doi.org/10.1016/j.neuroscience.2004.08.019.
Radzikowska, U., Golebski, K., 2023. Sex hormones and asthma: the role of estrogen in asthma development and severity. Allergy 78 (3), 620–622. https://doi.org/10.1111/all.15548.
Reyes-García, J., Flores-Soto, E., Carbajal-García, A., Sommer, B., Montaño, L., 2018. Maintenance of intracellular Ca^{2+} basal concentration in airway smooth muscle (Review). Int. J. Mol. Med. 42 (6), 2998–3008. https://doi.org/10.3892/ijmm.2018.3910.
Romero-Martínez, B.S., Sommer, B., Solís-Chagoyán, H., Calixto, E., Aquino-Gálvez, A., Jaimez, R., Gomez-Verjan, J.C., González-Avila, G., Flores-Soto, E., Montaño, L.M., 2023. Estrogenic modulation of ionic channels, pumps and exchangers in airway smooth muscle. Int. J. Mol. Sci. 24 (9), 7879. https://doi.org/10.3390/ijms24097879.
Sathish, V., Freeman, M.R., Long, E., Thompson, M.A., Pabelick, C.M., Prakash, Y.S., 2015. Cigarette smoke and estrogen signaling in human airway smooth muscle. Cell. Physiol. Biochem. 36 (3), 1101–1115. https://doi.org/10.1159/000430282.
Sathish, V., Thompson, M.A., Bailey, J.P., Pabelick, C.M., Prakash, Y.S., Sieck, G.C., 2009. Effect of proinflammatory cytokines on regulation of sarcoplasmic reticulum Ca^{2+} reuptake in human airway smooth muscle. Am. J. Physiol. Lung Cell Mol. Physiol. 29 (1), L26–L34. https://doi.org/10.1152/ajplung.00026.2009.
Semik-Orzech, A., Skoczyński, S., Pierzchała, W., 2017. Serum estradiol concentration, estradiol-toprogesterone ratio and sputum IL-5 and IL-8 concentrations are increased in luteal phase of the menstrual cycle in perimenstrual asthma patients. European Annals of Allergy and Clinical Immunology 49 (4), 161. https://doi.org/10.23822/eurannaci.1764-1489.09.
Sheridan, J.T., Gilmore, R.C., Watson, M.J., Archer, C.B., Tarran, R., 2013. 17β-Estradiol inhibits phosphorylation of stromal interaction molecule 1 (STIM1) protein. J. Biol. Chem. 288 (47), 33509–33518. https://doi.org/10.1074/jbc.m113.486662.
Somlyo, A.P., Somlyo, A.V., 2003. Ca^{2+} sensitivity of smooth muscle and nonmuscle myosin II: modulated by G proteins, kinases, and myosin phosphatase. Physiol. Rev. 83 (4), 1325–1358. https://doi.org/10.1152/physrev.00023.2003.
Stamatiou, R., Paraskeva, E., Papagianni, M., Molyvdas, P.A., Hatziefthimiou, A., 2011. The mitogenic effect of testosterone and 17β-estradiol on airway smooth muscle cells. Steroids 76 (4), 400–408. https://doi.org/10.1016/j.steroids.2010.12.010.
Stratton, R.C., Squires, P.E., Green, A.K., 2010. 17β-Estradiol elevates cGMP and, via plasma membrane recruitment of protein kinase GIα, stimulates Ca2+ efflux from rat hepatocytes. J. Biol. Chem. 285 (35), 27201–27212. https://doi.org/10.1074/jbc.m110.103630.
Szemraj, J., Kawecka, I., Lachowicz, L., Zylińska, L., 2003. Non-genomic effect of estradiol on plasma membrane calcium pump activity in vitro. Pol. J. Pharmacol. 55 (5), 887–893.
Sánchez-Ramos, J.L., Pereira-Vega, A.R., Alvarado-Gómez, F., Maldonado-Pérez, J.A., Svanes, C., Gómez-Real, F., 2017. Risk factors for premenstrual asthma: a systematic review and meta-analysis. Expet Rev. Respir. Med. 11 (1), 57–72. https://doi.org/10.1080/17476348.2017.1270762.
Townsend, E.A., Miller, V.M., Prakash, Y.S., 2012a. Sex differences and sex steroids in lung health and disease. Endocr. Rev. 33 (1), 1–47. https://doi.org/10.1210/er.2010-0031.
Townsend, E.A., Sathish, V., Thompson, M.A., Pabelick, C.M., Prakash, Y.S., 2012b. Estrogen effects on human airway smooth muscle involve cAMP and protein kinase A. Am. J. Physiol. Lung Cell Mol. Physiol. 303 (10), L923–L928. https://doi.org/10.1152/ajplung.00023.2012.
Townsend, E.A., Thompson, M.A., Pabelick, C.M., Prakash, Y.S., 2010. Rapid effects of estrogen on intracellular Ca^{2+} regulation in human airway smooth muscle. Am. J. Physiol. Lung Cell Mol. Physiol. 298 (4), L521–L530. https://doi.org/10.1152/ajplung.00287.2009.
Tran, D.N., Jung, E.-M., Ahn, C., Lee, J.-H., Yoo, Y.-M., Jeung, E.-B., 2018. Effects of bisphenol A and 4-tert-Octylphenol on embryo implantation failure in mouse. Int. J. Environ. Res. Publ. Health 15 (8), 1614. https://doi.org/10.3390/ijerph15081614.
Tran, Q.-K., Firkins, R., Giles, J., Francis, S., Matnishian, V., Tran, P., VerMeer, M., Jasurda, J., Burgard, M.A., Gebert-Oberle, B., 2016. Estrogen enhances linkage in the vascular endothelial calmodulin network via a feedforward mechanism at the G protein-coupled estrogen receptor 1. J. Biol. Chem. 291 (20), 10805–10823. https://doi.org/10.1074/jbc.m115.697334.
Varga, K., Hollósi, A., Pászty, K., Hegedűs, L., Szakács, G., Tímár, J., Papp, B., Enyedi, Á., Padányi, R., 2018. Expression of calcium pumps is differentially regulated by histone

deacetylase inhibitors and estrogen receptor alpha in breast cancer cells. BMC Cancer 18 (1). https://doi.org/10.1186/s12885-018-4945-x.

Vasudevan, N., Kow, L.-M., Pfaff, D.W., 2001. Early membrane estrogenic effects required for full expression of slower genomic actions in a nerve cell line. Proc. Natl. Acad. Sci. USA 98 (21), 12267–12271. https://doi.org/10.1073/pnas.221449798.

Warren, K.J., Deering-Rice, C., Hueckstead, T., Trivedi, S., Venosa, A., Reilly, C., Sanders, K., Clayton, F., Wyatt, T.A., Poole, J.A., Heller, N.M., Leung, D., Paine, R., 2023. Steady-state estradiol triggers a unique innate immune response to allergen resulting in increased airway resistance. Biol. Sex Differ. 14 (1) https://doi.org/10.1186/s13293-022-00483-7.

Watters, J.J., Campbell, J.S., Cunningham, M.J., Krebs, E.G., Dorsa, D.M., 1997. Rapid membrane effects of steroids in neuroblastoma cells: effects of estrogen on mitogen activated protein kinase signalling cascade and c-fos immediate early gene transcription. Endocrinology 138 (9), 4030–4033. https://doi.org/10.1210/endo.138.9.5489.

Webb, R.C., 2003. Smooth muscle contraction and relaxation. Adv. Physiol. Educ. 27 (1–4), 201–206. https://doi.org/10.1152/advan.00025.2003.

Wright, L.C., Chen, S., Roufogalis, B.D., 1993. Regulation of the activity and phosphorylation of the plasma membrane Ca^{2+}-ATPase by protein kinase C in intact human erythrocytes. Arch. Biochem. Biophys. 306 (1), 277–284. https://doi.org/10.1006/abbi.1993.1512.

Yang, H., Choi, K.C., Hyun, S.H., Jeung, E.B., 2011. Coexpression and estrogen-mediated regulation of TRPV6 and PMCA1 in the human endometrium during the menstrual cycle. Mol. Reprod. Dev. 78 (4), 274–282. https://doi.org/10.1002/mrd.21303.

Zhang, W.-B., Kwan, C.-Y., 2016. Pharmacological evidence that potentiation of plasmalemmal Ca^{2+}-extrusion is functionally coupled to inhibition of SR Ca^{2+}-ATPases in vascular smooth muscle cells. N. Schmied. Arch. Pharmacol. 389 (4), 447–455. https://doi.org/10.1007/s00210-016-1209-7.

International Journal of
Molecular Sciences

MDPI

Review

Estrogenic Modulation of Ionic Channels, Pumps and Exchangers in Airway Smooth Muscle

Bianca S. Romero-Martínez [1], Bettina Sommer [2], Héctor Solís-Chagoyán [3], Eduardo Calixto [4], Arnoldo Aquino-Gálvez [5], Ruth Jaimez [6], Juan C. Gomez-Verjan [7], Georgina González-Avila [8], Edgar Flores-Soto [1,*] and Luis M. Montaño [1,*]

1 Departamento de Farmacología, Facultad de Medicina, Universidad Nacional Autónoma de México, Ciudad de México 04510, Mexico
2 Laboratorio de Hiperreactividad Bronquial, Instituto Nacional de Enfermedades Respiratorias "Ismael Cosío Villegas", Ciudad de México 14080, Mexico
3 Neurociencia Cognitiva Evolutiva, Centro de Investigación en Ciencias Cognitivas, Universidad Autónoma del Estado de Morelos, Cuernavaca 62209, Mexico
4 Departamento de Neurobiología, Dirección de Investigación en Neurociencias, Instituto Nacional de Psiquiatría "Ramón de la Fuente Muñiz", Ciudad de México 14370, Mexico
5 Laboratorio de Biología Molecular, Departamento de Fibrosis Pulmonar, Instituto Nacional de Enfermedades Respiratorias Ismael Cosío Villegas, México City 14080, Mexico
6 Laboratorio de Estrógenos y Hemostasis, Facultad de Medicina, Universidad Nacional Autónoma de México, Ciudad de México 04510, Mexico
7 Dirección de Investigación, Instituto Nacional de Geriatría (INGER), Ciudad de México 10200, Mexico
8 Laboratorio de Oncología Biomédica, Instituto Nacional de Enfermedades Respiratorias "Ismael Cosío Villegas", México City 14080, Mexico
* Correspondence: edgarfs@comunidad.unam.mx (E.F.-S.); lmmr@unam.mx (L.M.M.); Tel.: +52-555-6232279 (L.M.M.)

check for updates

Citation: Romero-Martínez, B.S.; Sommer, B.; Solís-Chagoyán, H.; Calixto, E.; Aquino-Gálvez, A.; Jaimez, R.; Gomez-Verjan, J.C.; González-Avila, G.; Flores-Soto, E.; Montaño, L.M. Estrogenic Modulation of Ionic Channels, Pumps and Exchangers in Airway Smooth Muscle. *Int. J. Mol. Sci.* **2023**, *24*, 7879. https://doi.org/10.3390/ijms24097879

Academic Editors: László Csernoch and Péter Szentesi

Received: 8 February 2023
Revised: 28 February 2023
Accepted: 28 February 2023
Published: 26 April 2023

Abstract: To preserve ionic homeostasis (primarily Ca^{2+}, K^+, Na^+, and Cl^-), in the airway smooth muscle (ASM) numerous transporters (channels, exchangers, and pumps) regulate the influx and efflux of these ions. Many of intracellular processes depend on continuous ionic permeation, including exocytosis, contraction, metabolism, transcription, fecundation, proliferation, and apoptosis. These mechanisms are precisely regulated, for instance, through hormonal activity. The lipophilic nature of steroidal hormones allows their free transit into the cell where, in most cases, they occupy their cognate receptor to generate genomic actions. In the sense, estrogens can stimulate development, proliferation, migration, and survival of target cells, including in lung physiology. Non-genomic actions on the other hand do not imply estrogen's intracellular receptor occupation, nor do they initiate transcription and are mostly immediate to the stimulus. Among estrogen's non genomic responses regulation of calcium homeostasis and contraction and relaxation processes play paramount roles in ASM. On the other hand, disruption of calcium homeostasis has been closely associated with some ASM pathological mechanism. Thus, this paper intends to summarize the effects of estrogen on ionic handling proteins in ASM. The considerable diversity, range and power of estrogens regulates ionic homeostasis through genomic and non-genomic mechanisms.

Keywords: estrogen; airway smooth muscle; channels; exchangers; pumps; receptors

1. Introduction

Homeostasis is a state of cellular equilibrium maintained through regulatory mechanisms resistant to change that preserve the constant physiological conditions. The composition of the cytosol, the optimal internal cellular environment, differs significantly from that of the extracellular space, and these spaces are separated by a semipermeable lipid bilayer called cellular membrane that functions not only as a barrier between these two spaces but also prevents charged particles from crossing freely from one side to the other.

Several cellular functions, as for instance the action potential in the nerves, depend on ions permeating through the cellular membrane. Conceivably, the ionic composition on either side of the cell membrane is different and many cellular mechanisms work in accordance to maintain a constant concentration of them and consequently, an electrochemical gradient [1,2]. In order to maintain this balance, cells express a variety of proteins embedded in the cell membrane and in organelle membranes that function as gatekeepers of ions. Some of these proteins transport the ions in and out of these membranes in a highly controlled manner [1–3]. These proteins can be classified into three categories: ionic channels, pumps, and exchangers (Figure 1) [1,2].

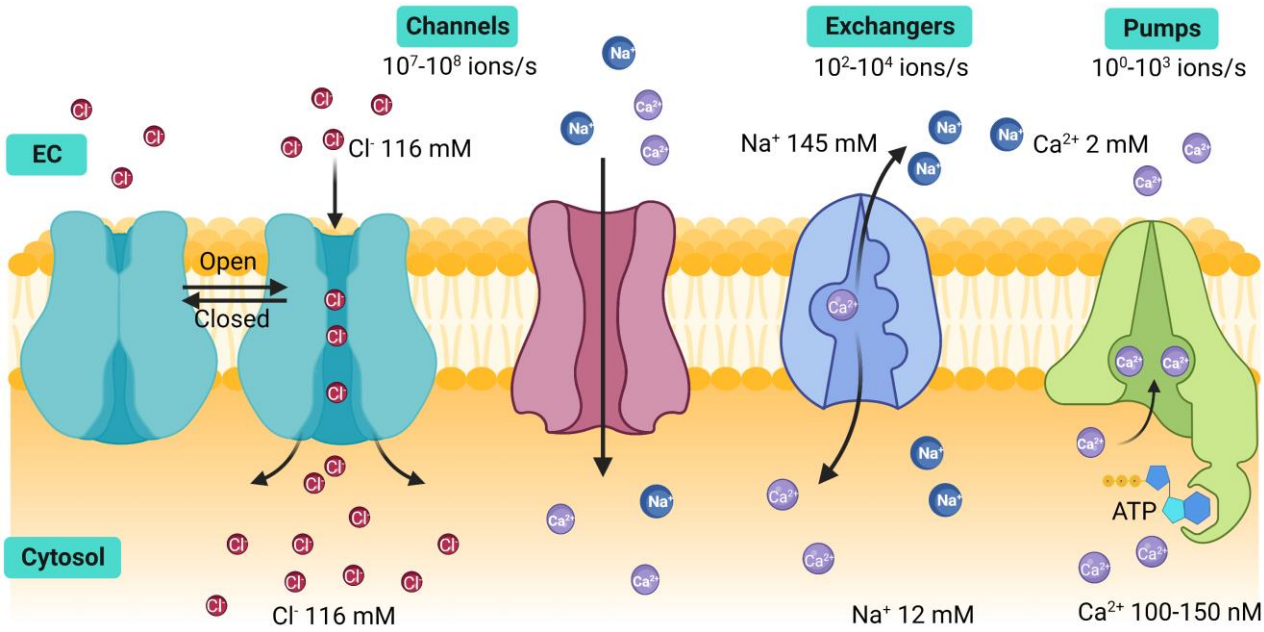

Figure 1. Ion transport proteins. Ion transport proteins are classified into three groups: channels, exchangers, and pumps. These three types of proteins maintain the homeostasis of the intracellular ions either through facilitated or active transport, and changes in the ionic intracellular concentrations can initiate cellular processes. In blue, a chlorine channel is represented; in red, a non-selective cation channel; in purple, the Na^+/Ca^{2+} exchanger; and in green, the plasma membrane Ca^{2+} ATPase. EC, extracellular; Cl^-, chloride, Na^+, sodium; Ca^{2+}, calcium; ATP, adenosine triphosphate.

Protein ion channels allow specific ions to flow across the cell membrane in favor of their electrochemical gradient, consequently generating transmembrane electric currents [3]. Ion channels are widely diverse, with several hundred genes in the human genome encoding them. Yet, they share certain structural generalities that characterize them, such as, for instance, being composed of several transmembrane segments, with a specific region that forms a pore across the membrane that serves as the passageway for the ions to cross at high speed. The channels dynamically alternate between an open or closed state through a "gating" process regulated by other segments of the channel that allow the flow of ions when needed [3,4]. In some cases, some ion channels may be in an inactive state, a circumstance that keeps them closed even during a process of resting membrane potential change. Therefore, ion channels are essential for the development of electrophysiological responses of excitable cells.

On the other hand, ion pumps do require a source of energy achieved through the hydrolysis of ATP, to move the ions against their electrochemical gradient; this process is referred to as active transport [3]. Pumps also utilize a gating system to regulate the passage of ions through their pore. However, unlike channels, pumps have a two-gate system that alternates between open and closed states. Gating reactions requiring ATP

are needed for the gates to alternate between open and closed states, limiting the speed of uphill movement of the ions [3].

The third type of transporters are exchangers. They transfer different ions in or out of the cytosol simultaneously, they do not require ATP as an energy source, and instead exploit the electrochemical gradient by moving the ions downhill of the concentration gradient. This type of transport is also known as facilitated transport. Three types of exchangers have been identified. Uniporters transport a single type of ion in one direction in favor of the concentration gradient. The second type are symporters, where two different types of ions are moved simultaneously across the membrane in the same direction. The last type are called antiporters, proteic structures apt to move different types of ions across the membrane in opposite directions (Figure 1) [3,5].

To maintain ionic homeostasis and provide a stable electrophysiological status in cells, these proteins are strictly regulated by numerous pathways, both extrinsic (autocrine, paracrine, endocrine signaling) and intrinsic cellular mechanisms and the electrochemical gradients [6]. Ion handling proteins can be regulated acutely (modulating its activity), or chronically (through modulation of quantity and subtype expression of the proteins). Acute regulation of ion handling proteins can be through direct interaction of the protein with the regulatory molecule, or indirectly, through second messengers and protein kinases [4]. Chronic regulation determines the number and kinds of ion transporters expressed in any given cell and requires three stages of regulation: developmental, homeostatic, and evolutionary [6]. Developmental regulation involves the activation of large quantities of genes necessary to express a specific cellular phenotype; these are tissue-specific patterns. Therefore, the quantity and subtypes of transporters expressed by any given cell type will vary from any other type. This expression of a defined genetic pattern certainly defines the cellular phenotype that best serves its function [6]. Meanwhile, homeostatic regulation refers to two main processes. The first keeps a certain phenotypic expression stable under physiological conditions, and the second oversees the plasticity of the transporter's expression in response to changes in the physiological stimuli [6].

In this sense, hormones have been recognized as one of the main homeostatic regulatory systems, and in recent years sex steroid hormones (SSHs) gained increasing interest for their role outside of reproductive physiology. SSHs have been implicated in regulating many critical physiological processes along every stage of life, including growth, regulation of homeostasis, reproduction, and aging [7,8]. Specifically, in lung physiology, SSHs participate in developmental stages from embryonic and onwards [9–11]. In women, significant hormonal changes occur during their reproductive life, initiating during puberty and lasting until menopause. Most of these changes are regulated through estrogens, SSHs that belong to a group of aromatized 18-carbon steroids whose induction and maintenance of various physiological processes makes them fundamental in reproduction, development of behaviors and several non-sexual processes [12]. Among the many organ systems in which estrogens exert their effect, the cardiovascular system has been abundantly studied, particularly vascular smooth muscle and cardiac muscle and the role estrogens play on their ion transporter regulation [13–15]. Many similarities in the activity of estrogen can be observed between vascular and airway smooth muscle (ASM), and owing to the tremendous amount of research dedicated to vascular diseases, it is quite enticing to apply the findings to ASM. However, key differences exist between these two cell types, and although year after year the research in the field of the role of SSHs in ASM grows, this topic still has much room for further investigation [11].

Here, we review emerging evidence suggesting estrogens influence airway smooth muscle function at the cellular level, modifying processes involved in intracellular ion homeostasis on different physiological and pathological conditions.

2. Estrogens Biosynthesis and Modes of Action

Estrogens belong to the family of SSHs derived from cholesterol, and they share a common structural base consisting of four rings called cyclopentanoperhydrophenan-

threne [7,8,12]. In women, their biosynthesis mainly occurs in the ovaries. However, extragonadal sites have been identified as, for instance, the adrenal glands, liver, heart, skin, brain, adipose tissue and lung, in which an aromatase enzyme is expressed; this enzyme also functions as the regulating step in estrogen production [7,8,12,16–18]. Local biosynthesis of estrogens can have tissue-specific effects that could participate in physiological processes and induction or maintenance of various diseases (Figure 2) [12,16].

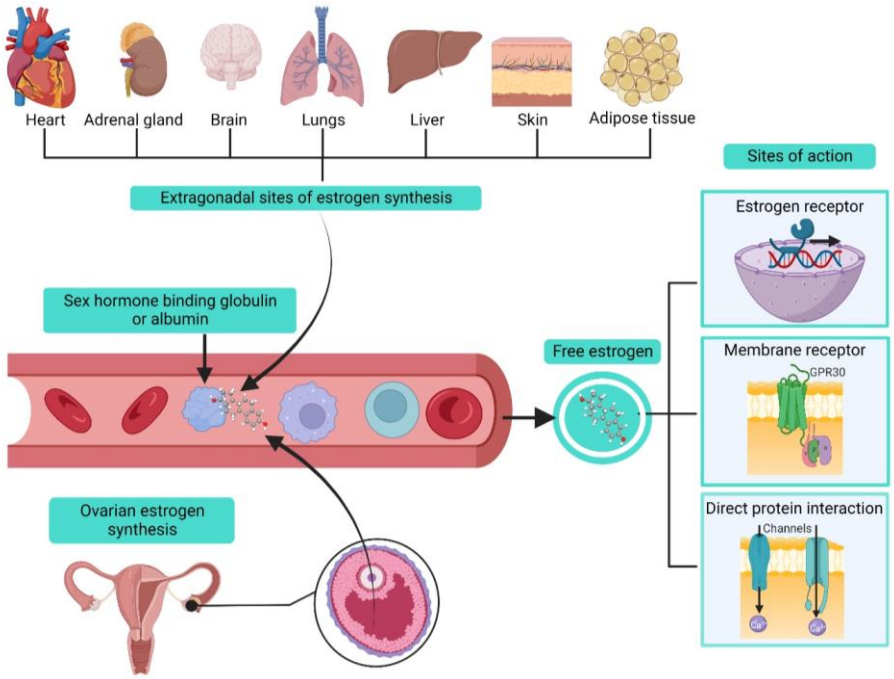

Figure 2. Estrogen biosynthesis and sites of action. The main site of estrogen synthesis are the ovaries. However, several extragonadal synthesis sites exist, and the main requirement for local estrogen production is the tissue expression of the aromatase enzyme. Once the estrogen is synthesized, it can have local activity or it can be liberated into the blood stream, where it will be carried to its action site bound to the sex hormone binding globulin or to albumin. When the estrogen reaches its target, it can produce its effect through three modes of action: through the activation of the estrogen receptors ERα and ERβ, or by interacting with its membrane receptor GPR30 or directly with its target protein. GPR30, G protein-coupled receptor 30.

During the reproductive lifetime of women, three main estrogens are physiologically synthesized: estrone (E1), 17β-estradiol (E2), and estriol (E3); E2 has the highest production representing the most abundant and potent estrogen during a woman's reproductive lifetime. In non-pregnant women, physiological circulating levels ranging from 80 pM–1.5 nM and going up to 150 nM during pregnancy [11,12]. In postmenopausal women, estradiol levels diminish, ranging between 40–120 pM [11].

Estrogens exert regulatory actions via long-term genomic and acute non-genomic actions [12,19]. Classical estrogen signaling (genomic effects) is mediated through the nuclear receptors ERα and ERβ, abundantly expressed in human ASM cells [11,12,19,20]. When ERs are activated by estrogen binding, they can lead to different signaling pathways, including gene transcription regulation either directly or through estrogen response elements (EREs) in the promoter region. ERs can also interact with other DNA-binding transcription factors and induce rapid effects involving phosphorylation processes [11,12,19]. Another estrogen receptor located at the cell membrane was identified. The activity of GPR30 can lead to the activation of numerous intracellular signaling pathways, including cyclic nucleotides, protein kinase C, protein kinase A, and protein kinase G [11,12,19]. However, it was demonstrated that the GPR30 was not significantly expressed in human ASM cells [21]. On the other hand, estrogens' non-genomic effects are rapid and take place outside the cell

nucleus and, as stated, can be initiated through estrogen membrane receptors. Another proposed mechanism of action is directly binding to its target protein [22]. Through these numerous mechanisms of action, estrogens are able to regulate ion transporters in ASM cells (Figure 2).

3. Airway Smooth Muscle Calcium Handling Mechanisms and Estrogens

Cell calcium (Ca^{2+}) homeostasis is maintained by a finely tuned Ca^{2+} signaling system made-up of numerous Ca^{2+} transporters (channels, exchangers, and pumps) regulating the influx and efflux of this cation from the cytoplasm to preserve its balance. Ca^{2+} homeostasis is essential for the cell. As a second messenger, Ca^{2+} signaling regulates various cellular processes that depend on the time of the Ca^{2+} and concentration. It is well known that Ca^{2+} regulates exocytosis, contraction, protein phosphorylation, dephosphorylation, metabolism, gene transcription, fecundation, cell proliferation, and even apoptosis [23]. In the ASM, Ca^{2+} homeostasis keeps intracellular basal Ca^{2+} concentrations (b[Ca^{2+}]i) at around 100–150 nM, while Ca^{2+} concentrations in the intracellular stores and extracellular space are higher (5–10 mM and 2 mM, respectively) creating a large chemical gradient in favor of Ca^{2+} influx into the cytosol [23,24]. In order to regulate [Ca^{2+}]i, numerous proteins exists to facilitate the cellular influx and efflux of Ca^{2+}. Among the calcium-handling proteins, we can include the voltage-dependent Ca^{2+} channels (VDCCs), store-operated Ca^{2+} channels (SOCCs), receptor-operated Ca^{2+} channel (ROCCs), transient receptor potential channels (TRPs), and the Na^+/Ca^{2+} exchanger in its reverse form (NCX_{REV}) as influx mechanisms located in the cellular membrane. On the other hand, the Na^+/Ca^{2+} Exchanger (NCX) and the plasma membrane Ca^{2+} ATPase (PMCA) are efflux mechanisms located in the cellular membrane. Meanwhile, the sarcoplasmic reticulum (SR) functions as the main internal Ca^{2+} store in the ASM. On the SR membrane, we can find the inositol 1,4,5-trisphosphate receptor (IP_3R) and the ryanodine receptors (RyR) as Ca^{2+} efflux mechanisms. In contrast, the sarcoplasmic reticulum Ca^{2+} ATPase (SERCA) acts as an intracellular Ca^{2+} extrusion mechanism (Figure 3) [23,24].

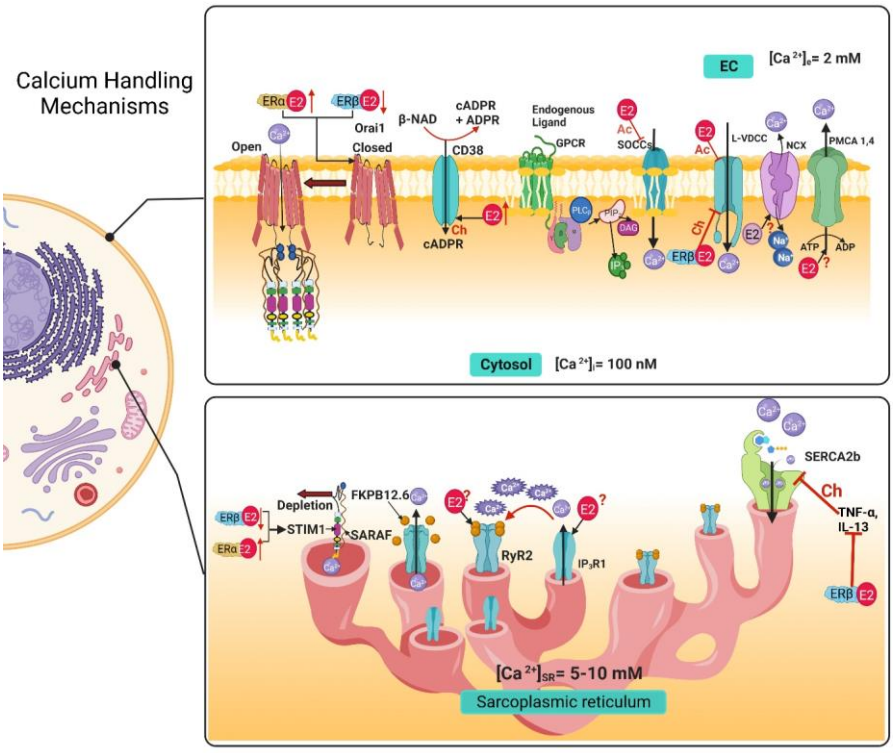

Figure 3. Calcium handling mechanisms in airway smooth muscle and their modulation by estrogens. E2 through non-genomic effects inhibits SOCCs, and the chronic exposure to an ERβ-specific agonist

decreases the expression of STIM1 and Orai1, and an ERα-specific agonist increases the expression of STIM1 and Orai1.The genomic effect of E2 increases the expression of CD38, although the non-genomic effect is still unknown. E2 acutely inhibits the LVDCC and the chronic exposure, via ERβ pathway, inhibits this channel. In the sarcoplasmic reticulum, the chronic exposure with an ERβ-specific agonist inhibits the increase in SERCA expression caused by exposure to TNF-α and IL-13. The genomic and non-genomic effects of E2 over RyR2, IP_3R1, NCX and PMCA are still not reported. EC, extracellular; Ac, Acute; Ch, Chronic; IP_3, inositol 1,4,5-trisphosphate; $[Ca^{2+}]i$, intracellular calcium concentration; $[Ca^{2+}]e$, extracellular calcium concentration; $[Ca^{2+}]SR$, sarcoplasmic reticulum calcium concentration; E2, 17β estradiol; ERα, estrogen receptor α; ERβ, estrogen receptor β; L-VDCC, L-type voltage dependent Ca^{2+} channel; SOCC, store-operated Ca^{2+} channel, NCX, Na^+/Ca^{2+} Exchanger; PMCA, plasma membrane Ca^{2+} ATPase; IP_3R, inositol 1,4,5-trisphosphate receptor; RyR, Ryanodine receptor; SERCA, sarcoplasmic reticulum Ca^{2+} ATPase; FKBP-12.6, 12.6 kDa FK506-binding protein; Orai1; STIM1, stromal interacting molecule; SARAF, Store-operated Ca^{2+} entry-associated regulatory factor.

3.1. Voltage-Dependent Ca^{2+} Channels

Extracellular Ca^{2+} entry is primordial in Ca^{2+} signaling, and its influx is primarily driven by an electrochemical gradient. In ASM, both L- type VDCCs (Long Lasting Currents voltage-dependent Ca^{2+} channels) and T-type VDCCs (Transient Currents voltage-dependent Ca^{2+} channels) are expressed, but L-VDCC is the predominant type in human ASM and various other species [24–33]. In the sense, the preincubation with E2 at physiological levels can inhibit L-VDCCs non-genomically (Figure 3) in a concentration-dependent manner in human ASM (hASM) stimulated with histamine, with a more pronounced effect when using an ERα-selective agonist, which was not observed when using an ERβ selective agonist (Table 1) [20]. This could be partially due to the localization of the receptors since ERβ is minimally present in the plasma membrane, where non-genomic effects could take place [20]. This effect seems to have a biphasic response since at supraphysiological levels, E2 also inhibits L-VDCCs non-genomically in guinea pig ASM, as demonstrated through electrophysiological studies (Table 1) [34]. Both estrogen receptors seem to have different signaling pathways. They serve distinct purposes, both in physiological and pathological conditions. For instance, in human ASM cells from an asthmatic, an increase in the expression of the different variants of both receptors at different degrees has been reported, although their role in asthma pathophysiology remains to be elucidated [21]. Furthermore, chronic exposure (24 h, genomic effect) to estrogens in hASM cells from asthmatics and non-asthmatics seems to have opposing effects on $[Ca^{2+}]i$. This phenomenon seems to depend on the type of receptor activated. An ERα-specific agonist ((R,R)-THC) augmented the $[Ca^{2+}]i$ response induced by histamine in both asthmatic and non-asthmatic hASM cells. Meanwhile, an ERβ-specific agonist (DPN), decreased the $[Ca^{2+}]i$ response induced by histamine in asthmatic and non-asthmatic hASM cells. The effect observed on the $[Ca^{2+}]i$ response with activation of ERβ signaling appears to implicate the inhibition of L-VDCC (Figure 3) (Table 1) [35]. Interestingly, E2, (as a non-selective ER agonist) at physiological concentrations did not show significant changes in the $[Ca^{2+}]i$ response to different agonists in ASM [35]. Unfortunately, the genomic effects of estrogen on L-VDCC expression, have not been explored in ASM cells yet. In comparison, ovariectomy (OVX) induced an increase in the channels' expression in rat aorta. Interestingly, treatment with E2 downregulated the channels' mRNA expression, and treatment with E2 and tamoxifen (an ER blocker) had a similar effect as E2 alone [36].

3.2. Store-Operated Calcium Channels

Another group of calcium channels that regulates Ca^{2+} influx to the cytosol is SOCCs, considered non-selective cation channels. Its activity depends on the SR Ca^{2+}depletion and its goal is to contribute to the refilling of internal Ca^{2+} stores [37]. To carry out their function following SR depletion, these channels must assemble into a complex formed by two proteins: Orai1 (calcium release-activated calcium channel protein 1) and STIM1 (stromal

interacting molecule) [37]. When at rest, STIM1 is bound to Ca^{2+}. When Ca^{2+} levels begin to diminish in the SR, STIM1 disassociates from Ca^{2+}, and this change causes STIM1 molecules to cluster and translocate to a region in proximity to the plasma membrane [37–39]. Orai1 is a transmembrane protein located in the plasma membrane. In basal conditions, this protein is a dimer, but when STIM1 clusters are formed, they interact with Orai1 and enable them to form tetramers, forming selective Ca^{2+} pores that allow Ca^{2+} influx [37,39]. This mechanism is negatively regulated by the SR transmembrane protein SARAF (store-operated Ca^{2+} entry-associated regulatory factor). When SARAF interacts with STIM1, it prevents spontaneous activation or the interaction between STIM1-Orai1 [37,40,41]. On the other hand, transient receptor potential canonical (TRPC) channels also play an important role in Ca^{2+} homeostasis, and it is known that the TRPC3 isoform prevails in ASM cells [24]. Recently, the STIM1-Orai1 complex was found to interact with TRPC channels required for their activation [42,43]. Other members of the TRP channel family are vanilloid (TRPV) receptors, ankyrin (TRPA) and melastatin (TRPM), of which TRPV1 and TRPV4 have been identified in ASM cells (Figure 3) [24,44–47].

Given the importance of SOCCs in Ca^{2+} homeostasis, the effects that E2 could have on their regulation is of increasing interest. Townsend et al. determined that the decrease in Ca^{2+} induced by the acute exposure to physiological concentrations of E2 observed in the Ca^{2+} response induced by histamine in hASM cells (Table 1) [20], was in part due to inhibition of SOCCs observed as a diminished SR refilling (Figure 3) [48]. On the other hand, the chronic effects of the estrogen receptor signaling on SOCCs modulation have also been explored in healthy and asthmatic hASM cells. The chronic exposure (24 h) to an ERβ-selective agonist (WAY-200070) downregulated the expression of STIM1 and Orai1 measured through Western blot (Figure 3), and consequently produced a decrease in $[Ca^{2+}]i$. This effect was observed in hASM from non-asthmatics, but was more pronounced in asthmatics [49]. When exposed to an ERα-selective agonist (propyl pyrazole triol at 10 nM) for 24 h, an opposite effect was observed. SOCCs Ca^{2+} influx was increased, and the expression of STIM1 and Orai1 was also increased (Figure 3) (Table 1) [49].

Cigarette smoke (CS) is a common risk factor associated with many airway diseases, and asthmatic women exposed to CS tend to have a worse asthmatic response; therefore, the effects of CS and E2 on ASM Ca^{2+} regulation were explored [50]. As a result, it was defined that, in hASM cells, a 24 h exposure to CS extract induces a significant increase in the Ca^{2+} response to histamine. On the other hand, acute exposure to nanomolar E2 concentrations inhibits the Ca^{2+} response to histamine partially via inhibition of SOCCs [20]. When exposed to CS extract, this E2 effect was blunted [50]. Chronic exposure to CS extract (24h exposure to 1% or 2% CS) also seems to increase the expression of ERα and ERβ, leading to investigate if a differential ER regulation was present. As observed before, the acute effect on Ca^{2+} was present when using an ERα-specific agonist but not an ERβ-selective agonist [20]. This effect was absent when the cells were previously exposed to CS extract [50]. Therefore, CS extract enhances $[Ca^{2+}]i$ through the dysregulation of ER signaling, and blunts the acute reduction in $[Ca^{2+}]i$ and subsequent force generation resultant from ERα activation, more so in asthmatic patients than in healthy subjects. E2 also non-genomically inhibited STIM1 phosphorylation, while pre-exposure to CS extract for 24 h abolished this E2 effect [50].

Studies in other cellular types point out the physiological implications of E2-mediated regulation of SOCCs. In airway epithelial cells, E2 (10 nM) acute (15 min) exposure can reduce STIM1 phosphorylation, preventing the formation of STIM1 clusters from interacting with and activating Orai1, decreasing SOCCs activity. This decrease in SOCCs influx also affects Ca^{2+} activated Cl^- channels colocalized with Orai1, impacting mucus hydration [51]. In mouse embryonic stem cells (mESCs), the treatment with physiological concentrations of E2 (1 pM and 1nM) during 24 h enhanced cellular proliferation in a concentration-dependent manner. The effect was through SOCCs activity and could be reverted by SOCCs blockers (2-APB 0.3 μM) [52]. As already mentioned, Ca^{2+} homeostasis disruption can lead to pathologies. Such is the case in various cancer types, where dysfunction of

Ca^{2+} homeostasis has been implicated. Epithelial ovarian cancer (EOC) is closely tied to E2 regulation, and the effects that E2 could have over Orai1 and the different pathological processes in EOC have been explored [53]. After 12 h exposure with E2 (at a micromolar range), Orai1 expression increased in SK-OV-3 cells (an EOC cell line), with the most significant effect observed at 1 μM, leading to an increase in $[Ca^{2+}]$i. E2, through Orai1, positively regulated cellular and migration (by CDK6 and MMP-1 pathways, respectively), and suppressed cellular proliferation apoptosis through caspase3 expression regulation [53]. In another study in EOC cells, the chronic exposure to E2 (10 nM–1 μM for 24, 48, and 72 h) increased the mRNA levels and protein expression of TRPC3, and via TRPC3 increased cellular proliferation and migration [54]. E2 upregulates TRPV1 expression, participating in pain induction, endometriosis and bone resorption. TRPV1 mRNA levels have been shown to be decreased by E2. Through GPR30, E2 modulates TRPV1 phosphorylation to participate in pain sensitization. Through non-genomic effects, E2 has been shown to both potentiate and decrease capsaicin-evoked currents of TRPV1 [55]. Yang et al., found that TRPV6 expression was increased in human endometrium after E2 treatment [56]. Similarly, in mouse uterine tissues, TRPV5 and TRPV6 were upregulated with E2 treatment; bisphenol A (BPA) that has estrogenic effects, also significantly increased TRPV5 and TRPV6 expression but not to the degree of E2 [57]. Upregulation of TRPA1 by E2 participates in the pathophysiology of endometriosis. Furthermore, through non-genomic effects, E2 increments TRPA1 activation in glucose-induced insulin secretion [55].

Through these studies, we can observe the diverse interactions that estrogens can have over SOCCs modulation and the repercussions in different pathological states.

3.3. Ryanodine Receptor

In the SR, one of the mechanisms in charge of the Ca^{2+} efflux to the cytosol is the RyR. In mammals, three isoforms are found -1, -2, and -3; in mouse ASM, RyR1, and RyR2 are the predominant isoforms, with minimal expression of RyR3 [23,24,58]. It has been found that he endogenous modulation of RyR activity in ASM cells is through the CD38/Cyclic ADP-ribose signaling pathway, regulating $[Ca^{2+}]$i. The membrane-bound protein CD38 synthesizes or degrades cADPR, which functions as a ligand for the protein FKBP-12.6 (12.6 kDa FK506-binding protein). In turn, FKBP112.6 binds to the RyR, providing stabilization and reducing the opening probability of the channel. When cADPR binds to the regulatory protein, this causes a conformational change in the RyR, activating Ca^{2+} release to the cytosol [59–61]. Alterations in this signaling pathway, such as the upregulation of CD38 induced by TNF-α, IL-1β, and IFN-γ, can lead to an asthmatic phenotype of the ASM cells, characterized by airway hyperresponsiveness (AHR) that might develop when an already enhanced $[Ca^{2+}]$i concentration is increased further after Gq protein coupled receptor (GPCR) activation [59,61]. Until now, no non-genomic effects of estrogens over RyRs in ASM cells have been reported. However, in rat cardiomyocytes, bisphenol A (BPA) and bisphenol S (BPS) (estrogenic endocrine-disrupting chemicals) have shown acute effects over RyR activity [62,63]. At nanomolar concentrations, both substances significantly altered characteristic RyR-mediated SR Ca^{2+} sparks by transiently and rapidly (30s–5 min) increasing the phosphorylation of RyR at the serine 2808 site through protein kinase A(PKA) activity, as well as phospholamban (PLB, a protein that binds to SERCA and regulates its activity) by Ca^{2+}/CaM-dependent protein kinase II (CAMKII). This effect was completely abolished when a selective-ERβ blocker was used (PHTPP), but not with a selective-ERα blocker (MPP), indicating that this effect is dependent on the ERβ signaling pathway [62,63].

In mouse ASM cells, long term exposure (24–48 h) to E2 (at physiological levels) was shown to upregulate the expression of CD38 (Figure 3) (Table 1) [64]. As mentioned before, CD38 is a key component in the mechanisms in charge of Ca^{2+} homeostasis by regulating the activity of RyRs. The genomic effect that estrogens could have directly on RyR expression in ASM cells has yet to be explored. In other models, estrogens have shown to impact RyR expression. In uterine arteries from pregnant sheep (a period of

higher estrogenic levels), all three isoforms of RyR were upregulated, causing an increase in Ca^{2+} sparks. Additionally, in uterine arteries from nonpregnant sheep treated ex vivo with estrogen and progesterone mimicking pregnancy conditions, a similar upregulation of RyR was observed [65]. In female rat cardiomyocytes, RyR2 is expressed at higher levels than in male rats [66–68]. In contrast, other reports state that in female cardiomyocytes, RyR2 phosphorylation by CaMKII/PKA is reduced, causing lower Ca^{2+} sparks [66,69,70]. Another possible mechanism of modulation through the ER signaling pathway is by direct protein–protein interaction. Recently, it was discovered that ERβ has an atypical non-genomic effect over the RyR, in the neuronal cell line HT-22. In these cells, RyR2 and ERβ have varying levels of co-localization, and in electrophysiological studies using RyRs from mouse brain incorporated into artificial lipid bilayers, the application of unliganded (E2-free) ERβ1 monomers caused a significant increase in single-channel currents under basal $[Ca^{2+}]$i of 100 nM. This effect caused by the addition of ERβ1 could indicate a synergic interaction with Ca^{2+} and RyR that increases the open probability of the channel and could potentiate RyR activity of Ca^{2+}-induced Ca^{2+}-release [71]. The modulatory activity that the complex E2-ERβ1, or the other isoforms of the ERβ and ERα, could have on the RyR remains to be determined. It might be possible that RyR-ERs interact in the ASM. This probability warrants further and more precise studies.

3.4. IP_3 Receptor

The other mechanism that releases Ca^{2+} from the SR is the IP_3R, activated by its agonist IP_3 (inositol 1,4,5-trisphosphate) [23,24,37]. As extensively known, when an agonist binds to a membrane GPCRs, phospholipase Cβ (PLCβ) is activated and hydrolyzes the lipid phosphatidylinositol 4,5-biphosphate, generating IP_3 and diacylglycerol (DAG) [23,24,37]. In mammals, three isoforms of the IP_3R are expressed (IP_3R1, -2, and -3); all isoforms have been identified in ASM (Figure 3) [24,72–75]. Afterward, IP_3 binds to the IP_3R in the SR, generating the release of Ca^{2+} from these internal stores. This pathway has usually been implicated in the agonist-induced contraction of the ASM. However, IP_3R participation in the bronchodilation mechanism induced by the TAS2R pathway (Type 2 taste receptor) has also been proposed [76,77].

The genomic and non-genomic effects that estrogens could have on the IP_3 signaling pathway in ASM cells remain to be explored, but estrogen modulation in other cell types has been reported (Figure 3). E2 (1 nM) increased IP_3 production after 6 h of exposure (non-genomic effect) in rat oviduct smooth muscle cells, a phenomenon mediated through an increase in PLC activity [78]. In HEPG2 cells (human hepatoma cell line), the addition of E2 (nanomolar range) induced a rapid increase in IP_3 production [79], which was also observed in female rat chondrocytes [80]. Treatment of rat osteoblasts with E2 (100 pM) caused rapid transient increases in $[Ca^{2+}]$i via the PLCβ-IP_3 pathway [81]. E2 treatment has been shown to cause rapid increases in $[Ca^{2+}]$i through an ER interaction with type 1a metabotropic glutamate receptors (mGluR1a), activating the PLCβ-IP_3 pathway in female rat astrocytes [82]. Among the genomic effects, it has been reported that IP_3R1 expression is suppressed after 48h exposure to E2 (10 nM) in human g-292 osteosarcoma cells and rat osteoblasts [83]. In rat choroidal plexus epithelial cells, E2 (nanomolar range) downregulated the expression of receptors TAS2R109 and -144, as well as PLCβ2, resulting in a decrease in $[Ca^{2+}]$i in response to TAS2R agonists [77,84].

3.5. Na^+/Ca^{2+} Exchanger

During the membrane depolarization phase in ASM, an accumulation of Na^+ underneath the plasma membrane takes place, influencing the Ca^{2+} homeostasis through the generation of local concentration gradients. The consequent modulation of the $[Ca^{2+}]$i through the Na^+ gradients results in various physiological processes, depending on the magnitude, time and region, including contraction, proliferation, protein synthesis and apoptosis, among others [85].

The NCX serves as one of the $[Ca^{2+}]i$ buffer mechanisms by extruding Ca^{2+} from the cytosol to the extracellular space [23,24]. The NCX carries three Na^+ ions into the cytosol while extruding one Ca^{2+}; three isoforms, NCX1, -2, and -3 are known, and the most prominent isoform in ASM is the variant NCX1.3 [24,86–89]. The participation of NCX in Ca^{2+} homeostasis in ASM seems to be minor (Figure 3) [24,90], and apparently its reverse mode (NCX_{rev}) has higher importance in ASM physiology. Interestingly, NCX_{rev} introduces Ca^{2+} and extrudes Na^+ [24]. NCX_{rev} plays a preponderant role in agonist-stimulated ASM, as for instance, an inhibitor of NCX_{rev} (KB-R7943, 10 μM) attenuated the $[Ca^{2+}]i$ increase and contraction induced by carbachol (CCh 100 μM) [91]. The Ca^{2+} influx caused by the removal of Na^+ in hASM and mouse ASM was blocked by KB-R7943 [91].

Seemingly, NCX_{rev} also has an important function during oscillatory contractions in mouse ASM induced by potassium channel blockade with tetraethylammonium chloride (TEA). In this experiment, two pattern changes of $[Ca^{2+}]i$ were induced. One was a high-frequency oscillation, and the other a low-frequency rhythmic oscillation. Both types of Ca^{2+} changes participate in triggering ASM contraction, and they might participate in other physiological processes in the ASM. Remarkably, these oscillations augment $[Ca^{2+}]i$, an increase that activates NCX, initiating the relaxation phase by extruding Ca^{2+} [92]. Alterations of the NCX also participate in pathological conditions; TNF-α or IL-13 treatment of hASM cells upregulated the expression of NCX1, and the treatment with KB-R7943 abolished methacholine induced AHR in an allergic mouse model [91,93]. This was also observed in a chronic allergen-induced AHR murine model, where NCX1 was upregulated and had higher NCX_{rev} activity [94].

The effects of E2 on NCX modulation have not been as extensively investigated as other mechanisms. The acute exposure to E2 in hASM cells did not have a significant effect on NCX (Table 1) [20], and the effects of a chronic exposure to E2 on NCX in ASM cells has not been explored yet (Figure 3). Likewise, the participation of NCX in other tissues' physiology is inconclusive. The chronic treatment with E2 (3 days) in prepubescent female rats resulted in downregulation of NCX1 expression in the esophagus [95]. In female rat cardiomyocytes, OVX (ovariectomy) caused downregulation of NCX expression that was reversed by E2 treatment [66,96]. Similarly, in female rabbit cardiomyocytes, NCX expression was greater than in males [66,97,98], and cardiomyocytes incubated with E2 1 nM during 24 h presented a 50% increase in NCX1 protein expression and I_{NCX} density mediated by ERs [98]. Contrary to these findings, OVX or E2 replacement therapy did not alter NCX expression in rat cardiomyocytes. However, NCX activity was significantly increased after OVX in a protein kinase A (PKA)-dependent way; this effect was reverted after E2 treatment [66,99]. Likewise, in cardiomyocytes from OVX guinea pigs, NCX activity was increased by 20%, and this effect was reverted with E2 treatment [66,100]. Moreover, E2 supplementation has been found to have a cardioprotective effect in ischemia/reperfusion injury models [101].

In this sense, NCX overexpression models after myocardial infarction (MI) caused an overload in $[Ca^{2+}]i$ in male mice but not in female mice. Male mice cardiomyocytes, when exposed to E2 (nanomolar range), decreased $[Ca^{2+}]i$ post-MI in a concentration-dependent manner [101]. Interestingly, in a group of female transgenic mice, the NCX overexpression did not lead to $[Ca^{2+}]i$ overload, indicating the protective role of E2 to compensate for the greater activity of NCX [101]. These findings point out that E2 exerts a protective function in cardiac myocytes. Indeed, further research clarified that post-MI E2-confered protection was mediated by NCX. In another study, it was confirmed that the myocardial contractile function (left ventricular developed pressure, dP/dt_{max}, dP/dt_{min}) in male transgenic NCX overexpression mice was significantly higher than in their WT counterparts, as well as in OVX transgenic females, but not in the transgenic or SHAM transgenic female groups. These results implicate NCX in both the contractile and relaxation aspects of the heartbeat. In the post-MI/reperfusion injury phase, the function recovery in transgenic males was lower than in WT males; however, female WT and transgenic NCX mice had a similar recovery, compared with the significantly diminished recovery

in the OVX group. This post-ischemic functional recovery pattern coincides with the lower recovery of energy metabolites (ATP and phosphocreatine) as well as the alternans (heartbeats of alternating large and small amplitude at equal intervals) observed only in the hearts of the male transgenic and female OVX transgenic mice, corresponding to $[Ca^{2+}]i$ overload. These findings suggest a protective role of estrogen over the NCX activity during ischemic/reperfusion injury [102].

Furthermore, E2′s protective capacities were also observed in neurons, where nanomolar concentrations of E2 exerted rapid effects over the NCX function, increasing the outward Ca^{2+} current and decreasing the Ca^{2+} influx mediated by NCX; this effect was potentiated by insulin-like growth factor 1 (IGF-1) [103]. These effects seem to be independent of the canonical estrogen signaling pathways, since the presence of an inhibitor of estrogen receptors (ICI182780, 10 μM) did not alter the results. The non-genomic activity of E2 over NCX in neurons leads to maintaining $[Ca^{2+}]i$ at lower levels, preventing the activation of Ca^{2+}-dependent apoptosis. These mechanisms could be especially useful to counteract the cytotoxicity induced by glutamate through NMDA or AMPA receptor activation [103,104].

3.6. Plasma Membrane Ca^{2+} ATPase

To restore $[Ca^{2+}]i$ to basal levels after increases induced by agonist stimulation, Ca^{2+} can be pumped across the membrane and out of the cell against its electrochemical gradient, expending ATP during the process [23,24,37,105]. This mechanism is achieved by the ASM plasma membrane ATPase (PMCA) that has four different isoforms: PMCA1, -2, -3 and -4, but only PMCA1 and PMCA4 are expressed in this tissue (Figure 3) [24,105]. PMCA activity in ASM cells has been implicated in many intracellular processes, including contraction regulation [24], cellular proliferation [105], and even apoptosis [105]. It is possible that dysfunction of this protein could lead to an increase in $[Ca^{2+}]i$ and favor AHR [24,105].

Modulation of PMCA in ASM cells by estrogen, either through genomic or non-genomic actions, has not been described (Figure 3). However, this phenomenon has been studied in other cellular types. For instance, in prepubescent female rats treated for 3 days with E2 (40 μg/kg/day), the PMCA1 expression in the esophagus was decreased [95]. In MCF-7 cells (breast cancer cell line), PMCA4b isoform expression was increased by E2 (1 nM) treatment in a way mediated by ERα [106]. Conversely, E2 treatment for 24 h decreased the expression of the isoforms PMCA2 and -4 in human fibroblast-like synovial cells (HFLS) and in mouse macrophage-like cells in a dose-dependent manner [107]. In another study, E2 exposure for 24 h did not alter PMCA expression in distal tubule kidney cells; however, PMCA activity was significantly enhanced [108]. In human endometrium, PMCA1 expression was significantly upregulated when treated with E2 (physiological range) for 48 h [56], compared to the decrease of PMCA1 expression in mouse uterus following E2 treatment [57]. E2 has also been described to participate in mechanical pain sensitivity through PMCA2. In female mice, OVX increased mechanical pain sensitivity through PMCA2; this was reversed with E2 supplementation, in a ER-mediated way [109]. It should be noted that alterations in the Ca^{2+} machinery might participate in various pathophysiological processes in accordance with the type of cell implicated.

3.7. Sarcoplasmic Reticulum Ca^{2+} ATPase

Another essential Ca^{2+}-pump that participates in intracellular Ca^{2+} reuptake that is located on the SR membrane of ASM cells is SERCA. It is in charge of driving Ca^{2+} ions against its electrochemical gradient by ATP consumption to reestablish b$[Ca^{2+}]i$ and restoring depleted Ca^{2+} internal stores [24,37,105]. Three isoforms of the SERCA protein are known: SERCA1, -2, and -3, with various alternative splicing isoforms. ASM expresses isoforms SERCA2a and 2b, which predominate [24,110,111]. Alterations in SERCA expression or activity can lead to increases in $[Ca^{2+}]i$, a phenomenon that has been linked to an asthmatic ASM phenotype that contributes to airway remodeling and hyperresponsiveness [24,105,111–113].

Interestingly, hASM cells exposed to E2 apparently showed no acute effects on SERCA activity (Figure 3) [20]. Contrastingly, the estrogen-induced genomic effects on SERCA were explored in hASM cells. They were treated with E2 (1 nM), ERα agonist (PPT, 10 nM) or an ERβ agonist (WAY, 10 nM) for 2 hrs, and then incubated with TNF-α or IL-13. The Ca^{2+} response to histamine in the presence of TNF-α or IL-13 was significantly higher compared to the vehicle. A similar response was observed in the E2 and PPT groups, but the effect was reverted in the WAY group, that showed a response similar to the vehicle group. The time of $[Ca^{2+}]$i decay in the response induced by histamine was higher in the group treated with TNF-α or IL-13. This response was reversed by a treatment with WAY but not by E2 or PPT (Figure 3) [35]. These results were attributed to the treatment's effects on SERCA2 expression, since there was a significant reduction in protein expression in the TNF-α or IL-13 treated cells, which was reverted in WAY treated cells but not in to those administered E2 or PPT (Table 1) [35].

The evidence indicates that $[Ca^{2+}]$i can be modulated by estrogens by the coordinated participation of several target proteins, and that changes in Ca^{2+} availability induced by estrogens is dynamic and additive exerted through genomic and non-genomic events.

Table 1. Summary of the effects of estrogens on the calcium handling mechanisms in the airway smooth muscle.

	Acute		*Chronic*	
Calcium Handling Mechanisms	**Pathway**	**Effect**	**Pathway**	**Effect**
Voltage-dependent Ca^{2+} channels (VDCCs)	ERα	Inhibition [20,34]	ERβ	Inhibition [35]
Store-Operated Calcium Channels (SOCCs)	ERα	Inhibition via STIM1 phosphorylation [20,50]	ERβ	Downregulated STIM1 and Orai1 expression [49]
			ERα	Upregulated STIM1 and Orai1 expression [49]
Ryanodine Receptor (RyR)	Unknown	Unknown	ERs	Upregulates CD38 expression [64]
IP_3 Receptor (IP_3R)	Unknown	Unknown	Unknown	Unknown
Na^+/Ca^{2+} Exchanger (NCX)	No effect	No effect [20]	Unknown	Unknown
Plasma Membrane Ca^{2+} ATPase (PMCA)	Unknown	Unknown	Unknown	Unknown
Sarcoplasmic Reticulum Ca^{2+} ATPase (SERCA)	No effect	No effect	ERβ	Upregulates SERCA2 expression [35]

4. Potassium Handling Mechanisms in Airway Smooth Muscle and Their Modulation by Estrogens

Airway basal tone and diameter represents a balance between constriction and relaxation of the ASM cells that allows adequate airflow through the respiratory tract. Potassium channels in ASM largely determine the membrane's voltage. K^+ electric conductance through the cell membrane is responsible for keeping the membrane potential at rest close to the equilibrium potential of K^+, thus playing an essential role as modulator of ASM homeostasis [114,115]. On the other hand, ionic currents through K^+ channels allow smooth muscle hyperpolarization, contributing to ASM relaxation. In fact, this is the mechanism of action of many bronchodilators as, for instance, β_2-adrenergic agonists, the main bronchodilators used in the therapy of asthma [114]. The family of potassium channels is incredibly varied, but the most significant in ASM are high-conductance Ca^{2+}-activated potassium channels (maxi-K, or BK_{Ca}), voltage-activated potassium channels (Kv), and ATP-regulated potassium channels (K_{ATP}), although the latter channels have been identified

in ASM cells, they do not seem to play a significant role in regulating airway contraction or relaxation [114–118]. To maintain the membrane potential at rest, ASM requires the participation of the Na^+/K^+ ATPase (NKA) [119,120], and some exchangers, such as the $Na^+/K^+/Cl^-$ cotransporter (NKCC) (Figure 4) [121].

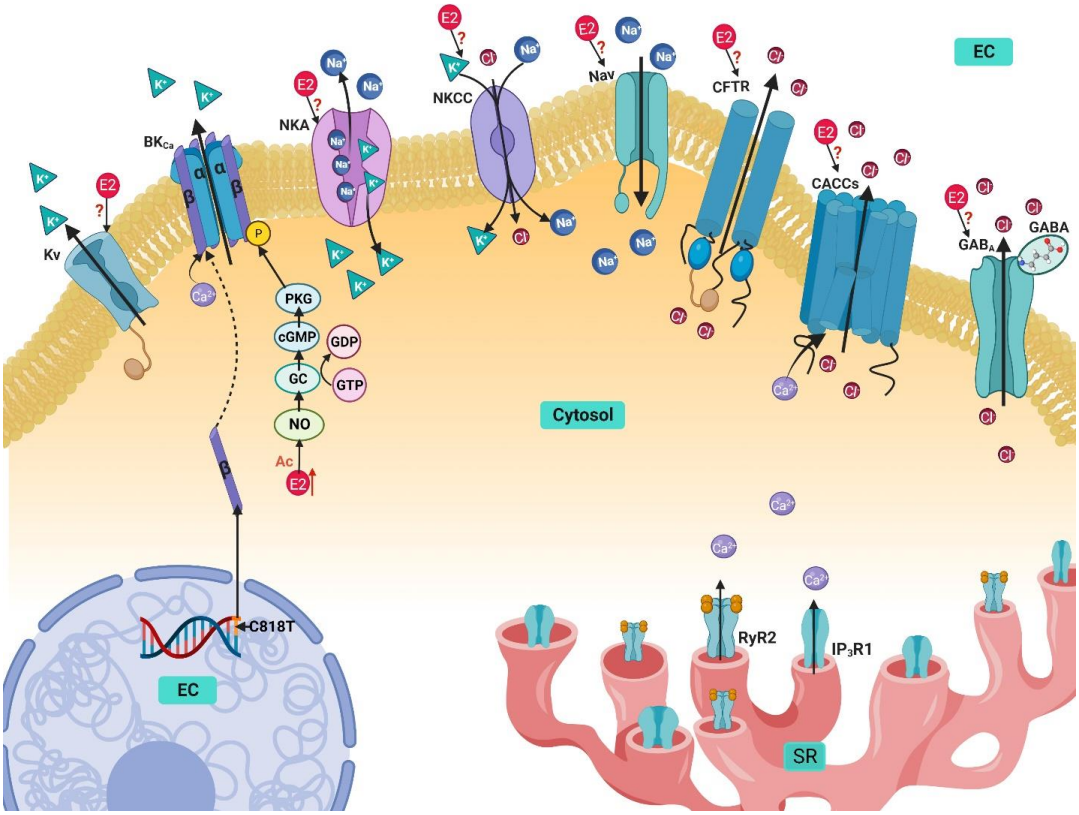

Figure 4. Potassium, sodium and chloride handling mechanisms in airway smooth muscle and their modulation by estrogens. Estrogen acutely increases the BK_{Ca} activity through the NO/GC/cGMP/PKG pathway phosphorylation of the β subunit, and when the SNP C818T is expressed, E2 compensates for the reduced activation of the channel through the activation of the NO/GC/cGMP/PKG pathway. The activity of E2 over the Kv, NKA, NKCC, Nav, CFTR, CACCs, and $GABA_A$ receptor proteins in the ASM is still unknown. EC, extracellular; E2, estradiol; Ac, Acute; SR, sarcoplasmic reticulum; Cl^-, chloride, K^+, potassium; Na^+, sodium; Ca^{2+}, calcium; P, phosphate; BK_{Ca}, high-conductance Ca^{2+}-activated K^+ channel; Kv, voltage-activated potassium channels; NKA, Na^+/K^+ ATPase; NKCC, $Na^+/K^+/Cl^-$ cotransporter; Nav, voltage-gated Na^+ channels; CACCs, Ca^{2+}-activated Cl^- channels; CFTR, cystic fibrosis transmembrane conductance regulator; GABA, gamma amino butyric acid; $GABA_A$, activated chloride channel; RyR2, ryanodine receptor 2; IP_3R, inositol 1,4,5-trisphosphate receptor; NO, nitric oxide; GC, guanyl cyclase; cGMP, cyclic guanosine monophosphate; PKG, protein kinase G; GTP, guanosine triphosphate; GDP, guanosine diphosphate.

4.1. Ca^{2+}-Activated K^+ Channels

The Ca^{2+}-activated K^+ channels (K_{Ca}) are constituted by three families: the large-conductance Ca^{2+}-activated K^+ channels (BK_{Ca}), the intermediate conductance (IK_{Ca}), and the small conductance (SK_{Ca}). BK_{Ca} have the highest importance in ASM cells [114]. In a cell at rest, Ca^{2+} ions that might activate BK_{Ca} usually are the result of Ca^{2+} sparks released from the SR that, after binding to the channel, raise the open-state probability of the channel (Figure 4) [114].

As already mentioned, β_2-adrenergic agonists are the main therapeutic option for bronchodilation (in asthma and chronic obstructive pulmonary disease [COPD]), and BK_{Ca} channel activation is one of the key mechanisms of action of these drugs [114,122]. BK_{Ca}

channels in ASM have also been involved in airway inflammation, as it has been reported that IL-4 induces rapid, large increases in the channel activity, which was reverted by the presence of IL-13 [123]. Many allergic mouse models display AHR development and maintenance mediated by the Th2-mediated cytokine pathway, particularly IL-13 and IL-4 [124]. Meanwhile, the intermediate conductance K^+ channel $IK_{Ca}3.1$ was identified to be involved in ASM cell proliferation, migration, and regulation of the expression of contractile phenotypic marker proteins (smooth muscle myosin heavy chain, smooth muscle α-actin, and myocardin), and is overexpressed in asthmatic mice [125–127]. The $IK_{Ca}3.1$ channel could be a potential therapeutic target for airway remodeling treatment in asthma and COPD.

Interestingly, the non-genomic activity of E2 on BK_{Ca} was examined in mouse ASM tracheal and bronchial rings incubated for 24 hrs in serum containing immunoglobulin E from healthy humans and asthmatic patients. A 30 min pretreatment with E2 (100 nM) attenuated the AHR induced by carbachol in the asthmatic group. The addition of a nonselective E2 receptor antagonist (ICI 182780) abolished this effect [128]. E2 was shown to stimulate the activity of BK_{Ca}, an effect that was corroborated through single-cell electrophysiological experiments. It was found to be mediated by the NOS (nitric oxide synthase)-cGMP (guanyl cyclase)-protein kinase G pathway when the addition of a PKG inhibitor (KT5823, 300 nM) attenuated the activation of BK_{Ca} by E2 [128]. Similarly, the effect of rapid modulation of BK_{Ca} channels by E2 was observed in hASM cells, but Seibold et al. demonstrated that it was linked to an African-specific single nucleotide polymorphism (SNP) in the KCNMB1 gene [129]. The SNP C818T of the KCNMB1 gene, which codes for the β1 subunit of the BK_{Ca} channel, is associated with reduced activation of the channel, leading to clinically significant functional impairment in male patients. On the contrary, in women, this effect was not observed; E2 can induce phosphorylation of the channel via NO/cGMP/PKG pathway to compensate for the SNP defect [129]. Meanwhile, in rat vascular smooth muscle cells, the acute application of E2, at micromolar concentrations, activates BK_{Ca} inducing vasorelaxation [130]. Similarly, in xenopus oocytes, E2 evokes rapid effects over BK_{Ca}, activating the channel, perhaps through direct binding [131].

However, the genomic effects of estrogens over BK_{Ca} in ASM have not been explored as has been the case in other tissues. The chronic treatment with E2 in OVX rats did not alter the expression of BK_{Ca} in vascular smooth muscle [36]. Nevertheless, in pregnant sheep uterine arteries, the expression of the β1 subunit of BK_{Ca} was increased, and myocytes of non-pregnant sheep treated with E2 reach a similar effect, leading to greater channel activity [132]. Through genomic effects, chronic incubation with E2 increased BK_{Ca} expression via ERβ in human and mouse neuroblastoma cell lines [133]. The same effect was observed in GT1-7 cells (gonadotropin-releasing hormone neuronal cell line) where three days of treatment with E2 at physiological levels induced an increase in BK_{Ca} currents mediated by ERβ, attributed to an increase in expression of the α- and β4-subunits of the BK_{Ca} channel [134]. In human uterine smooth muscle, E2 decreased the expression of BK_{Ca}, and reverted the altered expression of the channel in adenomyosis cases [135].

In MCF-7 cells, at physiological levels, E2 regulates cell proliferation in a dose-dependent manner by activating BK_{Ca} independently of ERs [136,137]. BK_{Ca} expression appears to be upregulated by E2 treatment in mice cervical cancer cells, which are estrogen-sensitive cancer cells. [136,138]. The endocrine-disrupting chemicals BPA, BPS, and BPF all demonstrated to regulate the expression of BK_{Ca}, diminishing it after 48 h through the activation of the ERβ pathway [139,140].

The microRNA (small non-coding RNA that regulate gene expression by repression or degradation of the mRNA) miR-16-5p has the potential to modulate the expression of $IK_{Ca}3.1$ [141,142], and E2 was shown to suppress miR-16 in MCF-7 cells via ERα [141,143], indicating a possible route through which E2 could regulate $IK_{Ca}3.1$ and cell proliferation in ASM cells. Indeed, it was demonstrated that, in asthmatic individuals, miR-16 was upregulated, and, through functional validation, resulted in reduced ASM cell growth [144]. Meanwhile, in another study, miR-16 was also associated with β-agonist resistance and

suppression of β_2 adrenergic receptors [145]. It would be interesting to explore how E2 (possibly via miR-16) modulates $IK_{Ca}3.1$ in ASM cells.

4.2. Voltage-Activated K^+ Channels

Voltage-activated K^+ channels (Kv) represent a crucial class of K^+ channels that regulate muscle tone by controlling resting membrane potential. They are also determinants in airway smooth muscle excitability and represent a significant target for different modulators and drugs that negatively regulate bronchoconstriction [115]. In mammals, 40 genes encode for the Kv channels, each gene corresponds to the α subunit. Kv channels are homotetramers of identical or similar α subunits, sometimes they can also contain auxiliary β subunits, adding to the wide diversity of this family (Figure 4) [146]. The Kv channels can be classified into 12 different subfamilies in accordance with their hydrophobic domain containing the six transmembrane segments [146]. Although all the K^+ channels share a similarity in the selectivity filter (SF) in the pore structure, the greatest divergence arises in the different gating mechanisms. In the Kv family, the channels are activated by the changes in the electric field built across the excitable cell membrane. The channel is activated by detecting changes in the membrane's voltage through its voltage-sensing domain (VSD), inducing a conformational change, propagated by a helical linker, that produces the opening of the pore and allows for the efflux of K^+ [146]. In ASM cells, various channels are present, including three channels from the shaker family (Kv1.1, Kv1.2, and Kv1.5), as well as the Kv7 channel [115,117]. Kv7 is present in guinea pig and human ASM cells, and through electrophysiological studies, it has been confirmed to contribute significantly to the maintenance of the resting membrane potential, airway diameter, and AHR regulation, although in mice, it did not appear to significantly impact membrane voltage or contraction by muscarinic agonists [117,147].

Regarding the influence that estrogens play on these channels, it was published that the expression of the Kv1.5 channel subtype in vascular smooth muscle cells was decreased in OVX rats, and this effect was reversed with the treatment of E2 or tamoxifen [36]. Contrastingly, in OVX rabbit hearts, chronic E2 treatment downregulated the expression of Kv1.5 and Kv7.1 [148]. E2 treatment augmented the expression of Kv7.5, but not Kv7.2 and 7.3, in OVX guinea pig neurons [149,150], and in mouse pancreatic β cells, BPA chronic treatment downregulated the expression of the KV2.1/2.2 channels [139].

The E2 treatment of HEK 293B cells (48 h) enhanced the activity of Kv11.1 channels but did not alter the expression of the channel. Instead, post-transcriptional modifications boosted the interaction between Kv11.1 and the chaperone proteins Hsp90 and Hsc70, improving trafficking of the channel to the membrane [136,151]. The hormonal regulation of the KCNH2 gene trafficking causes a shortening of the QT interval and could serve as a potential therapeutic target for patients at risk of presenting prolonged repolarization [136,151] In rat arterial smooth muscle, E2, at supraphysiological levels, inhibited Kv channel inhibition induced by serotonin independently of the ERs, via Src protein [136,152]. E2 could also modulate cellular proliferation through Kv10.1, in HeLa cells (cervical cancer cell line) E2 at picomolar levels upregulates the expression of Kv10.1 mediated by ERα [136,153,154]. Even though the effect that estrogens could exert over the Kv channels in ASM cells remains unknown, in other cellular models it has been defined that they participate both in physiological and pathological processes, and the same could be the case in ASM.

4.3. Na^+/K^+ ATPase

In ASM, the NKA is known to contribute to resting membrane potential regulation and maintenance of muscle tone. Its participation in spontaneous phasic activity during contraction has been recognized as well [119,120]. The ionic exchange of NKA extrudes 3 Na^+ molecules and pumps in 2 K^+ into the cytosol for every ATP used; it is an electrogenic pump that promotes a Na^+ outward current (Figure 4) [119]. During oscillatory contractions in mouse ASM induced by TEA, NKA has been identified to participate in

the relaxation phase of the oscillations. When activated, NKA reduces the differential potential of the cellular membrane, inactivating LVDCCs and causing relaxation [92]. It should be mentioned that TEA is a drug used to induce ASM contraction by depolarizing the membrane through the inhibition of K^+ channels. When activated by K^+, the pump induces muscle relaxation by hyperpolarizing the membrane. In accordance, inhibiting the ASM NKA pump with ouabain (100 μM) produces contraction [120,155–157]. The NKA also plays a role in AHR. In guinea pig ASM cells, bradykinin (an agonist of the bradykinin GPCR receptors, known to cause bronchoconstriction in asthmatics) increased the NKA activity mediated by the activation of the B2 receptors and stimulation of Na^+ influx through the Na^+-H^+ exchanger (NHX) [120]. NKA blockade with ouabain can alter ASM tone and induce muscle contraction by favoring the influx of Ca^{2+} through the VDCCs and NCX [85,120]. The differential regulation presented by the increase of NKA activity by bradykinin could lead to a negative feedback mechanism that opposes the contraction usually elicited by B2 receptor stimulation [120].

The effects of E2 on NKA activity has not been explored in ASM cells. In H9C2 rat cardiomyocytes, E2 enhanced the expression of NKA in a concentration-dependent manner [158,159]. In male rat cardiomyocytes, NKA activity, expression, and phosphorylation (possibly through Akt and ERK 1,2 regulation) were enhanced after 24 h E2 treatment [160]. A similar effect was observed in HSG and HeLa cells, where E2 treatment, through ERβ activation, upregulated the expression of the β1-subunit of NKA, and through the N-myc downstream-regulated Gene 2 (NDGR2) the degradation of the β1-subunit was decremented, enhancing NKA activity [158,161]. Moreover, in erythrocytes from women, NKA activity was enhanced when E2 levels were higher [158,162]. In female rat aorta, the activity of NKA is increased through NO, and an upregulation of the α2-isoform of NKA was noticed as well. Inversely, OVX blunted the effect [163]. Contrary to this, in another study, OVX increased the activity of NKA in rat vascular smooth muscle [164].

4.4. $Na^+/K^+/Cl^-$ Cotransporter

The $Na^+/K^+/Cl^-$ cotransporter (NKCC) facilitates the movement of Na^+, K^+, and Cl^- ions across the membrane in an electrically neutral way (Figure 4) [121]. It is expressed in ASM cells, and participates in different processes, including ASM cell proliferation, confirmed by its inhibition through loop diuretics treatment (bumetanide and furosemide) [165]. NKCC1 immunoreactivity was found in airway epithelial cells and alveolar type II cells, and in mice sensitized with ovalbumin (OVA) overexpression was seen. The inhibition of the cotransporter with furosemide reduced overall airway responsiveness and reverted the AHR induced by OVA sensitization [166].

The effect of E2 over the NKCC has been studied in other cell types. E2, at nanomolar concentrations, has a neuroprotective effect by decreasing edema formation after cerebral ischemia in rats by attenuating the NKCC activity [167]. After 24 h treatment with E2 (1 nM), NKCC expression decreased in bovine cerebral microvascular endothelial cells. Nevertheless, when endothelial cells were subjected to shear stress, E2 did not alter NKCC expression [168]. Contrary to this, in OVX rat hippocampus, the expression of NKCC decreased, and 24 h treatment with E2 reverted this effect [169]. In developing rat hypothalamus neurons, E2 treatment for 24 h significantly enhanced NKCC1 phosphorylation by increasing the expression of the kinases SPAK and OSR1 but did not modify the protein expression levels [170].

In rat aorta, the NKCC exchanger seems to participate in phenylephrine (PE) contraction in a gender-specific manner. In female rats, inhibition of NKCC1 did not modify the maximal contraction with PE, while OVX increased NKCC1 activity and E2 treatment blunted this effect [171]. The modulatory effect of E2 over the NKCC in ASM cells is still unknown but considering the significance that it has in the regulation of physiological and pathological processes in other cells model, it would be interesting to explore in the future the role it plays in the ASM.

5. Sodium Handling in Airway Smooth Muscle and Its Modulation by Estrogen

To initiate bronchoconstriction, an increase in $[Ca^{2+}]i$ is necessary, although it is not the only contributor to ASM contraction regulation. In the extracellular space, Na^+ concentration is the highest (140 mM), while the intracellular concentration is normally much lower, about 4–16 mM. This electrochemical gradient is usually utilized by excitable cells to generate action potentials and to facilitate the transport of energetically unfavorable solutes coupled to Na^+ [172]. In ASM cells, the membranal depolarization initiates contraction, and no single mechanism is in charge of maintaining the equilibrium of the membrane potential. Instead, many membrane mechanisms interact to balance it, including Na^+ channels that accelerate the rate of depolarization by influencing Ca^{2+} handling mechanisms [85]. As with other ion handling mechanisms, various proteins regulate the influx and efflux of Na^+ ions. In ASM cells, the main contributors for Na^+ influx are the NCX, the voltage-gated Na^+ channels (VGSC), and non-selective cation channels (NSCC), while Na^+ is extruded through the NKA [85].

Voltage-Gated Na^+ Channels

When bearing in mind excitable cells, such as neurons or myocytes, usually voltage gated sodium channels (VGSCs) are some of the first channels to consider. In ASM cells, VGSCs have already been identified to be functionally expressed in humans and rabbits, including the isoforms Nav1.2, 1.5, and 1.7 [85,173–175]. The contributors for the Na^+ currents observed in ASM cells appear to be Nav1.5 and 1.7 [173,175]. Additionally, oscillatory contractions in mouse ASM, Nav channels participate in the enhancement of the depolarization by activating LVDCCs; interestingly, when Nav were inhibited, the contractions disappeared [92]. Furthermore, the participation of these channels could be involved in pathological conditions, the increase in intracellular Na^+ concentration ($[Na^+]i$) activates the NCX_{REV}, increasing $[Ca^{2+}]i$ (Figure 4) [24,85,176]. Hence, the enhanced I_{Na} could participate in the dysfunction of cell contraction, excitation, and remodeling [176]. The chronic treatment of ASM cells with dexamethasone (1 µM for 24 h) diminished the expression of Nav1.7 channel and could prove beneficial in the detrimental mechanisms elicited by these channels in some pathologies [176].

Voltage-gated sodium channels also participated in pathologies like cancer, and it has been found that VGSCs are upregulated in these illnesses where they are indispensable for various pathophysiological mechanisms such as metastasis [177]. It is noteworthy to mention that in human breast cancer cells, the non-genomic effects of E2 through GPR30 increased the neonatal splice form of Nav1.5's (nNav1.5) activity, and this mechanism was crucial for cell adhesion and metastasis [178]. Moreover, E2 has been shown to exert non-genomic cardioprotective effects via Nav modulation. In cardiomyocytes from human inducible pluripotent stem cells (iPSC-CMs) and Chinese hamster ovarian (CHO) cells, E2 (micromolar concentrations) did not elicit changes by itself in Nav currents; however, it significantly reduced the high glucose or inflammatory mediators (bradykinin, histamine, serotonin, and ATP)-induced increments in Na+ currents that caused hyperexcitability and resulted in long QT3 arrhythmias, this effect was mediated by PKC/PKA activation [179].

E2 actions on VGSCs seemingly also participate in pain modulation. In adult dorsal root ganglion (DRG) neurons, ERs differentially regulate Nav expression [180]. In ERα knock out (ErαKO) and Erβ knock out (ERβKO) mice, the expression of Nav1.1, 1.7, 1.8, and 1.9 are upregulated, but in αERKO, the expression of Nav1.6 was decreased but not in βERKO [180]. Opposite to this, E2 treatment increased the expression of Nav1.7 in OVX rat trigeminal ganglions in a dose-dependent manner [181]. Meanwhile, a single acute E2 dose was proven to also modulate Nav activity. In patch-clamp studies, E2 at 10 nM increased Na+ inward currents in rat hypothalamic neurons [182].

6. Chlorine Handling Mechanisms in Airway Smooth Muscle and Their Modulation by Estrogen

Many ions participate in controlling the cellular electrochemical balance and its membrane potential, and Cl^- is no exception [183,184]. Intracellular concentrations of Cl^- are approximately 30–50 nM, in turn, the equilibrium potential of Cl^- ranges between −30 and −20 mV, more positive than the ASM resting membrane potential, which is around -60 mV. In an ASM at rest, Cl^- efflux will lead to membrane depolarization, but when the membrane depolarization is already in course, this Cl^- current will contribute to maintaining and enhancing the initial depolarization. Because of these mechanisms, Ca^{2+} enters through LVDCCs activation and a subsequently initiates an ASM contraction (Figure 4) [183–186]. Cl^- homeostasis is maintained through the coordinated activities of a series of proteins in charge of the influx and efflux of this ion through the membrane. It has been established that in ASM, the NKCC as well as several Cl^- channels participate in this anion's management. In fact, the following Cl^- channels have been identified in this cell type: Ca^{2+}-activated Cl^- channels (CACCs), ligand-gated Cl^- channels (gamma amino butyric acid receptor, GABA), and the cystic fibrosis transmembrane conductance regulator (CFTR) (Figure 4) [183,184].

Regarding smooth muscle physiology, Cl^- channels seem to effectively induce relaxation from a pre-contracted ASM, but apparently have minimal effects on basal tension and even might prevent contraction development [183,187]. This is probably related to the ASM Cl^- channels' localization, and the impact of the channel blockade on Ca^{2+} regulation at the membrane and SR level [187]. The blockade of the Cl^- channels potentiates the relaxation induced by β-agonists, especially when combining a Cl^- channel blocker with bumetanide (an NKCC blocker), and certainly this effect could be of therapeutic interest in the treatment of asthma [187]. Cl^- channel activity also participates closely in Ca^{2+} handling and contraction, not only through Cl^- channels present in the plasma membrane, but on the SR. In the SR, Ca^{2+} release is an electrogenic process, and modifications in charges (positive or negative) across the membrane will hinder this process. If the SR Cl^- fluxes are inhibited, Ca^{2+} sequestration and Ca^{2+} release induced by agonists will be reduced [183,188]. In ASM oscillatory contractions, Cl^- channels play a crucial role, especially in the rhythmic transitions of the membrane potential; this effect is clearly observed in the contraction induced by TEA (a K^+ channel blocker) [92,183]. During these oscillations, the $[Ca^{2+}]i$ increase induced by LVDCCs currents activate CACCs, and Cl^- ions participate in the contractile phase by favoring membrane depolarization and enhancing the contraction by further activating LVDCCs [92].

6.1. Ca^{2+} activated Cl^- Channels

CACCs have been shown to be present in ASM cells, and are activated by the increase in $[Ca^{2+}]i$ by activation of LVDCCs or Ca^{2+} release from the internal stores [185,186,188]. The participation of CACCs can be observed in various processes in ASM cells, including modulation of contraction–relaxation, maintenance of muscle tone and membrane potential, and membrane depolarization (Figure 4) [183,185,186,188,189]. The blockade of CACCs also potentiates the relaxant effect induced by β-agonists and could be of interest in the treatment of asthma [187]. One of the most important CACCs identified in ASM cells is TMEM16A (transmembrane protein with unknown function 16, Ano1); seemingly, this channel is involved in ASM tone modulation, and regulates the contraction induced by cholinergic agonists [190,191]. The participation of TMEM26A has also been observed in the relaxation by activation of the odorant pathway via the GPCR OR2W3, in which SOCCs activation initiates a tradeoff between CFTR in the SR and TMEM16A in the plasma membrane to induce relaxation [192].

Notwithstanding, no report exists on the estrogen's effect on CACCs in ASM cells. However, in HEK293T cells, estrogens inhibit TMEM16A. This inhibitory non-genomic effect of estrogen was observed with E2, E3, and estetrol (E4) at micromolar levels, with the most potent effect observed with E3 [193]. In female CF (cystic fibrosis) patients, periods

of E2 plasmatic levels elevation during the menstrual cycle coincided with the reduction of CACCs activity in airway epithelial cells, which caused subsequent mucus plugging. Tamoxifen treatment prevented this effect, and it even enhanced the Cl- currents [194]. In human bronchial epithelial cells, the acute application of E2 (10 nM) reduced ATP-induced CACC currents, but this effect was reverted with tamoxifen; in fact, the CACC currents were potentiated [195]. This estrogenic mechanism could be useful in the treatment of CF patients. This non-genomic effect of estrogens should be explored in ASM cells.

6.2. Cystic Fibrosis Transmembrane Conductance Regulator

In ASM cells, the CFTR channel is functionally expressed and plays a role in regulating muscle tone (Figure 4) [196–199]. In this sense, when compared to the WT littermates, FVB/N ΔF508 mice (deletion of the 508 codon) presented AHR with increased airway resistance against methacholine challenge. This increment in airway resistance developed in the absence of overt lung inflammation or an increase in ASM mass and was attributed to the altered airway mechanics [200]. A loss of CFTR, such as is the case in CF, leads to an "asthma-like" phenotype in patients that present AHR, and is attributed to be a consequence of a delayed Ca^{2+} reuptake and increased myosin light chain phosphorylation after cholinergic stimulation [197,198]. In addition, the CFTR channel and the TMEM16A jointly participate in the relaxation signaling pathway initiated by the odorant receptor OR2W3 in ASM cells [201].

In female CF patients, lung function was measured in correspondence to their menstrual cycle, and it was observed that the forced expiratory volume during one second and the forced vital capacity were significantly higher during the luteal phase when compared to ovulation and menstruation; this could be due to the higher estrogen levels, but the mechanism that could be at play or if it involves the ASM remains to be investigated [202]. In T84 epithelial cells, estrogen seems to modulate CFTR activity; E2 (micromolar levels) induced rapid and reversible inhibition of forskolin-stimulated Cl^- secretion, and this effect was also observed with other estrogen derivatives, including the stereoisomer 17α-estradiol that does not bind to the ERs, indicating that the genomic effect is through direct interaction of the estrogen with the CFTR protein [203]. In rats, an increment of CFTR expression in the uterus and ovary was observed after induced ovarian hyperstimulation syndrome (OHSS), in which E2 levels were found to be eight times higher than normal levels [204]. This was corroborated by E2 treatment of OVX rats that mimicked the results of OHSS and through measurement of CFTR activity in freshly isolated uterine epithelia [204]. In another study, CFTR expression was higher in women than in men in duodenal mucosa cells and in duodenocytes treated with E2 (1 nM) for 12 h, where a significant increase in expression mediated by ERα was observed [205]. This was also corroborated by measuring the activity of CFTR in OVX mice. Forskolin (a CFTR activator) stimulation response was markedly decreased, and this effect was reverted with E2 supplementation [205]. Similarly, peritoneal epithelial cells of rats with induced OHSS showed CFTR upregulation, and this genomic effect was reproduced by E2 treatment in OVX rats [206]. In pancreatic epithelial cells, E2 incubation (3.7 nM for 20 h), did not alter CFTR expression levels, but it inhibited cAMP-activation of CFTR and consequently led to cell volume reduction [207]. CFTR is also present in guinea pig cardiomyocytes, and the acute application of E2 (micromolar range) potentiates the I_{Cl} induced by isoprenaline in a concentration-dependent manner, independently of the ERs [208].

6.3. GABA-Activated Cl^- Channels

Another group of Cl^- channels are ionotropic receptors activated by a ligand. In ASM cells, ionotropic $GABA_A$ receptors have been identified to be functionally expressed in humans and guinea pigs, and GABA can relax the contraction induced by tachykinin in a concentration-dependent manner (Figure 4) [209]. Contrastingly, the activation of $GABA_A$ receptor does not affect ASM basal tone, nor does it seem effective in preventing a contraction, but when applied to a precontracted ASM, it induces relaxation effectively [210].

The $GABA_A$ receptors are heteromeric pentamers that can be composed of seven different classes of subunits (α1–6, β1–3, γ1–3, δ, π, ξ, and ρ1–3); the mixed composition of the receptor can affect its responsiveness to allosteric activation, particularly attributed to the α subunit [210]. In hASM cells, from the α subunit class, only α4 and α5 are expressed and integrate a hetero pentameric receptor [210], and selective targeting of this subunit with agonists results in activation of the Cl^- currents that generate hyperpolarization and relaxation of the precontracted smooth muscle [210,211]. When sensitized to house dust mite (HDM) antigen, $GABA_A$ receptor α4-subunit knockout mice in vivo models develop an increase in airway resistance, lung inflammation, and ASM proliferation, when compared to the WT mice [212]. The selective activation of the α subunit of the $GABA_A$ receptor could have bronchodilatory potential in asthma or COPD.

Although no reports have been made concerning the effect of estrogens on the modulation of the $GABA_A$ receptor in ASM cells, some effects have been observed in other tissues. In female rat brains, E2 treatment after OVX showed a significant increase of the α2 and the γ1 subunits only in regions that also expressed ERs, suggesting that the effect depends on the ER signaling [213]. The effect was also time-dependent, since there was a greater upregulation after 7 d of treatment compared to only 24 h [213]. Through genomic effects, E2 treatment also increased GABA binding sites in OVX rat brain, as soon as after 3 h of incubation, in a dose-dependent manner [214]. Conversely, another report failed to find a significant alteration in the rat brain expression of $GABA_A$ receptor in the OVX vs. OVX + E2 treated groups [215]. E2 regulation of $GABA_A$ receptor expression is also relevant in the developmental stages. In neonatal female rats, β-estradiol 3-benzoate (EB) treatment upregulated the expression of extrasynaptic α4/δ subunits but decreased the expression of synaptic α1/α4/γ2 subunits [216].

7. Conclusions

In summary, a wide range of evidence from different cell types and animal models indicate that estrogens have a promiscuous nature, being able to interact with a variety of regulatory proteins essential in the homeostasis of intracellular ions. The estrogenic effects are not clearly cut but are instead subject to the conditions and variables that surround them. The effects of estrogens can vary greatly depending on the concentration, time of exposure, type of estrogen, requirement or independence of ER signaling, and even cell type. In this context, the effects of estrogens in some proteins such as IP3 receptors, PMCA, SERCA, NKA, NKCC, VGSCs, and CACCs on ASM cells have not been explored in-depth. There is not a single regulatory protein in which at least one study of E2 modulation is reported. Thus, the necessity still exists to better understand the possible effects that estrogens could have in physiological and pathological conditions in ASM cells. In this sense, it seems that single-cell genomics studies and spatial transcriptomics analysis may be quite useful in the following years to unravel the punctual functions of estrogens, particularly on the surrounding tissues where they are synthesized.

Author Contributions: Conceptualization, B.S.R.-M., L.M.M. and E.F.-S.; investigation, B.S., R.J., A.A.-G., H.S.-C., G.G.-A. and B.S.R.-M.; data curation, J.C.G.-V. and E.C.; writing—original draft preparation, E.F.-S., E.C. and B.S.R.-M.; writing—review and editing, B.S.R.-M., E.F.-S., B.S. and L.M.M.; supervision B.S. and L.M.M.; funding acquisition, L.M.M. All authors have read and agreed to the published version of the manuscript.

Funding: This study was partly supported by grants from the Dirección General de Asuntos del Personal Académico (DGAPA), the Universidad Nacional Autónoma de México (IN200522) and CONACYT (137725) to L.M. Montaño.

Institutional Review Board Statement: Not applicable.

Informed Consent Statement: Not applicable.

Data Availability Statement: Not applicable.

Acknowledgments: Bianca S. Romero-Martínez is grateful to the Programa de Doctorado en Ciencias Biomédicas, Universidad Nacional Autónoma de México, for the instruction received during her Ph. D. degree studies. She received a fellowship from the Consejo Nacional de Ciencia y Tecnología, México (application # 2020-000013-01NACF-12778; CVU 469822. We are grateful to Maria del Pilar Gonzalez Romo and Rosalba Linares Sanchez for their administrative and technical support.

Conflicts of Interest: The authors declare no conflict of interest.

References

1. Nehrke, K. Membrane ion transport in non-excitable tissues. *WormBook* **2014**, 1–22. [CrossRef] [PubMed]
2. Janssen, L.J. Calcium Handling in Airway Smooth Muscle: Mechanisms and Therapeutic Implications. *Can. Respir. J.* **1998**, *5*, 491–498. [CrossRef] [PubMed]
3. Gadsby, D.C. Ion channels versus ion pumps: The principal difference, in principle. *Nat. Rev. Mol. Cell Biol.* **2009**, *10*, 344–352. [CrossRef] [PubMed]
4. Dascal, N. Ion-channel regulation by G proteins. *Trends Endocrinol. Metab.* **2001**, *12*, 391–398. [CrossRef]
5. Song, S.; Luo, L.; Sun, B.; Sun, D. Roles of glial ion transporters in brain diseases. *Glia* **2020**, *68*, 472–494. [CrossRef]
6. Rosati, B.; Mckinnon, D. Regulation of Ion Channel Expression. *Circ. Res.* **2004**, *94*, 874–883. [CrossRef]
7. Cole, T.J.; Short, K.L.; Hooper, S.B. The science of steroids. *Semin. Fetal Neonatal Med.* **2019**, *24*, 170–175. [CrossRef]
8. Miller, W.L.; Auchus, R.J. The Molecular Biology, Biochemistry, and Physiology of Human Steroidogenesis and Its Disorders. *Endocr. Rev.* **2011**, *32*, 81–151. [CrossRef]
9. Martin, Y.N.; Pabelick, C.M. Sex differences in the pulmonary circulation: Implications for pulmonary hypertension. *Am. J. Physiol.-Heart Circ. Physiol.* **2014**, *306*, H1253–H1264. [CrossRef]
10. Sathish, V.; Martin, Y.N.; Prakash, Y.S. Sex steroid signaling: Implications for lung diseases. *Pharmacol. Ther.* **2015**, *150*, 94–108. [CrossRef]
11. Townsend, E.A.; Miller, V.M.; Prakash, Y.S. Sex Differences and Sex Steroids in Lung Health and Disease. *Endocr. Rev.* **2012**, *33*, 1–47. [CrossRef] [PubMed]
12. Cui, J.; Shen, Y.; Li, R. Estrogen synthesis and signaling pathways during aging: From periphery to brain. *Trends Mol. Med.* **2013**, *19*, 197–209. [CrossRef] [PubMed]
13. Kurokawa, J.; Kodama, M.; Clancy, C.E.; Furukawa, T. Sex hormonal regulation of cardiac ion channels in drug-induced QT syndromes. *Pharmacol. Ther.* **2016**, *168*, 23–28. [CrossRef] [PubMed]
14. Yu, X.; Ma, H.; Barman, S.A.; Liu, A.T.; Sellers, M.; Stallone, J.N.; Prossnitz, E.R.; White, R.E.; Han, G. Activation of G protein-coupled estrogen receptor induces endothelium-independent relaxation of coronary artery smooth muscle. *Am. J. Physiol. Endocrinol. Metab.* **2011**, *301*, E882–E888. [CrossRef]
15. Tran, Q.K. Reciprocality Between Estrogen Biology and Calcium Signaling in the Cardiovascular System. *Front. Endocrinol.* **2020**, *11*, 568203. [CrossRef]
16. Mah, V.; Seligson, D.B.; Li, A.; Márquez, D.C.; Wistuba, I.I.; Elshimali, Y.; Fishbein, M.C.; Chia, D.; Pietras, R.J.; Goodglick, L. Aromatase Expression Predicts Survival in Women with Early-Stage Non–Small Cell Lung Cancer. *Cancer Res.* **2007**, *67*, 10484–10490. [CrossRef]
17. Mair, K.M.; Wright, A.F.; Duggan, N.; Rowlands, D.J.; Hussey, M.J.; Roberts, S.; Fullerton, J.; Nilsen, M.; Loughlin, L.; Thomas, M.; et al. Sex-Dependent Influence of Endogenous Estrogen in Pulmonary Hypertension. *Am. J. Respir. Crit. Care Med.* **2014**, *190*, 456–467. [CrossRef]
18. Martin, Y.N.; Manlove, L.; Dong, J.; Carey, W.A.; Thompson, M.A.; Pabelick, C.M.; Pandya, H.C.; Martin, R.J.; Wigle, D.A.; Prakash, Y.S. Hyperoxia-induced changes in estradiol metabolism in postnatal airway smooth muscle. *Am. J. Physiol.-Lung Cell. Mol. Physiol.* **2015**, *308*, L141–L146. [CrossRef]
19. Heldring, N.; Pike, A.; Andersson, S.; Matthews, J.; Cheng, G.; Hartman, J.; Tujague, M.; Ström, A.; Treuter, E.; Warner, M.; et al. Estrogen receptors: How do they signal and what are their targets. *Physiol. Rev.* **2007**, *87*, 905–931. [CrossRef]
20. Townsend, E.A.; Thompson, M.A.; Pabelick, C.M.; Prakash, Y.S. Rapid effects of estrogen on intracellular Ca^{2+} regulation in human airway smooth muscle. *Am. J. Physiol.-Lung Cell. Mol. Physiol.* **2010**, *298*, L521–L530. [CrossRef]
21. Aravamudan, B.; Goorhouse, K.J.; Unnikrishnan, G.; Thompson, M.A.; Pabelick, C.M.; Hawse, J.R.; Prakash, Y.S.; Sathish, V. Differential Expression of Estrogen Receptor Variants in Response to Inflammation Signals in Human Airway Smooth Muscle. *J. Cell. Physiol.* **2017**, *232*, 1754–1760. [CrossRef]
22. Kow, L.-M.; Pfaff, D.W. Rapid estrogen actions on ion channels: A survey in search for mechanisms. *Steroids* **2016**, *111*, 46–53. [CrossRef] [PubMed]
23. Berridge, M.J.; Bootman, M.D.; Roderick, H.L. Calcium signalling: Dynamics, homeostasis and remodelling. *Nat. Rev. Mol. Cell Biol.* **2003**, *4*, 517–529. [CrossRef] [PubMed]
24. Reyes-García, J.; Flores-Soto, E.; Carbajal-García, A.; Sommer, B.; Montaño, L. Maintenance of intracellular Ca^{2+} basal concentration in airway smooth muscle (Review). *Int. J. Mol. Med.* **2018**, *42*, 2998–3008. [CrossRef]
25. Janssen, L.J. T-type and L-type Ca^{2+} currents in canine bronchial smooth muscle: Characterization and physiological roles. *Am. J. Physiol.* **1997**, *272*, C1757–C1765. [CrossRef] [PubMed]

26. Montaño, L.M.; Barajas-Lopez, C.; Daniel, E.E. Canine bronchial sustained contraction in Ca^{2+}-free medium: Role of intracellular Ca^{2+}. *Can. J. Physiol. Pharmacol.* **1996**, *74*, 1236–1248. [CrossRef]
27. Sommer, B.; Flores-Soto, E.; Reyes-García, J.; Díaz-Hernández, V.; Carbajal, V.; Montaño, L.M. Na^{+} permeates through L-type Ca^{2+} channel in bovine airway smooth muscle. *Eur. J. Pharmacol.* **2016**, *782*, 77–88. [CrossRef]
28. Bean, B.P. Classes of calcium channels in vertebrate cells. *Annu. Rev. Physiol.* **1989**, *51*, 367–384. [CrossRef]
29. Yu, J.; Bose, R. Calcium channels in smooth muscle. *Gastroenterology* **1991**, *100*, 1448–1460. [CrossRef]
30. Green, K.A.; Small, R.C.; Foster, R.W. The properties of voltage-operated Ca^{2+}-channels in bovine isolated trachealis cells. *Pulm. Pharmacol.* **1993**, *6*, 49–62. [CrossRef]
31. Hisada, T.; Kurachi, Y.; Sugimoto, T. Properties of membrane currents in isolated smooth muscle cells from guinea-pig trachea. *Pflug. Arch. Eur. J. Physiol.* **1990**, *416*, 151–161. [CrossRef] [PubMed]
32. Kotlikoff, M.I. Calcium currents in isolated canine airway smooth muscle cells. *Am. J. Physiol.* **1988**, *254*, C793–C801. [CrossRef] [PubMed]
33. Marthan, R.; Martin, C.; Amédée, T.; Mironneau, J. Calcium channel currents in isolated smooth muscle cells from human bronchus. *J. Appl. Physiol.* **1989**, *66*, 1706–1714. [CrossRef] [PubMed]
34. Flores-Soto, E.; Reyes-García, J.; Carbajal-García, A.; Campuzano-González, E.; Perusquía, M.; Sommer, B.; Montaño, L.M. Sex steroids effects on guinea pig airway smooth muscle tone and intracellular Ca^{2+} basal levels. *Mol. Cell. Endocrinol.* **2017**, *439*, 444–456. [CrossRef]
35. Bhallamudi, S.; Connell, J.; Pabelick, C.M.; Prakash, Y.S.; Sathish, V. Estrogen receptors differentially regulate intracellular calcium handling in human nonasthmatic and asthmatic airway smooth muscle cells. *Am. J. Physiol.-Lung Cell. Mol. Physiol.* **2020**, *318*, L112–L124. [CrossRef] [PubMed]
36. Tsang, S.Y.; Yao, X.; Wong, C.M.; Chan, F.L.; Chen, Z.Y.; Huang, Y. Differential regulation of K^{+} and Ca^{2+} channel gene expression by chronic treatment with estrogen and tamoxifen in rat aorta. *Eur. J. Pharmacol.* **2004**, *483*, 155–162. [CrossRef] [PubMed]
37. Krebs, J.; Agellon, L.B.; Michalak, M. Ca^{2+} homeostasis and endoplasmic reticulum (ER) stress: An integrated view of calcium signaling. *Biochem. Biophys. Res. Commun.* **2015**, *460*, 114–121. [CrossRef]
38. Peel, S.E.; Liu, B.; Hall, I.P. A key role for STIM1 in store operated calcium channel activation in airway smooth muscle. *Respir. Res.* **2006**, *7*, 119. [CrossRef]
39. Peel, S.E.; Liu, B.; Hall, I.P. ORAI and Store-Operated Calcium Influx in Human Airway Smooth Muscle Cells. *Am. J. Respir. Cell Mol. Biol.* **2008**, *38*, 744–749. [CrossRef]
40. Palty, R.; Raveh, A.; Kaminsky, I.; Meller, R.; Reuveny, E. SARAF Inactivates the Store Operated Calcium Entry Machinery to Prevent Excess Calcium Refilling. *Cell* **2012**, *149*, 425–438. [CrossRef]
41. Albarran, L.; Regodón, S.; Salido, G.M.; Lopez, J.J.; Rosado, J.A. Role of STIM1 in the surface expression of SARAF. *Channels* **2017**, *11*, 84–88. [CrossRef] [PubMed]
42. Liao, Y.; Erxleben, C.; Yildirim, E.; Abramowitz, J.; Armstrong, D.L.; Birnbaumer, L. Orai proteins interact with TRPC channels and confer responsiveness to store depletion. *Proc. Natl. Acad. Sci. USA* **2007**, *104*, 4682–4687. [CrossRef]
43. Xiao, J.-H.; Zheng, Y.-M.; Liao, B.; Wang, Y.-X. Functional Role of Canonical Transient Receptor Potential 1 and Canonical Transient Receptor Potential 3 in Normal and Asthmatic Airway Smooth Muscle Cells. *Am. J. Respir. Cell Mol. Biol.* **2010**, *43*, 17–25. [CrossRef] [PubMed]
44. Yocum, G.T.; Chen, J.; Choi, C.H.; Townsend, E.A.; Zhang, Y.; Xu, D.; Fu, X.W.; Sanderson, M.J.; Emala, C.W. Role of transient receptor potential vanilloid 1 in the modulation of airway smooth muscle tone and calcium handling. *Am. J. Physiol.-Lung Cell. Mol. Physiol.* **2017**, *312*, L812–L821. [CrossRef]
45. Zhao, L.; Zhang, X.; Kuang, H.; Wu, J.; Guo, Y.; Ma, L. Effect of TRPV1 channel on the proliferation and apoptosis in asthmatic rat airway smooth muscle cells. *Exp. Lung Res.* **2013**, *39*, 283–294. [CrossRef]
46. Jia, Y.; Wang, X.; Varty, L.; Rizzo, C.; Yang, R.; Correll, C.; Phelps, P.; Egan, R.; Hey, J. Functional TRPV4 channels are expressed in human airway smooth muscle cells. *Am. J. Physiol.-Lung Cell. Mol. Physiol.* **2004**, *287*, L272–L278. [CrossRef] [PubMed]
47. Uchida, Y.; Izumizaki, M. Effect of menstrual cycle and female hormones on TRP and TREK channels in modifying thermosensitivity and physiological functions in women. *J. Therm. Biol.* **2021**, *100*, 103029. [CrossRef]
48. Flores-Soto, E.; Reyes-García, J.; Sommer, B.; Montaño, L.M. Sarcoplasmic reticulum Ca^{2+} refilling is determined by L-type Ca^{2+} and store operated Ca^{2+} channels in guinea pig airway smooth muscle. *Eur. J. Pharmacol.* **2013**, *721*, 21–28. [CrossRef] [PubMed]
49. Kalidhindi, R.; Ambhore, N.; Thompson, M.; Pabelick, C.; Prakash, Y.; Venkatachalem, S. Differential estrogen receptor signaling regulates store operated calcium entry in human airway smooth muscle. *Am. J. Respir. Crit. Care Med.* **2018**, *197*, A7259.
50. Sathish, V.; Freeman, M.R.; Long, E.; Thompson, M.A.; Pabelick, C.M.; Prakash, Y.S. Cigarette Smoke and Estrogen Signaling in Human Airway Smooth Muscle. *Cell. Physiol. Biochem.* **2015**, *36*, 1101–1115. [CrossRef]
51. Sheridan, J.T.; Gilmore, R.C.; Watson, M.J.; Archer, C.B.; Tarran, R. 17β-Estradiol Inhibits Phosphorylation of Stromal Interaction Molecule 1 (STIM1) Protein. *J. Biol. Chem.* **2013**, *288*, 33509–33518. [CrossRef] [PubMed]
52. Wong, C.K.; So, W.Y.; Law, S.K.; Leung, F.P.; Yau, K.L.; Yao, X.; Huang, Y.; Li, X.; Tsang, S.Y. Estrogen controls embryonic stem cell proliferation via store-operated calcium entry and the nuclear factor of activated T-cells (NFAT). *J. Cell. Physiol.* **2012**, *227*, 2519–2530. [CrossRef] [PubMed]
53. Lv, X.; Miao, C.; Liu, M.; Wang, X.; Wang, L.; Wang, D.J. 17β-Estradiol via Orai1 activates calcium mobilization to induce cell proliferation in epithelial ovarian cancer. *J. Biochem. Mol. Toxicol.* **2020**, *34*, e22603. [CrossRef] [PubMed]

54. Li, S.; Jiang, K.; Li, J.; Hao, X.; Chu, W.; Luo, C.; Zhu, Y.; Xie, R.; Chen, B. Estrogen enhances the proliferation and migration of ovarian cancer cells by activating transient receptor potential channel C3. *J. Ovarian Res.* **2020**, *13*, 20. [CrossRef]
55. Méndez-Reséndiz, K.A.; Enciso-Pablo, Ó.; González-Ramírez, R.; Juárez-Contreras, R.; Rosenbaum, T.; Morales-Lázaro, S.L. Steroids and TRP Channels: A Close Relationship. *Int. J. Mol. Sci.* **2020**, *21*, 3819. [CrossRef]
56. Yang, H.; Choi, K.C.; Hyun, S.H.; Jeung, E.B. Coexpression and estrogen-mediated regulation of TRPV6 and PMCA1 in the human endometrium during the menstrual cycle. *Mol. Reprod. Dev.* **2011**, *78*, 274–282. [CrossRef]
57. Tran, D.N.; Jung, E.-M.; Ahn, C.; Lee, J.-H.; Yoo, Y.-M.; Jeung, E.-B. Effects of Bisphenol A and 4-tert-Octylphenol on Embryo Implantation Failure in Mouse. *Int. J. Environ. Res. Public Health* **2018**, *15*, 1614. [CrossRef]
58. Lifshitz, L.M.; Carmichael, J.D.; Lai, F.A.; Sorrentino, V.; Bellvé, K.; Fogarty, K.E.; Zhuge, R. Spatial organization of RYRs and BK channels underlying the activation of STOCs by Ca^{2+} sparks in airway myocytes. *J. Gen. Physiol.* **2011**, *138*, 195–209. [CrossRef]
59. Jude, J.A.; Dileepan, M.; Panettieri, R.A.; Walseth, T.F.; Kannan, M.S. Altered CD38/Cyclic ADP-Ribose Signaling Contributes to the Asthmatic Phenotype. *J. Allergy* **2012**, *2012*, 289468. [CrossRef]
60. Fritz, N.; Macrez, N.; Mironneau, J.; Jeyakumar, L.H.; Fleischer, S.; Morel, J.-L. Ryanodine receptor subtype 2 encodes Ca^{2+} oscillations activated by acetylcholine via the M2 muscarinic receptor/cADP-ribose signalling pathway in duodenum myocytes. *J. Cell Sci.* **2005**, *118*, 2261–2270. [CrossRef]
61. Deshpande, D.A.; Walseth, T.F.; Panettieri, R.A.; Kannan, M.S. CD38-cyclic ADP-ribose-mediated Ca^{2+} signaling contributes to airway smooth muscle hyperresponsiveness. *FASEB J.* **2003**, *17*, 452–454. [CrossRef] [PubMed]
62. Gao, X.; Liang, Q.; Chen, Y.; Wang, H.-S. Molecular Mechanisms Underlying the Rapid Arrhythmogenic Action of Bisphenol A in Female Rat Hearts. *Endocrinology* **2013**, *154*, 4607–4617. [CrossRef]
63. Gao, X.; Ma, J.; Chen, Y.; Wang, H. Rapid responses and mechanism of action for low-dose bisphenol S on ex vivo rat hearts and isolated myocytes: Evidence of female-specific proarrhythmic effects. *Environ. Health Perspect.* **2015**, *123*, 571–578. [CrossRef]
64. Liu, Y.; Guo, Y.; Huang, W.; Deng, K.Y.; Qian, Y.; Xin, H.B. 17β-Estradiol Promotes Apoptosis in Airway Smooth Muscle Cells Through CD38/SIRT1/p53 Pathway. *Front. Endocrinol.* **2018**, *9*, 770. [CrossRef] [PubMed]
65. Hu, X.-Q.; Song, R.; Romero, M.; Dasgupta, C.; Huang, X.; Holguin, M.A.; Williams, V.; Xiao, D.; Wilson, S.M.; Zhang, L. Pregnancy Increases Ca^{2+} Sparks/Spontaneous Transient Outward Currents and Reduces Uterine Arterial Myogenic Tone. *Hypertension* **2019**, *73*, 691–702. [CrossRef] [PubMed]
66. Jiao, L.; Machuki, J.; Wu, Q.; Shi, M.; Fu, L.; Adekunle, A.; Tao, X.; Xu, C.; Hu, X.; Yin, Z.; et al. Estrogen and calcium handling proteins: New discoveries and mechanisms in cardiovascular diseases. *Am. J. Physiol.-Heart Circ. Physiol.* **2020**, *318*, H820–H829. [CrossRef]
67. Tappia, P.S.; Dent, M.R.; Aroutiounova, N.; Babick, A.P.; Weiler, H. Gender differences in the modulation of cardiac gene expression by dietary conjugated linoleic acid isomers. *Can. J. Physiol. Pharmacol.* **2007**, *3–4*, 465–475. [CrossRef]
68. Yaras, N.; Tuncay, E.; Purali, N.; Sahinoglu, B.; Vassort, G.; Turan, B. Sex-related effects on diabetes-induced alterations in calcium release in the rat heart. *Am. J. Physiol.-Heart Circ. Physiol.* **2007**, *293*, H3584–H3592. [CrossRef]
69. Bell, J.R.; Raaijmakers, A.J.; Curl, C.L.; Reichelt, M.E.; Harding, T.W.; Bei, A.; Ng, D.C.; Erickson, J.R.; Vila Petroff, M.; Harrap, S.B.; et al. Cardiac CaMKIIδ splice variants exhibit target signaling specificity and confer sex-selective arrhythmogenic actions in the ischemic-reperfused heart. *Int. J. Cardiol.* **2015**, *181*, 288–296. [CrossRef]
70. Farrell, S.R.; Ross, J.L.; Howlett, S.E. Sex differences in mechanisms of cardiac excitation-contraction coupling in rat ventricular myocytes. *Am. J. Physiol.-Heart Circ. Physiol.* **2010**, *299*, H36–H45. [CrossRef]
71. Rybalchenko, V.; Grillo, M.A.; Gastinger, M.J.; Rybalchenko, N.; Payne, A.J.; Koulen, P. The unliganded long isoform of estrogen receptor beta stimulates brain ryanodine receptor single channel activity alongside with cytosolic Ca^{2+}. *J. Recept. Signal Transduct. Res.* **2009**, *29*, 326–341. [CrossRef] [PubMed]
72. Narayanan, D.; Adebiyi, A.; Jaggar, J.H. Inositol trisphosphate receptors in smooth muscle cells. *Am. J. Physiol.-Heart Circ. Physiol.* **2012**, *302*, H2190–H2210. [CrossRef] [PubMed]
73. Song, T.; Hao, Q.; Zheng, Y.M.; Liu, Q.H.; Wang, Y.X. Inositol 1,4,5-trisphosphate activates TRPC3 channels to cause extracellular Ca^{2+} influx in airway smooth muscle cells. *Am. J. Physiol.-Lung Cell. Mol. Physiol.* **2015**, *309*, L1455–L1466. [CrossRef] [PubMed]
74. Wang, Y.X.; Zheng, Y.M.; Mei, Q.B.; Wang, Q.S.; Collier, M.L.; Fleischer, S.; Xin, H.B.; Kotlikoff, M.I. FKBP12.6 and cADPR regulation of Ca^{2+} release in smooth muscle cells. *Am. J. Physiol. Cell Physiol.* **2004**, *286*, C538–C546. [CrossRef]
75. Montaño, L.M.; Flores-Soto, E.; Reyes-García, J.; Díaz-Hernández, V.; Carbajal-García, A.; Campuzano-González, E.; Ramírez-Salinas, G.L.; Velasco-Velázquez, M.A.; Sommer, B. Testosterone induces hyporesponsiveness by interfering with IP_3 receptors in guinea pig airway smooth muscle. *Mol. Cell. Endocrinol.* **2018**, *473*, 17–30. [CrossRef]
76. Romero-Martínez, B.S.; Montaño, L.M.; Solís-Chagoyán, H.; Sommer, B.; Ramírez-Salinas, G.L.; Pérez-Figueroa, G.E.; Flores-Soto, E. Possible Beneficial Actions of Caffeine in SARS-CoV-2. *Int. J. Mol. Sci.* **2021**, *22*, 5460. [CrossRef]
77. Deshpande, D.A.; Wang, W.C.H.; Mcilmoyle, E.L.; Robinett, K.S.; Schillinger, R.M.; An, S.S.; Sham, J.S.K.; Liggett, S.B. Bitter taste receptors on airway smooth muscle bronchodilate by localized calcium signaling and reverse obstruction. *Nat. Med.* **2010**, *16*, 1299–1304. [CrossRef] [PubMed]
78. Reuquén, P.; Oróstica, M.L.; Rojas, I.; Díaz, P.; Parada-Bustamante, A.; Orihuela, P.A. Estradiol increases IP_3 by a nongenomic mechanism in the smooth muscle cells from the rat oviduct. *Reproduction* **2015**, *150*, 331–341. [CrossRef] [PubMed]
79. Marino, M.; Pallottini, V.; Trentalance, A. Estrogens cause rapid activation of IP_3-PKC-α signal transduction pathway in HEPG2 cells. *Biochem. Biophys. Res. Commun.* **1998**, *245*, 254–258. [CrossRef]

80. Ekstein, J.; Nasatzky, E.; Boyan, B.D.; Ornoy, A.; Schwartz, Z. Growth-plate chondrocytes respond to 17β-estradiol with sex-specific increases in IP_3 and intracellular calcium ion signalling via a capacitative entry mechanism. *Steroids* **2005**, *70*, 775–786. [CrossRef]
81. Le Mellay, V.; Grosse, B.; Lieberherr, M. Phospholipase C β and membrane action of calcitriol and estradiol. *J. Biol. Chem.* **1997**, *272*, 11902–11907. [CrossRef]
82. Micevych, P.; Soma, K.K.; Sinchak, K. Neuroprogesterone: Key to estrogen positive feedback? *Brain Res. Rev.* **2008**, *57*, 470–480. [CrossRef] [PubMed]
83. Kirkwood, K.L.; Homick, K.; Dragon, M.B.; Bradford, P.G. Cloning and characterization of the type I inositol 1,4,5-trisphosphate receptor gene promoter. Regulation by 17β-estradiol in osteoblasts. *J. Biol. Chem.* **1997**, *272*, 22425–22431. [CrossRef] [PubMed]
84. Tomás, J.; Santos, C.R.A.; Duarte, A.C.; Maltez, M.; Quintela, T.; Lemos, M.C.; Gonçalves, I. Bitter taste signaling mediated by Tas2r144 is down-regulated by 17β-estradiol and progesterone in the rat choroid plexus. *Mol. Cell. Endocrinol.* **2019**, *495*, 110521. [CrossRef]
85. Sommer, B.; Flores-Soto, E.; Gonzalez-Avila, G. Cellular Na+ handling mechanisms involved in airway smooth muscle contraction (Review). *Int. J. Mol. Med.* **2017**, *40*, 3–9. [CrossRef] [PubMed]
86. DiPolo, R.; Beaugé, L. Sodium/calcium exchanger: Influence of metabolic regulation on ion carrier interactions. *Physiol. Rev.* **2006**, *86*, 155–203. [CrossRef]
87. Philipson, K.D.; Nicoll, D.A. Sodium-calcium exchange: A molecular perspective. *Annu. Rev. Physiol.* **2000**, *62*, 111–133. [CrossRef]
88. Lytton, J. Na^+/Ca^{2+} exchangers: Three mammalian gene families control Ca^{2+} transport. *Biochem. J.* **2007**, *406*, 365–382. [CrossRef]
89. Algara-Suárez, P.; Mejía-Elizondo, R.; Sims, S.; Saavedra-Alanis, V.; Espinosa-Tanguma, R. The 1.3 isoform of Na^+-Ca^{2+} exchanger expressed in guinea pig tracheal smooth muscle is less sensitive to KB-R7943. *J. Physiol. Biochem.* **2010**, *66*, 117–125. [CrossRef]
90. Janssen, L.J.; Walters, D.K.; Wattie, J. Regulation of $[Ca^{2+}]$i in canine airway smooth muscle by Ca^{2+}-ATPase and Na^+/Ca^{2+} exchange mechanisms. *Am. J. Physiol.* **1997**, *273*, L322–L330. [CrossRef]
91. Wen, J.; Meng, X.; Xuan, B.; Zhou, T.; Gao, H.; Dong, H.; Wang, Y. Na^+/Ca^{2+} Exchanger 1 in Airway Smooth Muscle of Allergic Inflammation Mouse Model. *Front. Pharmacol.* **2018**, *9*, 1471. [CrossRef] [PubMed]
92. Xu, H.; Zhao, P.; Zhang, W.-J.; Qiu, J.-Y.; Tan, L.; Liu, X.-C.; Wang, Q.; Luo, X.; She, Y.-S.; Zang, D.-A.; et al. Generation and Role of Oscillatory Contractions in Mouse Airway Smooth Muscle. *Cell. Physiol. Biochem.* **2018**, *47*, 1546–1555. [CrossRef] [PubMed]
93. Sathish, V.; Delmotte, P.F.; Thompson, M.A.; Pabelick, C.M.; Sieck, G.C.; Prakash, Y.S. Sodium-calcium exchange in intracellular calcium handling of human airway smooth muscle. *PLoS ONE* **2011**, *6*, e23662. [CrossRef] [PubMed]
94. Rahman, M.; Inman, M.; Kiss, L.; Janssen, L.J. Reverse-mode NCX current in mouse airway smooth muscle: Na^+ and voltage dependence, contributions to Ca^{2+} influx and contraction, and altered expression in a model of allergen-induced hyperresponsiveness. *Acta Physiol.* **2012**, *205*, 279–291. [CrossRef] [PubMed]
95. Kim, K.; Lee, D.; Ahn, C.; Kang, H.Y.; An, B.S.; Seong, Y.H.; Jeung, E.B. Effects of estrogen on esophageal function through regulation of Ca^{2+}-related proteins. *J. Gastroenterol.* **2017**, *52*, 929–939. [CrossRef] [PubMed]
96. Chu, S.H.; Goldspink, P.; Kowalski, J.; Beck, J.; Schwertz, D.W. Effect of estrogen on calcium-handling proteins, β-adrenergic receptors, and function in rat heart. *Life Sci.* **2006**, *79*, 1257–1267. [CrossRef]
97. Sims, C.; Reisenweber, S.; Viswanathan, P.C.; Choi, B.R.; Walker, W.H.; Salama, G. Sex, age, and regional differences in L-type calcium current are important determinants of arrhythmia phenotype in rabbit hearts with drug-induced long QT type 2. *Circ. Res.* **2008**, *102*, e86–e100. [CrossRef]
98. Chen, G.; Yang, X.; Alber, S.; Shusterman, V.; Salama, G. Regional genomic regulation of cardiac sodium-calcium exchanger by oestrogen. *J. Physiol.* **2011**, *589*, 1061–1080. [CrossRef]
99. Kravtsov, G.M.; Kam, K.W.; Liu, J.; Wu, S.; Wong, T.M. Altered Ca2+ handling by ryanodine receptor and Na^+-Ca2+ exchange in the heart from ovariectomized rats: Role of protein kinase A. *Am. J. Physiol. Cell Physiol.* **2007**, *292*, C1625–C1635. [CrossRef]
100. Yang, H.Y.; Firth, J.M.; Francis, A.J.; Alvarez-Laviada, A.; MacLeod, K.T. Effect of ovariectomy on intracellular Ca^{2+} regulation in guinea pig cardiomyocytes. *Am. J. Physiol.-Heart Circ. Physiol.* **2017**, *313*, H1031–H1043. [CrossRef]
101. Sugishita, K.; Su, Z.; Li, F.; Philipson, K.D.; Barry, W.H. Gender influences $[Ca^{2+}]$i during metabolic inhibition in myocytes overexpressing the Na^+-Ca^{2+} exchanger. *Circulation* **2001**, *104*, 2101–2106. [CrossRef]
102. Cross, H.R.; Lu, L.; Steenbergen, C.; Philipson, K.D.; Murphy, E. Overexpression of the Cardiac Na^+/Ca^{2+} Exchanger Increases Susceptibility to Ischemia/Reperfusion Injury in Male, but Not Female, Transgenic Mice. *Circ. Res.* **1998**, *83*, 1215–1223. [CrossRef] [PubMed]
103. Sánchez, J.C.; López-Zapata, D.F.; Francis, L.; De Los Reyes, L. Effects of estradiol and IGF-1 on the sodium calcium exchanger in rat cultured cortical neurons. *Cell. Mol. Neurobiol.* **2011**, *31*, 619–627. [CrossRef] [PubMed]
104. Jeffs, G.J.; Meloni, B.P.; Bakker, A.J.; Knuckey, N.W. The role of the Na^+/Ca^{2+} exchanger (NCX) in neurons following ischaemia. *J. Clin. Neurosci. Off. J. Neurosurg. Soc. Australas.* **2007**, *14*, 507–514. [CrossRef]
105. Chen, Y.F.; Cao, J.; Zhong, J.N.; Chen, X.; Cheng, M.; Yang, J.; Gao, Y.D. Plasma membrane Ca^{2+}-ATPase regulates Ca^{2+} signaling and the proliferation of airway smooth muscle cells. *Eur. J. Pharmacol.* **2014**, *740*, 733–741. [CrossRef] [PubMed]
106. Varga, K.; Hollósi, A.; Pászty, K.; Hegedűs, L.; Szakács, G.; Tímár, J.; Papp, B.; Enyedi, Á.; Padányi, R. Expression of calcium pumps is differentially regulated by histone deacetylase inhibitors and estrogen receptor alpha in breast cancer cells. *BMC Cancer* **2018**, *18*, 1029. [CrossRef]

107. El-Beialy, W.; Galal, N.; Deyama, Y.; Yoshimura, Y.; Suzuki, K.; Tei, K.; Totsuka, Y. Effects of Estrogen on PMCA 2 and 4 in Human Fibroblast-like Synovial Cells and Mouse Macrophage-like Cells. *Endocr. J.* **2010**, *57*, 93–97. [CrossRef]
108. Dick, I.M.; Liu, J.; Glendenning, P.; Prince, R.L. Estrogen and androgen regulation of plasma membrane calcium pump activity in immortalized distal tubule kidney cells. *Mol. Cell. Endocrinol.* **2003**, *212*, 11–18. [CrossRef]
109. Khariv, V.; Acioglu, C.; Ni, L.; Ratnayake, A.; Li, L.; Tao, Y.-X.; Heary, R.F.; Elkabes, S. A link between plasma membrane calcium ATPase 2 (PMCA2), estrogen and estrogen receptor α signaling in mechanical pain. *Sci. Rep.* **2018**, *8*, 17260. [CrossRef]
110. Bobe, R.; Bredoux, R.; Corvazier, E.; Andersen, J.P.; Clausen, J.D.; Dode, L.; Kovács, T.; Enouf, J. Identification, Expression, Function, and Localization of a Novel (Sixth) Isoform of the Human Sarco/Endoplasmic Reticulum Ca^{2+} ATPase 3 Gene. *J. Biol. Chem.* **2004**, *279*, 24297–24306. [CrossRef]
111. Mahn, K.; Hirst, S.J.; Ying, S.; Holt, M.R.; Lavender, P.; Ojo, O.O.; Siew, L.; Simcock, D.E.; Mcvicker, C.G.; Kanabar, V.; et al. Diminished sarco/endoplasmic reticulum Ca^{2+} ATPase (SERCA) expression contributes to airway remodelling in bronchial asthma. *Proc. Natl. Acad. Sci. USA* **2009**, *106*, 10775–10780. [CrossRef]
112. Prakash, Y.S.; Sathish, V.; Thompson, M.A.; Pabelick, C.M.; Sieck, G.C. Asthma and sarcoplasmic reticulum Ca^{2+} reuptake in airway smooth muscle. *Am. J. Physiol.-Lung Cell. Mol. Physiol.* **2009**, *297*, L794. [CrossRef] [PubMed]
113. Carbajal, V.; Vargas, M.H.; lores-Soto, E.F.; Martínez-Cordero, E.; Bazán-Perkins, B.; Montaño, L.M. LTD_4 induces hyperresponsiveness to histamine in bovine airway smooth muscle: Role of SR-ATPase Ca^{2+} pump and tyrosine kinase. *Am. J. Physiol.-Lung Cell. Mol. Physiol.* **2005**, *288*, L84–L92. [CrossRef] [PubMed]
114. Kotlikoff, M.I. Potassium channels in airway smooth muscle: A tale of two channels. *Pharmacol. Ther.* **1993**, *58*, 1–12. [CrossRef] [PubMed]
115. Adda, S.; Fleischmann, B.K.; Freedman, B.D.; Yu, M.; Hay, D.W.; Kotlikoff, M.I. Expression and function of voltage-dependent potassium channel genes in human airway smooth muscle. *J. Biol. Chem.* **1996**, *271*, 13239–13243. [CrossRef]
116. Knox, A.J.; Tattersfield, A.E. Airway smooth muscle relaxation. *Thorax* **1995**, *50*, 894–901. [CrossRef]
117. Brueggemann, L.I.; Kakad, P.P.; Love, R.B.; Solway, J.; Dowell, M.L.; Cribbs, L.L.; Byron, K.L. Kv7 potassium channels in airway smooth muscle cells: Signal transduction intermediates and pharmacological targets for bronchodilator therapy. *Am. J. Physiol.-Lung Cell. Mol. Physiol.* **2012**, *302*, L120–L132. [CrossRef]
118. Isaac, L.; Mcardle, S.; Miller, N.M.; Foster, R.W.; Small, R.C. Effects of some K^+-channel inhibitors on the electrical behaviour of guinea-pig isolated trachealis and on its responses to spasmogenic drugs. *Br. J. Pharmacol.* **1996**, *117*, 1653–1662. [CrossRef]
119. Janssen, L.J.; Nana, R. Na^+/K^+ ATPase mediates rhythmic spontaneous relaxations in canine airway smooth muscle. *Respir. Physiol.* **1997**, *108*, 187–194. [CrossRef]
120. Dodson, A.M.; Rhoden, K.J. Bradykinin increases Na^+-K^+pump activity in cultured guinea-pig tracheal smooth muscle cells. *Br. J. Pharmacol.* **2001**, *133*, 1339–1345. [CrossRef]
121. Rhoden, K.J.; Douglas, J.S. Evidence of Na-K-Cl cotransport in airway smooth muscle. *Am. J. Physiol.* **1995**, *268*, L551–L557. [CrossRef] [PubMed]
122. Kume, H.; Hall, I.P.; Washabau, R.J.; Takagi, K.; Kotlikoff, M.I. β-adrenergic agonists regulate K_{Ca} channels in airway smooth muscle by cAMP-dependent and -independent mechanisms. *J. Clin. Investig.* **1994**, *93*, 371–379. [CrossRef] [PubMed]
123. Martin, G.; O'Connell, R.J.; Pietrzykowski, A.Z.; Treistman, S.N.; Ethier, M.F.; Madison, J.M. Interleukin-4 activates large-conductance, calcium-activated potassium (BK_{Ca}) channels in human airway smooth muscle cells. *Exp. Physiol.* **2008**, *93*, 908–918. [CrossRef] [PubMed]
124. Perkins, C.; Yanase, N.; Smulian, G.; Gildea, L.; Orekov, T.; Potter, C.; Brombacher, F.; Aronow, B.; Wills-Karp, M.; Finkelman, F.D. Selective stimulation of IL-4 receptor on smooth muscle induces airway hyperresponsiveness in mice. *J. Exp. Med.* **2011**, *208*, 853–867. [CrossRef]
125. Shepherd, M.C.; Duffy, S.M.; Harris, T.; Cruse, G.; Schuliga, M.; Brightling, C.E.; Neylon, C.B.; Bradding, P.; Stewart, A.G. $K_{Ca}3.1$ Ca^{2+}-Activated K^+ Channels Regulate Human Airway Smooth Muscle Proliferation. *Am. J. Respir. Cell Mol. Biol.* **2007**, *37*, 525–531. [CrossRef]
126. Yu, Z.H.; Wang, Y.X.; Song, Y.; Lu, H.Z.; Hou, L.N.; Cui, Y.Y.; Chen, H.Z. Up-regulation of $K_{Ca}3.1$ promotes human airway smooth muscle cell phenotypic modulation. *Pharmacol. Res.* **2013**, *77*, 30–38. [CrossRef]
127. Yu, Z.-H.; Xu, J.-R.; Wang, Y.-X.; Xu, G.-N.; Xu, Z.-P.; Yang, K.; Wu, D.-Z.; Cui, Y.-Y.; Chen, H.-Z. Targeted Inhibition of $K_{Ca}3.1$ Channel Attenuates Airway Inflammation and Remodeling in Allergic Asthma. *Am. J. Respir. Cell Mol. Biol.* **2013**, *48*, 685–693. [CrossRef]
128. Dimitropoulou, C.; White, R.E.; Ownby, D.R.; Catravas, J.D. Estrogen Reduces Carbachol-Induced Constriction of Asthmatic Airways by Stimulating Large-Conductance Voltage and Calcium-Dependent Potassium Channels. *Am. J. Respir. Cell Mol. Biol.* **2005**, *32*, 239–247. [CrossRef]
129. Seibold, M.A.; Wang, B.; Eng, C.; Kumar, G.; Beckman, K.B.; Sen, S.; Choudhry, S.; Meade, K.; Lenoir, M.; Watson, H.G.; et al. An african-specific functional polymorphism in KCNMB1 shows sex-specific association with asthma severity. *Hum. Mol. Genet.* **2008**, *17*, 2681–2690. [CrossRef]
130. Tsang, S.Y.; Yao, X.; Chan, H.Y.; Wong, C.M.; Chen, Z.Y.; Au, C.L.; Huang, Y. Contribution of K^+ channels to relaxation induced by 17β-estradiol but not by progesterone in isolated rat mesenteric artery rings. *J. Cardiovasc. Pharmacol.* **2003**, *41*, 4–13. [CrossRef]
131. Wong, C.M.; Tsang, S.Y.; Yao, X.; Chan, F.L.; Huang, Y. Differential effects of estrogen and progesterone on potassium channels expressed in Xenopus oocytes. *Steroids* **2008**, *73*, 272–279. [CrossRef] [PubMed]

132. Hu, X.-Q.; Xiao, D.; Zhu, R.; Huang, X.; Yang, S.; Wilson, S.; Zhang, L. Pregnancy Upregulates Large-Conductance Ca^{2+}-Activated K^+-Channel Activity and Attenuates Myogenic Tone in Uterine Arteries. *Hypertension* **2011**, *58*, 1132–1139. [CrossRef] [PubMed]
133. Li, X.T.; Qiu, X.Y. 17β-Estradiol Upregulated Expression of α and β Subunits of Larger-Conductance Calcium-Activated K^+ Channels (BK) via Estrogen Receptor β. *J. Mol. Neurosci.* **2015**, *56*, 799–807. [CrossRef]
134. Nishimura, I.; Ui-Tei, K.; Saigo, K.; Ishii, H.; Sakuma, Y.; Kato, M. 17β-Estradiol at Physiological Concentrations Augments Ca^{2+}-Activated K^+ Currents via Estrogen Receptor β in the Gonadotropin-Releasing Hormone Neuronal Cell Line GT1-7. *Endocrinology* **2008**, *149*, 774–782. [CrossRef]
135. Shi, J.; Jin, L.; Leng, J.; Lang, J. Response of potassium channels to estrogen and progesterone in the uterine smooth muscle cells of adenomyosis in vitro. *Zhonghua Fu Chan Ke Za Zhi* **2015**, *50*, 843–847.
136. Restrepo-Angulo, I.; Bañuelos, C.; Camacho, J. Ion Channel Regulation by Sex Steroid Hormones and Vitamin D in Cancer: A Potential Opportunity for Cancer Diagnosis and Therapy. *Front. Pharmacol.* **2020**, *11*, 152. [CrossRef]
137. Coiret, G.; Matifat, F.; Hague, F.; Ouadid-Ahidouch, H. 17-β-Estradiol activates maxi-K channels through a non-genomic pathway in human breast cancer cells. *FEBS Lett.* **2005**, *579*, 2995–3000. [CrossRef]
138. Ramírez, A.; Vera, E.; Gamboa-Domínguez, A.; Lambert, P.; Gariglio, P.; Camacho, J. Calcium-activated potassium channels as potential early markers of human cervical cancer. *Oncol. Lett.* **2018**, *15*, 7249–7254. [CrossRef] [PubMed]
139. Martinez-Pinna, J.; Marroqui, L.; Hmadcha, A.; Lopez-Beas, J.; Soriano, S.; Villar-Pazos, S.; Alonso-Magdalena, P.; Dos Santos, R.S.; Quesada, I.; Martin, F.; et al. Oestrogen receptor β mediates the actions of bisphenol-A on ion channel expression in mouse pancreatic beta cells. *Diabetologia* **2019**, *62*, 1667–1680. [CrossRef]
140. Marroqui, L.; Martinez-Pinna, J.; Castellano-Muñoz, M.; Dos Santos, R.S.; Medina-Gali, R.M.; Soriano, S.; Quesada, I.; Gustafsson, J.-A.; Encinar, J.A.; Nadal, A. Bisphenol-S and Bisphenol-F alter mouse pancreatic β-cell ion channel expression and activity and insulin release through an estrogen receptor ERβ mediated pathway. *Chemosphere* **2021**, *265*, 129051. [CrossRef]
141. Mohr, C.J.; Steudel, F.A.; Gross, D.; Ruth, P.; Lo, W.-Y.; Hoppe, R.; Schroth, W.; Brauch, H.; Huber, S.M.; Lukowski, R. Cancer-Associated Intermediate Conductance Ca^{2+}-Activated K^+ Channel $K_{Ca}3.1$. *Cancers* **2019**, *11*, 109. [CrossRef] [PubMed]
142. Sticht, C.; De La Torre, C.; Parveen, A.; Gretz, N. miRWalk: An online resource for prediction of microRNA binding sites. *PLoS ONE* **2018**, *13*, e0206239. [CrossRef] [PubMed]
143. Yu, X.; Zhang, X.; Dhakal, I.B.; Beggs, M.; Kadlubar, S.; Luo, D. Induction of cell proliferation and survival genes by estradiol-repressed microRNAs in breast cancer cells. *BMC Cancer* **2012**, *12*, 29. [CrossRef]
144. Davis, J.S.; Sun, M.; Kho, A.T.; Moore, K.G.; Sylvia, J.M.; Weiss, S.T.; Lu, Q.; Tantisira, K.G. Circulating microRNAs and association with methacholine PC_{20} in the Childhood Asthma Management Program (CAMP) cohort. *PLoS ONE* **2017**, *12*, e0180329. [CrossRef]
145. Yu, B.; Yao, L.; Liu, C.; Tang, L.; Xing, T. Upregulation of microRNA-16 alters the response to inhaled β-agonists in patients with asthma though modulating expression of ADRB2. *Mol. Med. Rep.* **2019**, *19*, 4027–4034. [CrossRef]
146. Taura, J.; Kircher, D.M.; Gameiro-Ros, I.; Slesinger, P.A. Comparison of K^+ Channel Families. In *Pharmacology of Potassium Channels*; Gamper, N., Wang, K., Eds.; Springer: Cham, Switzerland, 2021; Volume 267.
147. Evseev, A.I.; Semenov, I.; Archer, C.R.; Medina, J.L.; Dube, P.H.; Shapiro, M.S.; Brenner, R. Functional effects of KCNQ K^+ channels in airway smooth muscle. *Front. Physiol.* **2013**, *4*, 277. [CrossRef] [PubMed]
148. Drici, M.D.; Burklow, T.R.; Haridasse, V.; Glazer, R.I.; Woosley, R.L. Sex hormones prolong the QT interval and downregulate potassium channel expression in the rabbit heart. *Circulation* **1996**, *94*, 1471–1474. [CrossRef]
149. Roepke, T.A.; Malyala, A.; Bosch, M.A.; Kelly, M.J.; Rønnekleiv, O.K. Estrogen Regulation of Genes Important for K^+ Channel Signaling in the Arcuate Nucleus. *Endocrinology* **2007**, *148*, 4937–4951. [CrossRef]
150. Roepke, T.A.; Qiu, J.; Smith, A.W.; Ronnekleiv, O.K.; Kelly, M.J. Fasting and 17β-Estradiol Differentially Modulate the M-Current in Neuropeptide Y Neurons. *J. Neurosci.* **2011**, *31*, 11825–11835. [CrossRef]
151. Anneken, L.; Baumann, S.; Vigneault, P.; Biliczki, P.; Friedrich, C.; Xiao, L.; Girmatsion, Z.; Takac, I.; Brandes, R.P.; Kissler, S.; et al. Estradiol regulates human QT-interval: Acceleration of cardiac repolarization by enhanced KCNH2 membrane trafficking. *Eur. Heart J.* **2016**, *37*, 640–650. [CrossRef]
152. Kim, J.G.; Leem, Y.-E.; Kwon, I.; Kang, J.-S.; Bae, Y.M.; Cho, H. Estrogen modulates serotonin effects on vasoconstriction through Src inhibition. *Exp. Mol. Med.* **2018**, *50*, 1–9. [CrossRef]
153. Díaz, L.; Ceja-Ochoa, I.; Restrepo-Angulo, I.; Larrea, F.; Avila-Chávez, E.; García-Becerra, R.; Borja-Cacho, E.; Barrera, D.; Ahumada, E.; Gariglio, P.; et al. Estrogens and Human Papilloma Virus Oncogenes Regulate Human Ether-à-go-go-1 Potassium Channel Expression. *Cancer Res.* **2009**, *69*, 3300–3307. [CrossRef] [PubMed]
154. Carlson, A.E.; Brelidze, T.I.; Zagotta, W.N. Flavonoid regulation of EAG1 channels. *J. Gen. Physiol.* **2013**, *141*, 347–358. [CrossRef] [PubMed]
155. Souhrada, M.; Souhrada, J.F.; Cherniack, R.M. Evidence for a sodium electrogenic pump in airway smooth muscle. *J. Appl. Physiol. Respir. Environ. Exerc. Physiol.* **1981**, *51*, 346–352. [CrossRef] [PubMed]
156. Chideckel, E.W.; Frost, J.L.; Mike, P.; Fedan, J.S. The effect of ouabain on tension in isolated respiratory tract smooth muscle of humans and other species. *Br. J. Pharmacol.* **1987**, *92*, 609–614. [CrossRef]
157. Gunst, S.J.; Stropp, J.Q. Effect of Na-K adenosinetriphosphatase activity on relaxation of canine tracheal smooth muscle. *J. Appl. Physiol.* **1988**, *64*, 635–641. [CrossRef]

158. Obradovic, M.; Zafirovic, S.; Jovanovic, A.; Milovanovic, E.S.; Mousa, S.A.; Labudovic-Borovic, M.; Isenovic, E.R. Effects of 17β-estradiol on cardiac Na^{+}/K^{+}-ATPase in high fat diet fed rats. *Mol. Cell. Endocrinol.* **2015**, *416*, 46–56. [CrossRef]
159. Liu, C.G.; Xu, K.Q.; Xu, X.; Huang, J.J.; Xiao, J.C.; Zhang, J.P.; Song, H.P. 17β-oestradiol regulates the expression of Na^{+}/K^{+}-ATPase β1-subunit, sarcoplasmic reticulum Ca^{2+}-ATPase and carbonic anhydrase iv in H9C2 cells. *Clin. Exp. Pharmacol. Physiol.* **2007**, *34*, 998–1004. [CrossRef]
160. Obradovic, M.; Stewart, A.J.; Pitt, S.J.; Labudovic-Borovic, M.; Sudar, E.; Petrovic, V.; Zafirovic, S.; Maravic-Stojkovic, V.; Vasic, V.; Isenovic, E.R. In vivo effects of 17β-estradiol on cardiac Na^{+}/K^{+}-ATPase expression and activity in rat heart. *Mol. Cell. Endocrinol.* **2014**, *388*, 58–68. [CrossRef]
161. Li, Y.; Yang, J.; Li, S.; Zhang, J.; Zheng, J.; Hou, W.; Zhao, H.; Guo, Y.; Liu, X.; Dou, K.; et al. N-myc Downstream-regulated Gene 2, a Novel Estrogen-targeted Gene, Is Involved in the Regulation of Na^{+}/K^{+}-ATPase. *J. Biol. Chem.* **2011**, *286*, 32289–32299. [CrossRef]
162. Melis, M.G.; Troffa, C.; Manunta, P.; Pinna Parpaglia, P.; Soro, A.; Pala, F.; Madeddu, P.; Pazzola, A.; Tonolo, G.; Patteri, G. Influenze degli ormoni del ciclo mestruale sui trasporti cationici di membrana dei globuli rossi [Effect of menstrual cycle hormones on cation transport in the red-cell membrane]. *Boll. Della Soc. Ital. Di Biol. Sper.* **1990**, *66*, 679–684.
163. Palacios, J.; Marusic, E.T.; Lopez, N.C.; Gonzalez, M.; Michea, L. Estradiol-induced expression of N^{+}-K^{+}-ATPase catalytic isoforms in rat arteries: Gender differences in activity mediated by nitric oxide donors. *Am. J. Physiol.-Heart Circ. Physiol.* **2004**, *286*, H1793–H1800. [CrossRef] [PubMed]
164. Ribeiro Junior, R.F.; Fiorim, J.; Marques, V.B.; de Sousa Ronconi, K.; Botelho, T.; Grando, M.D.; Bendhack, L.M.; Vassallo, D.V.; Stefanon, I. Vascular activation of K^{+} channels and Na^{+}-K^{+} ATPase activity of estrogen-deficient female rats. *Vasc. Pharmacol.* **2017**, *99*, 23–33. [CrossRef] [PubMed]
165. Iwamoto, L.M.; Fujiwara, N.; Nakamura, K.T.; Wada, R.K. Na-K-2Cl cotransporter inhibition impairs human lung cellular proliferation. *Am. J. Physiol.-Lung Cell. Mol. Physiol.* **2004**, *287*, L510–L514. [CrossRef]
166. Wang, S.; Xiang, Y.Y.; Ellis, R.; Wattie, J.; Feng, M.; Inman, M.D.; Lu, W.Y. Effects of furosemide on allergic asthmatic responses in mice. *Clin. Exp. Allergy J. Br. Soc. Allergy Clin. Immunol.* **2011**, *41*, 1456–1467. [CrossRef]
167. O'Donnell, M.E.; Lam, T.I.; Tran, L.Q.; Foroutan, S.; Anderson, S.E. Estradiol Reduces Activity of the Blood–Brain Barrier Na–K–Cl Cotransporter and Decreases Edema Formation in Permanent Middle Cerebral Artery Occlusion. *J. Cereb. Blood Flow Metab.* **2006**, *26*, 1234–1249. [CrossRef]
168. Chang, E.; O'Donnell, M.E.; Barakat, A.I. Shear stress and 17β-estradiol modulate cerebral microvascular endothelial Na-K-Cl cotransporter and Na/H exchanger protein levels. *Am. J. Physiol. Cell Physiol.* **2008**, *294*, C363–C371. [CrossRef]
169. Nakamura, N.H.; Rosell, D.R.; Akama, K.T.; McEwen, B.S. Estrogen and ovariectomy regulate mRNA and protein of glutamic acid decarboxylases and cation-chloride cotransporters in the adult rat hippocampus. *Neuroendocrinology* **2004**, *80*, 308–323. [CrossRef]
170. Nugent, B.M.; Valenzuela, C.V.; Simons, T.J.; Mccarthy, M.M. Kinases SPAK and OSR1 Are Upregulated by Estradiol and Activate NKCC1 in the Developing Hypothalamus. *J. Neurosci.* **2012**, *32*, 593–598. [CrossRef]
171. Palacios, J.; Espinoza, F.; Munita, C.; Cifuentes, F.; Michea, L. Na^{+}-K^{+}-$2Cl^{-}$ cotransporter is implicated in gender differences in the response of the rat aorta to phenylephrine. *Br. J. Pharmacol.* **2006**, *148*, 964–972. [CrossRef]
172. Bers, D. Intracellular Na^{+} regulation in cardiac myocytes. *Cardiovasc. Res.* **2003**, *57*, 897–912. [CrossRef] [PubMed]
173. Bradley, E.; Webb, T.I.; Hollywood, M.A.; Sergeant, G.P.; McHale, N.G.; Thornbury, K.D. The cardiac sodium current Na(v)1.5 is functionally expressed in rabbit bronchial smooth muscle cells. *Am. J. Physiol. Cell Physiol.* **2013**, *305*, C427–C435. [CrossRef] [PubMed]
174. Snetkov, V.; Hirst, S.; Ward, J. Ion channels in freshly isolated and cultured human bronchial smooth muscle cells. *Exp. Physiol.* **1996**, *81*, 791–804. [CrossRef] [PubMed]
175. Jo, T.; Nagata, T.; Iida, H.; Imuta, H.; Iwasawa, K.; Ma, J.; Hara, K.; Omata, M.; Nagai, R.; Takizawa, H.; et al. Voltage-gated sodium channel expressed in cultured human smooth muscle cells: Involvement of SCN9A. *FEBS Lett.* **2004**, *567*, 339–343. [CrossRef]
176. Nakajima, T.; Jo, T.; Meguro, K.; Oonuma, H.; Ma, J.; Kubota, N.; Imuta, H.; Takano, H.; Iida, H.; Nagase, T.; et al. Effect of dexamethasone on voltage-gated Na^{+} channel in cultured human bronchial smooth muscle cells. *Life Sci.* **2008**, *82*, 1210–1215. [CrossRef]
177. Fraser, S.P.; Pardo, L.A. Ion channels: Functional expression and therapeutic potential in cancer. Colloquium on Ion Channels and Cancer. *EMBO Rep.* **2008**, *9*, 512–515. [CrossRef]
178. Fraser, S.P.; Ozerlat-Gunduz, I.; Onkal, R.; Diss, J.K.; Latchman, D.S.; Djamgoz, M.B. Estrogen and non-genomic upregulation of voltage-gated Na^{+} channel activity in MDA-MB-231 human breast cancer cells: Role in adhesion. *J. Cell. Physiol.* **2010**, *224*, 527–539. [CrossRef]
179. Fouda, M.A.; Ruben, P.C. Protein Kinases Mediate Anti-Inflammatory Effects of Cannabidiol and Estradiol Against High Glucose in Cardiac Sodium Channels. *Front. Pharmacol.* **2021**, *12*, 668657. [CrossRef]
180. Hu, F.; Wang, Q.; Wang, P.; Wang, W.; Qian, W.; Xiao, H.; Wang, L. 17β-Estradiol regulates the gene expression of voltage-gated sodium channels: Role of estrogen receptor α and estrogen receptor β. *Endocrine* **2012**, *41*, 274–280. [CrossRef]
181. Bi, R.-Y.; Meng, Z.; Zhang, P.; Wang, X.-D.; Ding, Y.; Gan, Y.-H. Estradiol upregulates voltage-gated sodium channel 1.7 in trigeminal ganglion contributing to hyperalgesia of inflamed TMJ. *PLoS ONE* **2017**, *12*, e0178589. [CrossRef]

182. Kow, L.M.; Devidze, N.; Pataky, S.; Shibuya, I.; Pfaff, D.W. Acute estradiol application increases inward and decreases outward whole-cell currents of neurons in rat hypothalamic ventromedial nucleus. *Brain Res.* **2006**, *1116*, 1–11. [CrossRef]
183. Gallos, G.; Yim, P.; Emala, C.W. Chloride in airway smooth muscle: The ignored anion no longer? *Am. J. Physiol.-Lung Cell. Mol. Physiol.* **2012**, *302*, L733–L735. [CrossRef] [PubMed]
184. Bulley, S.; Jaggar, J.H. Cl^- channels in smooth muscle cells. *Pflügers Arch.-Eur. J. Physiol.* **2014**, *466*, 861–872. [CrossRef] [PubMed]
185. Janssen, L.J.; Sims, S.M. Ca^{2+}-dependent Cl^- current in canine tracheal smooth muscle cells. *Am. J. Physiol.* **1995**, *269*, C163–C169. [CrossRef]
186. Kotlikoff, M.I.; Wang, Y.-X. Calcium Release and Calcium-Activated Chloride Channels in Airway Smooth Muscle Cells. *Am. J. Respir. Crit. Care Med.* **1998**, *158*, S109–S114. [CrossRef] [PubMed]
187. Danielsson, J.; Yim, P.; Rinderspacher, A.; Fu, X.W.; Zhang, Y.; Landry, D.W.; Emala, C.W. Chloride channel blockade relaxes airway smooth muscle and potentiates relaxation by β-agonists. *Am. J. Physiol.-Lung Cell. Mol. Physiol.* **2014**, *307*, L273–L282. [CrossRef]
188. Hirota, S.; Trimble, N.; Pertens, E.; Janssen, L.J. Intracellular Cl^- fluxes play a novel role in Ca^{2+} handling in airway smooth muscle. *Am. J. Physiol.-Lung Cell. Mol. Physiol.* **2006**, *290*, L1146–L1153. [CrossRef] [PubMed]
189. Gallos, G.; Remy, K.E.; Danielsson, J.; Funayama, H.; Fu, X.W.; Chang, H.Y.; Yim, P.; Xu, D.; Emala, C.W., Sr. Functional expression of the TMEM16 family of calcium-activated chloride channels in airway smooth muscle. *Am. J. Physiol.-Lung Cell. Mol. Physiol.* **2013**, *305*, L625–L634. [CrossRef]
190. Huang, F.; Zhang, H.; Wu, M.; Yang, H.; Kudo, M.; Peters, C.J.; Woodruff, P.G.; Solberg, O.D.; Donne, M.L.; Huang, X.; et al. Calcium-activated chloride channel TMEM16A modulates mucin secretion and airway smooth muscle contraction. *Proc. Natl. Acad. Sci. USA* **2012**, *109*, 16354–16359. [CrossRef]
191. Danielsson, J.; Kuforiji, A.S.; Yocum, G.T.; Zhang, Y.; Xu, D.; Gallos, G.; Emala, C.W. Agonism of the TMEM16A calcium-activated chloride channel modulates airway smooth muscle tone. *Am. J. Physiol.-Lung Cell. Mol. Physiol.* **2020**, *318*, L287–L295. [CrossRef]
192. Huang, C.; Wang, Y.; Li, X.; Ren, L.; Zhao, J.; Hu, Y.; Zhang, L.; Fan, G.; Xu, J.; Gu, X.; et al. Clinical features of patients infected with 2019 novel coronavirus in Wuhan, China. *Lancet* **2020**, *395*, 497–506. [CrossRef] [PubMed]
193. Kato, M.; Takayama, Y.; Sunagawa, M. The Calcium-Activated Chloride Channel TMEM16A is Inhibitied by Liquiritigenin. *Front. Pharmacol.* **2021**, *12*, 628968. [CrossRef] [PubMed]
194. Coakley, R.D.; Sun, H.; Clunes, L.A.; Rasmussen, J.E.; Stackhouse, J.R.; Okada, S.F.; Fricks, I.; Young, S.L.; Tarran, R. 17β-Estradiol inhibits Ca^{2+}-dependent homeostasis of airway surface liquid volume in human cystic fibrosis airway epithelia. *J. Clin. Investig.* **2008**, *118*, 4025–4035. [CrossRef]
195. Imberti, R.; Garavaglia, M.L.; Verduci, I.; Cannavale, G.; Balduzzi, G.; Papetti, S.; Mazzanti, M. Antiestrogen- and tamoxifen-induced effects on calcium-activated chloride currents in epithelial cells carrying the ΔF508-CFTR point mutation. *Respir. Res.* **2018**, *19*, 198. [CrossRef]
196. Vandebrouck, C.; Melin, P.; Norez, C.; Robert, R.; Guibert, C.; Mettey, Y.; Becq, F. Evidence that CFTR is expressed in rat tracheal smooth muscle cells and contributes to bronchodilation. *Respir. Res.* **2006**, *7*, 113. [CrossRef] [PubMed]
197. Michoud, M.-C.; Robert, R.; Hassan, M.; Moynihan, B.; Haston, C.; Govindaraju, V.; Ferraro, P.; Hanrahan, J.W.; Martin, J.G. Role of the Cystic Fibrosis Transmembrane Conductance Channel in Human Airway Smooth Muscle. *Am. J. Respir. Cell Mol. Biol.* **2009**, *40*, 217–222. [CrossRef]
198. Cook, D.P.; Rector, M.V.; Bouzek, D.C.; Michalski, A.S.; Gansemer, N.D.; Reznikov, L.R.; Li, X.; Stroik, M.R.; Ostedgaard, L.S.; Abou Alaiwa, M.H.; et al. Cystic Fibrosis Transmembrane Conductance Regulator in Sarcoplasmic Reticulum of Airway Smooth Muscle. Implications for Airway Contractility. *Am. J. Respir. Crit. Care Med.* **2016**, *193*, 417–426. [CrossRef]
199. Norez, C.; Jayle, C.; Becq, F.; Vandebrouck, C. Bronchorelaxation of the human bronchi by CFTR activators. *Pulm. Pharmacol. Ther.* **2014**, *27*, 38–43. [CrossRef] [PubMed]
200. Bazett, M.; Haston, C.K. Airway hyperresponsiveness in FVB/N delta F508 cystic fibrosis transmembrane conductance regulator mice. *J. Cyst. Fibros. Off. J. Eur. Cyst. Fibros. Soc.* **2014**, *13*, 378–383. [CrossRef]
201. Huang, J.; Lam, H.; Koziol-White, C.; Limjunyawong, N.; Kim, D.; Kim, N.; Karmacharya, N.; Rajkumar, P.; Firer, D.; Dalesio, N.M.; et al. The odorant receptor OR2W3 on airway smooth muscle evokes bronchodilation via a cooperative chemosensory tradeoff between TMEM16A and CFTR. *Proc. Natl. Acad. Sci. USA* **2020**, *117*, 28485–28495. [CrossRef]
202. Johannesson, M.; Lúdvíksdóttir, D.; Janson, C. Lung function changes in relation to menstrual cycle in females with cystic fibrosis. *Respir. Med.* **2000**, *94*, 1043–1046. [CrossRef] [PubMed]
203. Singh, A.K.; Schultz, B.D.; Katzenellenbogen, J.A.; Price, E.M.; Bridges, R.J.; Bradbury, N.A. Estrogen inhibition of cystic fibrosis transmembrane conductance regulator-mediated chloride secretion. *J. Pharmacol. Exp. Ther.* **2000**, *295*, 195–204. [PubMed]
204. Ajonuma, L.C.; Tsang, L.L.; Zhang, G.H.; Wong, C.H.Y.; Lau, M.C.; Ho, L.S.; Rowlands, D.K.; Zhou, C.X.; Ng, C.P.; Chen, J.; et al. Estrogen-Induced Abnormally High Cystic Fibrosis Transmembrane Conductance Regulator Expression Results in Ovarian Hyperstimulation Syndrome. *Mol. Endocrinol.* **2005**, *19*, 3038–3044. [CrossRef] [PubMed]
205. Jin, H.; Wen, G.; Deng, S.; Wan, S.; Xu, J.; Liu, X.; Xie, R.; Dong, H.; Tuo, B. Oestrogen upregulates the expression levels and functional activities of duodenal mucosal CFTR and SLC26A6. *Exp. Physiol.* **2016**, *101*, 1371–1382. [CrossRef]
206. Jin, P.-Y.; Lu, Y.-C.; Li, L.; Han, Q.-F. Co action of CFTR and AQP1 increases permeability of peritoneal epithelial cells on estrogen-induced ovarian hyper stimulation syndrome. *BMC Cell Biol.* **2012**, *13*, 23. [CrossRef]

207. Sweezey, N.B.; Gauthier, C.; Gagnon, S.; Ferretti, E.; Kopelman, H. Progesterone and estradiol inhibit CFTR-mediated ion transport by pancreatic epithelial cells. *Am. J. Physiol.* **1996**, *271*, G747–G754. [CrossRef]
208. Goodstadt, L.; Powell, T.; Figtree, G.A. 17β-estradiol potentiates the cardiac cystic fibrosis transmembrane conductance regulator chloride current in guinea-pig ventricular myocytes. *J. Physiol. Sci.* **2006**, *56*, 29–37. [CrossRef]
209. Mizuta, K.; Xu, D.; Pan, Y.; Comas, G.; Sonett, J.R.; Zhang, Y.; Panettieri, R.A.; Yang, J.; Emala, C.W. GABA_Areceptors are expressed and facilitate relaxation in airway smooth muscle. *Am. J. Physiol.-Lung Cell. Mol. Physiol.* **2008**, *294*, L1206–L1216. [CrossRef]
210. Gallos, G.; Yim, P.; Chang, S.; Zhang, Y.; Xu, D.; Cook, J.M.; Gerthoffer, W.T.; Emala, C.W., Sr. Targeting the restricted α-subunit repertoire of airway smooth muscle $GABA_A$ receptors augments airway smooth muscle relaxation. *Am. J. Physiol.-Lung Cell. Mol. Physiol.* **2012**, *302*, L248–L256. [CrossRef]
211. Gallos, G.; Yocum, G.T.; Siviski, M.E.; Yim, P.D.; Fu, X.W.; Poe, M.M.; Cook, J.M.; Harrison, N.; Perez-Zoghbi, J.; Emala, C.W., Sr. Selective targeting of the α5-subunit of $GABA_A$ receptors relaxes airway smooth muscle and inhibits cellular calcium handling. *Am. J. Physiol.-Lung Cell. Mol. Physiol.* **2015**, *308*, L931–L942. [CrossRef]
212. Yocum, G.T.; Turner, D.L.; Danielsson, J.; Barajas, M.B.; Zhang, Y.; Xu, D.; Harrison, N.L.; Homanics, G.E.; Farber, D.L.; Emala, C.W. $GABA_A$ receptor α_4 -subunit knockout enhances lung inflammation and airway reactivity in a murine asthma model. *Am. J. Physiol.-Lung Cell. Mol. Physiol.* **2017**, *313*, L406–L415. [CrossRef] [PubMed]
213. Herbison, A.; Fenelon, V. Estrogen regulation of $GABA_A$ receptor subunit mRNA expression in preoptic area and bed nucleus of the stria terminalis of female rat brain. *J. Neurosci.* **1995**, *15*, 2328–2337. [CrossRef] [PubMed]
214. Maggi, A.; Perez, J. Estrogen-induced up-regulation of gamma-aminobutyric acid receptors in the CNS of rodents. *J. Neurochem.* **1986**, *47*, 1793–1797. [CrossRef]
215. François-Bellan, A.M.; Segu, L.; Héry, M. Regulation by estradiol of $GABA_A$ and $GABA_B$ binding sites in the diencephalon of the rat: An autoradiographic study. *Brain Res.* **1989**, *503*, 144–147. [CrossRef] [PubMed]
216. Locci, A.; Porcu, P.; Talani, G.; Santoru, F.; Berretti, R.; Giunti, E.; Licheri, V.; Sanna, E.; Concas, A. Neonatal estradiol exposure to female rats changes $GABA_A$ receptor expression and function, and spatial learning during adulthood. *Horm. Behav.* **2017**, *87*, 35–46. [CrossRef] [PubMed]

biomedicines

MDPI

Article

Altered PLCβ/IP_3/Ca^{2+} Signaling Pathway Activated by GPRCs in Olfactory Neuronal Precursor Cells Derived from Patients Diagnosed with Schizophrenia

Zuly A. Sánchez-Florentino [1,2], Bianca S. Romero-Martínez [3], Edgar Flores-Soto [3], Luis M. Montaño [3], Bettina Sommer [4], Marcela Valdés-Tovar [5], Jesús Argueta [2], Eduardo Calixto [6], Arnoldo Aquino-Gálvez [7], Manuel Castillejos-López [8], Héctor Serrano [9], Juan C. Gomez-Verjan [10], Germán O. López-Riquelme [11], Gloria A. Benítez-King [2], Ruth Jaimez [3,*] and Héctor Solís-Chagoyán [12,*]

1 Posgrado en Biología Experimental, Universidad Autónoma Metropolitana-Iztapalapa, Mexico City 09340, CP, Mexico; zulyarmandosf@gmail.com
2 Laboratorio de Neurofarmacología, Subdirección de Investigaciones Clínicas, Instituto Nacional de Psiquiatría Ramón de la Fuente Muñiz, Mexico City 14370, CP, Mexico; jadclear@gmail.com (J.A.); bekin@imp.edu.mx (G.A.B.-K.)
3 Departamento de Farmacología, Facultad de Medicina, Universidad Nacional Autónoma de México, Mexico City 04510, CP, Mexico; biancasromero_@hotmail.com (B.S.R.-M.); edgarfloressoto@yahoo.com.mx (E.F.-S.); lmmr@unam.mx (L.M.M.)
4 Departamento de Investigación en Hiperreactividad Bronquial, Instituto Nacional de Enfermedades Respiratorias "Ismael Cosío Villegas", Mexico City 14080, CP, Mexico; bsommer195@gmail.com
5 Subdirección de Investigaciones Clínicas, Instituto Nacional de Psiquiatría Ramón de la Fuente Muñiz, Mexico City 14370, CP, Mexico; mvaldes_inprfm@yahoo.com
6 Departamento de Neurobiología, Dirección de Investigación en Neurociencias, Instituto Nacional de Psiquiatría Ramón de la Fuente Muñiz, Mexico City 14370, CP, Mexico; ecalixto@imp.edu.mx
7 Laboratorio de Biología Molecular, Departamento de Fibrosis Pulmonar, Instituto Nacional de Enfermedades Respiratorias "Ismael Cosío Villegas", Mexico City 14080, CP, Mexico; araquiga@yahoo.com.mx
8 Unidad de Epidemiología Hospitalaria e Infectología, Instituto Nacional de Enfermedades Respiratorias "Ismael Cosío Villegas", Mexico City 14080, CP, Mexico; mcastillejos@gmail.com
9 Departamento de Ciencias de la Salud, Universidad Autónoma Metropolitana-Iztapalapa, Mexico City 09340, CP, Mexico; hser@xanum.uam.mx
10 Dirección de Investigación, Instituto Nacional de Geriatría, Mexico City 10200, CP, Mexico; jverjan@inger.gob.mx
11 Laboratorio de Socioneurobiologia, Centro de Investigación en Ciencias Cognitivas, Universidad Autónoma del Estado de Morelos, Cuernavaca 62209, CP, Mexico; german.lopez@uaem.mx
12 Laboratorio de Neurobiología Cognitiva, Centro de Investigación en Ciencias Cognitivas, Universidad Autónoma del Estado de Morelos, Cuernavaca 62209, CP, Mexico
* Correspondence: jaimezruth@hotmail.com (R.J.); hector.solis@uaem.mx (H.S.-C.)

check for updates

Citation: Sánchez-Florentino, Z.A.; Romero-Martínez, B.S.; Flores-Soto, E.; Montaño, L.M.; Sommer, B.; Valdés-Tovar, M.; Argueta, J.; Calixto, E.; Aquino-Gálvez, A.; Castillejos-López, M.; et al. Altered PLCβ/IP_3/Ca^{2+} Signaling Pathway Activated by GPRCs in Olfactory Neuronal Precursor Cells Derived from Patients Diagnosed with Schizophrenia. *Biomedicines* **2024**, *12*, 2343. https://doi.org/10.3390/biomedicines12102343

Academic Editor: Andrei Surguchov

Received: 13 September 2024
Revised: 8 October 2024
Accepted: 13 October 2024
Published: 15 October 2024

Abstract: Background: Schizophrenia (SZ) is a multifactorial chronic psychiatric disorder with a worldwide prevalence of 1%. Altered expression of PLCβ occurs in SZ patients, suggesting alterations in the PLCβ/IP_3/Ca^{2+} signaling pathway. This cascade regulates critical cellular processes in all cell types, including the neuronal lineage; however, there is scarce evidence regarding the functionality of this transduction signaling in neuronal cells derived from SZ patients. **Objective**: We evaluated the functionality of the PLCβ/IP_3/Ca^{2+} pathway in olfactory neuronal precursor cells (hONPCs) obtained from SZ patients. **Methods**: Cryopreserved hONPCs isolated from SZ patients and healthy subjects (HS) were thawed. The cellular types in subcultures were corroborated by immunodetection of the multipotency and lineage markers SOX-2, Musashi-1, nestin, and β-III tubulin. The PLCβ/IP_3/Ca^{2+} pathway was activated by GPCR (G_q) ligands (ATP, UTP, serotonin, and epinephrine). In addition, PLCβ and IP_3R were directly stimulated by perfusing cells with the activators m-3M3FBS and ADA, respectively. Cytosolic Ca^{2+} was measured by microfluorometry and by Ca^{2+} imaging. The amount and subcellular distribution of the PLCβ1 and PLCβ3 isoforms were evaluated by confocal immunofluorescence. IP_3 concentration was measured by ELISA. **Results**: The results show that the increase of cytosolic Ca^{2+} triggered by GPCR ligands or directly through either PLCβ or IP_3R activation was significantly lower in SZ-derived hONPCs, regarding HS-derived cells.

Moreover, the relative amount of the PLCβ1 and PLCβ3 isoforms and IP_3 production stimulated with m-3M3FBS were reduced in SZ-derived cells. **Conclusions**: Our results suggest an overall functional impairment in the PLCβ/IP_3/Ca^{2+} signaling pathway in SZ-derived hONPCs.

Keywords: human olfactory neuronal stem cells; calcium signaling; PLCβ; IP_3; schizophrenia

1. Introduction

Schizophrenia (SZ) is a severe psychiatric disorder that usually presents its clinical onset in early adulthood and affects approximately 1% of the human population. The clinical symptoms that allow the diagnosis of this disorder are hallucinations, paranoia, inattention, decreased social interactions, lack of motivation, and cognitive impairment. SZ has a multifactorial etiology, and its development might have a complex genetic background but additionally involves diverse environmental risk factors [1,2]. Furthermore, SZ has been associated with altered neurotransmission mediated by serotonin, dopamine, glutamate, and GABA [3–5].

Diverse high-risk factors associated with SZ are encoded by genes related to calcium ion (Ca^{2+}) signaling, suggesting that alterations in the pathways activated by this cation can be characteristic of this disorder [6]. Ca^{2+} is a key intracellular messenger in all cell types; it is versatile and regulates multiple subcellular processes involved in essential functions, such as proliferation, migration, differentiation, neurotransmission, and cell death, among others. In this regard, several studies have shown that the pathophysiology of SZ has been related to processes dependent on Ca^{2+} signaling, such as dysfunction in neuromodulation mediated by dopamine, glutamate, serotonin, and GABA, leading to malfunctioning of interneurons and consequently cognitive, behavioral, and social dysfunction [7]. Interestingly, several of these extracellular signals are transduced through activation of the PLCβ enzyme, which generates the second messenger IP_3 and Ca^{2+} release from intracellular stores. In studies that analyze the expression of mRNA in biopsies of the orbitofrontal cortex, the deletion of the PLCβ1 gene in SZ patients has been suggested [8]; in addition, in post-mortem tissue, decreased levels of PLCβ1 mRNA expression in the dorsolateral prefrontal cortex [9], and lower levels of the PLCβ1 protein in the prefrontal cortex [10] were detected.

To the best of our knowledge, studies on the functionality of PLCβ in vivo in SZ patients are null. To overcome this limitation, models involving the isolation and culture of human cells from the neural lineage have been characterized, such as olfactory stem cells derived from the human olfactory epithelium (hOE) [11,12]. Experimental data suggest that isolated human olfactory neuronal precursor cells (hONPCs) that exhibit multipotent features can be propagated in culture and cryopreserved in biobanks. These hONPCs have been proposed to be a suitable model to study alterations found in neuropsychiatric and neurological diseases such as depression [13], Alzheimer's disease [14–16], bipolar disorder [17], Parkinson's disease [18], SZ [19–21], and in other pathologies such as fragile X syndrome [22], cannabis use [23], and COVID-19 and olfactory dysfunction [24].

The characteristics of hONPCs provide them with great potential as a human neural cell model, especially for studying neurodevelopmental disorders. The transcriptomic expression of these cells coincides with a mid-fetal stage of the brain. It has been used to describe the differential gene expression of multiple signaling pathway genes in SZ [20], which could serve for the further study and elucidation of the etiology of the disease and correlate embryonic and fetal events [20,25]. Furthermore, hONPCs have proven to be an effective model for studying cognition and neurodegenerative diseases, as Rantanen et al. observed while evaluating the transcriptomic profile of Alzheimer's disease (AD) patients and patients with moderate cognitive impairment [15]. Furthermore, the unique qualities of hONPCs allow the potential identification of target genes and signaling pathways in

diseased states, such as in SZ or AD, and the analysis of their possible role as therapeutic targets [21].

Due to the rigorous validation processes to which hONPCs have been subjected as a surrogate model, their robustness and reliability in providing consistent and accurate results in addressing pathophysiological mechanisms at the structural, cellular, and molecular levels have been guaranteed [12,26,27]. Therefore, the main objective of this study was to determine the functionality of the PLCβ/IP_3 pathway through stimulation of PLCβ or by activating some G protein-coupled receptors (GPCRs) in hONPCs isolated from SZ patients and healthy subjects (HS).

2. Materials and Methods

2.1. Human Olfactory Neural Precursor Cells

This study was carried out in accordance with the Helsinki Declaration for human research; the donors of the olfactory epithelium samples previously signed an informed consent letter. This research was approved by the Institutional Bioethics Committee (Project number: INPRFM IC 092010.0). Highly trained specialists from the Schizophrenia Clinic of the Instituto Nacional de Psiquiatría Ramón de la Fuente Muñiz (INPRFM) performed clinical patient evaluations and diagnoses and referred the patients to this study. Thus, we used a convenience non-probabilistic sampling method, with both controls and patients being Mexicans and matched by age (±6 years). The patients had a range of 0–18 years from the onset of symptoms to the sample collection; two patients were untreated (naïve), and four patients were treated with standard antipsychotic drugs (haloperidol, fluoxetine, risperidone) by the time of the sample collection. There were no observable differences related to the demographic characteristics of the populations (Table 1).

Table 1. Sociodemographic data of sample donors. Olfactory neural precursor cells were obtained from 6 subjects per group. Cryopreserved cells were used in this study. HS corresponds to healthy subjects and SZ to patients diagnosed with schizophrenia.

Diagnosis	Sex	Age	Age at Diagnosis	Pre-Existing Conditions	Family Psychiatric History	Treatment	Time of Evolution	Alcoholism	Smoking
HS	F	28							
HS	F	23						Yes	
HS	F	27				Ibuprofen Vitamin C		Yes	
HS	M	23							
HS	M	27		Hypoglycemia				Yes	
HS	M	28		Hypothyroidism		Levothyroxine Coenzyme Q Carnitine			
SZ	F	32	25			Haloperidol 50 mg, biperiden 4 mg, fluoxetine 20 mg	7		
SZ	F	27	26			Risperidone 2 mg, fluoxetine 20 mg, biperiden 2 mg	1		
SZ	M	20	20	ADHD care at age 8		Naïve	0		
SZ	M	28	27			Naïve	1	Yes	Yes
SZ	M	31	28			Risperidone 2 mg	3		
SZ	F	33	15	Obesity and hypothyroidism	Yes	Haloperidol 10 mg, fluoxetine 40 mg, akineton 2 mg, eutirox	18		

Samples of the olfactory epithelium were obtained by exfoliation of the nasal cavity, as reported by Benítez-King and coworkers (2011), from subjects without psychiatric diagnosis (healthy subjects: HS) and patients diagnosed with SZ [12]. Briefly, cells were obtained with an interdental brush and mechanically dissociated in Dulbecco's modified Eagle medium/F-12 nutrient mix (DMEM/F12), supplemented with 10% (*v*/*v*) fetal bovine serum, 2 mM L-glutamine, and 1% (*v*/*v*) penicillin–streptomycin. The dissociated cells were plated in a 4-well cell culture plate and incubated at 37 °C with 5% CO_2 until the culture reached confluence. The cultures were replated in 25 cm^2 cell culture flasks to obtain subcultures in different passages. These subcultures were cryopreserved in the supplemented DMEM/F12 medium with 8% DMSO. They were maintained submerged in liquid nitrogen in the cell bank of the Neuropharmacology Laboratory of the INPRFM. The experiments of this study were performed using cryopreserved subcultures of olfactory stem cells obtained from 6 HS and 6 SZ patients (Table 1); cells were thawed in passages 2 or 3, and experiments were carried out at passages 4–6.

2.2. Protein Detection by Immunofluorescence

Cells in passages 4–6 were placed on 12 mm diameter round coverslips and kept in culture with supplemented DMEM/F12 medium for three days with controlled temperature and CO_2, 37 °C and 5%, respectively. Then, cells were fixed with 4% paraformaldehyde and permeabilized with 0.2% Tween-20 in PBS for 30 min; non-specific protein binding was blocked with 5% BSA for 1 h. Primary and secondary antibodies were titrated to determine their optimal concentrations for detecting their epitopes. Three marker proteins for multipotent stem cells were immunodetected using a commercial kit (R&D Systems®, Cat. NC025; Minneapolis, MN, USA): anti-SOX-2 (1:60), anti-Musashi-1 (1:60), and anti-nestin (1:60) were incubated overnight. In addition, the isoforms 1 and 3 of the enzyme PLCβ were immunodetected with a rabbit monoclonal antibody (1:10; Abcam Carlsbad, CA, USA, Cat. EPR18714). Both SOX-2 and Musashi-1 primary antibodies were detected by the DyLight™ 488-conjugated donkey anti-goat IgG (1:500; Invitrogen, Carlsbad, CA, USA, Cat. SA5-1086), whereas for detection of anti-nestin, cells were incubated with an Alexa Fluor™ 488-conjugated goat anti-rabbit IgG (1:500; Invitrogen, Cat. A32723). In the case of PLCβ 1 and 3, the secondary antibody was an Alexa Fluor™ 680-conjugated donkey anti-rabbit IgG (1:500; Invitrogen Cat. A10043). Cells were incubated for 60 min with the secondary antibodies at room temperature, and the nuclei were counterstained with 150 nM of 4′,6-diamidino-2-phenylindole (DAPI) for 4 min. Finally, coverslips were mounted with ProLong™ Diamond Antifade Mountant (Thermo Fisher Scientific, Carlsbad, CA, USA, P36961). Labeling was observed on a ZEISS LSM 900 with a Airyscan 2 confocal microscope (Carl Zeiss Microscopy, Jena, Germany), and the images were analyzed by the ImageJ 1.53t and ZEN (blue edition, version 3.4.91) software. In all cases, non-specific fluorescence was assessed by omitting the primary antibodies, and, particularly for multipotent markers, J774A.1 mouse macrophages stimulated with LPS for 24 h were used as negative controls. Randomly chosen fields per subject were considered.

2.3. Quantification of Cytosolic Calcium Concentration by Microfluorometry

The functionality of various G protein-coupled receptors (particularly the Gq isoform) was examined by G protein activation in hONPCs from patients with SZ and HS. The cognate receptors present in these cells are described in Table S1 [23,28–30]. Cells in passages 3 to 5 at 80% confluence were detached with EDTA and a trypsin solution. Cells were seeded at 12,000 cells/cm^2 density on rat tail collagen-coated round coverslips; the cultures were maintained under a controlled environment at 37 °C and 5% CO_2 for three days with supplemented DMEM/F-12 medium.

Cells were incubated with 2.5 μM Fura 2-AM (Invitrogen), diluted in the supplemented DMEM/F-12 medium for 1 h at 37 °C and 5% CO_2. Then, coverslips with cells were placed in a perfusion chamber on an inverted microscope (Diaphot 200, Nikon, Tokio, Japan) and perfused with Krebs solution at 37 °C with a 2–2.5 mL/min flow. Krebs solution

contained (in mM): 118 NaCl, 25 $NaHCO_3$, 4.6 KCl, 1.2 KH_2PO_4, 1.2 $MgSO_4$, 11 glucose, and 2 $CaCl_2$; pH was adjusted by aerating the solution with carbogen. The cytosolic Ca^{2+} concentration was quantified using a microphotometer (model D-104, Photon Technology International, Ford, West Sussex, UK), applying alternating light stimuli of 340 and 380 nm wavelengths and quantifying the 510 nm fluorescence emitted by Fura 2 bound to Ca^{2+}. Light stimuli were applied at a frequency of 0.5 Hz, and intracellular Ca^{2+} concentration was calculated according to the Grynkiewicz formula [31]. The PLCβ/IP_3/Ca^{2+} pathway was stimulated by perfusing cells with either 300 μM ATP, 300 μM UTP, 10 μM serotonin (5-HT), or 10 μM epinephrine (EPI). Additionally, Ca^{2+} measurements were performed by activating the PLC enzyme with a stimulus of 10 μM m-3M3FBS (non-specific activator, Tocris, Avonmouth, Bristol. UK Cat. 1941) [32]. Finally, the IP_3R was stimulated directly with the specific activator adenophostin A hexasodium salt (32 nM ADA; Santa Cruz, Heidelberg, Germany, EU, Cat. sc-221213) [33]. Also, to evaluate GPCR ligand-induced Ca^{2+} responses not mediated through the PLCβ/IP_3 pathway, hONPCs were perfused with either 10 μM dopamine (DOPA) or 10 μM glutamate (GLU). To compare the increase in intracellular Ca^{2+} concentration, we calculated the difference of the maximal amplitude minus the basal concentration in each cell. Data were obtained from 3 random responses from 6 subjects per group.

2.4. Calcium Imaging by Fluorescence Microscopy

Cells in passages 4–6 at 12,000 cells/cm^2 density were cultured with supplemented DMEM/F-12 at 37 °C and 5% CO_2 for three days. The Ca^{2+} indicator Fluo 4-AM (4 μM; Invitrogen) diluted in culture medium was added and incubated for 30 min at 37 °C and 5% CO_2. Subsequently, cells were washed with Krebs solution at 37° C, and coverslips were placed in an epifluorescence microscope (Nikon Eclipse TE2000, Nikon, Tokyo, Japan). Intracellular Ca^{2+} increase was induced with either 300 μM ATP, 300 μM UTP, 10 μM 5-HT, 10 μM EPI, or 10 μM m-3M3FBS. Images were acquired with a Nikon digital camera (model DS-Ri2) and the NIS-Elements AR software (version 4.3); fluorescence was detected before stimulation (basal cytosolic Ca^{2+} concentration), and after 2 min (GPCR agonists) or 30 s (PLC activator), thapsigargin (1 μM, TG), and cyclopiazonic acid (10 μM, CPA) were added as the stimuli. The cells were manually segmented and the fluorescent marker intensity was quantified for each cell individually and represented as the mean fluorescence intensity in arbitrary units (MFI, AU, respectively). The images were analyzed using the software Fiji/ImageJ 1.54f. Data were obtained from 3 randomly selected fields from 6 subjects per group.

2.5. Measurement of IP_3 Concentration by ELISA

Cells in passages 4–6 were plated in 75 cm^2 culture flasks and cultured in supplemented DMEM/F12 medium. At 80% confluence, cells were stimulated with 10 μM m-3M3FBS for 20 min to activate PLC and increase the IP_3 concentration. Cultures were washed with 4 mL pre-cooled PBS, and cells were detached with a trypsin-containing solution. Suspended cells were counted with a hemocytometer and centrifuged for 5 min at 1000× *g*. The supernatant was discarded, and cells were washed three times with pre-cooled PBS (200 μL of pre-cooled PBS was added for 1×10^6 cells). Cells were frozen and thawed three times to be wholly lysed. The final centrifugation was performed at 4 °C and 1500× *g* for 10 min, and the supernatant was carefully collected.

The IP_3 immunoassay was performed according to the ELISA kit manufacturer's instructions (Abcam, Cat. ab287832). The optical density was measured at 450 nm, and measurements of IP_3 for standards and samples were performed in duplicate and averaged. Finally, a four-parameter logistic curve was plotted in GraphPad Prism software (version 9.3.1) to obtain a standard curve and interpolate the values from HS and SZ cultures; data were normalized by pg/10^6 cells and were obtained from 2 technical replicates of 4 subjects per group.

2.6. Statistical Analysis

Plotted data represent the mean ± standard error; data were compared using an unpaired Student's *t*-test with Welch's correction or a one-way analysis of variance (ANOVA). The significance of differences between groups was considered with $p < 0.05$. The sample size was determined using G*Power software (Version 3.1.9.6, Franz Faul, Universität Kiel, Germany) [34]. Using this software, we evaluated the effect of the population size using real data obtained in a pilot study. An a priori power analysis was performed, employing a two-tailed *t*-test or one-way ANOVA as applicable, with a significance level (α) set at 0.05. A power analysis (1-β) was selected at 80%. Statistical analysis was performed with GraphPad Prism software (version 9.3.1).

3. Results

3.1. Expression of Multipotency Markers in Cells from HS and SZ Patients

The present study found that hONPCs obtained from both HS and SZ exhibit characteristics of multipotent stem cells because they express molecular markers of multipotency, such as nestin, Musashi-1, and SOX-2 (Figure 1). Detecting these proteins suggests that cells from both patients and controls have equivalent characteristics of undifferentiated stem cells.

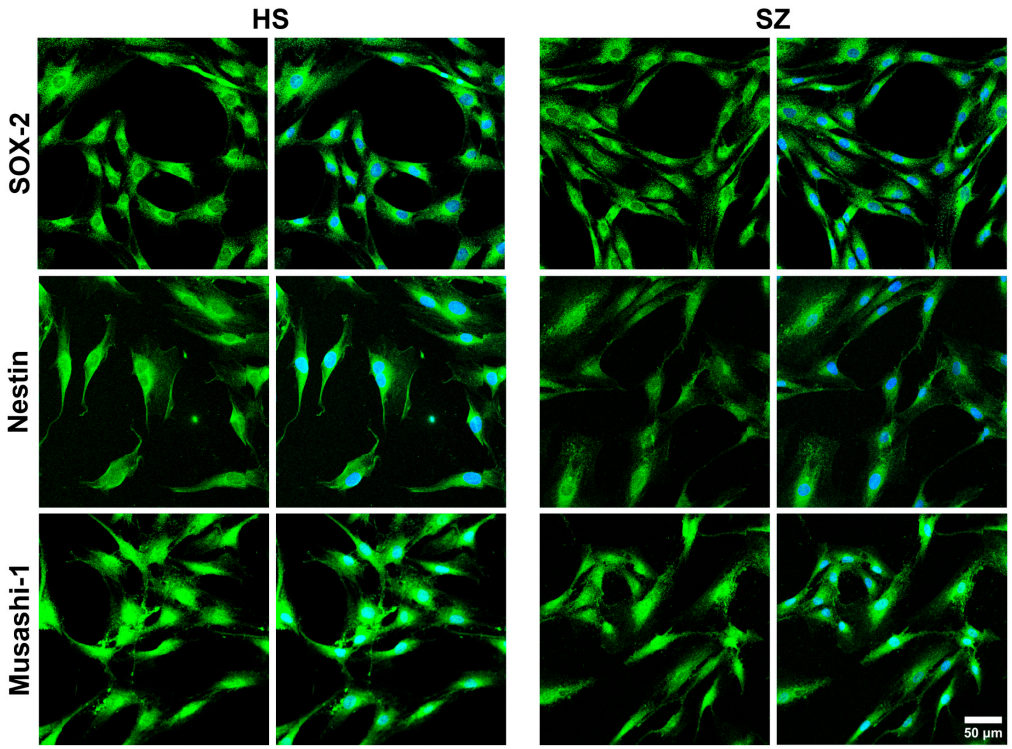

Figure 1. Determination of multipotency markers in hONPCs of HS and SZ patients. HS-derived and SZ patient-derived cells exhibit multipotent stem cell characteristics by expressing SOX-2, Musashi-1, and nestin. All cells express the three multipotency markers. DAPI-stained nuclei.

3.2. Olfactory Epithelium Single-Cell Ca^{2+} Response Induced by Gq-Coupled Agonists in HS and SZ Patients

In hONPCs, stimulation with GPCR ($G_{\alpha q}$) agonists (300 µM ATP, 300 µM UTP, 10 µM 5-HT or 10 µM EPI) induced a transient increase in the intracellular Ca^{2+} concentrations ($[Ca^{2+}]_i$) that returned to basal levels when the stimuli were removed (Figure 2). The Ca^{2+} responses induced by ATP, UTP, 5-HT, and EPI in HS-derived cells were higher than in SZ-derived cells. All groups were significantly diminished when comparing the $\Delta[Ca^{2+}]_i$ of the response induced by the different GPCR agonists from the SZ patients' cells regarding the HS-derived cells (Figure 2).

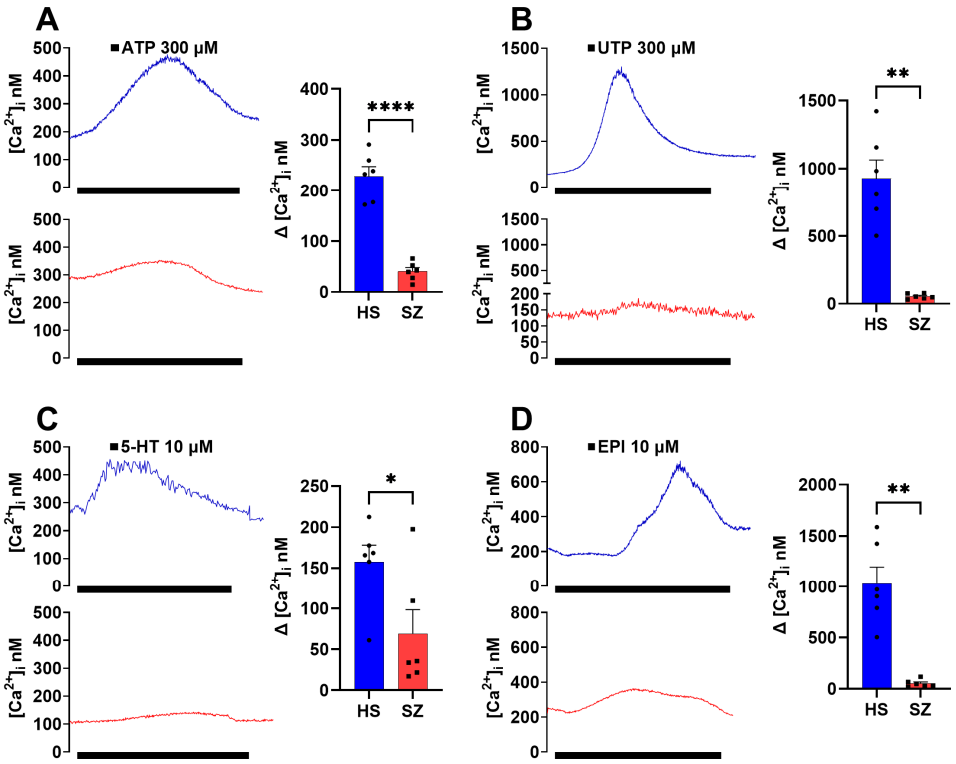

Figure 2. Increase in cytosolic Ca^{2+} induced by Gq-coupled agonists in single cells of the olfactory epithelium of HS and SZ patients. Cells were cultured for three days to assess changes in intracellular Ca^{2+} concentration ($[Ca^{2+}]_i$) induced by 300 µM ATP (**A**), 300 µM UTP (**B**), 10 µM serotonin (**C**), and 10 µM epinephrine (**D**) by microfluorometry using Fura 2-AM. The graphs represent the data obtained from six subjects per group. Each data point represents the average of three technical replicates for each subject. Data were expressed as mean ± SEM and compared using the Student's *t*-test with Welch's correction, * $p < 0.05$ ** $p < 0.01$ **** $p < 0.001$. HS = healthy subject (blue), SZ = schizophrenic patient (red).

3.3. Cellular Population Ca^{2+} Imaging after GPCR Agonist Stimulation in hONPCs from HS and SZ Patients

To corroborate the differences in the Ca^{2+} responses observed in the microfluorometric studies, we performed Ca^{2+} imaging with Fluo-4 loaded hONPCs at the population level (Figure 3). To explore the non-receptor-mediated Ca^{2+} response from the internal stores, the cells were stimulated with thapsigargin (1 µM, TG) or cyclopiazonic acid (10 µM, CPA); we observed significant differences between basal Ca^{2+} levels and the corresponding stimuli, but not when compared between groups (HS vs. SZ) (Figure 4). The basal Ca^{2+} levels and the ATP-induced Ca^{2+} responses in passage 1 cells were not different from those observed in passage 5 of HS- and SZ patient-derived cells (Figure 5). The Ca^{2+} response in HS cells treated with either ATP, UTP, 5-HT, or EPI was higher when compared to the SZ cells and results suggest that differences in Ca^{2+} responses were not dependent on culture passage. These results suggest a generalized pattern of dysfunction in the Ca^{2+} response induced by GPCR ($G_{\alpha q}$) agonists, probably via an alteration in the PLCβ/IP_3 pathway.

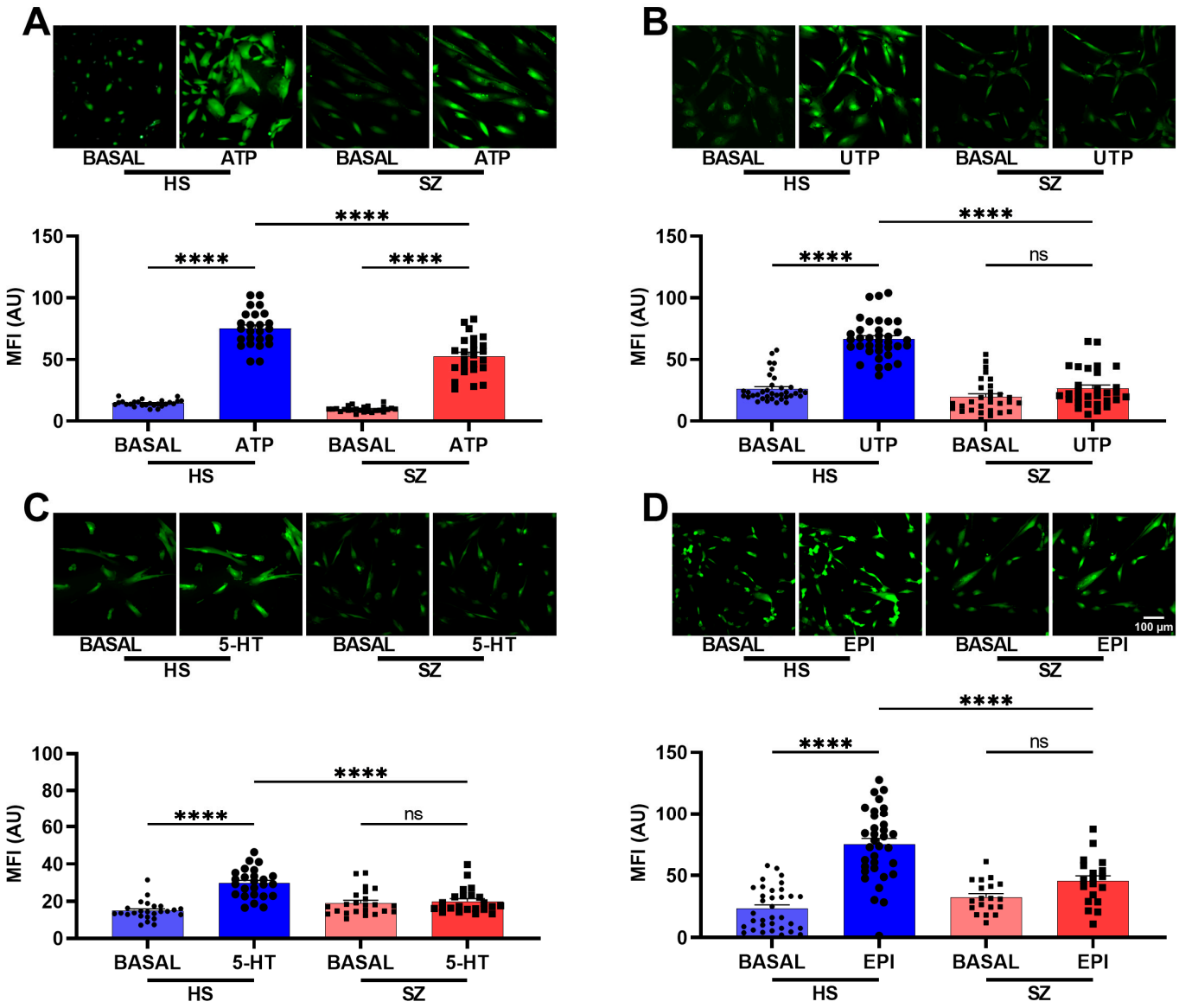

Figure 3. Intracellular calcium response after stimulation with G_q-coupled agonists in olfactory epithelial cell populations of HS and patients with SZ. The cells were incubated for 30 min with 4 µM Fluo 4-AM diluted in the culture medium at 37 °C and 5% CO_2. Images were captured before stimulation (basal) and 2 min after stimulation with either 300 µM ATP (**A**), 300 µM UTP (**B**), 10 µM serotonin (**C**), and 10 µM epinephrine (**D**) in HS-derived cells and SZ patient-derived cells. The graphs represent data obtained from at least 18 images (18–20 cells per image) per group. Data were expressed as mean ± SEM and compared using Brown–Forsythe one-way analysis of variance (ANOVA) and Dunnett's multiple comparison test, **** $p < 0.0001$. ns: not significant. Mean fluorescence intensity (MFI), arbitrary units (AU).

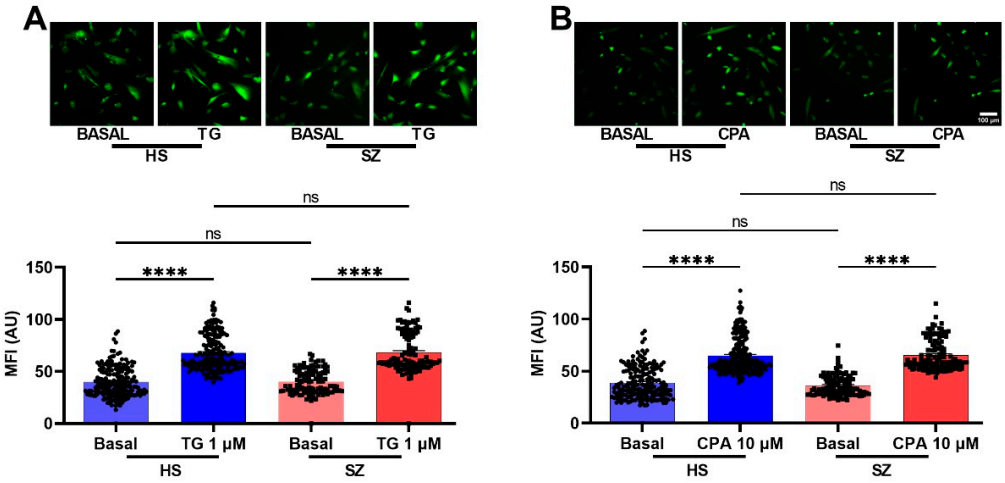

Figure 4. Intracellular calcium response after stimulation with thapsigargin and CPA in hONPCs of HS and patients with SZ. Images were captured before stimulation (basal) and 2 min after stimulation with either 1 µM thapsigargin (TG, left graph) (**A**), and 10 µM cyclopiazonic acid (CPA, right graph) (**B**) in HS and SZ derived cells. No significant differences were found when basal Ca^{2+} levels were compared (HS vs. SZ), neither when comparing treated cell responses. Highly significant differences were found when basal Ca^{2+} levels were compared with their respective treatment. The graphs represent data obtained from at least six images (18–20 cells per image) per group. Data were expressed as mean ± SEM and compared using the Kruskal–Wallis test and Dunn's multiple comparisons test, **** $p < 0.0001$. ns: not significant. Mean fluorescence intensity (MFI), arbitrary units (AU).

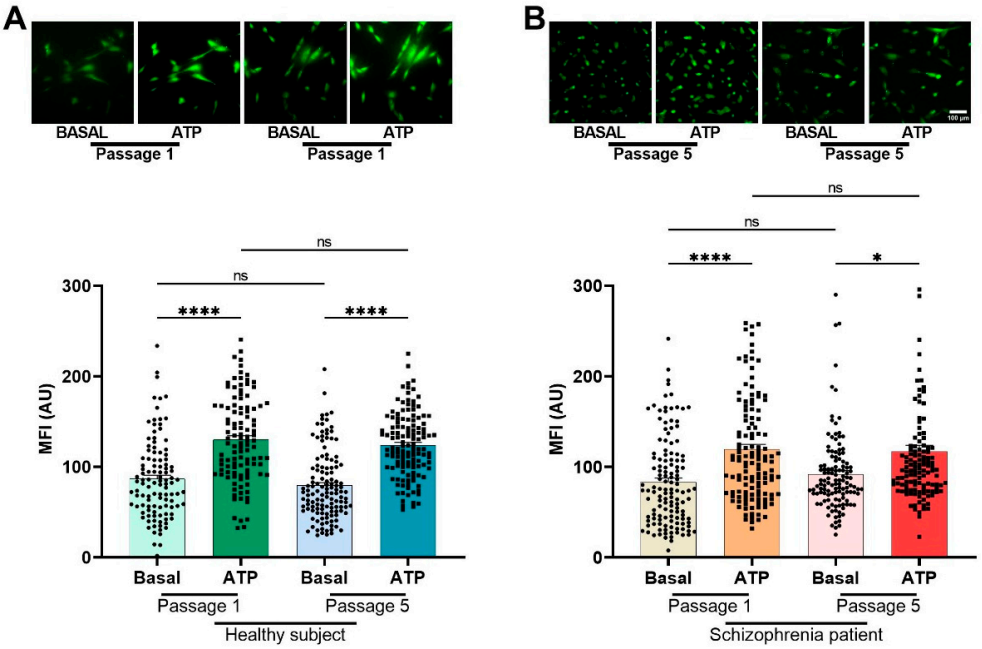

Figure 5. Intracellular calcium response after stimulation with ATP in olfactory epithelial precursor cell populations of HS (**A**) and SZ (**B**) patients in passage 1 and passage 5. The cells were incubated for 30 min with 4 µM Fluo 4-AM diluted in the culture medium at 37 °C and 5% CO_2. Images were captured before stimulation (basal) and 2 min after stimulation with 300 µM ATP. Each data point represents the mean fluorescence intensity (MFI) measurement of each cell. The MFI of at least 100 cells was determined. The graphs represent data obtained from at least six images (18–20 cells per image) per group. Data were expressed as mean ± SEM and compared using the Kruskal–Wallis and Dunn's multiple comparisons tests. **** $p < 0.0001$, * $p < 0.05$; not significant (ns). AU: arbitrary units.

3.4. Function and Expression of the PLCβ Protein in hONPCs

When a ligand (such as a neurotransmitter) binds to a GPCR ($G_{\alpha q}$) on the cell surface, it activates the $G_{\alpha q}$ protein subunit, subsequently activating PLCβ. Activated PLCβ cleaves phosphatidylinositol 4,5-bisphosphate (PIP2) into IP_3 and diacylglycerol (DAG). IP_3 then diffuses into the cytoplasm and binds to IP_3 receptors (IP_3R) on the endoplasmic reticulum, leading to the release of calcium ions from intracellular stores. To determine the functionality of PLCβ in the hONPCs, we stimulated isolated cells with 10 µM m-3M3FBS, an activator of PLCβ which is known to induce an intracellular Ca^{2+} increment [32]. In HS, the Ca^{2+} response was 696.2 ± 128.4 nM, n = 6, while in SZ patients this was, 239 ± 80.59 nM, n = 6, and we observed significant differences in the $\Delta[Ca^{2+}]_i$ ($p < 0.05$) (Figure 6A). Similarly, we explored the overall Ca^{2+} response through Ca^{2+} imaging. There was no difference in the basal Ca^{2+} levels; however, the difference in the response to m-3M3FBS between HS (70.24 ± 3.01 AU) and SZ patients (59. 98 ± 1.778 AU) was significant ($p < 0.001$) (Figure 6B).

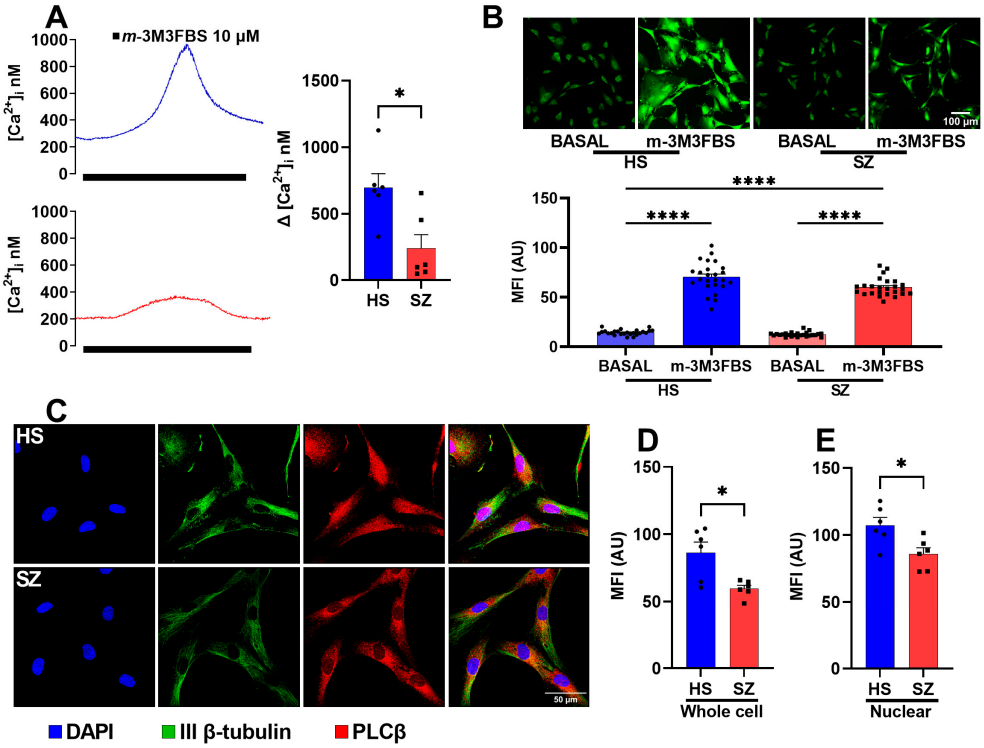

Figure 6. Cytosolic increase in Ca^{2+} after direct PLCβ stimulation and the amount of PLCβ protein in cultured cells from HS and patients with SZ. (**A**) Microfluorometric detection of changes in intracellular Ca^{2+} concentration ($[Ca^{2+}]_i$) induced by 10 µM m-3M3FBS. (**B**) Calcium images were captured before stimulation (basal) and 30 s after direct PLCβ stimulation (10 µM m-3M3FBS). (**C**) Immunofluorescent detection of PLCβ1 and 3; the panel shows representative images from cells detected by confocal microscopy. Neuronal-specific human IIIβ-tubulin (green) and PLCβ1 and 3 (red) were detected in the cells. Nuclei were counterstained with DAPI (blue). The mean fluorescence intensity of the whole cells (**D**) and of the nuclear zone (**E**) were compared. Data were expressed as mean ± SEM and compared using the Student's *t*-test with Welch's correction for panels (**A**,**D**,**E**) (* $p < 0.05$) or with one-way ANOVA and Tukey's multiple comparisons test for panel (**B**) (**** $p < 0.0001$).

Since PLCβ1 and PLCβ3 are expressed in various tissues with differential subcellular distribution (PLCβ1 in the nucleus and plasma membrane; PLCβ3 is nuclear) and have a higher sensitization to $G_{\alpha q}$-mediated activation relative to other isoenzymes [35–37], we detected their amount and distribution in hONPCs from HS and SZ patients by confocal immunofluorescence (Figure 6C). In the cells of SZ patients, we found a significant decrease

in the amount of PLCβ in the whole cell (SZ 57.58 ± 3.73 arbitrary units (AU) vs. HS 76.65 ± 7.261 AU) (Figure 6D). Interestingly, this pattern is also significantly lower at the subcellular level when comparing both groups at the nuclei (SZ 85.88 ± 5.7 AU vs. HS 107.2 ± 6.05 AU) (Figure 6E). These findings suggest that alterations in the expression of this protein may explain the decrease in $[Ca^{2+}]_i$ after a stimulus in the cells of SZ patients. Therefore, the altered Ca^{2+} response in the hONPCs of SZ patients could be independent of GPCR stimulation and directly caused by the lowered production of IP_3 via PLCβ activation. This could contribute to altered signaling pathways and cellular processes associated with SZ.

3.5. Production of IP_3 and IP_3 Receptor Function in hONPCs

IP_3 is produced through the action of PLCβ enzymes on PIP2, a phospholipid enriched at the cell membrane. In hONPCs (1×10^6), a 20 min incubation with m-3M3FBS (a PLC activator) was used to stimulate the production of IP_3; the intracellular concentration of inositol-triphosphate ($[IP_3]_c$) was determined by ELISA (Figure 7). In HS, the $[IP_3]_c$ was 646.1 ± 43.47 pg $IP_3/1 \times 10^6$ (n = 4), while in SZ patients it was 322.5 ± 81.36 pg $IP_3/1 \times 10^6$ (n = 4) (Figure 7A). We found significant differences among these groups in $[IP_3]_c$ production ($p < 0.05$). In addition, to determine the functionality of the IP_3R, we stimulated hONPCs with ADA (a potent IP_3R activator) to induce Ca^{2+} release from the sarcoplasmic reticulum [33]. In HS, the Δ fluorescence was 0.27 ± 0.04 (n = 8), and in the SZ patients, it was 0.16 ± 0.02 (n = 8) (Figure 7B). We found significant differences in the Δ fluorescence (340/380) ($p < 0.05$), showing a lower release of Ca^{2+} when the IP_3R was activated in SZ cells.

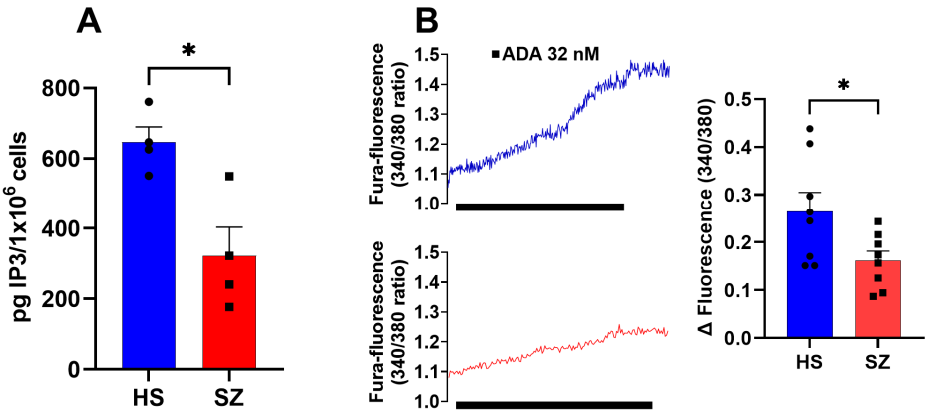

Figure 7. Effects of m-3M3FBS on the concentration of IP_3 in hONPCs. (**A**) Cells of HS and SZ patients were stimulated with 10 μM m-3M3FBS for 20 min to activate PLCβ and increase the IP_3 concentration. Data were normalized by pg $IP_3/10^6$ cells and obtained from two technical replicates of four subjects per group. (**B**) IP_3R was directly stimulated with 32 nM ADA. The graphs represent data obtained from eight responses from six subjects per group. Data were expressed as mean ± SEM and compared using the Student's *t*-test with Welch's correction, * $p < 0.05$.

3.6. Olfactory Epithelium Single Cell Ca^{2+} Response Independent of the $IP_3/IP_3R/Ca^{2+}$ Pathway in HS and SZ Patients

The Ca^{2+} responses in cells from HS induced by DOPA (51.54 ± 12.75 nM, n = 6) and GLU (131.1± 16.69 nM, n = 8) were similar to those observed for the SZ-cells: DOPA (31.80 ± 3.85 nM, n = 6) (Figure 8A), and GLU (106.8 ± 38.17 nM, n = 8) (Figure 8B), and no significant differences were observed when the Ca^{2+} responses were compared. This finding is understandable since the increase of cytosolic Ca^{2+} triggered upon ligand binding to the corresponding dopamine D_2R and glutamate NMDA receptors is not mediated by IP_3 production in hOE cells [30].

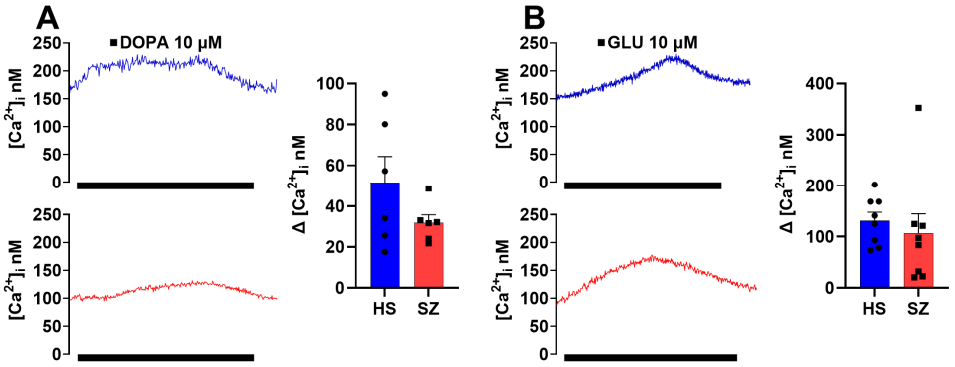

Figure 8. Increase in cytosolic Ca^{2+} induced by dopamine and glutamate in single cells of the olfactory epithelium of HS and SZ patients. Changes in intracellular Ca^{2+} concentration ($[Ca^{2+}]_i$) induced by 10 µM dopamine (**A**) and 10 µM glutamate (**B**) by microfluorometry using Fura 2-AM. The graphs represent data obtained from eight responses from six subjects per group. Data were expressed as mean ± SEM and compared using the Student's *t*-test with Welch's correction.

4. Discussion

hONPCs have different types of GPCRs with $G_{\alpha q}$ subunits. A cytosolic Ca^{2+} concentration increase was induced via the PLCβ/IP_3 pathway upon ligand stimulation of these GPCRs with several ligands such as ATP, UTP, EPI, or 5-HT. These responses were attenuated in SZ patient-derived hONPCs, and, furthermore, activating PLCβ produced a similar diminished response. Since the production of IP_3 and the function of IP_3R were also reduced in the SZ-derived cells, it could be assumed that the alteration in the signaling pathway is directly related to the PLCβ activity, not due to alterations in the internal Ca^{2+} stores. The Ca^{2+} response induced by DOPA and GLU, which receptors do not signal through the PLCβ/IP_3 pathway, consistently showed no difference between the HS and SZ groups. In this sense, a "convergent pathway hypothesis" can be suggested to emphasize the relevance of the PLCβ/IP_3 pathway as a critical point of convergence of various dysfunctional neurochemical signals in SZ.

Previously, Durante et al. identified specific molecular markers in multipotent cells of the olfactory neuroepithelium, including horizontal basal cells (TP63, KRT5, CXCL-14, SOX-2, MEG3), globose basal cells (HES6, ASCL1, CXCR4, SOX-2, EZH2, NEUROD-1, NEUROG-1), respiratory horizontal basal cells (KRT5, TP63, SOX-2), and sustentacular cells (CYP2A13, CYP2J2, GPX6, ERMN, SOX-2) [38]. It has been noted that the expression of specific markers is a particularly significant advantage of using hONPCs. In previous works, markers in these cells, including nestin, Musashi-1, OCT3/4, NANOG, Notch, SOX-2, NCAM, and the neuronal IIIβ-tubulin, not only enabled the determination of their potency but also facilitated the verification of their proper isolation [28,39]. We should highlight that cells analyzed in this work were from early passages and had not been modified by a transforming virus or chemical compound. Furthermore, for the pathway we were interested in, the responses from cells at passage 5 or higher passages were not different than those found in earlier passages, as shown in Figure 5.

In SZ, reports of altered neurotransmitter-mediated signaling pathways, i.e., muscarinic, purinergic, glutamatergic, serotonergic, dopaminergic, and GABAergic, have been published [3–5]. The activation of these pathways initiates various cellular processes regulated by Ca^{2+}, such as exocytosis, neuronal excitability, proliferation, differentiation, and neural plasticity [6,40,41]. SZ has been associated with Ca^{2+} signaling dysfunction, including the decreased activity of the NMDA receptor in early development stages [6]. There is evidence that the activity of NMDA receptors (NMDARs) is reduced when the phenotype of GABAergic inhibitory neurons is altered. There is also a decrease in the activity of serotonergic neurons located in the prefrontal cortex of patients with SZ [42,43]. Other proteins involved in Ca^{2+} signaling, such as the glutamate receptor mGluR5 [44] and muscarinic receptors [45], are also altered in SZ.

Interestingly, many extracellular signals involved in the pathogenesis of SZ are transduced through PLCβ-dependent pathways, implicating the function of this protein as a point of convergence in altered signaling. Four PLCβ isoenzymes (PLCβ1-4) encoded in different genes have been identified in mammals. These isoenzymes have differential distribution in tissues, e.g., PLCβ1 and PLCβ4 are found mainly in the brain, with exceptionally high expression in the cerebral cortex and hippocampus for PLCβ1 and in the cerebellum and retina for PLCβ4. On the other hand, PLCβ2 is preferentially present in hematopoietic cells, while PLCβ3 has ubiquitous expression. At the subcellular level, PLCβ1 is expressed on the plasma membrane, and all four PLCβ isoenzymes can be found in the nucleus. However, PLCβ1 appears to be the most abundant, followed by PLCβ3, PLCβ2, and finally PLCβ4 [36]. Dysregulation in the signaling associated with the different types of PLCβ is generally linked to various neuropsychiatric disorders, including epilepsy, Alzheimer's disease, Huntington's disease, bipolar disorder, depression, and SZ [8,46–48].

In this study, we observed an impaired function and a reduced amount of both the PLCβ1 and -β3 isoforms. PLCβ1 has been reported to be one of the first verifiable biomarkers that differentiate SZ from bipolar disorder [49]. In addition, studies performed on ex vivo samples from specific brain areas of SZ patients have reported alterations in PLCβ1, such as deletion of the PLCβ1 gene in the orbitofrontal cortex [46], decreased levels of PLCβ1 mRNA expression in the dorsolateral prefrontal cortex [9], and lower levels of the PLCβ1 protein in the prefrontal cortex [10]. In murine models, SZ-like behavior has been documented in phospholipase C β1 (PLCβ1(−/−)) knockout mice, such as hyperlocomotion, decreased exploration, nesting behavior, impaired working memory, and cognitive impairment, possibly due to abnormal cellular plasticity as a consequence of gene deletion and reduced mRNA and protein [50,51].

To the best of our knowledge, this is the first study providing evidence that the PLCβ signaling pathway is functionally impaired in cells from SZ patients, suggesting that previously reported abnormal levels of the enzyme may have a consequence on the functionality of its associated pathways, particularly in signal transduction through the PLCβ/IP_3/Ca^{2+} cascade. This signaling pathway aims to generate and control highly complex Ca^{2+} signals, and the resulting increase in the concentration of cytosolic Ca^{2+} modulates various cellular functions, such as gene expression, metabolism, secretion, neuronal excitation, and cell death, among others [52,53]. Thus, a functional impairment at the level of PLCβ/IP_3/Ca^{2+} might impact downstream elements of the signal transduction pathway, i.e., kinase activation, molecule translocation to specific subcellular compartments, cytoskeletal rearrangement, vesicle trafficking, etc.

We found a global change in the amount of PLCβ, and there are changes restricted to specific cellular compartments, such as the nucleus, where there is a reduced amount of PLCβ in SZ patients' cells. Therefore, the measurement of PLCβ isoforms in different cell fractions can provide us with information on how this decrease in protein can affect specific molecular and cellular processes.

The heterogeneity of pathology and the poor efficacy of current classical therapeutic options that often either have an incomplete effect or hard-to-manage side effects has given rise to the search for new cell signaling pathways and drug target identification. Through GWAS and cellular response phenotype models, a myriad of genetic risk loci have been identified in PBMCs and iPSC-derived CNS cells, highlighting mechanistic points of convergence, such as epitopes of the Akt/GSK-3β pathway, the phosphorylation of CrkL, 4EBP1, and PLC-γ1, among others. Furthermore, the identification of a new compound, or repurposing of drugs, directed at the genetic risk loci, presents the possibility of personalized targeted therapeutic approach that could overcome the drawbacks of the current pharmacological options, such as treatment resistance. Some of the identified drugs include corticosteroids (methylprednisolone and flunisolide), potassium channel blockers (ibutilide), calcium channel blockers (nicardipine, nisoldipine), and thapsigargin (directed at PLC-γ1) [54]. Notably, the animal knockout models of PLC-γ1 that presents manic-like behavioral changes [55] and altered cell responses to thapsigargin has been associated

with ATP2A2 mutations [56,57], indicating that PLC-γ1 could be a significant piece in the pathophysiology of SZ.

IP_3, an essential cellular second messenger, is generated in response to the activation of specific receptors on the cell membrane. This messenger plays a fundamental role in the release of calcium within the cell [36]. Some studies show that SZ patients have altered levels of calcium in platelets. However, these findings are inconsistent, and a clear association has not been established. Arranz et al. [58] found that platelets' IP_3 concentrations at baseline and post-treatment with antipsychotics were not significantly different when compared to controls. Meanwhile, Rípová et al. [59] determined that $[Ca^{2+}]_i$ was significantly higher in platelets of neuroleptic-treated patients than in controls. Differences in IP_3 levels were also found between controls and untreated and treated SZ patients. Studies have shown alterations in the levels and activity of enzymes involved in the synthesis and metabolism of IP_3 in patients with SZ [46,60]. These alterations could contribute to altered neuronal function and symptoms associated with the disease. Importantly, SZ is a complex and multifactorial disorder, and the exact relationship between IP_3 signaling dysfunction and SZ pathophysiology is not fully understood.

Our results provide new insights from an in vivo model that support the previous evidence obtained from the expression of PLCβ in postmortem brain tissues and clarify the divergent results that have been obtained up to now in the amount of IP_3 in platelets of SZ patients, which are limited to be a model that simulates characteristics of bioaminergic neurons and catecholamine regulation [61,62]. Specifically, one of the most outstanding results in this work is the dysfunction in PLCβ activity, which leads to deficiencies in the production of the second messenger IP_3 and the functionality of the IP_3R, subsequently leading to an alteration in the release of calcium from intracellular stores in hONPCs. These alterations are relevant to increasing our understanding of SZ pathophysiology and could be a prospect for therapeutic targets and diagnostic tools. Nevertheless, further research is required to determine how this specific dysfunction is related to other neurochemical, genetic, and environmental factors involved in the development and progression of SZ.

The DOPA and GLU stimuli in hONPCs showed no difference between HS and SZ patients. The phenotypic receptor expression varies greatly, regulated by acute and chronic mechanisms to best fit its specific functions according to cell type, species, and stage of development to maintain a stable phenotype under physiological conditions and have the capacity to oversee the plasticity of the expression under new stimuli [63]. hOE cells have been reported to predominantly express the D_2R isoform of the dopamine receptors, a G_{i}- and G_{o}-coupled receptor. In contrast, for glutamate receptors, the predominant isoform in these cells is the NMDA receptor, an ionotropic receptor [30]. Both receptors are independent of the PLCβ signaling pathway and could explain the lack of difference between the responses observed in our study.

Some limitations of using hONPCs as a study model for SZ include the lack of information about the functionality of different signaling pathways in these cells. Additionally, due to the undifferentiated nature of these cells, it is necessary to confirm the results through conventional SZ models based on differentiated dopaminergic and serotoninergic neurons [64]. Although the statistical power of the present study enables the identification of significant differences between groups, our sample size is relatively small, and there is a need to increase the number of subjects using methodologies that allow us to work with a larger sample. We acknowledge that, up to this point, due to the heterogeneous nature of the pathology, no shared molecular mechanism found in all individuals diagnosed with schizophrenia is known.

hONPCs are a suitable model for studying cellular and molecular processes in neuropsychiatric disorders [26]. Furthermore, considering that these precursor cells are multipotent, the signaling impairment through the $PLC\beta/IP_3/Ca^{2+}$ pathway may be conserved in their differentiated progeny, either neuronal or glial, implying that a broad spectrum of specialized functions could be altered. Thus, further research with hONPCs and their dif-

ferentiated progeny would provide a deeper insight into how the altered PLCβ/IP_3/Ca^{2+} pathway participates in diverse pathophysiological cellular processes in SZ.

5. Conclusions

The altered PLCβ/IP_3/Ca^{2+} pathway in hONPCs may have broader implications that could contribute to dysfunctions underlying the pathophysiology of SZ. The dysregulation of the PLCβ/IP_3/Ca^{2+} pathway and G_q ligand-triggered processes in these cells may impact their differentiation, migration, or survival, leading to structural and functional abnormalities in neuronal circuitries in SZ.

Supplementary Materials: The following supporting information can be downloaded at: https://www.mdpi.com/article/10.3390/biomedicines12102343/s1, Table S1: G protein coupled receptors present in diverse tissues. Those recognized in ONPCs are designated by *. Methodology: Cryopreservation.

Author Contributions: Conceptualization, Z.A.S.-F., B.S.R.-M., E.F.-S. and H.S.-C.; Formal analysis, Z.A.S.-F., B.S.R.-M., E.F.-S., L.M.M., B.S., M.V.-T., J.A., E.C., A.A.-G., M.C.-L., H.S., J.C.G.-V., G.O.L.-R., G.A.B.-K., R.J. and H.S.-C.; Funding acquisition, L.M.M., M.V.-T., G.A.B.-K. and R.J.; Methodology, Z.A.S.-F., B.S.R.-M., E.F.-S., L.M.M., B.S., M.V.-T., J.A., E.C., A.A.-G., M.C.-L., H.S., J.C.G.-V., G.O.L.-R., G.A.B.-K., R.J. and H.S.-C.; Writing—original draft, Z.A.S.-F., B.S.R.-M., E.F.-S., L.M.M., B.S., M.V.-T., J.A., E.C., A.A.-G., M.C.-L., H.S., J.C.G.-V., G.O.L.-R., G.A.B.-K., R.J. and H.S.-C.; Writing—review & editing, Z.A.S.-F., B.S.R.-M., E.F.-S., L.M.M., B.S., M.V.-T., J.A., E.C., A.A.-G., M.C.-L., H.S., J.C.G.-V., G.O.L.-R., G.A.B.-K., R.J. and H.S.-C. All authors have read and agreed to the published version of the manuscript.

Funding: This research was funded by Consejo Nacional de Ciencia y Tecnología (Grant 290526 to GBK), Consejo Nacional de Ciencia y Tecnología (Grant CF/2019/137725 to LMM), and Programa Presupuestario F003 Consejo Nacional de Ciencia y Tecnología (Grant 287115/CB2016 to MVT). The APC was funded by PAPIIT-UNAM 024/2016 Facultad de Medicina, UNAM to RJ.

Institutional Review Board Statement: This study was conducted in accordance with the Declaration of Helsinki and approved by the Ethics Committee of Instituto Nacional de Psiquiatría (protocol code INPRFM IC 092010.0, October 2021).

Informed Consent Statement: Informed consent was obtained from all subjects involved in this study.

Data Availability Statement: Data are available on request from the authors.

Acknowledgments: ZASF was supported by a Grant-in-aid (CVU 697823) from the National Council for Science, Humanities, and Technology (CONAHCYT). Bianca S. Romero Martinez is grateful to the Programa de Doctorado en Ciencias Biomédicas, Universidad Nacional Autónoma de México, for the instruction received during her Ph.D. degree studies. She received a fellowship from the Consejo Nacional de Ciencia y Tecnología, México (application # 2020-000013-01NACF-12778; CVU 469822). We are grateful to Maria del Pilar Romo and Rosalba Linares for their administrative and technical support.

Conflicts of Interest: The authors have declared that there are no conflicts of interest concerning the subject of this study.

References

1. Jauhar, S.; Johnstone, M.; McKenna, P.J. Schizophrenia. *Lancet* **2022**, *399*, 473–486. [CrossRef] [PubMed]
2. Stilo, S.A.; Murray, R.M. Non-Genetic Factors in Schizophrenia. *Curr. Psychiatry Rep.* **2019**, *21*, 100. [CrossRef] [PubMed]
3. Howes, O.D.; Mccutcheon, R.; Owen, M.J.; Murray, R.M. The Role of Genes, Stress, and Dopamine in the Development of Schizophrenia. *Biol. Psychiatry* **2017**, *81*, 9–20. [CrossRef] [PubMed]
4. Lewis, D.A.; Moghaddam, B. Cognitive dysfunction in schizophrenia: Convergence of gamma-aminobutyric acid and glutamate alterations. *Arch. Neurol.* **2006**, *63*, 1372–1376. [CrossRef]
5. Stahl, S.M. Beyond the dopamine hypothesis of schizophrenia to three neural networks of psychosis: Dopamine, serotonin, and glutamate. *CNS Spectr.* **2018**, *23*, 187–191. [CrossRef]
6. Berridge, M.J. Calcium signalling and psychiatric disease: Bipolar disorder and schizophrenia. *Cell Tissue Res.* **2014**, *357*, 477–492. [CrossRef]
7. Yang, A.; Tsai, S.-J. New Targets for Schizophrenia Treatment beyond the Dopamine Hypothesis. *Int. J. Mol. Sci.* **2017**, *18*, 1689. [CrossRef]

8. Lo Vasco, V.R.; Longo, L.; Polonia, P. Phosphoinositide-specific Phospholipase C β1 gene deletion in bipolar disorder affected patient. *J. Cell Commun. Signal* **2013**, *7*, 25–29. [CrossRef] [PubMed]
9. Udawela, M.; Scarr, E.; Hannan, A.J.; Thomas, E.A.; Dean, B. Phospholipase C beta 1 expression in the dorsolateral prefrontal cortex from patients with schizophrenia at different stages of illness. *Aust. N. Z. J. Psychiatry* **2011**, *45*, 140–147. [CrossRef]
10. Udawela, M.; Scarr, E.; Boer, S.; Um, J.Y.; Hannan, A.J.; Mcomish, C.; Felder, C.C.; Thomas, E.A.; Dean, B. Isoform specific differences in phospholipase C beta 1 expression in the prefrontal cortex in schizophrenia and suicide. *NPJ Schizophr.* **2017**, *3*, 19. [CrossRef]
11. Féron, F.; Perry, C.; Mcgrath, J.J.; Mackay-Sim, A. New Techniques for Biopsy and Culture of Human Olfactory Epithelial Neurons. *Arch. Otolaryngol.–Head Neck Surg.* **1998**, *124*, 861. [CrossRef] [PubMed]
12. Benitez-King, G.; Riquelme, A.; Ortiz-Lopez, L.; Berlanga, C.; Rodriguez-Verdugo, M.S.; Romo, F.; Calixto, E.; Solis-Chagoyan, H.; Jimenez, M.; Montano, L.M.; et al. A non-invasive method to isolate the neuronal linage from the nasal epithelium from schizophrenic and bipolar diseases. *J. Neurosci. Methods* **2011**, *201*, 35–45. [CrossRef] [PubMed]
13. Estrada-Reyes, R.; Quero-Chávez, D.B.; Alarcón-Elizalde, S.; Cercós, M.G.; Trueta, C.; Constantino-Jonapa, L.A.; Oikawa-Sala, J.; Argueta, J.; Cruz-Garduño, R.; Dubocovich, M.L.; et al. Antidepressant Low Doses of Ketamine and Melatonin in Combination Produce Additive Neurogenesis in Human Olfactory Neuronal Precursors. *Molecules* **2022**, *27*, 5650. [CrossRef]
14. Riquelme, A.; Valdés-Tovar, M.; Ugalde, O.; Maya-Ampudia, V.; Fernández, M.; Mendoza-Durán, L.; Rodríguez-Cárdenas, L.; Benítez-King, G. Potential Use of Exfoliated and Cultured Olfactory Neuronal Precursors for In Vivo Alzheimer's Disease Diagnosis: A Pilot Study. *Cell Mol. Neurobiol.* **2020**, *40*, 87–98. [CrossRef]
15. Rantanen, L.M.; Bitar, M.; Lampinen, R.; Stewart, R.; Quek, H.; Oikari, L.E.; Cunί-López, C.; Sutharsan, R.; Thillaiyampalam, G.; Iqbal, J.; et al. An Alzheimer's Disease Patient-Derived Olfactory Stem Cell Model Identifies Gene Expression Changes Associated with Cognition. *Cells* **2022**, *11*, 3258. [CrossRef]
16. Santillán-Morales, V.; Rodriguez-Espinosa, N.; Muñoz-Estrada, J.; Alarcón-Elizalde, S.; Acebes, Á.; Benítez-King, G. Biomarkers in Alzheimer's Disease: Are Olfactory Neuronal Precursors Useful for Antemortem Biomarker Research? *Brain Sci.* **2024**, *14*, 46. [CrossRef] [PubMed]
17. Solís-Chagoyán, H.; Calixto, E.; Figueroa, A.; Montaño, L.M.; Berlanga, C.; Rodríguez-Verdugo, M.S.; Romo, F.; Jiménez, M.; Gurrola, C.Z.; Riquelme, A.; et al. Microtubule organization and L-type voltage-activated calcium current in olfactory neuronal cells obtained from patients with schizophrenia and bipolar disorder. *Schizophr. Res.* **2013**, *143*, 384–389. [CrossRef]
18. Matigian, N.; Abrahamsen, G.; Sutharsan, R.; Cook, A.L.; Vitale, A.M.; Nouwens, A.; Bellette, B.; An, J.; Anderson, M.; Beckhouse, A.G.; et al. Disease-specific, neurosphere-derived cells as models for brain disorders. *Dis. Models Mech.* **2010**, *3*, 785–798. [CrossRef] [PubMed]
19. Galván-Arrieta, T.; Trueta, C.; Cercós, M.G.; Valdés-Tovar, M.; Alarcón, S.; Oikawa, J.; Zamudio-Meza, H.; Benítez-King, G. The role of melatonin in the neurodevelopmental etiology of schizophrenia: A study in human olfactory neuronal precursors. *J. Pineal Res.* **2017**, *63*, e12421. [CrossRef]
20. Evgrafov, O.V.; Armoskus, C.; Wrobel, B.B.; Spitsyna, V.N.; Souaiaia, T.; Herstein, J.S.; Walker, C.P.; Nguyen, J.D.; Camarena, A.; Weitz, J.R.; et al. Gene Expression in Patient-Derived Neural Progenitors Implicates WNT5A Signaling in the Etiology of Schizophrenia. *Biol. Psychiatry* **2020**, *88*, 236–247. [CrossRef]
21. Mihaljevic, M.; Lam, M.; Ayala-Grosso, C.; Davis-Batt, F.; Schretlen, D.J.; Ishizuka, K.; Yang, K.; Sawa, A. Olfactory neuronal cells as a promising tool to realize the "druggable genome" approach for drug discovery in neuropsychiatric disorders. *Front. Neurosci.* **2022**, *16*, 1081124. [CrossRef] [PubMed]
22. Abrams, M.T.; Kaufmann, W.E.; Rousseau, F.; Oostra, B.A.; Wolozin, B.; Taylor, C.V.; Lishaa, N.; Morel, M.L.; Hoogeveen, A.; Reiss, A.L. FMR1 gene expression in olfactory neuroblasts from two males with fragile X syndrome. *Am. J. Med. Genet.* **1999**, *82*, 25–30. [CrossRef]
23. Galindo, L.; Moreno, E.; López-Armenta, F.; Guinart, D.; Cuenca-Royo, A.; Izquierdo-Serra, M.; Xicota, L.; Fernandez, C.; Menoyo, E.; Fernández-Fernández, J.M.; et al. Cannabis Users Show Enhanced Expression of CB(1)-5HT(2A) Receptor Heteromers in Olfactory Neuroepithelium Cells. *Mol. Neurobiol.* **2018**, *55*, 6347–6361. [CrossRef]
24. Gunder, N.; Dörig, P.; Witt, M.; Welge-Lüssen, A.; Menzel, S.; Hummel, T. Future therapeutic strategies for olfactory disorders: Electrical stimulation, stem cell therapy, and transplantation of olfactory epithelium—An overview. *Hno* **2023**, *71*, 35–43. [CrossRef] [PubMed]
25. Yang, K.; Evgrafov, O.V. Editorial: Olfactory neuroepithelium-derived cellular models to study neurological and psychiatric disorders. *Front. Neurosci.* **2023**, *17*, 1203466. [CrossRef]
26. Borgmann-Winter, K.; Willard, S.L.; Sinclair, D.; Mirza, N.; Turetsky, B.; Berretta, S.; Hahn, C.-G. Translational potential of olfactory mucosa for the study of neuropsychiatric illness. *Transl. Psychiatry* **2015**, *5*, e527. [CrossRef]
27. Gao, Y.; Winstead, W.; Lei, Z.; Lu, C.; Roisen, F.J.; El-Mallakh, R.S. Olfactory Neuroepithelial Neural Progenitor Cells from Subjects with Bipolar I Disorder. *J. Cent. Nerv. Syst. Dis.* **2017**, *9*, 117957351769452. [CrossRef]
28. Solis-Chagoyan, H.; Flores-Soto, E.; Valdes-Tovar, M.; Cercos, M.G.; Calixto, E.; Montano, L.M.; Barajas-Lopez, C.; Sommer, B.; Aquino-Galvez, A.; Trueta, C.; et al. Purinergic Signaling Pathway in Human Olfactory Neuronal Precursor Cells. *Stem Cells Int.* **2019**, *2019*, 2728786. [CrossRef]
29. Harding, S.D.; Armstrong, J.F.; Faccenda, E.; Southan, C.; Alexander, S.P.; Davenport, A.P.; Spedding, M.; Davies, J.A. The IUPHAR/BPS Guide to PHARMACOLOGY in 2024. *Nucleic Acids Res.* **2024**, *52*, D1438–D1449. [CrossRef]

30. Borgmann-Winter, K.E.; Rawson, N.E.; Wang, H.Y.; Wang, H.; Macdonald, M.L.; Ozdener, M.H.; Yee, K.K.; Gomez, G.; Xu, J.; Bryant, B.; et al. Human olfactory epithelial cells generated in vitro express diverse neuronal characteristics. *Neuroscience* **2009**, *158*, 642–653. [CrossRef]
31. Grynkiewicz, G.; Poenie, M.; Tsien, R.Y. A new generation of Ca^{2+} indicators with greatly improved fluorescence properties. *J. Biol. Chem.* **1985**, *260*, 3440–3450. [CrossRef] [PubMed]
32. Bae, Y.S.; Lee, T.G.; Park, J.C.; Hur, J.H.; Kim, Y.; Heo, K.; Kwak, J.Y.; Suh, P.G.; Ryu, S.H. Identification of a compound that directly stimulates phospholipase C activity. *Mol. Pharmacol.* **2003**, *63*, 1043–1050. [CrossRef] [PubMed]
33. Hirota, J.; Michikawa, T.; Miyawaki, A.; Takahashi, M.; Tanzawa, K.; Okura, I.; Furuichi, T.; Mikoshiba, K. Adenophostin-medicated quantal Ca^{2+} release in the purified and reconstituted inositol 1,4,5-trisphosphate receptor type 1. *FEBS Lett.* **1995**, *368*, 248–252. [CrossRef] [PubMed]
34. Kang, H. Sample size determination and power analysis using the G*Power software. *J. Educ. Eval. Health Prof.* **2021**, *18*, 17. [CrossRef]
35. Fiume, R.; Keune, W.J.; Faenza, I.; Bultsma, Y.; Ramazzotti, G.; Jones, D.R.; Martelli, A.M.; Somner, L.; Follo, M.Y.; Divecha, N.; et al. Nuclear Phosphoinositides: Location, Regulation and Function. In *Phosphoinositides II: The Diverse Biological Functions*; Balla, T., Wymann, M., York, J.D., Eds.; Springer: Dordrecht, The Netherlands, 2012; pp. 335–361.
36. Jang, H.-J.; Yang, Y.R.; Cocco, L.; Ryu, S.H.; Suh, P.-G. Phosphoinositide-Specific Phospholipase C (PI-PLC). In *Encyclopedia of Signaling Molecules*; Choi, S., Ed.; Springer International Publishing: Cham, Switzerland, 2018; pp. 3973–3988.
37. Cocco, L.; Rubbini, S.; Manzoli, L.; Billi, A.M.; Faenza, I.; Peruzzi, D.; Matteucci, A.; Artico, M.; Gilmour, R.S.; Rhee, S.G. Inositides in the nucleus: Presence and characterisation of the isozymes of phospholipase β family in NIH 3T3 cells. *Biochim. Et Biophys. Acta (BBA)—Mol. Cell Biol. Lipids* **1999**, *1438*, 295–299. [CrossRef]
38. Durante, M.A.; Kurtenbach, S.; Sargi, Z.B.; Harbour, J.W.; Choi, R.; Goss, G.M.; Matsunami, H.; Goldstein, B.J. Single-cell analysis of olfactory neurogenesis and differentiation in adult humans. *Nat. Neurosci.* **2020**, *23*, 323–326. [CrossRef]
39. Ellis, P.; Fagan, B.M.; Magness, S.T.; Hutton, S.; Taranova, O.; Hayashi, S.; McMahon, A.; Rao, M.; Pevny, L. SOX2, a persistent marker for multipotential neural stem cells derived from embryonic stem cells, the embryo or the adult. *Dev. Neurosci.* **2004**, *26*, 148–165. [CrossRef]
40. Berridge, M.J.; Bootman, M.D.; Roderick, H.L. Calcium signalling: Dynamics, homeostasis and remodelling. *Nat. Rev. Mol. Cell Biol.* **2003**, *4*, 517–529. [CrossRef]
41. Berridge, M.J. The Inositol Trisphosphate/Calcium Signaling Pathway in Health and Disease. *Physiol. Rev.* **2016**, *96*, 1261–1296. [CrossRef]
42. Matsumoto, I.; Inoue, Y.; Iwazaki, T.; Pavey, G.; Dean, B. 5-HT2A and muscarinic receptors in schizophrenia: A postmortem study. *Neurosci. Lett.* **2005**, *379*, 164–168. [CrossRef]
43. Kang, K.; Huang, X.F.; Wang, Q.; Deng, C. Decreased density of serotonin 2A receptors in the superior temporal gyrus in schizophrenia--a postmortem study. *Prog. Neuropsychopharmacol. Biol. Psychiatry* **2009**, *33*, 867–871. [CrossRef] [PubMed]
44. Matosin, N.; Newell, K.A. Metabotropic glutamate receptor 5 in the pathology and treatment of schizophrenia. *Neurosci. Biobehav. Rev.* **2013**, *37*, 256–268. [CrossRef] [PubMed]
45. Scarr, E.; Dean, B. Muscarinic receptors: Do they have a role in the pathology and treatment of schizophrenia? *J. Neurochem.* **2008**, *107*, 1188–1195. [CrossRef] [PubMed]
46. Vasco, V.R.L.; Cardinale, G.; Polonia, P. Deletion of PLCB1 gene in schizophrenia-affected patients. *J. Cell. Mol. Med.* **2012**, *16*, 844–851. [CrossRef]
47. García del Caño, G.; Montaña, M.; Aretxabala, X.; González-Burguera, I.; López de Jesús, M.; Barrondo, S.; Sallés, J. Nuclear phospholipase C-β1 and diacylglycerol LIPASE-α in brain cortical neurons. *Adv. Biol. Regul.* **2014**, *54*, 12–23. [CrossRef]
48. Kurian, M.A.; Meyer, E.; Vassallo, G.; Morgan, N.V.; Prakash, N.; Pasha, S.; Hai, N.A.; Shuib, S.; Rahman, F.; Wassmer, E.; et al. Phospholipase C beta 1 deficiency is associated with early-onset epileptic encephalopathy. *Brain* **2010**, *133*, 2964–2970. [CrossRef] [PubMed]
49. Vakalopoulos, C. The effect of deficient muscarinic signaling on commonly reported biochemical effects in schizophrenia and convergence with genetic susceptibility loci in explaining symptom dimensions of psychosis. *Front. Pharmacol.* **2014**, *5*, 277. [CrossRef]
50. McOmish, C.E.; Burrows, E.; Howard, M.; Scarr, E.; Kim, D.; Shin, H.S.; Dean, B.; van den Buuse, M.; Hannan, A.J. Phospholipase C-beta1 knockout mice exhibit endophenotypes modeling schizophrenia which are rescued by environmental enrichment and clozapine administration. *Mol. Psychiatry* **2008**, *13*, 661–672. [CrossRef]
51. Koh, H.Y. Phospholipase C-β1 and schizophrenia-related behaviors. *Adv. Biol. Regul.* **2013**, *53*, 242–248. [CrossRef]
52. Wagner, L.E., 2nd; Yule, D.I. Differential regulation of the $InsP_3$ receptor type-1 and -2 single channel properties by $InsP_3$, Ca^{2+} and ATP. *J. Physiol.* **2012**, *590*, 3245–3259. [CrossRef]
53. Mikoshiba, K. Role of IP3 receptor signaling in cell functions and diseases. *Adv. Biol. Regul.* **2015**, *57*, 217–227. [CrossRef] [PubMed]
54. Lago, S.G.; Tomasik, J.; Van Rees, G.F.; Steeb, H.; Cox, D.A.; Rustogi, N.; Ramsey, J.M.; Bishop, J.A.; Petryshen, T.; Haggarty, S.J.; et al. Drug discovery for psychiatric disorders using high-content single-cell screening of signaling network responses ex vivo. *Sci. Adv.* **2019**, *5*, eaau9093. [CrossRef] [PubMed]

55. Yang, Y.R.; Jung, J.H.; Kim, S.-J.; Hamada, K.; Suzuki, A.; Kim, H.J.; Lee, J.H.; Kwon, O.-B.; Lee, Y.K.; Kim, J.; et al. Forebrain-specific ablation of phospholipase Cγ1 causes manic-like behavior. *Mol. Psychiatry* **2017**, *22*, 1473–1482. [CrossRef] [PubMed]
56. Gordon-Smith, K.; Green, E.; Grozeva, D.; Tavadia, S.; Craddock, N.; Jones, L. Genotype–phenotype correlations in Darier disease: A focus on the neuropsychiatric phenotype. *Am. J. Med. Genet. Part. B Neuropsychiatr. Genet.* **2018**, *177*, 717–726. [CrossRef]
57. Hayashi, A.; Kasahara, T.; Kametani, M.; Toyota, T.; Yoshikawa, T.; Kato, T. Aberrant endoplasmic reticulum stress response in lymphoblastoid cells from patients with bipolar disorder. *Int. J. Neuropsychopharmacol.* **2009**, *12*, 33. [CrossRef]
58. Arranz, B.; Rosel, P.; Sarró, S.; Ramirez, N.; Dueñas, R.; Cano, R.; María Sanchez, J.; San, L. Altered platelet serotonin 5-HT2A receptor density but not second messenger inositol trisphosphate levels in drug-free schizophrenic patients. *Psychiatry Res.* **2003**, *118*, 165–174. [CrossRef]
59. Rípová, D.; Strunecká, A.; Platilová, V.; Höschl, C. Phosphoinositide signalling system in platelets of schizophrenic patients and the effect of neuroleptic therapy. *Prostaglandins Leukot. Essent. Fat. Acids* **1999**, *61*, 125–129. [CrossRef]
60. Rípová, D.; Strunecká, A.; Nemcová, V.; Farská, I. Phospholipids and calcium alterations in platelets of schizophrenic patients. *Physiol. Res.* **1997**, *46*, 59–68.
61. Bondy, B.; Ackenheil, M.; Birzle, W.; Elbers, R.; Fröhler, M. Catecholamines and their receptors in blood: Evidence for alterations in schizophrenia. *Biol. Psychiatry* **1984**, *19*, 1377–1393.
62. Dreux, C.; Launay, J.M. Blood platelets: Neuronal model in psychiatric disorders. *Encephale* **1985**, *11*, 57–64.
63. Rosati, B.; Mckinnon, D. Regulation of Ion Channel Expression. *Circ. Res.* **2004**, *94*, 874–883. [CrossRef] [PubMed]
64. Sánchez-Florentino, Z.A.; Romero-Martínez, B.S.; Flores-Soto, E.; Serrano, H.; Montaño, L.M.; Valdés-Tovar, M.; Calixto, E.; Aquino-Gálvez, A.; López-Riquelme, G.O.; Alvarado, R.; et al. Potential of olfactory neuroepithelial cells as a model to study schizophrenia: A focus on GPCRs (Review). *Int. J. Mol. Med.* **2024**, *53*, 7. [CrossRef] [PubMed]

International Journal of
Molecular Sciences

MDPI

Review

Could Lower Testosterone in Older Men Explain Higher COVID-19 Morbidity and Mortalities?

Luis M. Montaño [1], Bettina Sommer [2], Héctor Solís-Chagoyán [3], Bianca S. Romero-Martínez [1], Arnoldo Aquino-Gálvez [4], Juan C. Gomez-Verjan [5], Eduardo Calixto [6], Georgina González-Avila [7] and Edgar Flores-Soto [1,*]

1 Departamento de Farmacología, Facultad de Medicina, Universidad Nacional Autónoma de Mexico, Mexico City 04510, Mexico; lmmr@unam.mx (L.M.M.); biancasromero_@hotmail.com (B.S.R.-M.)
2 Laboratorio de Hiperreactividad Bronquial, Instituto Nacional de Enfermedades Respiratorias "Ismael Cosío Villegas", Mexico City 14080, Mexico; bsommerc@hotmail.com
3 Laboratorio de Neurofarmacología, Instituto Nacional de Psiquiatría "Ramón de la Fuente Muñiz", Mexico City 14370, Mexico; hecsolch@imp.edu.mx
4 Laboratorio de Biología Molecular, Instituto Nacional de Enfermedades Respiratorias "Ismael Cosío Villegas", Mexico City 14080, Mexico; aaquino223@gmail.com
5 Dirección de Investigación, Instituto Nacional de Geriatría, Mexico City 10200, Mexico; jverjan@inger.gob.mx
6 Departamento de Neurobiología, Dir. Inv. en Neurociencias, Instituto Nacional de Psiquiatría "Ramón de la Fuente Muñiz", Mexico City 14370, Mexico; ecalixto@imp.edu.mx
7 Laboratorio de Oncología Biomédica, Instituto Nacional de Enfermedades Respiratorias "Ismael Cosío Villegas", Mexico City 14080, Mexico; ggonzalezavila22@gmail.com
* Correspondence: edgarfs@comunidad.unam.mx; Tel.: +52-5556232279

Citation: Montaño, L.M.; Sommer, B.; Solís-Chagoyán, H.; Romero-Martínez, B.S.; Aquino-Gálvez, A.; Gomez-Verjan, J.C.; Calixto, E.; González-Avila, G.; Flores-Soto, E. Could Lower Testosterone in Older Men Explain Higher COVID-19 Morbidity and Mortalities? *Int. J. Mol. Sci.* **2022**, *23*, 935. https://doi.org/10.3390/ijms23020935

Academic Editor: Evgenii Gusev

Received: 17 December 2021
Accepted: 7 January 2022
Published: 15 January 2022

Abstract: The health scourge imposed on humanity by the COVID-19 pandemic seems not to recede. This fact warrants refined and novel ideas analyzing different aspects of the illness. One such aspect is related to the observation that most COVID-19 casualties were older males, a tendency also noticed in the epidemics of SARS-CoV in 2003 and the Middle East respiratory syndrome in 2012. This gender-related difference in the COVID-19 death toll might be directly involved with testosterone (TEST) and its plasmatic concentration in men. TEST has been demonstrated to provide men with anti-inflammatory and immunological advantages. As the plasmatic concentration of this androgen decreases with age, the health benefit it confers also diminishes. Low plasmatic levels of TEST can be determinant in the infection's outcome and might be related to a dysfunctional cell Ca^{2+} homeostasis. Not only does TEST modulate the activity of diverse proteins that regulate cellular calcium concentrations, but these proteins have also been proven to be necessary for the replication of many viruses. Therefore, we discuss herein how TEST regulates different Ca^{2+}-handling proteins in healthy tissues and propose how low TEST concentrations might facilitate the replication of the SARS-CoV-2 virus through the lack of modulation of the mechanisms that regulate intracellular Ca^{2+} concentrations.

Keywords: testosterone; COVID-19; SARS-CoV-2; viral replication; calcium regulation; aging; inflammaging

1. Introduction

Despite the restrictive measures (i.e., isolation, social distancing) and massive vaccination campaigns, the number of people affected by the current COVID-19 pandemic is growing daily. As of 5 January 2022, there have been 295,577,202 confirmed cases of COVID-19, including 5,460,818 deaths, and these numbers are continuously evolving [1]. It is essential to evaluate the current guidelines and strategies in providing safe health services to ensure efficacy in the management of the current pandemic [2]. Global Health 50/50 points out that most data available indicate infection degree is equal for men (49.89%) and women (50.1%) and that no consistent pattern in terms of who is most likely to be diagnosed with COVID-19 exists [3]. This tendency was also reported by the World Health

Organization, which shows that there is little difference in the number of confirmed cases in men (49%) and those in women (51%) [4]; not surprisingly, the Mexican population follows the trend: from the total number of confirmed cases (4,008,648), 50.14% corresponds to females and 49.86% to males. The total number of deaths is 299,711 [1,5]. According to the Center for Systems Science and Engineering (CSSE) at Johns Hopkins University, in January 2022, confirmed cases in America were 105,416, 916 and USA had the highest incidence [1]. Global Health 50/50 reports that in this country male patients between 50 and 64 years of age presented a death toll almost two times higher than in women of the same age (293.26 vs. 170.66 per 100,000, respectively) [3]. Indeed, it has been observed that most COVID-19 fatalities were older males, even in those countries with a higher number of confirmed cases in women. Seemingly, once infected, men are at a higher risk of dying from COVID-19 than women, and this risk directly correlates with age (Figure 1) [3,6,7].

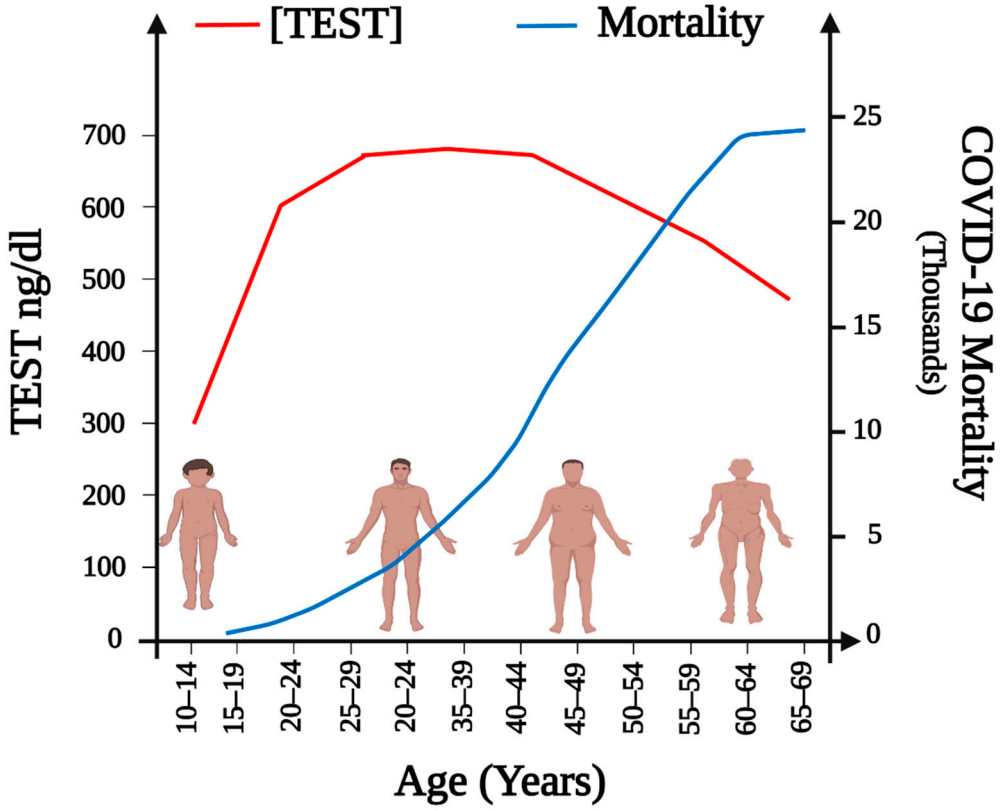

Figure 1. Association of TEST plasmatic concentrations and COVID-19 mortality in Mexican men by age group. Diminished TEST plasmatic concentrations have been associated with higher mortality by age group. In younger men TEST production could be affected during COVID-19 infection and lead to higher mortality. On the figure, the red line represents TEST plasmatic concentrations, and the blue line illustrates COVID-19 mortality in males.

The former fact has been noticed frequently since men with coronavirus infections have shown a lower survival rate than women. In the SARS-CoV epidemics of 2003 and the Middle East respiratory syndrome epidemics of 2012, men had substantially higher fatality rates than women, as in the current COVID-19 pandemic [8]. This gender-related difference in COVID-19 infection susceptibility, severity, and mortality has not been thoroughly explained, although it has been proposed, it might be attributed to genetic, immunological, and hormonal differences. Among these possibilities, the latter seems adequate to explain at least partially the gender-related observations. Furthermore, since the hormone steroid, testosterone (TEST) plasmatic concentrations decrease with aging and the presence of comorbidities (obesity, diabetes mellitus, and cardiovascular diseases) increases during the same period, both circumstances might worsen SARS-CoV-2 patients' prognosis

(Figure 1) [9–12]. Understandably, multiple studies have been carried out trying to predict the outcome of the disease in patients. In SARS-CoV-2 infected men, TEST has been reported to exert immunosuppressive effects [13] and modulate inflammation [14], which may contribute to attenuated antibody response and worsen the prognosis in comparison to women [14]. SARS-CoV-2 viral entry to host cells has been reported to be through the interaction of the viral spike protein (S) and the Angiotensin-Converting Enzyme 2 (ACE2) receptor, facilitated by the Type II Transmembrane Serine Protease (TMPRSS2) priming the S protein [15,16]. Male sex hormones are also believed to increase the expression of the ACE2 receptor, favoring the SARS-CoV-2 viral infectivity [15]. Furthermore, androgens, including TEST, are the only known promoters of the expression of TPMRSS2 through the activation of the androgen receptor (AR) [17,18]. Not only might TEST participate in the physiopathology of SARS-CoV-2, but the virus can interfere in the hormone's production [19–22]. However, when comparing young adult men with elderly patients, when TEST concentrations are progressively decreasing, we observe a greater severity and mortality; therefore, the above mentioned TEST immunosuppressive effects in COVID-19 patients might not be justified.

In this context, we propose that low plasmatic levels of TEST can be determinant in the infection's outcome and the replication of the SARS-CoV-2 virus through the modulation of the mechanisms that regulate intracellular Ca^{2+} concentrations ($[Ca^{2+}]i$) in host cells. In this regard, it has been reported that dysfunctional $[Ca^{2+}]i$ homeostasis mechanisms are necessary for the replication of certain viruses, such as influenza A virus (LVA) [23], Japanese encephalitis virus (JEV), Zika virus (ZIKV), dengue virus (DENV), and West Nile virus (WNV) [23–25]. Meanwhile, it was recently published that the over-activation of the ryanodine receptor (RyR) channel [26] and the voltage-dependent Ca^{2+} channel (VDCC) deregulate $[Ca^{2+}]i$ homeostasis playing an essential role in SARS-CoV-2 infection and cell replication [27]. It is not yet determined whether other cellular mechanisms are affected by SARS-CoV-2 infection and viral spread (Figure 2).

On the other hand, TEST modulates the activity of diverse proteins that regulate calcium homeostasis and its signaling. For instance, it has been reported that, in different systems, it blocks L-type voltage-dependent Ca^{2+} channels (L-VDCC), store-operated Ca^{2+} channels (SOCCs), transient receptor potential (TRP) channels, inositol 1,4,5-triphosphate receptors (IP_3R) and promotes prostaglandin E2 (PGE2) [28–31], contributing to maintaining the basal intracellular Ca^{2+} concentration ($b[Ca^{2+}]i$) and favoring the tissues basal functions (Figure 2) [28–32]. It is important to emphasize that these mechanisms are found in almost all tissues and cells of the body.

In summary, a wide range of evidence from different cell types points out that TEST interacts with various essential regulatory proteins that maintain $[Ca^{2+}]i$ homeostasis. Even though this androgen's physiological role has not been fully elucidated, some evidence hints at its detrimental role in COVID-19 patients warranting further research to understand better the possible effects that TEST could have on the infection and replication of the SARS-CoV-2 virus.

Nevertheless, age is the principal risk factor associated with an increase in severity and mortality in COVID-19 patients [9]. One contributing factor that could explain this matter is "inflammaging", a chronic inflammatory state observed in the elderly [9]. The decline in TEST levels is associated with age and can participate in the regulation of inflammaging in men [9]. Seemingly, TEST declining plasmatic concentrations in the older men could provide essential hints on the role of this androgen in the pathophysiology of COVID-19 patients.

Because of the above-described issues, we propose herein the following points: (1) SARS-CoV-2 replication depends on $[Ca^{2+}]i$ handling proteins; (2) TEST promotes calcium homeostasis at normal plasmatic concentrations; (3) Diminished plasmatic TEST concentrations dysregulate calcium homeostasis; finally, (4) TEST deficiency enhances inflammaging that exacerbates SARS-CoV-2 pathophysiology.

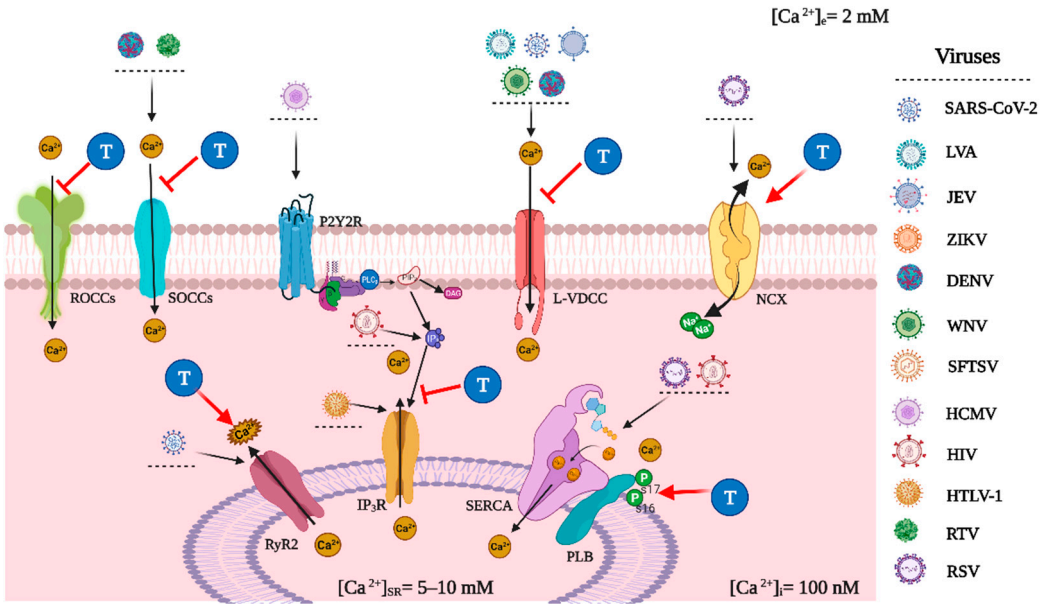

Figure 2. Viral hijacking of Ca^{2+} handling proteins and testosterone modulation. Schematic representation of various stages of the viral cycle targeting the Ca^{2+} apparatus in a host cell. Testosterone (T) can mitigate the dysfunction of Ca^{2+} homeostasis induced by the viral infection through the modulation of the activity and expression of various Ca^{2+} handling proteins. In the plasma membrane, T can acutely inhibit receptor operated calcium channels (ROCCs) in vascular smooth muscle (VSM), T also inhibits store operated calcium channels (SOCCs) acutely in airway smooth muscle (ASM) and VSM. T administered acutely inhibits L-Type voltage operated Ca^{2+} channels (L-VDCCs) in VSM and ASM, and, if chronically given, can downregulate L-VDCCs expression in cardiomyocytes. In these cells, T can upregulate the expression of the Na^+/Ca^{2+} exchanger (NCX). In the sarcoplasmic reticulum (SR), T can block the IP_3 receptor (IP_3R). In cardiomyocytes, chronic exposure to T increases the phosphorylation of phospholamban (PLB) sites s16 and s17, increasing sarcoplasmic reticulum Ca^{2+} ATPase (SERCA) activity, and can also increase the amplitude of Ca^{2+} sparks from the ryanodine receptor (RyR), probably due to an increase in Ca^{2+} content in the SR by the increased SERCA activity. Abbreviations on the figure: LVA, influenza A virus; JEV, Japanese encephalitis virus; ZIKV, Zika virus; DENV, dengue virus; WNV, West Nile virus; SFTSV, thrombocytopenia syndrome virus; HCMV, human cytomegalovirus; HIV, human immunodeficiency virus; HTLV-1, human T-cell lymphotropic virus type 1; RSV, respiratory syncytial virus; RTV, rotavirus; T, testosterone; GPCR, G-protein-coupled receptor; PLC-β, phospholipase C-β; IP_3, inositol1,4,5-trisphosphate; PIP, phosphatidyl inositol phosphate; DAG, diacylglycerol; b[Ca^{2+}]i, basal intracellular Ca^{2+} concentration; [Ca^{2+}]SR, sarcoplasmic reticulum Ca^{2+} concentration; [Ca^{2+}]e, extracellular Ca^{2+} concentration.

2. Calcium Signaling

The calcium ion (Ca^{2+}) is a versatile second messenger in all cell types and regulates multiple signaling processes responsible for essential cell functions. The processes it can regulate are time-dependent: in microseconds, exocytosis is generated, in milliseconds, it initiates contraction, and in minutes or hours, it originates events, such as fertilization, proliferation, transcription, gene regulation, and apoptosis [33,34]. Under resting conditions, cells maintain cytosolic Ca^{2+} concentrations ranging from 100 nM to 150 nM [35]; exquisitely regulated mechanisms maintain the equilibrium between the extracellular milieu (Ca^{2+} concentrations ~2 mM) and intracellular Ca^{2+} stores (Ca^{2+} concentrations ~5–10 mM) [36,37]. The homeostasis in Ca^{2+} signaling is determined by a balance between the proteins that increase Ca^{2+} within the cytoplasm: L-VDCC, SOCCs, receptor-operated Ca^{2+} channels (ROCCs), Na^+/Ca^{2+} exchanger in its reverse form (NCX_{REV}), IP_3 receptor (IP_3R), and ryanodine receptor (RyR) and proteins that decrease concentrations to basal levels: plasma membrane Ca^{2+} ATPase (PMCA), sarcoplasmic reticulum Ca^{2+} ATPase

(SERCA), Na^+/Ca^{2+} exchanger (NCX) and the mitochondrial uniporter [36,38–40] Importantly, alterations in this Ca^{2+}-dependent homeostatic mechanism might participate in various pathophysiological conditions, including viral infections [33].

3. Viral Modifications of Host Cell Calcium Homeostasis

Viruses are intracellular invasive particles that exploit the host cell's machinery to propagate the viral lifecycle; particularly the intracellular Ca^{2+} signaling system is hijacked during viral entry, viral gene replication, virion maturation, and release of various viral species [23,41]. Dysfunctions in the host cell's Ca^{2+} apparatus have been reported during a viral infection, leading to abnormal $[Ca^{2+}]i$ [23].

One of the primary viral targets of the Ca^{2+} apparatus are the VDCCs. Some studies have shown that the $Ca_v1.2$ channel serves as a receptor of the influenza A virus (IAV) and is necessary for its entry into the host cell [23]. This is further supported by the inhibition of IAV infection when VDCC blockers are used, such as verapamil [23,42]. VDCC blockers have also been shown to effectively inhibit the infection of the West Nile virus (NWV) and severe fever with thrombocytopenia syndrome virus (SFTSV) by inhibiting the virus-cell fusion step [23,43,44]. The increase in $[Ca^{2+}]i$ produced by certain viruses through VDCCs has also been demonstrated to be necessary for viral replication, and VDCC blockers have proven to be effective antiviral agents against Japanese encephalitis virus (JEV), ZIKV, DENV, and WNV [23,24,45]. It has been shown that Ca^{2+} binds to the fusion protein (FP) of MERS-CoV and the 2 FP domains on the S protein of SARS-CoV during the entry stage of both virus types [27,46,47], nevertheless, this phenomenon still requires further investigation. The use of VDCC blockers has also been associated with lower mortality and decreased risk for intubation in COVID-19 patients; therefore, Ca^{2+} could also potentially be involved in the viral entry stage (Figure 2) [48].

It was recently published that over-activation of the RyR channel and the associated alteration of $[Ca^{2+}]i$ homeostasis play an essential role in SARS-CoV-2 infection and intracellular replication. The TGF-β signaling pathway over-activation by this virus and reactive oxygen species (ROS) production leads to Ca^{2+} leak from RyR channels in the sarcoplasmic reticulum (SR). This effect is produced through oxidation and protein kinase A (PKA) phosphorylation, uncoupling the regulating protein calstabin (FKBP12.6) from the RyR channel, destabilizing the closed state and favoring an open state [49]. Another mechanism proposed for RyR channel dysfunction during SARS-CoV-2 infection is through cathepsin L13 (a protease expressed in the host cell's plasma membrane); this enzyme has also been shown to participate in the over-activation of RyR channels, promoting a leaky state. The increase in $[Ca^{2+}]i$ also favors cathepsin L13 activity that allows the viral entry through the cleavage and activation of the S protein. The increase in intracellular Ca^{2+} also promotes the release of the virus from the endosome into the host cell [26,50].

Ca^{2+} release from the SR can also be triggered through activation of the IP_3R, and it is a known target for some viruses during the early stages of viral infection to promote replication. The human cytomegalovirus (HCMV) interacts with $P2Y_2$ purinergic receptors to increase the production of IP_3 [51,52], while the human immunodeficiency virus (HIV) upregulates intracellular IP_3 [53] and the human T-cell lymphotropic virus type 1 (HTLV-1) directly activates the IP_3R (Figure 2) [54].

The final stage of the viral lifecycle consists of the extracellular release via exocytosis from the host cell, also called budding; in four hemorrhagic fever viruses, the STIM1/Orai1-mediated Ca^{2+} release is essential for this step [23,47,55]. This was also demonstrated when DENV yield was significantly reduced by SOCCs antagonists [56]. The influx of Ca^{2+} through SOCCs is a particular hallmark of rotavirus infection, and the mechanism for this action has been established to be through the activity of a nonstructural protein 4 (NSP4), a viroporin acting as an ion channel in the SR (Figure 2) [57,58].

In order to maintain proper intracellular Ca^{2+} homeostasis, calcium pumps and exchangers are required to decrease $[Ca^{2+}]i$, namely PMCA, SERCA, and NCX [33]. The disruption of any of these proteins would increase $[Ca^{2+}]i$, a phenomenon that has been

implicated in different stages of the viral cycle [25,59]. The participation of SERCA in the viral genome replication stage was demonstrated through a SERCA inhibitor that showed antiviral activity against respiratory syncytial virus (RSV) strains [60]. In AIDS transgenic mice that express replication-incompetent HIV-1, cardiac dysfunction has been linked to increased SERCA2 expression [61]. On the other hand, rotavirus infection activates NCX in its reverse mode (where one Ca^{2+} enters the cytosol and three Na^{+} ions are expelled) mediated by NSP4 (Figure 2) [62].

Interestingly, studies in structural homology, bioinformatics and metanalyses suggest that Ca^{2+} might participate in SARS-CoV-2 entry into host cells [25]. Furthermore, this is supported by studies showing that VDCC blockers inhibit viral cell entry [26,27]. Although further research is required to understand the extend of Ca^{2+} participation in SARS-CoV-2 pathogenesis, Ca^{2+} handling proteins could be a potential target in treating COVID-19 patients.

As the COVID-19 infection progresses, why men present disproportionately higher infection and mortality rates remain unclear. As of yet, no evidence links directly TEST and this higher susceptibility in men. Because it is well known that TEST physiologically participates in regulating Ca^{2+} handling proteins activity, these effects might help elucidate the paradigm concerning the relationship between TEST and COVID-19 severity and mortality in males. Conceivably, this androgen's plasmatic concentrations might correlate with COVID-19 severity, i.e., lower concentrations worsen the prognosis, particularly in older men.

4. Role of COVID-19 in Testosterone Production

As stated before, SARS-CoV-2 enters the cell through the ACE2-S protein complex; therefore, the targeted cells are those that express ACE2. This protein has been implicated in regulating two testicular functions: steroidogenesis and spermatogenesis and is expressed in four testicular cells: seminiferous duct cells, spermatogonia, Leydig cells, and Sertoli cells [63–66]. The expression of ACE2 seems to be linked with age, having a higher expression in younger men and indicating a high risk for potential infections of the testis in this population [63,65,67]. SARS-CoV-2 in semen samples and testicular biopsies of patients with COVID-19 were investigated. Interestingly, only two studies found the virus in semen [19,68,69], contradicting other reports that did not [20–22,70–74]. Indeed, more studies are needed to further clarify this issue.

Urogenital infections are known risk factors for male infertility, mainly due to the impact of inflammation on reproductive function [63,75,76]. Cytokines are known regulators of male reproduction system health [63,75], and local production in testis has been described [75,77]. Then again, the cytokine storm is a characteristic trait of COVID-19 infection, and, as one of its consequences, increased levels of seminal IL-6, TNF-α, and MCP-1 have been described [78]. COVID-19 can affect the proper testicular function and alter TEST production and male fertility, whether transiently or with more permanent implications. Additionally, fever, a prominent symptom in various infectious diseases including COVID-19, is linked with variations in semen and transient decline in male fertility [79,80]. Either by direct harm to the testicular cells, the SARS-CoV-2 virus entering the testicular cells, or the indirect consequence of the inflammatory response, evidence exists that COVID-19 might compromise male fertility. This illness´ effects on testicular function are observed in spermatogenesis alteration and testosterone production. Sperm quality in COVID-19 patients is altered, with a lower percentage of normal sperm morphology and count, and orchitis has been observed in some COVID-19 patients [20–22,78].

Various studies in COVID-19 male patients report low levels of circulating TEST, with most cases showing a normalization of TEST levels post-infection, although in approximately 50% of them not reaching standard levels during a 7-month follow-up, and up to 10% decreasing even further [20,81,82]. Long-term health implications of COVID-19 infection are still unknown, and male infertility as a possible sequel is investigated, especially with the rising interest in the chronic consequences that COVID-19 might pose. Such is the

case of the emerging "long-haul", a term used to describe the clinical duration of symptoms extending past the acute and post-acute infection, generally lasting around 28 days [83–85].

Severe COVID-19 cases are associated with impaired viral control and higher viral RNA load [86,87]. Interestingly, lower TEST levels have been found to correlate with COVID-19 severity [88], probably related to the fact that TEST could be implicated in viral replication regulation. COVID-19 adverse effects on TEST production will induce a worse infection.

5. Testosterone's Modes of Action at the Cellular Level

TEST binds to membrane-bound or nuclear receptors and triggers genomic (classical) effects that occur after a long period (hours to days). Meanwhile, nongenomic (non-classical) effects occur in a short period (seconds to minutes) and are independent of the androgen receptor (AR) occupancy by the male sex steroids [28,89]. The AR is present in almost all tissues and cell types, including the brain, heart, lung, and immune system cells [28,89,90].

TEST plays essential roles in Ca^{2+} homeostasis in several muscles, i.e., airway, cardiac and vascular. For instance, in airway smooth muscle (ASM), this androgen has benefic effects and seems to participate in the sexual dimorphism observed in many respiratory diseases, such as asthma that shows lower incidence in adult males than in females, as does symptom severity [91,92]. Some studies also point out that a single high dose of exogenous TEST induces significant bronchodilation [93], the therapeutic potential of this androgen that deserves further investigation.

In ASM, TEST tissular effects are related to the regulation of intracellular Ca^{2+} levels. We recently found that in this tissue, TEST inhibits L-VDCC and SOCCs [28–30]. Additionally, at physiological concentrations (nM, nmol/L), TEST induced a decrease in $[Ca^{2+}]i$ through the phospholipase C-β/inositol 1,4,5-trisphosphate (PLC_β/IP_3) signaling pathway, by blocking the IP_3R [31]. Also, in guinea pig ASM, TEST diminishes tone and $[Ca^{2+}]i$. These effects seem to occur by blocking L-VDCC and a constitutively active TRPC3 channel, and probably by PGE2 biosynthesis [28–31]. These mechanisms also favor ASM basal tone by keeping basal intracellular Ca^{2+} concentration ($b[Ca^{2+}]i$) in unstimulated tissues and by inducing relaxation in tissues pre-contracted with carbachol (CCh) or antigenic challenge (Figure 2) [93].

Additionally, we found that ASM chronic exposure to nanomolar concentrations of TEST induces β_2 adrenergic receptor expression, hence improving the salbutamol-induced relaxation [94]. This finding was further characterized by patch clamp studies that showed increases in the salbutamol-induced K^+ currents (IK^+); this rise was abolished when protein synthesis or transcription inhibitors were used during the TEST chronic exposure [94]. The increase in IK^+ induces ASM hyperpolarization diminishing the Ca^{2+} entry through voltage dependent channels, and therefore, contributing to keeping lower $[Ca^{2+}]i$.

Many studies have established TEST´s paramount role in immunity and inflammation. Hence, it has been demonstrated that TEST negatively regulates type 2 inflammation and the expression of IL-17A [95,96]. Furthermore, in human ASM, androgens diminish the intracellular Ca^{2+} increment induced by pro-inflammatory cytokines, such as tumor necrosis factor alpha (TNF-α) or interleukin-13 (IL-13) by a genomic effect [97]. All these effects diminish airway hyperresponsiveness and favor a milder asthmatic phenotype. Even though ACE2 expression in human ASM was just recently defined [98] and the entry of SARS-CoV-2 through its association has not been demonstrated yet, it is reasonable to propose that the above-described mechanisms could also be relevant in the SARS-CoV-2 infected males (Figure 3).

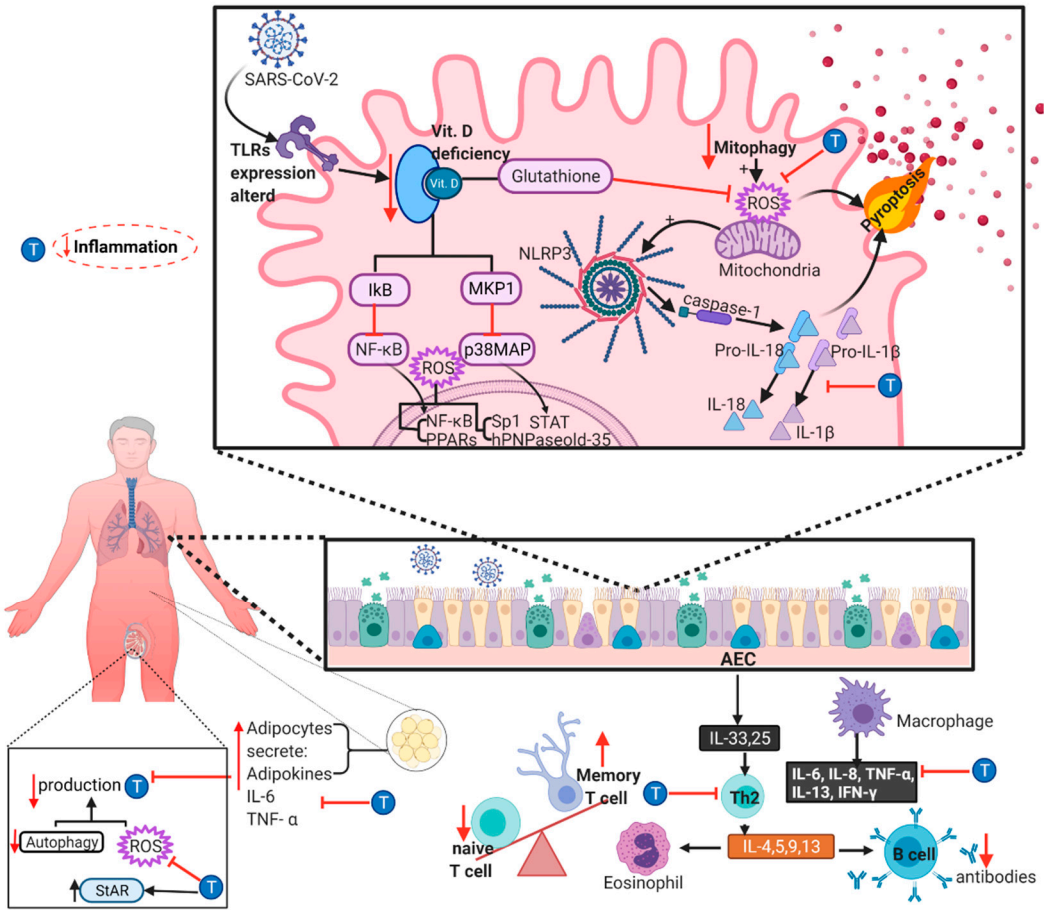

Figure 3. Testosterone mitigates the detrimental effects of inflammaging in COVID-19. Schematic representation of late-onset hypogonadism (LOH) produced by inflammaging markers, reverted with testosterone (T) supplementation, and increasing the steroidogenic acute regulatory protein (StAR) expression leading to T production. Inflammaging is characterized by alterations in autophagy and mitophagy activity, increased reactive oxygen species (ROS) production, cellular senescence, alteration of the expression of toll-like receptors (TLRs) and decrease in the concentration of vitamin D. The higher levels of ROS activate NLRP3, activating IL-1β and IL-18 production and pyroptosis, a mechanism that the StAR could block by inducing T production. ROS also activate the transcription factors hPNPaseold-35, NF-κB, AP-1, Sp1 and PPARs. The senescent adipocytes increase the secretion of adipokines and cytokines, such as IL-6 and TNF-α, that can also be inhibited by T. Immunosenescence can present alteration of the ratio of CD4+/CD8+ T cells, decrease immature T cells, increase memory T cells, alter Th2 response, and modify the production of pro-inflammatory cytokines. Abbreviations on the figure: T, testosterone; hPNPaseold-35, human polynucleotide phosphorylase; AP-1, activator protein 1; Sp1, specification protein 1; PPARs, peroxisomal proliferator-activated receptors; NLRP3, NOD-like receptor 3; Vit. D, vitamin D; ROS, reactive oxygen species; AEC, airway epithelial cells; StAR, steroidogenic acute regulatory protein.

The role of sex hormones has been extensively studied in physiological and pathological settings. Low levels of circulating TEST are associated with an increased cardiovascular risk by leading to an increase in inflammation, impaired metabolism, and mitochondrial dysfunction [99,100].

In male rodents, gonadectomy (GDX) reduced the expression of L-VDCC in the heart [101–103], and chronic exposure to dihydrotestosterone (DHT) increased the expression of $Ca_V1.2$ and peak $I_{Ca\text{-}L}$ (L-type Ca^{2+} current) in human ventricular myocytes [103,104]. The NCX protein has also been explored, though the evidence is contradictory. Some studies report that after 2–10 weeks of GDX the expression and activity of NCX were

unchanged [103,105–107]. In other works, there is evidence that after 2 or 16 weeks of GDX, a decrease in levels of mRNA of NCX occurs and that it could be reversed with supplementation of TEST [101–103]. At the moment, the effects of TEST in the regulation of NCX in cardiomyocytes are still unclear and require further investigation (Figure 2).

The administration of TEST at supraphysiological levels for two weeks appears to have a protective effect against myocardial ischemia-reperfusion injury, demonstrating an improvement in functional recovery compared to GDX and placebo groups [105]. The effect was partly attributed to the impact of TEST on $[Ca^{2+}]i$, reducing the end-ischemic $[Ca^{2+}]i$ and having a decreased $[Ca^{2+}]i$ overload in the postischemic period [105]. Worth mentioning is the $[Ca^{2+}]i$ homeostasis in contractile failure, the possibility of developing arrhythmias, and myocyte injury [105,108]. Although the protective effect of TEST in reperfusion injury is evident and is associated with $[Ca^{2+}]i$ handling, the effect cannot be attributed to a difference in protein expression of phospholamban (PLB), the NCX, RyR2, or SERCA2a. Yet, the possibility of changes in phosphorylation in any of these proteins remains [105–109]. Similarly, in another study, TEST did not alter protein expression of SERCA, its modulating components sarcolipin and heat shock protein 20 or NCX. However, in GDX rats, the phosphorylated Thr17 and Ser16 forms of PLB were significantly decreased, modulating SERCA activity [103,110,111]. Even though GDX does not modify the levels of expression of RyR, RyR-mediated Ca^{2+} release is decreased after GDX [103–106], with chronic testosterone exposure (24–30 h) increasing the amplitude of Ca^{2+} sparks [103,104]. The increase in SR Ca^{2+} release from individual Ca^{2+} sparks could be caused by an increase in SR Ca^{2+} content with exposure to TEST [103–106]; this increase in Ca^{2+} content is attributed to phosphorylation of PLB (Figure 2) [103,110,111].

COVID-19 patients appear to have cardiac dysfunction, leading to cardiac injury, with several studies demonstrating it through cardiac marker elevation and electrocardiogram (ECG) changes [112–115]. The incidence of cardiac injury is reported to be between 7.2% and 28%, but in severe and critical care patients, the incidence can be between 22% and 44% [112–118]. Arrhythmias can be a common symptom in COVID-19 patients, requiring close monitoring since they indicate myocardial injury associated with an unfavorable outcome. The incidence of arrhythmias has been reported to be between 17% and 24%, linked with intensive care unit (ICU) admission and death, exacerbating previously known cardiac comorbidities and unfortunately developing in patients without prior history of heart disease [112,115,119,120].

Cardiac arrhythmias could be caused by various factors present in COVID-19 patients, such as hypoxia, pro-inflammatory cytokines, direct myocardial injury, fever, electrolyte imbalances, plaque rupture, hypercoagulability, or many of the medications used to treat COVID-19 patients [115,121]. Concerning the induction of cardiac injury, SARS-CoV-2 has been shown to directly infect cardiomyocytes through internalization of the virus when the viral S protein binds to ACE2, aided by the TPMRSS2 [115,122,123]. Fever, a symptom often present in COVID-19 patients, has also been shown to trigger ventricular arrhythmias, especially in patients with underlying cardiomyopathies [115,124–126]. Specifically, pro-inflammatory cytokines can promote an arrhythmogenic state. In COVID-19 patients, some cytokine concentrations are elevated, such as IL-6, IL-1β, IL-2, IL-8, IL-17, G-CSF, GM-CSF, IP10, MCP1, CCL3 and TNF-α; all could lead to the generation of arrhythmias [113,115,127–129]. The acute administration of IL-6 increases L-type Ca^{2+} currents (I_{CaL}) in ventricular cardiomyocytes [115,130], and in chronic exposure, IL-6 has significantly down-regulated the expression of SERCA2 in ventricular myocytes [115,131]. Additionally, TNF-α reduces I_{CaL} and the expression of SERCA2a by increasing DNA methyltransferase levels, thus enhancing the methylation of its promoter region [115,126,132]. Furthermore, IL-1β has been shown to promote Ca^{2+} spark frequency [115,133]. Although the extent to which TEST plays a role in cardiomyocyte injury during SARS-CoV-2 infections remains uncertain, there exists evidence suggesting it could have a protective role and warrants further investigation.

Studies have demonstrated that TEST affects the cardiovascular system in health and disease. TEST may serve different functions in normal physiological conditions compared with pathophysiological states [134]. TEST concentrations in men remain relatively constant through the reproductive lifetime, in the range of 6–50 nM, and can influence the cardiovascular system functions, regulating vascular resistance, cardiac electrophysiology, and cardiac output, and TEST deficiency may contribute to developing hypertension [135–138]. Several epidemiological studies have shown an association of low testosterone with cardiovascular disease and conditions, such as metabolic syndrome and type 2 diabetes, which have increased cardiovascular risk [139,140].

It has been reported that TEST exhibits vasodilatory actions, both through acute and chronic mechanisms, and this effect can be observed in different species, including humans, and be reproduced in many vasculature types, i.e., thoracic, coronary, mesenteric, pulmonary, mammary, radial, and umbilical arteries [141–156].

Many of the mechanisms responsible for producing vasodilation have been deciphered and will be addressed below. One of the best-described mechanisms is acute TEST inhibition of the VDCCs. This effect can be obtained in various models, including rat aorta [157–160], porcine and rat coronary arteries [147,161,162], rat pulmonary artery [148,151], canine basilary artery [163], human umbilical artery (HUA) [164], and small porcine arteries [165], and can even potentiate the effect of nifedipine [166]. Moreover, TEST can regulate other Ca^{2+} handling proteins that participate in the vasodilatory effect, including the inhibition of ROCCs, which can be observed in rat aorta [157], porcine arteries [164,165], and HUA [164]. Similarly, SOCCs inhibition is observed in rat coronary, pulmonary and aorta arteries (Figure 2) [147,162].

In COVID-19, hypertension has been described as a morbidity risk factor and poor outcome [167]. As an essential vasodilator, TEST can mitigate the risk of hypertension, and its deficiency is linked to increased cardiovascular risk [140]. Moreover, ACE2 inhibitors and ARB (Angiotensin II receptor blocker) administration, two of the primary drug groups used in the treatment of hypertension, have shown to increase the expression of ACE2 [168–170]. This overexpression of ACE2 can increase the risk for potential infection by SARS-CoV-2. Therefore, TEST can indirectly mitigate the impact of COVID-19 by decreasing the cardiovascular risk or by lessening the necessity for ACE2 inhibitors or ARBs. The extent of hypertension's impact on the pathophysiology of COVID-19 is undoubtedly complex and possibly related to underlying comorbidities; this interesting fact remains a guideline for future studies.

In summary, the modulatory effects that physiological concentrations of TEST excerpt on the Ca^{2+} handling mechanisms that participate in the viral lifecycle could lessen the potential infection of SARS-CoV-2. Contrastingly, TEST deficiency has been shown to worsen comorbidities that pose a risk for COVID-19 severity and outcome, including those in the respiratory and cardiovascular systems. TEST plasmatic concentrations decrease with age, and therefore, might constitute a dominant risk factor observed to impact COVID-19 severity and mortality [168,169]. Besides, one of the primary hallmarks of aging is the so-called inflammaging, which also augments the risk of acquiring COVID-19.

6. Role of Inflammaging in the Pathogenesis of COVID

Young adults with COVID-19 and a favorable natural course of the disease, present a balance between the ratio of pro-inflammatory and anti-inflammatory cytokines, capable of modulating immune activity and reducing the response at the indicated time. A dysregulation of the immune response, as the chronic state of inflammation known as "inflammaging" in elderly patients, may contribute to the pathophysiology of SARS-CoV-2 [171,172]. Inflammaging has been associated with various pathologies, such as insulin resistance, type 2 diabetes mellitus, cardiovascular disease, Alzheimer's disease, and cancer [171,172]. Old age is characterized by this chronic state of inflammaging, in which a systemic increase in IL-6, IL-8, TNF-α, IL-13, IFN-γ, and acute phase proteins has been detected, and includes a series of systemic alterations, especially of the immune system. The sum of these factors

could favor viral infections as a result of alterations in autophagy and mitophagy activity, increased ROS production, cellular senescence that contributes to the pro-inflammatory profile related to aging, senescence of immune system cells, alteration of the expression of TLRs (toll-like receptors) and decrease in the concentration of vitamin D (Figure 3) [171,172].

Aging is associated with an increase in ROS production, which promotes the pro-inflammatory state through the synthesis of cytokines and the activation of transcription factors including human polynucleotide phosphorylase (hPNPaseold-35), NF-κB, activator protein 1 (AP-1), specificity protein 1 (Sp1), and peroxisomal proliferator-activated receptors (PPARs) [171]. One of the processes responsible for mitigating ROS production is mitochondrial autophagy, known as mitophagy. Autophagy is a catabolic exchange pathway in which dysfunctional or damaged cellular material is degraded; an alteration or decrease in this pathway has been associated with various pathologies characteristic of aging. When autophagic activity declines, it leads to an increase in ROS production. The lower autophagic activity and the enhanced ROS production lead to the activation of NOD-like receptors (NLR), especially NLRP3. As products of the activation of the NLRP3 receptor, the cytokines IL-1β and IL-18 also activate pyroptosis, a form of programmed cell death in which they release their pro-inflammatory cytosolic content to the extracellular space. There is an increase in the proportion of senescent cells in old age, these are characterized by having decreased cell viability and being more susceptible to cellular damage by ROS, and they can also produce cytokines, such as IL-1α, IL-1β, IL-6, IL-8, IL-18, CCL-2, TNF-α, GM-CSF, growth-regulated oncogene (GRO), MCP-2, MCP-3, MMP-1 and MMP-3 [171]. Above all, senescent adipocytes play an essential role in inflammaging. In old age, a redistribution of adipose tissue can be observed, with a decrement in subcutaneous regions and increases in the visceral areas; this could also be altered in age-related diseases, such as sarcopenia. This redistribution is associated with a dysfunction of adipose tissue, an increase in the production of adipokines and cytokines (especially IL-6 and TNF-α), metabolic dysfunction, and predisposes subjects to increased morbidity and mortality from several causes (Figure 3) [173].

Furthermore, immunosenescence also contributes to increasing the progressive loss of all immune effectors in both the innate and cellular immune systems [171,172]. An augmented activation and maturation of dendritic cells (DCs) by cytokines has been reported in this context. It has been described that the T cell population also undergoes essential changes that do not include decreases in cellular counts. There is a poor T cell mitogenic response, an alteration in the CD4+/CD8+ T cells ratio, a reduction of immature T cells, an increase in memory T cells, and the Th17/Treg cells ratio [171]. Macrophages show lower production of specific factors, for instance, fibroblast growth factor, vascular endothelial growth factor, epithelial growth factor, TGFß, toxic free radicals, and nitric oxide synthase expression, and a decrease in phagocytic and chemotactic activity. Lower production of antibodies and their protective effectiveness have been observed within the alterations in the B cell population, corresponding with the mitigated response of specific antigen antibodies, observed in old mice [171]. The changes observed by immunosenescence in older adults produce a chronic inflammatory profile, causing higher age-related morbidity and mortality in COVID -19 (Figure 3) [171,172].

Old age is also accompanied by vitamin D deficiency associated with several chronic degenerative diseases. The non-classical activities of this vitamin are related to immunoregulatory effects. In conjunction with its vitamin D receptor (VDR), it increases macrophages´ autophagic activity and the generation of antimicrobial products and favors a decrease in the expression of pro-inflammatory cytokine genes. These genes are silenced by higher glutathione levels, lowering ROS and suppressing the expression of NF-κB and p38 MAP kinase. Conceivably, elderly patients faced with SARS-CoV-2 infection would be unable to efficiently modulate the inflammatory response, most probably presenting an exacerbated response and severe tissue damage (Figure 3) [171].

A steady decline in TEST plasmatic concentration is associated with age, typically referred to as andropause, and is currently considered late-onset hypogonadism (LOH) [174].

This lowering of TEST plasmatic levels can have clinical repercussions and has been observed to decrease bone mineral density and lean body mass and increase the risk of metabolic syndrome and cardiovascular diseases [11,174,175]. The higher ROS production observed in inflammaging could also contribute to TEST deficiency, since high levels of ROS have been shown to disrupt the male reproductive hormonal profile: directly through oxidative stress and indirectly by acting on the hypothalamic axes of hormone release, decreasing luteinizing hormone (LH) secretion [176–179]. The treatment with TEST could be beneficial in hypogonadism, particularly in LOH, protecting against the effects of ROS on TEST production. The treatment with low doses of TEST has demonstrated a diminished ROS production in Leydig cells, preventing oxidative damage and upregulating the expression of the steroidogenic acute regulatory protein (StAR), which acts as the limiting-step enzyme in steroidogenesis, resulting in higher TEST synthesis and secretion (Figure 3) [180].

Similarly, TEST replacement therapy attenuated cognitive decline in rats by decreasing oxidative stress damage [181]. TEST production in Leydig cells depends on autophagy; another characteristic of inflammaging is altered autophagy, and disruption, especially in this site with high activity, and could lead to LOH [182]. Additionally, the senescent adipocytes observed in inflammaging can contribute to male infertility. Adipose tissue-mediated inflammation and oxidative stress in obese men can negatively impact TEST production and sperm quality, promoting LOH (Figure 3) [183,184].

Another aspect that has gained interest is the synchronicity between the decline of TEST plasmatic concentration and the development of a pro-inflammatory state [100]. In male diabetic patients, low levels of TEST are associated with a pro-inflammatory condition characterized by high TNF-α concentrations, an impaired metabolic profile, and mitochondrial dysfunction, leading to an increase in cardiovascular risk [99]. TEST deficiency has also been shown to increase IL-6 production in the bone marrow of young mice [9,185]. Inversely, TEST supplementation treatment could prove beneficial in reversing some of the detrimental immunological effects related to age, such as immunosenescence. TEST treatment can decrease the production of IL-6 and other pro-inflammatory cytokines in vitro and in vivo [9,186]. TEST treatment in men with hypogonadism significantly reduced the production of TNF-α and IL-1β and incremented the production of IL-10 (Figure 3) [9,187].

Similarly, in rat autoimmune orchitis, TEST treatment decreased CD4+ T cells, increased Treg cells, and decreased Th1 cytokine production (IFN-γ and IL-2) and other pro-inflammatory cytokines (MCP-1, TNF-α, IL-6) [9,188]. Moreover, the alterations in Th2 response related to aging could benefit from TEST modulation. TEST, through the AR activation, has been shown to suppress Th2-mediated inflammation indirectly by suppressing IL-4 production induced by allergen exposure in mice models [96]. Therefore, LOH could reasonably exacerbate the repercussions that inflammaging could have in the pathogenesis of COVID-19, and it would be interesting to investigate if TEST administration could be beneficial in older men suffering this illness (Figure 3).

At this point, it is important to distinguish between the chronological age (age measured in years from the date you are born to the present) and the biological age (age referred to different physiological and molecular processes, usually measured with distinct biological biomarkers, such as DNA methylation). This distinction may help us to better understand why the COVID-19 pandemic showed to be more lethal on subjects with several comorbidities, such as obesity, diabetes, or hypertension, most of which have shown an acceleration of age (residuals between chronological age estimation and biological age) [189–191].

In this sense, several studies have pointed out that biological age is strongly associated with the severity of the disease rather than with the calendar age. Moreover, in a recent article by Chiang-Ling et al., phenotypic age (PhenoAge) measured with several biomarkers and a machine-learning model [192], showed to be associated with severity of COVID-19 when data from the UK Biobank were combined with COVID-19 diagnoses of the UK National Health Service [193]. In this sense, a recent article reported that men

have accelerated biological aging during quarantine. Interestingly, this study found that biopsychological age might determine the risk to develop severe COVID-19 [194].

7. Conclusions

The higher severity and mortality observed in male COVID-19 patients could be linked to lower TEST protective effects. Illness severity has been associated with TEST deficiency, especially in elder patients. TEST might be modulating SARS-CoV-2 pathophysiology directly (regulating the viral life cycle) and indirectly (mitigating the exaggerated immunological response). The viral hijacking of the Ca^{2+} handling proteins might be a potential target for pharmacological treatment, and the modulatory actions of TEST over these mechanisms could prevent their viral-induced dysfunction. Further research on how low TEST plasmatic concentrations in elderly patients worsen SARS-CoV-2 symptoms is clearly needed.

Funding: This study was partly supported by grants from the Dirección General de Asuntos del Personal Académico (DGAPA), the Universidad Nacional Autónoma de México (IN204319, IN200522), and CONACYT (137725) to LM Montaño.

Acknowledgments: Bianca S. Romero-Martínez is grateful to the Programa de Doctorado en Ciencias Biomédicas, Universidad Nacional Autónoma de México, for the instruction received during her Ph.D. degree studies. She received a fellowship from the Consejo Nacional de Ciencia y Tecno-logía, México (application # 2020-000013-01NACF-12778; CVU 469822).

Conflicts of Interest: The authors declare no conflict of interest.

References

1. Dong, E.; Du, H.; Gardner, L. An interactive web-based dashboard to track COVID-19 in real time. *Lancet Infect. Dis.* **2020**, *20*, 533–534. [CrossRef]
2. Bordea, I.R.; Candrea, S.; Sălăgean, T.; Pop, I.D.; Lucaciu, O.; Ilea, A.; Manole, M.; Băbțan, A.M.; Sirbu, A.; Hanna, R. Impact of COVID-19 Pandemic on Healthcare Professionals and Oral Care Operational Services: A Systemic Review. *Risk Manag. Healthc. Policy* **2021**, *14*, 453–463. [CrossRef]
3. The Sex, Gender and Covid-19 Project. Available online: https://globalhealth5050.org/the-sex-gender-and-covid-19-project/about-us/ (accessed on 4 November 2021).
4. World Health Organization (WHO). Weekly Epidemiological Update on COVID-19—26 October 2021. Available online: https://www.who.int/publications/m/item/weekly-epidemiological-update-on-covid-19---26-october-2021 (accessed on 9 November 2021).
5. México, G.D. Covid-19 México. Available online: Datos.covid-19.conacyt.mx (accessed on 9 November 2021).
6. Wu, Z.; Mcgoogan, J.M. Characteristics of and Important Lessons From the Coronavirus Disease 2019 (COVID-19) Outbreak in China. *JAMA* **2020**, *323*, 1239. [CrossRef]
7. Richardson, S.; Hirsch, J.S.; Narasimhan, M.; Crawford, J.M.; Mcginn, T.; Davidson, K.W.; Barnaby, D.P.; Becker, L.B.; Chelico, J.D.; Cohen, S.L.; et al. Presenting Characteristics, Comorbidities, and Outcomes Among 5700 Patients Hospitalized With COVID-19 in the New York City Area. *JAMA* **2020**, *323*, 2052. [CrossRef] [PubMed]
8. Karlberg, J. Do Men Have a Higher Case Fatality Rate of Severe Acute Respiratory Syndrome than Women Do? *Am. J. Epidemiol.* **2004**, *159*, 229–231. [CrossRef]
9. Gomez, C.R.; Nomellini, V.; Kovacs, E.J. Sex Hormones and Immunosenescence. In *Handbook of Immunosenescence*; Springer: Cham, Switzerland, 2019. [CrossRef]
10. Vermeulen, A.; Verdonck, L.; Kaufman, J.M. A Critical Evaluation of Simple Methods for the Estimation of Free Testosterone in Serum. *J. Clin. Endocrinol. Metab.* **1999**, *84*, 3666–3672. [CrossRef] [PubMed]
11. Williamson, E.J.; Walker, A.J.; Bhaskaran, K.; Bacon, S.; Bates, C.; Morton, C.E.; Curtis, H.J.; Mehrkar, A.; Evans, D.; Inglesby, P.; et al. Factors associated with COVID-19-related death using OpenSAFELY. *Nature* **2020**, *584*, 430–436. [CrossRef] [PubMed]
12. Zhang, Y.; Wang, M.; Zhang, X.; Liu, T.; Libby, P.; Shi, G.P. COVID-19, the Pandemic of the Century and Its Impact on Cardiovascular Diseases. *Cardiol. Discov.* **2021**, *1*, 233–258. [CrossRef]
13. Foo, Y.Z.; Nakagawa, S.; Rhodes, G.; Simmons, L.W. The effects of sex hormones on immune function: A meta-analysis. *Biol. Rev.* **2017**, *92*, 551–571. [CrossRef]
14. Patil, A.; Tripathy, J.P.; Deshmukh, V.; Sontakke, B.; Tripathi, S.C. SeXX and COVID-19: Tussle between the two. *Monaldi Arch. Chest Dis.* **2020**, *90*, 2020060159. [CrossRef]
15. Asselta, R.; Paraboschi, E.M.; Mantovani, A.; Duga, S. ACE2 and TMPRSS2 variants and expression as candidates to sex and country differences in COVID-19 severity in Italy. *Aging* **2020**, *12*, 10087–10098. [CrossRef]

16. Bordea, I.R.; Xhajanka, E.; Candrea, S.; Bran, S.; Onișor, F.; Inchingolo, A.D.; Malcangi, G.; Pham, V.H.; Inchingolo, A.M.; Scarano, A.; et al. Coronavirus (SARS-CoV-2) Pandemic: Future Challenges for Dental Practitioners. *Microorganisms* **2020**, *8*, 1704. [CrossRef]
17. Hoffmann, M.; Kleine-Weber, H.; Schroeder, S.; Krüger, N.; Herrler, T.; Erichsen, S.; Schiergens, T.S.; Herrler, G.; Wu, N.-H.; Nitsche, A.; et al. SARS-CoV-2 Cell Entry Depends on ACE2 and TMPRSS2 and Is Blocked by a Clinically Proven Protease Inhibitor. *Cell* **2020**, *181*, 271–280.e8. [CrossRef]
18. Dalpiaz, P.L.M.; Lamas, A.Z.; Caliman, I.F.; Ribeiro, R.F.; Abreu, G.R.; Moyses, M.R.; Andrade, T.U.; Gouvea, S.A.; Alves, M.F.; Carmona, A.K.; et al. Sex Hormones Promote Opposite Effects on ACE and ACE2 Activity, Hypertrophy and Cardiac Contractility in Spontaneously Hypertensive Rats. *PLoS ONE* **2015**, *10*, e0127515. [CrossRef]
19. Li, D.; Jin, M.; Bao, P.; Zhao, W.; Zhang, S. Clinical Characteristics and Results of Semen Tests Among Men With Coronavirus Disease 2019. *JAMA Netw. Open* **2020**, *3*, e208292. [CrossRef]
20. Temiz, M.Z.; Dincer, M.M.; Hacibey, I.; Yazar, R.O.; Celik, C.; Kucuk, S.H.; Alkurt, G.; Doganay, L.; Yuruk, E.; Muslumanoglu, A.Y. Investigation of SARS-CoV-2 in semen samples and the effects of COVID-19 on male sexual health by using semen analysis and serum male hormone profile: A cross-sectional, pilot study. *Andrologia* **2021**, *53*, e13912. [CrossRef]
21. Holtmann, N.; Edimiris, P.; Andree, M.; Doehmen, C.; Baston-Buest, D.; Adams, O.; Kruessel, J.-S.; Bielfeld, A.P. Assessment of SARS-CoV-2 in human semen—A cohort study. *Fertil. Steril.* **2020**, *114*, 233–238. [CrossRef] [PubMed]
22. Yang, M.; Chen, S.; Huang, B.; Zhong, J.-M.; Su, H.; Chen, Y.-J.; Cao, Q.; Ma, L.; He, J.; Li, X.-F.; et al. Pathological Findings in the Testes of COVID-19 Patients: Clinical Implications. *Eur. Urol. Focus* **2020**, *6*, 1124–1129. [CrossRef]
23. Chen, X.; Cao, R.; Zhong, W. Host Calcium Channels and Pumps in Viral Infections. *Cells* **2019**, *9*, 94. [CrossRef] [PubMed]
24. Wang, S.; Liu, Y.; Guo, J.; Wang, P.; Zhang, L.; Xiao, G.; Wang, W. Screening of FDA-Approved Drugs for Inhibitors of Japanese Encephalitis Virus Infection. *J. Virol.* **2017**, *91*, e01055-17. [CrossRef] [PubMed]
25. Saurav, S.; Tanwar, J.; Ahuja, K.; Motiani, R.K. Dysregulation of host cell calcium signaling during viral infections: Emerging paradigm with high clinical relevance. *Mol. Asp. Med.* **2021**, *81*, 101004. [CrossRef]
26. Jiang, B.; Liang, S.; Liang, G.; Wei, H. Could dantrolene be explored as a repurposed drug to treat COVID-19 patients by restoring intracellular calcium homeostasis? *Eur. Rev. Med. Pharmacol. Sci.* **2020**, *24*, 10228–10238. [CrossRef]
27. Straus, M.R.; Bidon, M.K.; Tang, T.; Jaimes, J.A.; Whittaker, G.R.; Daniel, S. Inhibitors of L-Type Calcium Channels Show Therapeutic Potential for Treating SARS-CoV-2 Infections by Preventing Virus Entry and Spread. *ACS Infect. Dis.* **2021**, *7*, 2807–2815. [CrossRef]
28. Montaño, L.M.; Flores-Soto, E.; Sommer, B.; Solís-Chagoyán, H.; Perusquía, M. Androgens are effective bronchodilators with anti-inflammatory properties: A potential alternative for asthma therapy. *Steroids* **2020**, *153*, 108509. [CrossRef]
29. Flores-Soto, E.; Reyes-García, J.; Carbajal-García, A.; Campuzano-González, E.; Perusquía, M.; Sommer, B.; Montaño, L.M. Sex steroids effects on guinea pig airway smooth muscle tone and intracellular Ca^{2+} basal levels. *Mol. Cell. Endocrinol.* **2017**, *439*, 444–456. [CrossRef] [PubMed]
30. Perusquía, M.; Flores-Soto, E.; Sommer, B.; Campuzano-González, E.; Martínez-Villa, I.; Martínez-Banderas, A.I.; Montaño, L.M. Testosterone-induced relaxation involves L-type and store-operated Ca^{2+} channels blockade, and PGE2 in guinea pig airway smooth muscle. *Pflügers Arch.-Eur. J. Physiol.* **2015**, *467*, 767–777. [CrossRef] [PubMed]
31. Montaño, L.M.; Flores-Soto, E.; Reyes-García, J.; Díaz-Hernández, V.; Carbajal-García, A.; Campuzano-González, E.; Ramírez-Salinas, G.L.; Velasco-Velázquez, M.A.; Sommer, B. Testosterone induces hyporesponsiveness by interfering with IP3 receptors in guinea pig airway smooth muscle. *Mol. Cell. Endocrinol.* **2018**, *473*, 17–30. [CrossRef]
32. Flores-Soto, E.; Reyes-García, J.; Sommer, B.; Montaño, L.M. Sarcoplasmic reticulum Ca^{2+} refilling is determined by L-type Ca^{2+} and store operated Ca^{2+} channels in guinea pig airway smooth muscle. *Eur. J. Pharmacol.* **2013**, *721*, 21–28. [CrossRef] [PubMed]
33. Berridge, M.J.; Bootman, M.D.; Roderick, H.L. Calcium signalling: Dynamics, homeostasis and remodelling. *Nat. Rev. Mol. Cell Biol.* **2003**, *4*, 517–529. [CrossRef]
34. Bootman, M.D.; Lipp, P.; Berridge, M.J. The organisation and functions of local Ca^{2+} signals. *J. Cell Sci.* **2001**, *114*, 2213–2222. [CrossRef]
35. Reyes-García, J.; Flores-Soto, E.; Carbajal-García, A.; Sommer, B.; Montaño, L.M. Maintenance of intracellular Ca^{2+} basal concentration in airway smooth muscle (Review). *Int. J. Mol. Med.* **2018**, *42*, 2998–3008. [CrossRef]
36. Bazán-Perkins, B.; Flores-Soto, E.; Barajas-López, C.; Montaño, L.M. Role of sarcoplasmic reticulum Ca^{2+} content in Ca^{2+} entry of bovine airway smooth muscle cells. *Naunyn-Schmiedeberg's Arch. Pharmacol.* **2003**, *368*, 277–283. [CrossRef]
37. Clapham, D.E. Calcium Signaling. *Cell* **2007**, *131*, 1047–1058. [CrossRef]
38. Janssen, L.J.; Walters, D.K.; Wattie, J. Regulation of $[Ca^{2+}]i$ in canine airway smooth muscle by Ca^{2+}-ATPase and Na^{+}/Ca^{2+} exchange mechanisms. *Am. J. Physiol.* **1997**, *273*, L322–L330. [CrossRef]
39. Floyd, R.; Wray, S. Calcium transporters and signalling in smooth muscles. *Cell Calcium* **2007**, *42*, 467–476. [CrossRef]
40. Philipson, K.D.; Nicoll, D.A. Sodium-Calcium Exchange: A Molecular Perspective. *Annu. Rev. Physiol.* **2000**, *62*, 111–133. [CrossRef] [PubMed]
41. Clark, B.K.; Eisenstein, M.E. Targeting Host Store-Operated Ca^{2+} Release to Attenuate Viral Infections. *Curr. Top. Med. Chem.* **2013**, *13*, 1916–1932. [CrossRef] [PubMed]
42. Fujioka, Y.; Tsuda, M.; Nanbo, A.; Hattori, T.; Sasaki, J.; Sasaki, T.; Miyazaki, T.; Ohba, Y. A Ca^{2+}-dependent signalling circuit regulates influenza A virus internalization and infection. *Nat. Commun.* **2013**, *4*, 2763. [CrossRef]

43. Li, H.; Zhang, L.-K.; Li, S.-F.; Zhang, S.-F.; Wan, W.-W.; Zhang, Y.-L.; Xin, Q.-L.; Dai, K.; Hu, Y.-Y.; Wang, Z.-B.; et al. Calcium channel blockers reduce severe fever with thrombocytopenia syndrome virus (SFTSV) related fatality. *Cell Res.* **2019**, *29*, 739–753. [CrossRef] [PubMed]
44. Lavanya, M.; Cuevas, C.D.; Thomas, M.; Cherry, S.; Ross, S.R. siRNA Screen for Genes That Affect Junín Virus Entry Uncovers Voltage-Gated Calcium Channels as a Therapeutic Target. *Sci. Transl. Med.* **2013**, *5*, 204ra131–204ra201. [CrossRef]
45. Tammineni, E.R.; Carrillo, E.D.; Soto-Acosta, R.; Angel-Ambrocio, A.H.; García, M.C.; Bautista-Carbajal, P.; Del Angel, R.M.; Sánchez, J.A. The β_4 subunit of $Ca_V1.2$ channels is required for an optimal interferon response in cardiac muscle cells. *Sci. Signal.* **2018**, *11*, 1–14. [CrossRef]
46. Danta, C.C. Calcium Channel Blockers: A Possible Potential Therapeutic Strategy for the Treatment of Alzheimer's Dementia Patients with SARS-CoV-2 Infection. *ACS Chem. Neurosci.* **2020**, *11*, 2145–2148. [CrossRef]
47. Han, Z.; Madara, J.J.; Herbert, A.; Prugar, L.I.; Ruthel, G.; Lu, J.; Liu, Y.; Liu, W.; Liu, X.; Wrobel, J.E.; et al. Calcium Regulation of Hemorrhagic Fever Virus Budding: Mechanistic Implications for Host-Oriented Therapeutic Intervention. *PLoS Pathog.* **2015**, *11*, e1005220. [CrossRef] [PubMed]
48. Solaimanzadeh, I. Nifedipine and Amlodipine Are Associated With Improved Mortality and Decreased Risk for Intubation and Mechanical Ventilation in Elderly Patients Hospitalized for COVID-19. *Cureus* **2020**, *12*, e8069. [CrossRef] [PubMed]
49. Reiken, S.; Dridi, H.; Sittenfeld, L.; Liu, X.; Marks, A.R. Alzheimer's-like remodeling of neuronal ryanodine receptor in COVID-19. *bioRxiv* **2021**. [CrossRef]
50. Wei, H.; Liang, G.; Vera, R.M. Dantrolene repurposed to treat sepsis or septic shock and COVID-19 patients. *Eur. Rev. Med. Pharmacol. Sci.* **2021**, *25*, 3136–3144.
51. Chen, S.; Shenk, T.; Nogalski, M.T. P2Y2 purinergic receptor modulates virus yield, calcium homeostasis, and cell motility in human cytomegalovirus-infected cells. *Proc. Natl. Acad. Sci. USA* **2019**, *116*, 18971–18982. [CrossRef]
52. Keay, S.; Baldwin, B.R.; Smith, M.W.; Wasserman, S.S.; Goldman, W.F. Increases in $[Ca^{2+}]i$ mediated by the 92.5-kDa putative cell membrane receptor for HCMV gp86. *Am. J. Physiol.* **1995**, *269*, C11–C21. [CrossRef]
53. Ehrlich, L.S.; Medina, G.N.; Photiadis, S.; Whittredge, P.B.; Watanabe, S.; Taraska, J.W.; Carter, C.A. Tsg101 regulates $PI(4,5)P_2/Ca^{(2+)}$ signaling for HIV-1 Gag assembly. *Front. Microbiol.* **2014**, *5*, 234. [CrossRef]
54. Ding, W.; Albrecht, B.R.; Kelley, R.E.; Muthusamy, N.; Kim, S.-J.; Altschuld, R.A.; Lairmore, M.D. Human T-Cell Lymphotropic Virus Type 1 p12 I Expression Increases Cytoplasmic Calcium To Enhance the Activation of Nuclear Factor of Activated T Cells. *J. Virol.* **2002**, *76*, 10374–10382. [CrossRef]
55. Han, Z.; Harty, R.N. Influence of calcium/calmodulin on budding of Ebola VLPs: Implications for the involvement of the Ras/Raf/MEK/ERK pathway. *Virus Genes* **2007**, *35*, 511–520. [CrossRef]
56. Dionicio, C.L.; Peña, F.; Constantino-Jonapa, L.A.; Vazquez, C.; Yocupicio-Monroy, M.; Rosales, R.; Zambrano, J.L.; Ruiz, M.C.; Del Angel, R.M.; Ludert, J.E. Dengue virus induced changes in Ca^{2+} homeostasis in human hepatic cells that favor the viral replicative cycle. *Virus Res.* **2018**, *245*, 17–28. [CrossRef]
57. Michelangeli, F.; Ruiz, M.C.; del Castillo, J.R.; Ludert, J.E.; Liprandi, F. Effect of rotavirus infection on intracellular calcium homeostasis in cultured cells. *Virology* **1991**, *181*, 520–527. [CrossRef]
58. Pham, T.; Perry, J.L.; Dosey, T.L.; Delcour, A.H.; Hyser, J.M. The Rotavirus NSP4 Viroporin Domain is a Calcium-conducting Ion Channel. *Sci. Rep.* **2017**, *7*, 43487. [CrossRef]
59. Panda, S.; Behera, S.; Alam, M.F.; Syed, G.H. Endoplasmic reticulum & mitochondrial calcium homeostasis: The interplay with viruses. *Mitochondrion* **2021**, *58*, 227–242. [CrossRef] [PubMed]
60. Cui, R.; Wang, Y.; Wang, L.; Li, G.; Lan, K.; Altmeyer, R.; Zou, G. Cyclopiazonic acid, an inhibitor of calcium-dependent ATPases with antiviral activity against human respiratory syncytial virus. *Antivir. Res.* **2016**, *132*, 38–45. [CrossRef] [PubMed]
61. Lewis, W.; Grupp, I.L.; Grupp, G.; Hoit, B.; Morris, R.; Samarel, A.M.; Bruggeman, L.; Klotman, P. Cardiac Dysfunction Occurs in the HIV-1 Transgenic Mouse Treated with Zidovudine. *Lab. Investig.* **2000**, *80*, 187–197. [CrossRef] [PubMed]
62. Díaz, Y.; Peña, F.; Aristimuño, O.C.; Matteo, L.; De Agrela, M.; Chemello, M.E.; Michelangeli, F.; Ruiz, M.C. Dissecting the Ca^{2+} entry pathways induced by rotavirus infection and NSP4-EGFP expression in Cos-7 cells. *Virus Res.* **2012**, *167*, 285–296. [CrossRef] [PubMed]
63. Renu, K.; Subramaniam, M.D.; Chakraborty, R.; Myakala, H.; Iyer, M.; Bharathi, G.; Siva, K.; Vellingiri, B.; Valsala Gopalakrishnan, A. The role of Interleukin-4 in COVID-19 associated male infertility—A hypothesis. *J. Reprod. Immunol.* **2020**, *142*, 103213. [CrossRef]
64. Fan, C.; Lu, W.; Li, K.; Ding, Y.; Wang, J. ACE2 Expression in Kidney and Testis May Cause Kidney and Testis Infection in COVID-19 Patients. *Front. Med.* **2021**, *7*, 1045. [CrossRef]
65. Shen, Q.; Xiao, X.; Aierken, A.; Yue, W.; Wu, X.; Liao, M.; Hua, J. The ACE2 expression in Sertoli cells and germ cells may cause male reproductive disorder after SARS-CoV-2 infection. *J. Cell. Mol. Med.* **2020**, *24*, 9472–9477. [CrossRef]
66. Wang, Z.; Xu, X. scRNA-seq Profiling of Human Testes Reveals the Presence of the ACE2 Receptor, A Target for SARS-CoV-2 Infection in Spermatogonia, Leydig and Sertoli Cells. *Cells* **2020**, *9*, 920. [CrossRef]
67. Haghpanah, A.; Masjedi, F.; Alborzi, S.; Hosseinpour, A.; Dehghani, A.; Malekmakan, L.; Roozbeh, J. Potential mechanisms of SARS-CoV-2 action on male gonadal function and fertility: Current status and future prospects. *Andrologia* **2021**, *53*, e13883. [CrossRef] [PubMed]
68. Saylam, B.; Uguz, M.; Yarpuzlu, M.; Efesoy, O.; Akbay, E.; Çayan, S. The presence of SARS-CoV-2 virus in semen samples of patients with COVID-19 pneumonia. *Andrologia* **2021**, *53*, e14145. [CrossRef]

69. Song, C.; Wang, Y.; Li, W.; Hu, B.; Chen, G.; Xia, P.; Wang, W.; Li, C.; Diao, F.; Hu, Z.; et al. Absence of 2019 novel coronavirus in semen and testes of COVID-19 patients. *Biol. Reprod.* **2020**, *103*, 4–6. [CrossRef] [PubMed]
70. Banihani, S.A. Human semen quality as affected by SARS-CoV-2 infection: An up-to-date review. *Andrologia* **2021**, e14295. [CrossRef] [PubMed]
71. Paoli, D.; Pallotti, F.; Colangelo, S.; Basilico, F.; Mazzuti, L.; Turriziani, O.; Antonelli, G.; Lenzi, A.; Lombardo, F. Study of SARS-CoV-2 in semen and urine samples of a volunteer with positive naso-pharyngeal swab. *J. Endocrinol. Investig.* **2020**, *43*, 1819–1822. [CrossRef]
72. Ruan, Y.; Hu, B.; Liu, Z.; Liu, K.; Jiang, H.; Li, H.; Li, R.; Luan, Y.; Liu, X.; Yu, G.; et al. No detection of SARS-CoV-2 from urine, expressed prostatic secretions, and semen in 74 recovered COVID-19 male patients: A perspective and urogenital evaluation. *Andrology* **2021**, *9*, 99–106. [CrossRef]
73. Guo, L.; Zhao, S.; Li, W.; Wang, Y.; Li, L.; Jiang, S.; Ren, W.; Yuan, Q.; Zhang, F.; Kong, F.; et al. Absence of SARS-CoV-2 in semen of a COVID-19 patient cohort. *Andrology* **2021**, *9*, 42–47. [CrossRef]
74. Pan, F.; Xiao, X.; Guo, J.; Song, Y.; Li, H.; Patel, D.P.; Spivak, A.M.; Alukal, J.P.; Zhang, X.; Xiong, C.; et al. No evidence of severe acute respiratory syndrome–Coronavirus 2 in semen of males recovering from coronavirus disease 2019. *Fertil. Steril.* **2020**, *113*, 1135–1139. [CrossRef]
75. Loveland, K.L.; Klein, B.; Pueschl, D.; Indumathy, S.; Bergmann, M.; Loveland, B.E.; Hedger, M.P.; Schuppe, H.C. Cytokines in Male Fertility and Reproductive Pathologies: Immunoregulation and Beyond. *Front. Endocrinol.* **2017**, *8*, 307. [CrossRef] [PubMed]
76. Schuppe, H.-C.; Pilatz, A.; Hossain, H.; Diemer, T.; Wagenlehner, F.; Weidner, W. Urogenital Infection as a Risk Factor for Male Infertility. *Dtsch. Ärzteblatt Int.* **2017**, *114*, 339. [CrossRef]
77. Hedger, M.P.; Meinhardt, A. Cytokines and the immune-testicular axis. *J. Reprod. Immunol.* **2003**, *58*, 1–26. [CrossRef]
78. Li, H.; Xiao, X.; Zhang, J.; Zafar, M.I.; Wu, C.; Long, Y.; Lu, W.; Pan, F.; Meng, T.; Zhao, K.; et al. Impaired spermatogenesis in COVID-19 patients. *EClinicalMedicine* **2020**, *28*, 100604. [CrossRef]
79. Carlsen, E. History of febrile illness and variation in semen quality. *Hum. Reprod.* **2003**, *18*, 2089–2092. [CrossRef] [PubMed]
80. Jung, A.; Schuppe, H.-C.; Schill, W.-B. Fieber als Ursache einer temporären Fertilitätseinschränkung des Mannes. *Hautarzt* **2001**, *52*, 1090–1093. [CrossRef]
81. Salonia, A.; Pontillo, M.; Capogrosso, P.; Gregori, S.; Carenzi, C.; Ferrara, A.M.; Rowe, I.; Boeri, L.; Larcher, A.; Ramirez, G.A.; et al. Testosterone in males with COVID-19: A 7-month cohort study. *Andrology* **2021**, *10*, 34–41. [CrossRef]
82. Kadihasanoglu, M.; Aktas, S.; Yardimci, E.; Aral, H.; Kadioglu, A. SARS-CoV-2 Pneumonia Affects Male Reproductive Hormone Levels: A Prospective, Cohort Study. *J. Sex. Med.* **2021**, *18*, 256–264. [CrossRef]
83. Higgins, V.; Sohaei, D.; Diamandis, E.P.; Prassas, I. COVID-19: From an acute to chronic disease? Potential long-term health consequences. *Crit. Rev. Clin. Lab. Sci.* **2021**, *58*, 297–310. [CrossRef]
84. Callard, F.; Perego, E. How and why patients made Long Covid. *Soc. Sci. Med.* **2021**, *268*, 113426. [CrossRef]
85. Mendelson, M.; Nel, J.; Blumberg, L.; Madhi, S.A.; Dryden, M.; Stevens, W.; Venter, F.W.D. Long-COVID: An evolving problem with an extensive impact. *S. Afr. Med. J.* **2020**, *111*, 10. [CrossRef]
86. Bermejo-Martin, J.F.; González-Rivera, M.; Almansa, R.; Micheloud, D.; Tedim, A.P.; Domínguez-Gil, M.; Resino, S.; Martín-Fernández, M.; Ryan Murua, P.; Pérez-García, F.; et al. Viral RNA load in plasma is associated with critical illness and a dysregulated host response in COVID-19. *Crit. Care* **2020**, *24*, 691. [CrossRef]
87. Bermejo-Martin, J.F.; Almansa, R.; Tedim, A.P.; De La Fuente, A.; Eiros, J.M.; Torres, A.; Kelvin, D.J. Mounting evidence of impaired viral control in severe COVID-19. *Lancet Microbe* **2021**, *2*, e228–e229. [CrossRef]
88. Rastrelli, G.; Di Stasi, V.; Inglese, F.; Beccaria, M.; Garuti, M.; Di Costanzo, D.; Spreafico, F.; Greco, G.F.; Cervi, G.; Pecoriello, A.; et al. Low testosterone levels predict clinical adverse outcomes in SARS-CoV-2 pneumonia patients. *Andrology* **2021**, *9*, 88–98. [CrossRef] [PubMed]
89. Lucas-Herald, A.K.; Alves-Lopes, R.; Montezano, A.C.; Ahmed, S.F.; Touyz, R.M. Genomic and non-genomic effects of androgens in the cardiovascular system: Clinical implications. *Clin. Sci.* **2017**, *131*, 1405–1418. [CrossRef]
90. Markle, J.G.; Fish, E.N. SeXX matters in immunity. *Trends Immunol.* **2014**, *35*, 97–104. [CrossRef]
91. Kjellman, B.; Gustafsson, P.M. Asthma from childhood to adulthood: Asthma severity, allergies, sensitization, living conditions, gender influence and social consequences. *Respir. Med.* **2000**, *94*, 454–465. [CrossRef]
92. De Marco, R.; Locatelli, F.; Sunyer, J.; Burney, P. Differences in Incidence of Reported Asthma Related to Age in Men and Women. *Am. J. Respir. Crit. Care Med.* **2000**, *162*, 68–74. [CrossRef] [PubMed]
93. Espinoza, J.; Montaño, L.M.; Perusquía, M. Nongenomic bronchodilating action elicited by dehydroepiandrosterone (DHEA) in a guinea pig asthma model. *J. Steroid Biochem. Mol. Biol.* **2013**, *138*, 174–182. [CrossRef] [PubMed]
94. Carbajal-García, A.; Reyes-García, J.; Casas-Hernández, M.F.; Flores-Soto, E.; Díaz-Hernández, V.; Solís-Chagoyán, H.; Sommer, B.; Montaño, L.M. Testosterone augments β_2 adrenergic receptor genomic transcription increasing salbutamol relaxation in airway smooth muscle. *Mol. Cell. Endocrinol.* **2020**, *510*, 110801. [CrossRef]
95. Laffont, S.; Blanquart, E.; Guéry, J.C. Sex Differences in Asthma: A Key Role of Androgen-Signaling in Group 2 Innate Lymphoid Cells. *Front. Immunol.* **2017**, *8*, 1069. [CrossRef]
96. Fuseini, H.; Yung, J.A.; Cephus, J.Y.; Zhang, J.; Goleniewska, K.; Polosukhin, V.V.; Peebles, R.S.; Newcomb, D.C. Testosterone Decreases House Dust Mite–Induced Type 2 and IL-17A–Mediated Airway Inflammation. *J. Immunol.* **2018**, *201*, 1843–1854. [CrossRef] [PubMed]

97. Kalidhindi, R.; Katragadda, R.; Beauchamp, K.L.; Pabelick, C.M.; Prakash, Y.S.; Sathish, V. Androgen Receptor-Mediated Regulation of Intracellular Calcium in Human Airway Smooth Muscle Cells. *Cell. Physiol. Biochem.* **2019**, *53*, 215–228. [CrossRef] [PubMed]
98. Kalidhindi, R.S.R.; Borkar, N.A.; Ambhore, N.S.; Pabelick, C.M.; Prakash, Y.S.; Sathish, V. Sex steroids skew ACE2 expression in human airway: A contributing factor to sex differences in COVID-19? *Am. J. Physiol.-Lung Cell. Mol. Physiol.* **2020**, *319*, L843–L847. [CrossRef]
99. Rovira-Llopis, S.; Bañuls, C.; de Marañon, A.M.; Diaz-Morales, N.; Jover, A.; Garzon, S.; Rocha, M.; Victor, V.M.; Hernandez-Mijares, A. Low testosterone levels are related to oxidative stress, mitochondrial dysfunction and altered subclinical atherosclerotic markers in type 2 diabetic male patients. *Free Radic. Biol. Med.* **2017**, *108*, 155–162. [CrossRef] [PubMed]
100. Grandys, M.; Majerczak, J.; Zapart-Bukowska, J.; Duda, K.; Kulpa, J.K.; Zoladz, J.A. Lowered Serum Testosterone Concentration Is Associated With Enhanced Inflammation and Worsened Lipid Profile in Men. *Front. Endocrinol.* **2021**, *12*, 1088. [CrossRef] [PubMed]
101. Golden, K.L.; Marsh, J.D.; Jiang, Y. Castration Reduces mRNA Levels for Calcium Regulatory Proteins in Rat Heart. *Endocrine* **2002**, *19*, 339–344. [CrossRef]
102. Golden, K.L.; Marsh, J.D.; Jiang, Y.; Brown, T.; Moulden, J. Gonadectomy of adult male rats reduces contractility of isolated cardiac myocytes. *Am. J. Physiol. Endocrinol. Metab.* **2003**, *285*, E449–E453. [CrossRef] [PubMed]
103. Ayaz, O.; Howlett, S.E. Testosterone modulates cardiac contraction and calcium homeostasis: Cellular and molecular mechanisms. *Biol. Sex Differ.* **2015**, *6*, 9. [CrossRef]
104. Er, F.; Gassanov, N.; Brandt, M.C.; Madershahian, N.; Hoppe, U.C. Impact of dihydrotestosterone on L-type calcium channels in human ventricular cardiomyocytes. *Endocr. Res.* **2009**, *34*, 59–67. [CrossRef]
105. Callies, F.; Strömer, H.; Schwinger, R.H.; Bölck, B.; Hu, K.; Frantz, S.; Leupold, A.; Beer, S.; Allolio, B.; Bonz, A.W. Administration of testosterone is associated with a reduced susceptibility to myocardial ischemia. *Endocrinology* **2003**, *144*, 4478–4483. [CrossRef]
106. Tsang, S.; Wong, S.S.; Wu, S.; Kravtsov, G.M.; Wong, T.M. Testosterone-augmented contractile responses to alpha1- and beta1-adrenoceptor stimulation are associated with increased activities of RyR, SERCA, and NCX in the heart. *Am. J. Physiol. Cell Physiol.* **2009**, *296*, C766–C782. [CrossRef]
107. Weerateerangkul, P.; Shinlapawittayatorn, K.; Palee, S.; Apaijai, N.; Chattipakorn, S.C.; Chattipakorn, N. Early testosterone replacement attenuates intracellular calcium dyshomeostasis in the heart of testosterone-deprived male rats. *Cell Calcium* **2017**, *67*, 22–30. [CrossRef]
108. Murphy, J.G.; Marsh, J.D.; Smith, T.W. The role of calcium in ischemic myocardial injury. *Circulation* **1987**, *75*, V15–V24. [PubMed]
109. Vittone, L.; Mundiña-Weilenmann, C.; Said, M.; Ferrero, P.; Mattiazzi, A. Time course and mechanisms of phosphorylation of phospholamban residues in ischemia-reperfused rat hearts. Dissociation of phospholamban phosphorylation pathways. *J. Mol. Cell. Cardiol.* **2002**, *34*, 39–50. [CrossRef] [PubMed]
110. Sebag, I.A.; Gillis, M.A.; Calderone, A.; Kasneci, A.; Meilleur, M.; Haddad, R.; Noiles, W.; Patel, B.; Chalifour, L.E. Sex hormone control of left ventricular structure/function: Mechanistic insights using echocardiography, expression, and DNA methylation analyses in adult mice. *Am. J. Physiol.-Heart Circ. Physiol.* **2011**, *301*, H1706–H1715. [CrossRef] [PubMed]
111. Witayavanitkul, N.; Woranush, W.; Bupha-Intr, T.; Wattanapermpool, J. Testosterone regulates cardiac contractile activation by modulating SERCA but not NCX activity. *Am. J. Physiol.-Heart Circ. Physiol.* **2013**, *304*, H465–H472. [CrossRef] [PubMed]
112. Wang, D.; Hu, B.; Hu, C.; Zhu, F.; Liu, X.; Zhang, J.; Wang, B.; Xiang, H.; Cheng, Z.; Xiong, Y.; et al. Clinical Characteristics of 138 Hospitalized Patients With 2019 Novel Coronavirus–Infected Pneumonia in Wuhan, China. *JAMA* **2020**, *323*, 1061. [CrossRef]
113. Huang, C.; Wang, Y.; Li, X.; Ren, L.; Zhao, J.; Hu, Y.; Zhang, L.; Fan, G.; Xu, J.; Gu, X.; et al. Clinical features of patients infected with 2019 novel coronavirus in Wuhan, China. *Lancet* **2020**, *395*, 497–506. [CrossRef]
114. Yang, X.; Yu, Y.; Xu, J.; Shu, H.; Xia, J.A.; Liu, H.; Wu, Y.; Zhang, L.; Yu, Z.; Fang, M.; et al. Clinical course and outcomes of critically ill patients with SARS-CoV-2 pneumonia in Wuhan, China: A single-centered, retrospective, observational study. *Lancet Respir. Med.* **2020**, *8*, 475–481. [CrossRef]
115. Wang, Y.; Wang, Z.; Tse, G.; Zhang, L.; Wan, E.Y.; Guo, Y.; Lip, G.Y.H.; Li, G.; Lu, Z.; Liu, T. Cardiac arrhythmias in patients with COVID-19. *J. Arrhythmia* **2020**, *36*, 827–836. [CrossRef]
116. Shi, S.; Qin, M.; Shen, B.; Cai, Y.; Liu, T.; Yang, F.; Gong, W.; Liu, X.; Liang, J.; Zhao, Q.; et al. Association of Cardiac Injury With Mortality in Hospitalized Patients With COVID-19 in Wuhan, China. *JAMA Cardiol.* **2020**, *5*, 802. [CrossRef] [PubMed]
117. Zhou, F.; Yu, T.; Du, R.; Fan, G.; Liu, Y.; Liu, Z.; Xiang, J.; Wang, Y.; Song, B.; Gu, X.; et al. Clinical course and risk factors for mortality of adult inpatients with COVID-19 in Wuhan, China: A retrospective cohort study. *Lancet* **2020**, *395*, 1054–1062. [CrossRef]
118. Lake, M.A. What we know so far: COVID-19 current clinical knowledge and research. *Clin. Med.* **2020**, *20*, 124–127. [CrossRef] [PubMed]
119. Lei, S.; Jiang, F.; Su, W.; Chen, C.; Chen, J.; Mei, W.; Zhan, L.-Y.; Jia, Y.; Zhang, L.; Liu, D.; et al. Clinical characteristics and outcomes of patients undergoing surgeries during the incubation period of COVID-19 infection. *EClinicalMedicine* **2020**, *21*, 100331. [CrossRef] [PubMed]
120. Du, Y.; Tu, L.; Zhu, P.; Mu, M.; Wang, R.; Yang, P.; Wang, X.; Hu, C.; Ping, R.; Hu, P.; et al. Clinical Features of 85 Fatal Cases of COVID-19 from Wuhan. A Retrospective Observational Study. *Am. J. Respir. Crit. Care Med.* **2020**, *201*, 1372–1379. [CrossRef]

121. Long, B.; Brady, W.J.; Bridwell, R.E.; Ramzy, M.; Montrief, T.; Singh, M.; Gottlieb, M. Electrocardiographic manifestations of COVID-19. *Am. J. Emerg. Med.* **2021**, *41*, 96–103. [CrossRef]
122. Atri, D.; Siddiqi, H.K.; Lang, J.P.; Nauffal, V.; Morrow, D.A.; Bohula, E.A. COVID-19 for the Cardiologist: Basic Virology, Epidemiology, Cardiac Manifestations, and Potential Therapeutic Strategies. *JACC Basic Transl. Sci.* **2020**, *5*, 518–536. [CrossRef]
123. Chen, X.; Li, R.; Pan, Z.; Qian, C.; Yang, Y.; You, R.; Zhao, J.; Liu, P.; Gao, L.; Li, Z.; et al. Human monoclonal antibodies block the binding of SARS-CoV-2 spike protein to angiotensin converting enzyme 2 receptor. *Cell. Mol. Immunol.* **2020**, *17*, 647–649. [CrossRef]
124. D'Aloia, A.; Faggiano, P.; Brentana, L.; Boldini, A.; Curnis, A.; Bontempi, L.; Dei Cas, L. Recurrent ventricular fibrillation during a febrile illness and hyperthermia in a patient with dilated cardiomyopathy and automatic implantable cardioverter defibrillator. An example of reversible electrical storm. *Int. J. Cardiol.* **2005**, *103*, 207–208. [CrossRef]
125. Dinckal, M. Incessant monomorphic ventricular tachycardia during febrile illness in a patient with Brugada syndrome: Fatal electrical storm. *Europace* **2003**, *5*, 257–261. [CrossRef]
126. Vonderlin, N.; Siebermair, J.; Kaya, E.; Köhler, M.; Rassaf, T.; Wakili, R. Critical inflammatory mechanisms underlying arrhythmias. *Herz* **2019**, *44*, 121–129. [CrossRef] [PubMed]
127. Xu, Z.; Shi, L.; Wang, Y.; Zhang, J.; Huang, L.; Zhang, C.; Liu, S.; Zhao, P.; Liu, H.; Zhu, L.; et al. Pathological findings of COVID-19 associated with acute respiratory distress syndrome. *Lancet Respir. Med.* **2020**, *8*, 420–422. [CrossRef]
128. Schett, G.; Sticherling, M.; Neurath, M.F. COVID-19: Risk for cytokine targeting in chronic inflammatory diseases? *Nat. Rev. Immunol.* **2020**, *20*, 271–272. [CrossRef] [PubMed]
129. Wiersinga, W.J.; Rhodes, A.; Cheng, A.C.; Peacock, S.J.; Prescott, H.C. Pathophysiology, Transmission, Diagnosis, and Treatment of Coronavirus Disease 2019 (COVID-19). *JAMA* **2020**, *324*, 782. [CrossRef]
130. Hagiwara, Y.; Miyoshi, S.; Fukuda, K.; Nishiyama, N.; Ikegami, Y.; Tanimoto, K.; Murata, M.; Takahashi, E.; Shimoda, K.; Hirano, T.; et al. SHP2-mediated signaling cascade through gp130 is essential for LIF-dependent I CaL, $[Ca^{2+}]_i$ transient, and APD increase in cardiomyocytes. *J. Mol. Cell. Cardiol.* **2007**, *43*, 710–716. [CrossRef]
131. Alí, A.; Boutjdir, M.; Aromolaran, A.S. Cardiolipotoxicity, Inflammation, and Arrhythmias: Role for Interleukin-6 Molecular Mechanisms. *Front. Physiol.* **2019**, *9*, 1866. [CrossRef]
132. Kao, Y.H.; Chen, Y.C.; Cheng, C.C.; Lee, T.I.; Chen, Y.J.; Chen, S.A. Tumor necrosis factor-alpha decreases sarcoplasmic reticulum Ca^{2+}-ATPase expressions via the promoter methylation in cardiomyocytes. *Crit. Care Med.* **2010**, *38*, 217–222. [CrossRef]
133. Monnerat, G.; Alarcón, M.L.; Vasconcellos, L.R.; Hochman-Mendez, C.; Brasil, G.; Bassani, R.A.; Casis, O.; Malan, D.; Travassos, L.H.; Sepúlveda, M.; et al. Macrophage-dependent IL-1β production induces cardiac arrhythmias in diabetic mice. *Nat. Commun.* **2016**, *7*, 13344. [CrossRef]
134. Kelly, D.M.; Jones, T.H. Testosterone: A vascular hormone in health and disease. *J. Endocrinol.* **2013**, *217*, R47–R71. [CrossRef]
135. Pugh, P. Acute haemodynamic effects of testosterone in men with chronic heart failure. *Eur. Heart J.* **2003**, *24*, 909–915. [CrossRef]
136. Malkin, C.J.; Morris, P.D.; Pugh, P.J.; English, K.M.; Channer, K.S. Effect of testosterone therapy on QT dispersion in men with heart failure. *Am. J. Cardiol.* **2003**, *92*, 1241–1243. [CrossRef]
137. Schwartz, J.B.; Volterrani, M.; Caminiti, G.; Marazzi, G.; Fini, M.; Rosano, G.M.C.; Iellamo, F. Effects of testosterone on the Q-T Interval in older men and older women with chronic heart failure. *Int. J. Androl.* **2011**, *34*, e415–e421. [CrossRef]
138. Townsend, E.A.; Miller, V.M.; Prakash, Y.S. Sex Differences and Sex Steroids in Lung Health and Disease. *Endocr. Rev.* **2012**, *33*, 1–47. [CrossRef] [PubMed]
139. Zarotsky, V.; Huang, M.-Y.; Carman, W.; Morgentaler, A.; Singhal, P.K.; Coffin, D.; Jones, T.H. Systematic literature review of the risk factors, comorbidities, and consequences of hypogonadism in men. *Andrology* **2014**, *2*, 819–834. [CrossRef]
140. Jones, T.H.; Kelly, D.M. Randomized controlled trials—Mechanistic studies of testosterone and the cardiovascular system. *Asian J. Androl.* **2018**, *20*, 120–130. [CrossRef] [PubMed]
141. Yue, P.; Chatterjee, K.; Beale, C.; Poole-Wilson, P.A.; Collins, P. Testosterone relaxes rabbit coronary arteries and aorta. *Circulation* **1995**, *91*, 1154–1160. [CrossRef] [PubMed]
142. Tep-Areenan, P.; Kendall, D.A.; Randall, M.D. Testosterone-induced vasorelaxation in the rat mesenteric arterial bed is mediated predominantly via potassium channels. *Br. J. Pharmacol.* **2002**, *135*, 735–740. [CrossRef]
143. Chou, T.M.; Sudhir, K.; Hutchison, S.J.; Ko, E.; Amidon, T.M.; Collins, P.; Chatterjee, K. Testosterone induces dilation of canine coronary conductance and resistance arteries in vivo. *Circulation* **1996**, *94*, 2614–2619. [CrossRef]
144. Yildiz, O.; Seyrek, M.; Gul, H.; Un, I.; Yildirim, V.; Ozal, E.; Uzun, M.; Bolu, E. Testosterone relaxes human internal mammary artery in vitro. *J. Cardiovasc. Pharmacol.* **2005**, *45*, 580–585. [CrossRef]
145. Murphy, J.G.; Khalil, R.A. Decreased $[Ca^{2+}]_i$ during inhibition of coronary smooth muscle contraction by $_{17}$β-estradiol, progesterone, and testosterone. *J. Pharmacol. Exp. Ther.* **1999**, *291*, 44–52.
146. English, K.M.; Jones, R.D.; Jones, T.H.; Morice, A.H.; Channer, K.S. Aging reduces the responsiveness of coronary arteries from male Wistar rats to the vasodilatory action of testosterone. *Clin. Sci.* **2000**, *99*, 77–82. [CrossRef]
147. English, K.M.; Jones, R.D.; Jones, T.H.; Morice, A.H.; Channer, K.S. Testosterone acts as a coronary vasodilator by a calcium antagonistic action. *J. Endocrinol. Investig.* **2002**, *25*, 455–458. [CrossRef] [PubMed]
148. Perusquía, M.; Hernández, R.; Morales, M.A.; Campos, M.G.; Villalón, C.M. Role of endothelium in the vasodilating effect of progestins and androgens on the rat thoracic aorta. *Gen. Pharmacol.* **1996**, *27*, 181–185. [CrossRef]

149. Honda, H.; Unemoto, T.; Kogo, H. Different Mechanisms for Testosterone-Induced Relaxation of Aorta Between Normotensive and Spontaneously Hypertensive Rats. *Hypertension* **1999**, *34*, 1232–1236. [CrossRef] [PubMed]
150. Ding, A.Q.; Stallone, J.N. Testosterone-induced relaxation of rat aorta is androgen structure specific and involves K+ channel activation. *J. Appl. Physiol.* **2001**, *91*, 2742–2750. [CrossRef] [PubMed]
151. Jones, R.D.; English, K.M.; Pugh, P.J.; Morice, A.H.; Jones, T.H.; Channer, K.S. Pulmonary vasodilatory action of testosterone: Evidence of a calcium antagonistic action. *J. Cardiovasc. Pharmacol.* **2002**, *39*, 814–823. [CrossRef]
152. Rowell, K.O.; Hall, J.; Pugh, P.J.; Jones, T.H.; Channer, K.S.; Jones, R.D. Testosterone acts as an efficacious vasodilator in isolated human pulmonary arteries and veins: Evidence for a biphasic effect at physiological and supra-physiological concentrations. *J. Endocrinol. Investig.* **2009**, *32*, 718–723. [CrossRef]
153. Seyrek, M.; Yildiz, O.; Ulusoy, H.B.; Yildirim, V. Testosterone Relaxes Isolated Human Radial Artery by Potassium Channel Opening Action. *J. Pharmacol. Sci.* **2007**, *103*, 309–316. [CrossRef] [PubMed]
154. Cairrão, E.; Álvarez, E.; Santos-Silva, A.J.; Verde, I. Potassium channels are involved in testosterone-induced vasorelaxation of human umbilical artery. *Naunyn-Schmiedeberg's Arch. Pharmacol.* **2008**, *376*, 375–383. [CrossRef]
155. Cairrão, E.; Santos-Silva, A.J.; Verde, I. PKG is involved in testosterone-induced vasorelaxation of human umbilical artery. *Eur. J. Pharmacol.* **2010**, *640*, 94–101. [CrossRef]
156. Han, D.H.; Chae, M.R.; Jung, J.H.; So, I.; Park, J.K.; Lee, S.W. Effect of testosterone on potassium channel opening in human corporal smooth muscle cells. *J. Sex. Med.* **2008**, *5*, 822–832. [CrossRef]
157. Crews, J.K.; Khalil, R.A. Gender-specific inhibition of Ca^{2+} entry mechanisms of arterial vasoconstriction by sex hormones. *Clin. Exp. Pharmacol. Physiol.* **1999**, *26*, 707–715. [CrossRef]
158. Hu, Z.; Ma, R.; Gong, J. Investigation of testosterone-mediated non-transcriptional inhibition of Ca^{2+} in vascular smooth muscle cells. *Biomed. Rep.* **2016**, *4*, 197–202. [CrossRef]
159. Hall, J.; Jones, R.D.; Jones, T.H.; Channer, K.S.; Peers, C. Selective Inhibition of L-Type Ca^{2+} Channels in A7r5 Cells by Physiological Levels of Testosterone. *Endocrinology* **2006**, *147*, 2675–2680. [CrossRef] [PubMed]
160. Perusquía, M.; Herrera, N.; Ferrer, M.; Stallone, J.N. Antihypertensive effects of androgens in conscious, spontaneously hypertensive rats. *J. Steroid Biochem. Mol. Biol.* **2017**, *167*, 106–114. [CrossRef] [PubMed]
161. Crews, J.K.; Khalil, R.A. Antagonistic Effects of 17β-Estradiol, Progesterone, and Testosterone on Ca^{2+} Entry Mechanisms of Coronary Vasoconstriction. *Arterioscler. Thromb. Vasc. Biol.* **1999**, *19*, 1034–1040. [CrossRef] [PubMed]
162. Jones, R.D.; English, K.M.; Jones, T.H.; Channer, K.S. Testosterone-induced coronary vasodilatation occurs via a non-genomic mechanism: Evidence of a direct calcium antagonism action. *Clin. Sci.* **2004**, *107*, 149–158. [CrossRef] [PubMed]
163. Ramírez-Rosas, M.B.; Cobos-Puc, L.E.; Muñoz-Islas, E.; González-Hernández, A.; Sánchez-López, A.; Villalón, C.M.; Maassen-vandenbrink, A.; Centurión, D. Pharmacological evidence that Ca^{2+} channels and, to a lesser extent, K^+ channels mediate the relaxation of testosterone in the canine basilar artery. *Steroids* **2011**, *76*, 409–415. [CrossRef]
164. Perusquía, M.; Navarrete, E.; González, L.; Villalón, C.M. The modulatory role of androgens and progestins in the induction of vasorelaxation in human umbilical artery. *Life Sci.* **2007**, *81*, 993–1002. [CrossRef]
165. Navarro-Dorado, J.; Orensanz, L.M.; Recio, P.; Bustamante, S.; Benedito, S.; Martínez, A.C.; García-Sacristán, A.; Prieto, D.; Hernández, M. Mechanisms involved in testosterone-induced vasodilatation in pig prostatic small arteries. *Life Sci.* **2008**, *83*, 569–573. [CrossRef] [PubMed]
166. Saldanha, P.A.; Cairrão, E.; Maia, C.J.; Verde, I. Long- and short-term effects of androgens in human umbilical artery smooth muscle. *Clin. Exp. Pharmacol. Physiol.* **2013**, *40*, 181–189. [CrossRef] [PubMed]
167. Stanetić, K.; Stanetić, B.; Petrović, V.; Marković, B.; Kević, V.; Todorović, N.; Stanetić, M. The Influence of Different Risk Factors on COVID-19 Outcomes in Adult Patients—An Observational-Descriptive Study. *Acta Med. Acad.* **2021**, *50*, 308–316. [CrossRef] [PubMed]
168. Ferrario, C.M.; Jessup, J.; Chappell, M.C.; Averill, D.B.; Brosnihan, K.B.; Tallant, E.A.; Diz, D.I.; Gallagher, P.E. Effect of Angiotensin-Converting Enzyme Inhibition and Angiotensin II Receptor Blockers on Cardiac Angiotensin-Converting Enzyme 2. *Circulation* **2005**, *111*, 2605–2610. [CrossRef] [PubMed]
169. Furuhashi, M.; Moniwa, N.; Mita, T.; Fuseya, T.; Ishimura, S.; Ohno, K.; Shibata, S.; Tanaka, M.; Watanabe, Y.; Akasaka, H.; et al. Urinary Angiotensin-Converting Enzyme 2 in Hypertensive Patients May Be Increased by Olmesartan, an Angiotensin II Receptor Blocker. *Am. J. Hypertens.* **2015**, *28*, 15–21. [CrossRef]
170. Ramírez, L.M.M.; Flores-Soto, E. COVID-19 y su asociación con los inhibidores de la enzima convertidora de angiotensina y los antagonistas de los receptores para angiotensina II. *Rev. Fac. Med. UNAM* **2020**, *63*, 30–34.
171. Meftahi, G.H.; Jangravi, Z.; Sahraei, H.; Bahari, Z. The possible pathophysiology mechanism of cytokine storm in elderly adults with COVID-19 infection: The contribution of "inflame-aging". *Inflamm. Res.* **2020**, *69*, 825–839. [CrossRef]
172. Eshak, N.; Abdelnabi, M.; Beltagy, A. Inflamm-aging: The missing link to COVID-19 age-related mortality? *Southwest Respir. Crit. Care Chron.* **2020**, *8*, 66–67. [CrossRef]
173. Stout, M.B.; Justice, J.N.; Nicklas, B.J.; Kirkland, J.L. Physiological Aging: Links Among Adipose Tissue Dysfunction, Diabetes, and Frailty. *Physiology* **2017**, *32*, 9–19. [CrossRef]
174. Golan, R.; Scovell, J.M.; Ramasamy, R. Age-related testosterone decline is due to waning of both testicular and hypothalamic-pituitary function. *Aging Male* **2015**, *18*, 201–204. [CrossRef]

175. Dabaja, A.A.; Bryson, C.F.; Schlegel, P.N.; Paduch, D.A. The effect of hypogonadism and testosterone-enhancing therapy on alkaline phosphatase and bone mineral density. *BJU Int.* **2015**, *115*, 480–485. [CrossRef] [PubMed]
176. Darbandi, M.; Darbandi, S.; Agarwal, A.; Sengupta, P.; Durairajanayagam, D.; Henkel, R.; Sadeghi, M.R. Reactive oxygen species and male reproductive hormones. *Reprod. Biol. Endocrinol.* **2018**, *16*, 87. [CrossRef] [PubMed]
177. Spiers, J.G.; Chen, H.J.; Sernia, C.; Lavidis, N.A. Activation of the hypothalamic-pituitary-adrenal stress axis induces cellular oxidative stress. *Front. Neurosci.* **2015**, *8*, 456. [CrossRef]
178. Diamanti-Kandarakis, E.; Bourguignon, J.-P.; Giudice, L.C.; Hauser, R.; Prins, G.S.; Soto, A.M.; Zoeller, R.T.; Gore, A.C. Endocrine-Disrupting Chemicals: An Endocrine Society Scientific Statement. *Endocr. Rev.* **2009**, *30*, 293–342. [CrossRef]
179. Hardy, M.P.; Gao, H.-B.; Dong, Q.; Ge, R.; Wang, Q.; Chai, W.R.; Feng, X.; Sottas, C. Stress hormone and male reproductive function. *Cell Tissue Res.* **2005**, *322*, 147–153. [CrossRef]
180. Hwang, T.I.; Liao, T.-L.; Lin, J.-F.; Lin, Y.-C.; Lee, S.-Y.; Lai, Y.-C.; Kao, S.-H. Low-dose testosterone treatment decreases oxidative damage in TM3 Leydig cells. *Asian J. Androl.* **2011**, *13*, 432–437. [CrossRef] [PubMed]
181. Pintana, H.; Pongkan, W.; Pratchayasakul, W.; Chattipakorn, N.; Chattipakorn, S.C. Testosterone replacement attenuates cognitive decline in testosterone-deprived lean rats, but not in obese rats, by mitigating brain oxidative stress. *Age* **2015**, *37*, 84. [CrossRef]
182. Gao, F.; Li, G.; Liu, C.; Gao, H.; Wang, H.; Liu, W.; Chen, M.; Shang, Y.; Wang, L.; Shi, J.; et al. Autophagy regulates testosterone synthesis by facilitating cholesterol uptake in Leydig cells. *J. Cell Biol.* **2018**, *217*, 2103–2119. [CrossRef]
183. Kahn, B.E.; Brannigan, R.E. Obesity and male infertility. *Curr. Opin. Urol.* **2017**, *27*, 441–445. [CrossRef] [PubMed]
184. Liu, Y.; Ding, Z. Obesity, a serious etiologic factor for male subfertility in modern society. *Reproduction* **2017**, *154*, R123–R131. [CrossRef] [PubMed]
185. Zhang, J.; Pugh, T.D.; Stebler, B.; Ershler, W.B.; Keller, E.T. Orchiectomy Increases Bone Marrow Interleukin-6 Levels in Mice. *Calcif. Tissue Int.* **1998**, *62*, 219–226. [CrossRef]
186. Freeman, B.M.; Mountain, D.J.; Brock, T.C.; Chapman, J.R.; Kirkpatrick, S.S.; Freeman, M.B.; Klein, F.A.; Grandas, O.H. Low testosterone elevates interleukin family cytokines in a rodent model: A possible mechanism for the potentiation of vascular disease in androgen-deficient males. *J. Surg. Res.* **2014**, *190*, 319–327. [CrossRef]
187. Malkin, C.J.; Pugh, P.J.; Jones, R.D.; Kapoor, D.; Channer, K.S.; Jones, T.H. The Effect of Testosterone Replacement on Endogenous Inflammatory Cytokines and Lipid Profiles in Hypogonadal Men. *J. Clin. Endocrinol. Metab.* **2004**, *89*, 3313–3318. [CrossRef]
188. Fijak, M.; Schneider, E.; Klug, J.; Bhushan, S.; Hackstein, H.; Schuler, G.; Wygrecka, M.; Gromoll, J.; Meinhardt, A. Testosterone Replacement Effectively Inhibits the Development of Experimental Autoimmune Orchitis in Rats: Evidence for a Direct Role of Testosterone on Regulatory T Cell Expansion. *J. Immunol.* **2011**, *186*, 5162–5172. [CrossRef]
189. Horvath, S.; Erhart, W.; Brosch, M.; Ammerpohl, O.; Von Schonfels, W.; Ahrens, M.; Heits, N.; Bell, J.T.; Tsai, P.-C.; Spector, T.D.; et al. Obesity accelerates epigenetic aging of human liver. *Proc. Natl. Acad. Sci. USA* **2014**, *111*, 15538–15543. [CrossRef] [PubMed]
190. Smith, J.A.; Raisky, J.; Ratliff, S.M.; Liu, J.; Kardia, S.L.R.; Turner, S.T.; Mosley, T.H.; Zhao, W. Intrinsic and extrinsic epigenetic age acceleration are associated with hypertensive target organ damage in older African Americans. *BMC Med. Genom.* **2019**, *12*, 141. [CrossRef]
191. Joyce, B.T.; Gao, T.; Zheng, Y.; Ma, J.; Hwang, S.-J.; Liu, L.; Nannini, D.; Horvath, S.; Lu, A.T.; Bai Allen, N.; et al. Epigenetic Age Acceleration Reflects Long-Term Cardiovascular Health. *Circ. Res.* **2021**, *129*, 770–781. [CrossRef]
192. Levine, M.E.; Lu, A.T.; Quach, A.; Chen, B.H.; Assimes, T.L.; Bandinelli, S.; Hou, L.; Baccarelli, A.A.; Stewart, J.D.; Li, Y.; et al. An epigenetic biomarker of aging for lifespan and healthspan. *Aging* **2018**, *10*, 573–591. [CrossRef]
193. Kuo, C.-L.; Pilling, L.C.; Atkins, J.L.; Masoli, J.A.H.; Delgado, J.; Tignanelli, C.; Kuchel, G.A.; Melzer, D.; Beckman, K.B.; Levine, M.E. Biological Aging Predicts Vulnerability to COVID-19 Severity in UK Biobank Participants. *J. Gerontol. Ser. A* **2021**, *76*, e133–e141. [CrossRef]
194. Berezina, T.N.; Rybtsov, S. Acceleration of Biological Aging and Underestimation of Subjective Age Are Risk Factors for Severe COVID-19. *Biomedicines* **2021**, *9*, 913. [CrossRef]

International Journal of
Molecular Sciences

MDPI

Review

Theophylline: Old Drug in a New Light, Application in COVID-19 through Computational Studies

Luis M. Montaño [1], Bettina Sommer [2], Juan C. Gomez-Verjan [3], Genaro S. Morales-Paoli [3], Gema Lizbeth Ramírez-Salinas [4,5], Héctor Solís-Chagoyán [6], Zuly A. Sanchez-Florentino [6], Eduardo Calixto [7], Gloria E. Pérez-Figueroa [8,9], Rohan Carter [10], Ruth Jaimez-Melgoza [1], Bianca S. Romero-Martínez [1] and Edgar Flores-Soto [1,*]

1 Departamento de Farmacología, Facultad de Medicina, Universidad Nacional Autónoma de México, Ciudad de México 04510, CP, Mexico; lmmr@unam.mx (L.M.M.); jaimezruth@hotmail.com (R.J.-M.); biancasromero_@hotmail.com (B.S.R.-M.)
2 Laboratorio de Hiperreactividad Bronquial, Instituto Nacional de Enfermedades Respiratorias "Ismael Cosío Villegas", Ciudad de México 14080, CP, Mexico; bsommerc@hotmail.com
3 Dirección de Investigación, Instituto Nacional de Geriatría, Ciudad de México 10200, CP, Mexico; jver-jan@inger.gob.mx (J.C.G.-V.); mgenas.com@hotmail.com (G.S.M.-P.)
4 Laboratorio de Diseño y Desarrollo de Nuevos Fármacos e Innovación Biotecnológica (Laboratory for the Design and Development of New Drugs and Biotechnological Innovation), Escuela Superior de Medicina, Instituto Politécnico Nacional, Plan de San Luis y Díaz Mirón S/N, Col. Santo Tomas, Ciudad de México 11340, CP, Mexico; gemali86@hotmail.com
5 Departamento de Inmunología, Instituto de Investigaciones Biomédicas, Universidad Nacional Autónoma de México, Circuito Escolar s/n, Ciudad de México 14510, CP, Mexico
6 Laboratorio de Neurofarmacología, Instituto Nacional de Psiquiatría "Ramón de la Fuente Muñiz", Ciudad de México 14370, CP, Mexico; hecsolch@imp.edu.mx (H.S.-C.); zulyarmandosf@gmail.com (Z.A.S.-F.)
7 Departamento de Neurobiología, Dirección de Investigación en Neurociencias, Instituto Nacional de Psiquiatría "Ramón de la Fuente Muñiz", Ciudad de México 14370, CP, Mexico; ecalixto@imp.edu.mx
8 Instituto Nacional de Neurología y Neurocirugía, Unidad Periférica en el Estudio de la Neuroinflamación en Patologías Neurológicas, Ciudad de México 06720, CP, Mexico; gera.pfi3@gmail.com
9 Laboratorio de Investigación en Inmunología y Proteómica, Hospital Infantil de México Federico Gómez, Ciudad de México 06720, CP, Mexico
10 FRACGP/MBBS, Murchison Outreach Service Mount Magnet Western Australia, Mount Magnet, WA 6530, Australia; kingswood71@gmail.com
* Correspondence: edgarfs@comunidad.unam.mx; Tel.: +52-555-6232279

Abstract: Theophylline (3-methyxanthine) is a historically prominent drug used to treat respiratory diseases, alone or in combination with other drugs. The rapid onset of the COVID-19 pandemic urged the development of effective pharmacological treatments to directly attack the development of new variants of the SARS-CoV-2 virus and possess a therapeutical battery of compounds that could improve the current management of the disease worldwide. In this context, theophylline, through bronchodilatory, immunomodulatory, and potentially antiviral mechanisms, is an interesting proposal as an adjuvant in the treatment of COVID-19 patients. Nevertheless, it is essential to understand how this compound could behave against such a disease, not only at a pharmacodynamic but also at a pharmacokinetic level. In this sense, the quickest approach in drug discovery is through different computational methods, either from network pharmacology or from quantitative systems pharmacology approaches. In the present review, we explore the possibility of using theophylline in the treatment of COVID-19 patients since it seems to be a relevant candidate by aiming at several immunological targets involved in the pathophysiology of the disease. Theophylline down-regulates the inflammatory processes activated by SARS-CoV-2 through various mechanisms, and herein, they are discussed by reviewing computational simulation studies and their different applications and effects.

Keywords: theophylline; COVID-19; SARS-CoV-2; immunomodulatory effects; antiviral activity; molecular docking; network pharmacology; quantitative systems pharmacology

Citation: Montaño, L.M.; Sommer, B.; Gomez-Verjan, J.C.; Morales-Paoli, G.S.; Ramírez-Salinas, G.L.; Solís-Chagoyán, H.; Sanchez-Florentino, Z.A.; Calixto, E.; Pérez-Figueroa, G.E.; Carter, R.; et al. Theophylline: Old Drug in a New Light, Application in COVID-19 through Computational Studies. *Int. J. Mol. Sci.* **2022**, *23*, 4167. https://doi.org/10.3390/ijms23084167

Academic Editor: Evgenii Gusev

Received: 8 March 2022
Accepted: 4 April 2022
Published: 9 April 2022

1. Introduction

Theophylline (1,3-dimethyl-7H-purine-2,6-dione) is a dimethylxanthine derived from the xanthine purine base and composed of two methyl groups located at positions 1 and 3. Naturally, it is present in black tea (0.02–0.04% dry weight) [1,2] coffee (5 mg/kg) [3], chocolate, dried mate [4], and related foodstuffs [5]. Theophylline is rapidly and completely absorbed in the gastrointestinal tract after oral administration in solution reaching maximum serum levels around 1.5 and 2 h after intake. This alkaloid does not undergo any appreciable pre-systemic elimination, distributes freely into fat-free tissues, and is extensively metabolized in the liver involving at least two cytochrome P450 isozymes [6]. Theophylline serum half-life ranges from about 3 to 12.8 (average 7–9) h [7,8] and can be toxic in doses of 7.5 mg/kg or above [9]. Special consideration in the administration of theophylline must be taken in circumstances that can represent reduced drug clearance, for instance, in patients with liver or pulmonary disease (pneumonia, COPD) and heart failure. In contrast, an increased clearance can be expected in children <16 years and smokers [10]. Additionally, several drug interactions should be considered when theophylline is administrated, for example, decreased clearance in association with erythromycin, quinolones, allopurinol, cimetidine, serotonin uptake inhibitors, and the 5-lipoxygenase inhibitor zileuton, and a higher metabolism when administered in conjunction with phenytoin, phenobarbital, and rifampicin [10]. On the other hand, common side effects observed with theophylline treatment are headaches, gastrointestinal discomfort, insomnia, nausea, vomiting, and at higher doses, serious side effects such as seizures and cardiac arrhythmias, primarily due to antagonism of adenosine 1 receptor (A_1Rs), might develop. Low-dose, slow-release treatment seems to be well-tolerated in long-term treatments for COPD and asthmatic patients, reducing exacerbations and the probability of serious side effects [10,11].

The methylxanthines theophylline and dyphylline are used in the treatment of airway obstruction caused by clinical conditions such as asthma, infant apnea, chronic bronchitis, emphysema, and chronic obstructive pulmonary disease (COPD) [12,13] and have recently been proposed [14,15] and used as a supplement to treat coronavirus disease 2019 (COVID-19) patients [16–18]. Furthermore, recent studies have contributed to establishing theophylline's great therapeutic potential in the COVID-19 treatment. Wall et al. carried out a retrospective study on COVID-19 patients that required oxygen and received either theophylline or pentoxifylline. Patients with a history of asthma or COPD were given the former, and all other patients received pentoxifylline. Evaluations were done comparing C-reactive protein (CRP) concentrations and ROX score (defined as the ratio of oxygen saturation measured by pulse oximetry/FiO2 to respiratory rate) between a control group constituted by COVID-19 patients receiving standard medication and the group receiving xanthines from day 1 to day 4 of therapy, and results showed an increase in the ROX score (mean: 2.9) and a decrease in CRP (mean: −0.7) and mortality (24%) for the theophylline/pentoxifylline group. Even though it was a non-randomized study, the data obtained point out that this treatment could be associated with benefits for COVID-19 patients and warrants further research [16].

Additionally, Dahiya et al. reported the effects of theophylline or etophylline on sinus bradycardia, one of the most common arrhythmias found in COVID-19 patients. This symptom is possibly related to viral myocarditis, myocardial ischemia or might be a side effect of COVID-19 medication. Ten COVID-19 patients that developed sinus node dysfunction received etophylline or theophylline prolonged-release tablet (150 mg) once a day, and a normal heart rate was monitored 72 h after the treatment's initiation. Even though the studied population was small, it seems that if COVID-19 patients develop sinus bradycardia, a short lapse administration of either of these might be an effective treatment [18]. Theophylline relaxes smooth muscle and induces significant bronchodilation, provides a positive ionotropic effect, is a mild diuretic, and also shows cardiac and central nervous system (CNS) stimulant activities [10,19,20].

Theophylline´s relaxation of the bronchial smooth muscle and pulmonary blood vessels is mainly due to its activity as a phosphodiesterase inhibitor and adenosine receptor

antagonist. Additionally, it has been proven to be an effective anti-inflammatory and immunomodulatory agent [12].

The outbreak of COVID-19 in late December 2019 has brought significant harm and challenges around the world [21]. SARS-CoV-2 has four structural proteins: spike glycoprotein (S), small envelope glycoprotein (E), membrane glycoprotein (M), and nucleocapsid protein (N) that are re-sponsible for viral replication [22,23]. SARS-CoV-2 binds mainly to the angiotensin-converting enzyme 2 (ACE2) receptor to enter the cells, in a way like SARS-CoV; however, this process is facilitated by the proteolytic cleavage of the S protein´s receptor binding domain (RBD) by the transmembrane protease serine 2 (TMPRSS2) [22,24,25]. The RBD on the S protein of SARS-CoV-2 exclusively recognizes the ACE2 receptor on the host cell [24,25]. After entering the cell, the positive-sense viral RNA genome is released to the cell cytoplasm and translated and replicated forming progeny genomes and subgenomic mRNAs. The latter is translated to membrane proteins, protein N, and a variety of accessory proteins [24]. The synthetized membrane proteins (S, M, and E) are then incorporated into the rough endoplasmic reticulum (RER) and transferred to the endoplasmic reticulum-Golgi intermediate compartment (ERGIC). The N proteins and the genomic RNA simultaneously form nucleocapsids, which fuse at the ERGIC. Finally, the viruses are transported by vesicle to the plasma membrane and released out of the cell via exocytosis [16,22,26,27]. In severe COVID-19 cases, SARS-CoV-2 affects the lower respiratory tract and infects type II pneumocytes, leading to apoptosis and loss of surfactant and causing fatal pneumonia [28,29]. It has been described that the development of acute respiratory distress syndrome (ARDS) increases the chances of death in elderly patients, especially if they suffer from metabolic syndrome, type 2 diabetes mellitus, or other serious chronic diseases [22,28]; ARDS severity is related to acute lung damage and systemic microcirculatory abnormalities [28]. On the other hand, SARS-CoV-2 infection causes the phenomenon coined as "cytokine storm", which leads to the activation of macrophages and dendritic cells, as well as overproduction of cytokines in the center of COVID-19 classical general inflammation, increasing rapidly with pro-inflammatory tissue stress linked to systemic inflammation [28,30]. This issue is further described in subtopic 2.

Conceivably, the global spread of SARS-CoV-2 may continue for many months or years and will remain to have a serious impact on all human activities (health, social life, education, economy, etc.) [31,32]. The complexity and multifactorial characteristics of COVID-19 have encouraged different strategies to upgrade the clinical treatment of the disease. The use of social distancing, vaccines, antiviral drugs, and alternative clinical therapies has been paramount in preventing and treating COVID-19 in critically ill patients. Unfortunately, vaccinated people can still be infected by SARS-CoV-2, and too few antiviral treatments are available for COVID-19 patients. Therefore, the search for efficient treatments and beneficial dietary supplements continues to be an essential strategy in the fight against COVID-19 [33].

In this sense, we propose that the use of theophylline may provide health benefits against SARS-CoV-2, mainly through its bronchodilatory, immunomodulatory, anti-inflammatory, and antiviral effects proposed through in silico studies.

2. Immune Response in COVID-19 Patients

The immune response is induced by the presence of the virus detected by the host cell through pattern recognition receptors (PRR): Toll-like receptors (TLR), gene-I proteins inducible by retinoic acid (RIG-I), and NOD-like receptors (NLR) and other cytosolic viral sensors. When activated via adapter proteins, TLRs (primarily TLR3 and TLR7) activate the interferon regulatory factors (IRF3, IRF7) and a pro-inflammatory nuclear transcription factor (NF-κB). Consequently, the production and release of type I and III interferons (IFN-α/β and λ) are initiated, while NF-κB mediates the transcription of adhesion molecules, chemokines, colony-stimulating factors, and other cytokines that participate in the inflammatory response, including molecules that initiate neutrophil recruitment (Figure 1) [28,34–38].

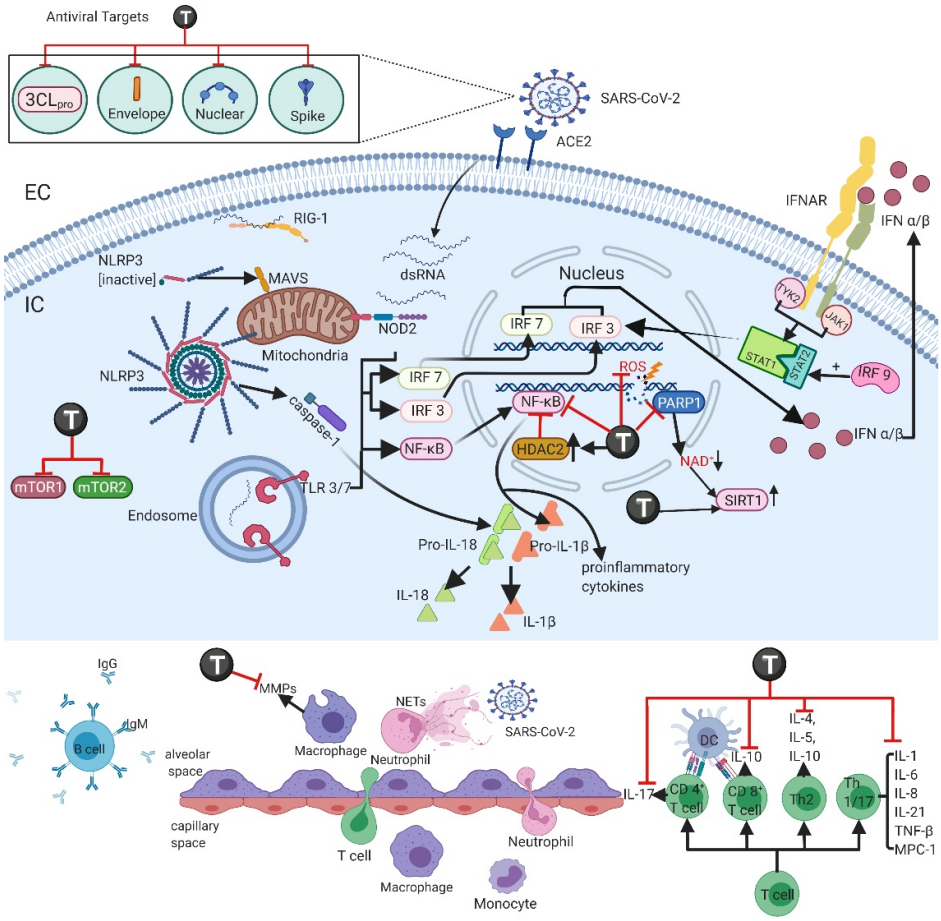

Figure 1. SARS-CoV-2 enters the cell through ACE2 found in the membrane of type II pneumocytes. The immune response is initiated through the activation of PRRS (TLR, NLR, RIG-1) located in the membrane and cytosol interacting with the viral RNA. The stimulation of these receptors leads to the activation of transcription regulating factors such as IRF 3/7 and NF-kB, which leads to the production of interferons type I/III and other pro-inflammatory cytokines. Theophylline modulation of HDAC2 inhibits NF-kB and inflammatory genes. DNA damage produced by ROS production activates PARP1, which leads to NAD^+ depletion, decreasing SIRT1 activity. Theophylline inhibits PARP1, decreases ROS production, and enhances SIRT1 expression and activity. mTOR inhibition by theophylline contributes to attenuating the inflammatory response. The production of these cytokines initiates the recruitment of neutrophils and recruitment and differentiation of monocytes into alveolar macrophages. The cytokine storm microenvironment produced as a result of the viral infection stimulates the activation and differentiation of cytotoxic $CD8^+$ and helper $CD4^+$ T cells necessary for viral clearance, initiating the production of cytokines, recruitment of monocytes and neutrophils, promoting the immune response. The proposed antiviral effects of theophylline are highlighted. In order to successfully limit the viral infection in later phases of the disease and to prevent future reinfections, the participation of the humoral response and production of antibodies is needed. Abbreviations: T—theophylline; PRRs—pattern recognition receptors; TLR—Toll-like receptors; RIG-1—gene-I proteins inducible by retinoic acid; NLR—NOD-like receptors; IRF 3/7—interferon regulatory factors; NF-κB—pro-inflammatory nuclear transcription factor; HDAC2—histone deacetylase 2; ROS—reactive oxygen species; PARP1—poly ADP ribose polymerase 1; SIRT1—sirtuin 1; mTOR—mechanistic target of rapamycin pathway; MMPs—matrix metalloproteinases.

Type I IFNs activate the JAK/STAT signaling pathway through IFNAR so that JAK1 and TYK2 kinase phosphorylate STAT 1 and 2. A complex among STAT 1/2 and IRF9 (the ISFG3 transcription factor) is formed and translocates to the nucleus to initiate transcription of IFN-stimulated genes. An effective type I IFN response in the early stages suppresses

viral replication and its spread; during SARS-CoV and MERS-CoV infection, this response is suppressed, and its inactivity is associated with the severity of the disease [22,34,37,38]. Many SARS-CoV-2 proteins (nsp1, nsp3, nsp5, nsp6, nsp9, nsp13, nsp14, nsp15, orf3b, orf6, orf9b, N, and M) have been identified to inhibit this signaling pathway at different points, hindering a proper type I IFN response [22]. These proteins inhibit IRF3 by blocking its nuclear translocation and phosphorylation, consequently impeding IFNs synthesis in ribosomes and their transport to the membrane. They also diminish ISG nuclear translocation and ISGF3 complex formation and block several points of the IFN I-III/IFN-R (Tyk2, Jak1)/ISGF3 (STAT1, STAT2, IRF9)/ISG signaling pathways [22]. During SARS-CoV or MERS-CoV infection, a delay in the IFN type I inflammatory response, essential in early viral control, is observed, causing an exaggerated inflammatory response by neutrophils and macrophages. In SARS-CoV-2 infection, transmission can occur even through asymptomatic individuals, probably due to a delay in the innate immune response and corresponding to the main cause of fatality in severe acute respiratory syndrome [37]. It is also known that, in the cytosol, free viral RNA induces a conformational change in the RIG-I receptor, thus interacting with mitochondrial antiviral signaling proteins (AVMs) in the epithelium and with NLR receptors in myeloid cells to activate inflammasomes. In this sense, NLRP3 activation leads to the production of IL-1β and IL-18 dependent on caspase 1 [22,35]. In SARS-CoV-2 infection, the N protein and Orf3a both activate NLRP3, contributing to augmenting the inflammatory response (Figure 1) [22].

Alveolar macrophages respond promptly to a viral threat through phagocytosis of opsonized viral particles or apoptotic infected cells (efferocytosis) and/or through the production and release of inflammatory cytokines. Type I IFNs released through pathways described previously induce recruitment and differentiation of circulating precursor monocytes to alveolar macrophages and dendritic cells (Figure 1) [34,35,37].

In SARS-CoV-2, a phenomenon known as "cytokine storm" frequently develops and is characterized by a high production of pro-inflammatory cytokines that play an important role in the pathophysiology of the infection. Circulating cytokines found during the cytokine storm are IL-2, IL-4, IL-6, IL-7, IL-10, TNF-α, IFN-γ, IP-10, MCP-1, MIP-1A, granulocyte colony-stimulating factor (G-CSF), and granulocyte macrophage CSF (CG-CSF) [22,37–39]. Circulating levels of these cytokines are associated with greater morbidity during the infectious process. It has been established that IL-6 promotes the recruitment, differentiation, and activity of monocytes and T cells; in COVID-19 patients, an elevation in its circulating concentration was reported in 52% of the cases studied [37,40,41]. On the other hand, it has been described that TNF-α increases cytotoxic activity, leukocyte cytokine production, and endothelial cell activity (Figure 1) [35,40].

Neutrophils are among the first immune cells to respond to an infectious threat. They engulf virions and viral particles that are inactivated by proteolytic enzymes, antimicrobial peptides, and reactive oxygen species (ROS), and they also secrete granules with antimicrobial peptides. Interestingly, neutrophils release extracellular neutrophil traps (NETs) that immobilize pathogens and prevent their further spread. Although these mechanisms are helpful in mitigating infection, an excessive neutrophilic response can harm the host and lead to further lung damage (Figure 1) [34,36,38].

The innate immune response is the first defense mechanism activated. However, to complete viral clearance, stop viral replication, and effectively eliminate viral infection, the antiviral response and the adaptive immune response are necessary. The microenvironment created by the cytokine storm stimulates the differentiation and maturation of $CD8^+$ cytotoxic T cells and $CD4^+$ helper T cells [22,35,37,38,42]. In SARS-CoV and SARS-CoV-2 infection, the depletion of $CD4^+$ T cells is associated with a reduction in the recruitment of lymphocytes, and of neutralizing and cytokine-producing antibodies, resulting in delayed viral clearance and strong immune-mediated interstitial pneumonitis [22,38]. $CD4^+$ T cells also produce interleukins via NF-κB, especially IL-17, which recruits monocytes, neutrophils, the differentiation of Th17, and the production of cytokines and chemokines such as IL-1, IL-6, IL-8, IL-21, TNF-β, and MCP-1 [22,38]. Th17 participation in the pathogenesis

of SARS-CoV-2 infection, especially in severe patients presenting a lower Treg/Th17 ratio, indicates that it negatively regulates Treg cells, promotes neutrophil migration and Th2 response, all these circumstances leading to an exaggerated immune response causing tissue damage and edema among the main complications of the disease (Figure 1) [22,43,44].

To limit infection in late stages and prevent reinfection in future times, the participation of the humoral immune response is required. In SARS-CoV infection, seroconversion is induced even as early as the fourth day of the infection onset, but in most patients, this response is evident by day 14. In preliminary studies in a patient with SARS-CoV-2, a specific IgM peak was observed on day 9 after the onset of the disease, changing to IgG predominance by the second week. A strong T-cell response correlated with higher neutralizing antibodies; however, a plasmatic Th2 cytokine pattern (IL-4, IL-5, IL-10) was observed in the group with higher lethality [22,37]. In severe cases of COVID-19, elevated levels of plasmatic CCR6+ Th17 were detected, indicating that the Th17 response is favored resulting in a pro-inflammatory response that might prompt pulmonary edema. Disproportionate elevation of the Th17 response is also observed in MERS-CoV and SARS-CoV infected patients [22,41,43,44]. Currently known memory T-cell responses against SARS-CoV are directed at structural proteins (such as the S, M, and N proteins). These responses last a long time, and the strongest reactions are directed against the spike protein [38,41]. Additional mechanisms activated during the response to SARS-CoV-2 and their potential as therapeutic targets are still unknown (Figure 1).

3. Immunomodulatory Effects of Theophylline

Theophylline is a well-known anti-inflammatory that exerts its effects through various mechanisms, with a notable history in the treatment of respiratory diseases with a strong inflammatory component, such as asthma and chronic obstructive pulmonary disease (COPD) and could therefore be beneficial in the treatment of COVID-19. In this sense, theophylline has been reported to have several interactions with different molecular targets (Figures 2 and 3), that interact differently with several immunological routes once such targets are reached (Table 1).

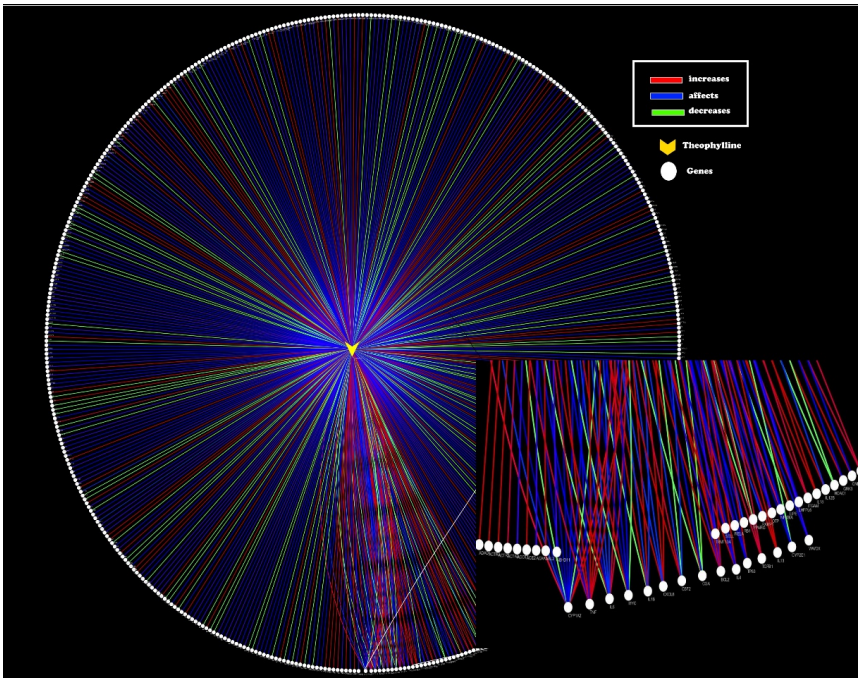

Figure 2. Pharmacological network biology analysis of theophylline-genes interaction. Node in yellow represents theophylline and white nodes represent genes that are modified to different degrees: somehow affected (blue), increased (red) or decreased activity (green) according to the Comparative Toxicogenomics Database [45].

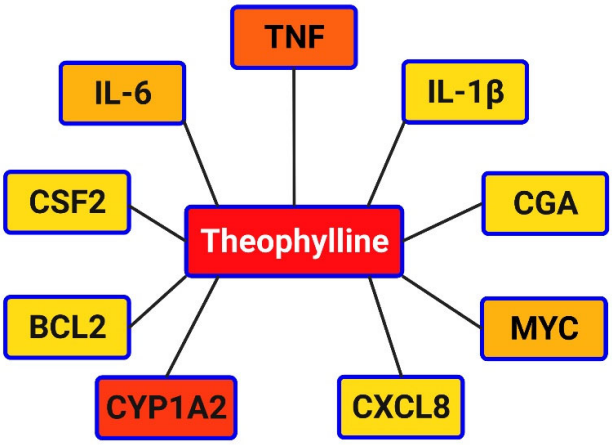

Figure 3. Network result from the most connected nodes. Color shades represent connection degrees from most connected (yellow) to less connected (red).

Table 1. Enrichment analysis of pathways altered by theophylline in humans.

Pathway	Pathway ID	Annotated Genes Quantity
Interleukin-10 signaling	REACT:R-HSA-6783783	10
Immune system	REACT:R-HSA-168256	45
Metabolism of proteins	REACT:R-HSA-392499	38
Interleukin-4 and 13 signaling	REACT:R-HSA-6785807	12
IL-17 signaling pathway	KEGG:hsa04657	11
NOD-like receptor signaling pathway	KEGG:hsa04621	13
Cytosolic DNA-sensing pathway	KEGG:hsa04623	9
Post-translational protein modification	REACT:R-HSA-597592	28
Inflammatory bowel disease (IBD)	KEGG:hsa05321	9
Jak-STAT signaling pathway	KEGG:hsa04630	12
Jak-STAT signaling pathway	KEGG:hsa04630	8
AGE-RAGE signaling pathway in diabetic complications	KEGG:hsa04933	7
Signaling by interleukins	REACT:R-HSA-449147	12
Longevity regulating pathway-multiple species	KEGG:hsa04213	6
Transcriptional misregulation in cancer	KEGG:hsa05202	8
Diseases of signal transduction	REACT:R-HSA-5663202	10
Cytokine signaling in immune system	REACT:R-HSA-1280215	27
Signaling by interleukins	REACT:R-HSA-449147	24
Innate immune system	REACT:R-HSA-168249	32
Interleukin-4 and 13 signaling	REACT:R-HSA-6785807	15
Cytokine-cytokine receptor interaction	KEGG:hsa04060	15
IL-17 signaling pathway	KEGG:hsa04657	11
Hematopoietic cell lineage	KEGG:hsa04640	11
Signal transduction	REACT:R-HSA-162582	33

In this context, several activities related to the immunological context of theophylline in humans and the importance in the treatment of COVID-19 must be mentioned.

3.1. Cytokine Inhibition

In COPD patients, continuous treatment with theophylline to maintain plasma levels of 9–11 mg/L for a 4-week period demonstrated a significant reduction in total inflammatory cells, predominantly in neutrophils, and lowering of IL-8, myeloperoxidase, and lactoferrin [46]. Additionally, theophylline produced a reduction in neutrophil chemotaxis induced by N-formyl-met-leu-phe and IL-8 [46]. This was also observed in airway smooth muscle cell cultures, where theophylline (10 μM) decreased TNF-α-induced IL-8 secretion via enhancing TNF-α-induced PP2A enzymatic activity [47]. Furthermore, the addition of low-dose theophylline (LDT) decreased IL-8 and IL-6 production in COPD patients

with lung fibrosis [48] and enhanced the anti-inflammatory effects of standard steroids treatment by further decreasing IL-8 sputum levels in COPD patients [49]. In the long-term theophylline treatment in COPD patients (12 months), IL-8, TNF-α, and neutrophil sputum levels were progressively reduced [50]. In human peripheral blood mononuclear cells (PBMCs), theophylline treatment significantly reduced IL-1β and TNF-α production, but not IL-8 production induced by lipo-polysaccharide (LPS) or recombinant human IL-1β. The lack of effect on IL-8 production could be limited to this cell group since it is not consistent with other studies [51]. In atopic asthmatics, theophylline at 150 mg daily for 3 weeks reduced circulating serum levels of IL-4 and IL-5 [52]. In PBMCs from asthmatic children stimulated with house dust mite, theophylline at 20 μg/mL significantly reduced IL-5 and IL-3 production and lymphocyte proliferation [53]. Not only is theophylline able to inhibit IL-5 production, but it can also inhibit IL-5 induced degranulation in eosinophils, having a synergic effect when used in combination with procaterol (a β-adrenergic agonist) (Figure 1) [54].

An additional mechanism through which theophylline inhibits TNF-α-induced activation of NF-κB in a dose-dependent manner preventing the translocation of the transcription factor into the nucleus is by protecting the IκBα protein from degradation [55–57]. The resultant inhibition of the NF-κB pathway causes the suppression of pro-inflammatory cytokines, including TNF-α, IL-8, and GM-CSF [57]. The NF-κB and the p38 mitogen-activated protein kinases (MAPK) pathway are also regulated through the activity of dual-specificity phosphatases (DUSPs) [58]. Both DUSP1 and DUSP5 overexpression can inhibit p38 MAPK, and DUSP5 can also inhibit NF-κB [58–60]. Moreover, in COVID-19 patients, high levels of DUSP1 and DUSP5 have been detected, especially in severe cases [58]. It is possible that theophylline administration to COVID-19 patients increases the expression of DUSP1 and DUSP5 [58] to such an extent that they contribute to the treatment of the illness.

On the other hand, theophylline's anti-inflammatory effects are also partially due to the increase in an anti-inflammatory cytokine (IL-10) secretion observed in asthmatics and COPD patients (Figure 1) [61,62].

3.2. Histone Deacetylase 2 Modulation

Another anti-inflammatory effect of theophylline is as a histone deacetylase (HDAC) activator. HDACs are a superfamily of enzymes that deacetylate histones to regulate gene expression [63,64]; specifically, HDAC2 modulates the inflammatory response in macrophages and monocytes by inhibition of NF-κβ, suppressing inflammatory genes and proteins (IL-8, GM-CSF) [63,64]. The effect of theophylline over HDAC2 is achieved at low doses (plasma concentration of 5 mg/L) [63–65]. In many respiratory diseases, including COPD, asthma, and viral infections such as by influenza A virus, the activity of HDACs is compromised [63,64,66]. Other components that decrease HDAC2 activity are reactive oxygen and nitrogen species (ROS and RNS), which are prominent in the inflammatory process of these diseases [67,68]. The mechanism by which theophylline regulates HDAC2 activity is by inhibiting oxidant-activated phosphoinositide-3-kinase-delta (PI3K-δ) [69]. In part, theophylline and other phosphodiesterase inhibitors (PDEIs) have been demonstrated to be HDAC2 modulators, which could be linked to IL-8, TNF-α, and ROS and RNS production since HDAC2 levels are linked to these [48,64,65,70]. As mentioned above, theophylline regulates IL-8 and TNF-α production and can also directly modulate ROS production in human monocytes via PDEI [71]. Through computational methods, cellular targets for SARS-CoV-2 miRNAs were identified. Among the targets, HDAC2 was identified to be the target for SARS-CoV-2-mir-D10-5p and SARS-CoV-2-mir-D6-3p. As an HDAC2 activator, theophylline might be influencing this pathway (Figure 1) [72].

3.3. Matrix Metalloproteinases Suppression

Matrix metalloproteinases (MMPs) are a family of Zn^{2+} and Ca^{2+} dependent proteolytic enzymes that participate in tissue remodeling through the ability to degrade

extracellular and membrane basement components. They are secreted by numerous cells (inflammatory cells, epithelial cells, stromal cells, fibroblasts, etc.) [73–75]. The dysregulation of MMPs can be linked to a variety of diseases, and therefore, the identification of elements that could alter MMP activity is of great interest. Many inflammatory components participate in the regulation of MMP activity, including inflammatory cytokines (IL-1β, IL-6, TNF-α, and IFN-γ), ROS, and RNS [73,76]. MMPs' participation in many respiratory diseases has been described, including tissue remodeling and acute lung injury [73–75]. Recently, an association between higher plasmatic MMP-2 and MMP-9 levels and COVID-19 severity was found, and it has even been proposed as a potentially accurate prognosis factor [77]. In human lung fibroblast, theophylline treatment can inhibit RNS-induced MMP-2 and MMP-9 release via the NF-κβ/TGF-b1 pathway and probably through HDCA2 activity as well [65]. Theophylline suppression of MMPs could be an additional therapeutic mechanism that might benefit COVID-19 patients (Figure 1).

3.4. SIRT1 Activation

The overactivation of PARP1 quickly causes NAD^+ depletion [78–80]. NAD^+ is involved in multiple metabolic processes as a cofactor, catalyzing electron transfer in metabolic reduction-oxygenation reactions, such as ATP production. Its lack or significant reduction could cause an energy crisis that would lead to cell apoptosis [78–80]. NAD^+ depletion could also lead to decreased sirtuin 1 (SIRT1) activity [78–80]. SIRT1 is an NAD^+-dependent deacetylase of nuclear proteins that regulates gene expression cytokines, tumor suppressors, and proto-oncogenes and modulates inflammatory processes, cell survival, and apoptosis [78–80]. COVID-19 pathophysiology includes not only increased ROS production that leads to depletion of NAD^+ but also decreased expression of SIRT1 [78–81]. PARP-1 activation and SIRT1 downregulation are important players in the inflammatory processes of many pulmonary diseases such as COPD, asthma, and some viral infections and have now been described in SARS-CoV-2 [78–82]. In human pulmonary epithelial cells, theophylline treatment inhibited PARP-1, preventing NAD^+ depletion [78], and in COPD patients, treatment with prednisolone together with theophylline increased SIRT1 expression [82,83]. Seemingly, targeting PARP-1 and SIRT1 with theophylline could also be beneficial in the treatment of COVID-19 patients (Figure 1).

3.5. mTOR Signaling Inhibition

Another prominent drug target gaining interest in the pathophysiology of COVID-19 is the mechanistic target of rapamycin (mTOR) pathway. mTOR is a serine/threonine protein kinase involved in the regulation of numerous intracellular processes, for instance, cell metabolism, proliferation, growth, and survival [84–86]. In order to exert its activity, mTOR binds to the multiprotein complexes mTOR complex 1 and complex 2 (mTORC1 and mTORC2); each complex participates in distinct signaling functions [84–86]. mTOR pathway has been characterized in immune cells. It is known that activation of mTORC1 controls IL-15-activated NK cell cytotoxicity and controls BCL6 expression to control B cells in the germinal line [84]. Inhibiting mTORC1 enhances dendritic cells' T-cell stimulatory activity and autophagy of macrophages and reduces antigen-specific memory B cell population after B cell activation [84]. In some severe cases of COVID-19, it was speculated that prior to exposure to other coronaviruses and because of antigenic epitope heterogeneity, antibody-dependent enhancement (ADE) could have developed [84,87]. Enhancement has been previously described in SARS-CoV, caused by the development of anti-spike protein antibodies, causing the infection of immune cells [84,87–89]. In the early stages of COVID-19 infection, blocking the activation of memory B cells through mTOR inhibitors could reduce cross-reactive antibodies to SARS-CoV-2 and mitigate the more severe symptomology [84]. On the other hand, mTORC2 regulates neutrophil and mast cells' chemotaxis and cell polarity [84]. Furthermore, the activation of the inflammasome NLRP3 and macrophage pyrosis is regulated through both mTORC1 and mTORC2 [90]. The mTOR pathway has been shown to be modulated through the increment in intracellu-

lar levels of cAMP [85,91,92]. The inhibition of mTORC1 seems to be mediated by cAMP via a PKA or PKB-dependent mechanism since cAMP activates the negative regulator of mTORC1, TSC1/2 [91,92]. This mechanism is not solely responsible for mTORC1 inhibition but can also be regulated by cAMP disturbing mTOR and Rheb co-localization through a Rag GTPase-dependent mechanism without the involvement of TSC1/2 [92]. Additionally, prolonged elevation of cAMP leads to mTORC2 inhibition and decreased activity of mTOR (Figure 1) [92].

Another concern of the mTOR pathway in the pathophysiology of SARS-CoV-2 is its participation in the viral life cycle. Viruses hijack the host cells transcription and translation machinery during its life cycle and mTOR is known to contribute to both DNA and RNA virus replication by acting on phosphoinositide 3-kinase (PI3K), Akt, or even mTOR directly [86,93]. Theophylline, by producing cAMP increments, activates PKA and PKB, inhibiting mTOR [91]. The inflammatory attenuation produced by mTOR signaling inhibition, as well as the interruption of the viral replication, are promising mechanisms of action of theophylline that might contribute to the treatment of SARS-CoV-2 pathophysiology (Figure 1).

4. In Silico Screening of Theophylline: Therapeutic Targets and Potential Agents

Recently published works have suggested theophylline´s potential antiviral activity using in silico molecular dynamics and molecular docking, and therefore originally performed studies are included herein. In silico studies to predict whether a ligand (drugs, biomolecules, or plant-derived compounds) can produce the expected biological effect are mainly done by structure-based drug design methods. Among the most used methods, we find the molecular docking and molecular dynamics simulation techniques [94,95]. Such techniques are widely used due to the range of applications in the analysis of molecular recognition events, such as binding energy, molecular interactions, and induced conformational changes [94]. To determine if theophylline is a feasible candidate to be used in the treatment against COVID-19, it was analyzed using structure-based techniques. Studies exploring this subject have analyzed the interactions of theophylline with different protein targets, for instance, the chymotrypsin-like protease protein (3CLpro) and the nucleocapsid protein (N) [15,96]. The interaction between the spike protein and ACE2 has gained particular interest for its potential to be used as a pharmacological target and has inspired the exploration of caffeine, another methylxanthine, as a possible pharmacological tool [13,97]. To expand the knowledge in this regard, we performed in silico experiments exploring the interaction of theophylline´s affinity for spike and envelope proteins. Original results from our team are shown in section theophylline affinity with spike and envelope proteins.

4.1. 3CLpro and Theophylline

The 3CLpro protein is a cysteine protease comprised of three domains and generates functional polypeptides playing an important role in viral transcription and replication. The active sites of 3CLpro are S1′, S1, S2, and S4 and are highly conserved in different coronaviruses such as MERS-CoV, SARS-CoV, and SARS-CoV-2 [98]. For the catalytic function of 3CLpro, the following amino acids are essential: Cys145, Glu166, and His41 [14]. Furthermore, there is no closely related homolog of 3CLpro in humans, making it an attractive target for innovative anti-COVID-19 drugs (Figure 1) [98].

In 2022, through molecular docking and molecular dynamics simulations, Elzupir et al. studied the interaction of bromotheophylline, pentoxifylline, and theophylline with the 3CLpro protein of the SARS-CoV-2 virus. These drugs formed a hydrogen bond with key residues for the inactivation of the 3CLpro protein; bromotheophylline and theophylline bound to amino acid Glu166, while pentoxifylline bound to Cys145. Theophylline forms a hydrogen bond with Glu166 and also establishes van der Waals forces with the amino acids Glu166, Cys145, and His41 [15]. Additionally, by means of molecular dynamics methods, the stability of the complexes between the 3CLpro protein and bromotheophylline, pen-

toxifylline, and theophylline was verified [15]. This study shows that theophylline and its derivatives are possible inhibitors of the enzymatic activity of the 3CLpro protein (Figure 1).

4.2. N-Protein and Theophylline

The N-protein conforms to the RNA package and participates in the release of viral particles. It contains two RNA-binding domains: the N-terminal domain (NTD) and the C-terminal domain (CTD), linked by a serine/arginine-rich domain (SRD) [99]. Due to the positively charged amino acids, the CTD and NTD domains bind to the viral RNA genome, and, in addition, the SRD improves the oligomerization capacity [99]. It has been shown that the N-protein promotes the activation of the NLRP3 inflammasome to induce hyperinflammation, facilitating the maturation of pro-inflammatory cytokines and aggravating lung lesions [100]. Several different inhibitors of this protein have been studied, and the interaction between N-protein and theophylline has been analyzed. In this context, Sarma et al. evaluated different bronchodilators able to inhibit the binding of viral RNA to the NTD of N-protein using in silico techniques and established that theophylline stably binds to the site that inhibits the interaction between RNA and protein N (Docking score: −3.763 kcal/mol and MM-GBSA −39.464 kcal/mol) [96]. Furthermore, they found that a derivative of theophylline (ZINC3118440) is a plausible inhibitor of the NTD site of the N-protein (Figure 1) [96].

4.3. Theophylline Affinity with Proteins Spike and Envelope

Our team performed molecular docking to predict the binding affinity between theophylline and two pharmacological targets, the S and E proteins.

Docking directed to sites of interest was carried out. In the case of the spike protein, the RBD binding site was explored, and for protein E, the affinity and mode of binding to this ion channel were predicted. The following (Figure 4) shows the binding modes of theophylline with the spike protein (Figure 4A) and protein E (Figure 4B). The delta G between the spike protein and theophylline was −5.4 kcal/mol, and Figure 4A illustrates that the binding is formed by four hydrogen bonds with amino acids Arg493B, Phe377A, Thr376A, and Phe375A, plus a Pi–Pi stacked interaction with Phe377A and Van de Waals forces with Phe456B, Tyr489B, Phe490B, and Ala484B. The structure and conformation of the spike protein that has been used to carry out the binding prediction belongs to the 7WK3 crystal that corresponds to the open conformation of the Omicron variant. According to molecular docking, theophylline is capable of binding to the spike protein of the Omicron variant.

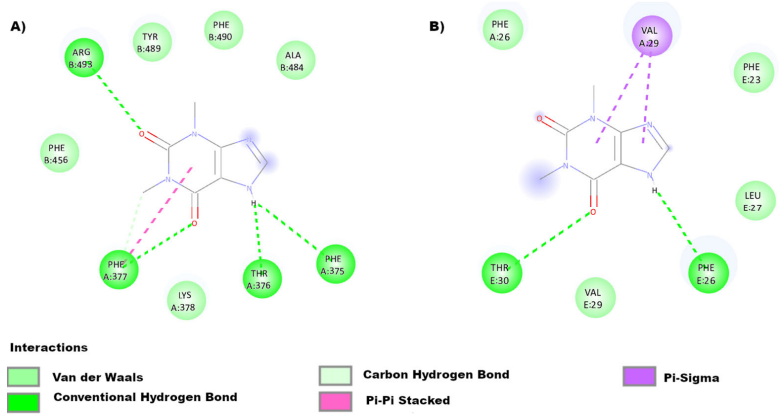

Figure 4. Molecular docking between theophylline and SARS-CoV-2 proteins (spike and protein E). In both couplings, we observe Van der Waals forces. (**A**) The interactions between theophylline and the spike protein show 4 hydrogen bonds and a Pi–Pi stacked interaction. (**B**) The relation with the E protein has Pi–sigma interactions and two hydrogen bonds. Molecular docking of protein E with theophylline showed that the delta G was −5.0 kcal/mol. (**B**) illustrates that the xanthine binds to amino acids Phe23E, Phe26A, Phe26E, Leu27E, Val29A, Val29E, and Thr30E (methodology in Supplementary Materials [101–103]).

In this sense, we may conclude that the spike protein and protein E are of pharmacological interest since they are the main structural proteins of the SARS-CoV-2 virus that participate in mechanisms of the viral cycle and are also involved in the inflammatory processes [95,104]. Interestingly, theophylline binds to amino acid Ala484, a mutation (E484A) found in the Omicron variant responsible for the greater resistance to neutralization by Bamlanivimab shown by this variety [105]. Theophylline also binds to amino acids close to Val25, responsible for inhibiting the ion channel function and oligomerization (Figure 1) [106,107]. Recently, in silico studies conducted by Rolta et al. showed an interesting binding affinity between caffeine, methylxanthine, theobromine, and theophylline with SARS-CoV-2 spike protein and S1 receptor-binding domain (S1RBD). Theoretically, all the above-mentioned phytocompounds could potentially prevent the binding of SARS-CoV-2 to the ACE2 receptor, sensibly diminishing the virus's infectious capacity. Notwithstanding these promising results, these methylxanthine derivatives must be probed in vitro and in vivo to confirm their therapeutic benefits against SARS-CoV-2 [108].

5. Quantitative-Systems Pharmacology Analysis

Theophylline plasma concentrations of 10–20 μg/mL are therapeutically relevant, with maximal bronchodilatory effects observed at 10 μg/mL [10,109,110]. Nevertheless, the anti-inflammatory effects of theophylline develop at lower doses, around 5–10 μg/mL [10,109,110]. To avoid unwanted side effects the range can be narrowed to 5–15 μg/mL, even though toxicity might be observed at concentrations as low as 15 μg/mL [10,109,110].

In this context, using PK-Sim (v 8.0) [111], we performed a quantitative-systems pharmacology (QSP) analysis where we simulated two scenarios: the first one was a healthy patient (>70 years old) that received two different doses of theophylline intravenously (IV), and the second was a patient with severe renal impairment (glomerular filtration rate [GFR] = 5 mL/min/100 g organ) [112] that also received theophylline (Figures 5 and 6).

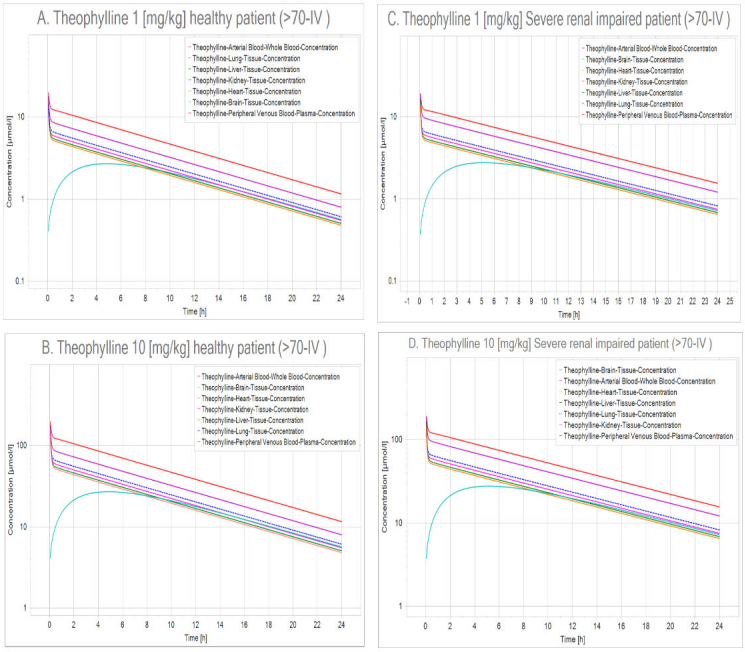

Figure 5. Physiologically based pharmacokinetic model (PBPK) simulation of theophylline at two concentrations modeled in a healthy patient and a patient with renal impairment. (**A**) Healthy patient dosed with 1 mg/kg, (**B**) Healthy patient that received 10 mg/kg, (**C**) Renal impaired patient administered 1 mg/kg. (**D**) Renal impaired patient dosed with 10 mg/kg. When results of the healthy patient were compared with those of the renal insufficiency patient, a slight increase in the time of theophylline body retention was observed in all organs studied (clearance reduction). Tissue concentration curves for the lungs (dotted blue curves) illustrate that the longest time for theophylline removal takes place in this tissue (Supplementary Materials Table S1).

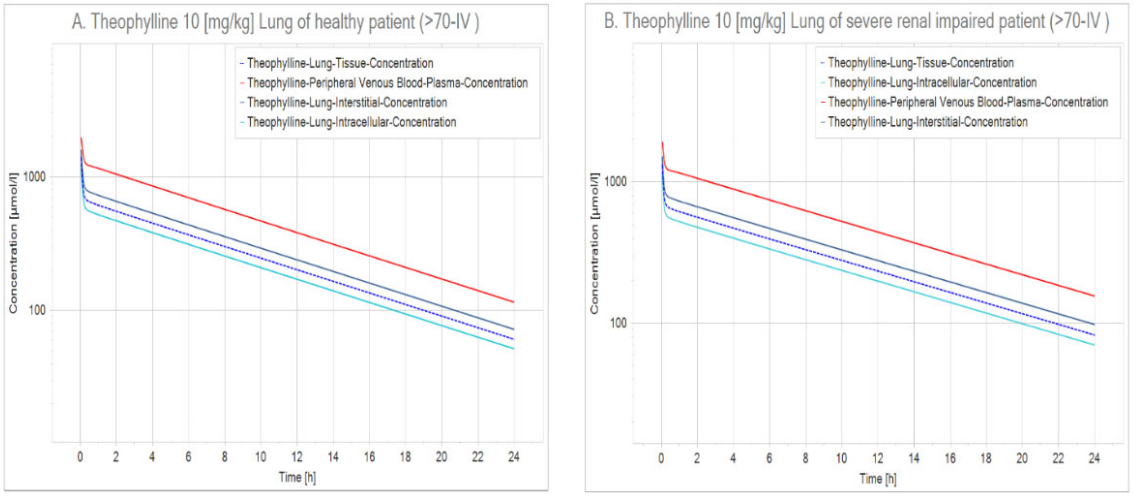

Figure 6. Physiologically based pharmacokinetics model (PBPK) simulation of 10 mg/kg theophylline in the lungs. (**A**) Kinetics in the lung of a healthy patient. (**B**) Kinetics in the lung of a patient with renal impairment. This figure shows that theophylline clearance is sensibly delayed in patients with impaired renal function. When comparing both charts, a decrease in the inclination of the lung concentration curves can be observed for the patient with renal failure. Noteworthy, renal elimination is the main route to excrete theophylline and consequently, a reduced clearance increases the time the drug remains in the body increasing the possibility of unwanted side effects (Supplementary Materials Table S2).

Massive albuminuria and subsequent development of proteinuria seen in SARS-CoV-2 show that renal involvement is common in this illness; it has been established that renal damage ranges from mild proteinuria to advanced acute kidney injury. SARS-CoV-2 binds to ACE2 receptors in many organs of the body, especially the proximal tubules of the kidney that have more ACE2 receptors than the lungs. Therefore, the virus has a great impact on the renal tubules [113], thus hindering theophylline clearance, leading to intoxication and aggravating existing renal failure that may lead to death. Notwithstanding, theophylline reaches therapeutic levels in peripheral blood during the first hours of administration, and the lung is one of the first organs reached by this methylxanthine. In this sense, theophylline seems to be at the interstisium during the first hours after administration, probably indicating that, if renal failure were present, it might be overcome before theophylline's toxic effects become risky.

6. Conclusions

Theophylline seems to be a relevant candidate for the treatment of COVID-19 patients since it aims several immunological targets involved in the pathophysiology of the disease. Through various mechanisms theophylline down-regulates the overactivation of the inflammatory processes activated by SARS-CoV-2. Additionally, it might have antiviral potential that could hinder the pathogenesis of the virus. Considering that many viral respiratory infections mount a similar host immune response [34,35], as was the case with the influenza, SARS-CoV, MERS or SARS-CoV-2 viruses; therefore, theophylline should be under consideration as a prime candidate in the drug discovery process for any future viral pathogens. Furthermore, COVID-19 is now also known to have long lasting clinical presentation, such as with "long-haul" cases [25,114–116], extending past the acute infection phase, and theophylline has proven to be effective in the chronic management of respiratory diseases, particularly those with an inflammatory component, such as asthma and COPD, and could also be repurposed for this case. Theophylline, offering multiple advantages with a known clinical use and an affordable price, should not be overlooked in the search for potential treatments for COVID-19 patients.

Supplementary Materials: The following supporting information can be downloaded at: https://www.mdpi.com/article/10.3390/ijms23084167/s1.

Author Contributions: Conceptualization, E.F.-S. and R.C.; investigation, G.S.M.-P., H.S.-C., Z.A.S.-F., E.C., G.E.P.-F., R.J.-M. and B.S.R.-M.; data curation, J.C.G.-V. and G.L.R.-S.; writing—Original draft preparation, E.F.-S., R.C. and B.S.R.-M.; writing—Review and editing, E.F.-S., B.S. and L.M.M.; supervision L.M.M.; funding acquisition, L.M.M. All authors have read and agreed to the published version of the manuscript.

Funding: This study was partly supported by grants from the Dirección General de Asuntos del Personal Académico (DGAPA), the Universidad Nacional Autónoma de México (IN204319, IN200522) and CONACYT (137725) to L.M. Montaño.

Institutional Review Board Statement: Not applicable.

Informed Consent Statement: Not applicable.

Data Availability Statement: Not applicable.

Acknowledgments: Bianca S. Romero-Martínez is grateful to the Programa de Doctorado en Ciencias Biomédicas, Universidad Nacional Autónoma de México, for the instruction received during her Ph. D. degree studies. She received a fellowship from the Consejo Nacional de Ciencia y Tecnología, México (application # 2020-000013-01NACF-12778; CVU 469822). Zuly A. Sánchez-Florentino is grateful to the Programa de Doctorado en Biología Experimental de la Universidad Autónoma Metropolitana, for the instruction received during his Ph. D. degree studies. He received a fellowship from the Consejo Nacional de Ciencia y Tecnología, México (CVU 697823).

Conflicts of Interest: The authors declare no conflict of interest.

References

1. Jalal, M.A.F.; Collin, H.A. Estimation of caffeine, theophylline and theobromine in plant material. *New Phytol.* **1976**, *76*, 277–281. [CrossRef]
2. Graham, H.N. Tea: The plant and its manufacture; chemistry and consumption of the beverage. *Prog. Clin. Biol. Res.* **1984**, *158*, 29–74.
3. Spiller, G.A. The chemical components of coffee. In *The Methylxanthine Beverages and Foods: Chemistry, Consumption, and Health Effects*; Spiller, G.A., Ed.; Liss: New York, NY, USA, 1984; pp. 91–147.
4. Graham, H.N. Mate. In *The Methylxanthine Beverages and Foods: Chemistry, Consumption, and Health Effects*; Spiller, G.A., Ed.; Liss: New York, NY, USA, 1984; pp. 179–183.
5. Hirsh, K. Central nervous system pharmacology of the dietary methylxanthines. In *The Methylxanthine Beverages and Foods: Chemistry, Consumption, and Health Effects*; Spiller, G.A., Ed.; Liss: New York, NY, USA, 1984; pp. 235–301.
6. Robson, R.A.; Miners, J.O.; Matthews, A.P.; Stupans, I.; Meller, D.; McManus, M.E.; Birkett, D.J. Characterisation of theophylline metabolism by human liver microsomes: Inhibition and immunochemical studies. *Biochem. Pharmacol.* **1988**, *37*, 1651–1659. [CrossRef]
7. Jenne, J.W.; Wyze, E.; Rood, F.S.; MacDonald, F.M. Pharmacokinetics of theophylline; Application to adjustment of the clinical dose of aminophylline. *Clin. Pharmacol. Ther.* **1972**, *13*, 349–360. [CrossRef]
8. Chrzanowski, F.A.; Niebergall, P.J.; Mayock, R.L.; Taubin, J.M.; Sugita, E.T. Kinetics of intravenous theophylline. *Clin. Pharmacol. Ther.* **1977**, *22*, 188–195. [CrossRef] [PubMed]
9. Hendeles, L.; Weinberger, M.; Bighley, L. Absolute bioavailability of oral theophylline. *Am. J. Health Pharm.* **1977**, *34*, 525–527. [CrossRef]
10. Barnes, P.J. Theophylline. *Am. J. Respir. Crit. Care Med.* **2013**, *188*, 901–906. [CrossRef] [PubMed]
11. Zhou, Y.; Wang, X.; Zeng, X.; Qiu, R.; Xie, J.; Liu, S.; Zheng, J.; Zhong, N.; Ran, P. Positive benefits of theophylline in a randomized, double-blind, parallel-group, placebo-controlled study of low-dose, slow-release theophylline in the treatment of COPD for 1 year. *Respirology* **2006**, *11*, 603–610. [CrossRef] [PubMed]
12. Jilani, T.N.; Preuss, C.V.; Sharma, S. Theophylline. In *StatPearls*; StatPearls: Treasure Island, FL, USA, 2022.
13. Romero-Martínez, B.S.; Montaño, L.M.; Solís-Chagoyán, H.; Sommer, B.; Ramírez-Salinas, G.L.; Pérez-Figueroa, G.E.; Flores-Soto, E. Possible Beneficial Actions of Caffeine in SARS-CoV-2. *Int. J. Mol. Sci.* **2021**, *22*, 5460. [CrossRef]
14. Gao, L.-Q.; Xu, J.; Chen, S.-D. In Silico Screening of Potential Chinese Herbal Medicine Against COVID-19 by Targeting SARS-CoV-2 3CLpro and Angiotensin Converting Enzyme II Using Molecular Docking. *Chin. J. Integr. Med.* **2020**, *26*, 527–532. [CrossRef] [PubMed]
15. Elzupir, A.O. Caffeine and caffeine-containing pharmaceuticals as promising inhibitors for 3-chymotrypsin-like protease of SARS-CoV-2. *J. Biomol. Struct. Dyn.* **2022**, *40*, 2113–2120. [CrossRef] [PubMed]

16. Wall, G.C.; Smith, H.L.; Trump, M.W.; Mohr, J.D.; DuMontier, S.P.; Sabates, B.L.; Ganapathiraju, I.; Kable, T.J. Pentoxifylline or theophylline use in hospitalized COVID-19 patients requiring oxygen support. *Clin. Respir. J.* **2021**, *15*, 843–846. [CrossRef] [PubMed]
17. Monserrat Villatoro, J.; Mejía-Abril, G.; Díaz García, L.; Zubiaur, P.; Jiménez González, M.; Fernandez Jimenez, G.; Cancio, I.; Arribas, J.R.; Fernández, C.S.; Mingorance, J.; et al. A Case-Control of Patients with COVID-19 to Explore the Association of Previous Hospitalisation Use of Medication on the Mortality of COVID-19 Disease: A Propensity Score Matching Analysis. *Pharmaceuticals* **2022**, *15*, 78. [CrossRef] [PubMed]
18. Dahiya, A.; Sharma, R.; Singh, A.; Joshi, P.; Wardhan, H. Role of Etophylline and Theophylline Prolonged Release Tablet in COVID-19 Associated Sinus Node Dysfunction. *J. Assoc. Physicians India* **2022**, *70*, 11–12.
19. Rabe, K.F.; Dent, G. Theophylline and airway inflammation. *Clin. Exp. Allergy* **1998**, *28* (Suppl. 3), 35–41. [PubMed]
20. Wettengel, R. Theophyllin–Rückblick, Standortbestimmung und Ausblick [Theophylline—Past present and future]. *Arzneimittelforschung* **1998**, *48*, 535–539. [PubMed]
21. Zhu, N.; Zhang, D.; Wang, W.; Li, X.; Yang, B.; Song, J.; Zhao, X.; Huang, B.; Shi, W.; Lu, R.; et al. A Novel Coronavirus from Patients with Pneumonia in China, 2019. *N. Engl. J. Med.* **2020**, *382*, 727–733. [CrossRef] [PubMed]
22. Gusev, E.; Sarapultsev, A.; Solomatina, L.; Chereshnev, V. SARS-CoV-2-Specific Immune Response and the Pathogenesis of COVID-19. *Int. J. Mol. Sci.* **2022**, *23*, 1716. [CrossRef] [PubMed]
23. Gorkhali, R.; Koirala, P.; Rijal, S.; Mainali, A.; Baral, A.; Bhattarai, H.K. Structure and Function of Major SARS-CoV-2 and SARS-CoV Proteins. *Bioinform. Biol. Insights* **2021**, *15*, 11779322211025876. [CrossRef] [PubMed]
24. Zhou, P.; Yang, X.-L.; Wang, X.-G.; Hu, B.; Zhang, L.; Zhang, W.; Si, H.-R.; Zhu, Y.; Li, B.; Huang, C.-L.; et al. A pneumonia outbreak associated with a new coronavirus of probable bat origin. *Nature* **2020**, *579*, 270–273. [CrossRef]
25. Montaño, L.M.; Sommer, B.; Solís-Chagoyán, H.; Romero-Martínez, B.S.; Aquino-Gálvez, A.; Gomez-Verjan, J.C.; Calixto, E.; González-Avila, G.; Flores-Soto, E. Could Lower Testosterone in Older Men Explain Higher COVID-19 Morbidity and Mortalities? *Int. J. Mol. Sci.* **2022**, *23*, 935. [CrossRef] [PubMed]
26. Masters, P.S. The Molecular Biology of Coronaviruses. *Adv. Virus Res.* **2006**, *66*, 193–292. [CrossRef] [PubMed]
27. Li, X.; Geng, M.; Peng, Y.; Meng, L.; Lu, S. Molecular immune pathogenesis and diagnosis of COVID-19. *J. Pharm. Anal.* **2020**, *10*, 102–108. [CrossRef]
28. Gusev, E.; Sarapultsev, A.; Hu, D.; Chereshnev, V. Problems of Pathogenesis and Pathogenetic Therapy of COVID-19 from the Perspective of the General Theory of Pathological Systems (General Pathological Processes). *Int. J. Mol. Sci.* **2021**, *22*, 7582. [CrossRef] [PubMed]
29. Gusev, E.; Solomatina, L.; Zhuravleva, Y.; Sarapultsev, A. The Pathogenesis of End-Stage Renal Disease from the Standpoint of the Theory of General Pathological Processes of Inflammation. *Int. J. Mol. Sci.* **2021**, *22*, 11453. [CrossRef] [PubMed]
30. To, K.K.-W.; Sridhar, S.; Chiu, K.H.-Y.; Hung, D.L.-L.; Li, X.; Hung, I.F.-N.; Tam, A.R.; Chung, T.W.-H.; Chan, J.F.-W.; Zhang, A.J.-X.; et al. Lessons learned 1 year after SARS-CoV-2 emergence leading to COVID-19 pandemic. *Emerg. Microbes Infect.* **2021**, *10*, 507–535. [CrossRef] [PubMed]
31. Gonzalez-Ramirez, J.A.; Ramírez-Nava, J.C.; Gonzalez-Lopez, S.; Sommer, B.; Solís-Chagoyán, H.; Montaño, L.M.; Romero-Martínez, B.S.; Flores-Soto, E. Hyperbaric oxygen therapy in overweight and obese patients with COVID-19. *World Acad. Sci. J.* **2021**, *3*, 61. [CrossRef]
32. Das, K.; Pingali, M.S.; Paital, B.; Panda, F.; Pati, S.G.; Singh, A.; Varadwaj, P.K.; Samanta, S.K. A detailed review of the outbreak of COVID-19. *Front. Biosci.* **2021**, *26*, 149–170. [CrossRef]
33. Imran, M.; Kumar Arora, M.; Asdaq, S.M.B.; Khan, S.A.; Alaqel, S.I.; Alshammari, M.K.; Alshehri, M.M.; Alshrari, A.S.; Mateq Ali, A.; Al-shammeri, A.M.; et al. Discovery, Development, and Patent Trends on Molnupiravir: A Prospective Oral Treatment for COVID-19. *Molecules* **2021**, *26*, 5795. [CrossRef] [PubMed]
34. Newton, A.H.; Cardani, A.; Braciale, T.J. The host immune response in respiratory virus infection: Balancing virus clearance and immunopathology. *Semin. Immunopathol.* **2016**, *38*, 471–482. [CrossRef]
35. Herold, S.; Becker, C.; Ridge, K.M.; Budinger, G.R.S. Influenza virus-induced lung injury: Pathogenesis and implications for treatment. *Eur. Respir. J.* **2015**, *45*, 1463–1478. [CrossRef] [PubMed]
36. Mizgerd, J.P. Acute Lower Respiratory Tract Infection. *N. Engl. J. Med.* **2008**, *358*, 716–727. [CrossRef] [PubMed]
37. Prompetchara, E.; Ketloy, C.; Palaga, T. Immune responses in COVID-19 and potential vaccines: Lessons learned from SARS and MERS epidemic. *Asian Pac. J. Allergy Immunol.* **2020**, *38*, 1–9. [CrossRef] [PubMed]
38. Li, G.; Fan, Y.; Lai, Y.; Han, T.; Li, Z.; Zhou, P.; Pan, P.; Wang, W.; Hu, D.; Liu, X.; et al. Coronavirus infections and immune responses. *J. Med. Virol.* **2020**, *92*, 424–432. [CrossRef]
39. Hu, B.; Huang, S.; Yin, L. The cytokine storm and COVID-19. *J. Med. Virol.* **2021**, *93*, 250–256. [CrossRef] [PubMed]
40. Pum, A.; Ennemoser, M.; Adage, T.; Kungl, A.J. Cytokines and Chemokines in SARS-CoV-2 Infections—Therapeutic Strategies Targeting Cytokine Storm. *Biomolecules* **2021**, *11*, 91. [CrossRef]
41. Luo, X.H.; Zhu, Y.; Mao, J.; Du, R.C. T cell immunobiology and cytokine storm of COVID-19. *Scand. J. Immunol.* **2021**, *93*, e12989. [CrossRef] [PubMed]
42. Ahmadpoor, P.; Rostaing, L. Why the immune system fails to mount an adaptive immune response to a COVID-19 infection. *Transpl. Int.* **2020**, *33*, 824–825. [CrossRef] [PubMed]

43. Wu, D.; Yang, X.O. TH17 responses in cytokine storm of COVID-19: An emerging target of JAK2 inhibitor Fedratinib. *J. Microbiol. Immunol. Infect.* **2020**, *53*, 368–370. [CrossRef] [PubMed]
44. Hotez, P.J.; Bottazzi, M.E.; Corry, D.B. The potential role of Th17 immune responses in coronavirus immunopathology and vaccine-induced immune enhancement. *Microbes Infect.* **2020**, *22*, 165–167. [CrossRef] [PubMed]
45. Davis, A.P.; Grondin, C.J.; Johnson, R.J.; Sciaky, D.; Wiegers, J.; Wiegers, T.C.; Mattingly, C.J. Comparative Toxicogenomics Database (CTD): Update 2021. *Nucleic Acids Res.* **2020**, *49*, D1138–D1143. [CrossRef] [PubMed]
46. Culpitt, S.V.; De Matos, C.; Russell, R.E.; Donnelly, L.E.; Rogers, D.F.; Barnes, P.J. Effect of Theophylline on Induced Sputum Inflammatory Indices and Neutrophil Chemotaxis in Chronic Obstructive Pulmonary Disease. *Am. J. Respir. Crit. Care Med.* **2002**, *165*, 1371–1376. [CrossRef] [PubMed]
47. Patel, B.S.; Rahman, M.M.; Rumzhum, N.N.; Oliver, B.G.; Verrills, N.M.; Ammit, A.J. Theophylline Represses IL-8 Secretion from Airway Smooth Muscle Cells Independently of Phosphodiesterase Inhibition. Novel Role as a Protein Phosphatase 2A Activator. *Am. J. Respir. Cell Mol. Biol.* **2016**, *54*, 792–801. [CrossRef]
48. Zhang, J.; Feng, M.-X.; Qu, J.-M. Low Dose Theophylline Showed an Inhibitory Effect on the Production of IL-6 and IL-8 in Primary Lung Fibroblast from Patients with COPD. *Mediat. Inflamm.* **2012**, *2012*, 492901. [CrossRef]
49. Cosio, B.G.; Iglesias, A.; Rios, A.; Noguera, A.; Sala, E.; Ito, K.; Barnes, P.J.; Agusti, A. Low-dose theophylline enhances the anti-inflammatory effects of steroids during exacerbations of COPD. *Thorax* **2009**, *64*, 424–429. [CrossRef] [PubMed]
50. Iiboshi, H.; Ashitani, J.-I.; Katoh, S.; Sano, A.; Matsumoto, N.; Mukae, H.; Nakazato, M. Long-term treatment with theophylline reduces neutrophils, interleukin-8 and tumor necrosis factor-α in the sputum of patients with chronic obstructive pulmonary disease. *Pulm. Pharmacol. Ther.* **2007**, *20*, 46–51. [CrossRef] [PubMed]
51. Yoshimura, T.; Usami, E.; Kurita, C.; Watanabe, S.; Nakao, T.; Kobayashi, J.; Yamazaki, F.; Nagai, H. Effect of Theophylline on the Production of Interleukin-1β, Tumor Necrosis Factor-α, and Interleukin-8 by Human Peripheral Blood Mononuclear Cells. *Biol. Pharm. Bull.* **1995**, *18*, 1405–1408. [CrossRef]
52. Kosmas, E.N.; Michaelides, S.A.; Polychronaki, A.; Roussou, T.; Toukmatzi, S.; Polychronopoulos, V.; Baxevanis, C.N. Theophylline induces a reduction in circulating interleukin-4 and interleukin-5 in atopic asthmatics. *Eur. Respir. J.* **1999**, *13*, 53–58.
53. Kimura, M.; Okafuji, I.; Yoshida, T. Theophylline suppresses IL-5 and IL-13 production, and lymphocyte proliferation upon stimulation with house dust mite in asthmatic children. *Int. Arch. Allergy Immunol.* **2003**, *131*, 189–194. [CrossRef] [PubMed]
54. Fujisawa, T.; Kato, Y.; Terada, A.; Iguchi, K.; Kamiya, H. Synergistic Effect of Theophylline and Procaterol On Interleukin-5-Induced Degranulation from Human Eosinophils. *J. Asthma* **2002**, *39*, 21–27. [CrossRef] [PubMed]
55. Ichiyama, T.; Hasegawa, S.; Matsubara, T.; Hayashi, T.; Furukawa, S. Theophylline inhibits NF-κB activation and IκBα degradation in human pulmonary epithelial cells. *Naunyn-Schmiedebergs Arch. Exp. Pathol. Pharmakol.* **2001**, *364*, 558–561. [CrossRef] [PubMed]
56. Umeda, M.; Ichiyama, T.; Hasegawa, S.; Kaneko, M.; Matsubara, T.; Furukawa, S. Theophylline Inhibits NF-κB Activation in Human Peripheral Blood Mononuclear Cells. *Int. Arch. Allergy Immunol.* **2002**, *128*, 130–135. [CrossRef]
57. Sagara, H.; Makino, S.; Chibana, N.; Ota, M.; Holgate, S.T.; Church, M.K.; Fukuda, T. Theophylline at Therapeutic Concentrations Inhibits NF-κB Activation in Human Lung Mast Cells. *Int. Arch. Allergy Immunol.* **2001**, *124*, 371–376. [CrossRef]
58. Goel, S.; Saheb Sharif-Askari, F.; Saheb Sharif Askari, N.; Madkhana, B.; Alwaa, A.M.; Mahboub, B.; Zakeri, A.M.; Ratemi, E.; Hamoudi, R.; Hamid, Q.; et al. SARS-CoV-2 Switches 'on' MAPK and NFκB Signaling via the Reduction of Nuclear DUSP1 and DUSP5 Expression. *Front. Pharmacol.* **2021**, *12*, 631879. [CrossRef] [PubMed]
59. Caunt, C.J.; Keyse, S.M. Dual-specificity MAP kinase phosphatases (MKPs): Shaping the outcome of MAP kinase signalling. *FEBS J.* **2013**, *280*, 489–504. [CrossRef] [PubMed]
60. Seo, H.; Cho, Y.-C.; Ju, A.; Lee, S.; Park, B.C.; Park, S.G.; Kim, J.-H.; Kim, K.; Cho, S. Dual-specificity phosphatase 5 acts as an anti-inflammatory regulator by inhibiting the ERK and NF-κB signaling pathways. *Sci. Rep.* **2017**, *7*, 17348. [CrossRef] [PubMed]
61. Takanashi, S.; Hasegawa, Y.; Kanehira, Y.; Yamamoto, K.; Fujimoto, K.; Satoh, K.; Okamura, K. Interleukin-10 level in sputum is reduced in bronchial asthma, COPD and in smokers. *Eur. Respir. J.* **1999**, *14*, 309–314. [CrossRef]
62. Cvietusa, P.; Mascali, J.J.; Negri, J.; Borish, L. Anti-inflammatory Effects of Theophylline: Modulation of Cytokine Production. *Ann. Allergy Asthma Immunol.* **1996**, *77*, 34–38. [CrossRef]
63. Ito, K.; Lim, S.; Caramori, G.; Cosio, B.; Chung, K.F.; Adcock, I.M.; Barnes, P.J. A molecular mechanism of action of theophylline: Induction of histone deacetylase activity to decrease inflammatory gene expression. *Proc. Natl. Acad. Sci. USA* **2002**, *99*, 8921–8926. [CrossRef] [PubMed]
64. Zheng, X.F.; Chen, D.D.; Zhu, X.L.; Le Grange, J.M.; Zhou, L.Q.; Zhang, J.N. Impacts of anti-inflammatory phosphodiesterase inhibitors on a murine model of chronic pulmonary inflammation. *Pharmacol. Res. Perspect.* **2021**, *9*, e00840. [CrossRef] [PubMed]
65. Sugiura, H.; Kawabata, H.; Ichikawa, T.; Koarai, A.; Yanagisawa, S.; Kikuchi, T.; Minakata, Y.; Matsunaga, K.; Nakanishi, M.; Hirano, T.; et al. Inhibitory effects of theophylline on the peroxynitrite-augmented release of matrix metalloproteinases by lung fibroblasts. *Am. J. Physiol. Lung Cell. Mol. Physiol.* **2012**, *302*, L764–L774. [CrossRef] [PubMed]
66. Nagesh, P.T.; Hussain, M.; Galvin, H.D.; Husain, M. Histone Deacetylase 2 Is a Component of Influenza A Virus-Induced Host Antiviral Response. *Front. Microbiol.* **2017**, *8*, 1315. [CrossRef]
67. Footitt, J.; Mallia, P.; Durham, A.; Ho, W.E.; Trujillo-Torralbo, M.-B.; Telcian, A.G.; Del Rosario, A.; Chang, C.; Peh, H.-Y.; Kebadze, T.; et al. Oxidative and Nitrosative Stress and Histone Deacetylase-2 Activity in Exacerbations of COPD. *Chest* **2016**, *149*, 62–73. [CrossRef] [PubMed]

68. Barnes, P.J. Inflammatory mechanisms in patients with chronic obstructive pulmonary disease. *J. Allergy Clin. Immunol.* **2016**, *138*, 16–27. [CrossRef]
69. To, Y.; Ito, K.; Kizawa, Y.; Failla, M.; Ito, M.; Kusama, T.; Elliott, W.M.; Hogg, J.C.; Adcock, I.M.; Barnes, P.J. Targeting Phosphoinositide-3-Kinase-δ with Theophylline Reverses Corticosteroid Insensitivity in Chronic Obstructive Pulmonary Disease. *Am. J. Respir. Crit. Care Med.* **2010**, *182*, 897–904. [CrossRef] [PubMed]
70. Ford, P.A.; Durham, A.L.; Russell, R.E.K.; Gordon, F.; Adcock, I.M.; Barnes, P.J. Treatment Effects of Low-Dose Theophylline Combined with an Inhaled Corticosteroid in COPD. *Chest* **2010**, *137*, 1338–1344. [CrossRef] [PubMed]
71. Chorostowska-Wynimko, J.; Kus, J.; Skopińska-Rózewska, E. Theophylline inhibits free oxygen radicals production by human monocytes via phosphodiesterase inhibition. *J. Physiol. Pharmacol.* **2007**, *58*, 95–103.
72. Aydemir, M.N.; Aydemir, H.B.; Korkmaz, E.M.; Budak, M.; Cekin, N.; Pinarbasi, E. Computationally predicted SARS-COV-2 encoded microRNAs target NFKB, JAK/STAT and TGFB signaling pathways. *Gene Rep.* **2021**, *22*, 101012. [CrossRef] [PubMed]
73. Asano, K.; Shikama, Y.; Shibuya, Y.; Nakajima, H.; Kanai, K.; Yamada, N.; Suzaki, H. Suppressive activity of tiotropium bromide on matrix metalloproteinase production from lung fibroblasts in vitro. *Int. J. Chronic Obstr. Pulm. Dis.* **2008**, *3*, 781–790. [CrossRef]
74. Davey, A.; McAuley, D.F.; O'Kane, C.M. Matrix metalloproteinases in acute lung injury: Mediators of injury and drivers of repair. *Eur. Respir. J.* **2011**, *38*, 959–970. [CrossRef] [PubMed]
75. Fligiel, S.E.; Standiford, T.; Fligiel, H.M.; Tashkin, D.; Strieter, R.M.; Warner, R.L.; Johnson, K.J.; Varani, J. Matrix metalloproteinases and matrix metalloproteinase inhibitors in acute lung injury. *Hum. Pathol.* **2006**, *37*, 422–430. [CrossRef] [PubMed]
76. Siwik, D.A.; Colucci, W.S. Regulation of Matrix Metalloproteinases by Cytokines and Reactive Oxygen/Nitrogen Species in the Myocardium. *Heart Fail. Rev.* **2004**, *9*, 43–51. [CrossRef] [PubMed]
77. D'Avila-Mesquita, C.; Couto, A.E.; Campos, L.C.; Vasconcelos, T.F.; Michelon-Barbosa, J.; Corsi, C.A.; Mestriner, F.; Petroski-Moraes, B.C.; Garbellini-Diab, M.J.; Couto, D.M.; et al. MMP-2 and MMP-9 levels in plasma are altered and associated with mortality in COVID-19 patients. *Biomed. Pharmacother.* **2021**, *142*, 112067. [CrossRef] [PubMed]
78. Moonen, H.J.; Geraets, L.; Vaarhorst, A.; Bast, A.; Wouters, E.F.; Hageman, G.J. Theophylline prevents NAD+ depletion via PARP-1 inhibition in human pulmonary epithelial cells. *Biochem. Biophys. Res. Commun.* **2005**, *338*, 1805–1810. [CrossRef] [PubMed]
79. Miller, R.; Wentzel, A.R.; Richards, G.A. COVID-19: NAD^+ deficiency may predispose the aged, obese and type2 diabetics to mortality through its effect on SIRT1 activity. *Med. Hypotheses* **2020**, *144*, 110044. [CrossRef]
80. Kouhpayeh, S.; Shariati, L.; Boshtam, M.; Rahimmanesh, I.; Mirian, M.; Zeinalian, M.; Salari-Jazi, A.; Khanahmad, N.; Damavandi, M.S.; Sadeghi, P.; et al. The Molecular Story of COVID-19; NAD+ Depletion Addresses All Questions in this Infection. *Preprints* **2020**. [CrossRef]
81. Bordoni, V.; Tartaglia, E.; Sacchi, A.; Fimia, G.M.; Cimini, E.; Casetti, R.; Notari, S.; Grassi, G.; Marchioni, L.; Bibas, M.; et al. The unbalanced p53/SIRT1 axis may impact lymphocyte homeostasis in COVID-19 patients. *Int. J. Infect. Dis.* **2021**, *105*, 49–53. [CrossRef] [PubMed]
82. Fukuda, Y.; Akimoto, K.; Homma, T.; Baker, J.R.; Ito, K.; Barnes, P.J.; Sagara, H. Virus-Induced Asthma Exacerbations: SIRT1 Targeted Approach. *J. Clin. Med.* **2020**, *9*, 2623. [CrossRef] [PubMed]
83. Hodge, G.; Tran, H.B.; Reynolds, P.N.; Jersmann, H.; Hodge, S. Lymphocyte senescence in COPD is associated with decreased sirtuin 1 expression in steroid resistant pro-inflammatory lymphocytes. *Ther. Adv. Respir. Dis.* **2020**, *14*, 175346662090528. [CrossRef]
84. Zheng, Y.; Li, R.; Liu, S. Immunoregulation with mTOR inhibitors to prevent COVID-19 severity: A novel intervention strategy beyond vaccines and specific antiviral medicines. *J. Med. Virol.* **2020**, *92*, 1495–1500. [CrossRef] [PubMed]
85. Ballou, L.M.; Lin, R.Z. Rapamycin and mTOR kinase inhibitors. *J. Chem. Biol.* **2008**, *1*, 27–36. [CrossRef]
86. Karam, B.S.; Morris, R.S.; Bramante, C.T.; Puskarich, M.; Zolfaghari, E.J.; Lotfi-Emran, S.; Ingraham, N.E.; Charles, A.; Odde, D.J.; Tignanelli, C.J. mTOR inhibition in COVID-19: A commentary and review of efficacy in RNA viruses. *J. Med. Virol.* **2021**, *93*, 1843–1846. [CrossRef] [PubMed]
87. Tetro, J.A. Is COVID-19 receiving ADE from other coronaviruses? *Microbes Infect.* **2020**, *22*, 72–73. [CrossRef] [PubMed]
88. Yip, M.S.; Leung, N.H.L.; Cheung, C.Y.; Li, P.H.; Lee, H.H.Y.; Daëron, M.; Peiris, J.S.M.; Bruzzone, R.; Jaume, M. Antibody-dependent infection of human macrophages by severe acute respiratory syndrome coronavirus. *Virol. J.* **2014**, *11*, 82. [CrossRef] [PubMed]
89. Jaume, M.; Yip, M.S.; Cheung, C.Y.; Leung, H.L.; Li, P.H.; Kien, F.; Dutry, I.; Callendret, B.; Escriou, N.; Altmeyer, R.; et al. Anti-Severe Acute Respiratory Syndrome Coronavirus Spike Antibodies Trigger Infection of Human Immune Cells via a pH- and Cysteine Protease-Independent FcγR Pathway. *J. Virol.* **2011**, *85*, 10582–10597. [CrossRef] [PubMed]
90. Yang, F.; Ye, X.-J.; Chen, M.-Y.; Li, H.-C.; Wang, Y.-F.; Zhong, M.-Y.; Zhong, C.-S.; Zeng, B.; Xu, L.-H.; He, X.-H.; et al. Inhibition of NLRP3 Inflammasome Activation and Pyroptosis in Macrophages by Taraxasterol Is Associated with Its Regulation on mTOR Signaling. *Front. Immunol.* **2021**, *12*, 632606. [CrossRef] [PubMed]
91. Scott, P.H.; Lawrence, J.C., Jr. Attenuation of Mammalian Target of Rapamycin Activity by Increased cAMP in 3T3-L1 Adipocytes. *J. Biol. Chem.* **1998**, *273*, 34496–34501. [CrossRef]
92. Xie, J.; Ponuwei, G.A.; Moore, C.E.; Willars, G.B.; Tee, A.; Herbert, T.P. cAMP inhibits mammalian target of rapamycin complex-1 and -2 (mTORC1 and 2) by promoting complex dissociation and inhibiting mTOR kinase activity. *Cell. Signal.* **2011**, *23*, 1927–1935. [CrossRef]

93. Le Sage, V.; Cinti, A.; Amorim, R.; Mouland, A.J. Adapting the Stress Response: Viral Subversion of the mTOR Signaling Pathway. *Viruses* **2016**, *8*, 152. [CrossRef] [PubMed]
94. Ferreira, L.G.; Dos Santos, R.N.; Oliva, G.; Andricopulo, A.D. Molecular Docking and Structure-Based Drug Design Strategies. *Molecules* **2015**, *20*, 13384–13421. [CrossRef] [PubMed]
95. Ramírez-Salinas, G.L.; Martínez-Archundia, M.; Correa-Basurto, J.; García-Machorro, J. Repositioning of Ligands That Target the Spike Glycoprotein as Potential Drugs for SARS-CoV-2 in an In Silico Study. *Molecules* **2020**, *25*, 5615. [CrossRef]
96. Sarma, P.; Shekhar, N.; Prajapat, M.; Avti, P.; Kaur, H.; Kumar, S.; Singh, S.K.; Kumar, H.; Prakash, A.; Dhibar, D.P.; et al. In-silico homology assisted identification of inhibitor of RNA binding against 2019-nCoV N-protein (N terminal domain). *J. Biomol. Struct. Dyn.* **2021**, *39*, 2724–2732. [CrossRef] [PubMed]
97. Mohammadi, S.; Heidarizadeh, M.; Entesari, M.; Esmailpour, A.; Esmailpour, M.; Moradi, R.; Sakhaee, N.; Doustkhah, E. In silico Investigation on the Inhibiting Role of Nicotine/Caffeine by Blocking the S Protein of SARS-CoV-2 Versus ACE2 Receptor. *Microorganisms* **2020**, *8*, 1600. [CrossRef] [PubMed]
98. Wu, Y.; Li, Z.; Zhao, Y.S.; Huang, Y.Y.; Jiang, M.Y.; Luo, H.B. Therapeutic targets and potential agents for the treatment of COVID-19. *Med. Res. Rev.* **2021**, *41*, 1775–1797. [CrossRef] [PubMed]
99. Zeng, W.; Liu, G.; Ma, H.; Zhao, D.; Yang, Y.; Liu, M.; Mohammed, A.; Zhao, C.; Yang, Y.; Xie, J.; et al. Biochemical characterization of SARS-CoV-2 nucleocapsid protein. *Biochem. Biophys. Res. Commun.* **2020**, *527*, 618–623. [CrossRef] [PubMed]
100. Pan, P.; Shen, M.; Yu, Z.; Ge, W.; Chen, K.; Tian, M.; Xiao, F.; Wang, Z.; Wang, J.; Jia, Y.; et al. SARS-CoV-2 N protein promotes NLRP3 inflammasome activation to induce hyperinflammation. *Nat. Commun.* **2021**, *12*, 4664. [CrossRef] [PubMed]
101. Webb, B.; Sali, A. Comparative Protein Structure Modeling Using MODELLER. *Curr. Protoc. Bioinform.* **2016**, *54*, 1–37. [CrossRef] [PubMed]
102. Berman, H.M.; Westbrook, J.; Feng, Z.; Gilliland, G.; Bhat, T.N.; Weissig, H.; Shindyalov, I.N.; Bourne, P.E. The Protein Data Bank. *Nucleic Acids Res.* **2000**, *28*, 235–242. [CrossRef]
103. Trott, O.; Olson, A.J. AutoDock Vina: Improving the speed and accuracy of docking with a new scoring function, efficient optimization, and multithreading. *J. Comput. Chem.* **2010**, *31*, 455–461. [CrossRef]
104. Duart, G.; García-Murria, M.J.; Grau, B.; Acosta-Cáceres, J.M.; Martínez-Gil, L.; Mingarro, I. SARS-CoV-2 envelope protein topology in eukaryotic membranes. *Open Biol.* **2020**, *10*, 200209. [CrossRef] [PubMed]
105. Laurini, E.; Marson, D.; Aulic, S.; Fermeglia, A.; Pricl, S. Molecular rationale for SARS-CoV-2 spike circulating mutations able to escape bamlanivimab and etesevimab monoclonal antibodies. *Sci. Rep.* **2021**, *11*, 20274. [CrossRef]
106. Nieto-Torres, J.L.; DeDiego, M.L.; Verdiá-Báguena, C.; Jimenez-Guardeño, J.M.; Regla-Nava, J.A.; Fernandez-Delgado, R.; Castaño-Rodriguez, C.; Alcaraz, A.; Torres, J.; Aguilella, V.M.; et al. Severe Acute Respiratory Syndrome Coronavirus Envelope Protein Ion Channel Activity Promotes Virus Fitness and Pathogenesis. *PLoS Pathog.* **2014**, *10*, e1004077. [CrossRef]
107. Schoeman, D.; Fielding, B.C. Coronavirus envelope protein: Current knowledge. *Virol. J.* **2019**, *16*, 69. [CrossRef] [PubMed]
108. Rolta, R.; Salaria, D.; Sharma, B.; Awofisayo, O.; Fadare, O.A.; Sharma, S.; Patel, C.N.; Kumar, V.; Sourirajan, A.; Baumler, D.J.; et al. Methylxanthines as Potential Inhibitor of SARS-CoV-2: An In Silico Approach. *Curr. Pharmacol. Rep.* **2022**, *8*, 149–170. [CrossRef] [PubMed]
109. Vassallo, R.; Lipsky, J.J. Theophylline: Recent Advances in the Understanding of Its Mode of Action and Uses in Clinical Practice. *Mayo Clin. Proc.* **1998**, *73*, 346–354. [CrossRef]
110. Senchina, D.S.; Hallam, J.E.; Kohut, M.L.; Nguyen, N.A.; Perera, M.A.D.N. Alkaloids and athlete immune function: Caffeine, theophylline, gingerol, ephedrine, and their congeners. *Exerc. Immunol. Rev.* **2014**, *20*, 68–93. [PubMed]
111. Willmann, S.; Lippert, J.; Sevestre, M.; Solodenko, J.; Fois, F.; Schmitt, W. PK-Sim®: A physiologically based pharmacokinetic'whole-body'model. *BIOSILICO* **2003**, *1*, 121–124. [CrossRef]
112. Hanke, N.; Türk, D.; Selzer, D.; Ishiguro, N.; Ebner, T.; Wiebe, S.; Müller, F.; Stopfer, P.; Nock, V.; Lehr, T. A comprehensive whole-body physiologically based pharmacokinetic drug–drug–gene interaction model of metformin and cimetidine in healthy adults and renally impaired individuals. *Clin. Pharmacokinet.* **2020**, *59*, 1419–1431. [CrossRef] [PubMed]
113. Ahmadian, E.; Hosseiniyan Khatibi, S.M.; Razi Soofiyani, S.; Abediazar, S.; Shoja, M.M.; Ardalan, M.; Zununi Vahed, S. Covid-19 and kidney injury: Pathophysiology and molecular mechanisms. *Rev. Med. Virol.* **2021**, *31*, e2176. [CrossRef] [PubMed]
114. Higgins, V.; Sohaei, D.; Diamandis, E.P.; Prassas, I. COVID-19: From an acute to chronic disease? Potential long-term health consequences. *Crit. Rev. Clin. Lab. Sci.* **2021**, *58*, 297–310. [CrossRef] [PubMed]
115. Callard, F.; Perego, E. How and why patients made Long Covid. *Soc. Sci. Med.* **2021**, *268*, 113426. [CrossRef] [PubMed]
116. Mendelson, M.; Nel, J.; Blumberg, L.; Madhi, S.A.; Dryden, M.; Stevens, W.; Venter, F. Long-COVID: An evolving problem with an extensive impact. *S. Afr. Med. J.* **2020**, *111*, 10–12. [CrossRef]

International Journal of
Molecular Sciences

MDPI

Review

Possible Beneficial Actions of Caffeine in SARS-CoV-2

Bianca S. Romero-Martínez [1], Luis M. Montaño [1], Héctor Solís-Chagoyán [2], Bettina Sommer [3], Gemma Lizbeth Ramírez-Salinas [4], Gloria E. Pérez-Figueroa [5] and Edgar Flores-Soto [1,*]

1 Departamento de Farmacología, Facultad de Medicina, Universidad Nacional Autónoma de México, CDMX CP 04510, Mexico; biancasromero_@hotmail.com (B.S.R.-M.); lmmr@unam.mx (L.M.M.)
2 Laboratorio de Neurofarmacología, Instituto Nacional de Psiquiatría Ramón de la Fuente Muñiz, CDMX CP 14370, Mexico; hecsolch@imp.edu.mx
3 Laboratorio de Hiperreactividad Bronquial, Instituto Nacional de Enfermedades Respiratorias "Ismael Cosío Villegas", CDMX CP 14080, Mexico; bsommerc@hotmail.com
4 Laboratorio de Diseño y Desarrollo de Nuevos Fármacos e Innovación Biotécnológica (Laboratory for the Design and Development of New Drugs and Biotechnological Innovation), Escuela Superior de Medicina, Instituto Politécnico Nacional, CDMX CP 11340, Mexico; gemali86@hotmail.com
5 Laboratorio de Investigación en Inmunología y Proteómica, Hospital Infantil de México Federico Gómez, CDMX CP 06720, Mexico; gera.pfi3@gmail.com
* Correspondence: edgarfloressoto@yahoo.com.mx; Tel.: +52-5556232279

Abstract: The COVID-19 pandemic has established an unparalleled necessity to rapidly find effective treatments for the illness; unfortunately, no specific treatment has been found yet. As this is a new emerging chaotic situation, already existing drugs have been suggested to ameliorate the infection of SARS-CoV-2. The consumption of caffeine has been suggested primarily because it improves exercise performance, reduces fatigue, and increases wakefulness and awareness. Caffeine has been proven to be an effective anti-inflammatory and immunomodulator. In airway smooth muscle, it has bronchodilator effects mainly due to its activity as a phosphodiesterase inhibitor and adenosine receptor antagonist. In addition, a recent published document has suggested the potential antiviral activity of this drug using in silico molecular dynamics and molecular docking; in this regard, caffeine might block the viral entrance into host cells by inhibiting the formation of a receptor-binding domain and the angiotensin-converting enzyme complex and, additionally, might reduce viral replication by the inhibition of the activity of 3-chymotrypsin-like proteases. Here, we discuss how caffeine through certain mechanisms of action could be beneficial in SARS-CoV-2. Nevertheless, further studies are required for validation through in vitro and in vivo models.

Keywords: caffeine; COVID-19; SARS-CoV-2; airway smooth muscle; immunomodulatory effects; antiviral activity

Citation: Romero-Martínez, B.S.; Montaño, L.M.; Solís-Chagoyán, H.; Sommer, B.; Ramírez-Salinas, G.L.; Pérez-Figueroa, G.E.; Flores-Soto, E. Possible Beneficial Actions of Caffeine in SARS-CoV-2. *Int. J. Mol. Sci.* **2021**, *22*, 5460. https://doi.org/10.3390/ijms22115460

Academic Editor: Michael Roth

Received: 6 April 2021
Accepted: 13 May 2021
Published: 22 May 2021

1. Introduction

In December 2019, a series of unexplained cases of atypical pneumonia were reported in Wuhan, China, with high transmission. This disease, which was subsequently named coronavirus disease 2019 (COVID-19), has spread rapidly worldwide, affecting a large part of the human population [1,2]. The World Health Organization (WHO) officially named the virus severe acute respiratory syndrome coronavirus 2 (SARS-CoV-2) [3]. SARS-CoV-2 belongs to the coronavirus family, a group of enveloped, single-stranded, positive-sense, RNA genome viruses. The virion contains four main structural proteins: the nucleocapsid (N) located in the nucleocapsid and in the viral envelope we can find the spike (S), membrane (M), and envelope (E) proteins. The S protein has been determined to facilitate viral entry into the host cell; this occurs through the complex formed by a receptor-binding domain (RBD; a subunit of the S protein) and the angiotensin-converting enzyme 2 (ACE2) found in the membrane of the host cell, mainly pneumocyte type II cells [1,4–6]. The number of patients is increasing day by day around the world, but some infected patients are asymptomatic or experience a mild disease course (fever, cough, chest tightness, dyspnea, etc.).

However, patients with severe symptoms may present severe respiratory tract infections, severe pneumonia, acute respiratory distress syndrome (ARDS), multiple organ failure, and death [7–11]. This is because the virus induces aberrant host immune responses, and modulation of the host immune response is the key to fight SARS-CoV-2 [12]. Among the theories, it is hypothesized that SARS-CoV-2 damages tissues due to the deterioration of inflammation mechanisms and cytokine storms given the pathophysiology of SARS-CoV-2 [13,14]. The WHO reported that as of 28 February 2021 there had been approximately 113,864,015 cases of COVID-19 and that the number of deaths had been approximately 2,526,793 worldwide. In Mexico, to this date there had been a total of 2,084,128 positive cases with a total of 185,257 deaths, and, unfortunately at the time of writing, the number of COVID-19 positive cases is increasing daily [15].

Many researchers, through their respective research areas, are facing and directing contributions to overcome the COVID-19 pandemic. Although the development and use of vaccines (with high efficiency) has been the first option, at the time of writing, only 0.67% of the world's population, according to the WHO, has been vaccinated. Therefore, current treatments are largely directed toward symptom management and vital support in severe cases [16]. Given the necessity for efficient therapeutic options in the intervention of SARS-CoV-2, two main routes in the drug discovery process for a viral infection are being undertaken: the discovery or synthesis of a new effective drug and the repurposing of an already existing drug. Drug discovery is a laborious process, usually taking several years and at large expense; therefore, taking into consideration the urgency arising from the pandemic currently plaguing our world, the option to repurpose already existing drugs or pharmacological compounds seems the more feasible option [17].

Until now, the therapeutic options to contain the COVID-19 pandemic have been based on prevention of transmission, detection of travelers, and public healthcare measures [17]. There is no effective treatment for SARS-CoV-2 infection and the drugs mainly used include antiviral protease inhibitors that impede the viral replication of SARS-CoV-2 by inactivating proteases essential for the replication [18]. The identification of specific drug targets that inhibit the life cycle of SARS-CoV-2 still require further investigation.

Another strategy is to use inflammation inhibitors, because experimental and clinical tests have shown that the damage caused by the virus is related to an altered inflammatory response and, in some patients, to an abnormal release of pro-inflammatory cytokines [18]. Low molecular heparins, plasma, and hyperimmune immunoglobulins are also utilized on a case-by-case basis, generally in severe COVID-19 patients, and are used to mitigate the complications and sequelae that can arise from the infection [18–20]. Although a variety of therapies may be a short-term strategy to deal with COVID-19, there is still an obvious lack of specific treatment for the disease [7]. Even if these anti-inflammatory agents are a promising line of treatment, they still require further study through randomized clinical trials.

Caffeine (1,3,7-trimethylxanthine) is a methylxanthine alkaloid found in the seed, fruit, and leaves of a variety of plants native to Africa, Southeast Asia, and South America. In addition to coffee and tea, it can also be found in cocoa beans, yerba mate leaves (used to make herbal teas), and guarana berries (used in various beverages and supplements). It is a common stimulant that is consumed daily around the world [21]; it can be synthesized and added to beverages and foods, including soft drinks, beverages, and tablets in a wide variety of over-the-counter formulations, such as combined diet aids and pain relievers. If consumed within the recommended dose (400 mg/day for adults), its most widely sought-after effect is as a mild stimulant of the central nervous system (CNS), due to its capacity to cross with ease the blood–brain barrier, which can cause a reduction in fatigue and increase wakefulness and awareness [22,23]. Caffeine is used successfully in the treatment of apnea of prematurity [24], exerting its antagonism on the adenosine receptors in the respiratory centers of the brainstem [25]. In chronic lung disease of prematurity, it inhibits non-selective phosphodiesterase and increases cyclic adenosine monophosphate levels (cAMP), directly relaxing the pulmonary vascular muscle of the baby and improving its

oxygenation [26]. In asthma, caffeine has been utilized in adults with mild asthma, showing a moderate improvement in lung function when low doses of 5 mg/kg of body weight are administered [27]. There are reports where people with exercise-induced bronchoconstriction (EIB) could alleviate it by ingesting caffeine before exercise (7 mg/kg) [28]. The mechanisms proposed for the bronchodilator effect are mostly through its activity as an inhibitor of phosphodiesterase and antagonism of the adenosine receptor [29]. It should be mentioned that consumed caffeine is easily distributed throughout the body and permeates through the cellular membrane due to its amphiphilic properties [30]. In the liver, it is metabolized by cytochrome P-450 (CYP) enzymes and biotransformed by CYP1A2 in three active metabolites, mainly paraxanthine (81.5%), theobromine (10.8%), and theophylline (5.4%), which are excreted in the urine [31]. A moderate consumption of caffeine is usually considered safe and acute toxicity is rare, but some of the symptomology that can be present are nausea, headaches, insomnia, nervousness, tachycardia, arrhythmias, gastrointestinal disturbances, and seizures. The consumption of caffeine in combination with alcohol could even result in death [23,32]. These could be the possible side effects if caffeine were to be used for treating COVID-19 patients.

We and other research groups have studied the pharmacological activities of caffeine in the smooth muscle of the respiratory tract, including mainly adenosine receptor antagonism, phosphodiesterase inhibition, and intracellular calcium release from the sarcoplasmic reticulum (SR), and as a taste receptor type 2 ligand (TAS2R) [33–36]. It is important to emphasize that these mechanisms are found in almost all tissues and cells of the body. Recently, caffeine has taken on an essential role in the fight against SARS-CoV-2 since it can play a role in the defense against this virus [6,7,36]. In this review, we analyze our experience in the handling of caffeine and the analysis of new experimental data that may have health benefits against SARS-CoV-2 in multiple organ systems, via inactivation of the virus, blocking the viral binding with ACE2, along with its immunomodulatory and anti-inflammatory roles, as well as benefits in patients with COVID-19, especially as caffeine is consumed daily.

2. Pharmacological Mechanisms of Caffeine in Airway Smooth Muscle

Recently, Kalidhindi et al., using confocal imaging, found that ACE2 is expressed in human airway smooth muscle (ASM), although an entry of SARS-CoV-2 has not been demonstrated [37]. The importance of these cells lies in the possibility that SARS-CoV-2 targets and damages the epithelial layers with subsequent influences on the underlying mesenchymal cells (ASM, fibroblasts), leading to an alteration in the reactivity of the airways, inflammation, and long-term fibrosis. In this context, SARS-CoV-2 can directly influence the functionality of multiple signaling pathways in lung cells, including ASM [37].

2.1. Adenosine Receptors

In the 1980s, it was found that adenosine administered by inhalation induces bronchoconstriction in subjects with asthma [38] and increases the concentrations of pro-inflammatory mediators such as histamine, tryptase, leukotrienes, and prostaglandins discharged from mast cells [39,40]. These findings pointed out that adenosine may result in bronchoconstriction through mast cell activation [41,42]. In asthmatics, adenosine concentrations are elevated in bronchoalveolar lavage fluid (BAL) [43] and in exhaled air condensate [44,45]. In conclusion, adenosine produces bronchoconstriction, inflammation, and mucus, which lead to airway obstruction. In addition, it may function as a paracrine mediator of the inflammatory response of the lung, especially in the allergic-asthma phenotype [38,46,47]. The effects of adenosine are exerted through G-protein-coupled receptors (GPCRs) and they have been classified into four subtypes, namely, adenosine receptors A_1, A_{2A}, A_{2B}, and A_3 [48]. When activated, these receptors increase or decrease the concentration of cAMP; subtypes A_1 and A_3 are coupled to Gi proteins that decrease the intracellular concentration of cAMP, while subtypes A_{2A} and A_{2B} are coupled to Gs proteins and can increase the intracellular concentration of cAMP [49] (Figure 1).

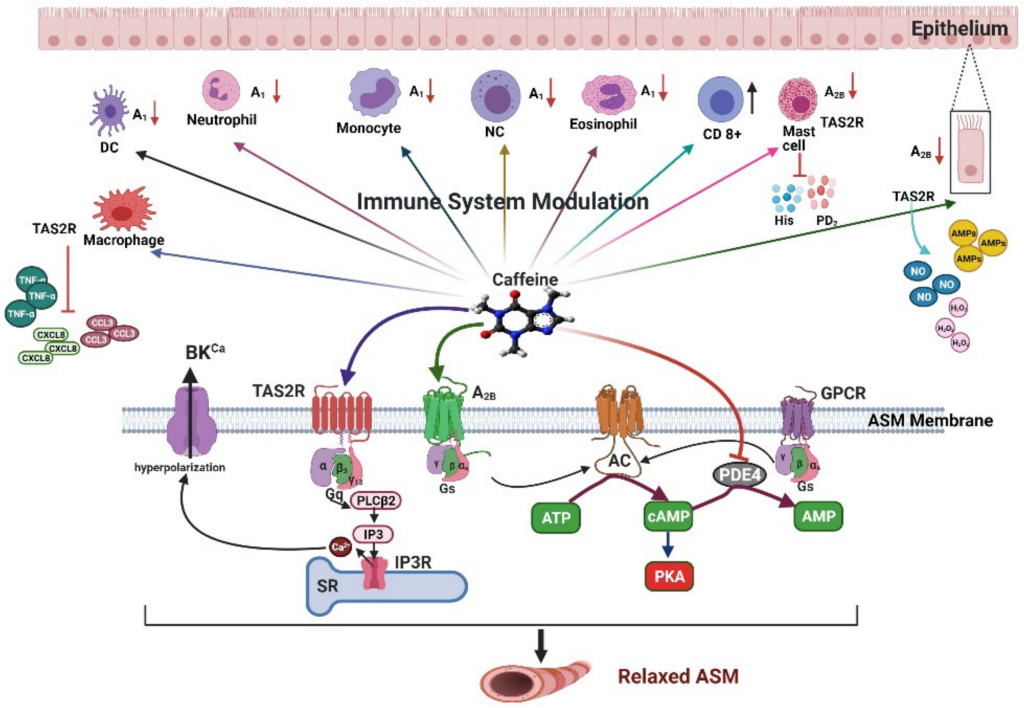

Figure 1. Schematic diagram of the immunomodulatory and bronchodilatory effects of caffeine. Various cells of the immune system express adenosine receptors (ARs) and TAS2R receptors that can modulate their activity; caffeine is a known antagonist of the AR receptor and an agonist of TAS2R receptors. Antagonism of A_1 and A_{2B} on immune cells will decrease pro-inflammatory activity. Caffeine activation of TAS2R in epithelial cells will increase the secretion of antimicrobial peptides (AMPs), NO, and H_2O_2, all of which have direct effects on the virus. In macrophages it inhibits pro-inflammatory cytokine production, and in mast cells it inhibits histamine and prostaglandin D_2 release. In ASM, caffeine can activate various pathways that promote bronchodilation: it activates TAS2R and A_2 receptors and inhibits PDE4 to induce relaxation. At high concentrations, it can also increase the open probability of RyR; this last mechanism has no therapeutic use. ASM, airway smooth muscle; AR, adenosine receptor; DC, dendritic cell; GPCRs, G-protein-coupled receptors; TAS2R, type 2 taste receptor; NC, natural killer cell; CD, lymphocyte CD 8+; His, histamine; PD2, prostaglandin D2; PDE4: phosphodiesterase 4; AMPs, antimicrobial peptides; IP_3, inositol 1,4,5-triphosphate; PLC-β_2, phospholipase C-β_2; SR, sarcoplasmic reticulum; PKA, protein kinase A; cAMP, cyclic adenosine monophosphate; GPCR, G-protein-coupled receptor; IP3R, IP_3 receptor.

The IC_{50} of caffeine has been reported in neuronal tissues to be 160–210 µM for A_{2B} receptors and 17 nM for A_{2A} receptors [50]. The adenosine receptor pathways are useful targets in asthma treatment through the effects observed in airway smooth muscle (ASM) or on various types of immune and non-immune cells [51]. Adenosine receptors have been reported to be expressed in most immune cells and participate in the regulation of various putative functions. A_{2A} is the most widely expressed, particularly in asthmatic patients, with the A_1, A_{2B}, and A_3 subtypes being expressed only in certain cell types [52]. Inhibition could lead to more refined asthma management. The selectivity of caffeine analogs for A_{2A} receptors has been found to be somewhat increased by the replacement of one or two methyl groups of caffeine with a propyl or propargyl substituent [53]. Indeed, 3,7-dimethyl-1-propargylxanthine (DMPX) has been successfully used as a selective A_2 antagonist [54]. On the other hand, caffeine-inspired non-xanthine heterocyclic antagonists for A_{2B} receptors have also been developed, including a variety of 9-deaza-xanthines and 9-deaza-adenines [55,56].

2.2. Cyclic Nucleotide Phosphodiesterases

There are 11 families of phosphodiesterase (PDE) genes (PDE1–PDE11), which encode the PDE proteins that hydrolyze cyclic adenosine monophosphate (cAMP) and cyclic guanosine monophosphate (cGMP) to inactive 5′ AMP and 5′ GMP, respectively, regulating their intracellular levels [57]. These cyclic nucleotides activate a variety of cellular processes including the relaxation of airway smooth muscle and the release of inflammatory mediators [58] (Figure 1). PDE inhibition represents a potential mechanism to modulate airway smooth muscle contraction and the release of inflammatory mediators [57]. PDE3 and PDE4 are located in the tracheal and vascular smooth muscle, and PDE4 has a wide distribution in tissues including brain, gastrointestinal (GI) tract, spleen, lung, heart, testis, and kidney [58]. Furthermore, PDE4 is expressed in almost all inflammatory cell types except platelets that contain PDE3 and PDE5 [57]. The IC_{50} of caffeine to inhibit phosphodiesterase ranges from 500 μM to 1 mM [59], while theophylline is considered a more potent PDE4 inhibitor due to a lower IC_{50} of 70 μM. Theophylline is considered a more potent PDE4 inhibitor because cAMP values of 40% equivalent to 18 μg/mL have been found in plasma levels; at this concentration, relaxation of the bronchial tissue is induced [60]. Recently, Sildenafil, an approved PDE5 inhibitor used in the treatment of erectile dysfunction and pulmonary hypertension [61] that improves pulmonary hemodynamics by reducing vascular resistance in idiopathic pulmonary fibrosis [62,63], has proven to be effective in the treatment of COVID-19 [64]. We believe that caffeine, through its PDE inhibitory capacity, could potentially have similar effects, although more research is needed in this regard.

2.3. Agonist of the Type 2 Taste Receptor

In ASM, the canonical signaling pathway for the type 2 taste receptor (TAS2R) is through the coupling of a bitter compound to a GPCR receptor, which activates the Gqα subunit gustducin. While Gβ3 and Gγ13 form a complex, the subunit Gα gustducin dissociates from the heterodimer Gβ3/Gγ13, which activates the phospholipase C-β_2 (PLC-β_2) responsible for hydrolyzing phosphatidylinositol-4,5-bisphosphate in inositol-1,4,5-triphosphate (IP_3) and diacylglycerol. The IP_3 will bind to the IP_3 receptor (IP3R) on the SR and allow the Ca^{2+} to be released (Figure 1). It has been proposed that this released Ca^{2+} induces the opening of high-conductance calcium-activated potassium channels (BK_{Ca}), which are responsible for the hyperpolarization of the membrane and the relaxation of ASM [61–65]. In ASM, the TAS2R subtypes that are expressed are 7, 10, 14, 43, and 46, and caffeine is a known agonist of the TAS2R receptors [62]. It has been seen that in ASM, caffeine reverses the agonist-induced bronchoconstriction by blocking Ca^{2+} oscillations, decreasing the sensitivity to Ca^{2+} via the inhibition of released Ca^{2+} by the IP3R [66]. In this context, caffeine may facilitate breathing by contributing to widening the airway caliber, although much more studies are needed.

3. Immunomodulatory Effects of Caffeine

Among the many possible benefits caffeine might indirectly have in the infection caused by SARS-CoV-2, a strong emphasis should be made in the immunomodulatory effects it possesses [34,67]. The application of a bolus of caffeine at a dose of 6 mg/kg produces an increase in the total lymphocyte and CD8+ lymphocyte count [68]. Exposure of human cells to high and prolonged concentrations of caffeine has been shown to promote NK cell activity [69,70]. NK cells and lymphocytes are among the first cells activated against a viral threat and play a crucial role in the pathophysiology of COVID-19 infection (Figure 2).

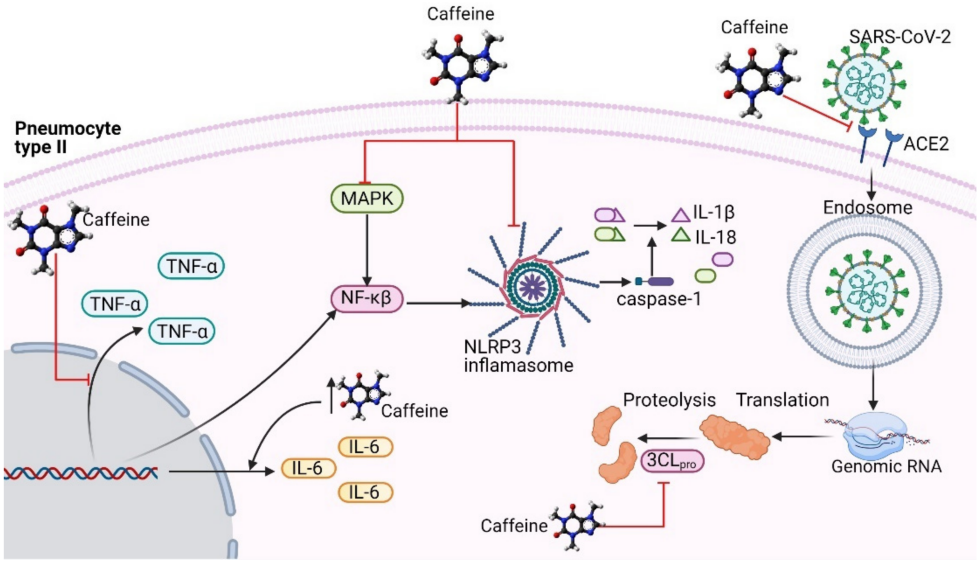

Figure 2. Schematic diagram of the proposed antiviral mechanisms of caffeine against SARS-CoV-2. Caffeine can inhibit the production of TNF-α and the expression of the inflammasome NLRP3 and its activity by the MAPK/NF-κβ pathway, decreasing the production of IL-1β and IL-18. Caffeine also inhibits viral entrance by blocking the RBD and ACE2 complex formation. Caffeine also inhibits $3CL_{pro}$, a protease required to release two polypeptides that are necessary for viral transcription and replication. TNF-α, tumor necrosis factor alpha; NF-κβ, nuclear factor kappa beta; ACE2, angiotensin-converting enzyme 2; NLRP3, inflammasome NOD-like receptor 3; IL-6, interleukin 6; IL-1β, interleukin 1 beta; IL-18, interleukin 18; MAPK, mitogen-activated protein kinase; $3CL_{pro}$, 3-chymotrypsin-like protease.

3.1. Adenosine Receptors

Some caffeine immunomodulatory effects can be attributed to its direct activity on immune cells, many of which express adenosine receptors, and caffeine is a well-known antagonist of these receptors. The stimulation of A_1 has been shown to promote the pro-inflammatory functions of neutrophils and eosinophils and promote monocyte phagocytosis, dendritic cell chemotaxis, and mucus production [52]. On the other hand, A_{2A} stimulation has been shown to inhibit degranulation from mast cells and neutrophils and neutrophil adherence to the endothelium; its activation has also been shown to inhibit IL-12 and TNF-α secretion from monocytes and macrophages and inhibits IL-6 and IL-8 secretion from endothelial cells [52].

On the other hand, A_{2B} stimulation promotes a pro-inflammatory state: in mast cells, it induces degranulation, cytokine secretion, and IgE synthesis, whereas in epithelial cells, it promotes IL-19 secretion. Moreover, VEGF and IL-8 secretion is promoted in endothelial cells, and IL-16 is secreted from bronchial smooth muscle and fibroblasts [52]. Little is known about the A_3 receptor functions, but its activity has been shown to be mainly inhibiting degranulation in neutrophils and inhibiting degranulation and chemotaxis in eosinophils.

It has been reported that adenosine plays a key role in regulating pulmonary inflammation and repair [71,72]. Remarkably, in acute inflammation, it significantly lowers cytokine production, immune cell migration, and vascular permeability, while during chronic inflammation, continuous, sustained adenosine stimulation increases cytokine secretion and immune cell infiltration into the lungs [73]. Interestingly, caffeine administration has been shown to partially revert the consequences of persistent adenosine stimulation [74], adding another interesting feature to the caffeine anti-inflammatory spectrum [75].

Thus, the participation of adenosine receptor pathways in the development of the cytokine storm in COVID-19 patients might be diminished through the protective effects of caffeine, limiting lung inflammation [52] (Figure 2).

3.2. Agonist of the Type 2 Taste Receptor

Anosmia and ageusia are characteristic symptoms of viral respiratory infections, particularly in that caused by SARS-CoV-2. TAS2R receptors are found to be expressed in many cell types, not only chemosensory epithelial cells but also throughout the airway and other systems, including leukocytes, mast cells, neutrophils, monocytes, eosinophils, and macrophages [64,76]. TAS2R agonists have demonstrated the inhibition of allergen-induced airway inflammation, inhibition of LPS-induced cytokine release, remodeling, and hyper-responsiveness [64,76]. Caffeine, being a known agonist of these receptors, could participate in accelerating the recovery of the sense of smell and could potentially contribute to mitigating the severity of the infection caused by SARS-CoV-2 due to the immunomodulatory effects attributed to these receptors [12,61]. In the first line of defense in the upper respiratory system against viral pathogens, the administration of caffeine has been demonstrated to modify certain immunological elements found in saliva, increasing the secretion of immunoglobulins and serum albumin, as well as lowering the levels of cystatin SN, a known inhibitor of protease [12,77]. In addition, the activation of TAS2Rs in epithelial cells of the upper respiratory tract has been shown to promote the secretion of antimicrobial peptides (AMPs), NO, and H_2O_2, which directly target viruses [78,79].

In macrophages, the activation of TAS2R has been shown to promote phagocytosis through NO and cAMP pathways, as well as the inhibition of TNF-α, CCL3, and CXCL8 production induced by LPS [61,64,80]. TAS2R agonists also inhibit pro-inflammatory cytokine production from leukocytes and IgE-mediated histamine and prostaglandin D_2 released by mast cells [61,81,82]. In a murine model, chronic or high acute doses of caffeine treatment protected against lung injury by lowering neutrophil recruitment and inhibiting secretion of TNF-α and IL-1 in an A_{2A}-independent manner but mediated through a cAMP pathway, possibly through the activation of TAS2R. However, a deleterious effect was observed when low acute doses of caffeine were administered, and this effect might be explained by the inhibition of the anti-inflammatory pathways mediated by the A_{2A} [83].

Similar results were observed in a previous study, where caffeine suppressed TNF-α plasma levels through the cAMP/PKA pathways, possibly through the activation of a TAS2R receptor [84] (Figure 2). Seemingly, caffeine can act as an immunosuppressor by reversing the overexpression of cytokines via TAS2R activation.

4. Probable Antiviral Activity of Caffeine in SARS-CoV-2 Infection

One of the first mechanisms that initiates the innate immune response is inflammasome NOD-like receptor 3 (NLRP3), an intracellular pattern recognition receptor (PRR) that recognizes pathogen-associated molecular patterns (PAMPs) and danger-associated molecular patterns (DAMPs) [85]. Caffeine has been shown to reduce its expression as well as suppress its activation through the mitogen-activated protein kinase (MAPK)/NF-κB signaling pathway. Consequently, the production of IL-1β and IL-18 is inhibited [67,86,87]. Notably, caffeine has also been observed to inhibit viral RNA synthesis and viral protein synthesis by some virus species such as the Newcastle disease virus, influenza virus, poliovirus, herpes simplex virus type 1 (HSV-1), human immunodeficiency virus (HIV), vaccinia virus, and polyomavirus [67,88–92]. In particular, an in vitro study showed that caffeine was able to inhibit the replication of the hepatitis C virus [67,93] (Figure 2).

4.1. Caffeine Might Be an Inhibitor of the RBD–ACE2 Complex

A key strategy in drug discovery against COVID-19 has been targeting the viral entrance into the host cell. Recently, Mohammadi et al. characterized the viral entrance through the formation of a complex between the RBD found in the S protein of the virus and the ACE2, the functional receptor for SARS-CoV-2 in the host cell's membrane. In a recent in silico study, caffeine was proposed as an effective inhibitor of the complex, both alone and in combination with antiviral agents [94].

The interactions between caffeine and caffeine in combination with antiviral agents with the RBD/ACE2 complex were evaluated through molecular dynamic (MD) simu-

lation and molecular docking. The two principal epitopes selected from the S protein crystal structure were recognized in the Protein Data Bank (PDB ID: 6VW1 and 6LZG). In addition, the interaction energies (IEs) were calculated between the RBD–ACE2 complex and the drug. From the data generated in MDs, the IE between caffeine and RBD–ACE2 complexes was calculated, showing a strong interaction with 6LZG. The results show that caffeine is especially efficient at interacting with 6LZG, thus blocking the formation of the RBD–ACE2 complex [94].

The possibility of using a combination of caffeine and antiviral agents was also explored through MD simulations and molecular docking, and it was shown that caffeine in combination with ribavirin has a synergic interaction in blocking the 6VW1 site, with a binding free energy of −6.76 (kcal/mol) and IE of −2000 (kcal/mol). Additionally, in the case of the 6VW1 complex, caffeine with favipiravir and ribavirin forms a more efficient structure against SARS-CoV-2 in terms of non-binding interaction energy, demonstrating a stable and promising binding tendency of caffeine with ACE2 and consequently possible inhibition of ACE2 against SARS-CoV-2 [94].

The most suitable interaction combination with ACE2 in absence of the S protein was also addressed. Among the various antiviral agents plus caffeine combinations explored, the strongest interaction was with ACE2 + remdesivir + caffeine with an IE value of −396.68 (kcal/mol). This negative value indicates that the complex is stable, preventing the formation of the S protein–ACE2 complex, and thus preventing the SARS-CoV-2 virus from infecting cells and continuing its viral cycle. Considering these results, the potential for the application of caffeine, both alone and in combination with antiviral agents, can be noticed, even more so since Tong et al. reported that ribavirin did not provide a survival benefit in comparison with the control treatment (involving only supportive therapy). As such, its in vivo activity against SARS-CoV-2 requires further investigation [95] (Figure 2).

4.2. Inhibition of 3-Chymotrypsin-Like Protease

One of the mechanisms necessary for the viral transcription and replication of SARS-CoV-2 depends on two polyproteins involved in the release of the functional polypeptide. Releasing these polypeptides requires the participation of 3-chymotrypsin-like protease ($3CL_{pro}$). Considering the importance of this protease, it has been investigated as a potential pharmacological target, searching for both existing drugs and natural compounds that could inhibit its activity [96,97]. Caffeine, other methylxanthines, and structurally similar compounds that possess a 4-pyridone ring in their structure have demonstrated an inhibitory effect on $3CL_{pro}$ through simulations of molecular dynamics and energy calculations [95]. The molecular docking between the $3CL_{pro}$ protein and caffeine shows an affinity of −5.6 kcal/mol and also forms hydrogen bonds with amino acids Cys145 and Glu166. These residues are key in the inhibition of the protease activity. This would prevent the generation of non-structural proteins that are essential for viral replication and thus the formation of new virions.

Finally, MD simulations were performed for the complexes formed in the dockings of the protein $3CL_{pro}$–caffeine and other similar compounds; these simulations were 200 ns [95]. The root-mean-square fluctuation (RMSF) values of the molecular dynamics of the $3CL_{pro}$–caffeine complexes were obtained; they demonstrated that the amino acids of the active site remained in stable conformation during simulation. Therefore, caffeine is recommended as a possible inhibitor of $3CL_{pro}$, further pointing out that this alkaloid has the potential to become a new therapeutic agent; however, further in vitro and in vivo studies are recommended to corroborate these findings [96] (Figure 2).

5. Conclusions

Despite the shared interests worldwide to provide effective therapeutic options against SARS-CoV-2, no specific antiviral treatment exists, and the primary options are based on symptomology treatment and vital support. In this review, we ascertained the possible health benefits that caffeine might provide, both directly and indirectly in terms of SARS-

CoV-2 infection, by favoring bronchodilatation and immunomodulation and probably by hindering viral intracellular transcription.

Funding: This study was partly supported by grants from the Dirección General de Asuntos del Personal Académico (DGAPA), the Universidad Nacional Autónoma de México (IN204319), and CONACYT (137725) to LM Montaño.

Acknowledgments: Bianca S. Romero-Martínez is grateful to the Programa de Doctorado en Ciencias Biomédicas, Universidad Nacional Autónoma de México, for the instruction received during her Ph.D. degree studies. She received a fellowship from the Consejo Nacional de Ciencia y Tecnología, México (application # 2020-000013-01NACF-12778; CVU 469822).

Conflicts of Interest: The authors declare that they have no competing interests.

References

1. Zhu, N.; Zhang, D.; Wang, W.; Li, X.; Yang, B.; Song, J.; Zhao, X.; Huang, B.; Shi, W.; Lu, R.; et al. A novel coronavirus from patients with pneumonia in China, 2019. *N. Engl. J. Med.* **2020**, *382*, 727–733. [CrossRef]
2. Cohen, J.; Normile, D. New SARS-like virus in China triggers alarm. *Science* **2020**, *367*, 234–235. [CrossRef]
3. Coronavirus Disease (COVID-19) Weekly Epidemiological Update and Weekly Operational Update. 2021. Available online: https://www.who.int/emergencies/diseases/novel-coronavirus-2019/situation-reports (accessed on 6 April 2021).
4. Cheng, V.C.C.; Lau, S.K.P.; Woo, P.C.Y.; Yuen, K.Y. Severe acute respiratory syndrome coronavirus as an agent of emerging and reemerging infection. *Clin. Microbiol. Rev.* **2007**, *20*, 660–694. [CrossRef] [PubMed]
5. Hoffmann, M.; Kleine-Weber, H.; Schroeder, S.; Krüger, N.; Herrler, T.; Erichsen, S.; Schiergens, T.S.; Herrler, G.; Wu, N.-H.; Müller, M.A.; et al. SARS-CoV-2 cell entry depends on ACE2 and TMPRSS2 and is blocked by a clinically proven protease inhibitor. *Cell* **2020**, *181*, 271–280. [CrossRef]
6. Li, Q.; Kang, C. Progress in developing inhibitors of SARS-CoV-2 3C-like protease. *Microorganisms* **2020**, *8*, 1250. [CrossRef] [PubMed]
7. Huang, C.; Wang, Y.; Li, X.; Ren, L.; Zhao, J.; Hu, Y.; Zhang, L.; Fan, G.; Xu, J.; Cao, B. Clinical features of patients infected with 2019 novel coronavirus in Wuhan, China. *Lancet* **2020**, *395*, 497–506. [CrossRef]
8. Ruan, Q.; Yang, K.; Wang, W.; Jiang, L.; Song, J. Clinical predictors of mortality due to COVID-19 based on an analysis of data of 150 patients from Wuhan, China. *Intensiv. Care Med.* **2020**, *46*, 846–848. [CrossRef]
9. Wang, L.; He, W.; Yu, X.; Hu, D.; Bao, M.; Liu, H.; Zhou, J.; Jiang, H. Coronavirus disease 2019 in elderly patients: Characteristics and prognostic factors based on 4-week follow-up. *J. Infect.* **2020**, *80*, 639–645. [CrossRef]
10. Rothan, H.A.; Byrareddy, S.N. The epidemiology and pathogenesis of coronavirus disease (COVID-19) outbreak. *J. Autoimmun.* **2020**, *109*, 102433. [CrossRef]
11. Velavan, T.P.; Meyer, C.G. The COVID-19 epidemic. *Trop. Med. Int. Health* **2020**, *25*, 278–280. [CrossRef]
12. Lin, L.; Lu, L.; Cao, W.; Li, T. Hypothesis for potential pathogenesis of SARS-CoV-2 infection—A review of immune changes in patients with viral pneumonia. *Emerg. Microbes Infect.* **2020**, *9*, 727–732. [CrossRef] [PubMed]
13. Wadman, M.; Couzin-Frankel, J.; Kaiser, J.; Matacic, C. How does coronavirus kill? Clinicians trace a ferocious rampage through the body, from brain to toes. *Sci. Biol. Coronavirus* **2020**. [CrossRef]
14. Conti, P.; Ronconi, G.; Caraffa, A.L.; Gallenga, C.E.; Ross, R.; Frydas, I.; Kritas, S.K. Induction of pro-inflammatory cytokines (IL-1 and IL-6) and lung inflammation by Coronavirus-19 (COVI-19 or SARS-CoV-2): Anti-inflammatory strategies. *J. Biol. Regul. Homeost Agents* **2020**, *34*, 327–331. [PubMed]
15. Dong, E.; Du, H.; Gardner, L. An interactive web-based dashboard to track COVID-19 in real time. *Lancet Infect. Dis.* **2020**, *20*, 533–534. [CrossRef]
16. Ramanathan, K.; Antognini, D.; Combes, A.; Paden, M.; Zakhary, B.; Ogino, M.; MacLaren, G.; Brodie, D.; Shekar, K. Planning and provision of ECMO services for severe ARDS during the COVID-19 pandemic and other outbreaks of emerging infectious diseases. *Lancet Respir. Med.* **2020**, *8*, 518–526. [CrossRef]
17. Pan, A.; Liu, L.; Wang, C.; Guo, H.; Hao, X.; Wang, Q.; Huang, J.; He, N.; Yu, H.; Lin, X.; et al. Association of Public Health Interventions with the Epidemiology of the COVID-19 Outbreak in Wuhan, China. *JAMA* **2020**, *323*, 1915. [CrossRef]
18. Stasi, C.; Fallani, S.; Voller, F.; Silvestri, C. Treatment for COVID-19: An overview. *Eur. J. Pharmacol.* **2020**, *889*, 173644. [CrossRef]
19. WHO Updates Clinical Care Guidance with Corticosteroid Recommendations. 2020. Available online: https://www.who.int/news-room/feature-stories/detail/who-updates-clinical-care-guidance-with-corticosteroid-recommendations (accessed on 6 April 2021).
20. Panel, C.-T.G. Coronavirus Disease 2019 (COVID-19) Treatment Guidelines. 2019. Available online: https://www.covid19treatmentguidelines.nih.gov/ (accessed on 6 April 2021).
21. Fredholm, B.B.; Bättig, K.; Holmén, J.; Nehlig, A.; Zvartau, E.E. Actions of caffeine in the brain with special reference to factors that contribute to its widespread use. *Pharmacol. Rev.* **1999**, *51*, 83–133.
22. Institute of Medicine Committee on Military Nutrition, R. *Caffeine for the Sustainment of Mental Task Performance: Formulations for Military Operations*; National Academies Press: Washington, DC, USA, 2001.

23. Nawrot, P.; Jordan, S.; Eastwood, J.; Rotstein, J.; Hugenholtz, A.; Feeley, M. Effects of caffeine on human health. *Food Addit. Contam.* **2003**, *20*, 1–30. [CrossRef]
24. Kreutzer, K.; Bassler, D. Caffeine for Apnea of Prematurity: A Neonatal Success Story. *Neonatology* **2014**, *105*, 332–336. [CrossRef]
25. Hedner, T.; Hedner, J.; Bergman, B.; Mueller, R.; Jonason, J. Characterization of adenosine-induced respiratory depression in the preterm rabbit. *Neonatology* **1985**, *47*, 323–332. [CrossRef]
26. Vyas-Read, S.; Kanaan, U.; Shankar, P.; Stremming, J.; Travers, C.; Carlton, D.P.; Fitzpatrick, A. Early characteristics of infants with pulmonary hypertension in a referral neonatal intensive care unit. *BMC Pediatr.* **2017**, *17*, 163. [CrossRef] [PubMed]
27. Welsh, E.J.; Bara, A.; Barley, E.; Cates, C.J. Caffeine for asthma. *Cochrane Database Syst. Rev.* **2010**, *2010*, CD001112. [CrossRef]
28. Kivity, S.; Ben Aharon, Y.; Man, A.; Topilsky, M. The effect of caffeine on exercise-induced bronchoconstriction. *Chest* **1990**, *97*, 1083–1085. [CrossRef] [PubMed]
29. Tilley, S.L. Methylxanthines in asthma. *Methylxanthines* **2011**, *200*, 439–456.
30. Willson, C. The clinical toxicology of caffeine: A review and case study. *Toxicol. Rep.* **2018**, *5*, 1140–1152. [CrossRef]
31. Campbell, M.E.; Grant, D.M.; Inaba, T.; Kalow, W. Biotransformation of caffeine, paraxanthine, theophylline, and theobromine by polycyclic aromatic hydrocarbon-inducible cytochrome(s) P-450 in human liver microsomes. *Drug Metab. Dispos.* **1987**, *15*, 237–249.
32. Ajjampur, K.; Subramaniam, A. The importance of early use of beta blockers and gastric decontamination in caffeine overdose: A case report. *Aust. Crit. Care* **2020**. [CrossRef] [PubMed]
33. Montaño, L.M.; Carbajal, V.; Arreola, J.L.; Barajas-López, C.; Flores-Soto, E.; Vargas, M.H. Acetylcholine and tachykinins involvement in the caffeine-induced biphasic change in intracellular Ca^{2+} in bovine airway smooth muscle. *Br. J. Pharmacol.* **2003**, *139*, 1203–1211. [CrossRef]
34. Flores-Soto, E.; Reyes-García, J.; Sommer, B.; Chavez, J.; Barajas-López, C.; Montaño, L.M. PPADS, a P2X receptor antagonist, as a novel inhibitor of the reverse mode of the Na^{+}/Ca^{2+} exchanger in guinea pig airway smooth muscle. *Eur. J. Pharmacol.* **2012**, *674*, 439–444. [CrossRef] [PubMed]
35. Soto, E.F.; Reyes-García, J.; Sommer, B.; Montaño, L.M. Sarcoplasmic reticulum Ca^{2+} refilling is determined by L-type Ca^{2+} and store operated Ca^{2+} channels in guinea pig airway smooth muscle. *Eur. J. Pharmacol.* **2013**, *721*, 21–28. [CrossRef] [PubMed]
36. Liu, L.; Zhang, C.; Chen, J.; Li, X. Rediscovery of caffeine: An excellent drug for improving patient outcomes while fighting WARS. *Curr. Med. Chem.* **2020**. [CrossRef] [PubMed]
37. Kalidhindi, R.S.R.; Borkar, N.A.; Ambhore, N.S.; Pabelick, C.M.; Prakash, Y.S.; Sathish, V. Sex steroids skew ACE2 expression in human airway: A contributing factor to sex differences in COVID-19? *Am. J. Physiol. Cell. Mol. Physiol.* **2020**, *319*, L843–L847. [CrossRef] [PubMed]
38. Cushley, M.J.; Tattersfield, A.E.; Holgate, S.T. Adenosine antagonism as an alternative mechanism of action of methylxanthines in asthma. *Agents Actions Suppl.* **1983**, *13*, 109–113. [PubMed]
39. Crimi, N.; Palermo, F.; Oliveri, R.; Maccarrone, C.; Palermo, B.; Vancheri, C.; Polosa, R.; Mistretta, A. Enhancing effect of dipyridamole inhalation on adenosine-induced bronchospasm in asthmatic patients. *Allergy* **1988**, *43*, 179–183. [CrossRef] [PubMed]
40. Bucchioni, E.; Csoma, Z.; Allegra, L.; Chung, K.; Barnes, P.; Kharitonov, S. Adenosine 5′-monophosphate increases levels of leukotrienes in breath condensate in asthma. *Respir. Med.* **2004**, *98*, 651–655. [CrossRef]
41. Polosa, R. Adenosine-receptor subtypes: Their relevance to adenosine-mediated responses in asthma and chronic obstructive pulmonary disease. *Eur. Respir. J.* **2002**, *20*, 488–496. [CrossRef] [PubMed]
42. Holgate, S.T. Adenosine provocation: A new test for allergic type airway inflammation. *Am. J. Respir. Crit. Care Med.* **2002**, *165*, 317–318. [CrossRef]
43. Driver, A.G.; Kukoly, C.A.; Ali, S.; Mustafa, S.J. Adenosine in bronchoalveolar lavage fluid in asthma. *Am. Rev. Respir. Dis.* **1993**, *148*, 91–97. [CrossRef]
44. Csoma, Z.; Huszár, É.; Vizi, É.; Vass, G.; Szabó, Z.; Herjavecz, I.; Kollai, M.; Horvath, I. Adenosine level in exhaled breath increases during exercise-induced bronchoconstriction. *Eur. Respir. J.* **2005**, *25*, 873–878. [CrossRef]
45. Huszár, É.; Vass, G.; Vizi, É.; Csoma, Z.; Barát, E.; Világos, G.M.; Herjavecz, I.; Horvath, I. Adenosine in exhaled breath condensate in healthy volunteers and in patients with asthma. *Eur. Respir. J.* **2002**, *20*, 1393–1398. [CrossRef]
46. Ali, S.; Mustafa, S.J.; Metzger, W.J. Adenosine receptor-mediated bronchoconstriction and bronchial hyperresponsiveness in allergic rabbit model. *Am. J. Physiol. Content* **1994**, *266*, 271–277. [CrossRef]
47. Dahlen, S.E.; Hansson, G.; Hedqvist, P.; Bjorck, T.; Granstrom, E.; Dahlen, B. Allergen challenge of lung tissue from asthmatics elicits bronchial contraction that correlates with the release of leukotrienes C4, D4, and E4. *Proc. Natl. Acad. Sci. USA* **1983**, *80*, 1712–1716. [CrossRef]
48. Olah, M.E.; Stiles, G.L. Adenosine receptor subtypes: Characterization and therapeutic regulation. *Annu. Rev. Pharmacol. Toxicol.* **1995**, *35*, 581–606. [CrossRef]
49. Fredholm, B.B.; Ijzerman, A.P.; Jacobson, K.A.; Linden, J.; Müller, C.E. International union of basic and clinical pharmacology. LXXXI. Nomenclature and classification of adenosine receptors—An update. *Pharmacol. Rev.* **2011**, *63*, 1–34. [CrossRef] [PubMed]
50. Conde, S.V.; Obeso, A.; Vicario, I.; Rigual, R.; Rocher, A.; Gonzalez, C. Caffeine inhibition of rat carotid body chemoreceptors is mediated by A2A and A2B adenosine receptors. *J. Neurochem.* **2006**, *98*, 616–628. [CrossRef] [PubMed]

51. Antonioli, L.; Blandizzi, C.; Pacher, P.; Haskó, G. The purinergic system as a pharmacological target for the treatment of immune-iediated inflammatory diseases. *Pharmacol. Rev.* **2019**, *71*, 345–382. [CrossRef] [PubMed]
52. Wilson, C.N.; Nadeem, A.; Spina, D.; Brown, R.; Page, C.P.; Mustafa, S.J. Adenosine receptors and asthma. *Handb. Exp. Pharmacol.* **2009**, *193*, 329–362.
53. Ukena, D.; Shamim, M.; Padgett, W.; Daly, J. Analogs of caffeine: Antagonists with selectivity for A2 adenosine receptors. *Life Sci.* **1986**, *39*, 743–750. [CrossRef]
54. Seale, T.W.; Abla, K.A.; Shamim, M.T.; Carney, J.M.; Daly, J.W. 3,7-Dimethyl-1-propargylxanthine: A potent and selective in vivo antagonist of adenosine analogs. *Life Sci.* **1988**, *43*, 1671–1684. [CrossRef]
55. Baraldi, P.G.; Romagnoli, R.; Preti, D.; Fruttarolo, F.; Carrion, M.D.; Tabrizi, M.A. Ligands for A2B adenosine receptor subtype. *Curr. Med. Chem.* **2006**, *13*, 3467–3482. [CrossRef]
56. Akkari, R.; Burbiel, J.C.; Hockemeyer, J.; Müller, C.E. Recent progress in the development of adenosine receptor ligands as antiinflammatory drugs. *Curr. Top. Med. Chem.* **2006**, *6*, 1375–1399. [CrossRef]
57. Maurice, D.H.; Ke, H.; Ahmad, F.; Wang, Y.; Chung, J.; Manganiello, V.C. Advances in targeting cyclic nucleotide phosphodiesterases. *Nat. Rev. Drug Discov.* **2014**, *13*, 290–314. [CrossRef]
58. Zhang, K.Y.; Ibrahim, P.N.; Gillette, S.; Bollag, G. Phosphodiesterase-4 as a potential drug target. *Expert Opin. Ther. Targets* **2005**, *9*, 1283–1305. [CrossRef] [PubMed]
59. Choi, O.H.; Shamim, M.T.; Padgett, W.L.; Daly, J.W. Caffeine and theophylline analogues: Correlation of behavioral effects with activity as adenosine receptor antagonists and as phosphodiesterase inhibitors. *Life Sci.* **1988**, *43*, 387–398. [CrossRef]
60. Rabe, K.F.; Magnussen, H.; Dent, G. Theophylline and selective PDE inhibitors as bronchodilators and smooth muscle relaxants. *Eur. Respir. J.* **1995**, *8*, 637–642.
61. Travadi, J.; Patole, S. Phosphodiesterase inhibitors for persistent pulmonary hypertension of the newborn: A review. *Pediatr. Pulmonol.* **2003**, *36*, 529–535. [CrossRef]
62. Rochwerg, B.; Neupane, B.; Zhang, Y.; Garcia, C.C.; Raghu, G.; Richeldi, L.; Brozek, J.; Beyene, J.; Schünemann, H. Treatment of idiopathic pulmonary fibrosis: A network meta-analysis. *BMC Med.* **2016**, *14*, 18. [CrossRef] [PubMed]
63. Prasad, S.; Wilkinson, J.; Gatzoulis, M.A. Sildenafil in primary pulmonary hypertension. *N. Engl. J. Med.* **2000**, *343*, 1342. [CrossRef]
64. Sansone, A.; Mollaioli, D.; Ciocca, G.; Limoncin, E.; Colonnello, E.; Vena, W.; Jannini, E. Addressing male sexual and reproductive health in the wake of COVID-19 outbreak. *J. Endocrinol. Investig.* **2021**, *44*, 223–231. [CrossRef] [PubMed]
65. Devillier, P.; Naline, E.; Grassin-Delyle, S. The pharmacology of bitter taste receptors and their role in human airways. *Pharmacol. Ther.* **2015**, *155*, 11–21. [CrossRef]
66. Deshpande, D.A.; Wang, W.C.; McIlmoyle, E.L.; Robinett, K.S.; Schillinger, R.M.; An, S.S.; Sham, J.S.K.; Liggett, S. Bitter taste receptors on airway smooth muscle bronchodilate by localized calcium signaling and reverse obstruction. *Nat. Med.* **2010**, *16*, 1299–1304. [CrossRef] [PubMed]
67. Meyerhof, W.; Batram, C.; Kuhn, C.; Brockhoff, A.; Chudoba, E.; Bufe, B.; Appendino, G.; Behrens, M. The molecular receptive ranges of human TAS2R bitter taste receptors. *Chem. Senses* **2010**, *35*, 157–170. [CrossRef]
68. Grassin-Delyle, S.; Abrial, C.; Fayad-Kobeissi, S.; Brollo, M.; Faisy, C.; Alvarez, J.-C.; Naline, E.; DeVillier, P. The expression and relaxant effect of bitter taste receptors in human bronchi. *Respir. Res.* **2013**, *14*, 134. [CrossRef] [PubMed]
69. Shaik, F.A.; Singh, N.; Arakawa, M.; Duan, K.; Bhullar, R.P.; Chelikani, P. Bitter taste receptors: Extraoral roles in pathophysiology. *Int. J. Biochem. Cell Biol.* **2016**, *77*, 197–204. [CrossRef] [PubMed]
70. Tan, X.; Sanderson, M.J. Bitter tasting compounds dilate airways by inhibiting airway smooth muscle calcium oscillations and calcium sensitivity. *Br. J. Pharmacol.* **2014**, *171*, 646–662. [CrossRef]
71. Monji, F.; Siddiquee, A.A.-M.; Hashemian, F. Can pentoxifylline and similar xanthine derivatives find a niche in COVID-19 therapeutic strategies? A ray of hope in the midst of the pandemic. *Eur. J. Pharmacol.* **2020**, *887*, 173561. [CrossRef]
72. Bishop, N.C.; Fitzgerald, C.; Porter, P.J.; Scanlon, G.A.; Smith, A.C. Effect of caffeine ingestion on lymphocyte counts and subset activation in vivo following strenuous cycling. *Graefe's Arch. Clin. Exp. Ophthalmol.* **2004**, *93*, 606–613. [CrossRef]
73. Chen, L.; Bell, E.M.; Browne, M.L.; Druschel, C.M.; Romitti, P.A.; Schmidt, R.J.; Burns, T.L.; Moslehi, R.; Olney, R.S.; National Birth Defects Prevention Study. Maternal caffeine consumption and risk of congenital limb deficiencies. *Birth Defects Res. Part A Clin. Mol. Teratol.* **2012**, *94*, 1033–1043. [CrossRef] [PubMed]
74. Dulson, D.K.; Bishop, N.C. Effect of a high and low dose of caffeine on human lymphocyte activation in response to antigen stimulation. *Appl. Physiol. Nutr. Metab.* **2016**, *41*, 224–227. [CrossRef]
75. Karmouty-Quintana, H.; Xia, Y.; Blackburn, M.R. Adenosine signaling during acute and chronic disease states. *J. Mol. Med.* **2013**, *91*, 173–181. [CrossRef] [PubMed]
76. Ter Horst, S.A.; Wagenaar, G.T.; De Boer, E.; Van Gastelen, M.A.; Meijers, J.C.; Biemond, B.J.; Ben, J.H.M.; Walther, F.J. Pentoxifylline reduces fibrin deposition and prolongs survival in neonatal hyperoxic lung injury. *J. Appl. Physiol.* **2004**, *97*, 2014–2019. [CrossRef] [PubMed]
77. Li, H.; Karmouty-Quintana, H.; Chen, N.-Y.; Mills, T.; Molina, J.; Blackburn, M.R.; Davies, J. Loss of CD73-mediated extracellular adenosine production exacerbates inflammation and abnormal alveolar development in newborn mice exposed to prolonged hyperoxia. *Pediatr. Res.* **2017**, *82*, 1039–1047. [CrossRef]

78. Chavez-Valdez, R.; Wills-Karp, M.; Ahlawat, R.; Cristofalo, E.A.; Nathan, A.; Gauda, E. Caffeine modulates TNF-alpha production by cord blood monocytes: The role of adenosine receptors. *Pediatr. Res.* **2009**, *65*, 203–208. [CrossRef] [PubMed]
79. Endesfelder, S.; Strauß, E.; Bendix, I.; Schmitz, T.; Bührer, C. Prevention of oxygen-induced inflammatory lung injury by caffeine in neonatal rats. *Oxidative Med. Cell. Longev.* **2020**, *2020*, 3840124. [CrossRef]
80. Nayak, A.P.; Villalba, D.; Deshpande, D.A. Bitter taste receptors: An answer to comprehensive asthma control? *Curr. Allergy Asthma Rep.* **2019**, *19*, 48. [CrossRef]
81. Dsamou, M.; Palicki, O.; Septier, C.; Chabanet, C.; Lucchi, G.; Ducoroy, P.; Chagnon, M.-C.; Morzel, M. Salivary protein profiles and sensitivity to the bitter taste of caffeine. *Chem. Senses* **2011**, *37*, 87–95. [CrossRef] [PubMed]
82. Lee, R.J.; Kofonow, J.M.; Rosen, P.L.; Siebert, A.P.; Chen, B.; Doghramji, L.; Xiong, G.; Adappa, N.D.; Palmer, J.N.; Kennedy, D.W.; et al. Bitter and sweet taste receptors regulate human upper respiratory innate immunity. *J. Clin. Investig.* **2014**, *124*, 1393–1405. [CrossRef]
83. Lee, R.J.; Xiong, G.; Kofonow, J.M.; Chen, B.; Lysenko, A.; Jiang, P.; Abraham, V.; Doghramji, L.; Adappa, N.D.; Palmer, J.N.; et al. T2R38 taste receptor polymorphisms underlie susceptibility to upper respiratory infection. *J. Clin. Investig.* **2012**, *122*, 4145–4159. [CrossRef]
84. Gopallawa, I.; Freund, J.R.; Lee, R.J. Bitter taste receptors stimulate phagocytosis in human macrophages through calcium, nitric oxide, and cyclic-GMP signaling. *Cell. Mol. Life Sci.* **2021**, *78*, 271–286. [CrossRef]
85. Orsmark-Pietras, C.; James, A.; Konradsen, J.R.; Nordlund, B.; Söderhäll, C.; Pulkkinen, V.; Pedroletti, C.; Daham, K.; Kupczyk, M.; Dahlén, B.; et al. Transcriptome analysis reveals upregulation of bitter taste receptors in severe asthmatics. *Eur. Respir. J.* **2013**, *42*, 65–78. [CrossRef] [PubMed]
86. Ekoff, M.; Choi, J.H.; James, A.; Dahlén, B.; Nilsson, G.; Dahlén, S.E. Bitter taste receptor (TAS2R) agonists inhibit IgE-dependent mast cell activation. *J. Allergy Clin. Immunol.* **2014**, *134*, 475–478. [CrossRef] [PubMed]
87. Li, J.; Li, G.; Hu, J.-L.; Fu, X.-H.; Zeng, Y.-J.; Zhou, Y.-G.; Xiong, G.; Yang, N.; Dai, S.-S.; He, F.-T. Chronic or high dose acute caffeine treatment protects mice against oleic acid-induced acute lung injury via an adenosine A2A receptor-independent mechanism. *Eur. J. Pharmacol.* **2011**, *654*, 295–303. [CrossRef] [PubMed]
88. Horrigan, L.A.; Kelly, J.P.; Connor, T.J. Caffeine suppresses TNF-α production via activation of the cyclic AMP/protein kinase A pathway. *Int. Immunopharmacol.* **2004**, *4*, 1409–1417. [CrossRef]
89. Im, H.; Ammit, A.J. The NLRP3 inflammasome: Role in airway inflammation. *Clin. Exp. Allergy* **2014**, *44*, 160–172. [CrossRef] [PubMed]
90. Guo, H.; Callaway, J.B.; Ting, J.P.Y. Inflammasomes: Mechanism of action, role in disease, and therapeutics. *Nat. Med.* **2015**, *21*, 677–687. [CrossRef] [PubMed]
91. Zhao, W.; Ma, L.; Cai, C.; Gong, X. Caffeine inhibits NLRP3 Iinflammasome activation by suppressing MAPK/NF-κB and A2aR signaling in LPS-induced THP-1 macrophages. *Int. J. Biol. Sci.* **2019**, *15*, 1571–1581. [CrossRef] [PubMed]
92. Dahl, J.; You, J.; Benjamin, T.L. Induction and utilization of an ATM signaling pathway by polyomavirus. *J. Virol.* **2005**, *79*, 13007–13017. [CrossRef] [PubMed]
93. Daniel, R.; Marusich, E.; Argyris, E.; Zhao, R.Y.; Skalka, A.M.; Pomerantz, R.J. Caffeine inhibits human immunodeficiency virus Type 1 transduction of nondividing cells. *J. Virol.* **2005**, *79*, 2058–2065. [CrossRef] [PubMed]
94. Mohammadi, S.; Heidarizadeh, M.; Entesari, M.; Esmailpour, A.; Esmailpour, M.; Moradi, R.; Sakhaee, N.; Doustkhah, E. In silico investigation on the inhibiting role of Nicotine/Caffeine by Blocking the S Protein of SARS-CoV-2 Versus ACE2 Receptor. *Microorganisms* **2020**, *8*, 1600. [CrossRef]
95. Tong, S.; Su, Y.; Yu, Y.; Wu, C.; Chen, J.; Wang, S.; Jiang, J. Ribavirin therapy for severe COVID-19: A retrospective cohort study. *Int. J. Antimicrob. Agents* **2020**, *56*, 106114. [CrossRef] [PubMed]
96. Elzupir, A.O. Caffeine and caffeine-containing pharmaceuticals as promising inhibitors for 3-chymotrypsin-like protease of SARS-CoV-2. *J. Biomol. Struct. Dyn.* **2020**, 1–8. [CrossRef] [PubMed]
97. Elmezayen, A.D.; Al-Obaidi, A.; Şahin, A.T.; Yelekçi, K. Potential inhibitors of coronavirus 3-chymotrypsin-like protease (3CL(pro)): An in silico screening of alkaloids and terpenoids from African medicinal plants. *J. Biomol. Struct. Dyn.* **2020**, *39*, 2980–2992. [CrossRef] [PubMed]